University of Salerno

Department of Chemistry and Biology "Adolfo Zambelli"

PhD Thesis in Chemistry

XXXIII Cycle

Study on Calixarene Threading: Towards Molecular Machines

Tutor:

Prof. Placido Neri

PhD Student:

Veronica Iuliano

8800100034

Co-Tutor:

Prof. Carmine Gaeta

Prof.ssa Carmen Talotta

Coordinator:

Prof. Claudio Pellecchia

Academic Year 2020/2021

Table of Contents

Abstract

Over the past three decades, the use of calixarenes as macrocyclic hosts in supramolecular chemistry has gained an increasing relevance, especially for the construction of molecular devices. Therefore, it is important to understand how to modify the supramolecular abilities of these macrocycles. In this PhD thesis, the threading abilities of calix[*n*]arenes with ammonium axles have been studied by modifying the calixarene scaffold. Initially, new hosts were obtained by functionalizing the upper rim, the lower rim, and the methylene bridges (**Figure A.1**). From these studies, important information was gained to obtain increasingly stable interpenetrated systems.

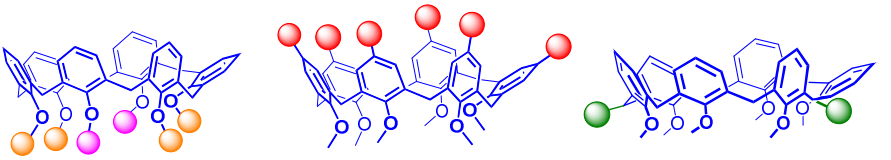

Figure A.1. Sketched functionalization for the new calixarene hosts here studied.

Subsequently, a trivalent calixarene host (**Figure A.2, left**) was studied which led to the formation of multicomponent systems such as pseudo[3]- and -[4]rotaxanes. Finally, studies on self-sorting processes in pseudo[3]rotaxane systems (**Figure A.2, right**) have been carried out. Thus, the peculiar ability of some diammonium axles to select the calixarene partner in the presence of other macrocycles has been highlighted. Furthermore, the selection takes place in a stereocontrolled way leading to the formation of selected stereo-adducts over those theoretically possible.

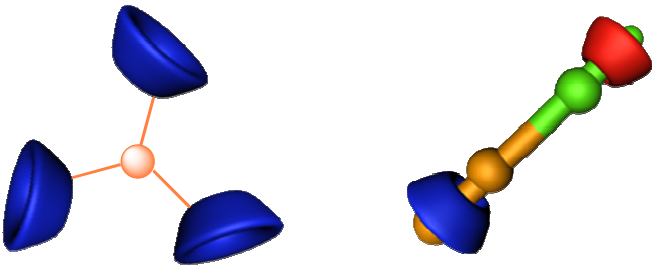

Figure A.2. Studied multivalent systems.

CHAPTER I

Introduction

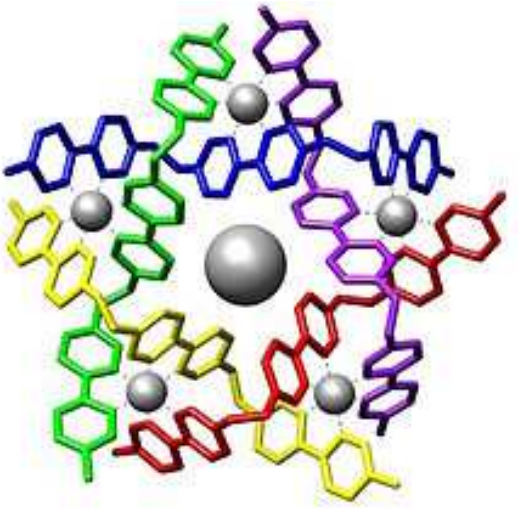

1.1 Supramolecular Chemistry

The importance of supramolecular chemistry has been recognized by awarding 2 Nobel prizes in this field. The first was awarded to Donald J. Cram, Jean-Marie Lehn, and Charles J. Pedersen in 1987 (**Figure 1.1a**), while the second was awarded to Jean-Pierre Sauvage, Sir J. Fraser Stoddart, and Bernard L. Feringa in 2016 (**Figure 1.1b**).

Figure 1.1. Chemistry Nobel prize winners in 1987 (a) and 2016 (b) years.

This branch of chemistry is a highly interdisciplinary one, which not only attracts the interest of organic, inorganic, and analytical chemists but also of biochemists, biologists, environmental scientists, engineers, material physicists, and theorists, even mathematicians, and various other researchers. Supramolecular chemistry has been defined, by Nobel laureate Jean Marie Lehn, as "*Chemistry beyond the molecule*"[1] and thus, a *supramolecule* is an organized, complex entity that is created from the association of two or more chemical species held together by secondary interactions.

Supramolecular structures are the result not only of additive but also cooperative interactions, including hydrogen bonding, hydrophobic interactions, and coordination. Their properties are different (often better) than the sum of the properties of each individual component. A well-known example of a cooperative supramolecular system, present in nature, is haemoglobin, a protein composed of four subunits appropriately assembled thanks to secondary interactions of supramolecular nature (**Figure 1.2**). In fact, in the active sites an allosteric regulation is imparted by the histidine 143 located proximally to the *eme* group. When O_2 binds to the first *eme*

[1](a) Lehn, J.-M. Supramolecular Chemistry: Concepts and Perspectives: A Personal Account; VCH: Weinheim ; New York, **1995**. (b) Ariga, K.;·Kunitake, T. Supramolecular Chemistry: Fundamentals and Applications; Springer-Verlag: Berlin/Heidelberg, **2006**.

group, the distance between His and iron atom increases causing important conformational changes in the other three subunits.

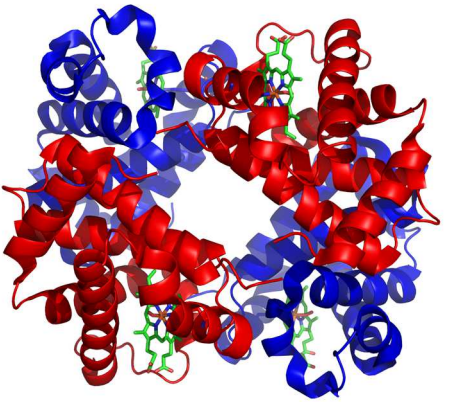

Figure 1.2. Representation of haemoglobin.

1.2 Molecular Recognition

Supramolecular chemistry is based on a general phenomenon known as molecular recognition. In fact, two entities that compose a supramolecular system are generally called molecular receptor and substrate. For a receptor (host) to recognize a determinate substrate (guest) an elevate number of non-covalent interactions must be created and a high degree of stereoelectronic complementarity must be present.

A definition of a host/guest complex was given by Nobel laureate D. J. Cram in 1986: "*The complexes are formed by two or more molecules or ions joined together in a single structural relationship by non-covalent forces. A molecular complex is composed of at least one host and one guest. A host-guest relationship implies a stereoelectronic complementarity between the link sites of the host and the guest* ".[2] The main molecular interactions involved in this type of process are of a secondary nature such as the ion-ion, dipole-dipole, dipole-hydrogen, hydrogen bonding, and van der Waals forces.[3] Examples are given by species containing an intramolecular cavity in which the substrate is able to fit (**Figure 1.3**).

[2] Cram, D.J., *Angew. Chem. Int. Ed. Engl.*, **1986**, *25*, 1039.
[3] Oshovsky, G. V.; Reinhoudt, D. N.; Verboom, W., *Supramolecular Chemistry in Water*, in *Angew. Chem. Int. Ed.*, **2007**.

Figure 1.3. Formation of Host/Guest complex.

The host can be represented by a large molecule or a molecular aggregate. A well-known example are enzymes (**Figure 1.4**),[4] which have a large central cavity with convergent bonding functions, for example Lewis bases or hydrogen bond donors. The guest, on the other hand, can be a monoatomic cation, a simple inorganic anion, or more complex molecules, such as hormones and neurotransmitters, that have divergent bonding functions such as Lewis acids or hydrogen bond acceptors. These molecular recognition phenomena are the basis of transport, regulation, enzymatic processes, translation and transcription of the genetic code, intramolecular, intermolecular, and cellular recognition. All these phenomena require an accurate manipulation of the energetic and stereochemical properties of non-covalent intermolecular forces to obtain highly efficient and selective receptor molecules.[5]

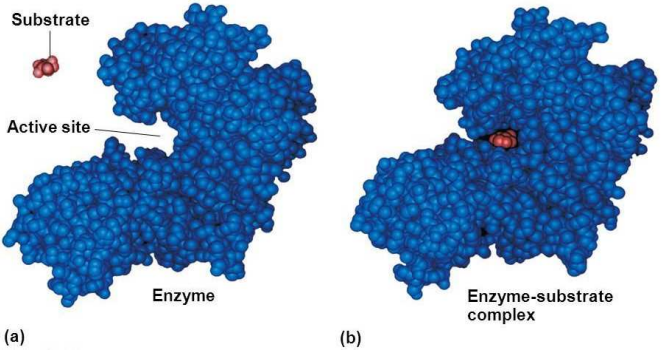

Figure 1.4. (a) The active site of the enzyme hexokinase (blue) and glucose (red) as substrate; (b) enzyme-substrate complex.

1.3 Interpenetrated and Interlocked Systems

From the initial studies on receptors, coordination chemistry, and molecular recognition through to pre-organization and self-assembly, supramolecular chemistry is now focusing on the complete control of increasingly complex molecules, supramolecules, and materials. Artificial systems possessing specific chemical-

[4] Campbell, N. A.; Reece, J. B. *Biology*, 7th ed.; Pearson, Benjamin Cummings: San Francisco, **2005**.
[5]. Lehn, J. Supramolecular Chemistry. *Science* **1993**, *260* (5115), 1762–1763.

physical and/or biological properties are designed. In the literature, there are a lot of examples of complex supramolecular architectures able to efficiently mimic biological systems or to perform specific movements following certain external stimuli. Recently, the interest has been focused on the study of interpenetrated and interlocked systems, such as pseudorotaxanes, rotaxanes, and catenanes (**Figure 1.5**)[6].

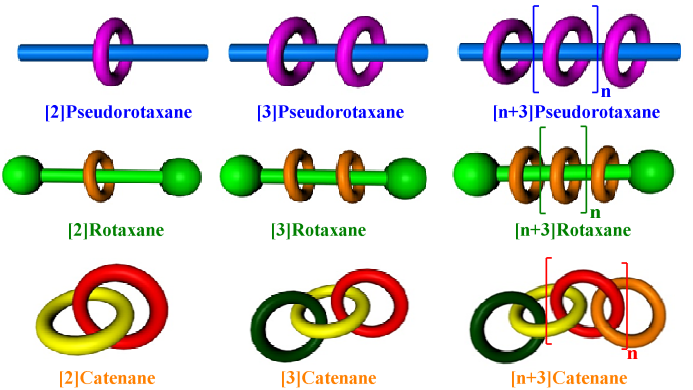

Figure 1.5. Interpenetrated and/or interlocked systems. Structure of [*n*]rotaxanes and [*n*]catenanes.

Rotaxanes are supramolecular systems consisting of a linear unit (axle) threaded through a cyclic one (wheel) and present at the ends of the linear system two bulky groups, called stoppers, that prevent the extraction of the two individual subunits. On the other hand, catenanes are made up of two cyclic components interpenetrating each other like in a chain.

A rotaxane without stoppers is called pseudorotaxane; in this case, you have an interpenetrated system in which the two supramolecular units that make it up are free to assemble and disassemble without any constraint.

1.3.1 Synthesis of rotaxanes

The synthesis of the first rotaxane was reported in 1967 by Harrison and Harrison[7] who proposed a statistical approach for their construction. In the statistical threading method, the two halves of a molecule in the shape of a balance wheel react in the presence of a macrocycle. The process is purely statistical with no apparent attraction between linear species and cyclic molecules. In this pioneering work, Harrison and coworkers also introduced the concept of slipping (**Figure 1.6**), a process in which the blocking groups (BG) pass through the cyclic unit having similar size. In these

[6] Sauvage, J.-P.; Dietrich-Buchecker, C.; *Molecular Catenanes, Rotaxanes and Knots: A Journey Through the World of Molecular Topology*; Wiley-VCH: Weinheim, **1999**.
[7] Harrison, I. Thomas.; Harrison, Shuyen. *J. Am. Chem. Soc.* **1967**, *89* (22), 5723–5724.

cases, the formation yield of the rotaxane species depends on the largeness of the macrocycle.

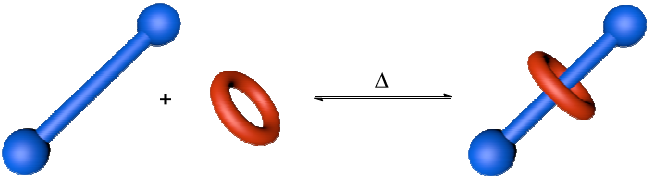

Figure 1.6. The slipping process.

Later, Schill and Zollenkopf introduced the chemical conversion method.[8] The basic idea is described in **Figure 1.7**. In the first instance, a cyclic molecule is connected to a linear system suitably functionalized at the ends with X groups. Then the system is made to react with a molecule (BG) bearing a functional group suitable to react with the ends of the linear system. The cyclic system may be crossed by the linear system or not. The last step involves the splitting of the chemical bond between the linear units and the cyclic part, leading to the formation of the rotaxane species. This strategy, in which numerous synthetic steps are involved, is not effective either in terms of time or overall yield.

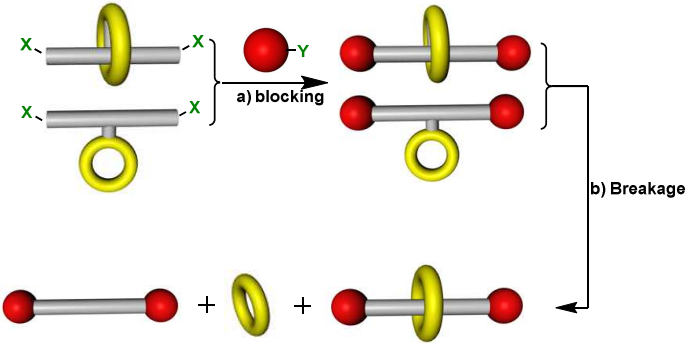

Figure 1.7. Chemical conversion method.

Subsequently, significant progress was made in this area when the threading of the linear species into the cyclic one was directed by control of enthalpic factors. This approach differs substantially from the statistical threading because in this case there are intermolecular interactions between linear and cyclic species. Therefore, it is usually more effective and gives higher yields. There are several types of attractive forces used in the synthesis of rotaxanes which include hydrogen bonds, metal-ligand interactions, hydrophilic or hydrophobic interactions, π–π stacking, or a combination of them (**Figure 1.8**).

[8] Schill, G.; Zollenkopf, H. *Nachr. Chem. Tech.* **1967**, *15*, 149–152.

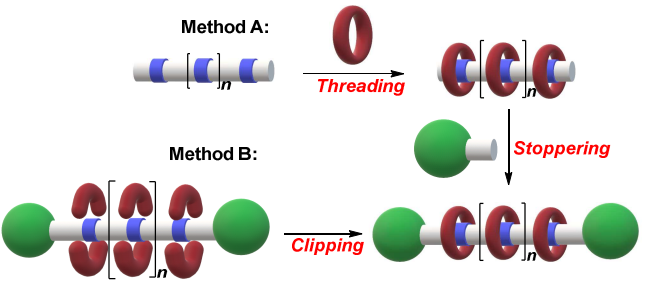

Figure 1.8. Threading controlled by enthalpy factors.

1.3.2 Synthesis of catenanes

The synthesis of the first catenane system dates to 1960,[9] when Wasserman succeeded, with a statistical approach, to synthesize and characterize the first example of artificial [2]catenane (**Figure 1.9**). A cyclization by acyloin condensation was carried out on a di-ester with thirty-eight carbon atoms. The product was then reduced with a Clemmensen reaction. Wasserman's success encouraged other scholars to seek synthetic pathways that lead to interlocked adduct with much higher yields.

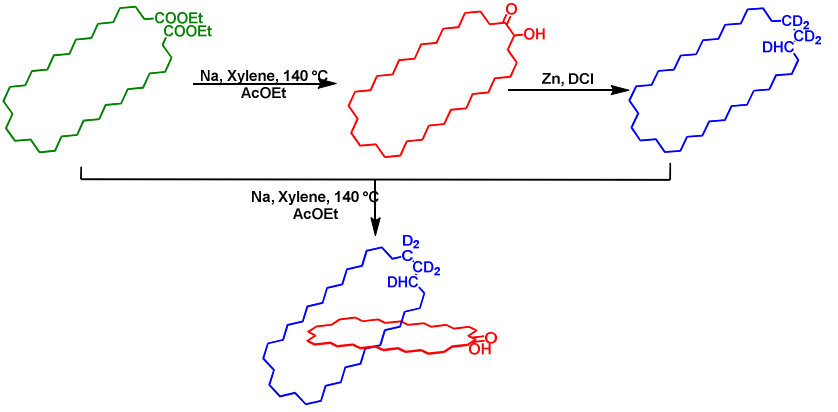

Figure 1.9. Synthesis of the first [2]catenane by Wasserman in 1960.

The first covalent template synthesis of a [2]catenane proposed by Schill and Lüttingraus[10] dates to 1964 (**Figure 1.10**). The adopted strategy exploits the use of the acetal of di(12-chlorododecyl) ketone with a catechol bearing a cyclic system. The introduction of an amino group to give intramolecular nucleophilic substitution followed by the removal of the acetal and the subsequent oxidation of the phenol led to the desired architecture. The role of the acetal intermediate in this methodology is

[9] Wasserman, E. *J. Am. Chem. Soc.* **1960**, *82* (16), 4433–4434.
[10] Schill, G.; Lüttringhaus, A. *Angew. Chem. Int. Ed. Engl.* **1964**, *3* (8), 546–547.

crucial, as the intramolecular cyclization on nitrogen is forced by the tetrahedral geometry of the protected carbonyl carbon. This type of synthesis was subsequently exploited for the construction of the first [3]catenane.[11]

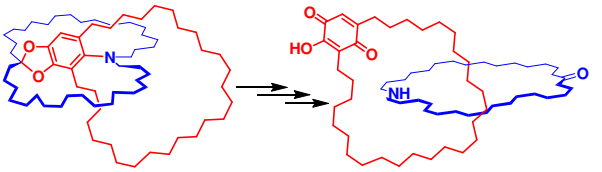

Figure 1.10. Synthesis of the "original [2]catenanes" by Schill and Lüttringhaus in 1964.

Finally, in 1987, Sauvage and coworkers[12] developed an efficient template synthesis of a [2]catenane by exploiting the use of metals as coordination centers (**Figure 1.11**). This approach was then extended to the synthesis of other [*n*]catenane systems.

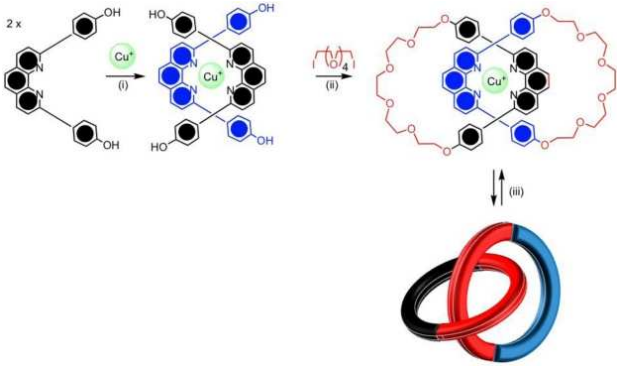

Figure 1.11. Sauvage's copper (I) template synthesis of an interlocked catenane in two sequential steps: (i) coordination of the disubstituted phenanthroline ligand to the metal; (ii) mechanical interlocking by a covalent bond forming reaction; (iii) Demetallation leads to a specific conformational change.

1.4 Artificial Molecular Machines

The haemoglobin, previously mentioned, is not only a complex supramolecular system but can be defined as a real molecular machine. Molecular machine is an assembly of a discrete number of molecular components designed to perform mechanical-like movements due to appropriate external stimuli. In detail, this protein can transport oxygen inside the cells and carbon dioxide out of them through the movement of its subunits. Drawing inspiration from nature, supramolecular chemists

[11] Schill, G.; Rissler, K.; Fritz, H.; Vetter, W. *Angew. Chem. Int. Ed. Engl.* **1981**, *20* (2), 187–189.
[12] Dietrich-Buchecker, C. O.; Sauvage, J. Pierre. *Chem. Rev.* **1987**, *87* (4), 795–810.

for years have focused their attention on the creation of artificial molecular machines because they can have wide applications in the field of electronics, sensors, drug delivery and catalysis. These molecular devices can make movements that can be translational or rotational. Rotational molecular machines can be based, for example, on the cis/trans switch of double bonds thanks to photochemical stimuli or on the H-bond formation by a pH-responsive rotary switch. Instead, translational molecular machines include interpenetrated and/or interlocked systems such as pseudorotaxanes, rotaxanes, and catenanes.

1.4.1 Rotational molecular machines

Concerning rotational molecular machines, the Nobel prize winner Bernard L. Feringa, conducted an exhaustive study on the synthesis of molecular rotor systems.[13] In particular, he developed unidirectional motors able to perform repetitive unidirectional rotary movement, using light and mild heating (35−65 °C) as the power input (**Scheme 1.1**).

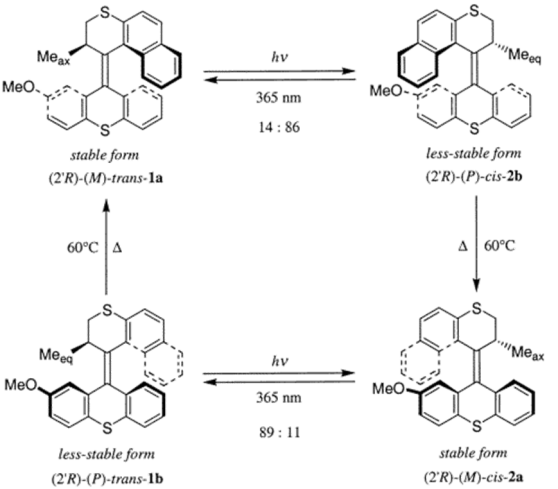

Scheme 1.1. Mechanism of the Feringa molecular rotor system.

The work of Feringa has open the way to an entire research field devoted to the synthesis of rotational molecular machines. Subsequent studies[14] reported the synthesis of nanocars consisting of a carbon core that is the Feringa's rotational system and 4 carborane units as wheels at the ends (**Figure 1.12**). When irradiated with UV light at 365 nm (or heating at 65 °C) the double bond isomerizes bringing the nanocar to make a real movement on the surface (**Figure 1.13**).

[13]Koumura, N.; Geertsema, E. M.; van Gelder, M. B.; Meetsma, A.; Feringa, B. L. *J. Am. Chem. Soc.* **2002**, *124* (18), 5037–5051.
[14]Morin, J.-F.; Shirai, Y.; Tour, J. M. *Org. Lett.* **2006**, *8* (8), 1713–1716.

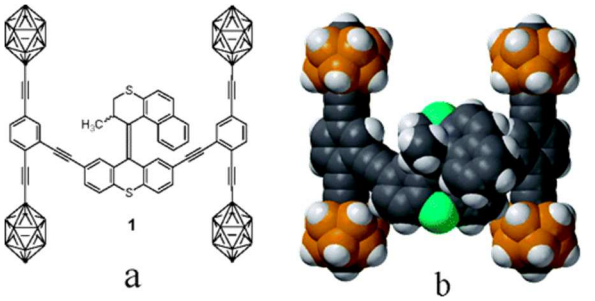

Figure 1.12. (a) Structure of motorized nanocar 1. (b) The space-filling model of 1.

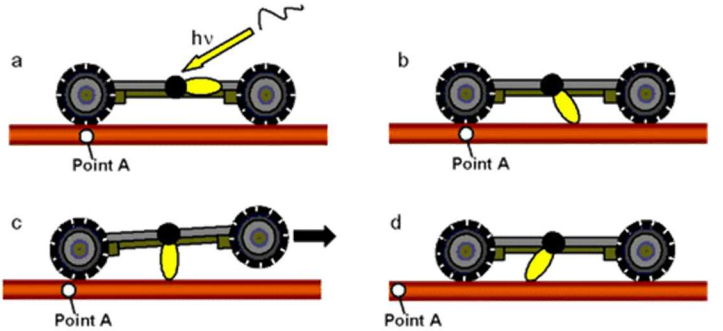

Figure 1.13. Proposed propulsion scheme for the motorized nanocar 1 where (a) 365 nm light would impinge upon the motor which in conjunction with a heated substrate (at least 65 °C) (b) affording motor rotation and (c) sweeping across the surface to (d) propel the nanocar forward.

At the same time, Ivan Aprahamian reported a new type of chemically induced rotary switch using a hydrazone block.[15] In particular, the switching process is activated by a Lewis acid. Therefore, this molecular device is able to control the E/Z isomerization in hydrazones by the pH response. Furthermore, this isomerization is reversible thanks to heating as described in **Scheme 1.2**.

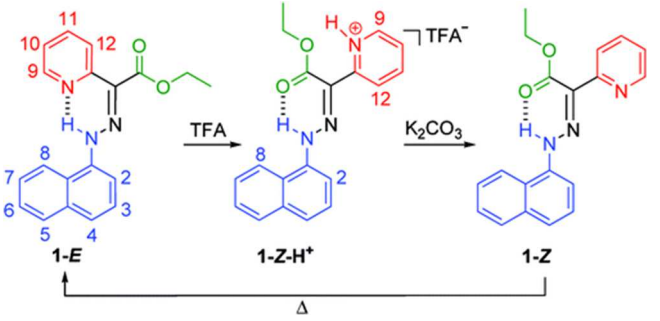

Scheme 1.2. Aprahamian's rotary system.

[15]Landge, S. M.; Aprahamian, I. *J. Am. Chem. Soc.* **2009**, *131* (51), 18269–18271.

In 2016,[16] a robotic arm capable of carrying a small molecule was reported David Leigh (**Figure 1.14**).

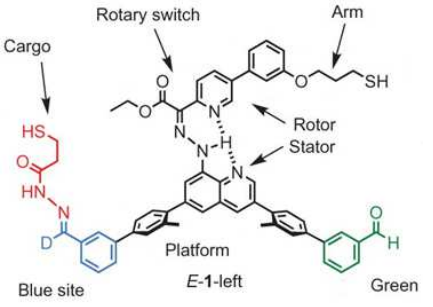

Figure 1.14. Leigh's robotic arm.

A pH-responsive, three-step rotary switch was realized, which steers a molecular robotic arm that can grip or release a cargo through disulfide bond formation. A dynamic hydrazone linkage was used to bind the cargo to the platform sites (**Scheme 1.3**).

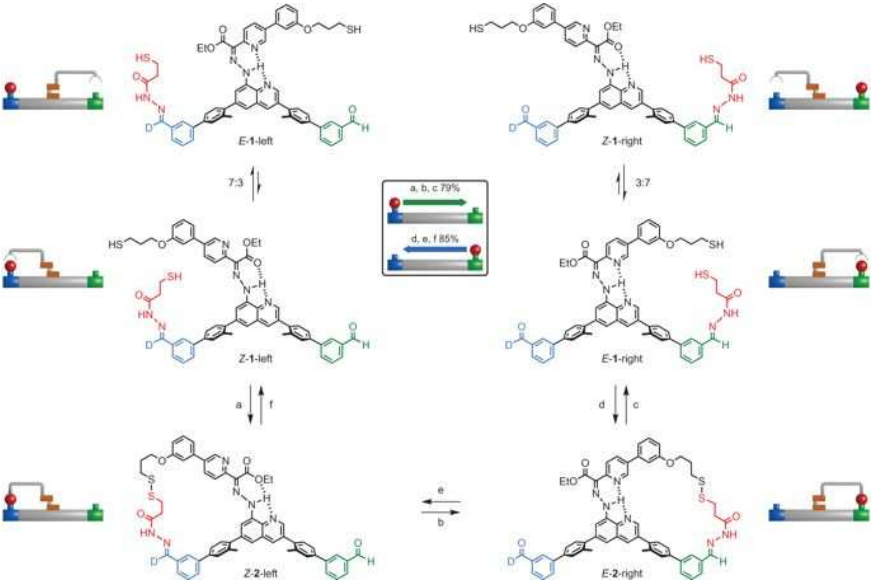

Scheme 1.3. Mechanism of Leigh's robotic arm.

[16]Kassem, S.; Lee, A. T. L.; Leigh, D. A.; Markevicius, A.; Solà, J. *Nat. Chem.* **2016**, *8* (2), 138–143.

1.4.2 Translational molecular machines

David Leigh has also conducted significant studies on translational molecular machines. In 2014[17] he reported an artificial molecular machine that can pick up and assemble reactive groups in sequence, by traveling along a track. In this case, the reacting groups are different amino acids. This molecular device is based on an interpenetrated system constituted by a cyclic unit and a linear system (**Figure 1.15**). The cyclic unit carries a thiolate group that iteratively removes amino acids from the strand and transfers them to a peptide-elongation site through native chemical ligation.

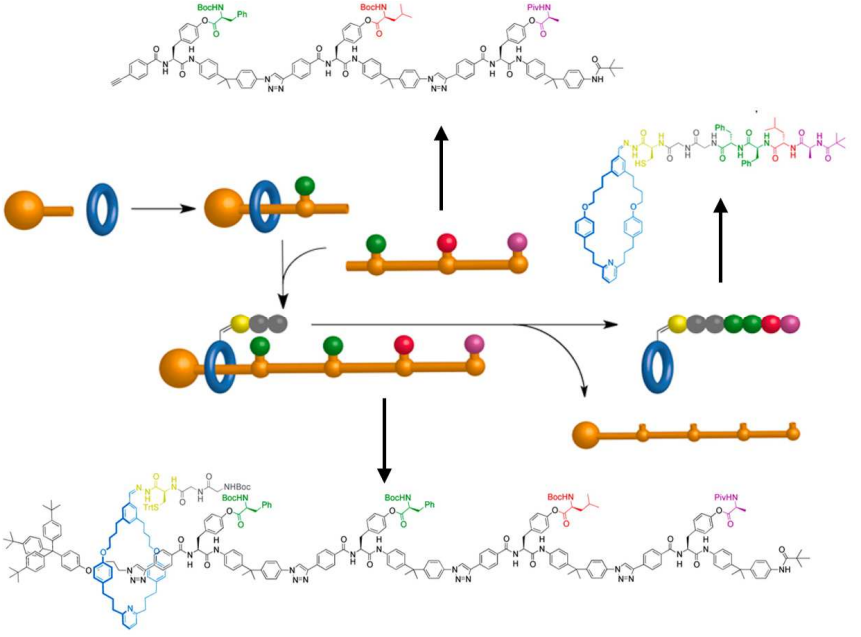

Figure 1.15. The ribosome-like translational machine by Leigh.

In 2017,[18] Leigh has also synthesized an artificial translational molecular machine able to carry out the autonomous sequential synthesis of peptides containing β3-amino acids (**Figure 1.16**).

[17]De Bo, G.; Kuschel, S.; Leigh, D. A.; Lewandowski, B.; Papmeyer, M.; Ward, J. W. *J. Am. Chem. Soc.* **2014**, *136* (15), 5811–5814.
[18]De Bo, G.; Gall, M. A. Y.; Kitching, M. O.; Kuschel, S.; Leigh, D. A.; Tetlow, D. J.; Ward, J. W. *J. Am. Chem. Soc.* **2017**, *139* (31), 10875–10879.

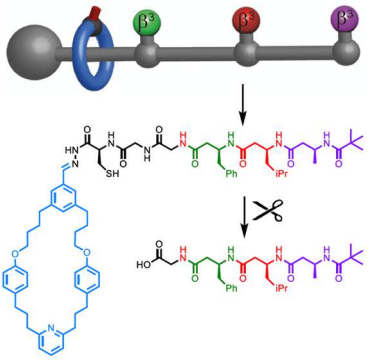

Figure 1.16. Translational molecular machine performing an autonomous sequential synthesis.

Other important contributions in the field of molecular machines are due to Nobel Prize winner Sir. Fraser Stoddart, who has synthesized and studied a huge number of supramolecular systems by exploiting mostly π-π interactions between electron rich and electron poor aromatic units. Thanks to this secondary interaction Sir F. Stoddart has managed to synthesize highly complex interpenetrated and interlocked structures (**Figure 1.17**).[19]

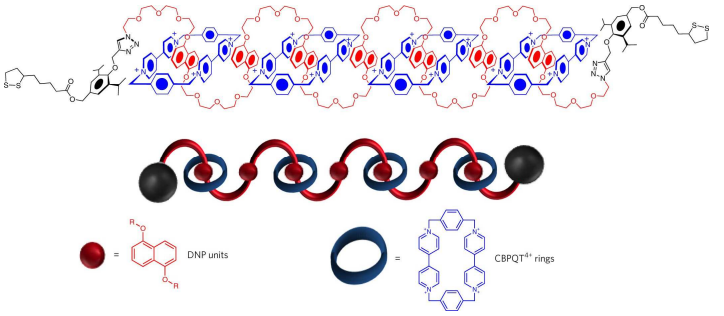

Figure 1.17. [5]Rotaxane system of Stoddart.

In 2015,[20] an interesting artificial molecular pump was reported by Stoddart. Its design was inspired by the Na^+/K^+ pump present in living organisms. In detail, a dumbbell-shaped molecular pump comprises a redox-switchable viologen recognition site, linked by bismethylene chains to a 3,5–dimethylpyridinium, and a tetracationic ring as cyclic unit (**Figure 1.18**). The threading of the macrocycle in the linear system occurs thanks to a reduction/oxidation cycle. The pump withstands up to two

[19]Sluysmans, D.; Hubert, S.; Bruns, C. J.; Zhu, Z.; Stoddart, J. F.; Duwez, A.-S. *Nat. Nanotechnol.* **2018**, *13* (3), 209–213.
[20]Cheng, C.; McGonigal, P. R.; Schneebeli, S. T.; Li, H.; Vermeulen, N. A.; Ke, C.; Stoddart, J. F. *Nat. Nanotechnol.* **2015**, *10* (6), 547–553.

oxidation reduction cycles and works against a local concentration gradient in order to accumulate potential energy.

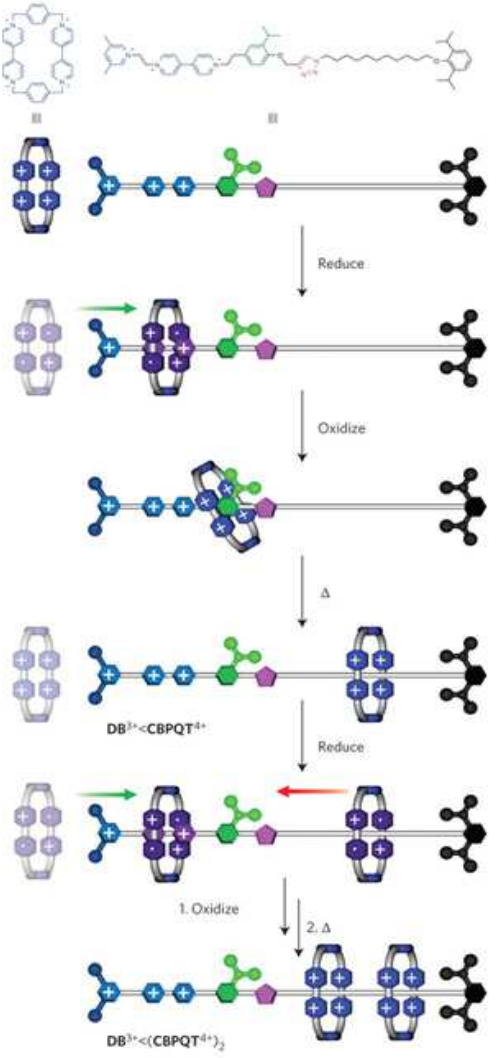

Figure 1.18. Mechanism of artificial molecular pump.

Another example of molecular devices realized by Stoddart is the molecular elevator[21] (**Figure 1.19**). This machine uses an acid-base stimulus and is based on a guest bearing three linear axles, each containing an ammonium and a viologen recognition site. The second component is a host platform made up by 3 crown ethers and having

[21] Badjić, J. D., Balzani, V., Credi, A., Silvi, S., & Stoddart, J. F.. *Science* **2004**, *303*(5665), 1845.

a size of only 3.5 × 2.5 nm. The platform is initially located closest to the ammonium sites, thanks to H-bonding interactions between the crown oxygen atoms and the ammonium groups.

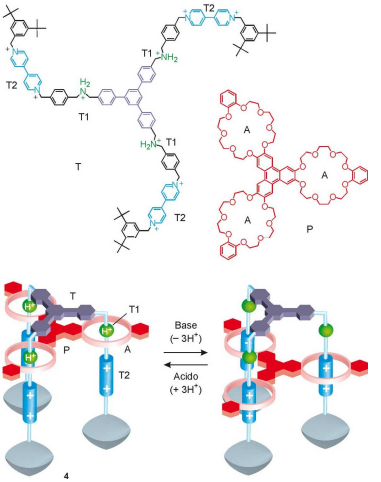

Figure 1.19. (a) Linear and cyclic units of Stoddart's molecular elevator; (b) Stoddart's molecular elevator.

Following the ammonium deprotonation by a base, the platform moves towards the electronic-poor viologen units of the linear system, thus carrying out a displacement of 0.7 nm. In the same vein of this work, in 2008, Stoddart devised an additional machine known as molecular muscle[22] (**Figure 1.20**).

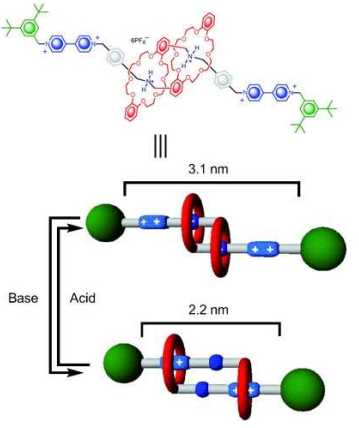

Figure 1.20. Stoddart's molecular muscle.

[22]. Wu, J.; Leung, K. C.-F.; Benítez, D.; Han, J.-Y.; Cantrill, S. J.; Fang, L.; Stoddart, J. F. *Angew. Chem. Int. Ed.* **2008**, *47* (39), 7470.

This system exploits the same approach previously seen, i.e. the movement of a cyclic unit from an ammonium site to a viologen unit by following a change in pH. Due to its structure, the interlocked system passes from an extended (3.1 nm) to a contracted (2.2 nm) form.

CHAPTER II

Calix[n]arenes

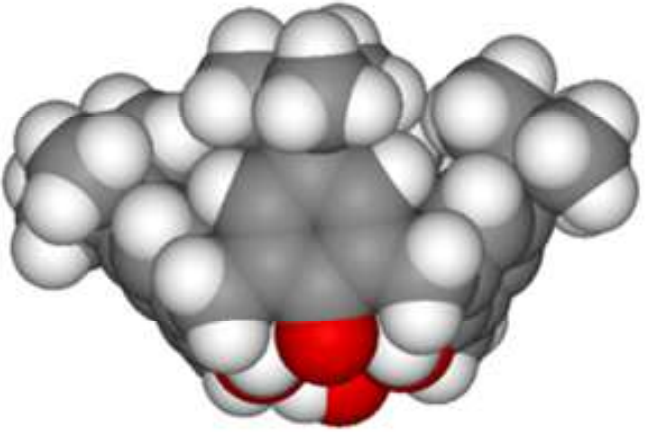

2.1 Synthesis of Calix[*n*]arenes

Among the macrocycles known in the literature for their ability to form interpenetrated and interlocked systems, there are cucurbituryls, [23] crown ethers,[24] cyclodextrins,[25] and calixarenes. [26] Calixarenes are a particular class of macrocycles that belong to the metacyclophane family. They are obtained by phenol/formaldehyde condensation and are widely used in supramolecular chemistry, where they have found many applications. Calix[*n*]arenes have the general structure **1** reported in **Figure 2.1** in which the number *n* of phenolic units ranges from 4 to 20. In addition, these macrocycles have a three-dimensional structure with two distinct portions indicated as upper rim and lower rim (**Figure 2.1**). However, the most studied members are those constituted by 4-8 aromatic units.

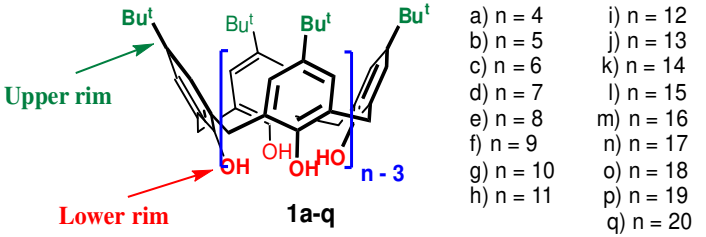

Figure 2.1. The calix[*n*]arene family (*n* = 4-20).

These macrocycles also have a high conformational freedom, which allows them to assume different conformations thanks to the free rotation around the Ar-CH_2-Ar bonds (**Figure 2.2**).

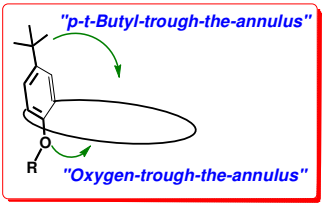

Figure 2.2. Conformational interconversion in *p-tert*-butylcalix[*n*]arenes.

---

[23] Lagona, J.; Mukhopadhyay, P.; Chakrabarti, S.; Isaacs, L. *Angew. Chem. Int. Ed.* **2005**, *44*, 4844.
[24] Gokel, G. W. *Crown Ethers and Cryptands* Royal Society of Chemistry, Cambridge, **1991**
[25] Szejtli, J. *Cyclodextrin Technology* in *Topics in Inclusion Science;* (Ed: Davies, J. E.), Kluwer, Dordecht, **1988**.
[26] a) Gutsche, C. D. *Calixarenes* (Ed.: J. F. Stoddart), Royal Society of Chemistry, Cambridge, **1989**; b) Gutsche, C. D. *Calixarenes Revisited* (Ed.: J. F. Stoddart), Royal Society of Chemistry, Cambridge, **1998**; c) Bunzli J.-C. G.; Harrowfield, J.; *Calixarenes: A Versatile Class of Macrocyclic Compounds* (Eds.: Vicens, J.; Böhmer, V.), Kluwer, Dordrecht, **1991**; d) Gutsche, C. D. *Calixarenes – An Introduction, 2nd ed.,* Royal Society of Chemistry, Cambridge, **2008**; e) Neri, P.; Sessler, J. L.; Wang, M.-X.; *Calixarenes and Beyond*; Springer Verlag, **2016.**

In particular, calix[6]arenes gives rise to eight discrete conformations (**Figure 2.3**): *cone, partial-cone, 1,2-alternate, 1,3-alternate, 1,4-alternate, 1,2,3-alternate, 1,2,4-alternate,* and *1,3,5-alternate*.

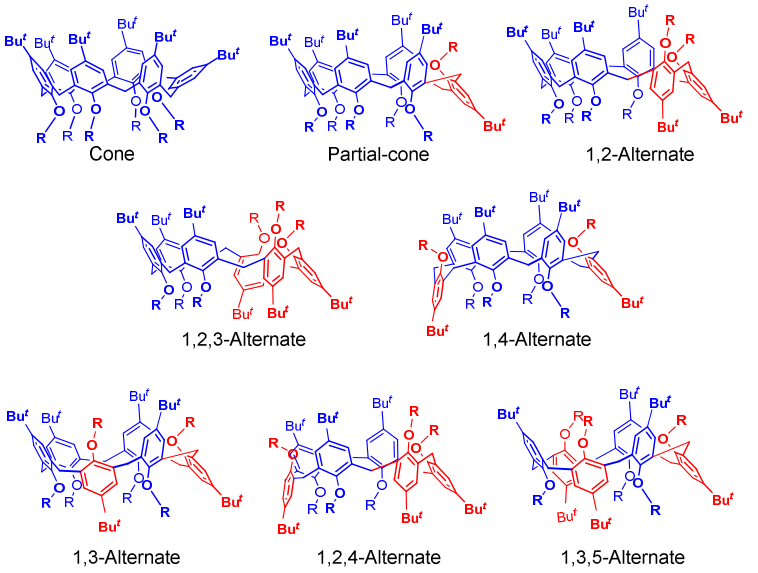

Figure 2.3. The possible 8 discrete conformations of a calix[6]arene macrocycle.

Their three-dimensional structure, the possibility of being easily functionalized at both the lower and upper rim, their conformational flexibility, and the presence of the central cavity which gives them complexing properties explain the extensive studies and use of these molecules. A classic type of functionalization of calixarenes at the lower rim exploits the acidity of the phenolic groups, which, once deprotonated by suitable bases, can behave as nucleophiles in alkylation/acylation reactions in the presence of alkyl or acyl halides.

The basic calixarene macrocycles can be obtained using two different synthetic strategies:

- One-pot procedure
- Multi-step synthesis and fragment condensation

2.1.1 One-pot procedure

Through the one-pot procedure, calixarene macrocycles are obtained by direct reaction between the *p-tert*-butylphenol and formaldehyde in basic or acid

conditions.[27] The one-pot procedure has been optimized for *p-tert*-butylphenol as starting material and gives rise to the *p-tert*-butylcalix[n]arene macrocycle. By varying the reaction conditions, as the source of formaldehyde, solvent, temperature, and base, the individual members of the calix[*n*]arene family (**Figure 2.1**) can be selectively obtained as shown in **Scheme 2.1**.

In detail, *p-tert*-butylcalix[4]arene **1a** is obtained by reaction between *p-tert*-butylphenol and a commercial solution of formaldehyde in water in the presence of sodium hydroxide (45 equiv.). The reaction mixture is heated for 2 h at 110-120 °C leading to the formation of a viscous paste called "the precursor". Subsequently, the mixture is refluxed in diphenyl ether for 2 h. In these conditions, the cyclic tetramer **1a** is recovered by precipitation from ethyl acetate and recrystallized from toluene. The amount of hydroxide ion and the nature of its cation plays an important role in addressing the synthesis toward a specific macrocycle. In particular, the presence of NaOH as base allows the synthesis in high yields of the cyclic octamer **1e** in xylene as solvent and tetramer **1a** in diphenyl ether as solvent, while using KOH in xylene as solvent, high yields (80-85%) of the cyclic hexamer **1c** can be obtained.

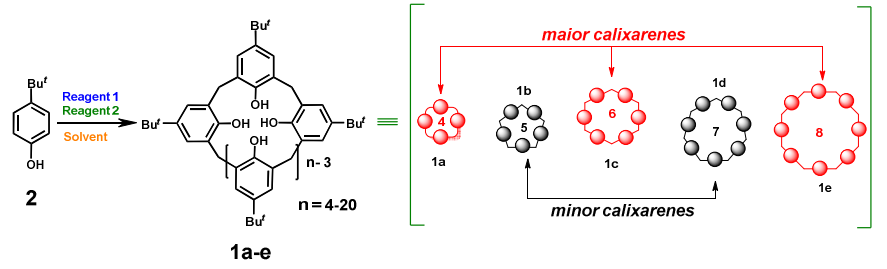

	1a	1b	1c	1d	1e
Reagent 1 =	formaldehyde	formaldehyde	formaldehyde	*s*-trioxane	formaldehyde
Reagent 2 =	NaOH	KOH	KOH	p-TsOH	NaOH
Solvent =	diphenyl ether	tetrahydronaphthalene	xylene	chloroform	xylene

Scheme 2.1. One-pot procedure for calix[n]arenes.

[27] a) Gutsche, C. D.; Iqbal, M., *p-tert*-Butylcalix[4]arene, *Org. Synth.* 68 (1990) 234-237. (b) Gutsche, C. D.; Dhawan, B.; Leonis, M., *p-tert*-Butylcalix[6]arene, *Org. Synth.* 68 (1990) 238-242. c) Munch J. H.; Gutsche, C. D., *p-tert*-butylcalix[8]arene, *Org. Synth.* 68 (1990) 243-246. (d) Stewart, D. R.; Gutsche, C. D., The one-step Synthesis of p-tert-butylcalix[5]arene. Organic Preparations and Procedures International 25 (1993) 137-139. e) Stewart, D. R.; Gutsche, C. D., Isolation, characterization, and conformational characteristics of *p-tert*-butylcalix[9–20]arenes, *J. Am. Chem. Soc.* 121 (1999) 4136-4146. f) Bew, S. P.; Sharma, S. V., An expedient one-pot synthesis of *para-tert*-butylcalix[8]- and [9]arene, *Chem. Commun.* (2007) 975–977. g) Dumazet, I.; Regnouf De-Vains, J.-B.; Lamartine, R., Synthesis and characterization of *p-tert*-butylcalix[9]arene, *p-tert*-butylcalix[10]arene, *p-tert*-butylcalix[11]arene and *p-tert*-butylcalix[12]arene, *Synthetic Commun.* 27 (1997) 2547–2555.

2.1.2 Multi-step synthesis and fragment condensation

Historically, the main advantage of the multistep synthesis is that it makes available calixarene derivatives bearing differently *p*-substituted phenol units. The first example of multi-step synthesis of calixarenes was reported by Hayes and Hunter, that synthesized the *p*-methylcalix[4]arene **8** by a 10-steps procedure (**Scheme 2.2**).

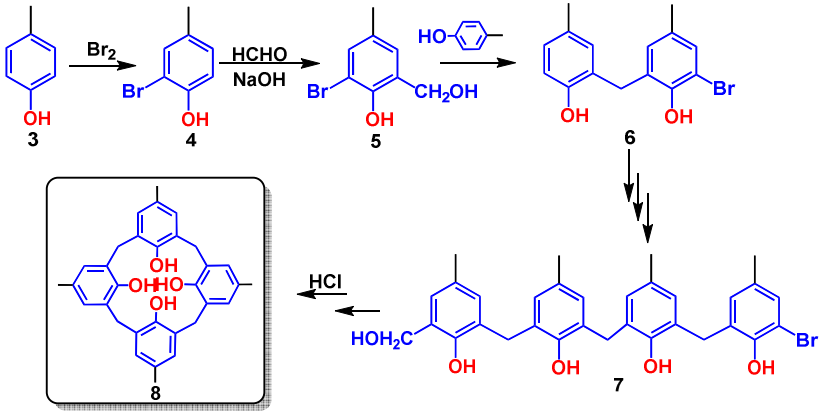

Scheme 2.2. Synthesis of *p*-methylcalix[4]arene with a non-convergent stepwise approach.

The multi-step syntheses were long and tedious so many efforts were devoted to improving this strategy.[28] Thus, Böhmer and coworkers[29] developed convergent syntheses that require fewer reaction steps. In detail, this method is identified in four different ways as: 3+1, 2+2, 2+1+1, and 1+1+1+1 *fragment condensation* (**Scheme 2.3**).

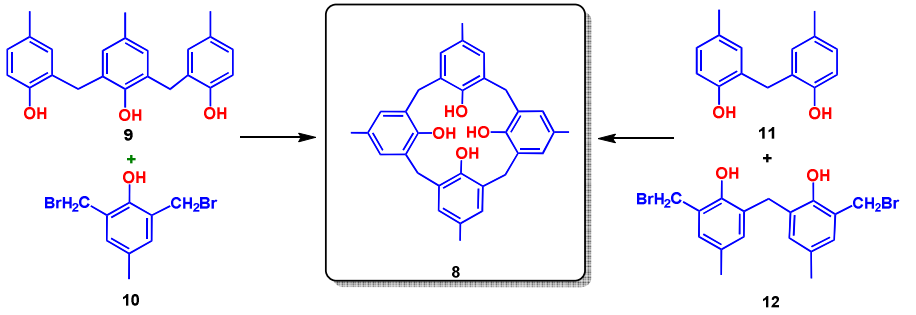

Scheme 2.3. Examples of 3+1 and 2+2 fragment condensation.

---

[28] No, K. H.; Gutsche, C. D., Calixarenes. 8. Short, stepwise synthesis of *p*-phenylcalix[4]arene, *p*-phenyl-*p*-*tert* -butylcalix[4]arene, and derived products, *J. Org. Chem.* 47 (1982) 2713-2719.

[29] Böhmer, V., Special calixarenes by directed syntheses, *Liebigx Ann./Recueil* (1997) 2019-2030. Böhmer, V.; Chhim, P.; Kämmerer, H., A new synthetic access to cyclic oligonuclear phenolic compounds *Makromol. Chem.* 180 (1979) 2503-2506. Goldmann, H.; Vogt, W.; Paulus, E.; Böhmer, V., A series of calix[4]arenes, having two opposite para positions connected by an aliphatic chain, *J. Am. Chem. Soc.* 110 (1988) 6811-6817.

2.2 Supramolecular systems based on calixarenes

2.2.1 Interpenetrated systems based on calix[6]arenes

The first example of a calixarene-based pseudorotaxane was reported by Arduini et al. in 2000.[30] In detail, a pseudo[2]rotaxane **13⊂14** was obtained by exploiting the presence of ureido groups at the upper rim of the macrocycle that dissociate the ion pair of the linear system (**Figure 2.4**). This approach, however, limits the functionalization of the upper rim.

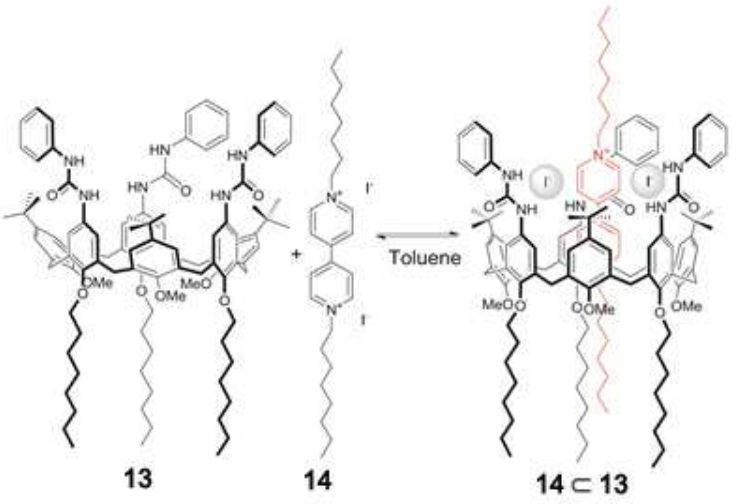

Figure 2.4. Self-assembly in toluene of calix[6]arene-based wheel **13** and viologen-based axle **14**.

In 2010, the threading of dialkylammonium axles through the cavity of calix[6- or -7]arene was studied by Gaeta et al.[31] This threading is possible by exploiting the poorly coordinating tetrakis[3,5-bis(trifluoromethyl)phenyl]borate anion (TFPB) (**Figure 2.5**), known in the literature as "superweak anion".[32]

---

[30] Arduini, A.; Ferdani, R.; Pochini, A.; Secchi, A.; Ugozzoli, F. *Angew. Chem. Int. Ed.* **2000**, 39, 3453–3456.

[31] Gaeta, C.; Troisi, F.; Neri, P. *Org. Lett.* **2010**, *12* (9), 2092–2095.

[32] a) Strauss, S. H.; *Chem. Rev.*, **1993**, *93*, 927; b) Hirochika, N.; Suzuki, H.; Norob, J.; Kimura, T.; *Chem. Commun.*, **2005**, 2963; c) Nishida, H.; Takada, N.; Yoshimura, M.; Sonoda, T.; Kobayashi, H.; *Bull. Chem. Soc. Jpn.*, **1984**, *57*, 2600; d) Blight, B. A.; Camara-Campos, A.; Djurdjevic, S.; Kaller, M.; Leigh, D. A.; McMillan, F. M.; McNab, H.; Slawin, A. M.; *J. Am. Chem. Soc.*, **2009**, *131*, 14116.

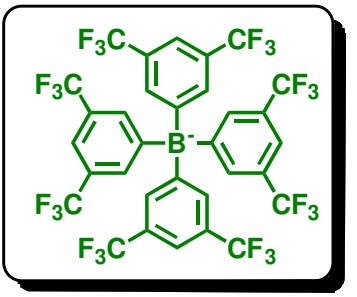

Figure 2.5. Structure of tetrakis[3,5-bis(trifluoromethyl)phenyl]borate anion.

The use of the superweak anion allows to dialkylammonium species to be present in solution as a weakly associated ion pair and drastically improve the hydrogen bonding interactions with the calixarene oxygens leading to the formation of interpenetrated systems (**Figure 2.6**).

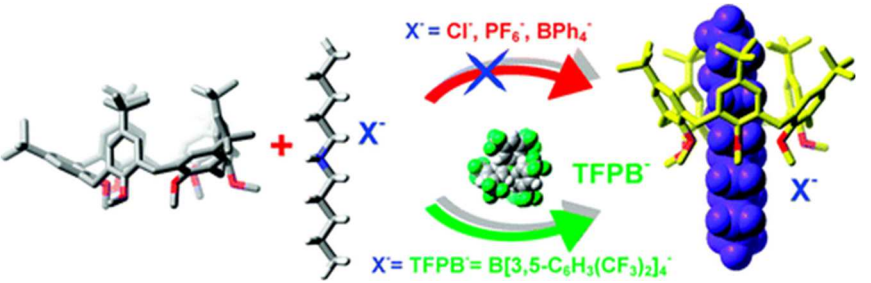

Figure 2.6. Anion influence on the through-the-annulus threading of calix[6]arene macrocycle

The formation of interpenetrated species, related to the threading of dipentylammonium and dibenzylammonium TFPB salts through the cavity of hexamethoxy-*p*-*terz*-butylcalix[6]arene (**Scheme 2.4**), was deduced from the analysis of ^{1}H-NMR spectra. In both cases, an AX system related to $ArCH_2Ar$ bridges was observed in the 3-4 ppm region, which is indicative of the presence of a cone conformation of the calix[6]arene. Furthermore, the high-field signals of the spectrum attributable to the aliphatic protons strongly shielded by the calixarene aromatic walls (the protons α, β, γ, δ, and ε resonating between 0.5 and -1.2 ppm) are particularly diagnostic (**Figure 2.7b**). In a similar way, the high-field shift of the benzyl protons shielded by the calixarene cavity (o, m, and p), was a clear evidence of the presence of the aromatic system inside the calixarene cavity (**Figure 2.7a**).

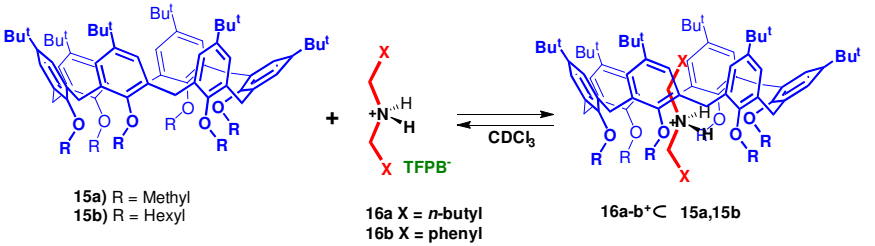

Scheme 2.4. Threading of symmetric salts in the calixarene cavity.

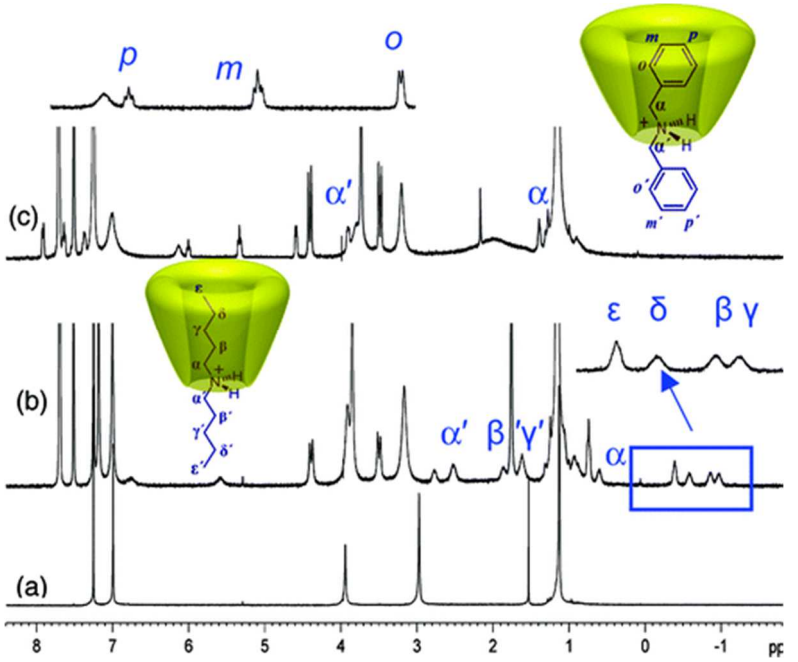

Figure 2.7. ^{1}H NMR spectra ($CDCl_3$, 400 MHz, 298 K) of (a) **15a**, b) equimolar solution (3 mM) of **15a** and di-n-pentylammonium TFPB−, **16a**, (c) equimolar solution (3 mM) of **15a** and dibenzylammonium TFPB−, **16b**.

The threading of non-symmetrical alkyl-benzyl-ammonium axles was also studied. In this case, given the natural directionality of the calixarene macrocycle, two isomeric pseudorotaxane species will be possible, namely the *endo*-alkyl or *endo*-benzyl one, in which the alkyl or benzyl group, respectively, is included inside the macrocycle cavity (**Scheme 2.4**). The study proved that the *endo*-alkyl adduct is usually preferred (**Figure 2.8**), leading to the so-called "endo-*alkyl rule*".

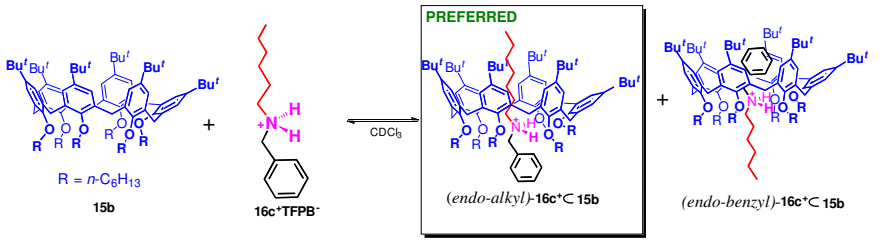

Scheme 2.5. Threading of asymmetric salt in the calixarene cavity.

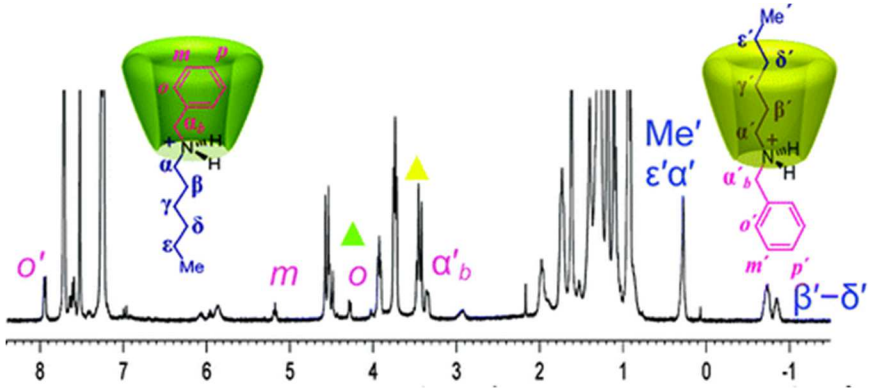

Figure 2.8. ^{1}H NMR spectra ($CDCl_3$, 400 MHz, 298 K) of equimolar solution (3 mM) of **15b** and *n*-hexylbenzylammonium **16c**$^+$TFPB$^-$.

This phenomenon has laid the foundations for further threading studies with dicationic axles, carrying a different sequence of the alkylbenzyl unit. In this way, the first examples of calixarene-based pseudo[3]rotaxanes were obtained.[33] In addition, an efficient and rational control of the "sequential stereoisomerism" was developed by playing on the nature of the linear system. Several different stereosequences have been obtained by using the alkylbenzylammonium unit as the coding language (**Figure 2.9**).

[33] Talotta, C.; Gaeta, C.; Pierro, T.; Neri, P. *Org. Lett.* **2011**, *13* (8), 2098–2101.

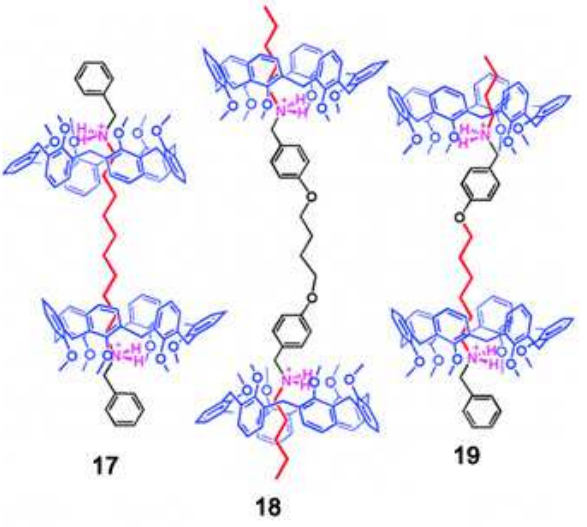

Figure 2.9. Sequential isomers by threading between bis-ammonium axles and pHcalix[6]arene hexametoxy.

The study of calixarene threading has allowed the creation of increasingly complex supramolecular architectures such as the first examples of calixarene-based handcuff pseudorotaxane[34] (**Figure 2.10**). Thanks to possibility to control the threading directionality by exploiting the "*endo*-alkyl rule" a predefined orientational isomer was obtained.

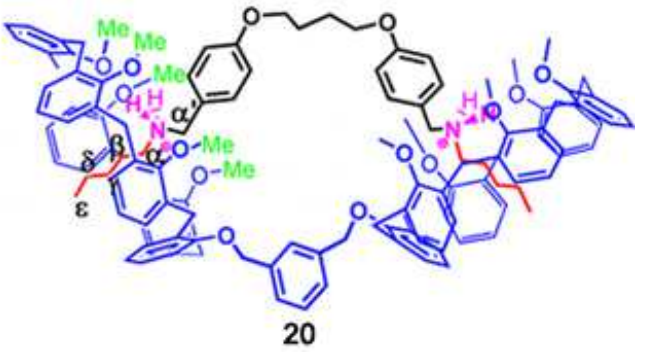

Figure 2.10. Handcuff interpenetrated system.

[34] Ciao, R.; Talotta, C.; Gaeta, C.; Margarucci, L.; Casapullo, A.; Neri, P. *Org. Lett.* **2013**, *15* (22), 5694–5697.

2.2.2 Interlocked systems based on calix[6]arenes

Thanks to the possibility of threading calixarene macrocycle with viologen-based axles, over the years, it has been possible to synthesize different interlocked systems as rotaxanes and catenanes. To this end, a linear system bearing terminal hydroxyl functions was used. Subsequently at the formation of pseudorotaxane system, the introduction at the ends of the axle of two sufficiently bulky groups (threading/stoppering approach) led to the formation of rotaxane system **21**[35] (**Figure 2.11**).

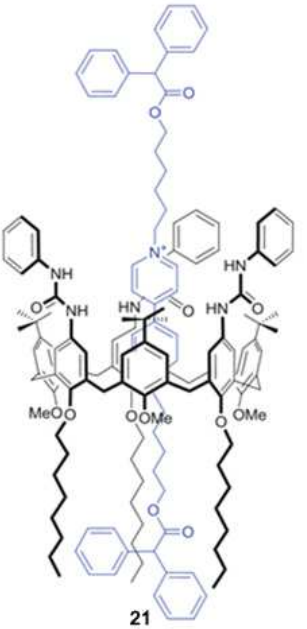

Figure 2.11. Rotaxane formed by calixarene and viologen axles **21**.

In the case of calix[6]arene catenane, after the threading of tris(*N*-phenylureido)calix[6]arene a subsequent cyclization by metathesis reaction led to the interlocked system[36] (**Figure 2.12a**).

Catenane **22** was studied by UV-visible absorption spectroscopy in acetonitrile. The absorption spectrum (**Figure 2.12b**) shows an intense band in the UV region (λmax = 260 nm, ε = 86000 M^{-1} cm^{-1}) and a weaker band in the visible region (λmax = 470 nm, ε = 600 M^{-1} cm^{-1}). In particular, the latter band is attributed to the interaction of the charge transfer between the viologen unit and the calixarene rings.

[35] Arduini, A.; Calzavacca, F.; Pochini, A.; Secchi, A. *Chem. - Eur. J.* **2003**, *9* (3), 793–799.
[36] Orlandini, G.; Zanichelli, V.; Secchi, A.; Arduini, A.; Ragazzon, G.; Credi, A.; Venturi, M.; Silvi, S. *Supramol. Chem.* **2016**, *28*, 427–435.

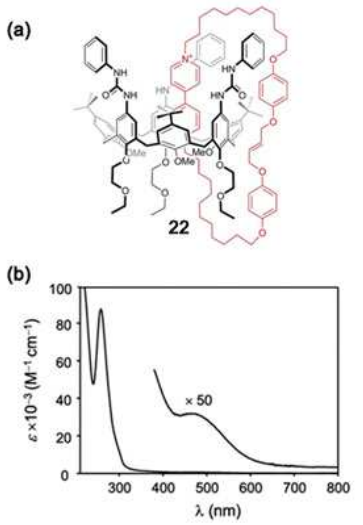

Figure 2.12. (a) Catenane formed by Calixarene and Viologen Axles **22**. (b) Absorption spectrum of catenane **22** in acetonitrile.

The "superweak anion" approach has also allowed the synthesis of interlocked systems. In 2011, Neri and coworkers[37] synthesized a calix[2]rotaxane by using a similar threading/stoppering approach (**Scheme 2.5**).

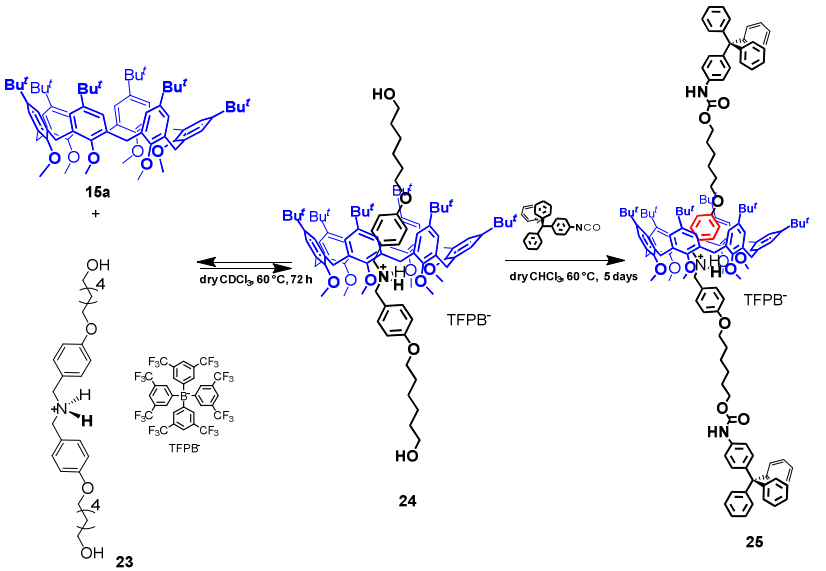

Scheme 2.6. Synthesis of calix[2]rotaxane **25**.

[37] Pierro, T.; Gaeta, C.; Talotta, C.; Casapullo, A.; Neri, P. *Org. Lett.* **2011**, *13* (10), 2650–2653.

Further studies conducted on calix[2]rotaxane **25** have shown that by changing the protonation state of the ammonium site, the cyclic unit can carry out translational movements along the linear system acting as a nanosized molecular shuttle. In detail, by mixing calix[2]rotaxane **25** with 1,5 equiv of phosphazene base P1-*t*-Bu (*N*-*tert*-butyl-*N*′,*N*′,*N*″,*N*″,*N*‴,*N*‴-hexamethylphosphorimidic triamide important changes in the proton spectrum were observed indicating the displacement of the calixarene macrocycle from the initial central dibenzylammonium station to a new position where an aliphatic chain is inside the calixarene cavity. Because of the unsymmetrical nature of the macrocycle, there are two different (no equivalent) aliphatic sites on the linear component. Therefore, two possible translational isomers can be formed where the wheel can be found on the upper station **26U** or on the lower station **26L** (**Scheme 2.6**).

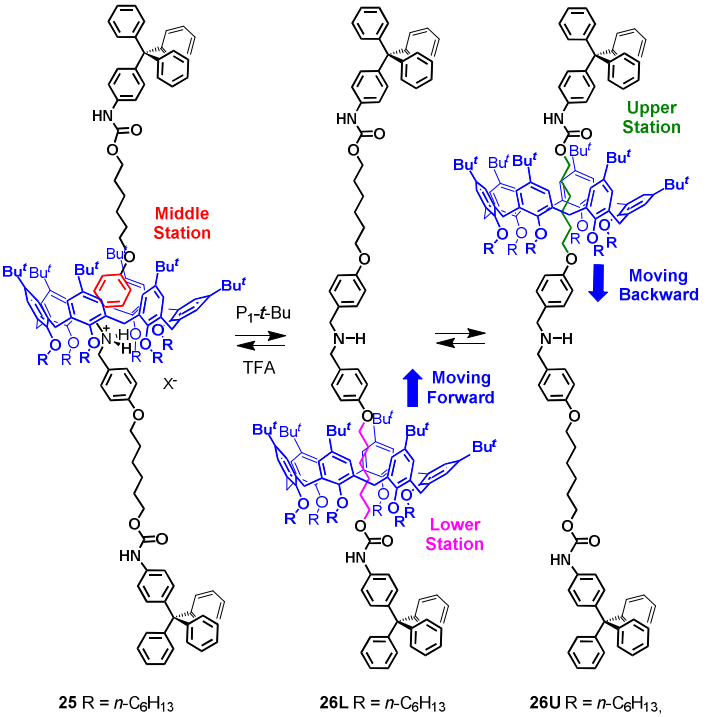

Scheme 2.7. Formation of **25U** and **25L** derivatives following the use of the P1-t-Bu base on derivative **12**.

DFT studies indicated that **25L** is the preferred isomer thanks to H-bonding interactions between calix[6]arene oxygen atoms and the NH urethane at the lower station (**Figure 2.13**).

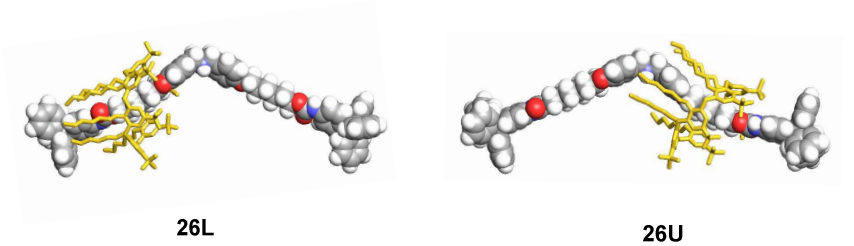

Figure 2.13. Low energy structures of isomers **25U** (right) and **25L** (left).

Afterwards, in 2013, the same group synthesized the first examples of calix[2]catenanes[38] (**Figure 2.14**) using a threading/cyclization approach. In detail, after the threading of linear system inside the cavity of hexamethoxycalix[6]arene, a urethane macrocyclization reaction was performed.

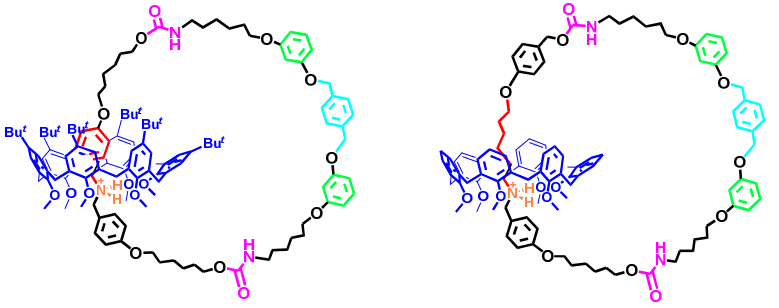

Figure 2.14. Calix[2]catenanes through-the-annulus threaded, **27** and **28**.

The interlocked systems described so far are all made up by 2 units, but further studies have reported the formation of calixarene-based [3]rotaxane systems.[39] In fact, the sequential stereoisomerism observed for the [3]pseudorotaxanes previously described, led to the synthesis of the first examples of [3]rotaxanes in a stereoprogrammed way (**Figure 2.15**).

[38] Gaeta, C.; Talotta, C.; Mirra, S.; Margarucci, L.; Casapullo, A.; Neri, P. *Org. Lett.* **2013**, *15* (1), 116–119
[39] Talotta, C.; Gaeta, C.; Neri, P. *Org. Lett.* **2012**, *14* (12), 3104–3107.

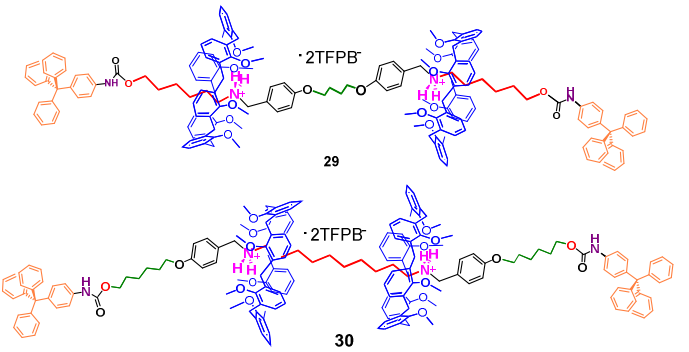

Figure 2.15. Stereoprogrammed [3]rotaxane systems.

Finally, an interlocked system was also obtained using a double calixarene. By mixing the host with a bis-ammonium linear axle having terminal hydroxyl sites, the interpenetrated system was initially obtained, which was stoppered to give a handcuff rotaxane (**Figure 2.16**)

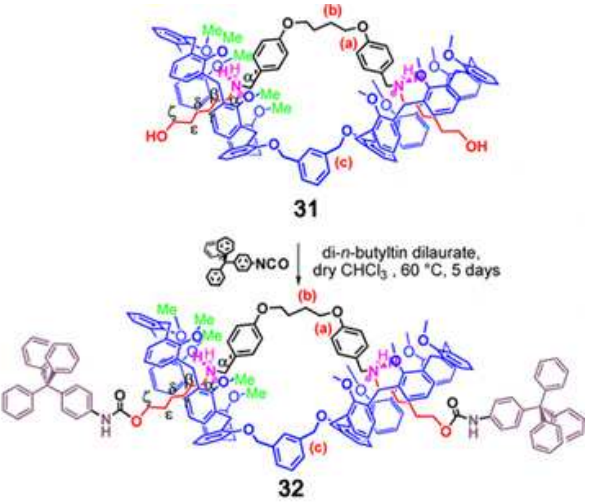

Figure 2.16. Handcuff interlocked system.

2.2.3 Interpenetrated systems based on calix[5]arenes

Interpenetrated systems based on the smaller calix[5]arene macrocycle have been largely less studied. In a very recent joint work by the Neri and Parisi groups, the "superweak anion approach" was extended to calix[5]arenes.

Initially, the threading of calix[5]arene **33** with a dipentyl ammonium axle was studied. The typical shielded signals related to the aliphatic chain within the calixarene cavity clearly evidenced the pseudorotaxane formation (**Figure 2.17**).

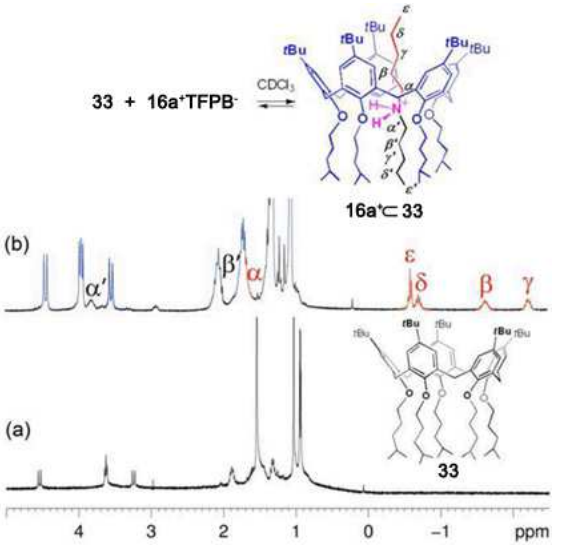

Figure 2.17. High-field regions of the ^{1}H NMR spectra (300 MHz, $CDCl_3$, 298 K) of (a) **33** and (b) an equimolar solution (4.5 mM) of **33** and **16a**$^+$TFPB$^-$ after 18 h at rt.

Subsequently, the study was extended to non-symmetrical alkylbenzylammonium axles. As previously described, it is well known that calix[6]arenes follows the so-called "*endo*-alkyl rule"; therefore it was of some interest to investigate the behavior of the smaller calix[5]arene analogues.[40]

In detail, the threading study of penta-penta-*O*-(4-methylpentyl)-*p*-*tert*-butylcalix[5]arene **33** with pentylbenzylammonium **16d**$^+$ evidenced the selective formation of *endo*-alkyl pseudorotaxane **16d**$^+$⊂**33** (**Figure 2.18**), confirming that the above rule also applies to calix[5]arene macrocycle.

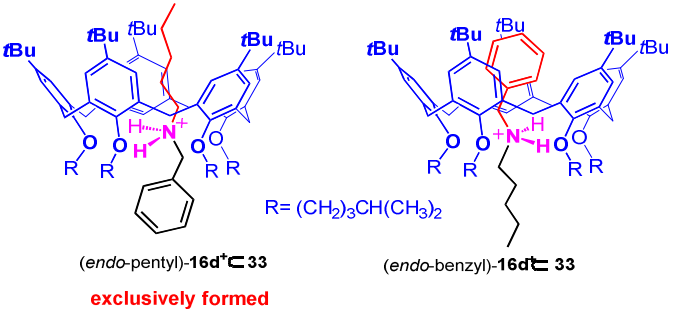

Figure 2.18. Endo-pentyl-/endo-benzyl pseudorotaxane stereoisomers, potentially obtainable by directional threading of the pentylbenzylammonium axle through the calix[5]arene wheels.

[40] De Rosa, M.; Talotta, C.; Gaeta, C.; Soriente, A.; Neri, P.; Pappalardo, S.; Gattuso, G.; Notti, A.; Parisi, M. F.; Pisagatti, I. *J. Org. Chem.* **2017**, *82* (10), 5162–5168.

From the study of dibenzylammonium axle, it was understood that the calix[5]arene lower rim, being narrower than the calix[6]arene one, cannot be crossed by the benzyl portion, while it is easily accessible to thin aliphatic chains (**Figure 2.19**).

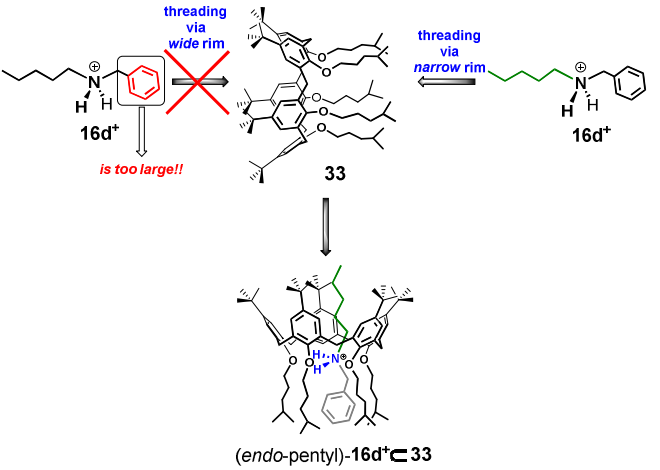

Figure 2.19. Unidirectional threading mode of **16d**$^{+}$ through the narrow rim of **33**.

This is the first example of unidirectional threading observed for calix[5]arenes. This important information can be considered as an additional rule, which could contribute to enriching the molecular code previously introduced. The application of this code could lead to more complex architectures mimicking those observed in biological systems.

CHAPTER III

Goals and Outline – Part I

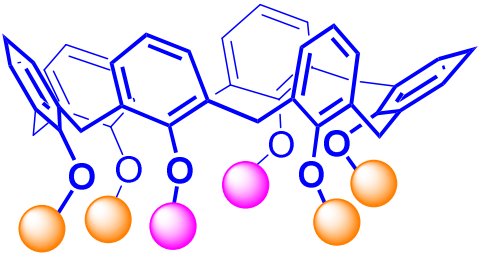

3.1 Goals and Outline – Part I

Given the extensive studies conducted on the threading of calix[*n*]arenes and given the importance of interpenetrated supramolecular systems in various fields, the aim of the present PhD thesis was to further investigate the threading abilities of this family of macrocycles in order to provide useful information for the future construction of mechanically interlocked molecular machines (MIMs) based on these macrocycles.

On this basis, this thesis will describe the synthesis of various calixarene derivatives specifically functionalized at the lower and upper rims and at methylene bridges (**Figure 3.1**). How these functionalization affect the threading ability of the macrocycles is also reported.

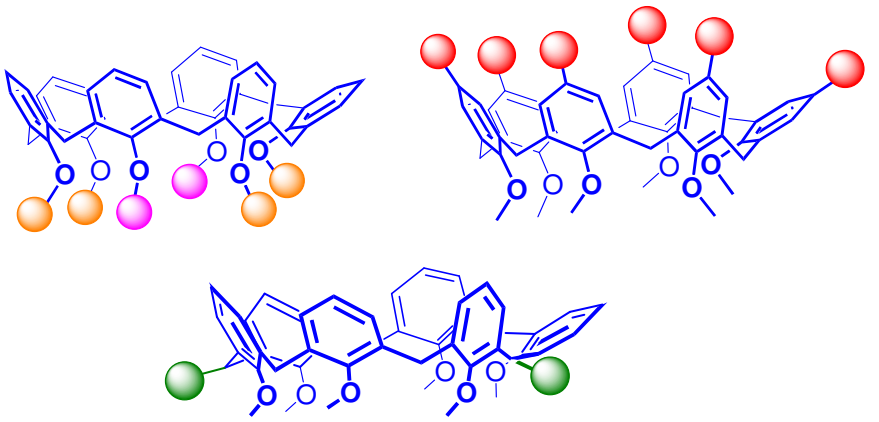

Figure 3.1. Calixarene derivatives functionalized.

All the new derivatives were characterized through NMR spectroscopy, mass spectrometry and, where necessary, also with UV/vis studies. Preliminary threading studies were also carried out by exploiting the "superweak anion approach".

CHAPTER IV

Functionalization to improve the threading ability of calix[6]arene macrocycle

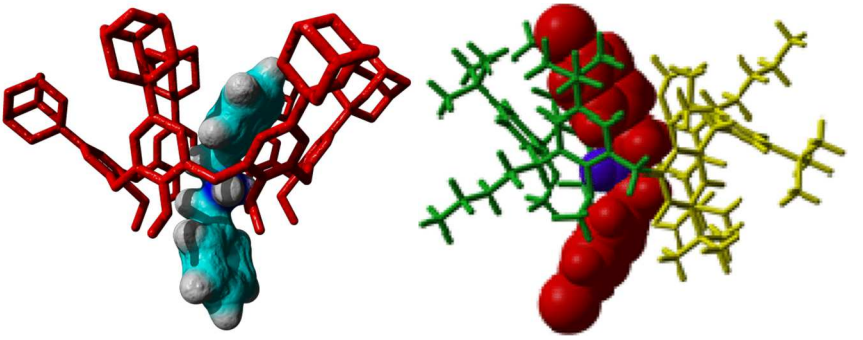

4.1 Chemical modification of calixarene macrocycle

Calixarenes have been extensively studied in the literature thanks to their high synthetic versatility. In fact, these macrocycles can be easily functionalized (**Figure 4.1**) at:

- Lower rim, with alkylation or acylation reactions.
- Upper rim, by aromatic electrophilic substitutions (halogenation, nitration, sulfonation, etc.).
- Methylene bridge, through nucleophilic substitution reactions.
- Aromatic walls, by reduction or oxidation of the phenol rings.

Thus, by introducing specific functional groups, it is possible to get hosts for anion or cation recognition or to obtain useful building blocks for self-assembly processes.

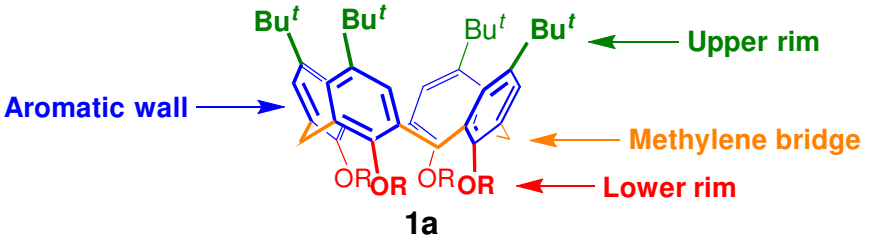

Figure 4.1. Functionalization of calixarene macrocycle.

4.2 Lower and Upper Rim Functionalization

The most popular and widely studied functionalization concerns the alkylation of the lower rim of calix[*n*]arenes by Williamson ether synthesis.

Using appropriate reaction conditions, partially and/or totally *O*-alkylated derivatives can be obtained directly from the native calix[*n*]arenes. The reaction outcome is dependent on several factors, such as the nature of the *p*-substituent at the upper rim, solvent, temperature, and base.

Totally *O*-alkylated calix[*n*]arene derivatives are obtained in the presence of a strong base with an excess of alkylating agent.[41] Instead, partial alkylation of calixarenes can be carried out in the presence of a weak base. In case of calix[6]arene, potassium trimethylsilanolate is used as a weak base. After the first alkylation, the second

[41] (a) Van Loon, J. D.; Arduini, A.; Coppi, L.; Verboom, W.; Pochini, A.; Ungaro, R.; Harkema, S.; Reinhoudt, D. N., *J. Org. Chem.* **1990**, *55*, 5639-5646. (b) Iwamoto, K.; Araki, K.; Shinkai, S. *J. Org. Chem.* **1991**, *56*, 4955-4962. (c) Araki, K.; Iwamoto, K.; Shinkai, S.; Matsuda, T., *Chem. Lett.* **1989** 1747-1750. (d) Kelderman, E.; Derhaeg, L.; Heesink, G. J. T.; Verboom, W.; Engbersen J. F. J.; Van Hulst, N. F.; Persoons, A.; Reinhoudt, D. N., *Angew. Chem., Int. Ed. Engl.* **1992**, *31*, 1075-1077.

deprotonation preferentially involves the distal OH group, to give an anion stabilized by two H-bonds with the proximal OH groups (**Scheme 4.1**). In addition to the pKa of the hydroxyl groups, the bulky effect of the base is also exploited.

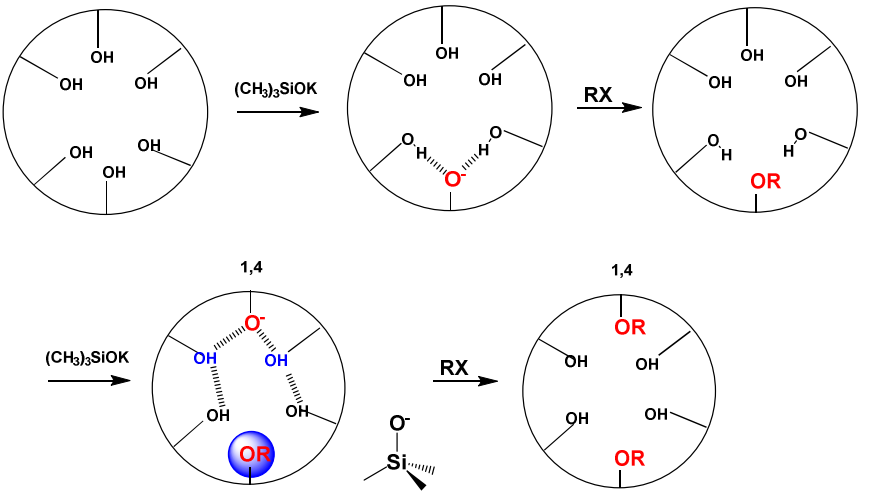

Scheme 4.1. Mechanism of weak-base-promoted regioselective 1,4-dialkylation of calix[6]arenes.

It is also possible to introduce substituents on the upper rim of the calixarene macrocycles. Luckily, it is possible to replace the *tert*-butyl with other groups. For this kind of approach, in a first instance, the *p-tert*-butyl group can be easily removed by a complete or selective reaction of de-*tert*-butylation, using a Lewis acid catalyst such as $AlCl_3$ (reverse Friedel-Crafts reaction) in the presence of phenol (**Scheme 4.2**). Subsequent electrophilic substitution reactions allow the introduction of new groups at the para-position. New functionalities can be introduced by acylation, bromination, formylation, diazo coupling, nitration, sulfonation, Claisen rearrangement, and Mannich reaction.[42]

[42] (a) Gutsche, C. D.; Levine, J. A. *J. Am. Chem. Soc.* **1982**, *104*, 2652-2653. (b) Gutsche, C. D.; Pagoria, P. F. *J. Org. Chem.* **1985**, *50*, 5795-5802. (c) Shinkai, S.; Tsubaki, T.; Sone, T.; Manabe, O. *Tetrahedron Lett.* **1985**, *26*, 3343-3344. (d) Morzherin, Y.; Rudkevich, D. M.; Verboom, W.; Reinhoudt, D. N. *J. Org. Chem* **1993** *58*, 7602-7605. (e) Gutsche, C. D.; Lin, L.-G. *Tetrahedron* **1986** *42*, 1633-1640. (f) Arduini, A.; Fanni, S.; Manfredi, G.; Pochini, A.; Ungaro, R.; Sicuri, A. R.; Ugozzoli, F. *J. Org. Chem.* **1995**, *60*, 1448-1453. (g) Shinkai, S.; Araki, K.; Shibata, J.; Tsugawa, D.; Manabe, O. *J. Chem. Soc., Perkin Trans.* **1990**, *1*, 3333-3337.(h) Verboom, W.; Durie, A.; Egberink, R. J. M.; Asfari, Z.; Reinhoudt, D. N. *J. Org. Chem.* **1992**, *57* 1313-1316. (i) Shinkai, S.; Koreishi, H.; Ueda, K.; Arimura, T.; Manabe, O. *J. Am. Chem. Soc.* **1987**, *109*, 6371-6376. (l) Almi, M.; Arduini, A.; Casnati, A.; Pochini, A.; Ungaro, R. *Tetrahedron* **1989**,*45*, 2177-2182. (m) Gutsche, C. D.; Nam, K. C. *J. Am. Chem. Soc.* **1988**, *110* 6153-6162. (n) Gutsche, C. D.; Levine, J. A.; Sujeeth, P. K. *J. Org. Chem.* **1985**, *50* 5802-5806.

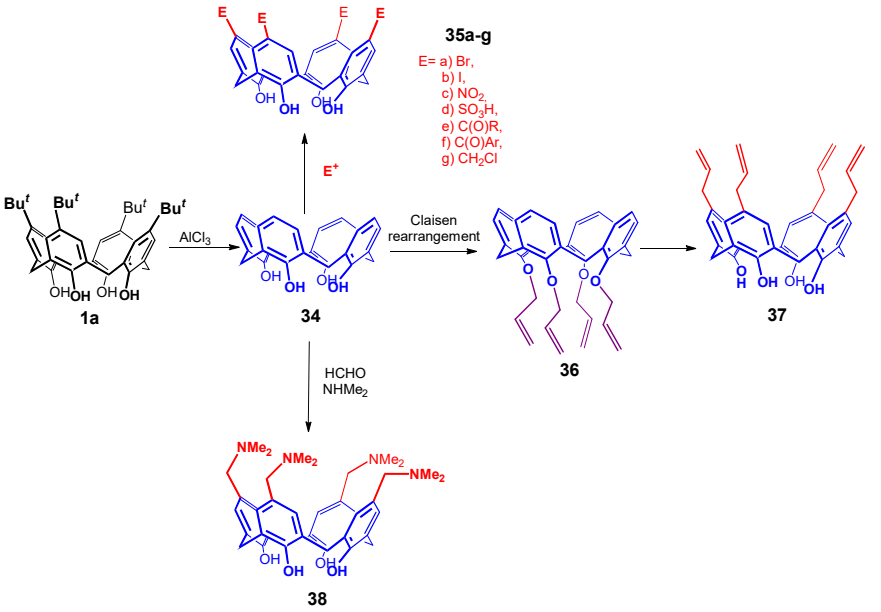

Scheme 4.2. Examples of upper rim functionalization.

An interesting substituent that can be introduced on the upper rim of the calixarene is the adamantane group. Introduction of a bulky lipophilic group increase the size of the hydrophobic cavity, and functional groups present in the adamantane fragment provide the possibility for further modification and conformational organization of the molecule. To obtain this substitution, a convenient synthesis is the direct adamantylation of an unsubstituted calix[*n*]arene with 1-hydroxyadamantanes in trifluoroacetic acid (**Scheme 4.3**).[43]

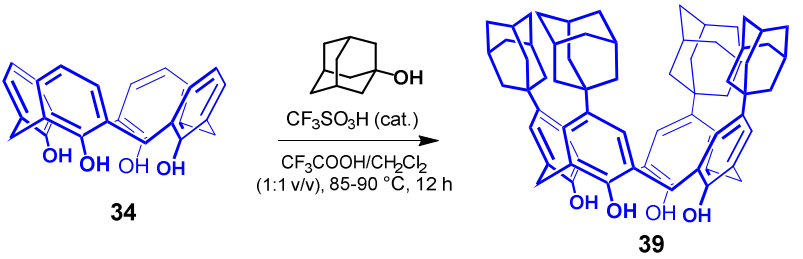

Scheme 4.3. Synthesis of derivative **39**.

[43] (a) Lubitov, I. E.; Shokova, E. A.; Kovalev, V. V. *Synlett* **1993**, 647-648. (b) Shokova, E. A.; Motornaya, A. E.; Shestakova, A. K.; Kovalev, V. V. *Tetrahedron Letters* **2004**, *45* (34), 6465–6469. (c) Shokova, E. A.; Khomich, E. V.; Akhmetov, N. N.; Vatsuro, I. M.; Luzikov, Y. N.; Kovalev, V. V. *Russ. J. Org. Chem.* **2003**, *39*, 368–383.

4.3 Influence of *exo*-Adamantyl Groups and *endo*-OH Functions on the Threading of Calixarene[44]

From previous studies it is known that calixarene derivatives bearing the *p-tert*-butyl groups at the upper rim (derivatives **15a-c**) give rise to more stable pseudorotaxane complexes than those formed by the corresponding *p*-H-macrocycles (derivatives **15d,e**) due to more favourable van der Waals interactions with the cationic axle. Based on these observations, it was decided to expand the previous knowledge by evaluating how a different substitution at the lower/upper rim of the macrocycle affects the threading of ammonium axles.

In particular, it was decided to study the threading of calix[6]arenes (**Figure 4.2**) bearing *p*-adamantyl units at the upper rim, derivatives **15f,g**. In addition, it was evaluated if the substitution of a few of the OR groups at the lower rim with the OH ones could also lead to thermodynamically stable pseudorotaxane complexes.

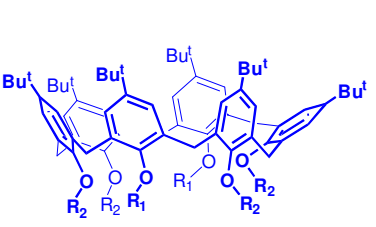

15a) R1= R2= Methyl
15b) R1= R2= Hexyl
15c) R1= H; R2= Hexyl

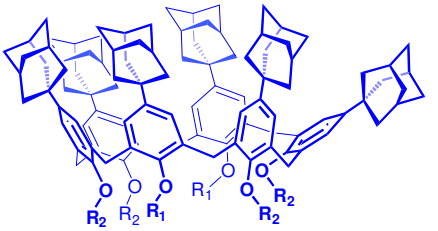

15f) R1= R2= Methyl
15g) R1= H; R2= Hexyl

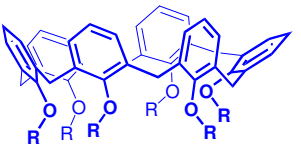

15d) R= Methyl
15e) R= Hexyl

Figure 4.2. Structures of calix[6]arene wheels **15a-g**.

4.3.1 Synthesis of derivatives 15f and 15g

The synthesis of hexamethoxy-*p*-adamantylcalixarene **15f** was obtained by exhaustive methylation with MeI, promoted by NaH in DMF (**Scheme 4.4**) of the corresponding hexol.

[44] Iuliano, V.; Talotta, C.; Gaeta, C.; Hickey, N.; Geremia, S.; Vatsouro, I.; Kovalev, V.; Neri, P. *J. Org. Chem.* **2020**, *85* (19), 12585–12593.

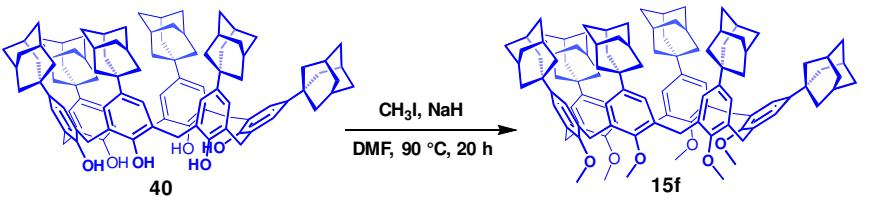

Scheme 4.4. Synthesis of derivative **15f**.

The new derivative was fully characterized by NMR spectroscopy and mass spectrometry. Furthermore, its structure was also confirmed by X-ray diffraction studies which also evidenced its preferential conformation. In fact, in accordance with other calix[6]arene examples, **15f** adopts a centrosymmetric 1,2,3-alternate conformation in the solid state (**Figure 4.3**).

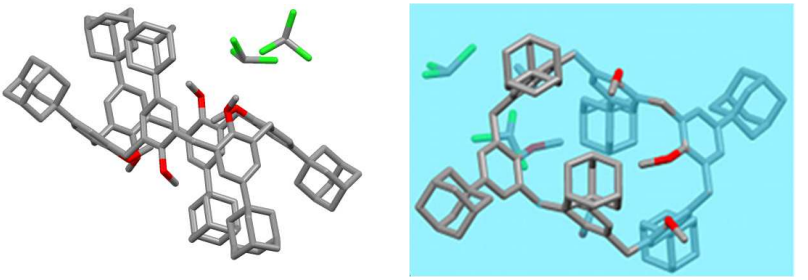

Figure 4.3. X-Ray structure of derivative **15f**.

In a similar way, derivative **15g** was synthesized by a selective alkylation at the 1,2,4,5-positions by using NaH in DMF (**Scheme 4.5**).

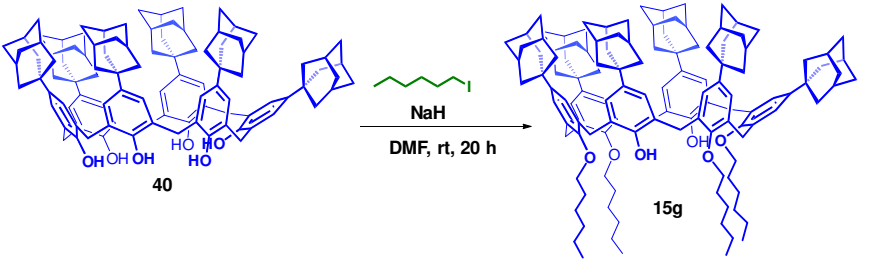

Scheme 4.5. Synthesis of derivative **15g**.

The characterization of derivative **15g** was made less easy by the broad appearance of its ^{1}H NMR signals at room temperature, due to a conformational mobility close to the NMR time scale. During these studies, unusual signals were observed in the negative region of the ^{1}H NMR spectrum, which could be attributed to one of the hexyl chain self-included within the calix[6]arene cavity (**Figure 4.4a**). Consequently, we can anticipate that **15g** must assume a particular conformation in solution. To determine this conformation, an NMR study was performed at 243 K (**Figure 4.4b-e**). From a detailed analysis, it was found that **15g** adopts a partial-cone

conformation with a hexyl chain self-included inside the cavity (corresponding to a pseudo[1]rotaxane complex).

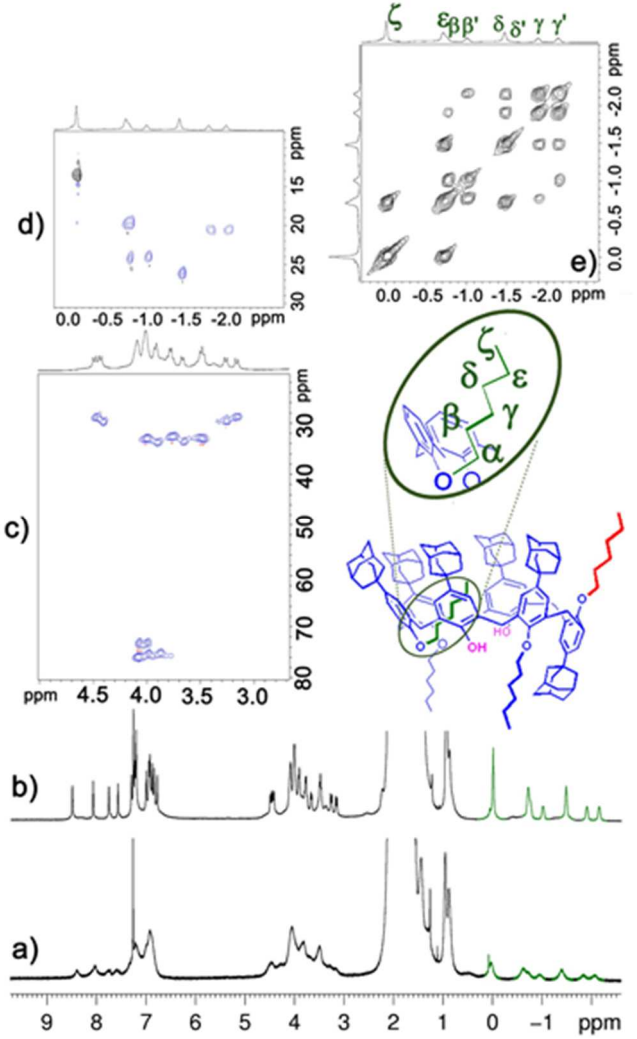

Figure 4.4. ^{1}H NMR spectra ($CDCl_3$, 600 MHz) of pseudo[1]rotaxane derivative **15g** at 298 K (a) and 243 K (b); c,d) different portions of its HSQC spectrum ($CDCl_3$, 600 MHz, 243 K); e) portion of its COSY−45 spectrum ($CDCl_3$, 600 MHz, 243 K).

A conclusive confirmation of the peculiar conformation adopted by **15g** was obtained by X-ray studies. In fact, **15g** exhibits an asymmetric partial-cone conformation, with just one of the phenyl rings with inverted orientation with respect to the other five in the solid state (**Figure 4.5**). This phenyl is opposite to a phenyl group bearing a self-included hexyloxy chain in the macrocycle. The partial-cone conformation, combined with the mixed hydroxy/hexyloxy substitution pattern at the lower rim (1,2,4,5-

tetrahexyloxy) results in an asymmetric C_1 molecular point symmetry. Since it crystallized in the P -1 space group, the structure is therefore composed by racemic pairs of inherently chiral **15g** molecules.

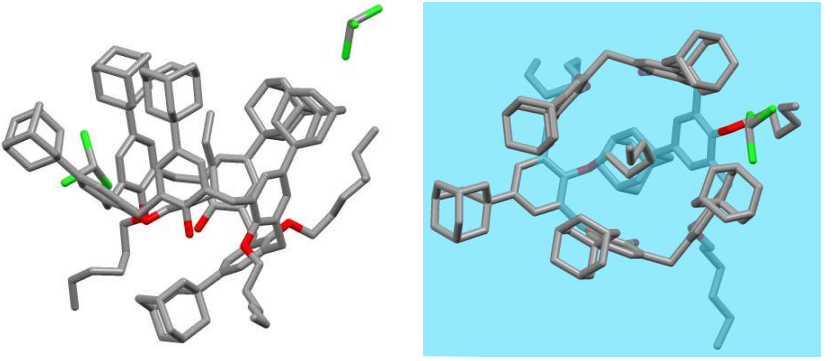

Figure 4.5. X-Ray structure of derivative **15g**.

Finally, in order to make a comparative threading study, the *p-tert*-butyl-calix[6]arene analogue **15c** was also synthesized.

1,2,4,5-tetrahexyloxy-*p-tert*-butylcalix[6]arene-diol **15c** was obtained (**Scheme 4.6**) starting from *p-tert*-butilcalix[6]arene, 2 out of 6 hydroxyl groups were protected by benzylation at the 1,4-positions (90 % yield).

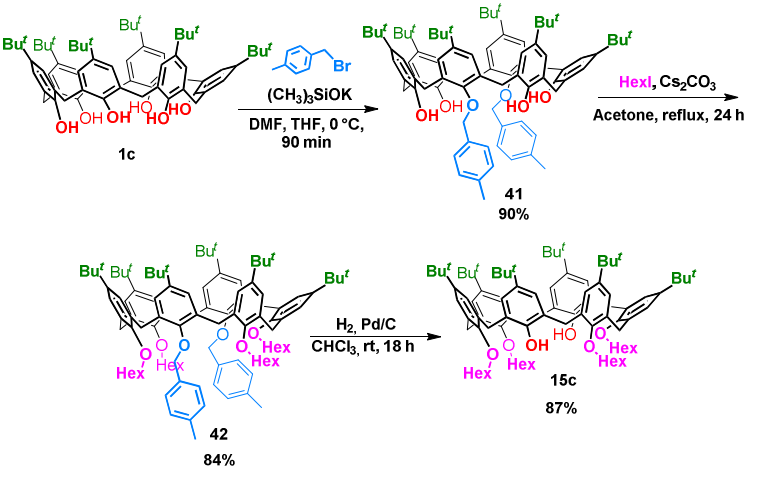

Scheme 4.6. Synthesis of derivative **15c**.

Subsequently, the known 1,4-dibenzyl derivative **41**,[45] was first tetralkylated with hexyl iodide (84 % yield) and then debenzylated with H_2 Pd/C (87 % yield). The characterization of **15c** was very similar to that of **15g** for what concerns the broad

[45] Kanamathareddy, S.; Gutsche, C. D. *J. Org. Chem.* **1992**, *57* (11), 3160–3166.

appearance of its ^{1}H and ^{13}C NMR signals at room temperature, due to a conformational mobility close to the NMR time scale. The similarity was also extended to the unusual signals in the negative region of the spectrum due to the self-included hexyl chain. Also, in this case, a low temperature NMR study confirmed the peculiar partial-cone conformation (**Figure 4.6**). This result leads to suppose that this conformational feature could be characteristic of calix[6]arenes 1,2,4,5-tetrasubstituted with long alkyl chains.

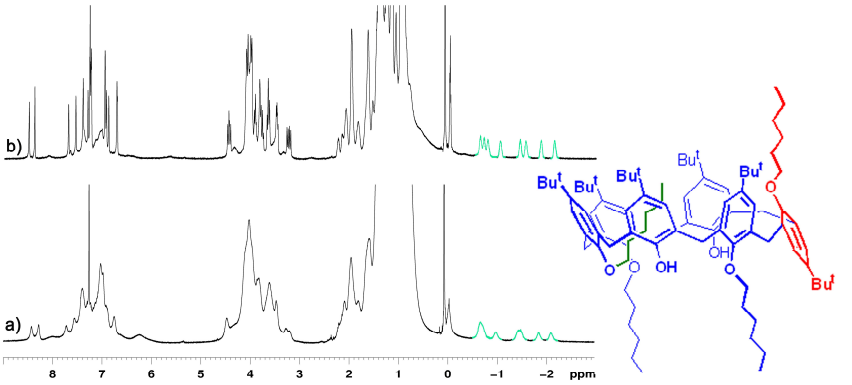

Figure 4.6. ^{1}H NMR spectra ($CDCl_3$, 600 MHz) of pseudo[1]rotaxane derivative **15c** at 298 K (a) and 243 K (b)

4.3.2 Threading of Derivatives 15f and 15g

Initially, the threading properties of derivative **15f** were studied by using three types of linear systems: an axle with two aliphatic chains (**16a**$^{+}$) or two benzyl groups (**16b**$^{+}$), and a mixed alkylbenzylammonium one (**16e**$^{+}$) (**Figure 4.7**).

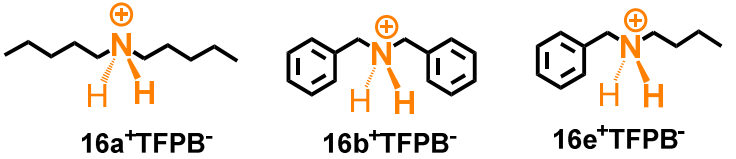

Figure 4.7. Linear systems.

By mixing host **15f** with axle **16b**, drastic changes in the proton spectrum are observed, which confirmed the **16b**$^{+}\subset$ **15f** psuedorotaxane formation. In detail, the appearance of a well-spaced AX system (at 3.46/4.39 ppm, $\Delta\delta$ = 0.93 ppm) for the $ArCH_2Ar$ groups of the calix wheel indicates that the latter has a cone shape in the supramolecular system **16b**$^{+}\subset$ **15f** (**Figure 4.8**).

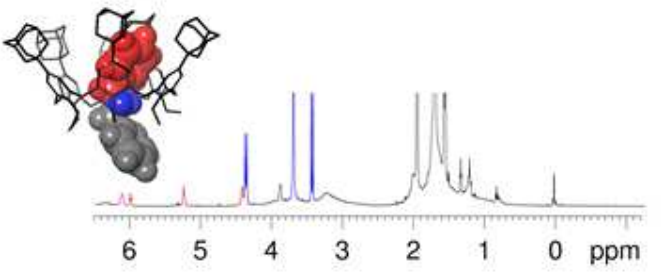

Figure 4.8. ^{1}H NMR spectrum of **16b$^+$⊂ 15f** ($CDCl_3$, 600 MHz, 298 K).

The most important proof of the formation of the interpenetrated system is the presence of the guest signal to unusual chemical shifts for aromatic protons due to the shielding of the calixarene cavity (at 4.44, 5.26, and 6.00 ppm; ortho-, meta- and para-BnH, respectively) while the other outside the calix cavity resonated at more typical values (7.90, 7.64, and 7.50 ppm, ortho-, meta-, and para-BnH, respectively). Once the characterization of the new supramolecular system was complete, it was possible to determine the association constant by means of a competition experiment with the native hexahexyloxy-*p*-tert-butylcalix[6]arene **15b.** The NMR spectrum of the mixture 1:1:1 of **15f/15b/16b$^+$** indicated that pseudorotaxane **16b$^+$⊂ 15b** was favoured over **16b$^+$⊂ 15f** in a 1:0.8 ratio (**Figure 4.9**). An apparent association constant value of 7.4±0.2×10^4 M^{-1} was calculated from this competition experiment for the **16b$^+$⊂ 15f** complex, which is significantly higher than that previously observed for **16b$^+$⊂ 15a** (2.5 x 10^3 M^{-1}).

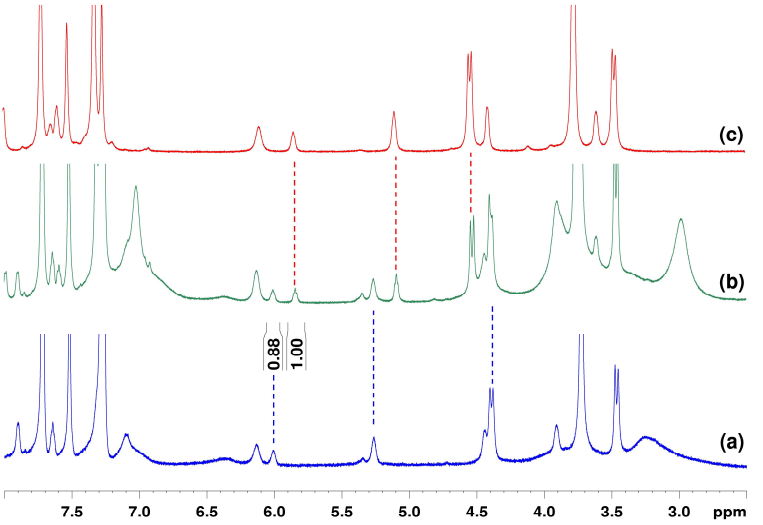

Figure 4.9. ^{1}H NMR spectra ($CDCl_3$, 600 MHz, 298 K) of (a) 1:1 solution of **15f** and **16b$^+$**TFPB$^-$, (b) 1:1:1 solution of **15f**, **15b** and **16b$^+$**TFPB$^-$, (c) 1:1 solution of **15b** and **16b$^+$**TFPB$^-$.

Subsequently, the threading study of **15f** was extended to the dipentylammonium axle **16a**$^+$ by using similar experimental conditions. The formation of pseudorotaxane **16a**$^+\subset$ **15a** was confirmed by the ^{1}H NMR spectrum (**Figure 4.10**), which shows shielded signals related to the aliphatic chain inside the calixarene cavity between 0.6 and -1.0 ppm.

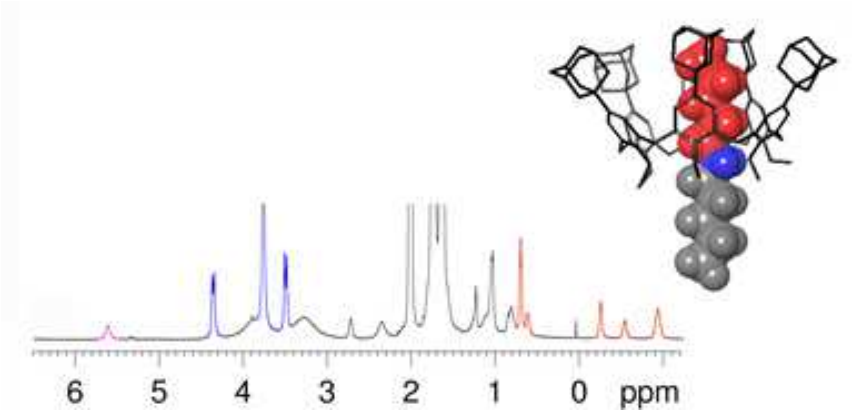

Figure 4.10. ^{1}H NMR spectrum of **16a**$^+\subset$ **15f** ($CDCl_3$, 600 MHz, 298 K).

Also, in this case, the association constant was calculated by a competition experiment with **15b** (**Figure 4.11**). The value of the constant is 5.0±0.2 x 10^4 M^{-1}, which was again higher than that of **16a**$^+\subset$ **15a** (4.4±0.2 x 10^2 M^{-1}).

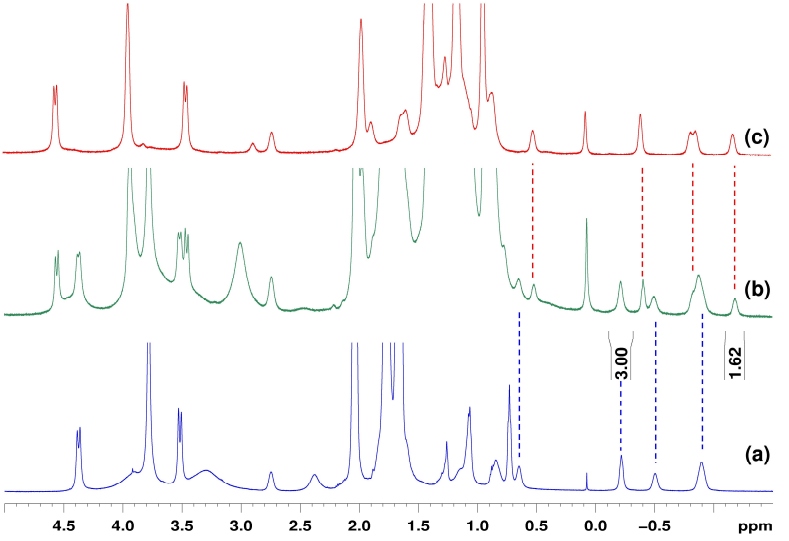

Figure 4.11. ^{1}H NMR spectra ($CDCl_3$, 600 MHz, 298 K) of (a) 1:1 solution of **15f** and **16a**$^+$$TFPB^-$, (b) 1:1:1 solution of **15f**, **15b** and **16a**$^+$$TFPB^-$, (c) 1:1 solution of **15b** and **16a**$^+$$TFPB^-$.

Finally, to verify if the "*endo*-alkyl rule" mentioned in Chapter 1 is also valid for *p*-adamantylcalix[6]arenes, it was studied the threading of **15f** with butylbenzylammonium axle **16e**$^+$. The presence of up-field shifted resonances in the negative region of the proton spectrum demonstrated the preferential formation of the *endo*-alkyl **16e**$^+\subset$ **15f** pseudorotaxane. Furthermore, once again the association constant (**Figure 4.15**) of **16e**$^+\subset$ **15f** (determined by a competition experiment) was higher than that of **16e**$^+\subset$ **15a (Figure 4.12)**.

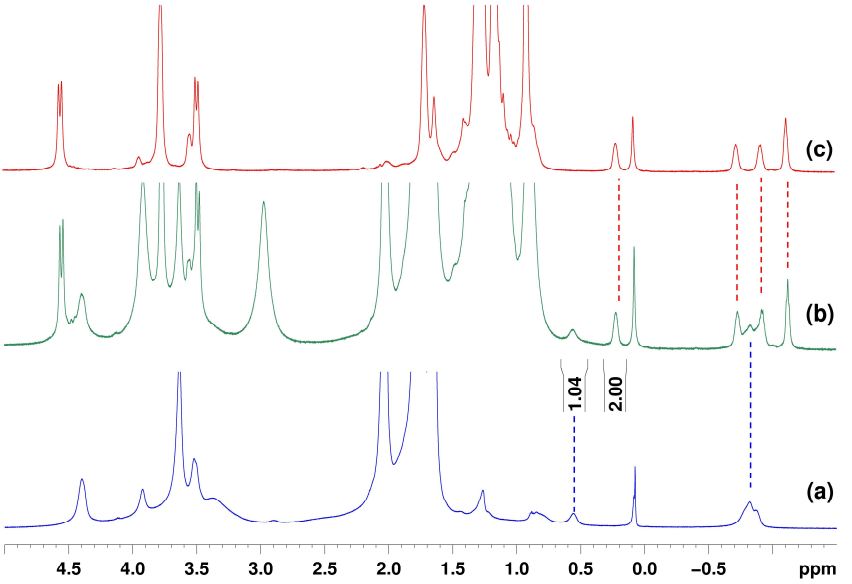

Figure 4.12. ^{1}H NMR spectra ($CDCl_3$, 600 MHz, 298 K) of (a) 1:1 solution of **15f** and **16a**$^+$TFPB$^-$, (b) 1:1:1 solution of **15f**, **15b** and **16a**$^+$TFPB$^-$, (c) 1:1 solution of **15b** and **16a**$^+$TFPB$^-$.

The threading study with the above three axles was then extended to 1,2,4,5-tetrahexyloxy-*p*-adamantyl-calix[6]arene-diol **15g** (**Figure 4.13**). The formation of a pseudo[2]rotaxane system was observed in all the three instances. It is noteworthy that the free host has a partial cone conformation with one of the hexyl chains shielded inside the macrocycle cavity (**Figure 4.13a**) while when the axis penetrates the macrocycle and the host-guest complex is formed, the calixarene assumes a cone conformation (**Figure 4.13b-d**). Also, in this case, the threading with the asymmetric linear system confirmed the *endo*-alkyl rule (**Figure 4.13d**). Subsequently, the apparent association constants (**Figure 4.15**) were determined also by competition experiments.

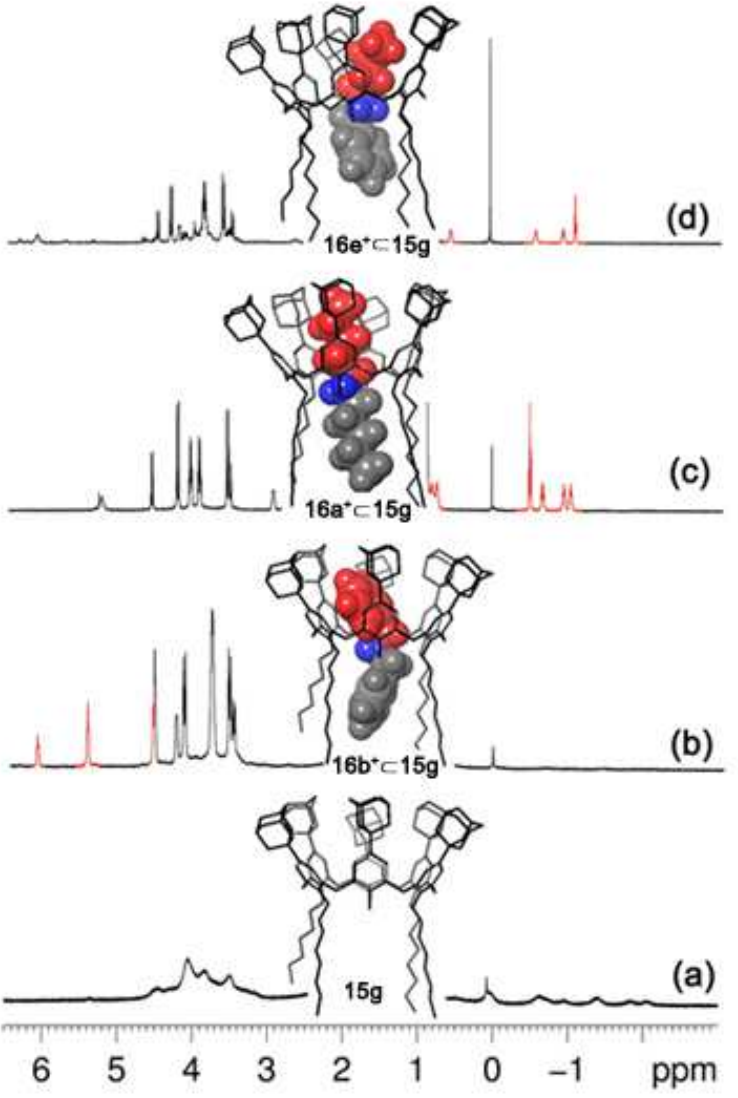

Figure 4.13. Portions of ^{1}H NMR spectra ($CDCl_3$, 600 MHz, 298 K) of **15g** (a), **16b⁺⊂ 15g** (b), **16a⁺⊂ 15g** (c), and **16e⁺⊂ 15g** (d).

The effect of the adamantyl group on the threading of derivative **15g** was also studied. As for the previous macrocycle, threading was observed with all the above three linear axles and once again the *endo*-alkyl rule was respected. Association constant values were calculated by quantitative ^{1}H NMR experiments using TCE as the internal standard for **16b⁺⊂ 15g** and **16e⁺⊂ 15g**. In this case, the following equation was used to obtain the moles of the complex:

$$\frac{G_a}{G_b} = \frac{F_a}{F_b} \times \frac{N_b}{N_a} \times \frac{M_a}{M_b}$$

Instead for **16a⁺⊂ 15g,** the association constant was determined by a competition experiment.

Preliminary threading tests with the ammonium axes used previously were also carried out for derivative **15c** (**Figure 4.14**).

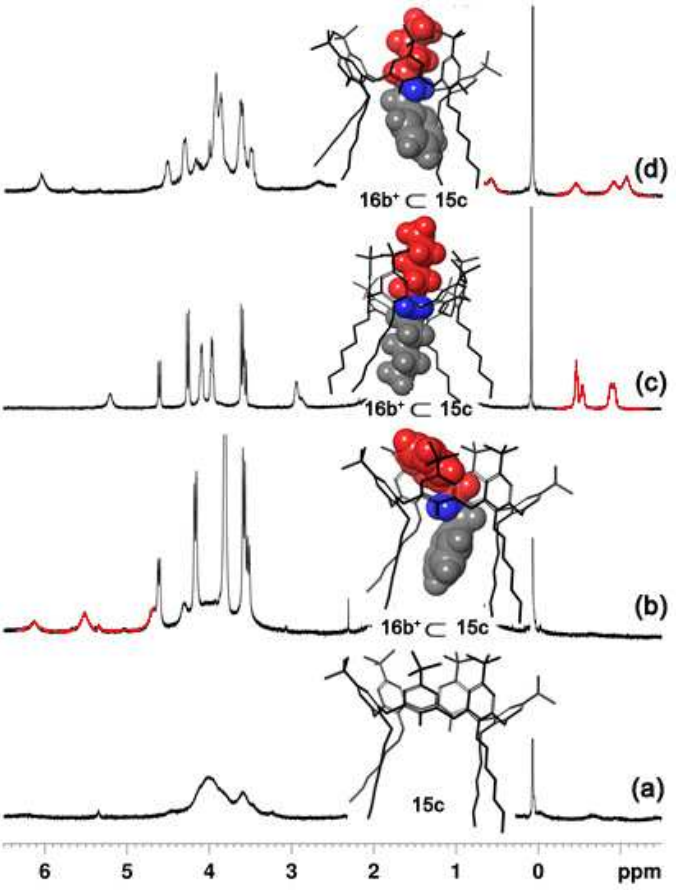

Figure 4.14. Portions of ^{1}H NMR spectra of (a) **15c**, (b) **16b⁺ ⊂ 15c**, (c) **16a⁺ ⊂ 15c** and (d) **16e⁺ ⊂ 15c** ($CDCl_3$, 600 MHz, 298 K).

Comparing the association constants (**Figure 4.15**) obtained for derivative **15g** with those of **15c** it was confirmed that the adamantyl group leads to higher constants than the tert-butyl one. In detail, association constant of 8.5×10^4 was found for **16b⁺ ⊂ 15g**, which is higher than that of **16b⁺ ⊂ 15c** (2.5×10^3). Similar results were found by

comparing **16a**$^+$ ⊂ **15g** (3.4×10^5) with **16a**$^+$ ⊂ **15c** (7.1×10^3) and **16e**$^+$ ⊂ **15g** (9.3×10^4) with **16e**$^+$ ⊂ **15c** (1.2×10^3).

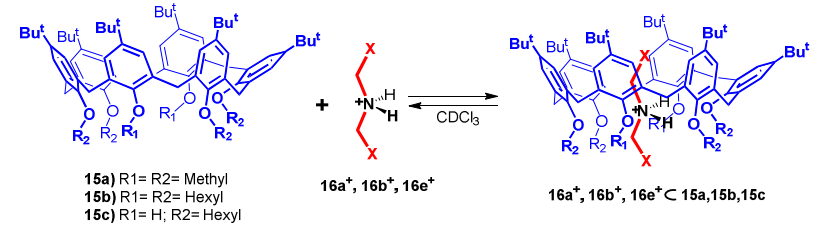

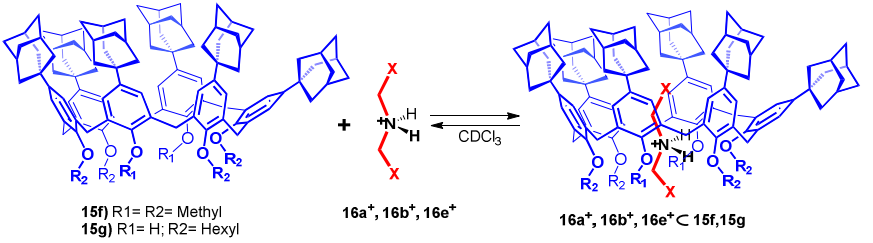

K_{app}

⊂	15a	15b	15f	15g	15c
16b$^+$	$2.5\pm0.2\times10^3$	$1.2\pm0.2\times10^5$	$7.4\pm0.2\times10^4$	$8.5\pm0.2\times10^4$	$2.5\pm0.2\times10^3$
16a$^+$	$4.4\pm0.2\times10^2$	$3.5\pm0.1\times10^4$	$5.0\pm0.2\times10^4$	$3.4\pm0.2\times10^5$	$7.1\pm0.2\times10^3$
16e$^+$	$6.5\pm0.2\times10^4$	$5.1\pm0.2\times10^5$	$1.4\pm0.2\times10^5$	$9.3\pm0.2\times10^4$	$1.0\pm0.2\times10^3$

Figure 4.15. Threading of calix[6]-wheels and K_{app} values measured for the formation of the corresponding pseudorotaxanes.

At this point, attention was paid to the effect on the threading efficiency of the substitution of a few of the OR groups at the *endo*-rim of the calix[6]-wheel with the OH ones. The threading ability of 1,2,4,5-tetrahexyloxycalix[6]arene-diol **15c** was compared with that of the corresponding hexahexyloxy-ether **15b**, both bearing *exo*-*tert*-butyl groups (**Figure 4.15**). An apparent association constant of 2.5×10^3 was found for **16b**$^+$⊂ **15c** which is significantly less stable with respect to **16b**$^+$⊂ **15b** (1.2×10^5). As expected, this can be attributed to the less favourable interactions between the OH groups and the guest in comparison with the OR ones. A similar result was observed for the complexation of dipentylammonium axle **16a**$^+$ with 1,2,4,5-tetrahexyloxycalix[6]arene-diol **15c**, which gave an apparent association constant of 7.1×10^3 for **16a**$^+$⊂ **15c** with respect to the value of 3.5×10^4 for **16a**$^+$⊂ **15b**.

4.3.3 Computational Studies

Further insights on the higher stability of pseudorotaxanes **16b**$^+$⊂ **15f** and **16a**$^+$⊂ **15f** were obtained by DFT calculations at the B3LYP/6-31G(d,p) level of theory using Grimme's dispersion corrections (IOp(3/124 = 3). As can be seen from the energy-

minimized structures (**Figure 4.16**) the p-adamantyl groups of host **15f** are all well-disposed around the endo-cavity portion of the guest **16b**$^+$ or **16a**$^+$.

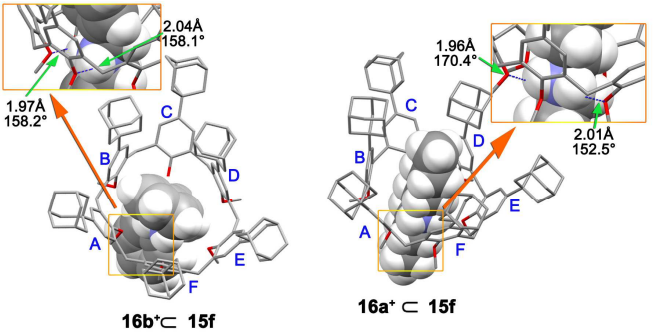

	16b$^+$⊂ 15f	16a$^+$⊂ 15f
A (°)	51.6(1)	53.4(1)
B (°)	84.9(1)	85.4(1)
C (°)	42.1(1)	39.3(1)
D (°)	80.3(1)	88.8(1)
E (°)	56.0(1)	47.2(1)
F (°)	51.0(1)	62.8(1)

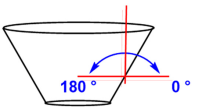

Figure 4.16. DFT-optimized structure of **16b**$^+$**⊂ 15f** and **16a**$^+$**⊂ 15f** pseudorotaxanes at the B3LYP/6-31G(d,p)-IOp(3/124=3) level of theory.

In detail, pseudo[2]rotaxane **16b**$^+$**⊂ 15f** is stabilized by two H-bonding interactions between the ammonium group and the calixarene oxygen atoms with an average N···O distance of 2.05 Å and an average N-H···O angle of 158.05°. Additional C-H···π interactions were identified between the α and β methylene groups of the benzyl unit of **16b**$^+$ inside the calix cavity and the aromatic rings of 15f with an average C-H···π centroid distance of 3.16 Å and an average C-H···π centroid angle of 155°. As a result of these contributions, the calix[6]arene macrocycle is fixed in a cone conformation. In particular, two of the six Ar rings (B and D) are almost orthogonally ori-ented with respect to the average plane defined by the six bridging methylene carbon atoms (canting angles[46] of 84.9°(1) and 80.3°(1), respectively, while the other A, C, E, F rings are more outwards tilted (canting angles of 51.6°(1), 42.1°(1), 56.0°(1), and 51.0°(1), respectively). As concerns the DFT-optimized structure of **16a**$^+$**⊂ 15f** pseudorotaxane, two H-bonding interactions were identified between the NH_2^+ group of **16a**$^+$ and the oxygen atoms of calix-wheel **15f**, with a longer average distance of 1.98 Å and an average angle of 161.45°. Also in this case, the calix[6]arene macrocycle is fixed in a cone conformation with D and E rings almost orthogonal with respect to the mean plane de-fined by all bridging methylenes

[46] Lipkowitz, K. B.; Pearl, G. Structural features of solid-state calix[4]arene in the cone conformation. *J. Org. Chem.* **1993**, *58*, 6729-6736.

(canting angle 85.4°(1) and 88.8°(1), respectively), while the other A, B, C, E rings are more opened with canting angle values of 47.2°(1), 62.8°(1), 53.4°(1), and 39.3°(1), respectively.

To further investigate the energy contribution due to non-covalent interactions (NCI)[47], a SOPT analysis[48] of the Fock matrix in the NBO basis was carried out. Interestingly, the SOPT analysis conducted on **16b⁺⊂ 15f** pseudo[2]rotaxane (**Figure 4.17**) indicates that there is an articulate network of hydrogen bonding, C-H···π, and π···π interactions.

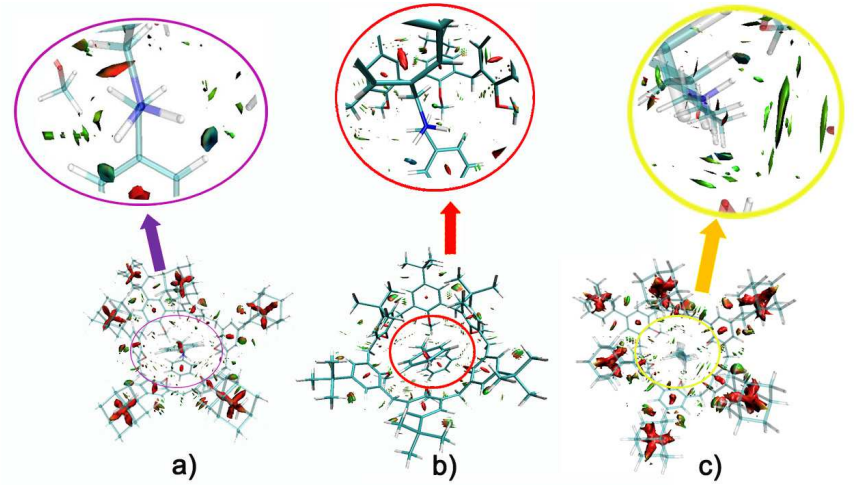

Figure 4.17. Non-covalent interaction plot by the sign of the second Hessian eigenvalue (gradient isosurfaces (s = 0.6 a.u.) for **16b⁺⊂ 15f** (a), **16b⁺⊂ 15a** (b) and **16a⁺⊂ 15f** (c). In the coloring isosurface blue and green colors represent strong and medium interactions (H-bonding and van der Waals).

The overall energy analysis indicates that the total energetic contribution due to secondary non-covalent interactions (NCI) is 34.09 kcal/mol. Very interestingly, a similar analysis for the corresponding tert-butylated **16b⁺⊂ 15a** pseudo[2]rotaxane gives a lower total energy contribution of 26.66 Kcal/mol. Instead, in the case of **16a⁺⊂ 15f**, the SOPT analysis indicated an energy contribution of 30.18 Kcal/mol for the secondary interactions.

DFT calculations at the B3LYP/6-31G(d,p) level of theory using Grimme's dispersion corrections (IOp(3/124 = 3)) were also performed on pseudorotaxanes **16b⁺⊂ 15g** and **16a⁺⊂ 15g** and the corresponding energy-minimized structure are reported in **Figure 4.18**. For both the two supramolecular adducts, it is possible to observe the typical

[47] Weinhold, F.; Landis, C. R. *Valency and Bonding: A Natural Bond Orbital Donor-Acceptor Perspective*, 1st ed.; Cambridge University Press, **2005.**
[48] Johnson, E. R.; Keinan, S.; Mori-Sánchez, P.; Contreras-García, J.; Cohen, A. J.; Yang, W. Revealing Noncovalent Interactions. *J. Am. Chem. Soc.* **2010**, *132* (18), 6498–6506.

network of H-bonding interactions between the am-monium group and the oxygen atoms of the calixarene macrocycle (**16b⁺⊂ 15g**: average N···O distance 1.73 Å, average N-H···O angle 166.45°; **16a⁺⊂ 15g**: average N···O distance 1.91 Å, average N-H···O angle 166.15°). Several non-covalent interactions were identified between the endo-cavity benzyl unit of **16b⁺** (or the endo-cavity alkyl chain of **16a⁺**) and the aromatic rings of **15g**. All these interac-tions contributes to fix the calix[6]arene macrocycle in the cone conformation. An interesting observation was found for the two distal unsubstituted phenolic rings A and D of both pseudorotaxanes. These ArOH units are more tilted outwards the cavity with a canting angles18 in the range 25.9°-29.7° (**Figure 4.18**).

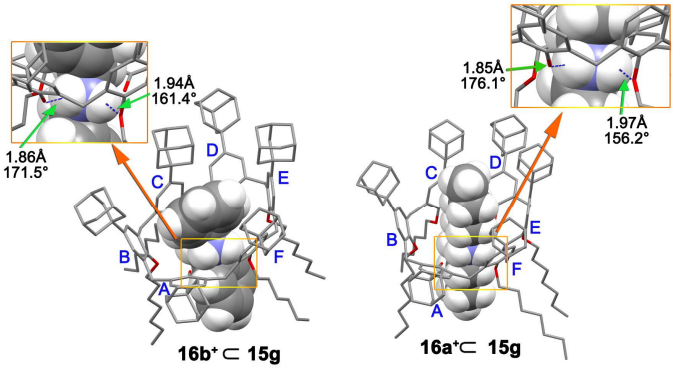

	16b⁺⊂15g	16a⁺⊂15g
A (°)	29.2(1)	29.1(1)
B (°)	64.9(1)	66.2(1)
C (°)	84.3(1)	85.0(1)
D (°)	29.7(1)	25.9(1)
E (°)	78.4(1)	85.0(1)
F (°)	58.8(1)	61.2(1)

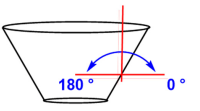

Figure 4.18. DFT-optimized structure of **16b⁺⊂ 15g** and **16a⁺⊂ 15g** pseudorotaxanes at the B3LYP/6-31G(d,p)-IOp(3/124) level of theory.

In conclusion, these studies demonstrated that *exo*-adamantyl groups give rise to a more efficient threading with respect to the *exo-tert*-butyl ones leading to apparent association constants more than one order of magnitude higher. This higher thermodynamic stability can be ascribed to the more favorable van der Waals interactions of *exo*-adamantyls versus *exo-tert*-butyls with the cationic axle. In addition, it was also demonstrated that *endo*-OH functions give rise to a less efficient threading with respect to the *endo*-OR ones, in line with what was known from the complexation of alkali metal cations.

4.4 Methylene bridge functionalization

In the previous paragraph, it was observed how the introduction of a bulky group to the upper rim and the complete alkylation of the lower rim leads to a higher association constant with ammonium axles. On this basis it was then decided to investigate the influence of substituents at the methylene bridges.

The introduction of substituents at the methylene bridges is an interesting method for reducing the conformation flexibility of calixarene macrocycle. Macrocycles with a higher pre-organization are particularly interesting for their higher selectivity and efficiency in molecular recognition.

For the preparation of methylene-functionalized calixarenes, several synthetic strategies have been developed. The "fragment condensation" method[49] introduced by Böhmer *et al.* requires the use of fragments specifically functionalized, that subsequently are cyclocondensed to give substituted calixarenes. Generally, this reaction involves a Friedel-Crafts alkylation which is conducted in the presence of a Lewis acid (**Scheme 4.7**).

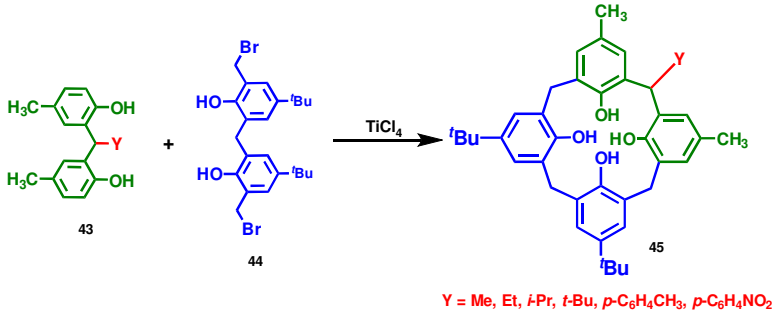

Scheme 4.7. "Fragment condensation" method.

Unlike calix[4]arenes, which can adopt a thermodynamically stable and fixed cone conformation, calix[6]arenes are more flexible and therefore present greater difficulties concerning the substitution of the methylene bridge. In 2015, Singh[50] described the first example of a symmetrical substitution of the methylene bridges of a calix[6]arene. This work shows that such alkylation leads to two different conformationally stable calix[6]arene isomers which have been isolated and characterized by VT NMR spectroscopy and by X-ray analysis. The implemented

[49] (a) Tabatabai, M.; Vogt, W.; Böhmer, V. *Tet. Lett.* **1990**, *31*, 3295. (b) Sartori, G.; Maggi, R.; Bigi, F.; Arduini, A.; Pastorio, A.; Porta, C. *J. Chem. Soc., Perkin Trans. 1,* **1994**, 1657. (c) Biali, S. E.; Böhmer, V.; Cohen, S.; Ferguson, G.; Grüttner, C.; Grynszpan, F.; Paulus, E. F.; Thondorf, I.; Vogt, W. *J. Am. Chem. Soc. 1996*, **118**, 12938. (d) Bergamaschi, M.; Bigi, F.; Lanfranchi, M.; Maggi, R.; Pastorio, A.; Pellinghelli, M. A.; Peri, F.; Porta, C.; Sartori, G. *Tetrahedron* **1997**, *53*, 13037. (e) For a review on the synthesis of calixarenes via the stepwise and fragment condensation methods see: Böhmer, V. *Liebigs Ann./Recueil* **1997**, 2019.

[50] Arora, S.; Sharma, S.; Mithu, V. S.; Hee-Lee, C.; Singh, K. *Chem. Commun.* **2015**, *51* (20), 4227–4230.

synthesis consists of two steps. The first step involves alkylation at the lower rim with MeI in the presence of NaH as a base. Subsequently, an alkylation step is carried out on the methylene bridge by deprotonating the latter with a mixture of *n*BuLi-TMEDA (**Scheme 4.8**). This approach leads to the preferential formation of two conformers showing a high degree of conformational stability: a distorted cone and a 1,2,3-alternate isomer.

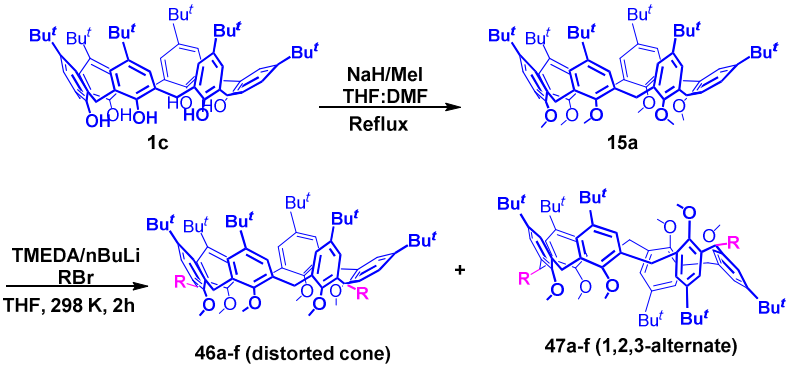

R=(a) Et; (b) *n*-pentyl; (c) *n*-decyl; (d) Bn; (e) CH_2COOEt; (f) allyl

Scheme 4.8. Synthesis of hexamethoxycalix[6]arene **15a** and disubstituted calix[6]arenes **46a-f** (distorted cone) and **47a-f** (1,2,3-alternate) conformers.

These derivatives can be isolated by chromatography and it is possible to distinguish them by observing the AX system of the methylene bridge in the proton spectrum (**Figure 4.19**).

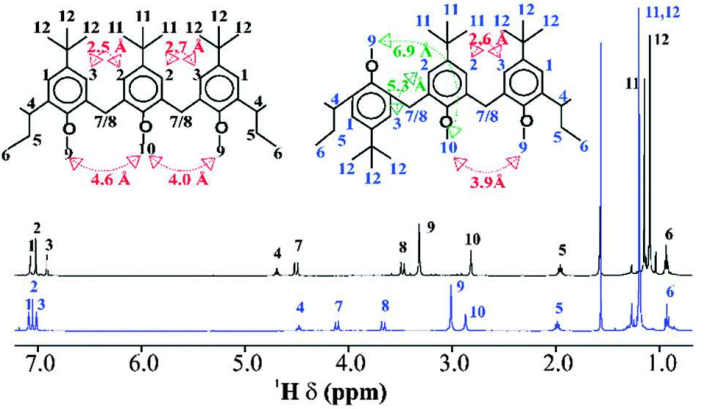

Figure 4.19. Comparison of ^{1}H NMR spectra of two stable conformers, distorted cone and 1,2,3-alternate.

Furthermore, the structures of these isomers were also confirmed by single-crystal X-ray analysis (**Figure 4.20**).

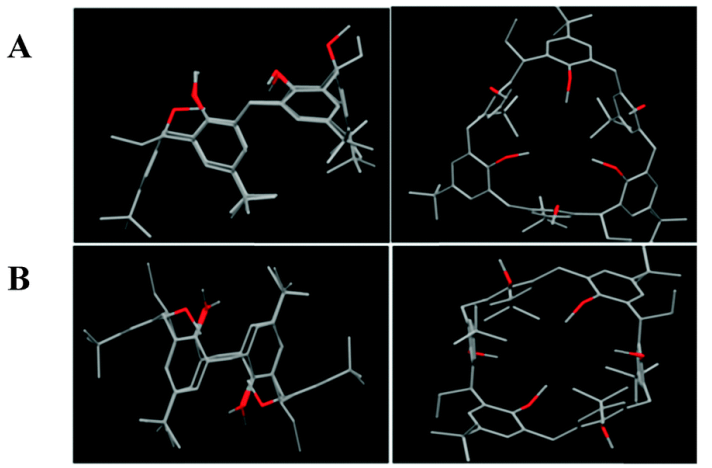

Figure 4.20. Stereo views of **46a** (distorted cone conformation) (A) and **47a** (1,2,3-alternate conformation) (B) as deduced from single crystal X-ray structures

In a similar way, Biali[51] also investigated the alkylation of the bridge of calix[6]arenes. In fact, by using a comparable approach, he was able to synthesize several calix[6]arenes having different groups on the methylene bridge such as OH, Cl, etc ... (**Scheme 4.9**).

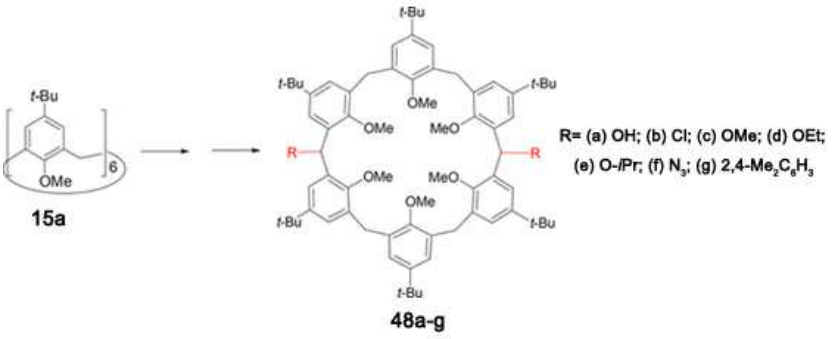

Scheme 4.9. Synthesis of derivative **48**.

Also, in this case, two conformationally stable isomers were obtained which can be identified both by NMR spectroscopy (**Figure 4.21**) and by X-ray analysis.

[51] Shalev, O.; Biali, S. E. *Org. Lett.* **2018**, *20* (8), 2324–2327.

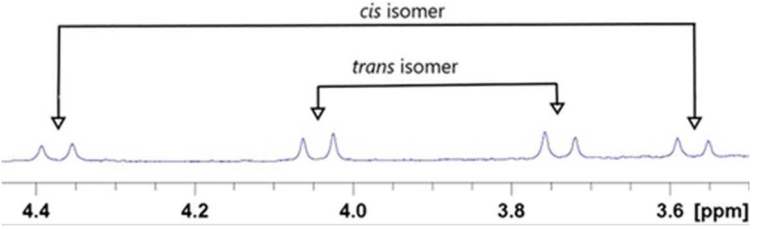

Figure 4.21. ^{1}H NMR spectrum of the methylene region of the crude mixture of dihydroxycalix[6]arene derivative **48a**.

In conclusion, both these works show the versatility of this synthetic approach for the synthesis of conformationally stable calix[6]arene macrocycles.

Therefore, with the aim to evaluate the threading ability of this conformationally stable calixarenes in comparison with the mobile ones, it was decided to investigate this synthetic approach to obtain calix[6]arenes in a cone and 1,2,3-alternate conformation.

4.5 Conformationally stable calix[6]arenes[52]

4.5.1 Synthesis of conformationally stable derivatives

Our attention was focused on derivatives **46g** and **47g** bearing a *p*-methylbenzyl substituent and derivatives **46h** and **47h** bearing a butyl chain at the methylene bridge (**Figure 4.22**).

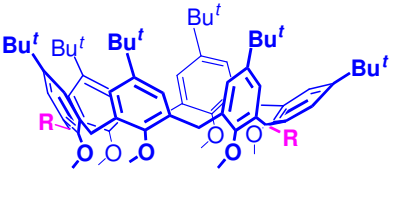

46g) R=*p*-methylbenzyl
46h) R=*n*-butyl

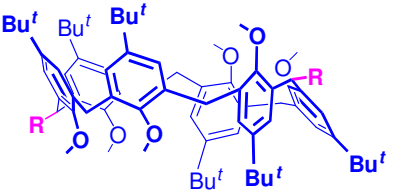

47g) R=*p*-methylbenzyl
47h) R=*n*-butyl

Figure 4.22. Derivatives **46g,h** and **47g,h**.

Derivatives **46g/47g** and **46h/47h** were synthesized by following the procedure reported by Singh and co-workers. In detail, *p*-tert-butylcalix[6]arene hexamethyl ether **15a** was first treated with *n*-BuLi/TMEDA and the anion was then reacted with

[52] Tranfić Bakić, M.; Iuliano, V.; Talotta, C.; Geremia, S.; Hickey, N.; Spinella, A.; De Rosa, M.; Soriente, A.; Gaeta, C.; Neri, P. *J. Org. Chem.* **2019**, *84* (18), 11922–11927.

the corresponding alkyl halide electrophile, leading to derivatives **46g,h** and **47g,h** fixed in the cone or 1,2,3-alternate conformation, respectively (**Scheme 4.10**).

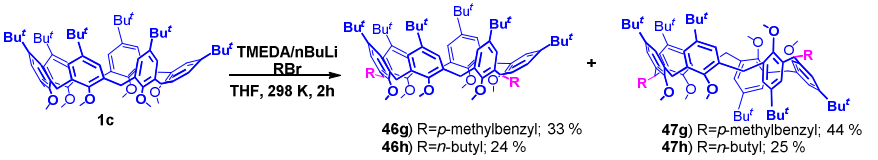

Scheme 4.10. Synthesis of derivatives **46g/46h** and **47g/47h**.

Also, in this case, the two cis/trans isomers blocked in a different conformation were separated by chromatography and fully characterized by NMR spectroscopy and by mass spectrometry. Furthermore, the X-ray structures were also obtained for derivatives **47h** and **46h**, confirming their conformation (**Figure 4.23**).

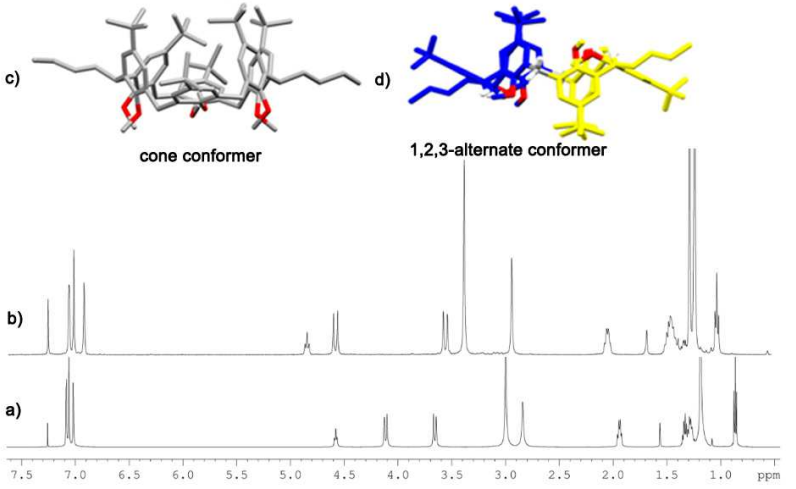

Figure 4.23. (a) ^{1}H NMR Spectra of **47h** (b) and **46h**. (c) X-ray structures of **47h** (d) and **46h**.

4.5.2 Threading Studies of derivatives 46g,h and 47g,h

Initially, threading studies on derivatives **46g,h** and **47g,h** were carried out by using ammonium axles having TFPB as counteranion (**Figure 4.24**).

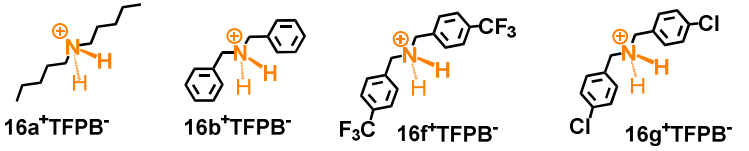

Figure 4.24. Ammonium linear systems.

Initially, it was studied the threading ability of cone derivative **46g** with dibenzylammonium axle **16b**$^{+}\cdot$TFPB^{-}. When host and guest were mixed (1:1 ratio) in

chloroform, important changes appeared in the ^{1}H NMR spectrum (**Figure 4.25**) indicative of the formation of pseudorotaxane **16b$^+$⊂46g**.

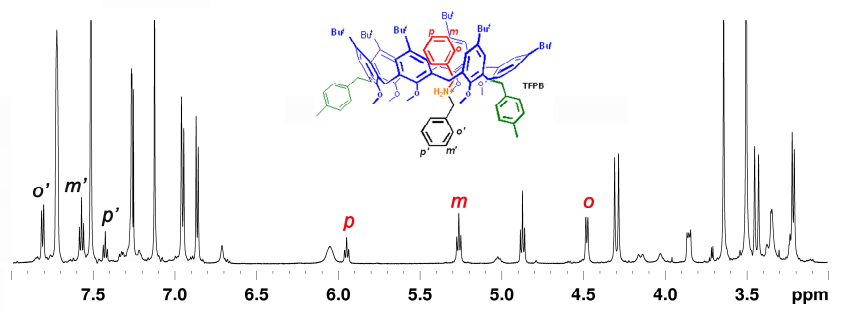

Figure 4.25. Portion of ^{1}H NMR spectrum of mixture 1:1 of **46g** and **16b$^+$** ($CDCl_3$, 600 MHz, 298 K).

The complex **16b$^+$⊂46g** was completely characterized by 1D and 2D NMR. The presence of shielded signals in the proton spectrum related to the portion of the axle inside the calixarene cavity at 4.48, 5.27, and 5.95 ppm (*ortho*-, *meta*-, and *para*-BnH, respectively), was easily evidenced. Furthermore, the other benzyl resonances were seen at regular chemical shift values (7.43, 7.58, and 7.81 ppm, o', p', m', respectively). An apparent association constant of 2.6±0.2×10^5 M^{-1} was determined for pseudorotaxane **16b$^+$⊂46g** by integration of the free and complexed ^{1}H NMR signals of the host (**Figure 4.26**).

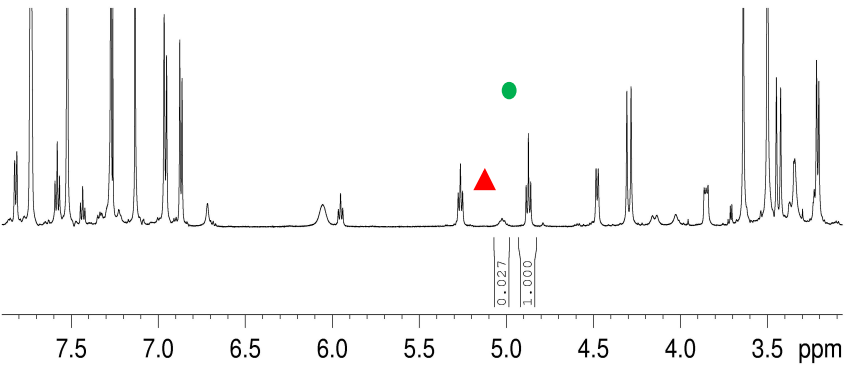

Figure 4.26. Portion of ^{1}H NMR spectrum (600 MHz, $CDCl_3$, 298 K) of a 1:1 mixture of **46g** (3.2 ×10^{-3} M) and **16b$^+$**TFPB$^-$ (3.2 ×10^{-3} M). Complexed ArCH(R)Ar (▲) and free ArCH(R)Ar (●) signals of host **46g**.

This value is significantly higher than that observed for **16b$^+$⊂ 15a** (2.5 x 10^3 M^{-1}). Subsequently, **46g** was tested with dibenzyl axles **16f** and **16g** bearing electron withdrawing groups in para (**Figure 4.27**).

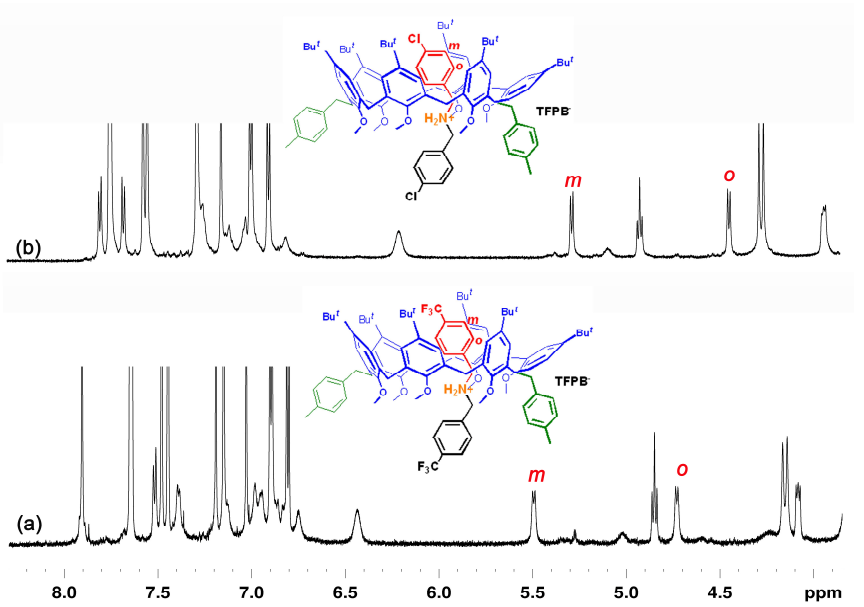

Figure 4.27. Portion of ^{1}H NMR spectra of (a) mixture 1:1 of **46g** and **16f**$^+$, (b) mixture 1:1 of **46g** and **16g**$^+$ ($CDCl_3$, 600 MHz, 298 K).

In both cases, clear evidence of pseudorotaxane formation were observed. For **16f**$^+$**⊂46g,** shielded signals related to the portion of the axle inside the calixarene cavity were observed at 4.73 and 5.50 ppm (*ortho*- and *meta*-BnH, respectively). Instead, for **16g**$^+$**⊂46g,** they resonated at 4.44 and 5.24 ppm (*ortho*- and *meta*-BnH, respectively). Association constant values were determined by quantitative ^{1}H NMR experiments using 1,1,2,2-tetrachloroethane as the internal standard (**Figure 4.28**).

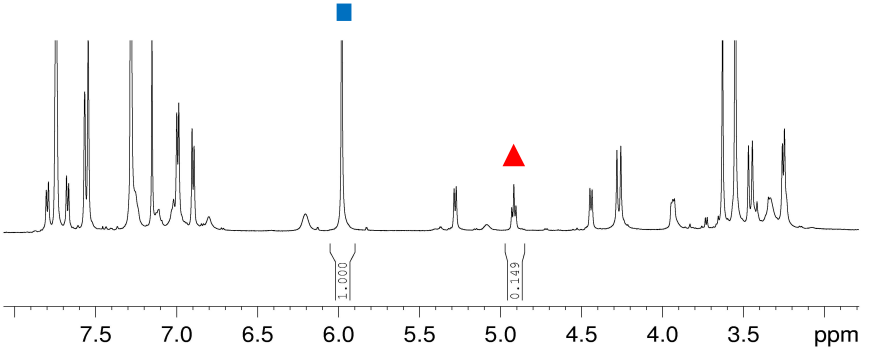

Figure 4.28. ^{1}H NMR spectrum (600 MHz, $CDCl_3$, 298 K) of an equimolar solution (3.2 mM) of **46g** and **16g**$^+$$TFPB^-$ in 0.5 mL of $CDCl_3$ containing 1 μL of 1,1,2,2-Tetrachloroethane. Complex **16g**$^+$**⊂46g** (▲) and 1,1,2,2-tetrachloroethane (■).

Finally, the proton NMR spectrum of a 1:1 mixture of derivatives **46g** and **3** in chloroform also indicated the formation of the corresponding interpenetrated system

(**Figure 4.29**). Particularly diagnostic was the presence of shielded aliphatic signals between 0.6 and -1.0 ppm.

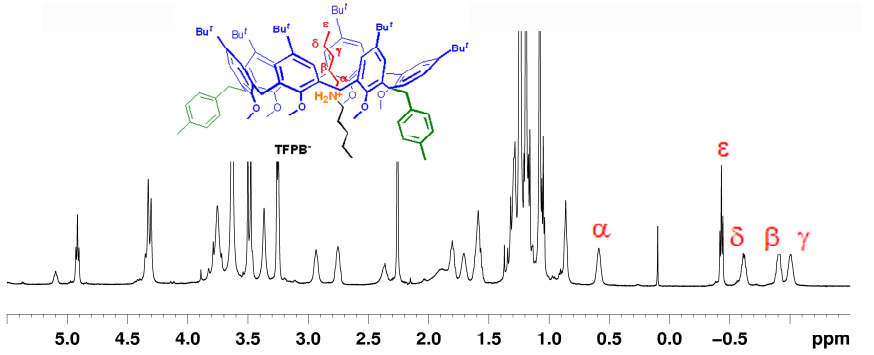

Figure 4.29. Portion of ^{1}H NMR spectrum of mixture 1:1 of **46g** and **16a**$^{+}$ ($CDCl_3$, 600 MHz, 298 K).

Also, for this supramolecular system, the apparent association constant was determined by integration of free and complexed ^{1}H NMR signals of host (**Figure 4.30**).

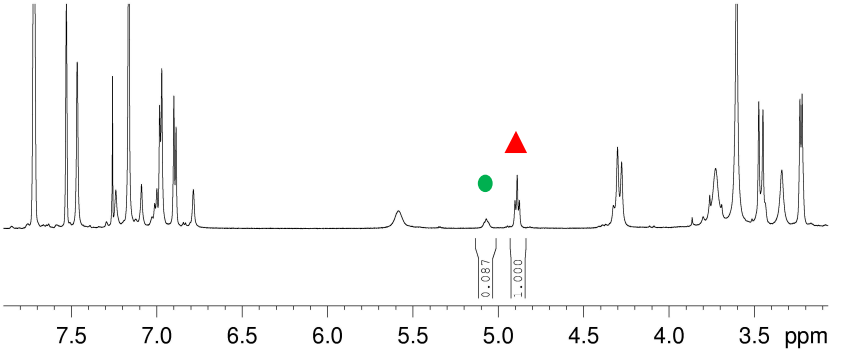

Figure 4.30. Portion of ^{1}H NMR spectrum (600 MHz, $CDCl_3$, 298 K) of a 1:1 mixture of **46g** (3.2×10^{-3} M) and **16a**$^{+}$TFPB^{-} (3.2×10^{-3} M). Complexed ArCH(R)Ar (▲) and free ArCH(R)Ar (●) signals of host **46g**.

The threading study was then extended to host **46h** and to the other ammonium guests. All the apparent association constants are collected in the table reported in **Figure 4.31**.

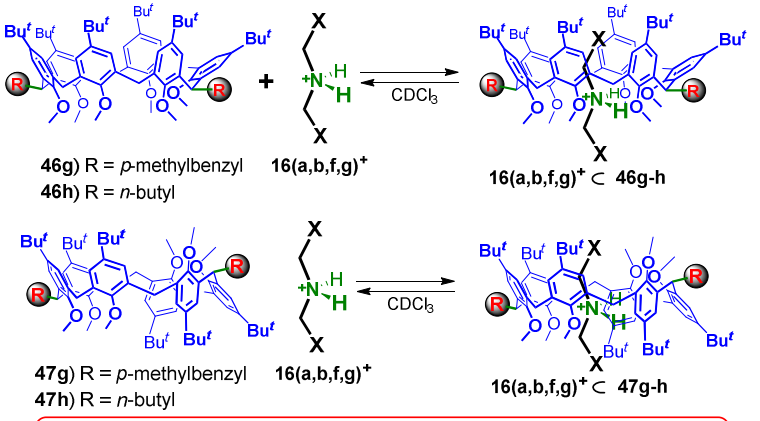

	K_{app}				
⊂	**46g**	**46h**	**47g**	**47h**	**15a**
16a$^+$	$6.2\pm0.2\times10^4$	$6.2\pm0.2\times10^3$	*<10*	*<10*	$4.4\pm0.2\times10^2$
16b$^+$	$2.6\pm0.2\times10^5$	$9.3\pm0.1\times10^3$	*<10*	*<10*	$2.5\pm0.2\times10^3$
16f$^+$	$1.7\pm0.2\times10^3$	$3.5\pm0.2\times10^2$	$8.0\pm0.2\times10^2$	$1.2\pm0.2\times10^3$	
16g$^+$	$2.3\pm0.2\times10^4$	$1.8\pm0.2\times10^4$	$2.2\pm0.2\times10^2$	$4.5\pm0.2\times10^2$	

Figure 4.31. Threading of calix[6]-wheels substituted at the methylene bridges and K_{app} values measured for the formation of the corresponding pseudorotaxanes.

By comparing the corresponding values, we can state that the more preorganized cone conformers have higher constants than the mobile native hexamethoxycalix[6]arene. Moreover, derivative **46g**, with the bigger *p*-methylbenzyl substituent, gives pseudorotaxane adducts 10-100 times more stable than derivative **46h**, bearing the smaller *n*-butyl group.

The threading studies on conformationally stable 1,2,3-alternate calix[6]arene derivatives **47g**,**c** gave unexpected results. In fact, no significant threading was observed with the common axles **16b** and **16a**, but interesting spectral changes were observed with linear systems **16f**,**f** (**Figure 4.32**).

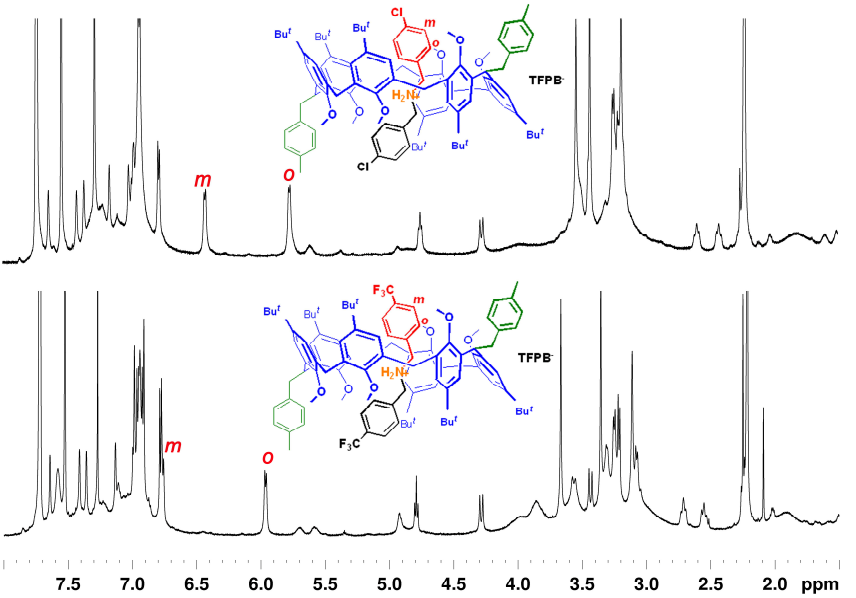

Figure 4.32. Portion of ^{1}H NMR spectra of (a) mixture 1:1 of **47g** and **16f**$^{+}$, (b) mixture 1:1 of **47g** and **16g**$^{+}$ ($CDCl_3$, 600 MHz, 298 K).

This behaviour can be ascribed to a positive cooperativity between the H-bonds, established by ammonium group with calix[6]arene oxygen atoms, and π-π interactions between the aromatic electron-poor ring of the axle and the electron-rich calixarene rings. These observations were confirmed by DFT studies (at the B3LYP/6-31G(d,p) IOp(3/124=3) level of theory **Figure 4.33**).

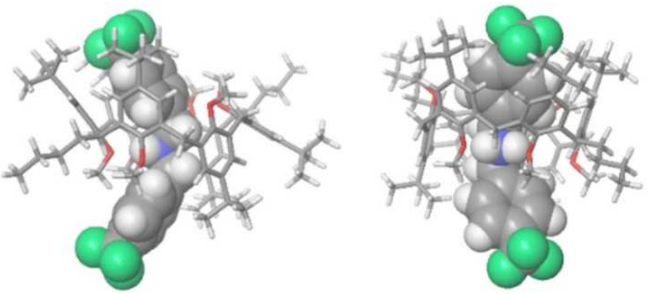

Figure 4.33. Different views of the DFT-optimized structure of **16f**$^{+}$ ⊂ **47h** pseudorotaxane

Finally, another noteworthy feature concerns the signals of the axle. In fact, only one pattern of benzyl signals is observed in the proton spectrum of the complex **16f**$^{+}$⊂**47h**, whereas two distinct patterns were expected on a structural basis. This can be explained by a fast rototranslational motion of the dibenzylammonium axles **16f**$^{+}$ inside the cavity of the calix[6]-wheel **47h** in 1,2,3-alternate conformation. This

observation clearly implies than in the **16f⁺⊂47h** pseudorotaxane the two ¾-cone subcavities (red and blue in **Figure 4.34**) became equivalent.

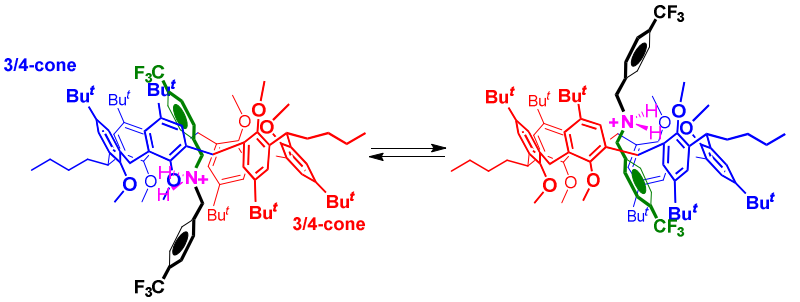

Figure 4.34. Rototranslation motion of the dibenzylammonium axles **16f⁺** inside the cavity of the calix[6]-wheel **47h** in 1,2,3-alternate conformation.

4.6 Conclusion

In conclusion, a careful study on the threading properties of specific calix[6]arene derivatives has been reported in this chapter.

Initially, the attention was focused on calixarene derivatives bearing adamantyl groups at the upper rim. It was observed that such large group as leads to an increase in the association constant by one order of magnitude. This higher thermodynamic stability has been ascribed to the more favourable van der Waals interactions of adamantyls with respect to *tert*-butyls groups at upper rim with the ammonium axle. Subsequently, it was noted that OH functions at the calixarene lower rim give rise to a less efficient threading with respect to the OR ones.

Finally, an in-depth study was carried out on calixarenes alkylated at the methylene bridges. In particular, the first examples of pseudorotaxanes constituted by calix[6]arene-wheels substituted at the methylene bridges, were obtained. Furthermore, it was observed that the greater preorganization of the macrocycle in the cone conformation leads to higher threading constants with ammonium axles. Afterwards, the NMR features of the threading process between ammonium axles bearing an electron poor ring and calix-wheels in the stable 1,2,3-alternate conformation, have been described in detail. An unusual rototraslation motion of the axle was evidenced, which could be blocked at low temperatures.

4.7 Experimental Section

4.7.1 General comments

Reactions under anhydrous conditions were conducted under an inert atmosphere (nitrogen) using dry solvents. The commercial reagents were purchased by Aldrich and TCIchemicals and were used without further purification. The reactions were controlled by thin-layer chromatography (TLC) with Macherey-Nagel plates coated with silica gel (0.25 mm) with fluorescence indicator UV254 and visualized using UV light and nebulisation with an indicator solution of H_2SO_4-$Ce(SO_4)_2$. The reaction temperatures were measured externally using electronic thermometers. The reaction products were purified by Macherey-Nagel silica gel chromatography (60, 70-230 mesh). NMR spectra were recorded on Bruker Avance-600 spectrometer [600 (^{1}H) and 150 MHz (^{13}C)], Bruker Avance-400 spectrometer [400 (^{1}H) and 100 MHz (^{13}C)]. Chemical shifts are reported relative to the residual solvent peak ($CHCl_3$: δ 7.26, $CDCl_3$: δ 77.16) Standard pulse programs, provided by the manufacturer, were used for 2D NMR experiments. High-resolution Mass spectra were acquired with a Bruker Solarix spectrometer equipped with a Tesla magnet. It was used a MALDI as methods of sample ionization. DHB was used as matrix. Samples were prepared in $CHCl_3$ (1 mg / mL).

4.7.2 Influence of *exo*-Adamantyl Groups

4.7.2.1 Synthesis of derivatives 15f, 15g, 15c.

Derivative 15f

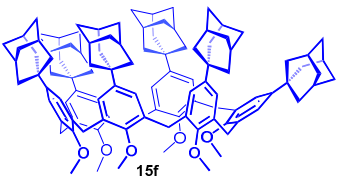

To a stirred suspension of p-adamantylcalix[6]arene **40** (0.432 g, 0.30 mmol) in DMF (50 mL) sodium hydride (60 % in mineral oil, 0.720 g, 18.0 mmol) was added. The mixture was stirred for 15 min at room temperature. Dimethylsulfate (2.72 mL, 28.8 mmol) was added and the reaction mixture was stirred at 90 °C for 20 h. After cooling, the reaction was quenched by addition of methanol (10 mL). The solvents were evaporated under reduced pressure, and the residue was parted between dichloromethane and 2 M HCl. The organic phase was washed with water, dried with $MgSO_4$, and concentrated to almost dryness. The residue was purified by column chromatography (SiO_2, gradient from hexane to hexane/THF (25:1)). Yield 0.214 g (47%). **^{1}H NMR** (600 MHz, $CDCl_3$, 298 K): δ 7.02 (s, 12H, ArH), 3.91 (s, 12H, $ArCH_2Ar$), 2.92 (s, 18H, OCH_3), 2.02 (bs, 18H, Ad), 1.83–1.62 (m, 72H; Ad). **^{13}C NMR** (150 MHz, $CDCl_3$, 298 K): δ 154.2, 145.9, 133.5,

125.7, 59.9, 43.4, 36.8, 35.7, 31.4, 29.0. **HRMS** (m/z) calcd for $C_{108}H_{132}KO_6$ 1564.9689 found 1564.9690.

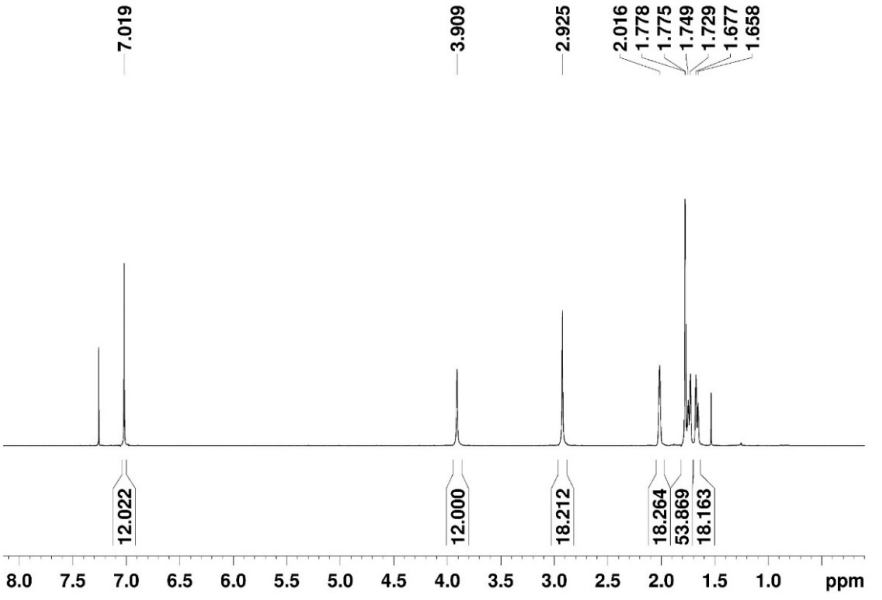

Figure 4.35. ^{1}H NMR spectrum of derivative **15f** (600 MHz, $CDCl_3$, 298K).

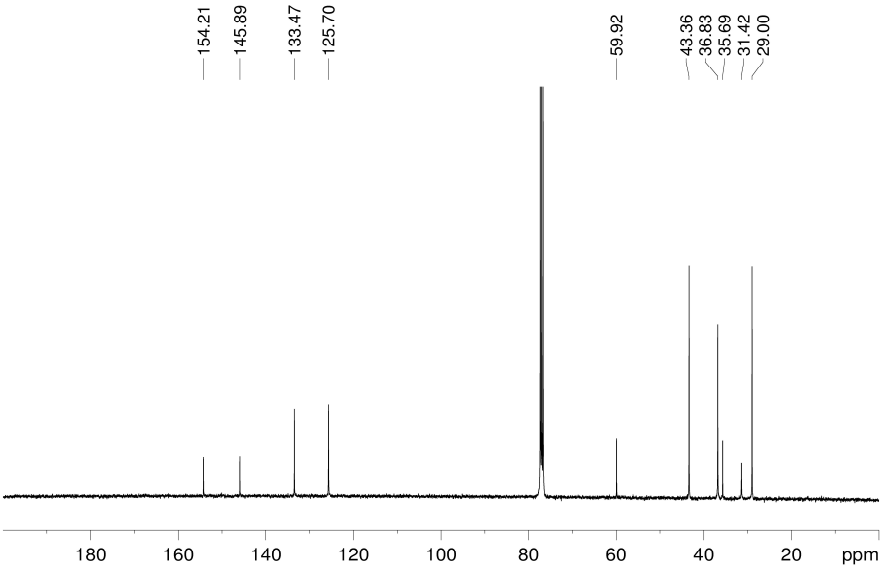

Figure 4.36. ^{13}C NMR spectrum of derivative **15f** (150 MHz, $CDCl_3$, 298K).

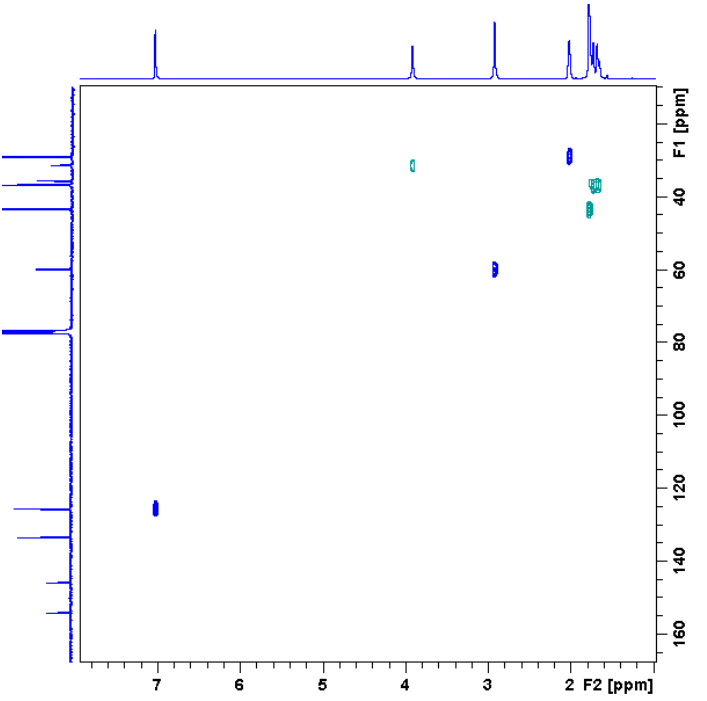

Figure 4.37. 2D HSQC spectrum of derivative **15f** (600 MHz, $CDCl_3$, 298K).

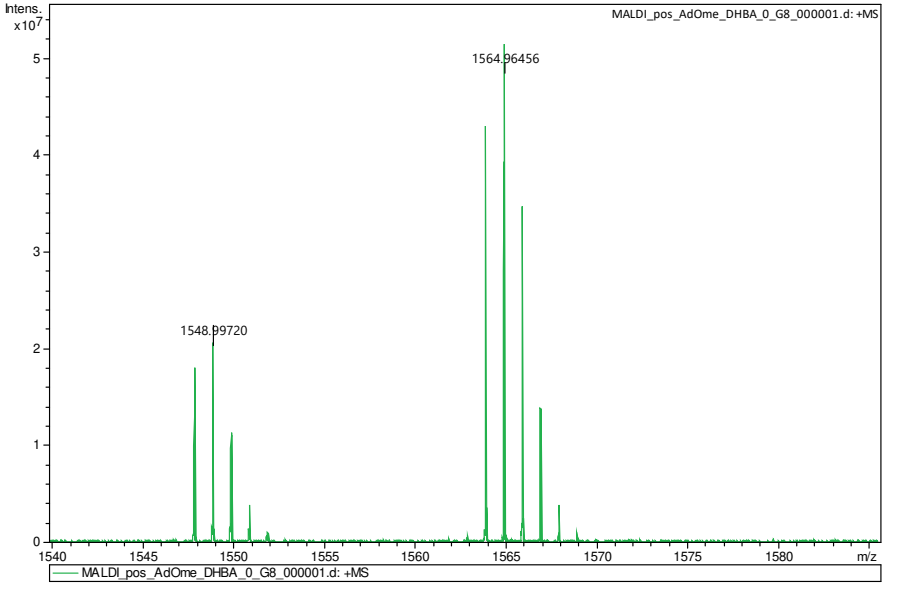

Figure 4.38. HR-MS spectrum of derivative **15f**.

Derivative 15g

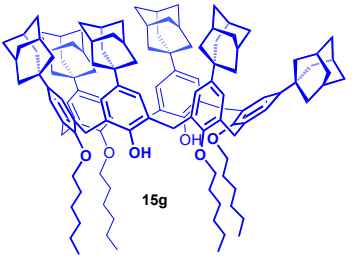

To a stirred suspension of p-adamantylcalix[6]arene **40** (0.432 g, 0.30 mmol) in DMF (15 mL) sodium hydride (60 % in mineral oil, 0.288 g, 7.2 mmol) was added. The mixture was stirred for 15 min at room temperature. 1-Bromohexane (1.01 mL, 7.2 mmol) was added and the reaction mixture was stirred at 90 °C for 20 h. After cooling, the reaction was quenched by addition of methanol (30 mL). The solid formed was collected, washed with methanol, dried, and dissolved in dichloromethane. The solution was washed with 2 M HCl, water, dried with $MgSO_4$, and the solvent was evaporated under reduced pressure. The residue was purified by column chromatography (SiO_2, 1st column: gradient from hexane to hexane/THF (50:1), 2nd column: gradient from hexane to hexane/chloroform (3:2). Yield 0.177 g (33%). **^{1}H NMR** (600 MHz, TCDE, 373 K): δ 7.54 (bs, 2H, ArOH) 6.98-6.83 (overlapped, 12H, ArH), 3.75-3.49 (overlapped, 20H, ArCH_2Ar, -O$CH_2$$(CH_2)_4CH_3$), 1.91-0.69 (overlapped, 134H, $OCH_2(CH_2)_4CH_3$, $OCH_2(CH_2)_4CH_3$, Ad). **^{13}C NMR** (150 MHz, TCDE, 373 K): δ 150.8, 148.3, 144.2, 140.1, 131.2, 130.8, 125.4, 124.2, 122.4, 72.4, 41.8, 41.6, 35.3, 34.0, 33.8, 30.0, 29.4, 27.7, 27.6, 27.5, 23.4, 20.5, 12.1. **HRMS** (m/z) clcd for $C_{126}H_{168}NaO_6$ 1801.2757 found 1801.2725.

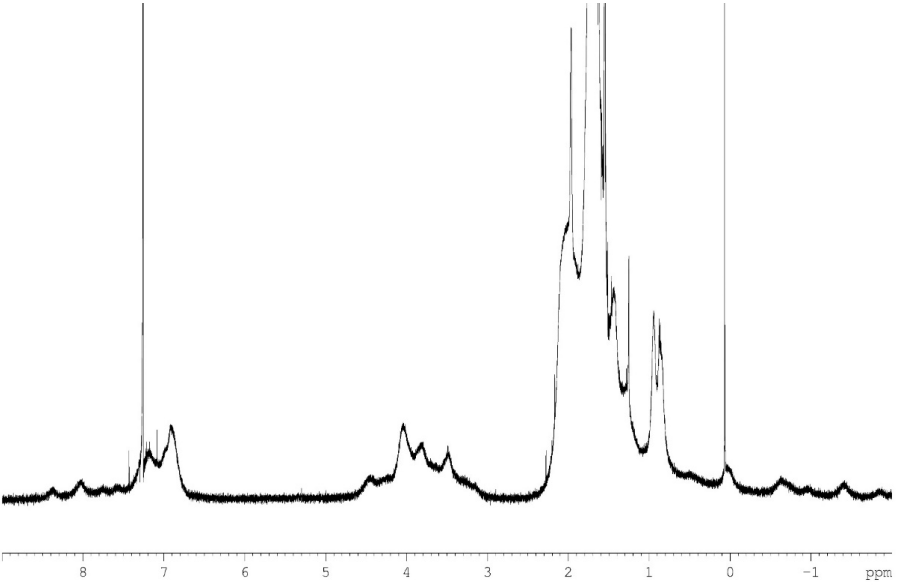

Figure 4.39. ^{1}H NMR spectrum of derivative **15g** (600 MHz, $CDCl_3$, 298K).

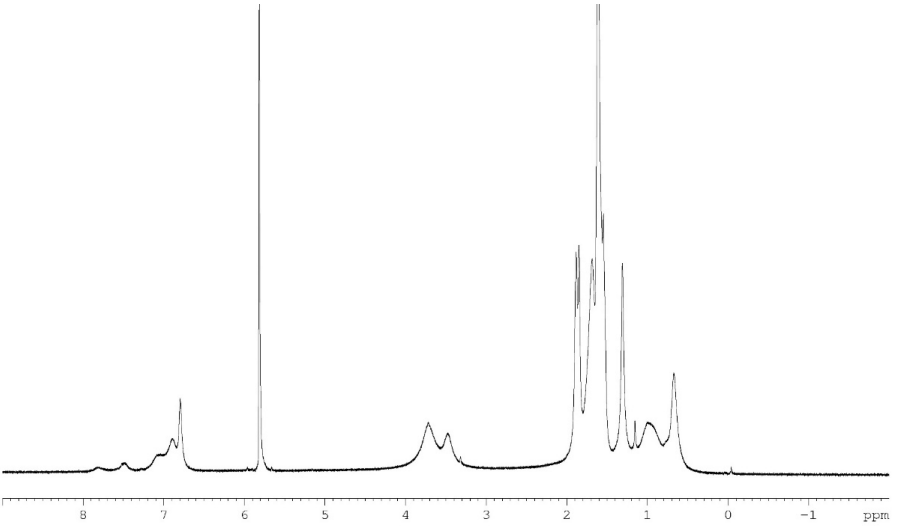

Figure 4.40. ^{1}H NMR spectrum of derivative **15g** (600 MHz, TCDE, 373K).

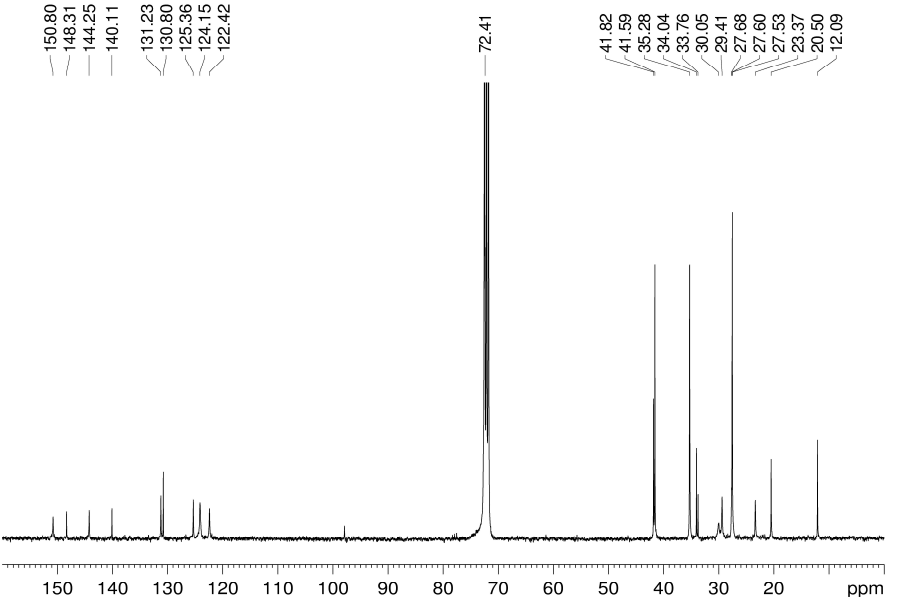

Figure 4.41. ^{1}H NMR spectrum of derivative **15g** (600 MHz, TCDE, 373K).

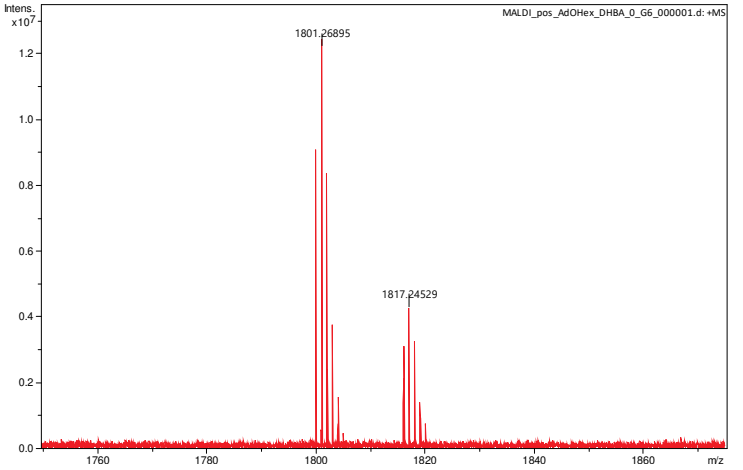

Figure 4.42. HR-MS spectrum of derivative **15g**.

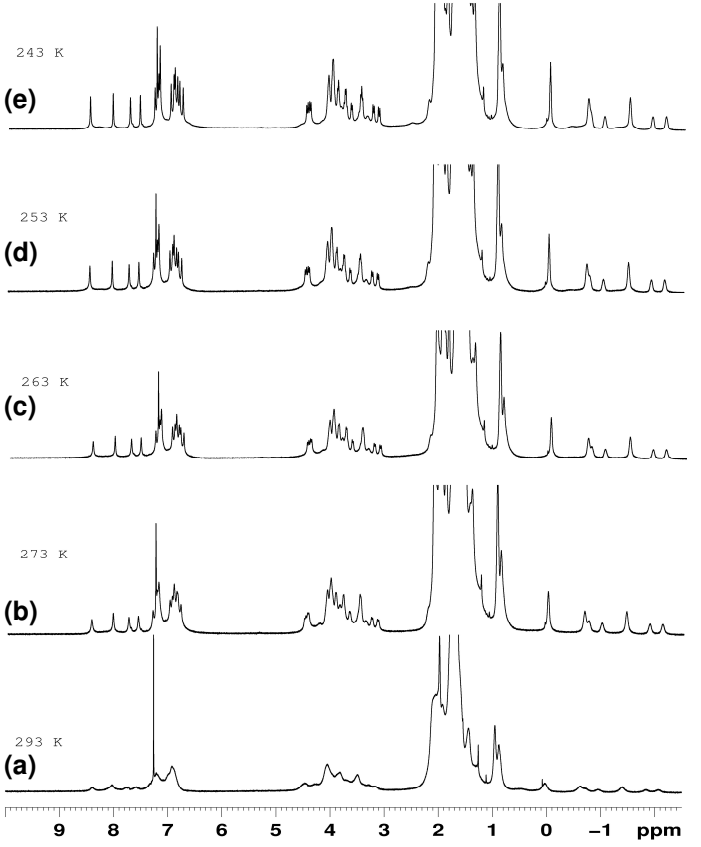

Figure 4.43. ^{1}H NMR spectra of derivative **15g** at different temperature: (a) 293 K, (b) 273 K, (c) 263 K, (d) 253 K, (e) 243 K (600 MHz, $CDCl_3$).

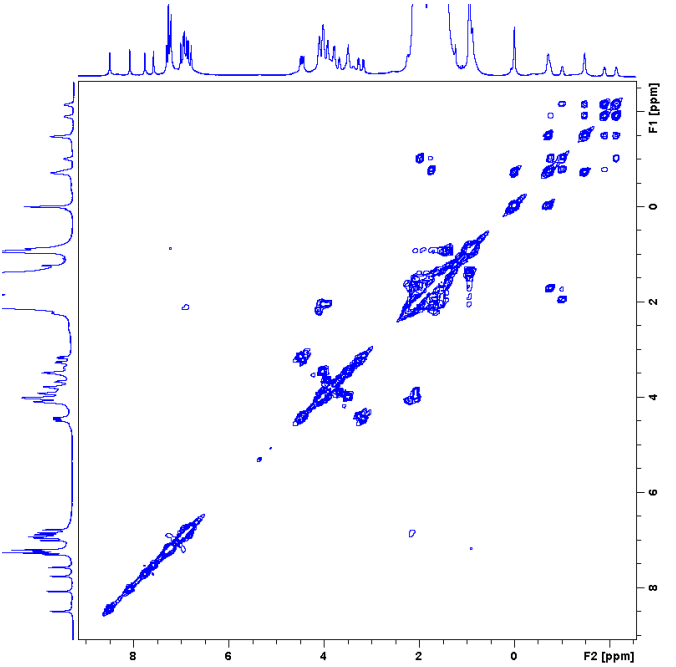

Figure 4.44. 2D COSY spectrum of derivative **15g** (600 MHz, $CDCl_3$, 243 K).

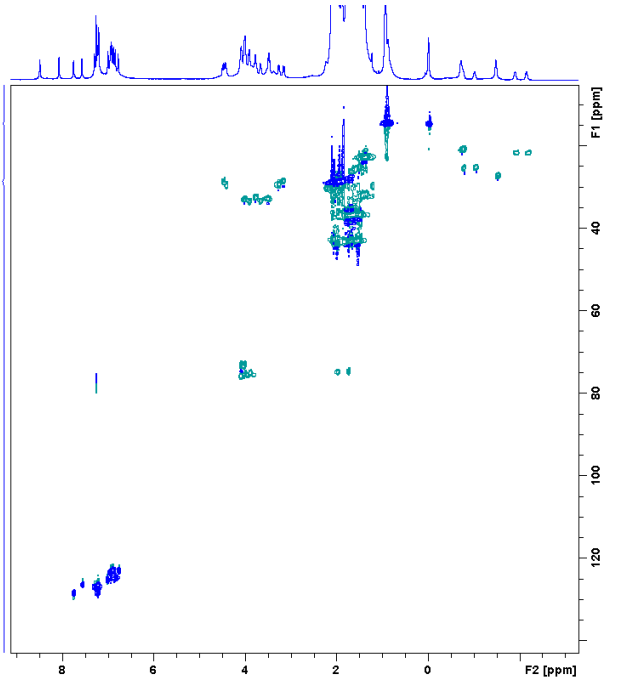

Figure 4.45. 2D HSQC spectrum of derivative **15g** (600 MHz, $CDCl_3$, 243 K).

Derivative 42

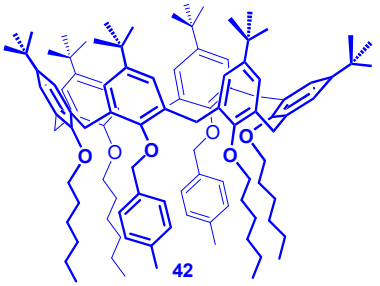

In a dry round flask, derivative **41** (1.05 g, 1.29 mmol) was dissolved in Acetone dry (70 mL). Subsequently, Cs_2CO_3 (12.65 g, 38.8 mmol) were added at room temperature. Afterwards, Hexyl iodide (9.55 mL, 64.7 mmol) was added to the reaction mixture. Stirring was continued for 24 hours at reflux. After the reaction was stopped by addition of 1 N HCl and the solution was extracted with chloroform. The organic phase was dried over anhydrous Na_2SO_4, filtered and evaporated of the solvent. The raw was purified through precipitation by methanol. Derivative **42** was obtained with 90 % yield. **^{1}H NMR** (300 MHz, TCDE, 373 K): δ 7.27 (bd, 4H, Ar'H), 7.03 (bd, 4H, Ar'H), 6.92 (bs, 4H, ArH), 6.89 (bs, 4H, ArH), 6.81 (bs, 4H, ArH), 4.65 (s, 4H, CH_2PhCH_3), 3.77 (overlapped, 12H, $ArCH_2Ar$), 3.19 (bt, 8H, -$OCH_2(CH_2)_4CH_3$), 2.23 (s, 6H, -$OBnCH_3$), 1.31-0.97 (overlapped, 86H, -$OCH_2(CH_2)_4CH_3$, -$C(CH_3)_3$,), 0.74 (bt, 12H, -$OCH_2(CH_2)_4CH_3$). **^{13}C NMR** (75 MHz, TCDE, 373 K): δ 151.8, 151.1, 143.5, 143.1, 135.3, 133.6, 131.3, 131.2, 131.1, 127.1, 126.6, 124.2, 123.9, 72.9, 72.4, 32.1, 30.1, 29.7, 28.0, 24.2, 20.7, 19.2, 12.1. **HRMS** (m/z) clcd for $C_{106}H_{148}KO_6$ 1557.0941 found 1557.0962.

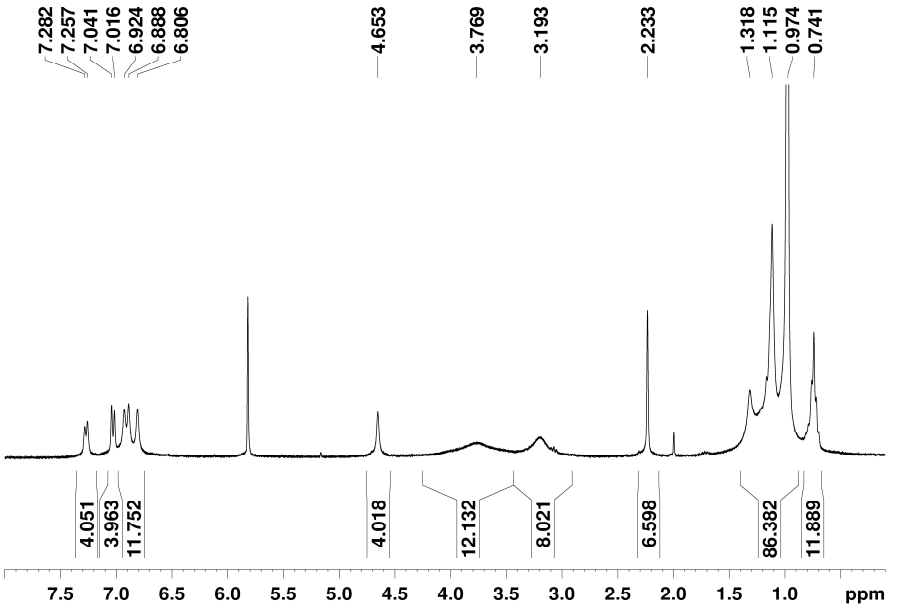

Figure 4.46. ^{1}H NMR spectrum of derivative **42** (600 MHz, TCDE, 373K).

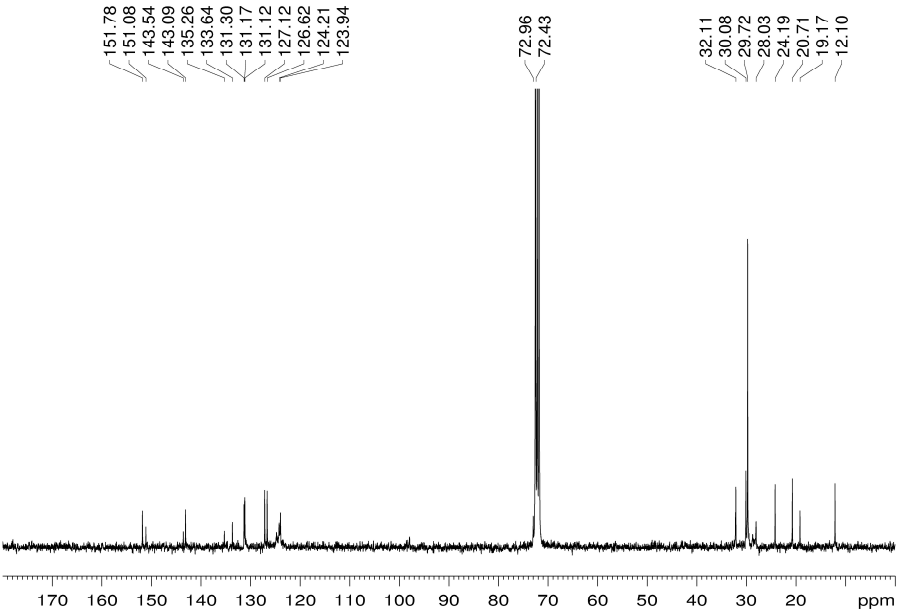

Figure 4.47. ^{1}H NMR Spectrum of derivative **42** (600 MHz, TCDE, 373 K).

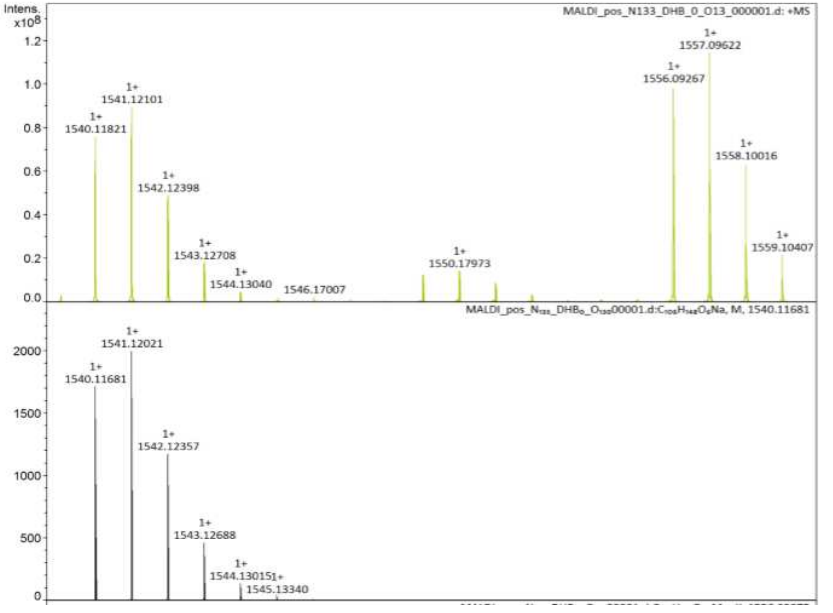

Figure 4.48. HR-MS spectrum of derivative **42**.

Derivative 15c

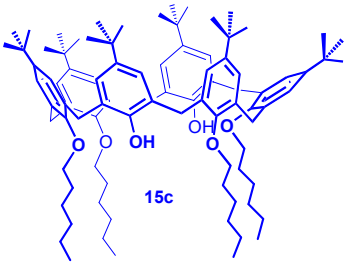

In a round flask, derivative **44** (0.50 g, 0.45 mmol) was dissolved in chloroform (50 mL). Subsequently, Pd/c was added. Stirring was continued for 18 hours at room temperature under H_2. After this time, the reaction was stopped by filtration on celite. The solvent was evaporated under reduced pressure. Derivative **15c** was obtained with 95 % yield. **^{1}H NMR** (600 MHz, TCDE, 373 K): δ 6.97-6.62 (overlapped, 14H, ArH, ArOH), 3-73-3.60 (overlapped, 20H, $ArCH_2Ar$, $-OCH_2(CH_2)_4CH_3$), 1.15-0.74 (overlapped, 98H, $-OCH_2(CH_2)_4CH_3$, $-OCH_2(CH_2)_4CH_3$, $-C(CH_3)_3$,). **13C NMR** (150 MHz, TCDE, 373 K): δ 151.2, 150.4, 146.2, 142.0, 132.9, 132.5, 126.8, 126.1, 125.2, 33.8, 33.6, 31.5, 31.2, 29.8, 29.5, 25.4, 22.3, 13.8. **HRMS** (m/z) clcd for $C_{90}H_{132}KO_6$ 1347.9655 found 1347.9635.

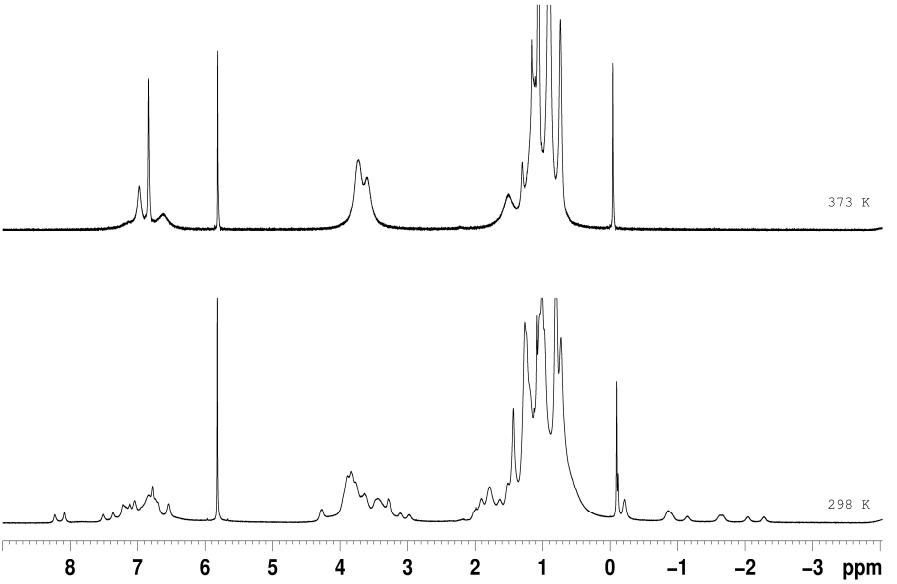

Figure 4.49. ^{1}H NMR spectra of derivative **15c** (600 MHz, TCDE).

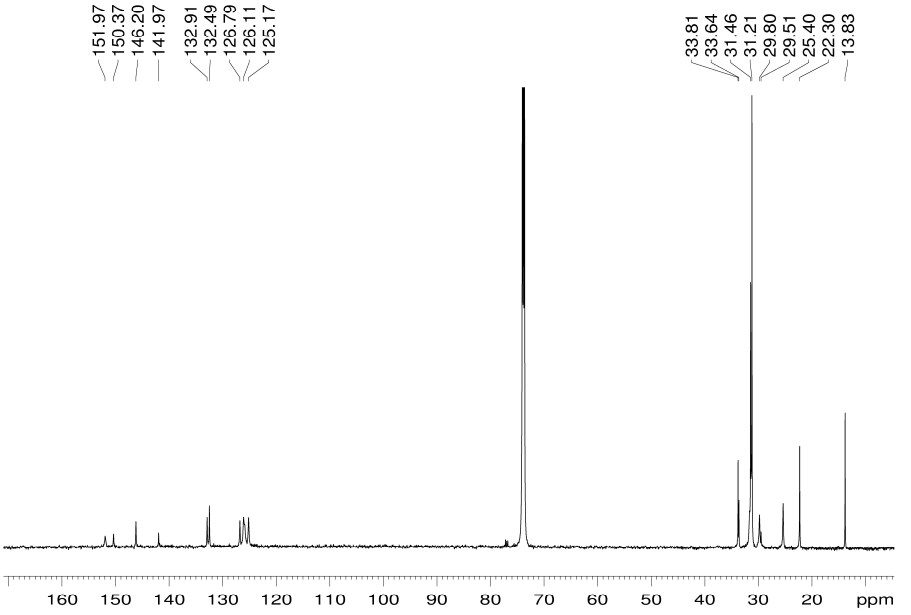

Figure 4.50. ^{13}C NMR spectrum of derivative **15c** (600 MHz, TCDE, 373 K).

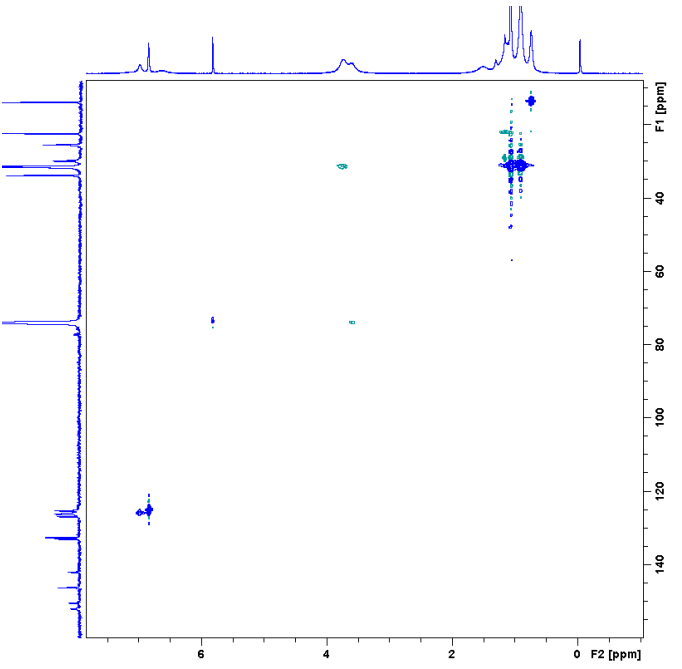

Figure 4.51. 2D HSQC spectrum of derivative **15c** (600 MHz, TCDE, 373 K).

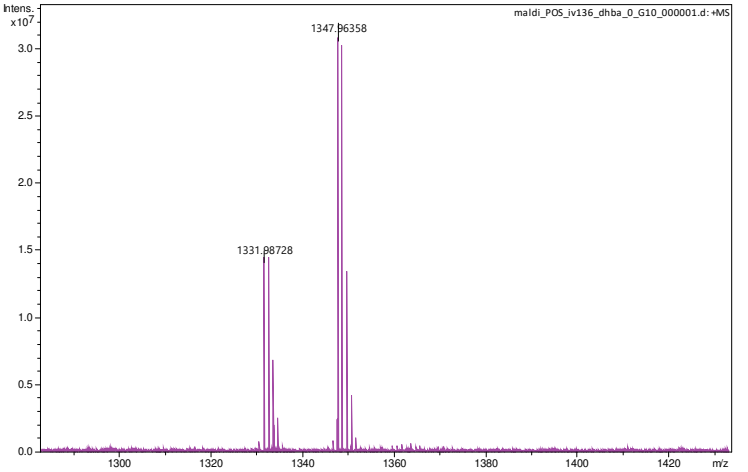

Figure 4.52. HR-MS spectrum of derivative **15c**.

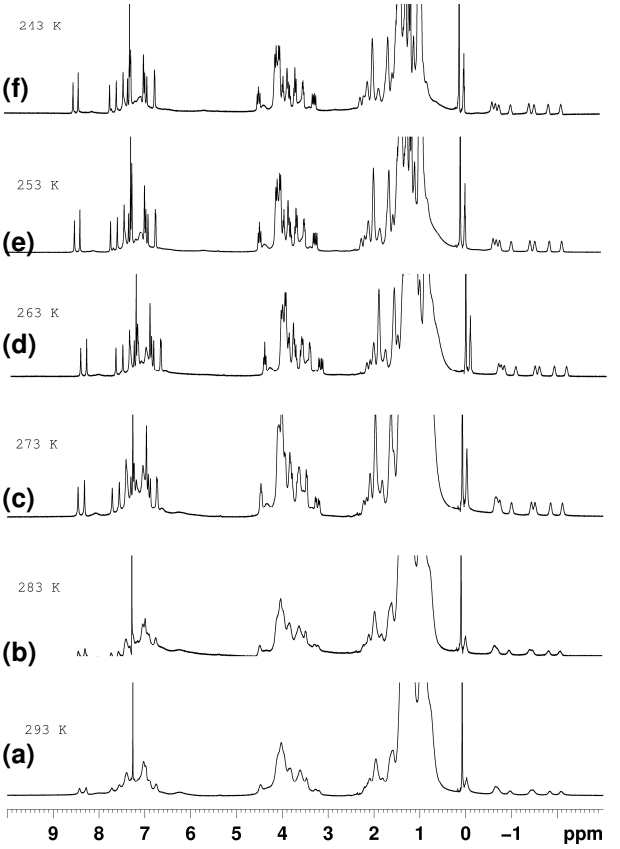

Figure 4.53. ^{1}H NMR spectrum of derivative **15c** at different temperature: (a) 293 K, (b) 283 K, (c) 273 K, (d) 263 K, (e) 253 K, (f) 243 K (600 MHz, $CDCl_3$).

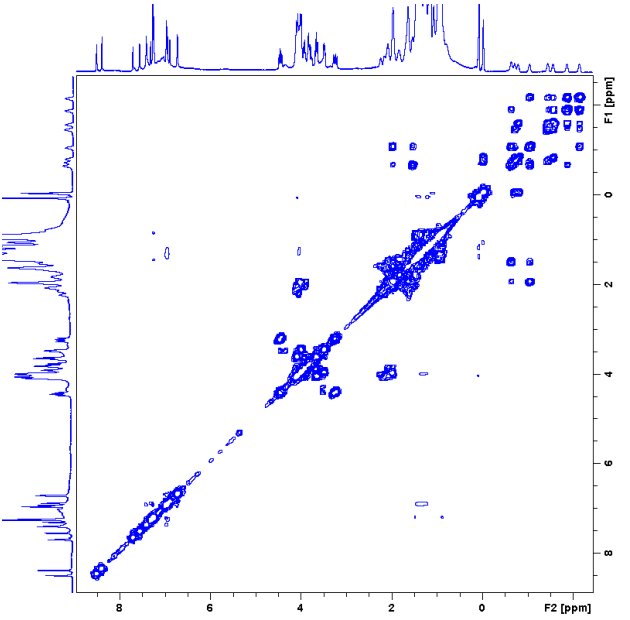

Figure 4.54. 2D COSY spectrum of derivative **15c** (600 MHz, $CDCl_3$, 243 K).

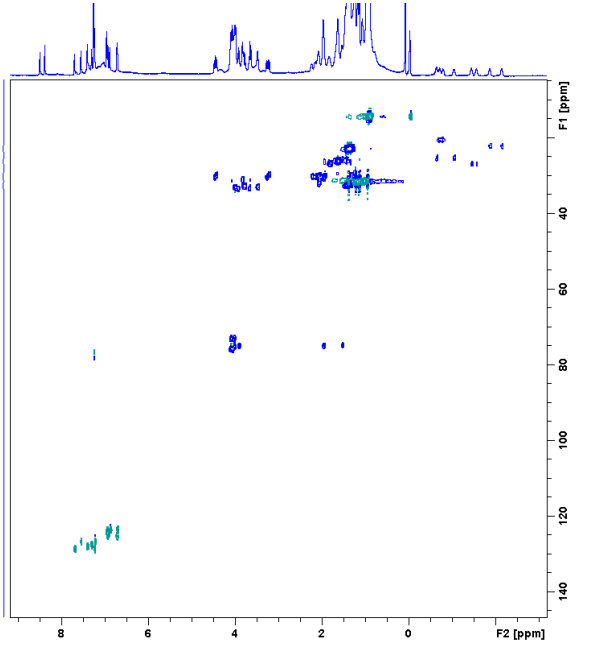

Figure 4.55. 2D HSQC spectrum of derivative **15c** (600 MHz, $CDCl_3$, 243 K).

4.7.2.2 Synthesis of pseudo[2]rotaxanes

A 1:1 mixture of calix[6]arene derivative and TFPB linear system was dissolved in 0.5 mL of $CDCl_3$.In detail, in **Table 4.1** we reported concentration using for calix[6]arene derivative and for axles. Then, the solution was transferred in an NMR tube for 1D and 2D NMR spectra acquisition.

Table 4.1. Amount of hosts and guests for complexation experiments.

Pseudo[2]rotaxanes	**Calix[6]arenes**		**Axles**		**$CDCl_3$**
	(mg)	**(mmol)**	**(mg)**	**(mmol)**	**(ml)**
$16e^+ \subset 15b$	4.02	$2.7 \cdot 10^{-3}$	2.78	$2.7 \cdot 10^{-3}$	0.5
$16b^+ \subset 15f$	4.01	$2.6 \cdot 10^{-3}$	2.78	$2.6 \cdot 10^{-3}$	0.5
$16a^+ \subset 15f$	4.00	$2.6 \cdot 10^{-3}$	2.68	$2.6 \cdot 10^{-3}$	0.5
$16e^+ \subset 15f$	4.01	$2.6 \cdot 10^{-3}$	2.70	$2.6 \cdot 10^{-3}$	0.5
$16b^+ \subset 15g$	4.00	$2.2 \cdot 10^{-3}$	2.38	$2.2 \cdot 10^{-3}$	0.5
$16a^+ \subset 15g$	4.02	$2.2 \cdot 10^{-3}$	2.30	$2.2 \cdot 10^{-3}$	0.5
$16e^+ \subset 15g$	4.01	$2.2 \cdot 10^{-3}$	2.32	$2.2 \cdot 10^{-3}$	0.5
$16b^+ \subset 15c$	4.02	$3.0 \cdot 10^{-3}$	3.24	$3.0 \cdot 10^{-3}$	0.5
$16a^+ \subset 15c$	4.01	$3.0 \cdot 10^{-3}$	3.12	$3.0 \cdot 10^{-3}$	0.5
$16e^+ \subset 15c$	4.03	$3.0 \cdot 10^{-3}$	3.14	$3.0 \cdot 10^{-3}$	0.5

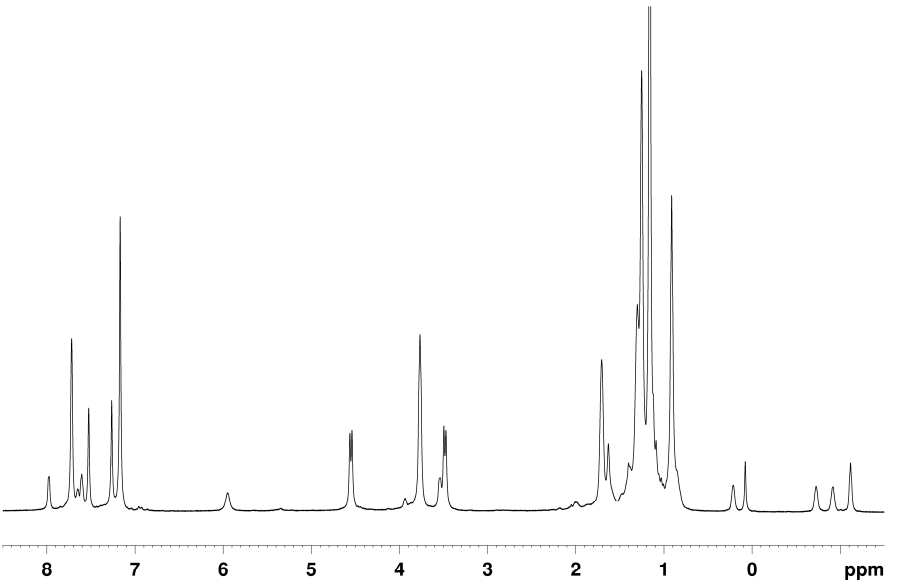

Figure 4.56. ^{1}H NMR spectrum of derivative **16e^{+}⊂ 15b** (600 MHz, $CDCl_3$, 298 K).

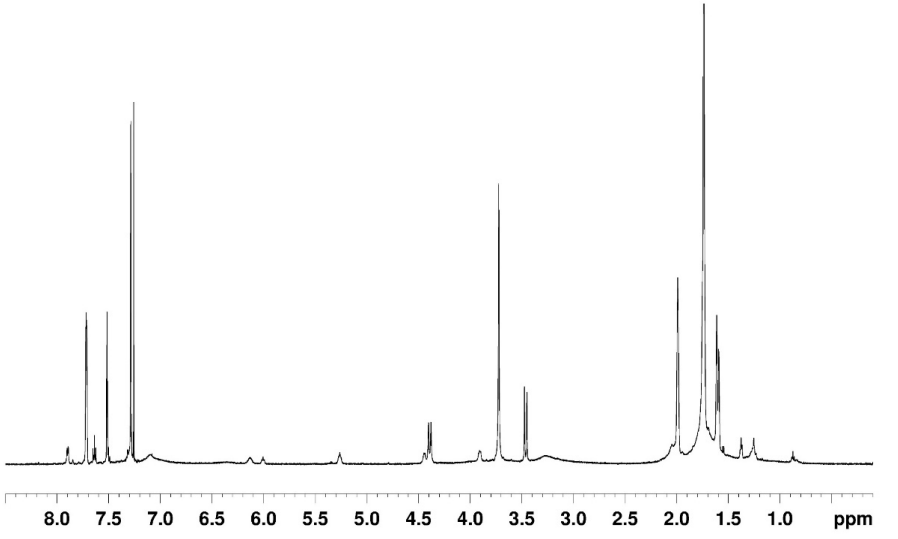

Figure 4.57. ^{1}H NMR spectrum of derivative **16b^{+}⊂ 15f** (600 MHz, $CDCl_3$, 298 K).

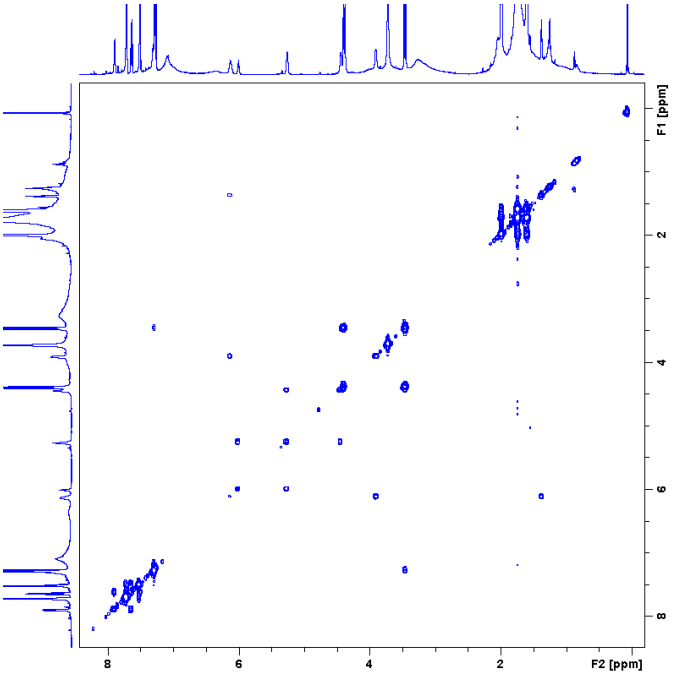

Figure 4.58. 2D COSY spectrum of derivative **16b$^+$⊂ 15f** (600 MHz, $CDCl_3$, 298 K).

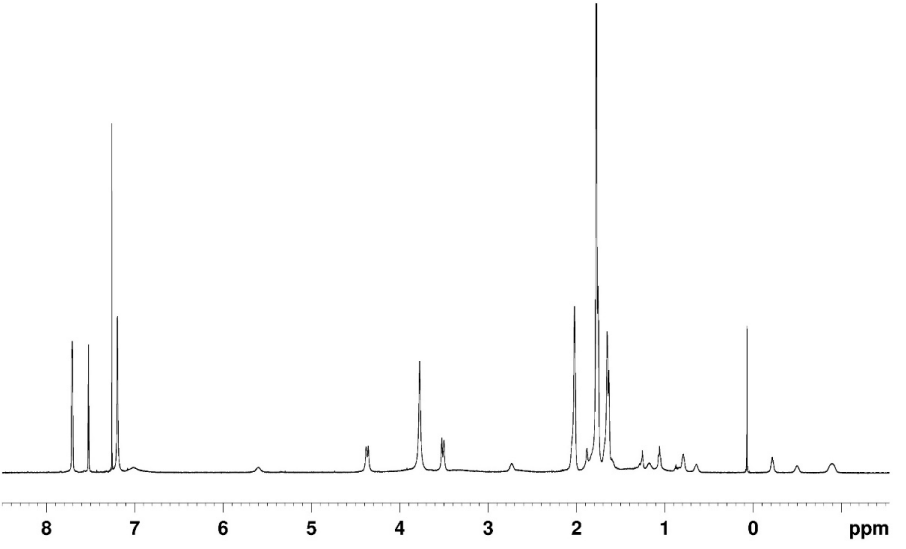

Figure 4.59. ^{1}H NMR spectrum of derivative **16a$^+$⊂ 15f** (600 MHz, $CDCl_3$, 298 K).

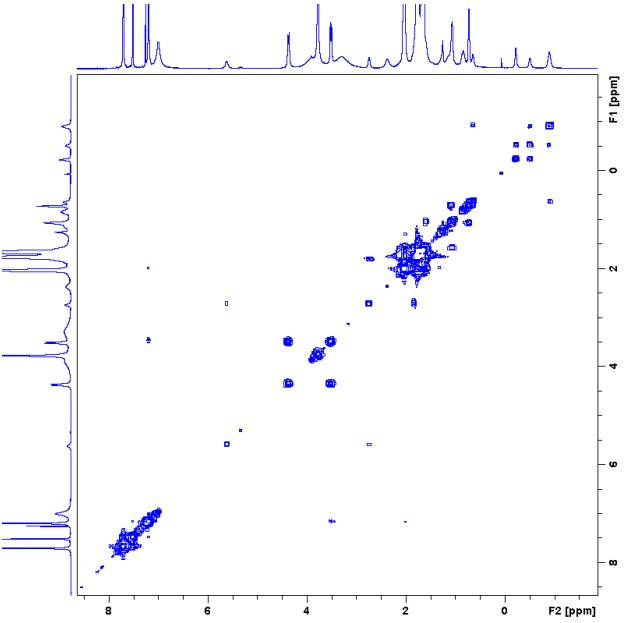

Figure 4.60. 2D COSY spectrum of derivative **16a^{+}⊂ 15f** (600 MHz, $CDCl_3$, 298 K).

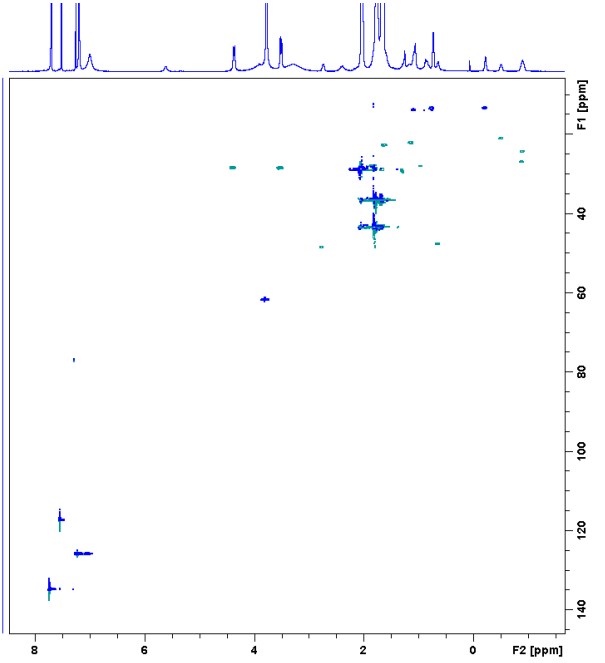

Figure 4.61. 2D HSQC spectrum of derivative **16a^{+}⊂ 15f** (600 MHz, $CDCl_3$, 298 K).

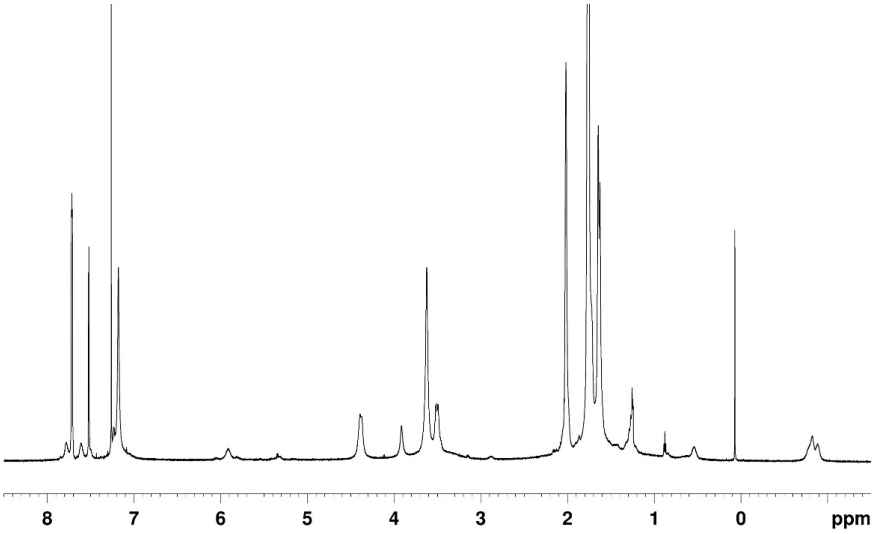

Figure 4.62. ^{1}H NMR spectrum of derivative **16e^{+}⊂ 15f** (600 MHz, $CDCl_3$, 298 K).

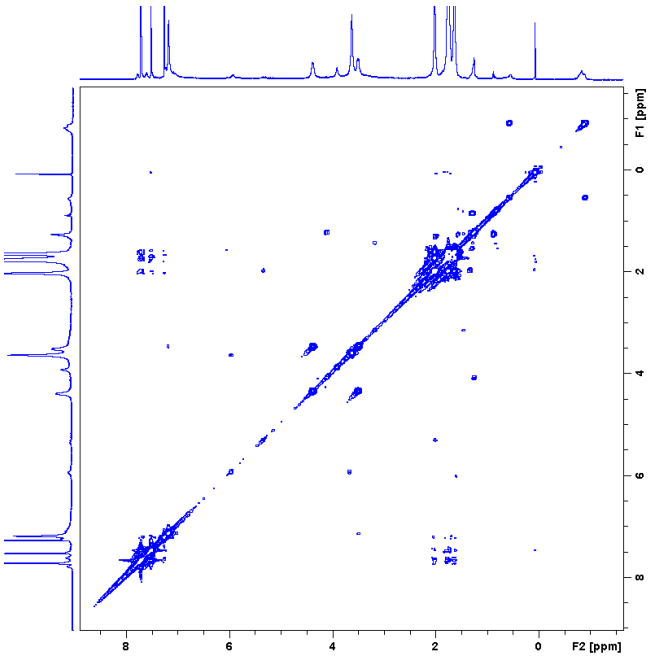

Figure 4.63. 2D COSY spectrum of derivative **16e^{+}⊂ 15f** (600 MHz, $CDCl_3$, 298 K).

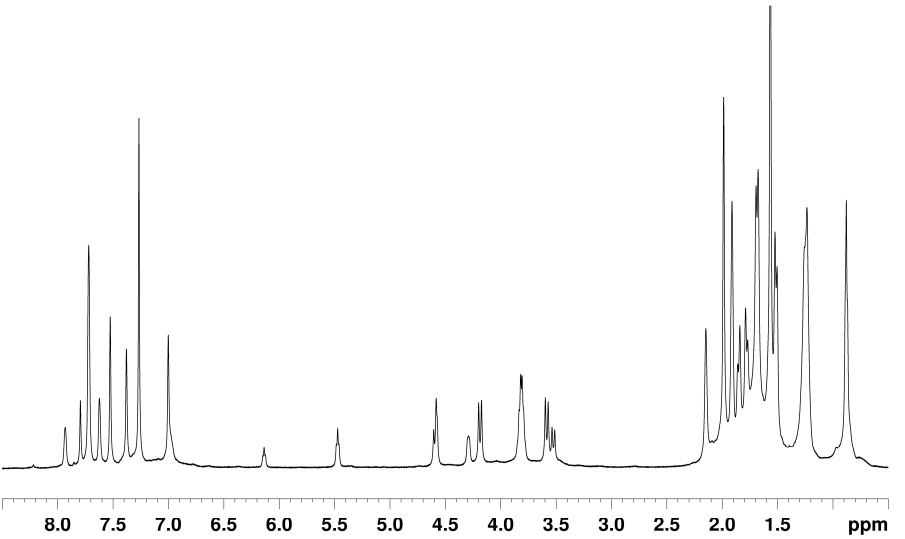

Figure 4.64. ^{1}H NMR spectrum of derivative **16b^{+}⊂ 15g** (600 MHz, $CDCl_3$, 298 K).

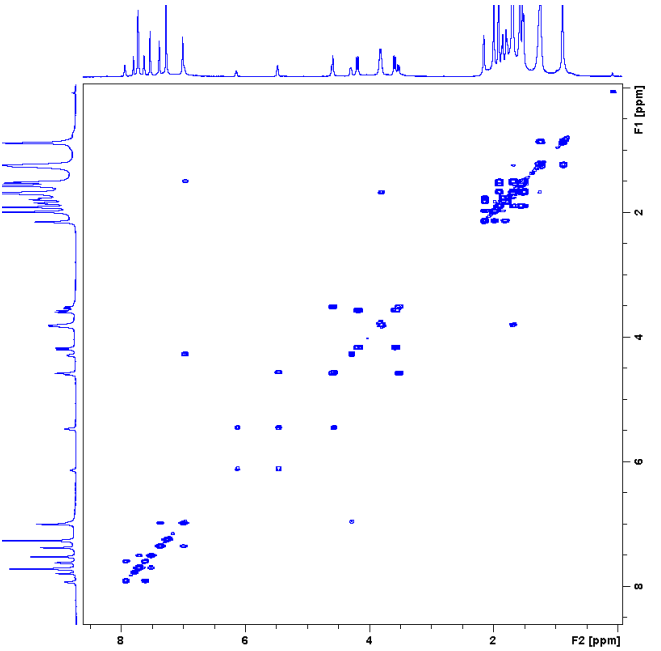

Figure 4.65. 2D COSY spectrum of derivative **16b^{+}⊂ 15g** (600 MHz, $CDCl_3$, 298 K).

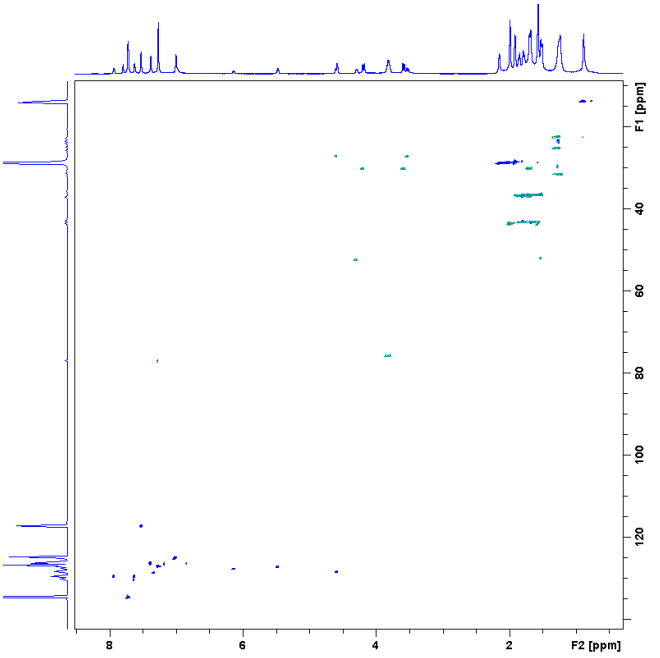

Figure 4.66. 2D HSQC spectrum of derivative **16b$^+$⊂ 15g** (600 MHz, $CDCl_3$, 298 K).

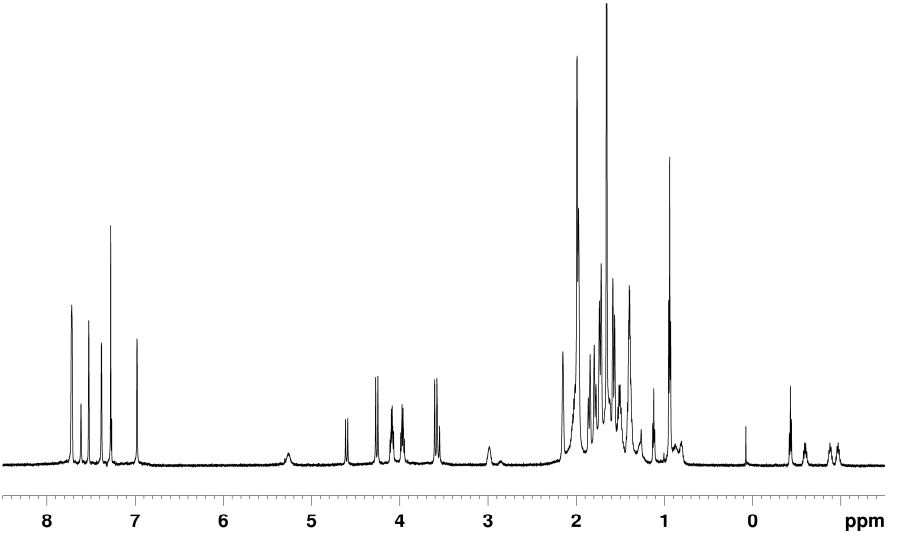

Figure 4.67. ^{1}H NMR spectrum of derivative **16a$^+$⊂ 15g** (600 MHz, $CDCl_3$, 298 K).

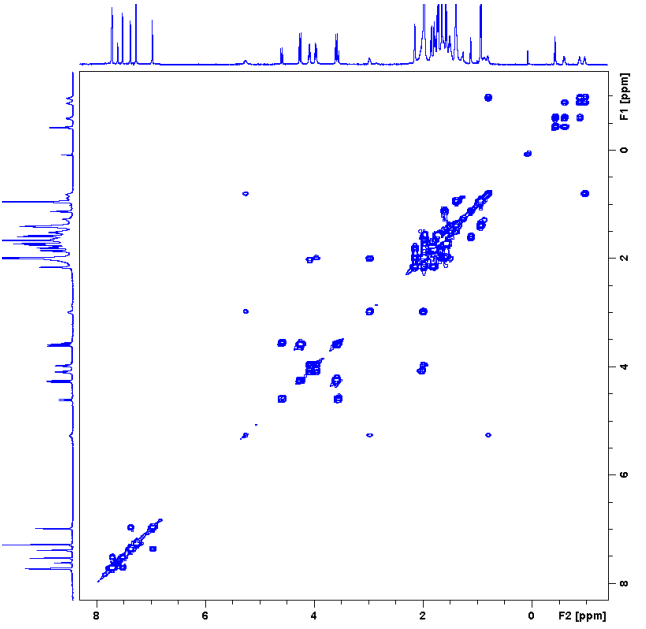

Figure 4.68. 2D COSY spectrum of derivative **16a**$^{+}$**⊂ 15g** (600 MHz, $CDCl_3$, 298 K).

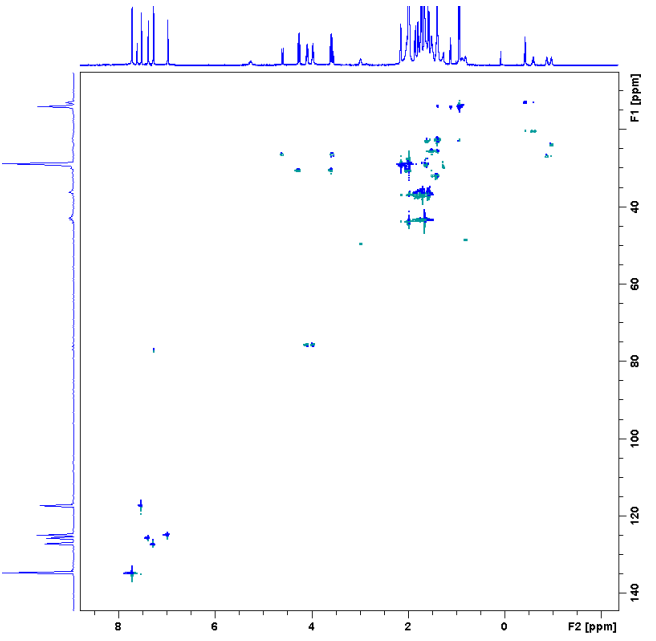

Figure 4.69. 2D HSQC spectrum of derivative **16a**$^{+}$**⊂ 15g** (600 MHz, $CDCl_3$, 298 K).

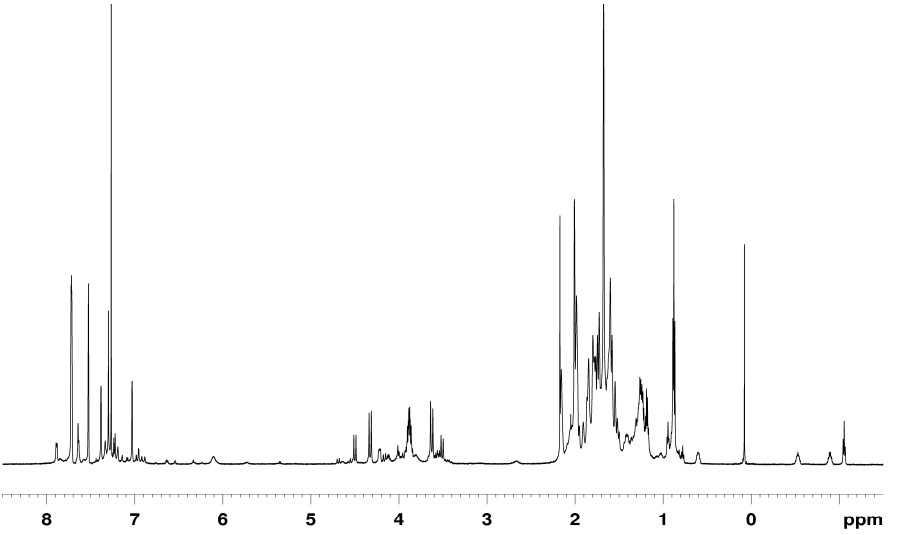

Figure 4.70. ^{1}H NMR spectrum of derivative **16e^{+}⊂ 15g** (600 MHz, $CDCl_3$, 298 K).

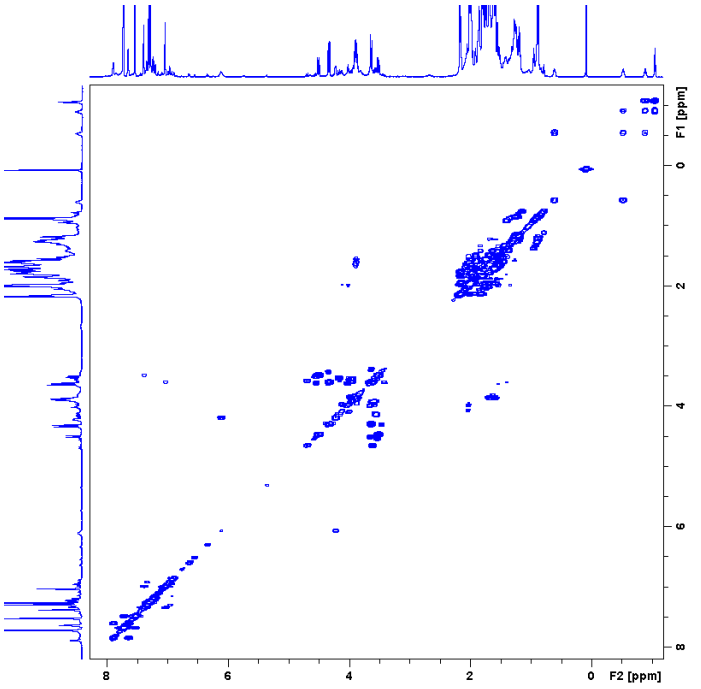

Figure 4.71. 2D COSY spectrum of derivative **16e^{+}⊂ 15g** (600 MHz, $CDCl_3$, 298 K).

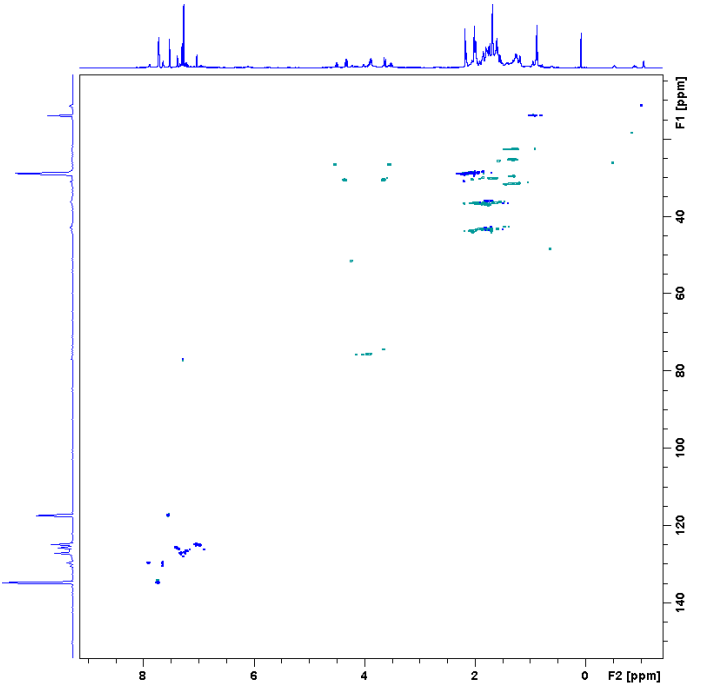

Figure 4.72. 2D HSQC spectrum of derivative **16e⁺⊂ 15g** (600 MHz, $CDCl_3$, 298 K).

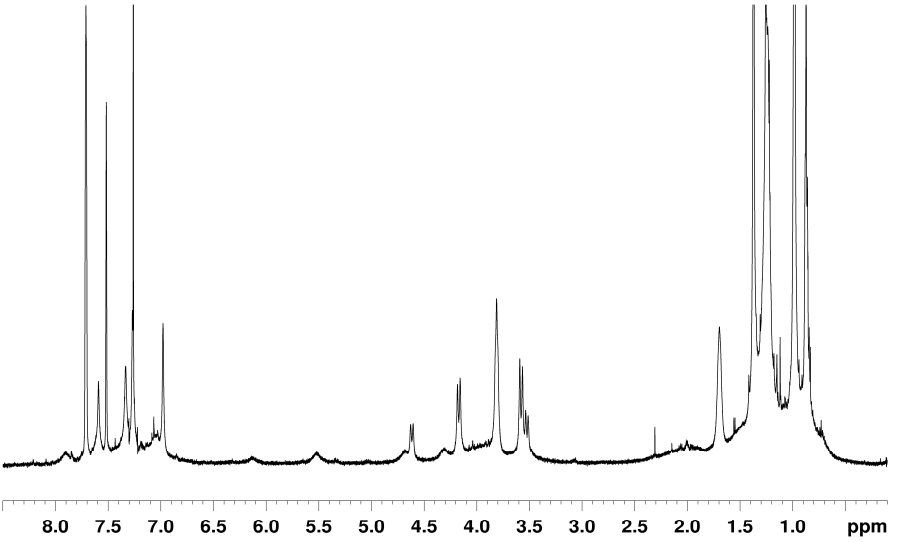

Figure 4.73. ^{1}H NMR spectrum of derivative **16b⁺⊂ 15c** (600 MHz, $CDCl_3$, 298 K).

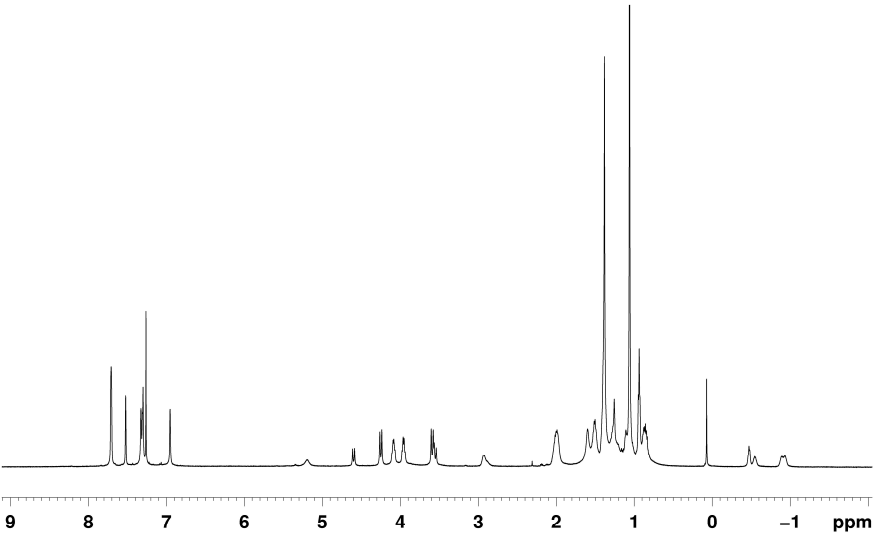

Figure 4.74. ^{1}H NMR spectrum of derivative **16a^{+}⊂ 15c** (600 MHz, $CDCl_3$, 298 K).

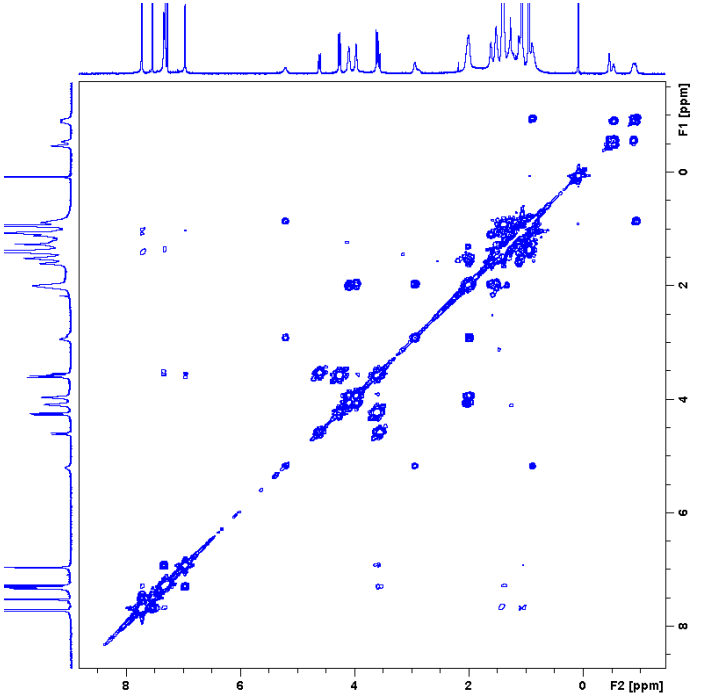

Figure 4.75. 2D COSY spectrum of derivative **16a^{+}⊂ 15c** (600 MHz, $CDCl_3$, 298 K).

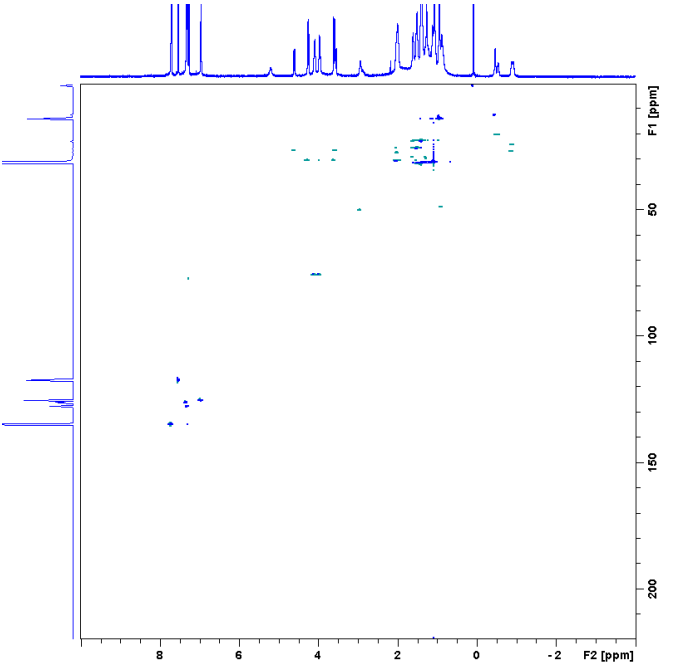

Figure 4.76. 2D HSQC spectrum of derivative **16a^{+}⊂ 15c** (600 MHz, $CDCl_3$, 298 K).

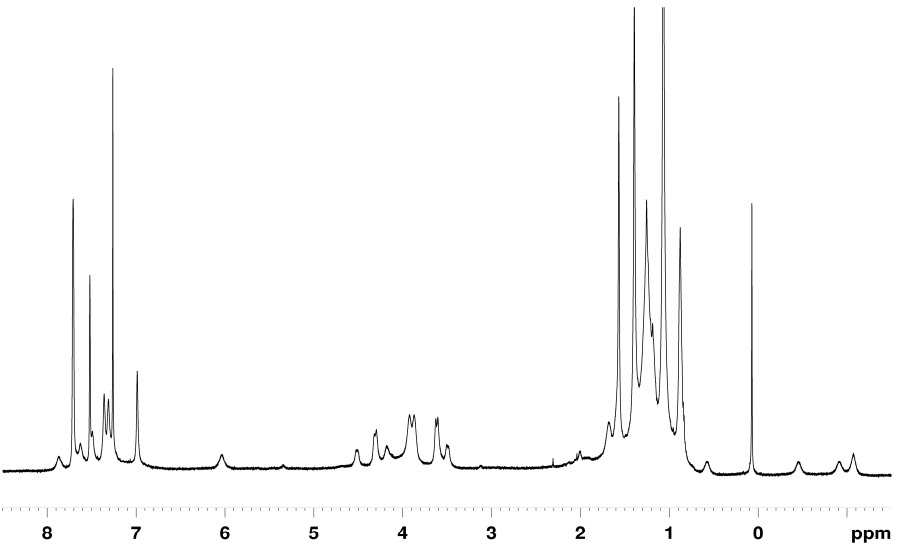

Figure 4.77. ^{1}H NMR spectrum of derivative **16e^{+}⊂ 15c** (600 MHz, $CDCl_3$, 298 K).

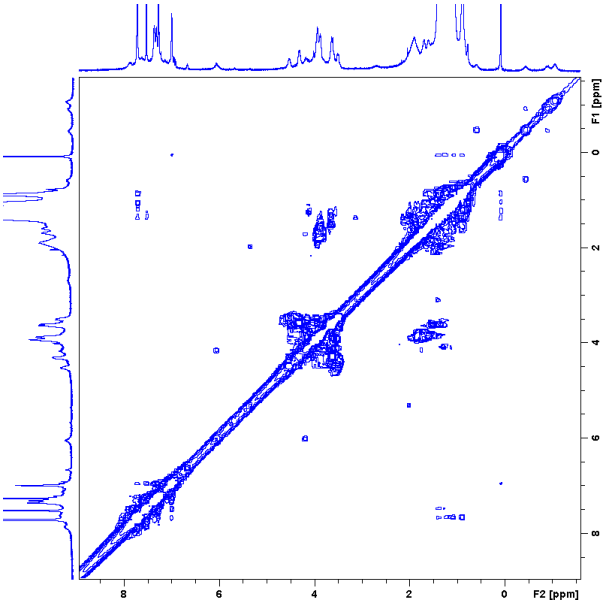

Figure 4.78. 2D COSY spectrum of derivative **16e$^+$⊂ 15c** (600 MHz, $CDCl_3$, 298 K).

4.7.2.3 ^{1}H NMR determination of K_{ass} values

The association constant values of complexes were calculated by means of three methods:

a) ^{1}H NMR competition experiments. In this case, was performed an analysis of a 1:1:1 mixture of host, and two guests (or two host and one guest) in an NMR tube using 0.5 mL of $CDCl_3$ as solvent. The following equation was used to obtain K_{ass} value.

$$K_{A\subset H}=\frac{[HG_A]}{[H][G_A]} \quad \text{and} \quad K_{B\subset H}=\frac{[HG_B]}{[H][G_B]} \longrightarrow K_{rel}=\frac{K_{A\subset H}}{K_{B\subset H}}=\frac{[HG_A][H][G_B]}{[HG_B][H][G_A]} \longrightarrow$$

$$\begin{matrix}[HG_A]=[G_B]\\ [HG_B]=[G_A]\end{matrix} \longrightarrow \quad K_{rel}=\frac{K_{A\subset H}}{K_{B\subset H}}=\frac{[HG_A]^2}{[HG_B]^2}$$

b) Quantitative ^{1}H NMR experiments using TCE as the internal standard. In this case, ^{1}H NMR experiments were carried out on a 1:1 mixture of host and guest in 0.5 mL of $CDCl_3$ containing 1 µL of 1,1,2,2-tetrachloroethane (d= 1.586 g/mL) as internal standard.

c) Integration of free and complexed ^{1}H NMR signals of host or guest. In this case, an equimolar solution of host and guest was solubilized in $CDCl_3$ and equilibrated in a NMR tube.

Table 4.2. K_{rel} calculated by ^{1}H NMR competition experiments.

	$K_{4^+\subset 1a}$ (6.5×10^4 M^{-1})	$K_{4^+\subset 1b}$ (5.1×10^5 M^{-1})	$K_{2^+\subset 1f}$ (7.4×10^4 M^{-1})	$K_{3^+\subset 1f}$ (5.0×10^4 M^{-1})	$K_{2^+\subset 1g}$ (8.5×10^4 M^{-1})	$K_{3^+\subset 1h}$ (7.1×10^3 M^{-1})
$K_{2^+\subset 1b}$ (1.2×10^5 M^{-1})[a]			$K_{rel} = \frac{K_{2^+@1f}}{K_{2^+@1b}} = 0.62$		$K_{rel} = \frac{K_{2^+@1g}}{K_{2^+@1b}} = 0.71$	
$K_{3^+\subset 1b}$ (3.5×10^4 M^{-1})[a]				$K_{rel} = \frac{K_{3^+@1f}}{K_{3^+@1b}} = 1.43$		$K_{rel} = \frac{K_{2^+@1g}}{K_{3^+@1g}} = 0.20$
$K_{4^+\subset 1f}$ (1.4×10^5 M^{-1})		$K_{rel} = \frac{K_{4^+@1f}}{K_{4^+@1b}} = 3.64$				
$K_{3^+\subset 1g}$ (3.4×10^5 M^{-1})					$K_{rel} = \frac{K_{2^+@1g}}{K_{3^+@1g}} = 0.25$	
$K_{4^+\subset 1g}$ (9.3×10^4 M^{-1})		$K_{rel} = \frac{K_{4^+@1b}}{K_{4^+@1g}} = 5.48$			$K_{rel} = \frac{K_{2^+@1g}}{K_{3^+@1g}} = 0.91$	
$K_{7^+\subset 1a}$ (3.4×10^2 M^{-1})[b]	$K_{rel} = \frac{K_{4^+@1b}}{K_{4^+@1g}} = 180.6$					

K_{ass} value of $16h^+\subset 15a$

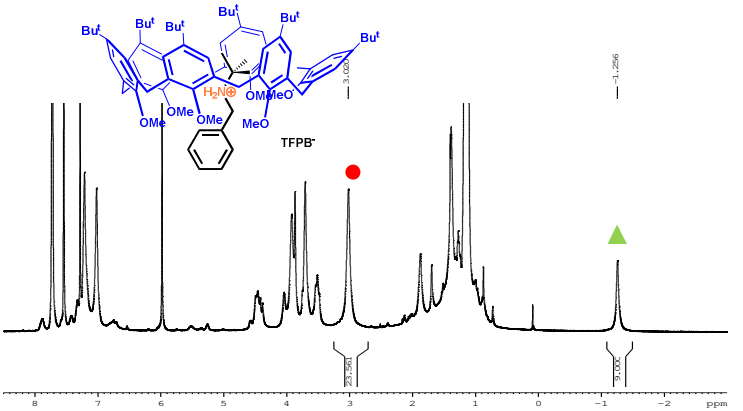

Figure 4.79. ^{1}H NMR spectrum of equimolar solution ($3.8 \cdot 10^{-3}$ M) of **15a** and **16h**$^+$·TFPB$^-$. The association constant K_{ass} value was calculated by integration of complexed (▲) and free derivative **15a** (●) ($CDCl_3$, 400 MHz, 298 K).

K_{ass} value of 16e$^+$⊂ 15b

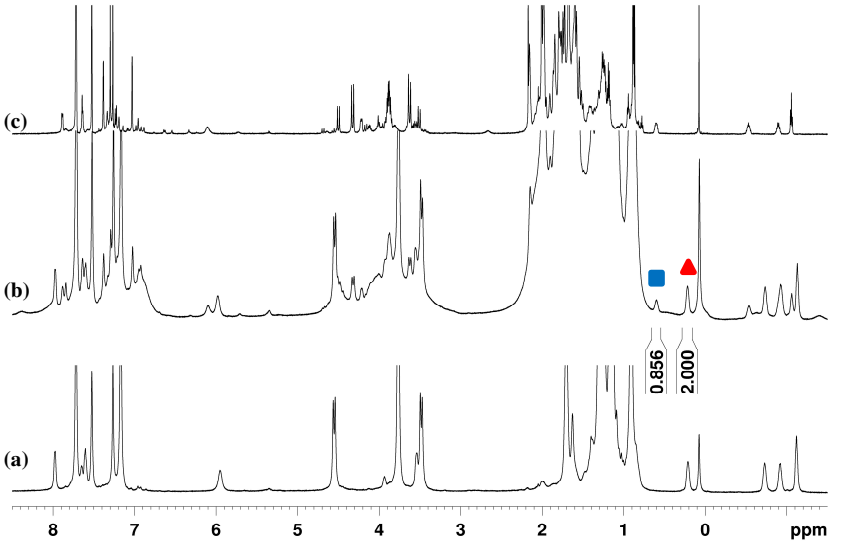

Figure 4.80. ^{1}H NMR spectrum of (a) an equimolar solution (4.5 mM) of 16e$^+$ and 15b in 0.5 mL of $CDCl_3$; (b) an equimolar solution (4.5 mM) of **16e$^+$**, **15g** and **15b** in 0.5 mL of $CDCl_3$. (c) an equimolar solution (4.5 mM) of **16e$^+$** and **15g** in 0.5 mL of $CDCl_3$.The association constant K_a value was calculated by integration of signal of complex **16e$^+$⊂15b** (▲) and complex **16e$^+$⊂ 15g** (■) (600 MHz, $CDCl_3$, 298 K).

K_{ass} value of 16b$^+$⊂ 15f

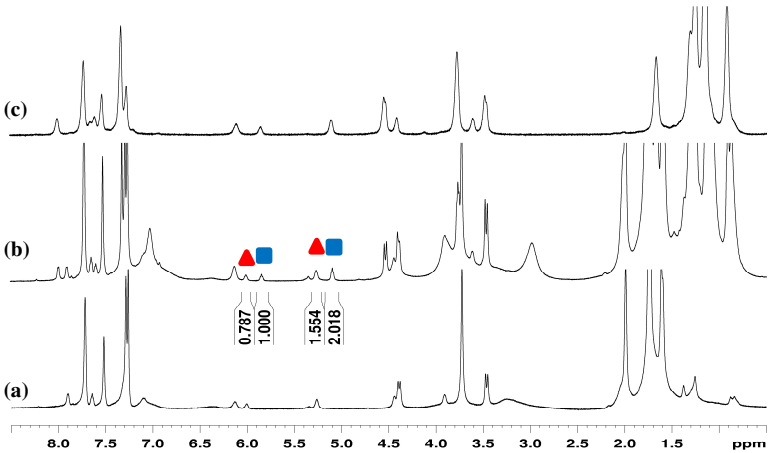

Figure 4.81. ^{1}H NMR spectrum of (a) an equimolar solution (4.5 mM) of **16b$^+$** and **15f** in 0.5 mL of $CDCl_3$; (b) an equimolar solution (4.5 mM) of **16b$^+$**, **15f** and **15b** in 0.5 mL of $CDCl_3$. (c) an equimolar solution (4.5 mM) of **16b$^+$** and **15b** in 0.5 mL of $CDCl_3$.The association constant K_a value was calculated by integration of signal of complex **16b$^+$⊂15f** (▲) and complex **16b$^+$⊂15b** (■) (600 MHz, $CDCl_3$, 298 K).

K_{ass} value of $16a^{+}\subset$ 15f

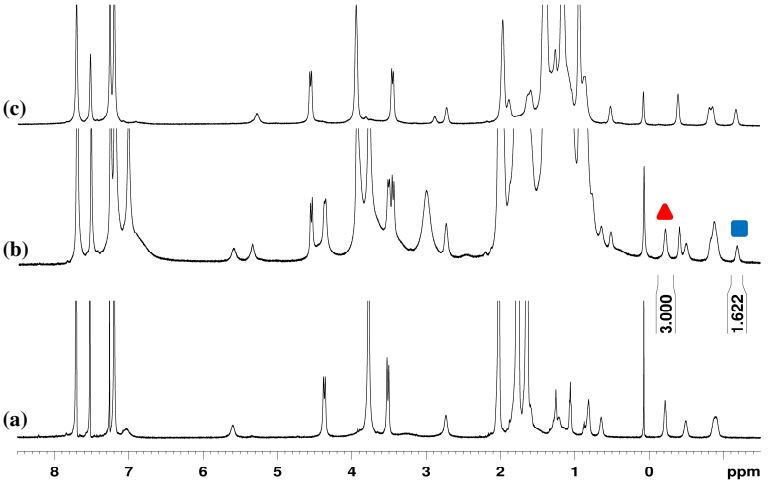

Figure 4.82. ^{1}H NMR spectrum of (a) an equimolar solution (4.5 mM) of **16a**$^{+}$ and **15f** in 0.5 mL of $CDCl_3$; (b) an equimolar solution (4.5 mM) of **16a**$^{+}$, **15f** and **15b** in 0.5 mL of $CDCl_3$. (c) an equimolar solution (4.5 mM) of **16a**$^{+}$ and **15b** in 0.5 mL of $CDCl_3$.The association constant K_a value was calculated by integration of signal of complex **16a**$^{+}\subset$**15f** (▲) and complex **16a**$^{+}\subset$**15b** (■) (600 MHz, $CDCl_3$, 298 K).

K_{ass} value of $16e^{+}\subset$ 15f

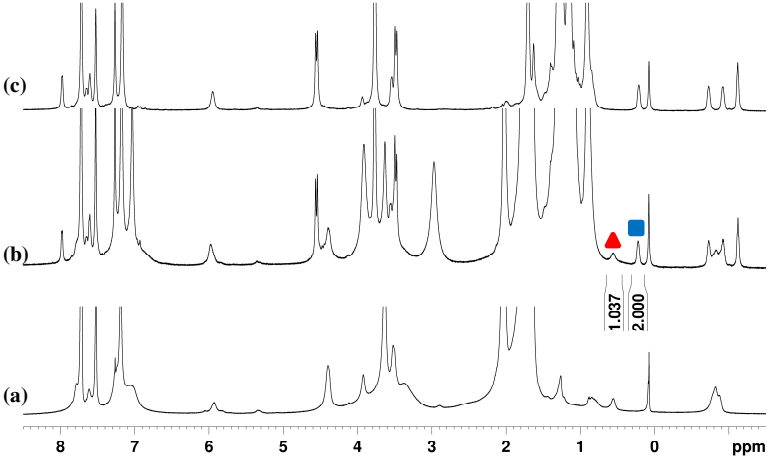

Figure 4.83. ^{1}H NMR spectrum of (a) an equimolar solution (4.5 mM) of **16e**$^{+}$ and **15f** in 0.5 mL of $CDCl_3$; (b) an equimolar solution (4.5 mM) of **16e**$^{+}$, **15f** and **15b** in 0.5 mL of $CDCl_3$. (c) an equimolar solution (4.5 mM) of **16e**$^{+}$ and **15b** in 0.5 mL of $CDCl_3$.The association constant K_a value was calculated by integration of signal of complex **16e**$^{+}\subset$**15f** (▲) and complex **16e**$^{+}\subset$**15b** (■) (600 MHz, $CDCl_3$, 298 K).

K_{ass} value of $16b^{+}\subset$ 15g

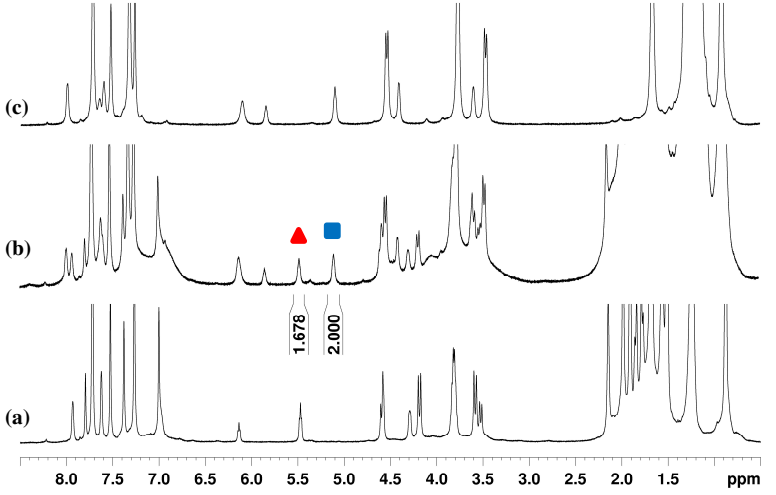

Figure 4.84. ^{1}H NMR spectrum of (a) an equimolar solution (4.5 mM) of **16b^{+}** and **15g** in 0.5 mL of $CDCl_3$; (b) an equimolar solution (4.5 mM) of **16b^{+}**, **15g** and **15b** in 0.5 mL of $CDCl_3$. (c) an equimolar solution (4.5 mM) of **16b^{+}** and **15b** in 0.5 mL of $CDCl_3$.The association constant K_a value was calculated by integration of signal of complex **16b$^{+}\subset$15g** (▲) and complex **16b$^{+}\subset$15b** (■) (600 MHz, $CDCl_3$, 298 K).

K_{ass} value of $16a^{+}\subset$ 15g

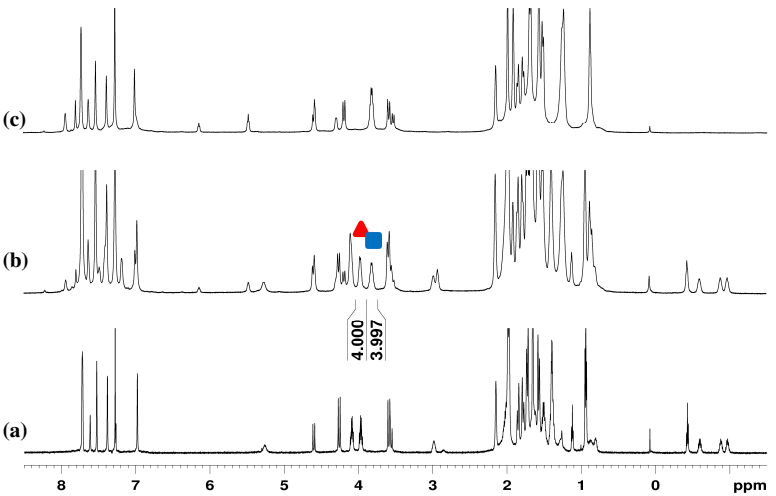

Figure 4.85. ^{1}H NMR spectrum of (a) an equimolar solution (4.5 mM) of **16a^{+}** and **15g** in 0.5 mL of $CDCl_3$; (b) an equimolar solution (4.5 mM) of **16a^{+}**, **15g** and **16b^{+}** in 0.5 mL of $CDCl_3$. (c) an equimolar solution (4.5 mM) of **16b^{+}** and **15g** in 0.5 mL of $CDCl_3$.The association constant K_a value was calculated by integration of signal of complex **16a$^{+}\subset$15g** (▲) and complex **16b$^{+}\subset$ 15g** (■) (600 MHz, $CDCl_3$, 298 K).

K_{ass} value of 16e$^+$⊂ 15g

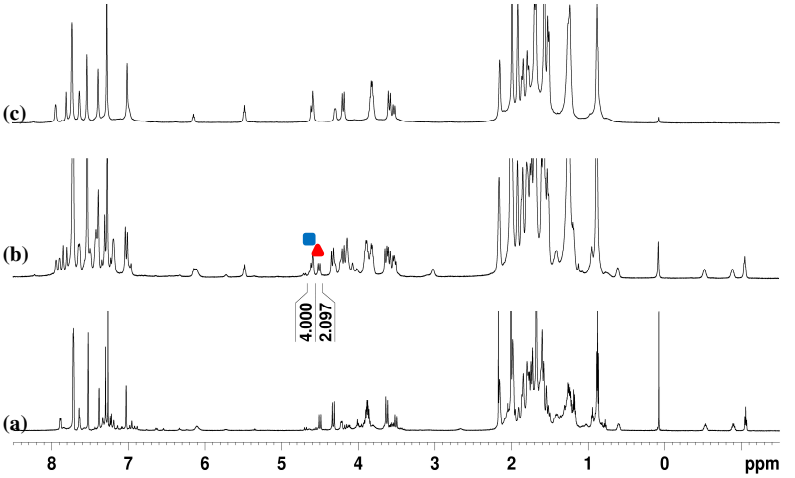

Figure 4.86. ^{1}H NMR spectrum of (a) an equimolar solution (4.5 mM) of **16e$^+$** and **15g** in 0.5 mL of $CDCl_3$; (b) an equimolar solution (4.5 mM) of **16e$^+$**, **15g** and **16b$^+$** in 0.5 mL of $CDCl_3$. (c) an equimolar solution (4.5 mM) of 16b$^+$ and 15g in 0.5 mL of $CDCl_3$.The association constant K_a value was calculated by integration of signal of complex **16e$^+$⊂15g** (▲) and complex **16b$^+$⊂15g** (■) (600 MHz, $CDCl_3$, 298 K).

K_{ass} value of 16a$^+$⊂ 15c

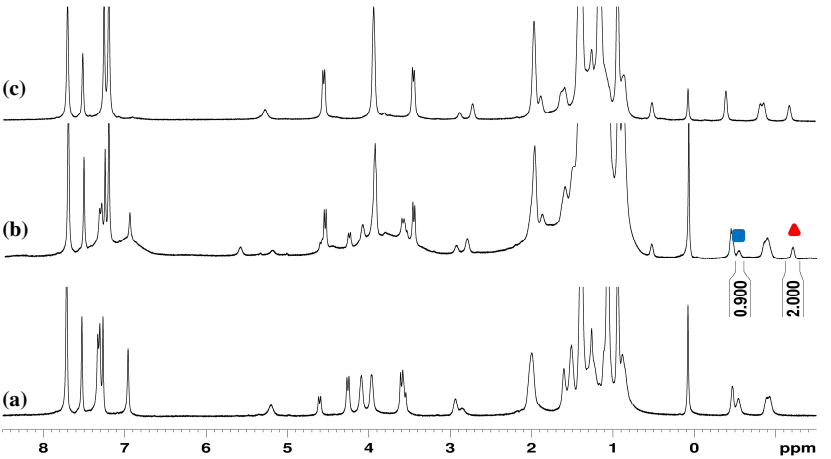

Figure 4.87. ^{1}H NMR spectrum of (a) an equimolar solution (4.5 mM) of **16a$^+$** and **15c** in 0.5 mL of $CDCl_3$; (b) an equimolar solution (4.5 mM) of **16a$^+$**, **15c** and **15b** in 0.5 mL of $CDCl_3$. (c) an equimolar solution (4.5 mM) of **16a$^+$** and **15b** in 0.5 mL of $CDCl_3$.The association constant K_a value was calculated by integration of signal of complex **16a$^+$⊂15c** (▲) and complex **16a$^+$⊂15b** (■) (600 MHz, $CDCl_3$, 298 K).

K_{ass} value of 16e$^+$⊂ 15a

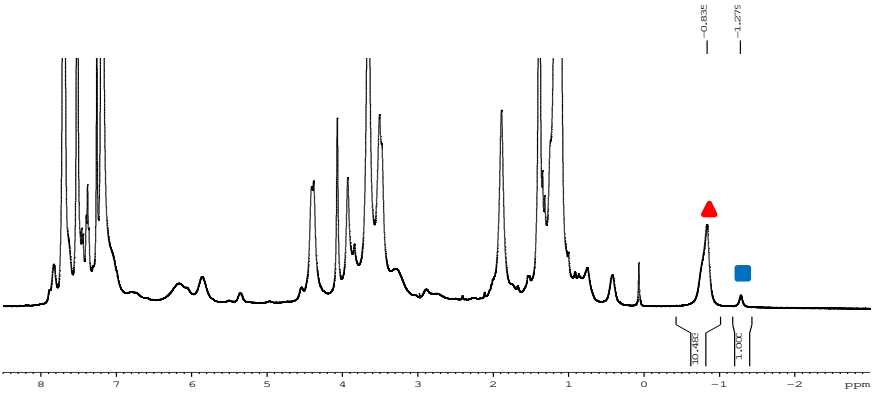

Figure 4.88. ^{1}H NMR spectrum of an equimolar solution (4.5 mM) of **16e$^+$**, **15a** and **16h$^+$** in 0.5 mL of $CDCl_3$. The association constant K_a value was calculated by integration of signal of complex **16e$^+$⊂15a** (▲) and complex **16h$^+$⊂15a** (■) (400 MHz, $CDCl_3$, 298 K).

K_{ass} value of 16b$^+$⊂ 15c

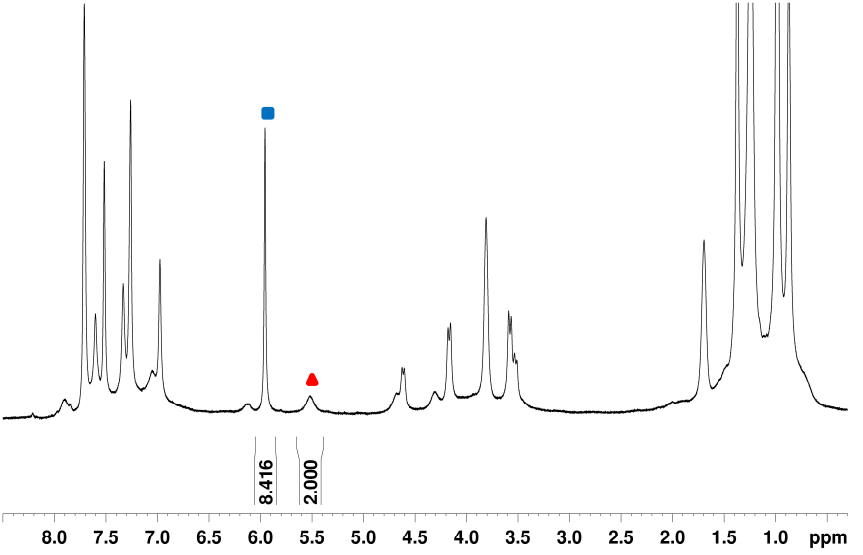

Figure 4.89. ^{1}H NMR spectrum of an equimolar solution (6.1 mM) of **16b$^+$** and **15c** in 0.5 mL of $CDCl_3$ containing 1 μL of TCE. The association constant K_a value was calculated by integration of signal of complex **16b$^+$⊂15c** (▲) and TCE (■) (600 MHz, $CDCl_3$, 298 K).

K_{ass} value of $16e^{+}\subset 15c$

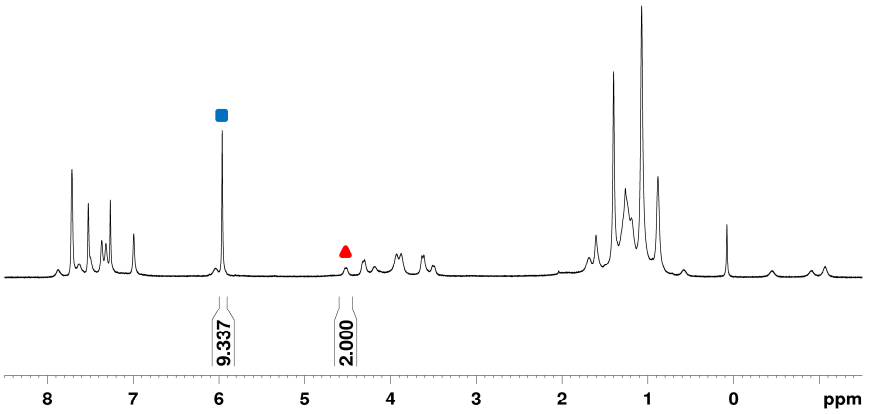

Figure 4.90. ^{1}H NMR spectrum of an equimolar solution (6.1 mM) of **16b^{+}** and **15c** in 0.5 mL of $CDCl_3$ containing 1 µL of TCE. The association constant K_a value was calculated by integration of signal of complex **16b$^{+}\subset$15c** (▲) and TCE (■) (600 MHz, $CDCl_3$, 298 K).

4.7.2.4 Crystallographic information of derivatives 15f and 15g

Colourless single crystals suitable for X-ray investigation were obtained by slow evaporation of $CHCl_3$/MeOH solutions containing **15f** or **15g**. Data collections were carried out at the Macromolecular crystallography XRD1 beamline of the Elettra Synchrotron (Trieste, Italy), employing the rotating-crystal method with a Dectris Pilatus 2M area detector. Single crystals investigated were dipped in a cryo-protectant (PEG200 for **15f** and Paratone for **15g**), mounted on a loop, and flash-frozen under a liquid nitrogen stream at 100 K. Diffraction data were indexed and integrated using the XDS package,[53] while scaling was carried out with XSCALE.[54] The structures were solved using the SHELXT package;[55] and structure refinement was performed with SHELXL-14,[56] operating through the WinGX GUI,[57] by full-matrix least-squares methods on F2. Both molecules crystallized in the $P\bar{1}$ space group. The **15f** molecule exhibits a 1,2,3-alternate conformation; while the **15g** molecule has a partial-cone formation, with one of the hexyloxy substituted inverted with respect to the other five aryl groups in the macrocycle. Details of the refinement of the thermal parameters of non-hydrogen atoms are outlined below. All hydrogen atoms were placed at the

[53] Kabsch, W. *Acta Crystallogr., Sect. D: Biol. Crystallogr.* **2010**, *66*, 125–132.
[54] Kabsch, W. *Acta Crystallogr., Sect. D: Biol. Crystallogr.* **2010**, *66*, 133–144.
[55] Sheldrick, G. M. Acta Cryst. **2015**, A71, 3-8.
[56] Sheldrick, G. M. *Acta Cryst.* **2008**, *A64*, 112–122.
[57] Farrugia, L.J. *J. Appl. Cryst.* **2012**, *45*, 849–854.

geometrically calculated positions and refined using the riding model. Crystal data and final refinement details for the structures are reported in **Table 4.3** and **Table 4.4**.

Crystal Structure of 15f: The triclinic (space group $P\bar{1}$) asymmetric unit contains a 1/2 molecule of **15f** which lies on a centre of inversion and two co-crystallized $CHCl_3$ solvent molecules encapsulated in the calixarene ring. The structure exhibits no appreciable disorder and all non-hydrogen atoms were refined anisotropically at full occupancy.

Crystal Structure of 15g: The triclinic (space group $P\bar{1}$) asymmetric unit contains one molecule of **15g** and four $CHCl_3$ molecules modelled with partial occupancy. The **15g** molecule shows several types of disorder. The most significant disorder is attributed to the superimposition on the same site of the two enantiomeric forms of **15g**, which results in a partial occupation of the hexyloxy groups (2, 3 and 5, 6) located on each side of a plane containing the inverted phenyl group and its facing phenyl group with self-included hexyl chain. Each of the four affected positions (2, 3, 5, and 6) was refined with a hydrogen atom and a hexyl group at 50% of occupancy factors, with the overlapped oxygen atoms at full occupation. In addition, two of these hexyl substituents show two-position disorder for all six carbon atoms, which were refined at 30 and 20% of occupancy factors in both cases. A similar two-position disorder is present for all six carbon atoms of the hexyloxy group bonded to the inverted phenyl group; as well as all six hexyloxy carbon atoms of its facing phenyl group. These were refined at 50% of occupancy factors in both cases. Finally, one of the adamantyl groups shows a two-position disorder of all its carbon atoms (except for the atom bonded to the phenyl ring) which was refined at 60 and 40% of occupancy factors. Significant disorder and partial occupancy are also observed for the solvent molecules. One fully occupied $CHCl_3$ molecule site shows a three-position disorder, modelled at 40, 40, and 20% of occupancy factors; while a second, partially occupied site shows a two-position disorder modelled at 50 and 40% of occupancy factors. Finally, two further $CHCl_3$ sites were modelled at 20 and 15% of occupancy factors. These two partially occupied sites are superimposed on sites of the partially occupied hexyl groups discussed above. To maintain a regular geometry, DFIX and DANG were applied to all partially occupied atoms discussed above. In addition, the thermal parameters of all partially occupied carbon atoms were refined isotropically, while all other non-hydrogen atoms were refined anisotropically.

Table 4.3. Dihedral angles, θ, between the mean plane of the bridging methylene groups and the mean planes of the six aryl rings for 15f and 15g. Absolute angle value greater/smaller than 90° indicates outward/inward orientation of the adamantly group, while a negative sign indicates an inverted orientation of the adamantly group with respect to a given orientation of the macrocycle.

Crystal	**Dihedral angles, θ [°]**					
15f[a]	1	2	3	1'	2'	3'
	96	132	72	-96	-132	-72
15g	1	2	3	4	5	6
	-46	94	98	158	96	98

[a] 1', 2', and 3' are generated by inversion of 1, 2, and 3, respectively. See the main text and Figure 1 for full details on the designation of the six aryl rings.

Table 4.4. Crystal data and structure refinement for **15f** and **15g**.

	15f	**15g**
Empirical formula	$C_{108}H_{136}O_6$, 4($CHCl_3$)	$C_{126}H_{168}O_6$, 2.25($CHCl_3$)
Formula weight	2003.6	2047.17
Temperature (K)	100(2)	100(2)
Wavelength (Å)	0.7	0.7
Crystal system	Triclinic	Triclinic
Space group	P -1	P -1
Unit cell dimensions (Å, °)	a = 12.338 (2) b = 15.813 (3) c = 15.8860 (6) α = 62.331(11) β = 80.881 (10) γ = 68.02 (3)	a = 12.959 (4) b = 15.165 (3) c = 29.378 (7) α = 75.80 (3) β = 86.69 (2) γ = 86.896 (10)
Volume (Å^3)	2544.9 (9)	5583 (3)
Z	1	2
ρ_{calcd} (g/cm^3)	1.307	1.218
μ (mm^{-1})	0.361	0.216
F(000)	1060	2205
Reflections collected	48310	45006
Independent reflections	13952	12925
Data / restraints / parameters	13952 / 0 / 590	12925 / 1496 / 1417
GooF	1.038	1.042
R1 / wR2 [I>2σ(I)]	0.042 / 0.0436	0.1007/ 0.1598
R1 / wR2 all data	0.1192 / 0.1208	0.2737 / 0.3254
Largest. Diff. peak/hole (e Å^{-3})	0.798 / -1.035	0.666 / -0.413
CCDC code	1988954	1988955

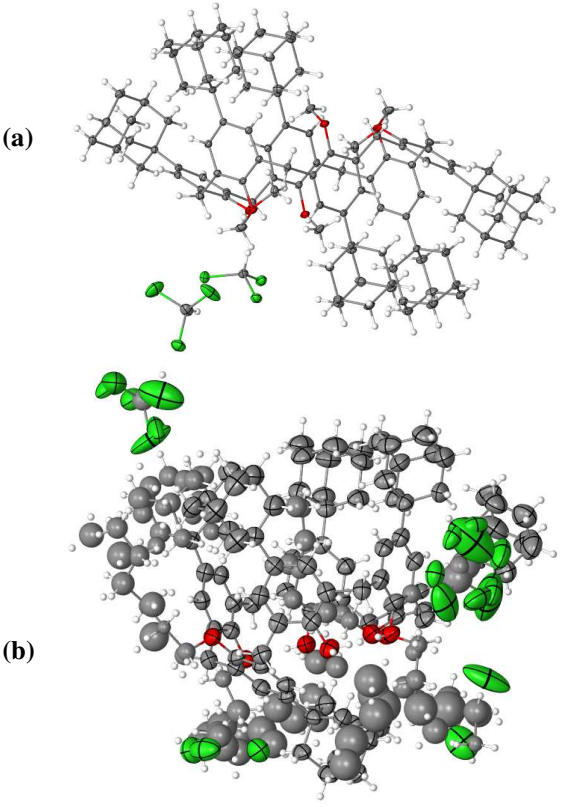

Figure 4.91. ORTEP drawing of **15f** (a) and **15g** (b) (ellipsoids at 50% probability).

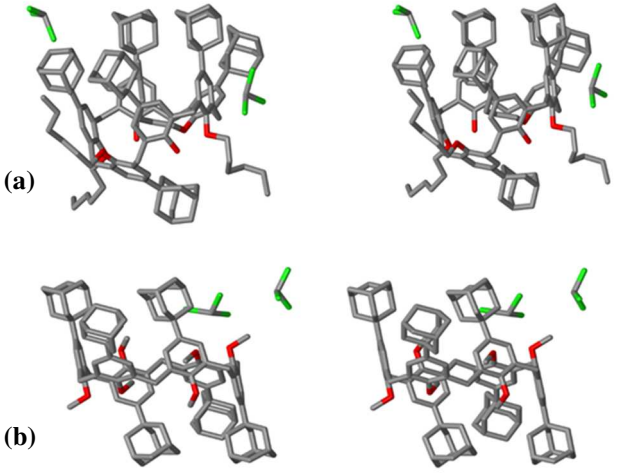

Figure 4.92. Stereo view of **15f** (a) and **15g** (b).

4.7.2.5 Computational Details

Atomic coordinates of 16b⁺⊂15f

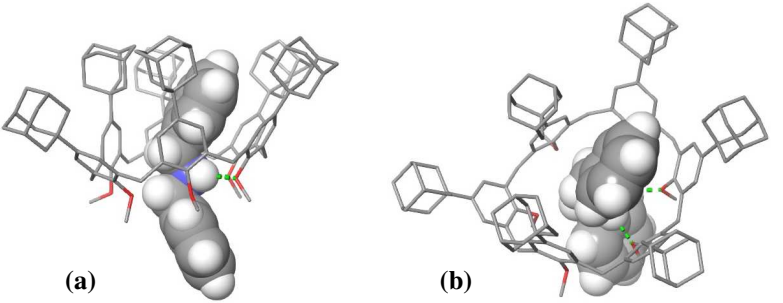

Figure 4.93. (a) Side view and (b) top view of complex **16b⁺⊂15f**.

.

O	1.94906300	-3.35100600	3.48040200
O	-1.95177000	-4.54301100	3.35087300
O	3.07972200	-0.09508900	3.71918800
O	0.73302200	2.70082900	3.60103900
O	-3.14748500	2.94777500	3.79683600
O	-3.95509600	-0.77741400	3.37511900
C	-1.89716200	-4.24972600	1.99269400
C	-2.36357500	3.91343300	0.32900900
H	-1.62079600	4.50443000	-0.19161800
C	-2.99881600	-3.62531800	1.37653100
C	2.42832900	-5.30266600	0.39276500
H	1.89260100	-6.06591500	-0.16001800
C	-2.25348300	3.80216000	1.72134100
C	-2.90157700	-3.29781700	0.02298500
C	-3.22105300	3.05162900	2.40903200
C	-0.72597300	-4.53055600	1.27230100
C	1.17167100	3.53768600	2.56595600
C	4.71517800	-0.95911800	2.15928800
C	-0.67981300	-4.18229900	-0.08397200
H	0.22780300	-4.39871100	-0.63098400
C	-5.08842100	-2.17296600	1.76183300
C	3.78468800	-3.37216800	1.89577200
C	0.72060900	5.27120300	0.96701500
H	0.02667500	5.99399800	0.54805000
C	-4.27322300	-3.37880000	2.18206000
H	-4.91202200	-4.26811300	2.09752700
H	-3.98939100	-3.30348300	3.23221100
C	1.81947600	-4.78856700	1.54524100
C	2.52040800	-3.83579200	2.30102300
C	3.68791800	-4.87926200	-0.04632900
C	-4.88070000	-0.91462400	2.34039000
C	4.33539900	-3.90452800	0.72582100
C	0.25654000	4.43371900	1.98446500
C	5.62966300	-0.70262300	1.13530500
H	6.21387200	-1.53308300	0.75238400
C	-4.25413100	2.39012000	1.72019700
C	2.04582700	5.24272700	0.50470800
C	-1.17225100	4.55502200	2.49219000
H	-1.22218400	4.22434800	3.52769900
C	-1.75573000	-3.57577700	-0.73938600
C	4.00088700	0.13063800	2.68671800
C	2.51123800	3.48102600	2.15347000
C	-5.59555900	0.21332900	1.90479100
C	-4.31666300	2.53325400	0.33317100
H	-5.11759700	2.02666700	-0.19420200
C	0.43478900	-5.25880500	1.94826600
H	0.29914900	-5.16705300	3.02519400
C	4.18961000	1.43766300	2.21171700
C	-5.31309600	1.59015600	2.47747700
H	-4.99168300	1.50393900	3.51464400
H	-6.24894500	2.16321100	2.47632500
C	2.91634600	4.33900100	1.12135500
H	3.95694700	4.31928900	0.82450300
C	4.56803000	-2.36616700	2.73239900
H	4.09795500	-2.29987800	3.71037300
H	5.57644200	-2.76864200	2.88432800
C	5.11166600	1.63059100	1.17482200

H	5.27900700	2.64117300	0.82603500
C	2.26902700	-4.15475900	4.62345800
H	3.34000700	-4.11023800	4.85497600
H	1.69921100	-3.75731200	5.46579500
C	-6.56674500	0.03697700	0.91529200
H	-7.14180900	0.90609900	0.60820900
C	-3.39923400	3.30831000	-0.39142000
C	-6.83497700	-1.20951500	0.32798400
C	5.84672000	0.58152200	0.61417700
C	-6.06916300	-2.29515200	0.76697400
H	-6.23471000	-3.28021400	0.34498100
C	-3.89444600	3.94814200	4.49679500
H	-4.96235200	3.89241700	4.25576800
H	-3.53108400	4.95537600	4.26085400
C	3.52818400	2.62611400	2.90489800
H	4.33449100	3.29766600	3.22717300
H	3.04818600	2.25624700	3.80566900
C	0.88624600	3.27896400	4.90929100
H	1.93333500	3.53226500	5.10502900
H	0.28264900	4.18694300	5.00977500
C	-2.46914200	-5.83946100	3.66451600
H	-3.49727000	-5.96018000	3.30386200
H	-1.84828500	-6.63385800	3.23320100
H	-1.43277700	5.62152300	2.48759700
H	0.35653000	-6.32793600	1.71015100
C	9.43331800	1.99809800	-1.51814800
C	9.35781400	0.51828500	-1.09514400
C	8.96774100	-0.34571800	-2.31168300
C	7.59520300	0.10921900	-2.84863800
C	7.67171600	1.58933200	-3.27015400
C	8.05706700	2.44593600	-2.04841900
H	10.19827100	2.13238000	-2.29317300
H	9.73166700	2.62084800	-0.66481200
C	8.29825700	0.35354000	0.01332800
H	10.33179700	0.19348600	-0.70876700
H	8.92991600	-1.40560200	-2.02667300
H	9.72805700	-0.25581500	-3.09756400
H	7.31300100	-0.50765000	-3.71109500
C	6.53156200	-0.05479700	-1.74408800
H	8.41152700	1.71798800	-4.07011000
H	6.70513800	1.91811800	-3.67441900
C	6.99720400	2.27481700	-0.94023200
H	8.09915100	3.50339800	-2.33738800
H	6.02261500	2.62360300	-1.30712200
C	6.89133600	0.79507000	-0.48999800
H	7.26425700	2.90764000	-0.08403100
H	8.57117900	0.95056900	0.89294800
H	8.26889100	-0.69248100	0.34131800
H	6.44789600	-1.11329800	-1.46860600
H	5.54603000	0.25315500	-2.11742400
C	-10.03760100	-0.04849300	-2.41960400
C	-8.69761800	-0.50519000	-3.03191300
C	-8.82721300	-1.95781100	-3.52946700
C	-9.19020400	-2.87111100	-2.34216400
C	-10.53402300	-2.42072500	-1.73667100
C	-10.40499100	-0.96865500	-1.23746800
H	-10.82825100	-0.07760200	-3.17986500
H	-9.96260700	0.99281200	-2.07922800
C	-7.59092500	-0.42623900	-1.96068100
H	-8.43159500	0.15133200	-3.87012200
H	-7.88464000	-2.28683900	-3.98660500
H	-9.59861200	-2.02461000	-4.30693800
H	-9.26999900	-3.90962800	-2.68650600
C	-8.08529900	-2.78635500	-1.26868800
H	-11.33020700	-2.49417300	-2.48815300
H	-10.81659600	-3.08222200	-0.90744400
C	-9.30165800	-0.89073700	-0.16259400
H	-11.35553600	-0.64234300	-0.79750700
H	-9.55760800	-1.52916900	0.69272700
C	-7.92644600	-1.33679300	-0.74236500
H	-9.23299200	0.13442100	0.22061900
H	-7.47363600	0.61311800	-1.62995600
H	-6.62610800	-0.73316300	-2.38646500
H	-7.13577600	-3.13558000	-1.69553600
H	-8.33111700	-3.46027600	-0.43785600
H	5.32045700	-3.56325100	0.42536900
C	-4.94207200	4.22551300	-2.16667000
C	-5.18504400	4.40974700	-3.67801900
C	-5.21245900	3.02916600	-4.36427800
C	-3.86094000	2.31857600	-4.14695300
C	-3.61280500	2.13039600	-2.63600100
C	-3.58683500	3.50210700	-1.90195200
H	-5.76409000	3.64757700	-1.72755700
H	-4.93710900	5.19915800	-1.65984700
C	-4.05122900	5.26147100	-4.28115000
H	-6.14711000	4.91574500	-3.82657100
H	-5.40893600	3.14491200	-5.43767100
H	-6.02956100	2.41994500	-3.95541900
H	-3.88187400	1.33424600	-4.63130900
C	-2.72847200	3.17112300	-4.75102400

H	-4.39617900	1.49077100	-2.21270700
H	-2.65944700	1.61280700	-2.46761200
C	-2.46624500	4.35938400	-2.54391400
H	-1.49120000	3.88056200	-2.38224800
C	-2.70412800	4.54666800	-4.05681000
H	-2.42521000	5.34396300	-2.06019200
H	-4.03523700	6.25507800	-3.81459400
H	-4.22236500	5.41607600	-5.35393700
H	-2.88121600	3.29579400	-5.83051800
H	-1.76298100	2.66412900	-4.62183200
H	-1.89026200	5.15524600	-4.47074400
C	6.69902100	-5.45703900	-3.16827000
C	5.35181700	-4.82761600	-3.57830900
C	4.63158100	-4.29431300	-2.32325000
C	4.36533400	-5.44074200	-1.30303200
C	5.73006400	-6.09391900	-0.93239000
C	6.44782200	-6.62325600	-2.19067900
H	7.34212300	-4.70102900	-2.69804800
H	7.23193400	-5.81807000	-4.05680600
C	4.47217900	-5.89310900	-4.26065200
H	5.52861600	-3.99448100	-4.27024800
H	3.67648500	-3.82908700	-2.60150200
H	5.23971300	-3.51033100	-1.85502800
C	3.50785600	-6.51640100	-2.01798900
H	6.37082900	-5.36352400	-0.42374900
H	5.55844500	-6.91083600	-0.21978700
C	5.56801800	-7.68745800	-2.87463300
H	7.40533300	-7.06907300	-1.89416000
H	5.40025300	-8.53319600	-2.19528300
C	4.22240200	-7.05223300	-3.27611400
H	6.07632800	-8.08700400	-3.76112300
H	4.96441500	-6.26695800	-5.16719500
H	3.51774400	-5.45072100	-4.57551700
H	2.53705400	-6.09100400	-2.30467000
H	3.30451600	-7.34886400	-1.33200800
H	3.58420600	-7.80803300	-3.75018000
C	4.17143200	8.48364600	-1.59334300
C	4.40147600	7.03901000	-2.07867400
C	3.55612500	6.77810100	-3.34061600
C	2.06505400	6.96737700	-3.00093200
C	1.82702200	8.40968700	-2.50911000
C	2.68087300	8.67344700	-1.25207300
H	4.47639100	9.19587400	-2.37026000
H	4.79099500	8.69017500	-0.71099400
C	3.99202800	6.05026500	-0.96715100
H	5.46391100	6.89179500	-2.30912600
H	3.73347200	5.76017300	-3.71231000
H	3.85253700	7.46583300	-4.14247500
H	1.45444800	6.77540100	-3.89219600
C	1.66184900	5.97364100	-1.89250400
H	2.08823800	9.12466700	-3.29927900
H	0.76336700	8.56140600	-2.28267300
C	2.27750700	7.68404000	-0.13984200
H	2.50953700	9.69739800	-0.89770700
H	1.22661500	7.84335700	0.12954000
C	2.49486300	6.21088500	-0.59830500
H	2.86605300	7.87050600	0.76765600
H	4.61587900	6.22349800	-0.08071200
H	4.18577400	5.02231400	-1.30158900
H	1.81542400	4.94180000	-2.23605300
H	0.59197300	6.07862700	-1.67509300
C	-3.10158900	-2.15355200	-4.65580300
C	-1.96313200	-1.37640900	-3.96423300
C	-0.61350100	-1.76902200	-4.59533700
C	-0.39025400	-3.28243500	-4.41179600
C	-1.52289000	-4.06083900	-5.10929800
C	-2.87278200	-3.66833500	-4.47794900
H	-3.13803900	-1.90067400	-5.72320100
H	-4.07097100	-1.86542800	-4.22704000
C	-1.94704400	-1.71503800	-2.45935900
H	-2.12571000	-0.29847800	-4.08567500
H	0.20131900	-1.20553800	-4.12198600
H	-0.60424100	-1.51196900	-5.66235700
H	0.57601600	-3.56900000	-4.84635900
C	-0.37985100	-3.62174700	-2.90723900
H	-1.52802600	-3.83902500	-6.18405600
H	-1.35823000	-5.14147500	-5.00773600
C	-2.85766300	-4.01245100	-2.97477300
H	-3.68407100	-4.22439800	-4.96421700
H	-2.71205300	-5.09116800	-2.83308200
C	-1.72458900	-3.23937900	-2.23611100
H	-3.82930000	-3.76602100	-2.52984200
H	-2.89355000	-1.40299500	-2.00172800
H	-1.15116500	-1.15404800	-1.95321800
H	0.44494800	-3.08747800	-2.41800100
H	-0.19122600	-4.69567700	-2.77884000
H	-3.75104000	-2.81353600	-0.44610800
H	-2.45839500	-5.92470300	4.75314200
H	0.54468100	2.53507800	5.62771400
H	-3.75620900	3.75555500	5.56303600

H	1.98862500	-5.20202900	4.46711100
C	3.64013600	-0.01442600	5.03910600
C	-4.53410300	-0.99586700	4.66946400
H	-3.73396400	-0.87275000	5.40095900
H	-5.32909200	-0.26955900	4.87498700
H	-4.95275600	-2.00514600	4.75330200
H	4.38181000	-0.80352000	5.20304800
H	4.11956000	0.95622700	5.20298200
H	2.81396800	-0.13493500	5.74110100
C	-0.64483400	-0.96304600	4.05705900
N	0.20816500	-0.22437900	3.03556800
C	-0.21293800	-0.63275900	1.62800600
H	0.13453000	0.80059800	3.16289000
C	1.68466500	-0.78639300	-0.02158000
C	2.41078600	-0.28356300	-1.10070500
C	2.08104200	0.95799200	-1.64693600
C	1.02372000	1.69605100	-1.11213900
C	0.29300800	1.19233100	-0.03665400
C	0.62183900	-0.05087600	0.51999800
H	1.93399200	-1.76010000	0.38816600
H	3.22919200	-0.86422100	-1.51325100
H	2.64268000	1.34690700	-2.49123700
H	0.76215000	2.66127400	-1.53321500
H	-0.54430700	1.76145500	0.35651000
C	0.29902300	-0.47302600	7.71937200
C	0.27437000	-0.96284100	6.41278000
C	-0.56850000	-0.39198800	5.45008700
C	-1.39755500	0.67886000	5.81869300
C	-1.37478100	1.16524700	7.12757800
C	-0.52778900	0.59277200	8.07895800
H	0.95005600	-0.93108600	8.45772600
H	0.90164000	-1.80589200	6.13859100
H	-2.05957800	1.13371800	5.08525500
H	-2.02538900	1.98866500	7.40667700
H	-0.51935600	0.96823500	9.09759200
H	-1.25736300	-0.32567900	1.54198500
H	-0.17753200	-1.72364700	1.61745300
H	-0.30645800	-2.00035800	4.02220800
H	-1.66940100	-0.91900300	3.67946700
H	1.21123400	-0.42708500	3.20197000

Energy = -5244.36186 a.u.

0 imaginary frequency

Atomic coordinates of 16a⁺⊂15f

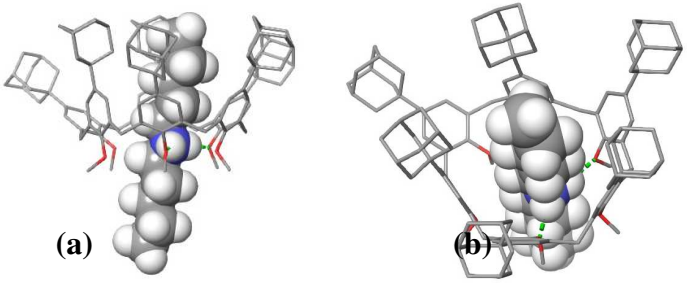

Figure 4.94. (a) Side view and (b) top view of complex **16a⁺⊂15f**.

O	-4.00373000	-0.83691400	3.14430300
O	-2.64973200	2.92111300	3.86896100
O	-2.56792600	-3.89509300	3.38674500
O	1.70487800	-2.62620100	3.58958300
O	3.60713800	0.23939300	4.01544900
O	1.48086500	2.79660800	3.76555200
C	-2.71889600	3.06163500	2.48321100
C	5.48703600	-0.84875800	1.04021300
H	5.82665400	-1.77667400	0.59250700
C	-1.68288900	3.73937000	1.81062300
C	-6.53099200	0.67526700	0.93051900
H	-6.92893400	1.66310100	0.72591000
C	4.75972600	-0.92122000	2.23030400
C	-1.75169100	3.82956300	0.41853300
C	4.34356400	0.28191300	2.82906400
C	-3.79191900	2.49036200	1.78296000

C	2.21726200	-3.38333800	2.52229400
C	-3.54230100	-3.46408200	1.21763300
C	-3.81718100	2.61895900	0.38921900
H	-4.64803500	2.17307400	-0.14150100
C	0.82198700	4.42163900	2.09429400
C	-5.48895700	-1.84368200	1.53495800
C	4.05560300	-4.01757800	1.11355800
H	5.10349800	-3.91767600	0.84908200
C	-0.59816700	4.43912800	2.62932900
H	-0.89512700	5.49080300	2.74445100
H	-0.61729500	4.00194300	3.62603300
C	-5.49942900	0.57254700	1.87634800
C	-5.00220000	-0.69768600	2.18559300
C	-7.05900800	-0.43923400	0.27084000
C	1.81346400	3.62144300	2.67941600
C	-6.50584000	-1.69005800	0.59117600
C	3.56381000	-3.22157400	2.15136800
C	-3.37429700	-3.38423600	-0.16602700
H	-4.23979500	-3.11662500	-0.76475700
C	4.63586800	1.52140200	2.24051000
C	3.26879400	-4.96402900	0.44077200
C	4.49153400	-2.26858800	2.89396200
H	4.08842700	-2.08539800	3.88699200
C	-2.81904800	3.29420800	-0.32007600
C	-2.43557900	-3.82080500	2.00262700
C	1.38460600	-4.30934500	1.87737800
C	3.14397000	3.64450300	2.22592600
C	5.36702900	1.53588300	1.04570200
H	5.60555100	2.49901300	0.61141800
C	-4.93278300	1.81207900	2.53832900
H	-4.57403500	1.57013000	3.53857200
C	-1.18102600	-4.07243700	1.41831400
C	4.24022900	2.83417800	2.90776700
H	3.94139100	2.62334200	3.93177900
H	5.13398200	3.46649100	2.95822600
C	1.93811600	-5.09011800	0.85174500
H	1.30048900	-5.83456200	0.38971700
C	-4.91039200	-3.21362400	1.83781400
H	-4.83397800	-3.36000500	2.91526600
H	-5.60930400	-3.97038100	1.46258300
C	-1.05972700	-3.96436000	0.02731300
H	-0.09168000	-4.15423600	-0.41686800
C	-4.51383000	-1.08587100	4.45634500
H	-5.22174100	-1.92195800	4.46397600
H	-3.66047200	-1.34008600	5.08620100
C	3.45555100	4.49460600	1.16174400
H	4.48791600	4.53516800	0.82875900
C	5.81674900	0.36710400	0.42341000
C	2.50525400	5.32305500	0.54639300
C	-2.14979500	-3.64332900	-0.79465500
C	1.19860800	5.27024300	1.04290800
H	0.44170300	5.92696100	0.63108500
C	4.40861500	0.26079700	5.20247100
H	5.01335600	1.17312800	5.26172800
H	5.07982200	-0.60458700	5.25077500
C	-0.04442900	-4.54390100	2.32538500
H	-0.16367200	-5.62707600	2.47026600
H	-0.20695100	-4.09337800	3.30388500
C	1.85600600	-3.27491700	4.86247500
H	1.33610100	-4.23804400	4.87548200
H	2.91213300	-3.43952500	5.10049300
C	-3.33070000	3.94095200	4.60710500
H	-2.91078600	4.93232500	4.39934200
H	-4.40187900	3.95537100	4.37653200
H	5.45364800	-2.77735600	3.02566500
H	-5.74590000	2.54026400	2.65968900
C	-1.57931100	-5.00526900	-4.94211000
C	-3.00606200	-4.69198100	-4.45173700
C	-3.43625800	-3.30251800	-4.96425300
C	-2.46052600	-2.23322300	-4.43218500
C	-1.03576800	-2.54934200	-4.92670000
C	-0.61091700	-3.93462000	-4.40210300
H	-1.54918000	-5.02215200	-6.03891900
H	-1.27244600	-6.00206800	-4.59938700
C	-3.03145400	-4.69922900	-2.91047600
H	-3.70125700	-5.45447800	-4.82459500
H	-4.45934700	-3.07866800	-4.63455400
H	-3.44611800	-3.29084700	-6.06151300
H	-2.76615400	-1.24296600	-4.79417200
C	-2.48358800	-2.23453200	-2.88951600
H	-1.00307100	-2.53542400	-6.02355300
H	-0.33552900	-1.77905700	-4.57851300
C	-0.64284400	-3.93877700	-2.85905000
H	0.41023300	-4.15869000	-4.73611900
H	0.07373100	-3.20047300	-2.47468300
C	-2.06418000	-3.62418900	-2.32733700
H	-0.31691300	-4.92109500	-2.49271000
H	-2.74370600	-5.68754400	-2.52928800
H	-4.05239200	-4.51259000	-2.55746100
H	-3.48781400	-1.97290500	-2.53590600

H	-1.80394900	-1.46537200	-2.49911600
C	5.06581400	7.29824600	-2.40131700
C	3.97354100	6.34269100	-2.92422200
C	2.77813700	7.16331200	-3.44573500
C	2.20913600	8.01856000	-2.29699000
C	3.29763900	8.97998900	-1.78083700
C	4.49291400	8.16019200	-1.25789300
H	5.42422600	7.94138100	-3.21474800
H	5.93176200	6.72444100	-2.04537400
C	3.50447600	5.42252400	-1.77884100
H	4.38036600	5.72475400	-3.73447800
H	2.00243000	6.49354400	-3.84035800
H	3.09400500	7.80776600	-4.27560600
H	1.34793200	8.59481500	-2.65684500
C	1.74673200	7.09890400	-1.14782800
H	3.62144300	9.65092100	-2.58630600
H	2.89458800	9.61427400	-0.98067900
C	4.02533900	7.24437600	-0.10830600
H	5.26959000	8.83693700	-0.88077600
H	3.62947400	7.84548300	0.72036500
C	2.92507600	6.25550100	-0.59706900
H	4.88222000	6.68730100	0.28924500
H	4.34571100	4.81122200	-1.42974400
H	2.73748400	4.72494500	-2.14046100
H	0.94960900	6.43579000	-1.50995500
H	1.31634700	7.71067900	-0.34441900
H	-6.88550800	-2.58396400	0.10402000
C	8.07128900	-0.25429100	-0.53986200
C	8.95032700	-0.29410600	-1.80628000
C	9.16749300	1.14009100	-2.32651500
C	7.80207300	1.77055300	-2.66468900
C	6.92262000	1.80492100	-1.39726200
C	6.67925200	0.37642400	-0.84609300
H	8.56604700	0.32676600	0.24902300
H	7.94325900	-1.27039900	-0.14735700
C	8.24901900	-1.13492400	-2.89228100
H	9.91738800	-0.74718000	-1.55517900
H	9.80815700	1.12737500	-3.21714900
H	9.68617700	1.74266100	-1.56958600
H	7.94826600	2.79751900	-3.02176200
C	7.10536600	0.93579700	-3.75668300
H	7.41462500	2.42137400	-0.63380600
H	5.96181100	2.28387000	-1.62910000
C	6.00313200	-0.45636900	-1.97416800
H	5.02609100	-0.01709600	-2.21161400
C	6.88729200	-0.49835800	-3.23714500
H	5.81161500	-1.47854100	-1.62563500
H	8.10629700	-2.16519500	-2.53980900
H	8.87713500	-1.19112800	-3.79017200
H	7.71656400	0.92065500	-4.66778400
H	6.14301700	1.39086300	-4.02591000
H	6.38327000	-1.09793400	-4.00554200
C	-10.04784100	-1.70073200	-2.66647500
C	-8.85929400	-0.85624200	-3.16994300
C	-7.71972800	-0.90292700	-2.13176500
C	-8.19256900	-0.34191800	-0.75788000
C	-9.41908000	-1.17738800	-0.28433400
C	-10.55501000	-1.13008300	-1.32636100
H	-9.74113900	-2.74745800	-2.53987800
H	-10.85571800	-1.69431700	-3.40903400
C	-9.31264800	0.60300700	-3.36900000
H	-8.49373400	-1.26351200	-4.12108800
H	-6.85959200	-0.31805600	-2.48393800
H	-7.37084800	-1.93610200	-2.01482600
C	-8.67479300	1.11366000	-0.98551900
H	-9.11976700	-2.21818900	-0.11234000
H	-9.77063500	-0.78848800	0.68000800
C	-11.00729000	0.32925300	-1.52682300
H	-11.39747000	-1.73233400	-0.96406100
H	-11.39052000	0.73949300	-0.58343900
C	-9.81353200	1.16731900	-2.02512700
H	-11.82977300	0.37554600	-2.25175300
H	-10.11050200	0.65309200	-4.12068800
H	-8.47935300	1.20969300	-3.74778300
H	-7.83745700	1.73518300	-1.32971300
H	-9.02578700	1.54325200	-0.03830500
H	-10.12461000	2.21122800	-2.15611800
C	4.74063700	-8.44843100	-1.82275600
C	3.53126200	-7.67826400	-2.38782600
C	3.99836800	-6.74291900	-3.52012900
C	5.02232000	-5.73706900	-2.95893000
C	6.23391500	-6.50055000	-2.38632000
C	5.76416200	-7.44357800	-1.25987200
H	5.20119900	-9.05809500	-2.61015700
H	4.41544700	-9.13925100	-1.03407900
C	2.87874300	-6.84391900	-1.26590700
H	2.79063500	-8.38775600	-2.77688100
H	3.14012900	-6.20933000	-3.94960600
H	4.44807300	-7.32811000	-4.33200100
H	5.35456800	-5.06206400	-3.75760600

C	4.36435900	-4.90463300	-1.83969200
H	6.72540600	-7.07710700	-3.17990700
H	6.97939200	-5.79229000	-2.00065700
C	5.10719900	-6.61585100	-0.13642100
H	6.62530400	-7.98368800	-0.84736800
H	5.84656100	-5.92788600	0.29073100
C	3.88154700	-5.81972800	-0.67535400
H	4.78139900	-7.27326500	0.67991100
H	2.51883800	-7.51398400	-0.47434200
H	2.00153200	-6.31971900	-1.66755100
H	3.50945100	-4.34126700	-2.23581600
H	5.08020900	-4.16450000	-1.46074800
C	-1.68981900	4.66566300	-4.32292700
C	-1.65702100	3.14746300	-4.05353400
C	-2.91278900	2.49069400	-4.65861600
C	-4.16865800	3.10166600	-4.00736700
C	-4.20686300	4.61727100	-4.28485700
C	-2.95185300	5.27594900	-3.68008100
H	-1.68597000	4.85684300	-5.40342800
H	-0.78867900	5.14190100	-3.91295400
C	-1.62838500	2.89436200	-2.53209000
H	-0.75719800	2.71203900	-4.50706100
H	-2.88913500	1.40551300	-4.49117700
H	-2.93605900	2.64566600	-5.74468400
H	-5.06705200	2.62787200	-4.42234600
C	-4.13447300	2.85510700	-2.48463900
H	-4.24938700	4.80275000	-5.36555200
H	-5.11247600	5.05937200	-3.84970800
C	-2.92363000	5.02785100	-2.15840800
H	-2.97505900	6.35698500	-3.86595500
H	-3.80796600	5.47173500	-1.68353300
C	-2.88176600	3.50292300	-1.83999900
H	-2.04987700	5.52551400	-1.72033700
H	-0.71533100	3.32616600	-2.10380000
H	-1.59467500	1.81578900	-2.33012700
H	-4.14013500	1.77521700	-2.28741500
H	-5.04362400	3.26896000	-2.02989900
H	-0.95507700	4.34734600	-0.10264500
H	-3.19435100	3.70634000	5.66509100
H	1.41382800	-2.61739700	5.61320500
H	3.71926700	0.22962500	6.04953200
H	-5.02065300	-0.20146900	4.86376900
C	-2.94342600	-5.18412000	3.88037200
C	1.64419800	3.44021100	5.03920400
H	1.49723700	2.67828700	5.80637200
H	2.64823500	3.86376400	5.13960200
H	0.90821100	4.24012300	5.17317500
H	-3.01852500	-5.09393000	4.96632600
H	-3.91280400	-5.50021400	3.47699100
H	-2.19581800	-5.94723800	3.63374800
C	1.66859000	0.34147500	-2.96855000
H	1.23781900	-0.62311400	-3.25825300
H	2.55452800	0.50673700	-3.59004100
C	2.02201300	0.36516500	-1.47973400
H	0.93849200	1.11894900	-3.21836500
H	2.49313700	1.32450600	-1.22798100
C	0.81360300	0.14744800	-0.55987100
H	2.77471200	-0.40481900	-1.26842600
C	1.21334100	0.16465500	0.92090500
H	0.06444600	0.92775000	-0.74550700
H	0.33262900	-0.81085900	-0.79843800
C	0.01529300	-0.00837200	1.84645900
H	1.94202100	-0.63245400	1.10991200
H	1.71543900	1.11274100	1.14734500
N	0.43888500	0.03800900	3.29493000
H	-0.72154600	0.78754000	1.71087800
H	-0.48161800	-0.97049400	1.69555200
C	-0.70143100	-0.16648800	4.25757700
C	-0.25393500	0.04661600	5.70167600
H	-1.49024300	0.53730800	3.98232700
H	-1.07421500	-1.17995700	4.08766000
C	-1.34961100	-0.30954300	6.71499600
H	0.64387600	-0.55130600	5.90776100
H	0.03095400	1.09643800	5.83554000
C	-0.92496700	-0.06674700	8.16924100
H	-2.24937700	0.27999300	6.49542600
H	-1.63190300	-1.36401900	6.59035700
C	-2.01735600	-0.42619400	9.18015800
H	-0.01944300	-0.65012700	8.38452100
H	-0.64391500	0.98786300	8.29198300
H	-1.68466100	-0.24113800	10.20563000
H	-2.92356400	0.16623000	9.01300200
H	-2.29431700	-1.48359700	9.10675400
H	1.14326700	-0.70320900	3.45354400
H	0.89955000	0.94743000	3.48556800

Energy = -5096.78470 a.u.

0 imaginary frequency

Atomic coordinates of $16b^{+}\subset 15g$

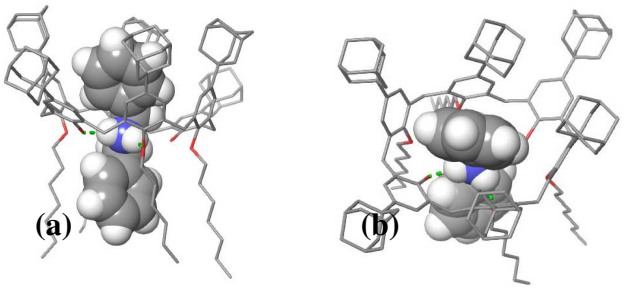

Figure 4.95. (a) Side view and (b) top view of complex **$16b^{+}\subset 15g$**.

O	-2.93958800	2.86748200	-2.22744000	C	3.34104900	2.85249200	0.74342200
O	0.81715800	4.19662500	-1.54954800	C	-2.50745400	-0.69735600	-3.00410500
O	-3.62773400	-0.55038100	0.91983600	C	-0.88171500	-3.04849300	3.35689700
O	-2.75495000	-1.49205700	3.46595000	C	-5.55812300	-1.71433300	-1.95427800
O	0.42874700	0.54486000	3.75862500	H	-5.85300600	-1.31477000	-2.92098300
O	1.96381200	2.99592300	0.65247500	C	2.75214900	0.15021500	3.16539200
C	1.58237800	3.67442700	-2.60399100	C	-1.13123400	-5.08978200	1.99661100
C	2.40311800	-2.55453000	3.80616000	C	-0.06379500	-2.20906200	4.34127600
H	2.26553100	-3.58578100	4.10675100	H	-0.66787500	-1.35466300	4.63677400
C	2.98118000	3.70337600	-2.49368300	C	3.15042900	2.63222700	-4.69481300
C	-0.70834900	0.52787100	-3.99869600	C	-4.38770500	-1.38221700	0.12705900
H	0.21168800	0.56356300	-4.56585400	C	-2.99996800	-3.52412100	2.21545500
C	1.29576000	-1.69731600	3.87914000	C	3.85863000	2.15292700	1.84992300
C	3.73675700	3.16055500	-3.53551300	C	3.80345400	-0.76217200	3.06112800
C	1.50279100	-0.33850400	3.59623100	H	4.76579700	-0.39830400	2.72312800
C	0.94262200	3.12878300	-3.72620700	C	-0.57170800	3.07668700	-3.84243500
C	-2.20493200	-2.70138100	3.02630300	H	-1.02329300	3.83000700	-3.19854200
C	-4.76760800	-0.90064900	-1.13902600	C	-4.78921600	-2.66189800	0.54513400
C	1.75169500	2.64277500	-4.76367500	C	2.94999700	1.65627300	2.96268700
H	1.25674300	2.27140400	-5.65325100	H	1.97167200	2.11872600	2.84350400
C	4.19577000	3.44158100	-0.20074600	H	3.34857100	2.05653800	3.90553500
C	-3.05991300	0.47284800	-2.48322200	C	-2.44203000	-4.70069100	1.70394900
C	-0.38123700	-4.24334200	2.82919400	H	-3.06903800	-5.32311300	1.07582200
H	0.63069900	-4.53055500	3.09008600	C	-4.33405700	0.46117600	-1.63761600
C	3.67963400	4.35505300	-1.30631700	H	-4.20474200	1.15134000	-0.80029900
H	4.53822700	4.91215700	-1.69169800	H	-5.15347300	0.87828100	-2.23738700
H	3.01949400	5.10763600	-0.86259500	C	-5.56761400	-3.44174500	-0.31985800
C	-1.22859900	1.73586100	-3.51174700	H	-5.87037900	-4.42161100	0.03223600
C	-2.41551000	1.69554600	-2.76267600	C	-3.90571800	3.53810400	-3.06166100
C	-1.33436700	-0.70135900	-3.77637000	H	-3.41515300	3.89115700	-3.97967900

C	-4.49790700	4.70125500	-2.28137200
H	-4.69037600	2.83045300	-3.35964900
C	5.24821400	2.05417500	1.96967900
H	5.64396900	1.57487200	2.85961000
C	3.67000200	-2.11589900	3.40873200
C	6.14157500	2.57890700	1.02555400
C	-5.97476800	-2.99971400	-1.58195000
C	5.57754400	3.27271900	-0.04830300
H	6.21997700	3.74025100	-0.78584600
C	0.47597400	1.33737800	4.98022100
H	1.17457800	0.85366500	5.67120700
C	-0.90192000	1.46331500	5.61021700
H	0.87157200	2.33024600	4.73842000
C	-4.46211500	-3.19601600	1.93141700
H	-5.04128100	-4.11328600	2.07417200
H	-4.83439700	-2.49360800	2.68277000
C	-3.47619700	-1.55433800	4.72228000
H	-4.04713400	-2.48969400	4.76536600
C	-4.39564000	-0.34739200	4.82464800
H	-2.75108800	-1.57117600	5.54601000
C	0.44670700	5.59304500	-1.72353400
H	0.01938400	5.71446600	-2.72497100
C	-0.55505800	5.98450300	-0.65187000
H	1.35103300	6.21317200	-1.67281200
H	0.09518200	-2.82005700	5.23925300
H	-0.83834300	3.34218300	-4.87400500
H	-3.49686800	-0.91004500	1.81924000
H	1.68854500	3.55766500	-0.10617300
C	-0.86367900	2.35654200	6.85929200
H	-1.59819200	1.87978000	4.87480800
H	-1.27158500	0.46691500	5.87975800
C	-2.22387700	2.48822600	7.55483400
H	-0.13061500	1.95713600	7.57421300
H	-0.50410600	3.35583100	6.57855100
C	-2.18821900	3.38140400	8.80114400
H	-2.95700600	2.88915800	6.84078200
H	-2.58635100	1.48928900	7.83689400
C	-3.54827000	3.50659900	9.49363700
H	-1.45142500	2.98189600	9.51073200
H	-1.82647100	4.37974700	8.51986800
H	-4.29926500	3.93609000	8.82068600
H	-3.91838700	2.52826600	9.82059500
H	-3.48883900	4.14965900	10.37699800
C	-5.18300400	-0.32145100	6.14165300
H	-3.79601400	0.56516100	4.72601100
H	-5.09280300	-0.35822300	3.97634400
C	-6.13384200	0.87724600	6.25043800
H	-5.76025200	-1.25100000	6.24172800
H	-4.48184600	-0.30571100	6.98747500
C	-6.92671000	0.91017100	7.56232800
H	-5.55532100	1.80702000	6.15212200
H	-6.83338900	0.86231300	5.40277400
C	-7.87854300	2.10769000	7.67257800
H	-7.50284300	-0.02060500	7.66178000
H	-6.22673800	0.92515000	8.40986900
C	-8.66992200	2.13105300	8.98341300
H	-7.30136300	3.03775100	7.57654300
H	-8.57562000	2.09456000	6.82372000
H	-9.33830300	2.99634300	9.03102300
H	-9.28457700	1.23048100	9.09133500
H	-8.00102600	2.17974800	9.84994100
C	-5.54961800	5.47563800	-3.08637800
H	-4.94144800	4.31411500	-1.35560100
H	-3.68649400	5.37703400	-1.98132500
C	-6.15273900	6.65599400	-2.31436400
H	-5.09956500	5.84493900	-4.01848400
H	-6.35505400	4.79189900	-3.38838400
C	-7.20395000	7.43477900	-3.11397500
H	-6.60404700	6.28648500	-1.38274600
H	-5.34707300	7.33980600	-2.01058700
C	-7.80867900	8.61565700	-2.34447800
H	-6.75236700	7.80316100	-4.04613300
H	-8.00889700	6.75071500	-3.41811800
C	-8.85690500	9.38807600	-3.15057600
H	-8.26075900	8.24677400	-1.41372700
H	-7.00389400	9.29882000	-2.04016300
H	-9.26867900	10.22264300	-2.57457600
H	-8.42603900	9.79972300	-4.07015400
H	-9.69182700	8.73983000	-3.43924100
H	-1.43113800	5.32941800	-0.73185800
H	-0.11669200	5.80724900	0.33761000
C	-0.98314100	7.45435900	-0.77017900
C	-2.01773500	7.86551900	0.28530800
H	-0.09931500	8.10145500	-0.68415300
H	-1.39632000	7.63667000	-1.77210800
C	-2.43512400	9.33754900	0.18629500
H	-2.90695400	7.22707400	0.18743000
H	-1.61279900	7.66640800	1.28737300
C	-3.47216400	9.75191800	1.23758400
H	-2.83887600	9.53449900	-0.81717100

H	-1.54540300	9.97568500	0.28409100
C	-3.88385300	11.22316600	1.13209800
H	-4.36122700	9.11429400	1.13864600
H	-3.06820000	9.55525800	2.24011200
H	-4.62319700	11.48688400	1.89473000
H	-3.02167100	11.88678300	1.26182100
H	-4.32418400	11.44257800	0.15299900
C	-9.37102700	-5.31269700	-3.16591800
C	-9.07860200	-3.92266900	-3.76394900
C	-8.33501800	-4.08630600	-5.10519300
C	-7.00853700	-4.83807300	-4.87142800
C	-7.30248400	-6.22714900	-4.27280700
C	-8.04110200	-6.05579400	-2.93110600
H	-10.01140500	-5.89028400	-3.84453700
H	-9.91948800	-5.21001800	-2.22046400
C	-8.20116000	-3.11597100	-2.78511900
H	-10.02068900	-3.38447200	-3.92739400
H	-8.13817700	-3.10224700	-5.55094900
H	-8.96022000	-4.63852500	-5.81821300
H	-6.47528500	-4.95046100	-5.82386800
C	-6.12780600	-4.03441500	-3.89319100
H	-7.91308400	-6.81818600	-4.96712100
H	-6.36589600	-6.78002600	-4.12205000
C	-7.16352700	-5.24435200	-1.95557200
H	-8.24171300	-7.04094200	-2.49181400
H	-6.22932400	-5.78816000	-1.76223300
C	-6.84582200	-3.83805300	-2.52528800
H	-7.68479500	-5.14903800	-0.99421700
H	-8.72471400	-2.97633100	-1.83053400
H	-8.01814000	-2.11385400	-3.19185300
H	-5.88632500	-3.05951300	-4.33360100
H	-5.17287600	-4.55156400	-3.72889900
C	9.94739600	1.43996600	2.86561600
C	9.55372700	0.74850100	1.54427100
C	10.33254000	1.38524900	0.37710500
C	9.98939500	2.88555700	0.29664200
C	10.39181400	3.57831200	1.61346100
C	9.61209800	2.94307500	2.78108000
H	11.01894600	1.30293000	3.05781800
H	9.41253100	0.97984400	3.70713600
C	8.04010800	0.92160800	1.30517100
H	9.78664100	-0.32236300	1.60419300
H	10.07532100	0.88619000	-0.56644400
H	11.41174200	1.25212600	0.52391800
H	10.52975000	3.34328100	-0.54120300
C	8.47385400	3.05908900	0.06591300
H	11.47172200	3.47633100	1.77886300
H	10.17840000	4.65362800	1.55643000
C	8.09808100	3.11975200	2.54535700
H	9.88724100	3.43613800	3.72173300
H	7.84163700	4.18599000	2.49930700
C	7.65548500	2.42819500	1.22172300
H	7.54224000	2.69975600	3.39255300
H	7.48323000	0.43874500	2.11787200
H	7.74070500	0.41924900	0.37599100
H	8.19158500	2.59408500	-0.88798100
H	8.24139000	4.12875400	-0.01601400
H	-3.01316900	-1.63284200	-2.79656400
C	5.94428300	-2.50320300	4.44084100
C	7.21330300	-3.37937500	4.44716500
C	7.85239000	-3.36760300	3.04381800
C	6.84865500	-3.92863000	2.01623800
C	5.57763200	-3.05497700	2.00544400
C	4.90334700	-3.03189300	3.40759900
H	6.21181900	-1.46663400	4.20205200
H	5.48725300	-2.48729900	5.43871000
C	6.83843900	-4.82457500	4.82869600
H	7.92271400	-2.97523300	5.18004200
H	8.76998400	-3.96932200	3.04199700
H	8.14253900	-2.34465600	2.76880500
H	7.29928500	-3.91541000	1.01572400
C	6.47429100	-5.37361000	2.39844100
H	5.83326000	-2.03624900	1.69130000
H	4.86239700	-3.43853000	1.26783800
C	4.56661900	-4.49564600	3.79309200
H	3.83469200	-4.90956900	3.08609000
C	5.83287300	-5.37720700	3.79941500
H	4.10428200	-4.52431500	4.78808900
H	6.40207100	-4.84927300	5.83567600
H	7.73620600	-5.45482300	4.85513200
H	7.36648900	-6.01225800	2.38990300
H	5.77646800	-5.79168800	1.66080400
H	5.54971800	-6.40103300	4.07359000
C	-1.16438200	-4.95360100	-4.80542600
C	-0.10874700	-4.41498000	-3.81872800
C	-0.58771600	-3.07122700	-3.23263700
C	-0.80773700	-2.01951200	-4.35926100
C	-1.84581400	-2.59524200	-5.36864100
C	-1.36252500	-3.93952900	-5.95035900
H	-2.11573100	-5.12512700	-4.28426600

H	-0.84414600	-5.92204800	-5.21061400
C	1.22829900	-4.20603500	-4.55533000
H	0.02952900	-5.13241300	-2.99888400
H	0.14800400	-2.68729900	-2.51585800
H	-1.51939600	-3.22794300	-2.67657200
C	0.53649300	-1.84773000	-5.11209200
H	-2.81290900	-2.73280700	-4.87001100
H	-2.00819300	-1.86857800	-6.17528400
C	-0.02523700	-3.73102300	-6.68756700
H	-2.11668700	-4.31744100	-6.65195600
H	-0.15790100	-3.02712900	-7.51955200
C	1.02354800	-3.19013900	-5.69579900
H	0.31930000	-4.67757700	-7.12313000
H	1.59342100	-5.15901500	-4.95929800
H	1.99049500	-3.84036600	-3.85480500
H	1.29564400	-1.44381800	-4.42956900
H	0.41692100	-1.12379900	-5.92887700
H	1.97457800	-3.02534400	-6.21842500
C	-0.49291800	-9.38916500	1.28876900
C	-0.83373000	-8.50368100	0.07399000
C	0.45395100	-8.18716800	-0.71087600
C	1.43548600	-7.43359000	0.20711300
C	1.77810300	-8.31181300	1.42785700
C	0.48786900	-8.63580200	2.20828300
H	-0.04819200	-10.33474400	0.95402500
H	-1.40738300	-9.64459300	1.83961900
C	-1.48073700	-7.18986400	0.55918600
H	-1.54359400	-9.02817100	-0.57739400
H	0.21944700	-7.57896600	-1.59465100
H	0.91243500	-9.11501000	-1.07545700
H	2.35288500	-7.19711900	-0.34686400
C	0.78487900	-6.11996400	0.68654200
H	2.26369500	-9.23953300	1.10006000
H	2.49369200	-7.79189900	2.07905700
C	-0.16402700	-7.32420500	2.69144300
H	0.72955800	-9.25662100	3.07989400
H	0.51798800	-6.80227200	3.37373100
C	-0.52016100	-6.40220100	1.48704200
H	-1.07554200	-7.54023200	3.26330200
H	-2.41011600	-7.42167100	1.09489600
H	-1.75378600	-6.57221000	-0.30642300
H	0.55257500	-5.47420900	-0.17054500
H	1.49580400	-5.56887500	1.31505700
C	6.77082300	1.51847300	-6.88286200
C	5.84487800	0.38246300	-6.40184900
C	5.00005200	-0.12918100	-7.58467000
C	4.14972100	1.02961600	-8.14090600
C	5.07542000	2.16038700	-8.63058000
C	5.91950400	2.67369100	-7.44816700
H	7.45684200	1.14418500	-7.65298400
H	7.39212600	1.87766600	-6.05173600
C	4.91121100	0.91519400	-5.29580200
H	6.44837800	-0.43862500	-5.99491500
H	4.35123500	-0.95279200	-7.25816400
H	5.65230700	-0.53004600	-8.37060800
H	3.53440700	0.66908100	-8.97435600
C	3.21990800	1.56585400	-7.03238000
H	5.72898200	1.79272500	-9.43153500
H	4.48104700	2.97972200	-9.05531700
C	4.98535700	3.21154100	-6.34519600
H	6.57595200	3.48504500	-7.78611000
H	4.38382400	4.04556600	-6.72895200
C	4.03671400	2.09111500	-5.82397400
H	5.58493500	3.61118200	-5.51860300
H	5.50924500	1.24899900	-4.43888200
H	4.25604400	0.11261700	-4.93151300
H	2.54275200	0.76497700	-6.70725100
H	2.59475200	2.37114500	-7.43952700
H	4.81871300	3.18487500	-3.44302400
C	-1.51242800	2.11019700	0.86314300
N	-0.29166500	1.22159800	0.99154500
C	-0.35143800	0.09010400	-0.02962900
H	0.57034800	1.77937200	0.84063800
C	1.21467900	-1.87960400	0.15714700
C	2.39543900	-2.53634800	-0.19217200
C	3.34326100	-1.89914900	-0.99345900
C	3.10728300	-0.60091600	-1.45103000
C	1.92059300	0.04826900	-1.11762100
C	0.96783600	-0.58182800	-0.30371000
H	0.47920800	-2.38589200	0.77464400
H	2.56863500	-3.54789400	0.15941600
H	4.26095400	-2.41274600	-1.26374500
H	3.83591200	-0.09760400	-2.07847300
H	1.72723400	1.04163300	-1.50970300
C	-3.32845700	3.98780200	3.61498700
C	-3.02817600	3.07834900	2.59920000
C	-1.74837500	3.04001500	2.02953500
C	-0.76532500	3.91937200	2.50721600
C	-1.06209800	4.81667800	3.53444200
C	-2.34510100	4.85904500	4.08556800

H	-4.32857900	4.01382700	4.03676400
H	-3.79267100	2.39598100	2.23787700
H	0.23190800	3.90975300	2.07689500
H	-0.29287900	5.49265800	3.89610000
H	-2.57625700	5.56828500	4.87433200
H	-0.73521900	0.54960300	-0.94181900
H	-1.10730100	-0.60482800	0.33714200
H	-2.36050300	1.43462100	0.74526800
H	-1.38506800	2.66017000	-0.07360200
H	-0.21877500	0.86077000	1.96019800

Energy = -6070.07984 a.u.

0 imaginary frequency

Atomic coordinates of 16a^{+}⊂15g

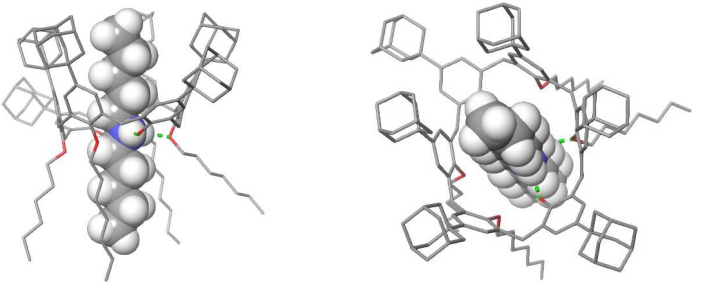

Figure 4.96. (a) Side view and (b) top view of complex 16a^{+}⊂15g.

O	-1.08033400	-3.49913700	1.12055800
O	2.55843800	-3.07442700	2.37696500
O	-2.65013300	-1.36732500	-2.11363200
O	-1.46851600	-0.10852500	-4.24865800
O	2.44932600	0.02846700	-3.95335900
O	3.52759200	-1.35961900	0.27467100
C	2.34972100	-1.99610700	3.24478400
C	1.55127700	3.34458100	-2.62956500
H	0.82810700	4.12865700	-2.82132200
C	3.41910800	-1.11154300	3.46195600
C	-2.24040300	-1.70866600	4.12179600
H	-1.88665900	-1.51788300	5.12731200
C	1.49443700	2.18504000	-3.40982500
C	3.18969100	0.02627400	4.23482700
C	2.45581000	1.18408000	-3.17656300
C	1.08591900	-1.78028300	3.81675400
C	-1.89740900	1.22375900	-4.12713500
C	-4.49076900	-1.69838300	-0.61947900
C	0.91154400	-0.61997300	4.58435300
H	-0.05981900	-0.44445100	5.02563500
C	5.27449500	-0.52866700	1.75203900
C	-3.16147100	-2.32255600	1.54790200
C	-1.47015300	3.57995600	-4.11400700
H	-0.77741400	4.40201600	-4.26272300
C	4.81366600	-1.39386200	2.91405800
H	5.52901400	-1.25984600	3.73132300
H	4.88779900	-2.44735500	2.62702600
C	-1.39466200	-2.41496400	3.25352400
C	-1.89480900	-2.76073300	1.98743200
C	-3.51731400	-1.28098400	3.74674900
C	4.63188600	-0.56977700	0.50438000
C	-3.93467800	-1.57691300	2.43958300
C	-0.97431300	2.27814100	-4.23844800
C	-5.82780400	-1.44925700	-0.29393700
H	-6.24922500	-1.99028600	0.54797300
C	3.40601900	1.31027700	-2.14854600
C	-2.81690400	3.86628700	-3.83849000
C	0.49366400	2.03169100	-4.55505500
H	0.61314100	1.02638400	-4.95393100
C	1.94036600	0.30366500	4.80783600
C	-3.95711700	-1.07009700	-1.76053800
C	-3.25668200	1.45710400	-3.88589700
C	5.11143200	0.20515700	-0.56621500
C	3.41595800	2.48966400	-1.39645300
H	4.15968500	2.58210300	-0.61649500
C	-0.00513500	-2.84716800	3.69773300
H	0.35126700	-3.60559100	3.00684800
C	-4.75304500	-0.22277100	-2.54793400

C	4.42941000	0.19769600	-1.91733400
H	3.94437300	-0.76519800	-2.09067500
H	5.20817700	0.28222000	-2.68715800
C	-3.68790600	2.77912800	-3.72209100
H	-4.74214500	2.94469300	-3.53172900
C	-3.68955700	-2.72240700	0.16624800
H	-2.85332600	-3.05579500	-0.44778300
H	-4.33376000	-3.60250400	0.29889500
C	-6.07294900	0.01978200	-2.14810500
H	-6.66962400	0.67164900	-2.77595600
C	-1.43816900	-4.89576100	0.94144700
H	-2.52215500	-4.97552100	0.81215600
C	-0.98000700	-5.80882200	2.07309400
H	-0.96763200	-5.18769800	-0.00211900
C	6.25118800	0.98782100	-0.36403000
H	6.62003200	1.56022700	-1.21106800
C	2.52012800	3.53944400	-1.63544800
C	6.92709200	1.05682700	0.86219700
C	-6.64670300	-0.57564000	-1.02169700
C	6.40381900	0.28534800	1.90436800
H	6.88664100	0.28975300	2.87533700
C	3.28699100	0.09275600	-5.12488600
H	2.94065500	0.90535100	-5.77880400
C	3.22122000	-1.24537400	-5.84407900
H	4.31846400	0.32490500	-4.82948500
C	-4.27903500	0.32649800	-3.88717400
H	-5.16507500	0.68919100	-4.41587900
H	-3.90297700	-0.50611500	-4.49045100
C	-1.47060600	-0.62690400	-5.60568700
H	-2.44081400	-0.41345500	-6.07052900
C	-1.19863100	-2.12138200	-5.56242900
H	-0.70304300	-0.10120400	-6.18516900
C	3.01672300	-4.30222300	2.99086700
H	2.22057000	-4.69843000	3.63373600
C	3.37371300	-5.28856900	1.89013900
H	3.88354100	-4.09180500	3.62981500
H	0.78135000	2.72755700	-5.35406600
H	-0.10075600	-3.32702300	4.68116300
H	-2.38122300	-0.94301700	-2.95955600
H	3.38785700	-2.00881700	0.98925500
C	4.08144500	-1.27970600	-7.11397700
H	3.54392700	-2.03302800	-5.15188900
H	2.17423800	-1.45854100	-6.09813700
C	4.00997300	-2.62155900	-7.85341000
H	3.76646100	-0.47496900	-7.79280500
H	5.12697700	-1.06540700	-6.85305800
C	4.87025900	-2.66827900	-9.12211900
H	4.32198300	-3.42757800	-7.17387400
H	2.96389300	-2.83512700	-8.11727400
C	4.79052300	-4.01017600	-9.85551900
H	4.55962100	-1.86115000	-9.79911300
H	5.91489500	-2.45656600	-8.85759900
H	5.12926800	-4.83303000	-9.21597900
H	3.76306800	-4.23336600	-10.16476400
H	5.41438800	-4.01078000	-10.75448900
C	-1.19868400	-2.75517900	-6.96063800
H	-0.22963600	-2.28975600	-5.07644300
H	-1.95875100	-2.60513300	-4.93466900
C	-0.94362200	-4.26753000	-6.93608000
H	-2.16164000	-2.55862800	-7.45151200
H	-0.43486700	-2.26827700	-7.58272000
C	-0.93418300	-4.90785500	-8.32932800
H	0.01756500	-4.46470400	-6.43997800
H	-1.71142300	-4.75358500	-6.31757900
C	-0.68374100	-6.42077200	-8.30514700
H	-1.89292500	-4.70722600	-8.82796100
H	-0.16465800	-4.42297700	-8.94684700
C	-0.67334300	-7.05293900	-9.69992500
H	0.27380900	-6.62043500	-7.80487800
H	-1.45426500	-6.90431200	-7.68936200
H	-0.49293700	-8.13107300	-9.64806900
H	-1.63019500	-6.90060400	-10.21146200
H	0.11013300	-6.61494600	-10.32837900
C	-1.39916800	-7.26603100	1.82760300
H	0.11102400	-5.75058300	2.16946100
H	-1.40699400	-5.45856100	3.02045300
C	-0.93649800	-8.22137200	2.93514700
H	-2.49279000	-7.32060100	1.73607700
H	-0.99589900	-7.60737600	0.86363600
C	-1.35593000	-9.67729000	2.69952900
H	0.15810000	-8.16862300	3.02486200
H	-1.33673500	-7.87846100	3.89945400
C	-0.88924900	-10.63458300	3.80325000
H	-2.45046800	-9.73030100	2.61311100
H	-0.95935100	-10.01838700	1.73252800
C	-1.31286400	-12.08621000	3.56154900
H	0.20471000	-10.58132000	3.88893700
H	-1.28554500	-10.29298500	4.76900400
H	-0.96485000	-12.74243500	4.36519200
H	-2.40343400	-12.17732700	3.50737700

H	-0.90273700	-12.46796500	2.61981600
H	2.49674700	-5.43014400	1.24505600
H	4.15774000	-4.84985100	1.25932900
C	3.84310100	-6.64114800	2.44227100
C	4.22155600	-7.64263200	1.34377400
H	4.70662800	-6.48627700	3.10360100
H	3.05262300	-7.07395700	3.07147300
C	4.68772000	-8.99776800	1.88909900
H	3.35914400	-7.79505200	0.67904600
H	5.01450700	-7.21010100	0.71766900
C	5.06939700	-10.00039100	0.79304200
H	3.89442200	-9.43021900	2.51552000
H	5.54857000	-8.84435500	2.55508800
C	5.53418600	-11.35072100	1.34597500
H	4.20883300	-10.15332000	0.12738700
H	5.86245600	-9.56767100	0.16824500
H	5.79890200	-12.04228900	0.54015500
H	6.41535300	-11.23470200	1.98674300
H	4.74989100	-11.82499600	1.94656200
C	-11.05062100	-0.49785400	-1.11994200
C	-10.34845100	-1.49137400	-0.17414500
C	-10.36385400	-0.93178600	1.26302800
C	-9.62722400	0.42289400	1.29702600
C	-10.32901700	1.41536500	0.34992200
C	-10.30604800	0.85122500	-1.08411600
H	-12.09613100	-0.36017300	-0.81675000
H	-11.06535100	-0.89537000	-2.14311300
C	-8.88944500	-1.69344600	-0.63162400
H	-10.86798600	-2.45733200	-0.19976800
H	-9.88338600	-1.64091700	1.95021900
H	-11.39798000	-0.80702000	1.60792500
H	-9.63265300	0.82065100	2.31993800
C	-8.16712700	0.22505300	0.84163200
H	-11.36416800	1.58101600	0.67389800
H	-9.82499100	2.39021500	0.38213700
C	-8.84533100	0.64597400	-1.53647000
H	-10.79186400	1.55915800	-1.76694400
H	-8.32375400	1.61220100	-1.54130900
C	-8.10512200	-0.34793000	-0.60480700
H	-8.83510700	0.26940800	-2.56754600
H	-8.86268000	-2.10716100	-1.64791100
H	-8.39881700	-2.42764100	0.01895800
H	-7.65583500	-0.45541900	1.53411500
H	-7.62419800	1.17869900	0.87714200
C	10.17635600	3.78656200	-0.21513700
C	9.11342700	4.29533100	0.78004600
C	9.67542300	4.22644100	2.21323100
C	10.03707000	2.76599800	2.54734800
C	11.10608000	2.26063800	1.55857000
C	10.54489300	2.32799800	0.12490000
H	11.06997200	4.42186700	-0.16955500
H	9.79344900	3.85011400	-1.24237800
C	7.85233800	3.41288700	0.68031100
H	8.84592100	5.33142000	0.53669300
H	8.93445000	4.60661300	2.92880500
H	10.56288600	4.86552600	2.30383400
H	10.42493800	2.70702900	3.57194600
C	8.77645000	1.88297400	2.43989800
H	12.01416800	2.87139900	1.63966500
H	11.39233100	1.22973400	1.80458700
C	9.28622500	1.44260300	0.02356300
H	11.29779700	1.96261500	-0.58472700
H	9.53669700	0.39754100	0.24706300
C	8.18155400	1.92677200	1.00906000
H	8.90418600	1.46041900	-1.00438100
H	7.43071000	3.48794200	-0.32953500
H	7.07984400	3.77361100	1.37230100
H	8.02706600	2.22474000	3.16611000
H	9.03349900	0.84939400	2.70573400
H	-4.90240900	-1.22445900	2.10478300
C	2.92001400	6.01586500	-1.92555000
C	2.98788800	7.39098200	-1.23110000
C	4.10333800	7.37495800	-0.16798000
C	3.79587900	6.28253800	0.87521400
C	3.72316700	4.90816000	0.17778600
C	2.60808300	4.88472800	-0.89932800
H	3.87054700	5.79574900	-2.42821300
H	2.14963200	6.03348400	-2.70615700
C	1.63566600	7.69140700	-0.55316200
H	3.20360800	8.16096600	-1.98238100
H	4.17561400	8.35485600	0.32072700
H	5.07456500	7.18279600	-0.64210200
H	4.59441800	6.25591000	1.62719900
C	2.44944600	6.58901700	1.55895000
H	4.69367400	4.68517700	-0.28262300
H	3.53730100	4.12549900	0.92494400
C	1.26511400	5.22522200	-0.19342200
H	1.03931300	4.44600000	0.54423600
C	1.33328000	6.60295000	0.49666700
H	0.44340500	5.21943900	-0.91999100

H	0.83513000	7.72477300	-1.30451200
H	1.66373700	8.67897700	-0.07552000
H	2.49709400	7.55776900	2.07236900
H	2.23277800	5.83193100	2.32475200
H	0.36831600	6.81061900	0.97647700
C	-7.12224500	0.72135400	5.21897700
C	-5.84567900	1.57216800	5.06114300
C	-4.85435600	0.84608300	4.12855300
C	-4.46430600	-0.54618500	4.70579200
C	-5.76805700	-1.37789600	4.89893000
C	-6.75739800	-0.64719900	5.82916300
H	-7.60724000	0.58342000	4.24337300
H	-7.84405200	1.24038300	5.86210900
C	-5.19358400	1.78147200	6.44161300
H	-6.10203600	2.54422800	4.62143100
H	-3.94774500	1.45041600	3.99754600
H	-5.30137200	0.73057500	3.13393700
C	-3.84219500	-0.31836400	6.10754900
H	-6.24215400	-1.56026700	3.92693000
H	-5.51201100	-2.36172000	5.31302300
C	-6.10494400	-0.43717000	7.20917000
H	-7.66291200	-1.25723800	5.93672100
H	-5.86012300	-1.40597400	7.66366300
C	-4.82855400	0.41065100	7.04361200
H	-6.80610800	0.06473000	7.88765700
H	-5.88132400	2.31598900	7.10887600
H	-4.29454500	2.40451200	6.34509500
H	-2.92155700	0.27330700	6.01672500
H	-3.56341700	-1.28163400	6.55418400
H	-4.35002400	0.55173100	8.02060500
C	-4.94662400	7.64136200	-4.62253900
C	-5.22573400	6.92097000	-3.28880700
C	-4.43384800	7.60443000	-2.15702000
C	-2.92757600	7.52408400	-2.47148600
C	-2.64070300	8.23928900	-3.80763300
C	-3.44050900	7.56055300	-4.93830500
H	-5.26486100	8.68949500	-4.55929600
H	-5.52816500	7.18009500	-5.43130000
C	-4.79667000	5.44327400	-3.40168900
H	-6.29889800	6.96136000	-3.06497000
H	-4.64684400	7.11633300	-1.19686400
H	-4.74488100	8.65195500	-2.05783300
H	-2.35468900	8.00157700	-1.66651200
C	-2.50390000	6.04513000	-2.57949200
H	-2.91656000	9.29871000	-3.73441800
H	-1.56616300	8.20601500	-4.03155000
C	-3.01701300	6.08178300	-5.05178600
H	-3.23406700	8.06453200	-5.89057600
H	-1.95330900	6.02280200	-5.31217000
C	-3.28359500	5.32288200	-3.71766300
H	-3.56701600	5.58950100	-5.86409600
H	-5.38288500	4.95571500	-4.19133400
H	-5.02475300	4.92206900	-2.46263400
H	-2.68647700	5.52607000	-1.62924700
H	-1.42507400	5.98642300	-2.76888800
C	2.95270600	3.99123900	6.93428700
C	1.98753400	4.09953500	5.73590500
C	0.54099800	4.22931300	6.25056300
C	0.18577400	2.98436500	7.08642500
C	1.14368100	2.88117000	8.28963300
C	2.59099700	2.75119500	7.77696700
H	2.89113600	4.89712900	7.55037100
H	3.98918100	3.91807400	6.57953900
C	2.11036100	2.83528900	4.86085000
H	2.24628100	4.97872900	5.13201600
H	-0.15410400	4.32997900	5.40644200
H	0.43499400	5.13573400	6.85985700
H	-0.84867900	3.06249000	7.44392400
C	0.31656800	1.71850700	6.21356100
H	1.04519700	3.76865400	8.92732700
H	0.88226300	2.01322100	8.90886200
C	2.71613100	1.48456600	6.90631800
H	3.27905200	2.66927200	8.62746700
H	2.47789900	0.59085800	7.49733900
C	1.76148300	1.55579800	5.67671200
H	3.75298900	1.37004600	6.56864500
H	3.12875300	2.76131100	4.46171800
H	1.43848800	2.90576400	3.99486000
H	-0.38940000	1.77646000	5.37405000
H	0.03778000	0.83912000	6.80863900
H	4.02163600	0.70574900	4.39597900
C	-1.64699400	3.99182500	2.23232900
H	-0.70091300	4.18984300	2.74868600
H	-2.45750600	4.33723600	2.88191200
C	-1.79992800	2.50595300	1.89746400
H	-1.66287000	4.60729000	1.32612300
H	-2.76779700	2.34027900	1.40613100
C	-0.68187000	1.96170700	0.99898500
H	-1.82813400	1.91915900	2.82495100
C	-0.90100000	0.48854000	0.63142900

H	-0.62084300	2.56128400	0.08177100
H	0.28537900	2.07400000	1.50737700
C	0.20905900	-0.05398100	-0.26354500
H	-0.96613600	-0.11135700	1.54552700
H	-1.86473400	0.38875600	0.11660900
N	-0.10855300	-1.44586700	-0.75420300
H	0.33822000	0.56189200	-1.15742900
H	1.17187800	-0.11362200	0.24912800
C	0.90943800	-1.99286000	-1.72216700
C	0.63413400	-3.45624600	-2.05660100
H	0.87934800	-1.35882800	-2.61093100
H	1.88503600	-1.86992700	-1.24755000
C	1.68968700	-4.02988300	-3.01207900
H	0.63312700	-4.04393200	-1.12995500
H	-0.36545900	-3.55669700	-2.49992700
C	1.44578200	-5.50257200	-3.36456700
H	1.71292800	-3.43278500	-3.93297600
H	2.68326400	-3.92346600	-2.55597500
C	2.51024200	-6.07743000	-4.30337400
H	1.41432200	-6.09540000	-2.44024600
H	0.45478900	-5.60482000	-3.82667500
H	2.30866400	-7.12693500	-4.53768600
H	2.54423500	-5.52644700	-5.25007900
H	3.50772800	-6.02269500	-3.85359100
H	-0.20811100	-2.10493800	0.03531600
H	-1.04430800	-1.42881200	-1.20426700

Energy = -5922.50258 a.u.

0 imaginary frequency

Atomic coordinates of 16b⁺⊂15a

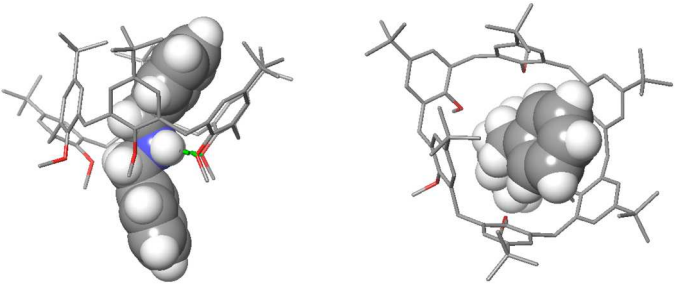

Figure 4.97. (a) Side view and (b) top view of complex **16b⁺⊂15a**.

O	2.10354300	-4.25711300	2.20165200
O	-1.81854600	-3.24451700	2.40789200
O	3.90857900	-0.42692100	2.12990900
O	2.90749100	3.39136700	2.35844800
O	-0.88652500	2.93951600	2.27744800
O	-3.08435800	-0.00604400	2.59311500
C	-2.39402300	-3.72098000	1.22834300
C	-1.13915000	5.30341500	-0.53504700
H	-0.49925200	6.01861200	-1.03956400
C	-3.68707800	-3.31365800	0.86757300
C	0.85023500	-3.92905200	-1.24081400
H	-0.04707600	-4.16368800	-1.80261800
C	-0.58531600	4.56581500	0.52022400
C	-4.24086400	-3.83333300	-0.31228100
H	-5.24643300	-3.52963200	-0.57475400
C	-1.42103500	3.67660100	1.21272000
C	-1.65720800	-4.60850700	0.41986700
C	2.94847000	3.34766800	0.96651900
C	5.17805500	-1.80803300	0.61064300
C	-2.26589800	-5.10828900	-0.73363200
H	-1.70940200	-5.82561700	-1.32997600
C	-4.78929200	-0.98510300	1.18589400
C	3.14541600	-3.32609900	0.23458100
C	2.00965900	3.94577900	-1.16765000
H	1.24217500	4.46355500	-1.73412000
C	-4.50373400	-2.37409500	1.75064400
H	-5.46786800	-2.85514800	1.95346700
H	-3.98898200	-2.27092000	2.70281100
C	0.88986600	-4.27291900	0.11320000
C	2.05452700	-3.96649900	0.84314800
C	1.92531200	-3.30587500	-1.89264800
C	-4.09061000	0.15105700	1.63021000

C	3.05622200	-3.00664900	-1.12565600
H	3.90329300	-2.51191300	-1.58316200
C	1.93869800	3.99274000	0.22712000
C	6.20210300	-1.90588900	-0.34233700
H	6.44780800	-2.89423300	-0.71500500
C	-2.77875100	3.52287800	0.87719500
C	3.03706800	3.27567800	-1.84946700
C	0.85796700	4.80016200	0.94170600
H	0.96266900	4.61025900	2.00815300
C	-3.56116300	-4.74009200	-1.12952900
C	4.86737700	-0.54344500	1.12450400
C	3.98121500	2.64499100	0.32637900
C	-4.38139600	1.43592000	1.14689200
C	-3.27281400	4.28229000	-0.18700600
H	-4.32566300	4.19649400	-0.43202000
C	-0.24900800	-5.03563800	0.79011500
H	-0.10246100	-4.95245900	1.86597500
C	5.51046000	0.61203800	0.65304700
C	-3.70724300	2.67020500	1.74095800
H	-3.14447000	2.35108300	2.61309900
H	-4.50601100	3.33093100	2.10199100
C	3.99710500	2.61787700	-1.07367200
H	4.79484700	2.06824500	-1.55673600
C	-4.17904800	-5.34825300	-2.40260700
C	6.52798100	0.46100000	-0.29331300
H	7.04605300	1.35538700	-0.62855600
C	2.65973000	-5.53595200	2.52230200
H	2.64239100	-5.61938400	3.61093500
H	2.06841200	-6.35071000	2.08734600
C	-5.40416000	1.55991800	0.19685100
H	-5.65577900	2.55313200	-0.15173600
C	-2.47979000	5.17954500	-0.91637800
C	-6.13370200	0.46442900	-0.27340000
C	6.90924300	-0.79002600	-0.80293700
C	-5.80529100	-0.79621000	0.24641400
H	-6.37946600	-1.66252300	-0.06656700
C	-1.00879700	3.59835800	3.55064700
H	-0.56244800	2.93837000	4.29327500
H	-2.05989700	3.77950300	3.79859700
C	1.84389700	-3.01244300	-3.40360500
C	-7.28777700	0.60170400	-1.28512600
C	-3.11050600	6.02513600	-2.04023200
C	0.62453500	-2.11170100	-3.70579500
H	-0.31628300	-2.57377700	-3.39427900
H	0.55676600	-1.91690700	-4.78169900
H	0.70580600	-1.14864400	-3.19192000
C	3.64911700	4.47181400	2.93512100
H	4.71322500	4.40845900	2.68058100
H	3.26297600	5.44251000	2.60219500
C	1.69094800	-4.34946300	-4.16853000
H	2.54300500	-5.01032000	-3.97943300
H	1.63541100	-4.16724900	-5.24729500
H	0.78221600	-4.88344900	-3.87463400
C	-3.74637700	5.09845200	-3.10275100
H	-4.22099700	5.69479100	-3.88910200
H	-4.51285100	4.44632700	-2.67383400
H	-2.99039600	4.46185400	-3.57416300
C	-2.07689100	-4.08829100	3.53794000
H	-3.14507900	-4.10769000	3.78459300
H	-1.74090300	-5.11495100	3.35587700
C	-5.59784900	-4.81544600	-2.67733900
H	-6.29074400	-5.05840100	-1.86517300
H	-5.99157500	-5.27235400	-3.59014700
H	-5.60567300	-3.73004400	-2.82479500
C	-3.29152200	-5.00571700	-3.62274500
H	-3.21070100	-3.92209400	-3.75954500
H	-3.72099500	-5.43071100	-4.53613000
H	-2.27925800	-5.40744400	-3.51783700
C	3.10540900	-2.30195000	-3.92984000
H	2.99868600	-2.11041400	-5.00197800
H	4.00530600	-2.91024400	-3.79337000
H	3.26589300	-1.33777700	-3.43567400
C	3.10856900	3.32992200	-3.38822700
C	-4.26330900	-6.88555200	-2.24630700
H	-3.27803900	-7.33532800	-2.09275300
H	-4.69633000	-7.33523200	-3.14612200
H	-4.89305000	-7.15955400	-1.39385200
C	-4.20756500	6.93462800	-1.43576800
H	-3.78785800	7.60598200	-0.67987800
H	-5.00395500	6.35328000	-0.96167000
H	-4.66555400	7.54907000	-2.21822200
C	-2.07809000	6.92365900	-2.74716300
H	-1.63084700	7.65169600	-2.06287600
H	-2.56778200	7.48697400	-3.54712700
H	-1.27159300	6.33941200	-3.20295400
C	-8.60370700	0.11546900	-0.63193500
H	-8.84615600	0.71204300	0.25328300
H	-8.54450100	-0.93234200	-0.32307200
H	-9.43477700	0.20569000	-1.33948000
C	-7.49125300	2.05652400	-1.74859200

H	-7.75633700	2.71798600	-0.91741100
H	-8.30958100	2.10022300	-2.47348900
H	-6.59714200	2.45761100	-2.23783400
C	4.23856200	2.44850800	-3.95315300
H	4.23794500	2.50620000	-5.04589200
H	4.11238300	1.39638600	-3.67672300
H	5.22498400	2.77633900	-3.61051500
C	1.77545500	2.85151900	-4.00666700
H	0.93485500	3.48382900	-3.70596700
H	1.54524800	1.82345500	-3.71003300
H	1.83346900	2.88414000	-5.09984400
C	-6.98731700	-0.26119600	-2.53346600
H	-7.80298400	-0.17690600	-3.25934500
H	-6.87861400	-1.32050500	-2.28187600
H	-6.06402300	0.06600500	-3.02288000
C	3.37208700	4.79258300	-3.82178400
H	2.57698700	5.46396800	-3.48320400
H	3.42734100	4.86330700	-4.91357800
H	4.31740900	5.15996700	-3.40981700
H	1.07443000	5.86518200	0.78834000
C	8.06278400	-0.89003900	-1.81864600
C	7.72440600	-0.04996900	-3.07289400
C	9.35987600	-0.34635000	-1.17317100
C	8.32140000	-2.34017300	-2.26886100
H	9.14688800	-2.36027900	-2.98676200
H	8.60115600	-2.98514300	-1.42963000
H	7.44700700	-2.77753400	-2.76217400
H	8.53838000	-0.11279400	-3.80300900
H	6.80981500	-0.41246300	-3.55373900
H	7.58028200	1.00718900	-2.83055100
H	10.19152000	-0.40564600	-1.88344400
H	9.25725700	0.69959800	-0.86928300
H	9.63006400	-0.92767600	-0.28577300
H	-0.14275300	-6.09929600	0.53878800
H	-1.51780800	-3.67586400	4.38027700
H	3.69413100	-5.62414600	2.17062800
H	3.53311900	4.38942100	4.01795000
H	-0.47995800	4.55684100	3.54756100
C	-3.55363200	0.08116600	3.94867900
H	-2.67715400	0.00230300	4.59273700
H	-4.05497000	1.03791300	4.12784100
H	-4.25354800	-0.72984000	4.17605400
C	4.47199600	-0.55729500	3.44338400
H	5.20901700	0.23097400	3.63668400
H	3.64938500	-0.46540700	4.15375000
H	4.95896900	-1.53043700	3.57227800
C	5.09686200	1.98774700	1.13865700
H	5.97709300	2.64299500	1.11108100
H	4.77104900	1.93730500	2.17733400
C	4.41108200	-3.04143800	1.04156300
H	5.08023700	-3.90791000	0.95731200
H	4.12597100	-2.97322100	2.09221900
C	0.65364100	-0.66735800	2.78357500
N	-0.27596000	0.01398700	1.79107100
C	0.09918500	-0.39220100	0.37016800
H	-1.26099700	-0.23170200	2.00469200
C	-0.66426100	1.29994000	-1.33742600
C	-1.51521100	1.69504600	-2.36905400
C	-2.56257400	0.86536400	-2.77087400
C	-2.75884700	-0.36215800	-2.13707100
C	-1.90996400	-0.75843700	-1.10491500
C	-0.85883700	0.07163000	-0.69349200
H	0.16151900	1.94160700	-1.04619500
H	-1.35334100	2.64763100	-2.86127000
H	-3.21724700	1.17113400	-3.58163000
H	-3.56766500	-1.01610200	-2.44573900
H	-2.05436700	-1.72382000	-0.63223600
C	1.30738900	1.53644900	5.82056800
C	1.31935400	1.05154700	4.51095400
C	0.5861000	-0.09853200	4.17823200
C	-0.14627600	-0.75108900	5.17841700
C	-0.15900700	-0.26395000	6.48637100
C	0.56870900	0.88245700	6.80919600
H	1.88439300	2.42157700	6.07130300
H	1.90320900	1.56671000	3.75113800
H	-0.69565000	-1.65463400	4.93069900
H	-0.72377800	-0.78516100	7.25329800
H	0.56951000	1.25773300	7.82790400
H	0.17003200	-1.48148100	0.38675300
H	1.10139800	0.01162200	0.21102800
H	1.66148900	-0.56569300	2.37310000
H	0.37600700	-1.72303300	2.76506300
H	-0.24507800	1.04311800	1.90015000

Energy = -3850.69576 a.u.

0 imaginary frequency.

Non-covalent interactions

NBO second-order perturbation theory analysis was performed via single point energy calculations using the M06-2X/dgdzvp//M06-2X/dgdzvp:PM6 method. The non-covalent interaction (NCI) index was analyzed with the Multiwfn program[58] and its plot was graphed with VMD program.[59] The reduced density gradient (RDG) analysis-based NCI results for **16b⁺⊂15f**, and **16a⁺⊂15f**. are reported in Figure S60. The strongest interactions associated with the many hydrogen bonds existing between phenolic oxygen and ammonium site.

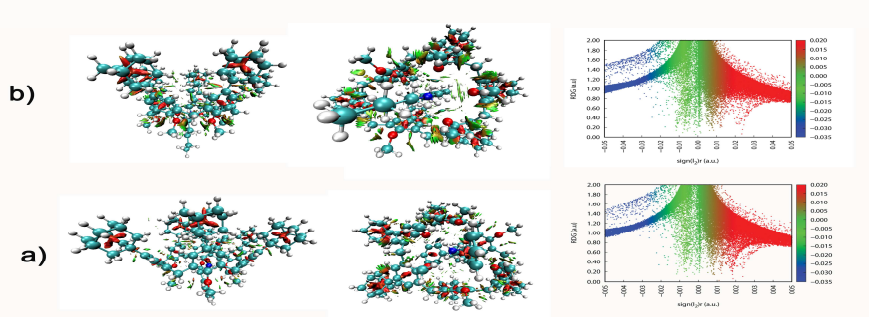

Figure 4.98. Non-covalent interaction plot and plot of the reduced density gradient (RDG) versus the electron density multiplied by the sign of the second Hessian eigenvalue (gradient isosurfaces (s = 0.6 a.u.) for **16b⁺⊂15f** (a) and **16a⁺⊂15f** (b). In the coloring scheme blue and green colors represent strong and medium interactions (H-bonding and van der Waals).

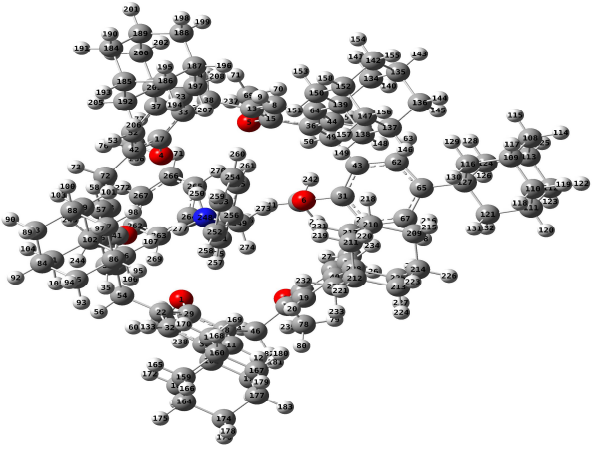

Figure 4.99. Minimized Structure with labels of **16b⁺ ⊂15f**.

[58] Lu, T.; Chen, F. W. *J. Comput. Chem.* **2012**, *33*, 580-592.
[59] Humphrey, W. ; Dalke, A.; Schulten, K.; *J. Mol. Graph.* **1996**, *14*, 33-38.

Table 4.5. Secondary orbital interactions for **16b**$^{+}$ ⊂ **15f**.

n	*Type Donor*	*Type Acceptor*	*E Kcal/mol*
1	BD (2) C 7 - C 16	/***. BD*(1) C 249 - H 274	0.56
2	BD (2) C 8 - C 64	/***. BD*(1) C 255 - H 261	0.41
3	BD (2) C 13 - C 15	/***. BD*(1) C 255 - H 261	0.08
4	BD (2) C 17 - C 33	/***. BD*(2) C 254 - C 255	0.21
5	BD (2) C 17 - C 33	/***. BD*(1) C 255 - H 261	0.08
6	BD (2) C 18 - C 34	/***. BD*(2) C 251 - C 256	0.09
7	BD (2) C 18 - C 34	/***. BD*(2) C 252 - C 253	0.05
8	BD (2) C 19 - C 40	/***. BD*(1) C 249 - H 274	0.09
9	BD (2) C 22 - C 32	/***. BD*(1) C 251 - H 257	0.22
10	BD (2) C 28 - C 29	/***. BD*(1) C 251 - H 257	0.30
11	BD (1) C 59 - H 61	/***. BD*(1) C 263 - H 269	0.61
12	BD (1) C 59 - H 238	/***. BD*(1) C 263 - H 269	0.08
13	BD (1) C 150 - H 151	/***. BD*(1) C 254 - H 260	0.11
14	BD (1) C 197 - H 207	/***. BD*(1) C 254 - H 260	0.15
15	BD (1) C 239 - H 246	/***. BD*(2) C 263 - C 264	0.17
16	BD (1) C 240 - H 241	/***. BD*(2) C 265 - C 266	0.15
17	CR (1) O 3	/***. BD*(1) N 248 - H 277	0.14
18	LP (1) O 1	/***. BD*(1) C 247 - H 275	0.54
19	LP (1) O 1	/***. BD*(1) N 248 - H 277	0.17
20	LP (2) O 1	/***. BD*(1) C 247 - H 275	0.25
21	LP (1) O 2	/***. BD*(1) C 247 - H 275	0.07
22	LP (1) O 3	/***. BD*(1) N 248 - H 277	0.09
23	LP (2) O 3	/***. BD*(1) N 248 - H 277	10.36
24	LP (1) O 4	/***. BD*(1) N 248 - H 250	0.27
25	LP (2) O 4	/***. BD*(1) N 248 - H 250	8.34
26	LP (1) O 5	/***. BD*(1) C 265 - H 270	1.76
27	LP (2) O 5	/***. BD*(1) C 265 - H 270	0.11
28	LP (1) O 6	/***. BD*(1) C 247 - H 276	2.62
29	LP (2) O 6	/***. BD*(1) C 247 - H 276	0.95
30	BD*(2) C 8 - C 64	/***. BD*(1) C 255 - H 261	0.12
	unit 2 to unit 1		
31	BD (1) N 248 - H 277	/***. BD*(1) O 3 - C 41	0.08
32	BD (1) N 248 - H 277	/***. BD*(1) O 3 - C 239	0.11
33	BD (2) C 251 - C 256	/***. BD*(2) C 41 - C 48	0.05
34	BD (2) C 251 - C 256	/***. BD*(1) C 217 - H 231	0.12
35	BD (2) C 252 - C 253	/***. BD*(1) C 211 - H 219	0.06
36	BD (1) C 252 - H 258	/***. BD*(1) C 96 - H 107	0.06
37	BD (1) C 254 - H 260	/***. BD*(1) C 150 - H 151	0.10
38	BD (1) C 254 - H 260	/***. BD*(1) C 197 - H 207	0.09
39	BD (1) C 255 - H 261	/***. BD*(2) C 8 - C 64	0.07
40	BD (2) C 263 - C 264	/***. BD*(1) C 239 - H 246	0.47
41	BD (1) C 263 - H 269	/***. BD*(1) C 59 - H 61	0.41
42	BD (1) C 263 - H 269	/***. BD*(1) C 239 - H 246	0.14
43	BD (1) C 264 - C 265	/***. RY*(1) H 236	0.07
44	BD (2) C 265 - C 266	/***. BD*(1) C 75 - H 236	1.16
45	BD (2) C 265 - C 266	/***. BD*(1) C 240 - H 241	0.32
46	BD (1) C 265 - H 270	/***. BD*(1) C 240 - H 241	0.07
47	BD*(2) C 251 - C 256	/***. BD*(2) C 18 - C 34	0.70
48	BD*(2) C 251 - C 256	/***. BD*(2) C 19 - C 40	0.12
49	BD*(2) C 252 - C 253	/***. BD*(2) C 57 - C 66	0.26
50	BD*(2) C 263 - C 264	/***. BD*(1) C 239 - H 246	0.31
51	BD*(2) C 265 - C 266	/***. BD*(1) C 240 - H 241	0.17

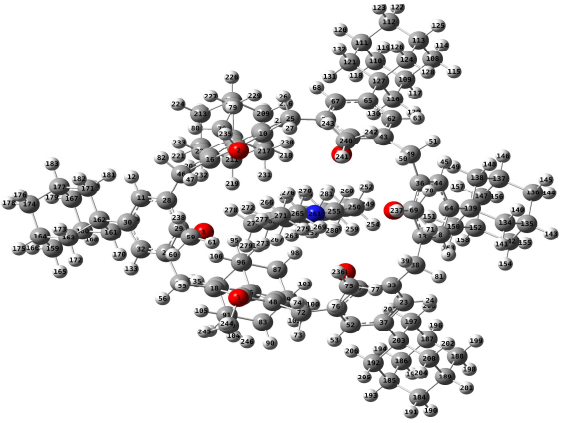

Figure 4.100. Minimized Structure with labels of **16a⁺⊂15f**.

Table 4.6. Secondary orbital interactions for **16a⁺ ⊂ 15f**

n	*Type Donor*	*Type Acceptor*	*E Kcal/mol*
1	BD (2) C 7 - C 16	***. BD*(1) C 258 - H 262	0,13
2	BD (2) C 8 - C 13	***. BD*(1) C 255 - H 259	0,16
3	BD (2) C 10 - C 14	***. BD*(1) C 258 - H 262	0,16
4	BD (2) C 15 - C 36	***. BD*(1) C 255 - H 260	0,15
5	BD (2) C 17 - C 42	***. BD*(1) C 255 - H 259	0,07
6	BD (2) C 21 - C 31	***. BD*(1) C 255 - H 260	0,17
7	BD (2) C 41 - C 48	***. BD*(1) C 258 - H 263	0,22
8	BD (2) C 57 - C 66	***. BD*(1) C 253 - H 257	0,09
9	BD (1) C 75 - H 76	***. BD*(1) C 265 - H 269	0,06
10	BD (1) C 75 - H 236	***. BD*(1) C 265 - H 269	0,45
11	BD (1) C 87 - H 98	***. BD*(1) C 247 - H 248	0,37
12	BD (1) C 96 - H 107	***. BD*(1) C 253 - H 257	0,06
13	BD (1) C 150 - H 151	***. BD*(1) C 250 - H 254	0,1
14	BD (1) C 210 - H 218	***. BD*(1) C 247 - H 251	0,09
15	BD (1) C 217 - H 231	***. BD*(1) C 253 - H 256	0,22
16	BD (1) C 240 - H 241	***. BD*(1) C 265 - H 270	0,66
17	BD (1) C 240 - H 242	***. BD*(1) C 265 - H 270	0,09
18	CR (1) O 4	***. BD*(1) N 261 - H 280	0,11
19	CR (1) O 6	***. BD*(1) N 261 - H 281	0,15
20	LP (1) O 1	***. BD*(1) C 264 - H 266	0,08
21	LP (1) O 2	***. BD*(1) C 264 - H 266	0,66
22	LP (2) O 2	***. BD*(1) C 264 - H 266	0,09
23	LP (1) O 3	***. BD*(1) C 264 - H 267	0,08
24	LP (1) O 4	***. BD*(1) N 261 - H 280	1,69
25	LP (2) O 4	***. BD*(1) N 261 - H 280	8,68
26	LP (1) O 5	***. BD*(1) N 261 - H 280	0,48
27	LP (1) O 5	***. BD*(1) N 261 - H 281	0,25
28	LP (2) O 5	***. BD*(1) N 261 - H 280	0,2
29	LP (2) O 6	***. BD*(1) N 261 - H 281	11,61
30	BD*(2) C 8 - C 13	***. BD*(1) C 255 - H 259	0,07
31	BD*(2) C 17 - C 42	***. BD*(1) C 255 - H 259	0,07
32	BD*(2) C 21 - C 31	***. BD*(1) C 255 - H 260	0,11
	unit 2 to unit 1		
33	BD (1) C 247 - H 248	***. BD*(1) C 87 - H 98	0,41
34	BD (1) C 247 - H 249	***. BD*(1) C 87 - H 98	0,05
35	BD (1) C 247 - H 251	***. BD*(1) C 210 - H 218	0,09
36	BD (1) C 250 - H 254	***. BD*(1) C 150 - H 151	0,13
37	BD (1) C 253 - H 256	***. BD*(1) C 217 - H 231	0,13
38	BD (1) C 253 - H 257	***. BD*(1) C 96 - H 107	0,07
39	BD (1) C 255 - H 260	***. BD*(2) C 21 - C 31	0,07
40	BD (1) N 261 - H 280	***. BD*(1) O 4 - C 17	0,07

41	BD (1) N 261 - H 280	***. BD*(1) O 4 - C 75	0,07
42	BD (1) N 261 - H 281	***. BD*(1) O 6 - C 31	0,08
43	BD (1) N 261 - H 281	***. BD*(1) O 6 - C 240	0,1
44	BD (1) C 265 - H 269	***. BD*(1) C 75 - H 236	0,5
45	BD (1) C 265 - H 270	***. BD*(1) C 75 - H 236	0,06
46	BD (1) C 265 - H 270	***. BD*(1) C 240 - H 241	0,49
47	BD (1) C 268 - H 272	***. BD*(1) C 59 - H 61	0,07
48	BD (1) C 268 - H 273	***. BD*(1) C 59 - H 61	0,21

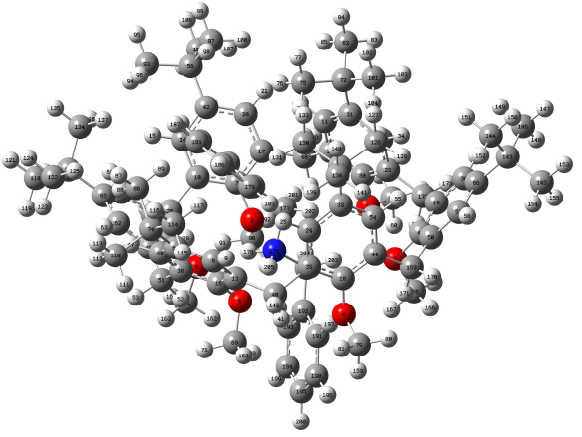

Figure 4.101. Minimized Structure with labels of **16b⁺⊂15a**.

Table 4.7. Secondary orbital interactions for **16b⁺⊂15a**.

n°	*Type Donor*	*Type Acceptor*	*E Kcal/mo)*
1	BD (2) C 13 - C 16	/***. BD*(2) C 179 - C 184	0,26
2	BD (2) C 13 - C 16	/***. BD*(1) C 179 - H 185	0,11
3	BD (2) C 24 - C 35	/***. BD*(1) C 179 - H 185	1,11
4	BD (2) C 32 - C 45	/***. BD*(2) C 182 - C 183	0,08
5	BD (2) C 38 - C 46	/***. BD*(2) C 180 - C 181	0,08
6	BD (2) C 62 - C 65	/***. BD*(2) C 182 - C 183	0,07
7	BD (1) C 86 - H 89	/***. BD*(1) C 180 - H 186	0,17
8	BD (1) C 90 - H 92	/***. BD*(1) C 193 - H 198	0,07
9	BD (1) C 90 - H 157	/***. BD*(1) C 193 - H 198	0,54
10	BD (1) C 130 - H 131	/***. BD*(1) C 180 - H 186	0,14
11	BD (1) C 134 - H 137	/***. BD*(1) C 182 - H 188	0,05
12	BD (1) C 161 - H 162	/***. BD*(2) C 192 - C 193	0,19
13	BD (1) C 165 - H 167	/***. BD*(2) C 190 - C 191	0,16
14	CR (1) O 5	/***. BD*(1) N 176 - H 205	0,09
15	CR (1) O 6	/***. BD*(1) N 176 - H 178	0,17
16	LP (1) O 1	/***. BD*(1) C 175 - H 204	0,06
17	LP (1) O 2	/***. BD*(1) C 175 - H 204	0,59
18	LP (1) O 2	/***. BD*(1) N 176 - H 178	0,12
19	LP (2) O 2	/***. BD*(1) C 175 - H 204	0,21
20	LP (2) O 3	/***. BD*(1) C 175 - H 203	0,95
21	LP (1) O 4	/***. BD*(1) C 191 - H 197	1,55
22	LP (2) O 4	/***. BD*(1) C 191 - H 197	0,21
23	LP (1) O 5	/***. BD*(1) N 176 - H 205	0,76
24	LP (2) O 5	/***. BD*(1) N 176 - H 205	6,16
25	LP (2) O 6	/***. BD*(1) N 176 - H 178	9,08
26	BD*(2) C 24 - C 35	/***. BD*(1) C 179 - H 185	0,09
	unit 2 to unit 1		
27	BD (1) C 175 - H 203	/***. BD*(1) O 3 - C 43	0,07

28	BD (1) N 176 - H 178	/***. BD*(1) O 6 - C 32	0,1
29	BD (1) N 176 - H 178	/***. BD*(1) O 6 - C 161	0,13
30	BD (1) N 176 - H 205	/***. BD*(1) O 5 - C 16	0,07
31	BD (1) N 176 - H 205	/***. BD*(1) O 5 - C 69	0,08
32	BD (2) C 179 - C 184	/***. BD*(2) C 13 - C 16	0,07
33	BD (2) C 179 - C 184	/***. BD*(2) C 38 - C 46	0,05
34	BD (2) C 179 - C 184	/***. BD*(1) C 75 - H 78	0,18
35	BD (1) C 179 - H 185	/***. BD*(2) C 24 - C 35	0,06

36	BD (1) C 180 - H 186	/***. BD*(1) C 86 - H 89	0,13
37	BD (1) C 180 - H 186	/***. BD*(1) C 130 - H 131	0,09
38	BD (2) C 182 - C 183	/***. BD*(1) C 75 - H 76	0,09
39	BD (2) C 190 - C 191	/***. BD*(1) C 165 - H 167	0,33
40	BD (2) C 192 - C 193	/***. BD*(1) C 161 - H 162	0,61
41	BD (2) C 182 - C 183	/***. BD*(1) C 75 - H 76	0,09
42	BD (2) C 190 - C 191	/***. BD*(1) C 69 - H 70	1,44

4.7.3 Conformationally stable calix[6]arenes

4.7.3.1 Synthesis of Derivatives 46g and 47g

In a dry round flask, under N_2, hexamethoxycalix[6]arene **1** (0.502 g, 0.45 mmol) was dissolved in freshly distilled THF (50 mL). Subsequently, TMEDA (0.57 mL, 3.59 mmol) and *n*-BuLi (1.50 mL of a solution 2.5 M in hexane, 3.59 mmol) were added at room temperature. A persistent blood red colored anion was generated. Afterwards, a solution of *p*-methylbenzyl bromide (0.724 g, 3.59 mmol) in THF dry (20 mL) was added dropwise to the reaction mixture. It is observed a gradually change color of mixture, first to green and later to pale yellow. Stirring was continued for an hour at room temperature. After the reaction was stopped by addition of 1 N HCl and the solution was extracted with ethyl acetate. The organic phase was dried over anhydrous Na_2SO_4, filtered and evaporated of the solvent. The raw was purified through chromatography column on silica gel and using solvent mixture 74 % hexane / 21 % chloroform / 5 % ethyl acetate as eluens. *cone* **46g** was isolated with 25 % yield, and *1,2,3-alternate* **47g** conformer with 22 % yield.

Derivative 46g

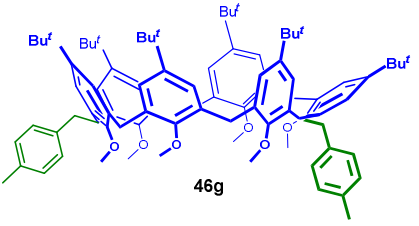

^{1}H NMR (600 MHz, $CDCl_3$, 298 K) δ: 7.16 (s, 4H, Ar*H*), 7.04 (d, J = 7.6 Hz, 4H, Ar*H*), 7.02 (s, 4H, Ar*H*), 6.96 (d, J = 7.6 Hz, 4H, Ar*H*), 6.86 (s, 4H, Ar*H*), 5.13 (bt, 2H, ArC*H*(*p*-MeBn)Ar), 4.41 and 3.45 (AX system, J = 15.3 Hz, 8H, $ArCH_2Ar$), 3.23-3.19 (overlapped, $-CH_2Ph$, 16H, $-OCH_3$), 2.70 (s, 6H, $-OCH_3$), 2.23 (s, 6H, $-BnCH_3$), 1.16 (s,18H, $-C(CH_3)_3$,), 1.07 (s, 36H, $-C(CH_3)_3$). **^{13}C NMR** (150 MHz, $CDCl_3$, 298 K): δ 154.0, 153.6, 145.7, 145.2, 137.9, 136.5, 135.0, 133.1, 133.1, 128.9, 128.7, 126.3, 125.3, 123.9, 60.2, 60.0, 41.9, 34.2,

34.1, 31.4, 31.4, 29.9, 20.9. **HRMS** (*m*/*z*) clcd for $C_{88}H_{112}NaO_6$ 1287.8351 found 1287.8379.

Derivative 47g

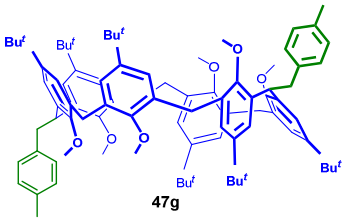

^{1}H NMR (600 MHz, $CDCl_3$, 298 K): δ 7.12 (s, 4H, Ar*H*), 7.02-7.02 (overlapped, 8H, Ar*H*), 6.96-6.94 (overlapped, 8H, Ar*H*), 4.89 (bt, 2H, ArC*H*(*p*-MeBn)Ar), 4.05 and 3.64 (AX system, J = 14.8 Hz, 8H, , $ArCH_2Ar$), 3.25 (d, J = 7.3 Hz, 4H, -CH_2Ph), 2.96 (s, 12H, -OCH_3), 2.80 (s, 6H, -OCH_3), 2.22 (s, 6H, -BnCH_3), 1.17 (s, 18H, -$C(CH_3)_3$), 1.15 (s, 36H, -$C(CH_3)_3$). **^{13}C NMR** (150 MHz, $CDCl_3$, 298 K): δ 154.2, 154.1, 145.7, 145.3, 137.9, 136.7, 135.0, 133.5, 133.1, 128.9, 128.7, 126.3, 125.8, 124.4, 69.0, 60.1, 59.6, 40.9, 34.2, 34.1, 31.4, 20.9. **Elemental Analysis:** Calcd for $C_{88}H_{112}O_6$ C, 83.50; H, 8.92; O, 7.58, Found: C, 83.48; H, 8.93; O, 7.59.

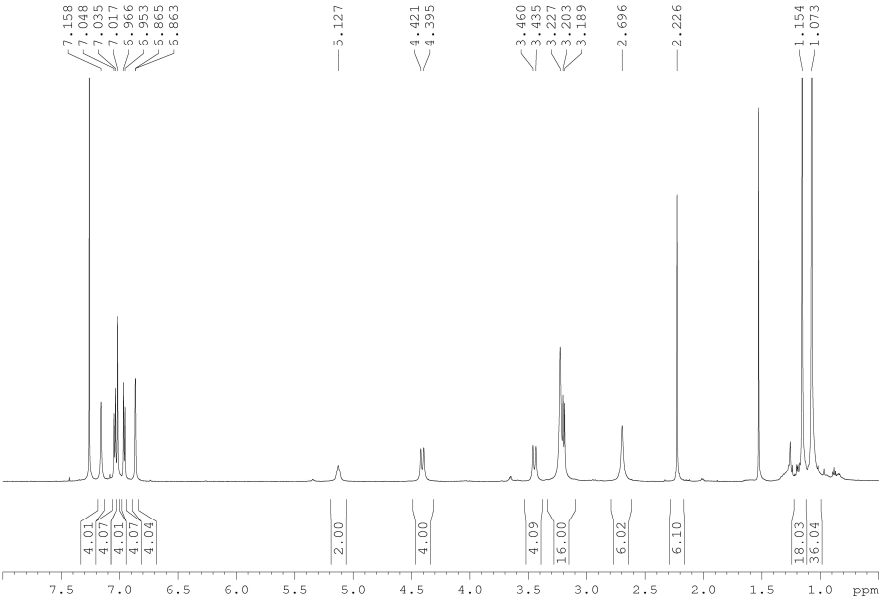

Figure 4.102. ^{1}H NMR spectrum of derivative **46g** (600 MHz, $CDCl_3$, 298 K).

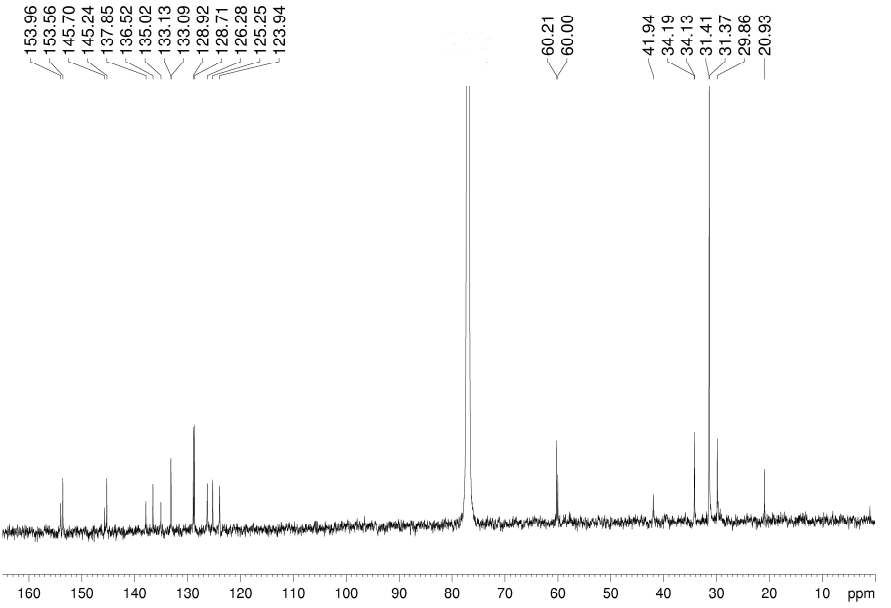

Figure 4.103. ^{13}C NMR spectrum of derivative **46g** (150 MHz, $CDCl_3$, 298 K).

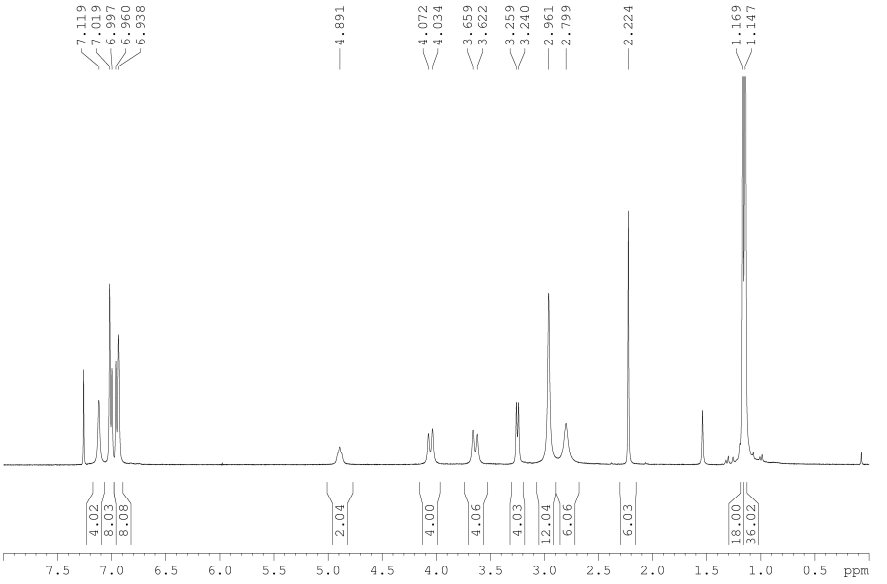

Figure 4.104. ^{1}H NMR spectrum of derivative **47g** (400 MHz, $CDCl_3$, 298 K).

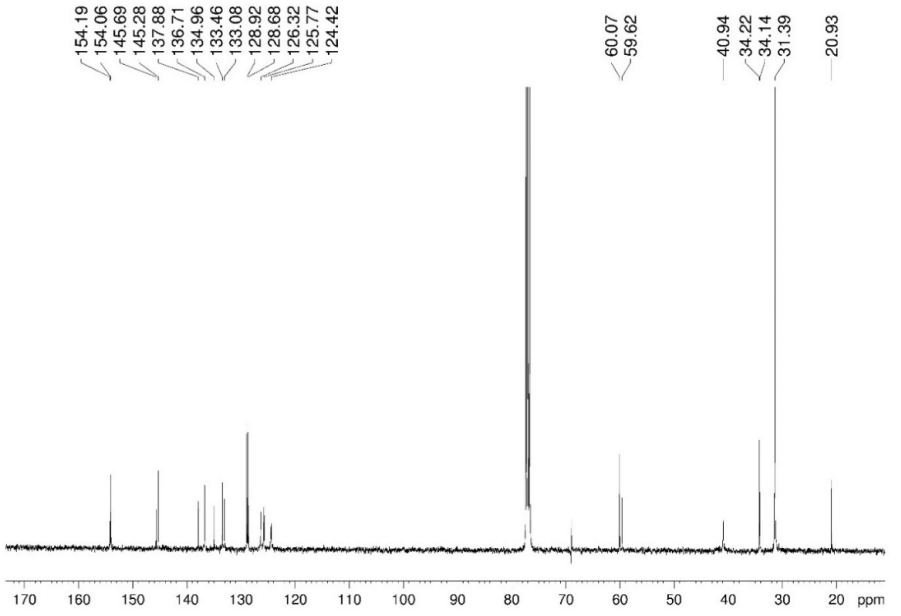

Figure 4.105. ^{13}C NMR spectrum of derivative **47g** (100 MHz, $CDCl_3$, 298 K).

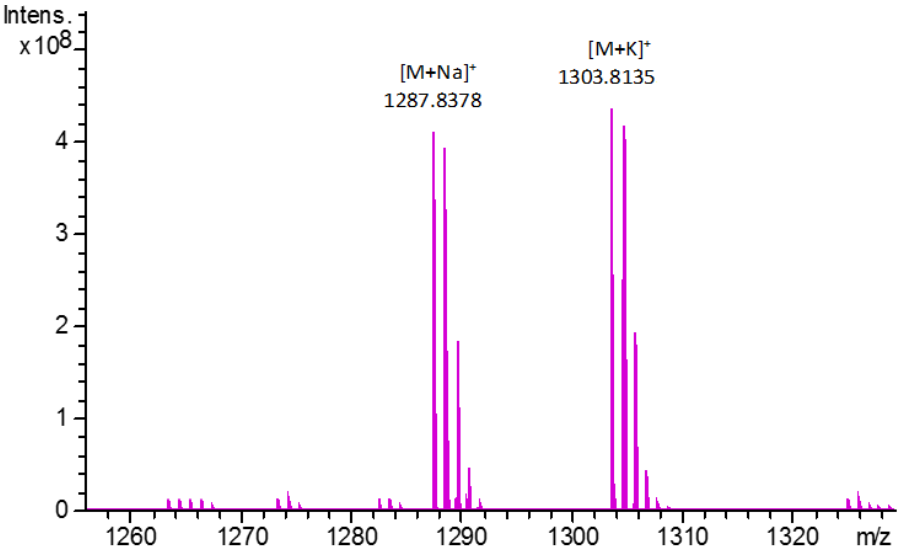

Figure 4.106. MALDI-MS spectrum of derivative **46g**.

4.7.3.2 Synthesis of Derivatives 46h and 47h

In a dry round flask, under N_2, hexamethoxycalix[6]arene **1** (1.575 g, 0.94 mmol) was dissolved in freshly distilled THF (150 mL). Subsequently, TMEDA (1.73 mL, 7.52 mmol) and *n*-BuLi (4.50 mL of a solution 2.5 M in hexane, 7.52 mmol) were added at room temperature. A persistent blood red coloured anion was generated. Afterwards, a solution of 1-bromobutane (1.23 mL, 7.60 mmol) in THF dry (60 mL) was added dropwise to the reaction mixture. It was observed a gradually change colour of mixture, first to green and later to pale yellow. Stirring was continued for an hour at room temperature. After the reaction was stopped by addition of 1 N HCl and the solution was extracted with ethyl acetate. The organic phase was dried over anhydrous Na_2SO_4, filtered, and evaporated of the solvent. The raw was purified through chromatography column on silica gel and using solvent mixture 74:21:5 hexane/chloroform/ethyl acetate as eluents., *cone* **46h** was isolated with 27 % yield and *1,2,3-alternate* **47h** conformer with 10 % yield.

Derivative 46h

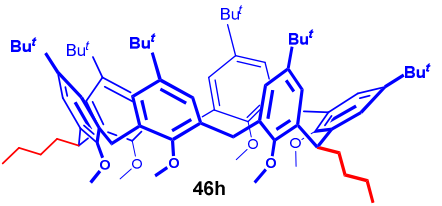

^{1}H NMR (600 MHz, $CDCl_3$, 298 K): δ 7.06 (s, 4H, Ar*H*), 7.01 (s, 4H, Ar*H*), 6.92 (s, 4H, Ar*H*), 4.78 (t, J_{ab} = 7.6 Hz, 2H, ArC*H*(*n*Bu)Ar), 4.51 and 3.46 (AX system, J = 15.3 Hz, 8H, , $ArCH_2Ar$), 3.28 (s,12H , OCH_3), 2.83 (s, 6H, OCH_3), 1.92 (q, J_{ba} = 7.6 Hz, J_{bc} = 14.7, 4H, -$CH_2CH_2CH_2CH_3$), 1.34 - 1.28 (m, 8H, -$CH_2CH_2CH_2CH_3$), 1.13 (s, 18H, -$C(CH_3)_3$), 1.06 (s, 36H , -$C(CH_3)_3$), 0.86 (t, -$CH_2CH_2CH_2CH_3$, J = 7.1 Hz, 6H). **^{13}C NMR** (150 MHz, $CDCl_3$, 298 K): δ 153.8, 153.5, 145.7, 145.4, 137.4, 133.2, 133.1, 126.1, 125.2, 123.4, 69.0, 60.3, 60.1, 36.9, 36.4, 34.2, 34.1, 31.4, 30.5, 29.8, 22.7, 14.0. **HRMS** (*m/z*) clcd for $C_{80}H_{112}O_6Na$ 1191.8351 found 1191.8399.

Derivative 47h

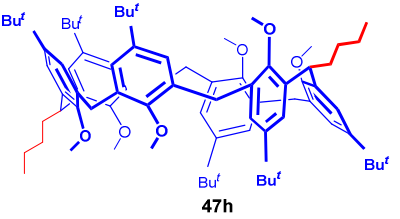

^{1}H NMR (600 MHz, $CDCl_3$, 298 K): δ 7.08-7.02 (overlapped, 12H, Ar*H*), 4.58 (t, J_{ab} = 7.6 Hz, 2H, ArC*H*(*n*Bu)Ar), 4.11 and 3.66 (AX system, J = 15.0 Hz, 8H, $ArCH_2Ar$), 3.00 (s, 12H, OCH_3), 2.84 (s, 6H, OCH_3), 1.93 (q, J_{ba} = 7.6 Hz, J_{bc} = 14.9, 4H, -$CH_2CH_2CH_2CH_3$), 1.34 - 1.28 (m, 8H, -$CH_2CH_2CH_2CH_3$), 1.19 (s, 54H, -$C(CH_3)_3$), 0.86 (t, J = 7.1 Hz, 6H, -$CH_2CH_2CH_2CH_3$). **^{13}C NMR** (150 MHz, $CDCl_3$, 298 K): δ 154.5, 154.3, 145.8, 145.6, 137.5, 133.7, 133.4, 126.6, 126.0, 124.0,

60.3, 59.8, 38.0, 35.7, 34.4, 34.3, 32.2, 31.6, 30.7, 22.9, 14.2. **Elemental Analysis**: Calcd for $C_{80}H_{112}O_6$ C, 82.14; H, 9.65; O, 8.21, Found: C, 82.13; H, 9.67; O, 8.20.

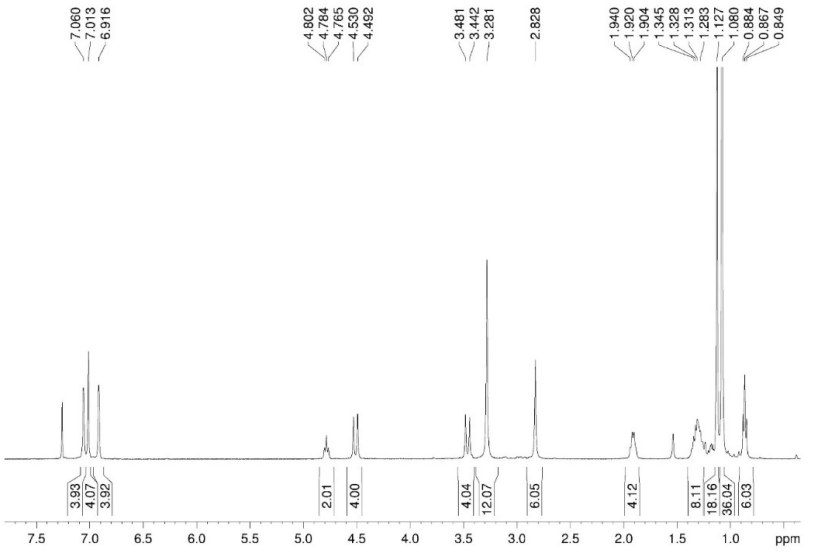

Figure 4.107. ^{1}H NMR spectrum of derivative **46h** (600 MHz, $CDCl_3$, 298 K).

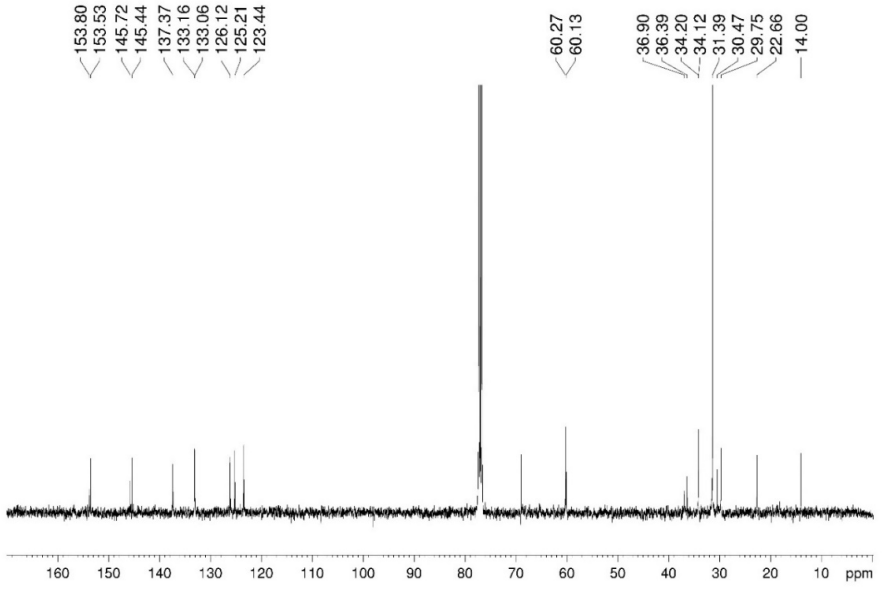

Figure 4.108. ^{13}C NMR spectrum of derivative **46h** (100 MHz, $CDCl_3$, 298 K).

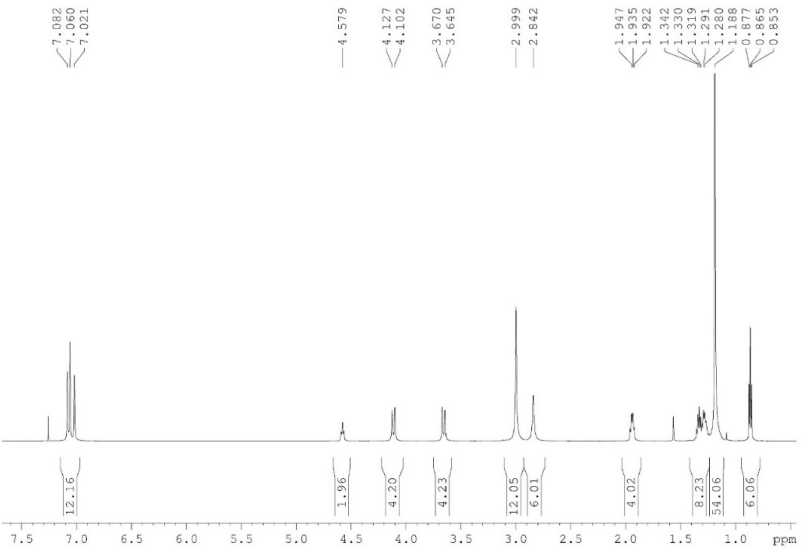

Figure 4.109. ^{1}H NMR spectrum of derivative **47h** (600 MHz, $CDCl_3$, 298 K).

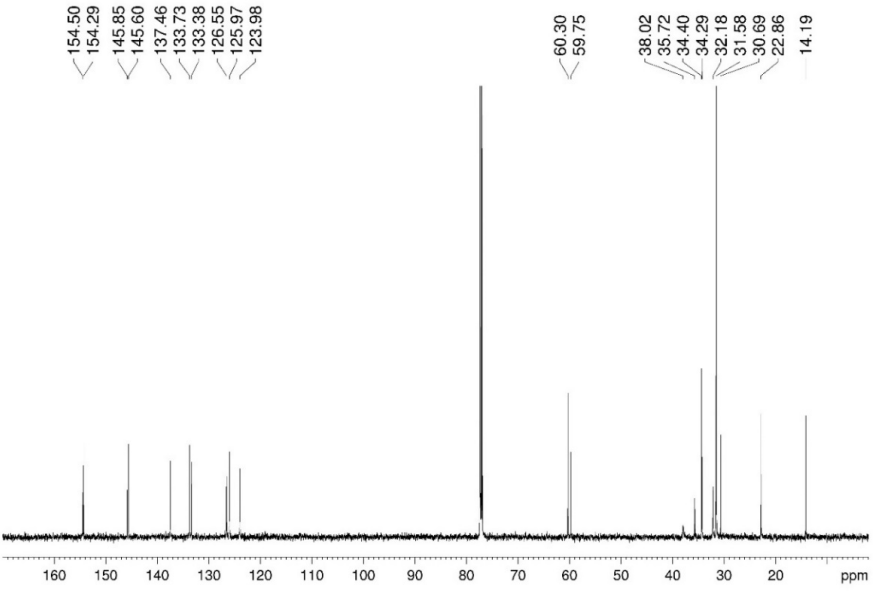

Figure 4.110. ^{13}C NMR spectrum of derivative **47h** (150 MHz, $CDCl_3$, 298 K).

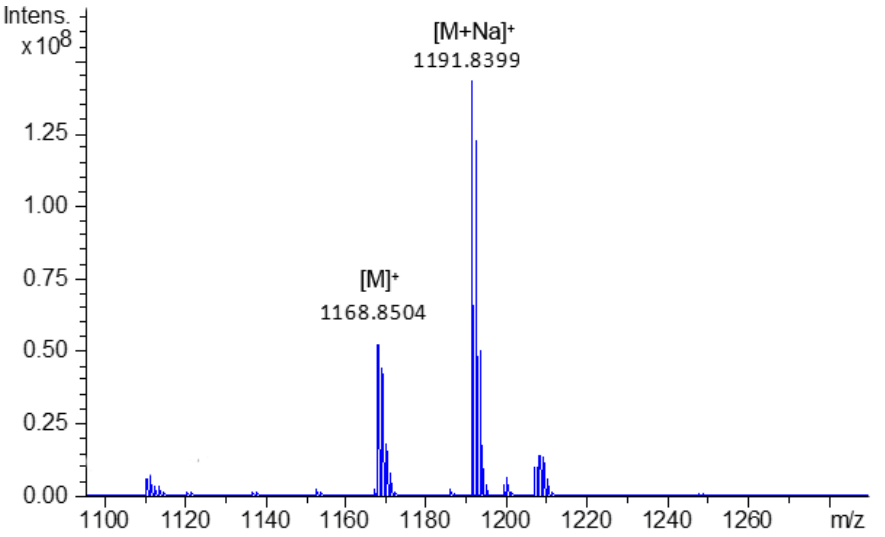

Figure 4.111. MALDI-MS Spectrum of derivative **46h**.

4.7.3.3 Synthesis of pseudo[2]rotaxanes

A 1:1 mixture of calix[6]arene derivative and TFPB linear system was dissolved in 0.5 mL of $CDCl_3$.In detail, in **Table 4.8** we reported concentration using for calix[6]arene derivative and for axles. Then, the solution was transferred in an NMR tube for 1D and 2D NMR spectra acquisition.

Table 4.8. Amount of hosts and guests for complexation experiments.

Pseudo[2]rotaxanes	Calix[6]arenes		Axles		$CDCl_3$
	(mg)	(mmol)	(mg)	(mmol)	(ml)
16b$^+$⊂46g	2.09	$1.6 \cdot 10^{-3}$	1.87	$1.6 \cdot 10^{-3}$	0.5
16f$^+$⊂46g	2.09	$1.6 \cdot 10^{-3}$	2.04	$1.6 \cdot 10^{-3}$	0.5
16g$^+$⊂46g	2.01	$1.6 \cdot 10^{-3}$	1.78	$1.6 \cdot 10^{-3}$	0.5
16a$^+$⊂46g	2.08	$1.6 \cdot 10^{-3}$	1.77	$1.6 \cdot 10^{-3}$	0.5
16b$^+$⊂47g	2.08	$1.6 \cdot 10^{-3}$	1.84	$1.6 \cdot 10^{-3}$	0.5
16f$^+$⊂47g	2.08	$1.6 \cdot 10^{-3}$	2.06	$1.6 \cdot 10^{-3}$	0.5
16g$^+$⊂47g	2.00	$1.6 \cdot 10^{-3}$	1.77	$1.6 \cdot 10^{-3}$	0.5

16a$^+$⊂47g	2.08	$1.6 \cdot 10^{-3}$	1.74	$1.6 \cdot 10^{-3}$	0.5
16b$^+$⊂46h	2.01	$1.7 \cdot 10^{-3}$	1.84	$1.7 \cdot 10^{-3}$	0.5
16f$^+$⊂46h	2.01	$1.7 \cdot 10^{-3}$	2.05	$1.7 \cdot 10^{-3}$	0.5
16g$^+$⊂46h	2.01	$1.7 \cdot 10^{-3}$	1.93	$1.7 \cdot 10^{-3}$	0.5
16a$^+$⊂46h	2.03	$1.7 \cdot 10^{-3}$	1.74	$1.7 \cdot 10^{-3}$	0.5
16b$^+$⊂47h	2.02	$1.7 \cdot 10^{-3}$	1.84	$1.7 \cdot 10^{-3}$	0.5
16f$^+$⊂47h	2.02	$1.7 \cdot 10^{-3}$	2.06	$1.7 \cdot 10^{-3}$	0.5
16g$^+$⊂47h	2.01	$1.7 \cdot 10^{-3}$	1.93	$1.7 \cdot 10^{-3}$	0.5
16a$^+$⊂47h	2.03	$1.7 \cdot 10^{-3}$	1.78	$1.7 \cdot 10^{-3}$	0.5

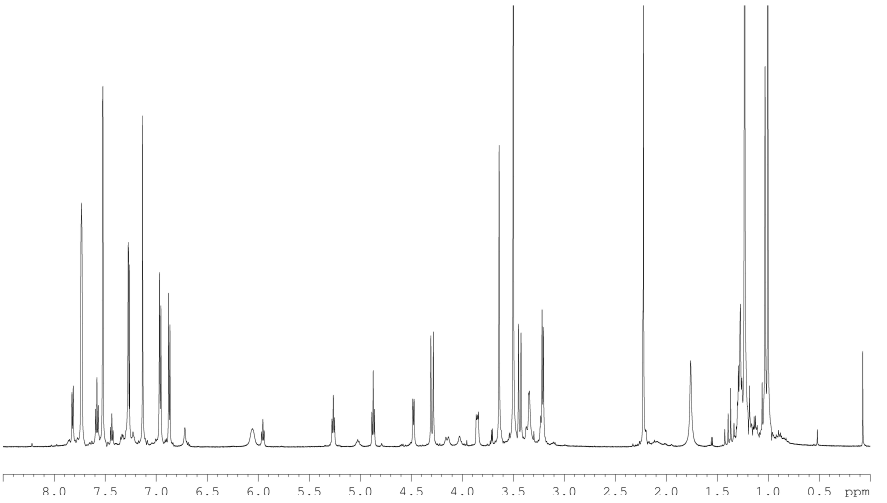

Figure 4.112. ^{1}H NMR spectrum (600 MHz, $CDCl_3$, 298 K) of 1:1 solution of **46g** (3.2 mM) and **16b$^+$**TFPB$^-$ (3.2 mM).

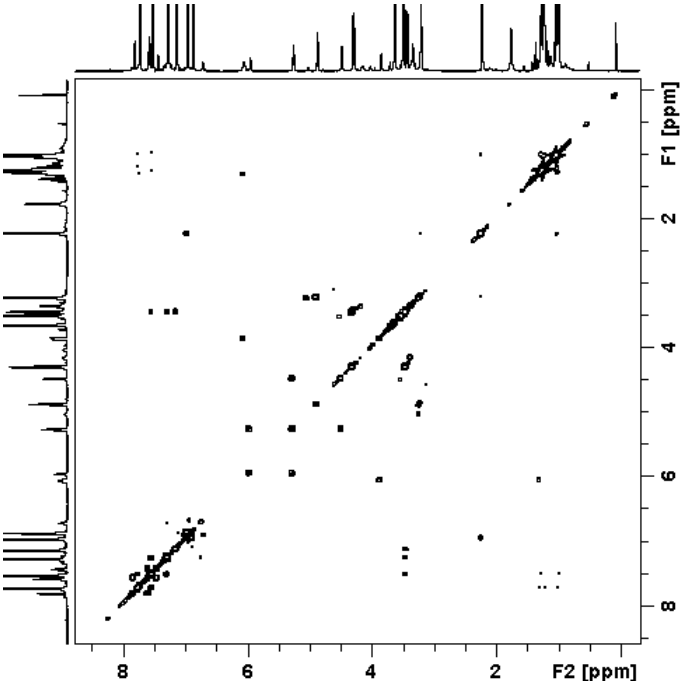

Figure 4.113. 2D COSY spectrum of derivative **16b**$^{+}$**⊂46g** (600 MHz, $CDCl_3$, 298 K).

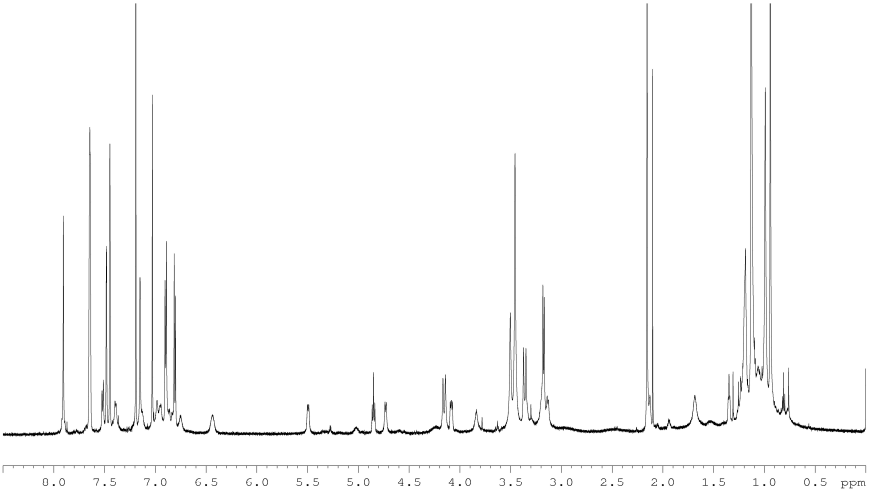

Figure 4.114. ^{1}H NMR spectrum (600 MHz, $CDCl_3$, 298 K) of 1:1 solution of **46g** (3.2 mM) and **16f**$^{+}$TFPB^{-} (3.2 mM).

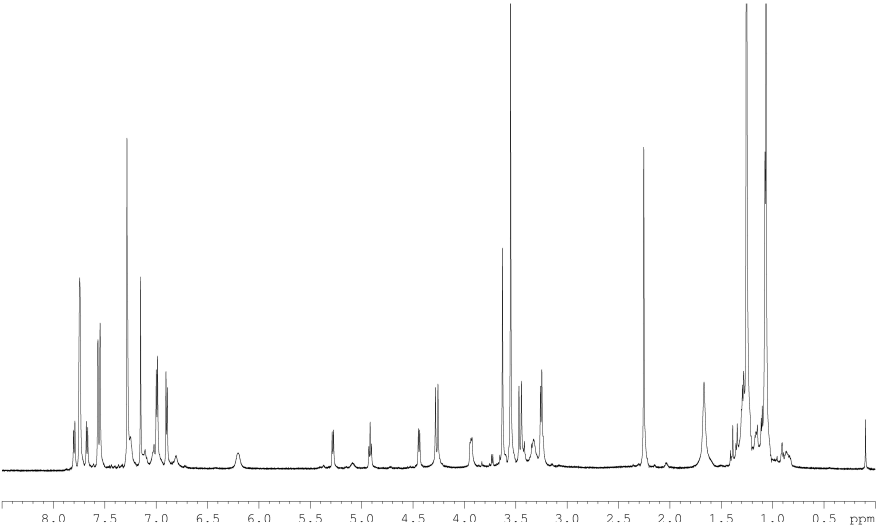

Figure 4.115. ^{1}H NMR spectrum (600 MHz, $CDCl_3$, 298 K) of 1:1 solution of **46g** (3.2 mM) and **16g**$^{+}$TFPB^{-} (3.2 mM).

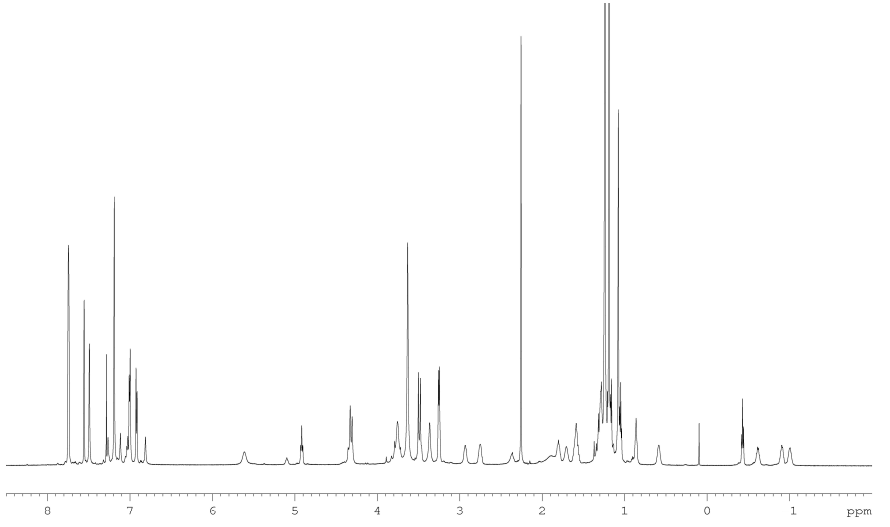

Figure 4.116. ^{1}H NMR spectrum (600 MHz, $CDCl_3$, 298 K) of 1:1 solution of **46g** (3.2 mM) and **16a**$^{+}$TFPB^{-} (3.2 mM).

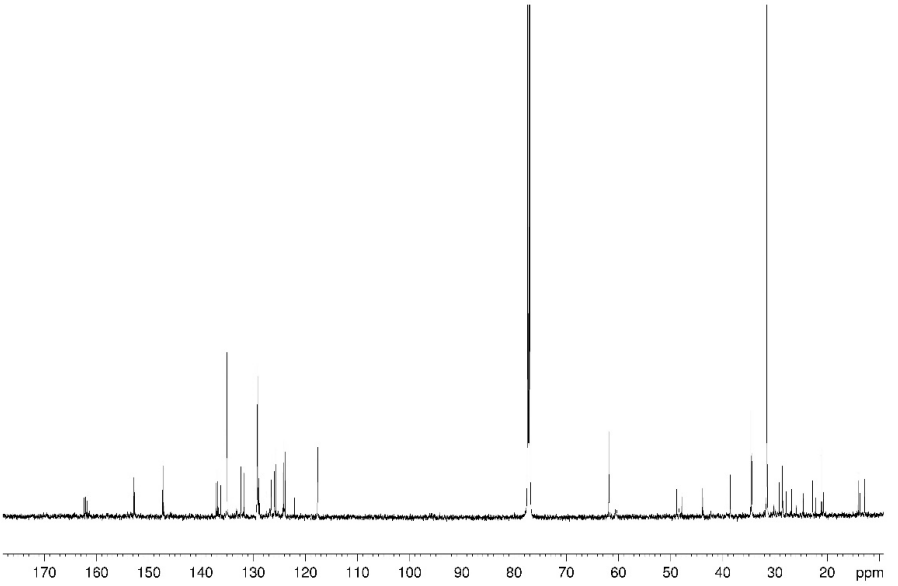

Figure 4.117. ^{13}C NMR spectrum of derivative **16a**$^{+}$ ⊂ **46g** (150 MHz, $CDCl_3$, 298 K).

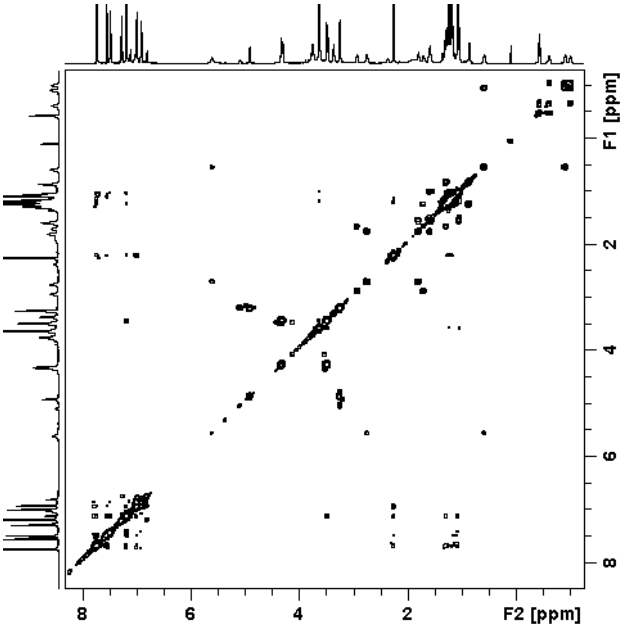

Figure 4.118. 2D COSY spectrum of derivative **16a**$^{+}$⊂ **46g** (600 MHz, $CDCl_3$, 298 K).

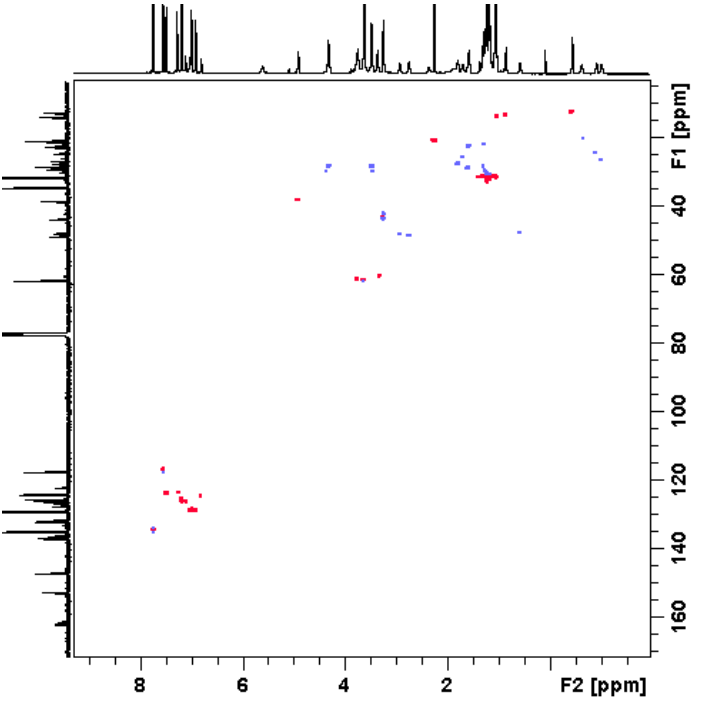

Figure 4.119. 2D HSQC spectrum of derivative **16a**$^{+}$ ⊂ **46g** (600 MHz, $CDCl_3$, 298 K).

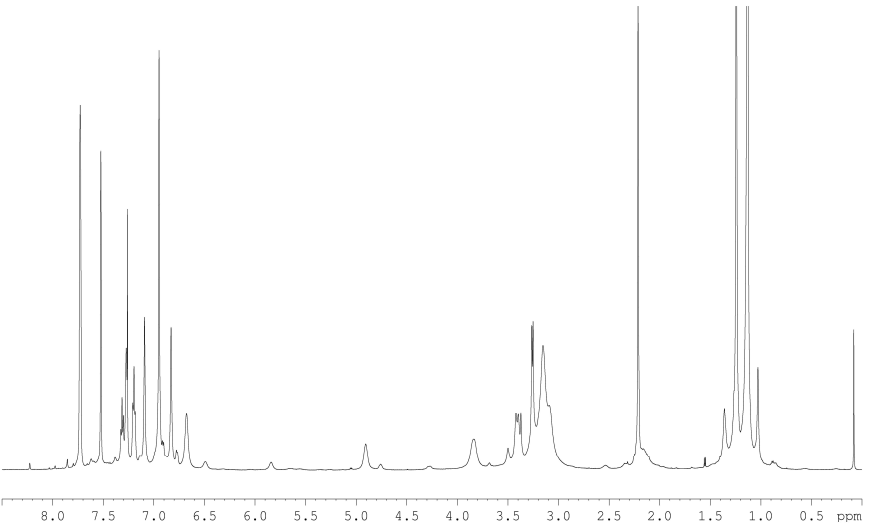

Figure 4.120. ^{1}H NMR spectrum (600 MHz, $CDCl_3$, 298 K) of 1:1 solution of **47g** (3.2 mM) and **16b**$^{+}$TFPB^{-} (3.2 mM).

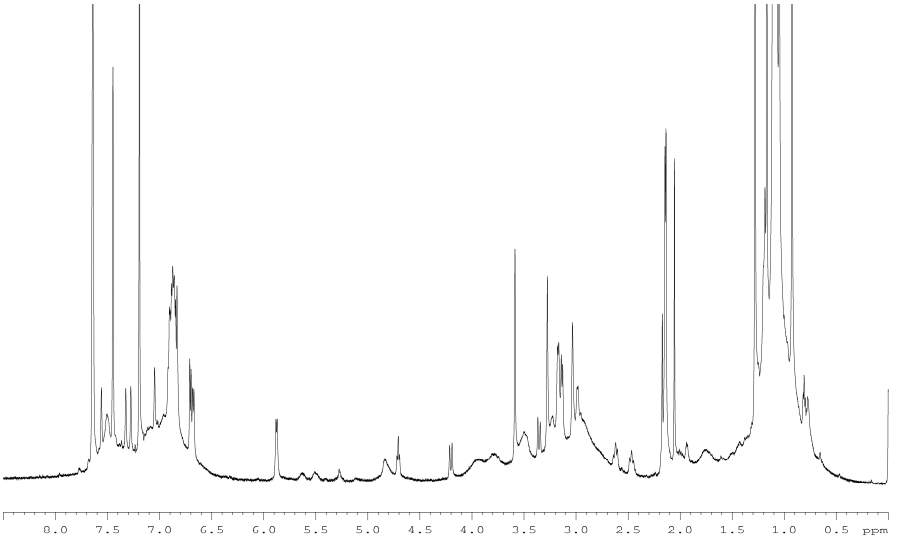

Figure 4.121. ^{1}H NMR spectrum (600 MHz, $CDCl_3$, 298 K) of 1:1 solution of **47g** (3.2 mM) and **16f**$^{+}$TFPB^{-} (3.2 mM).

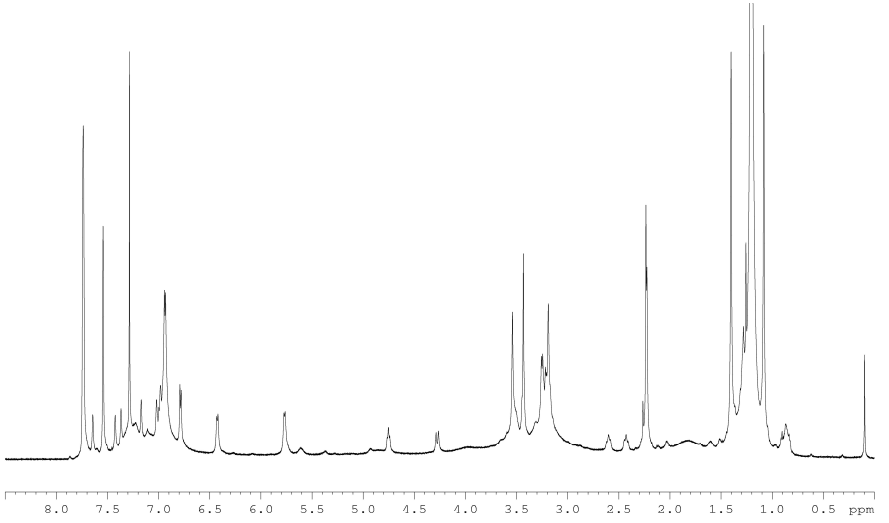

Figure 4.122. ^{1}H NMR spectrum (600 MHz, $CDCl_3$, 298 K) of 1:1 solution of **47g** (3.2 mM) and **16g**$^{+}$TFPB^{-} (3.2 mM).

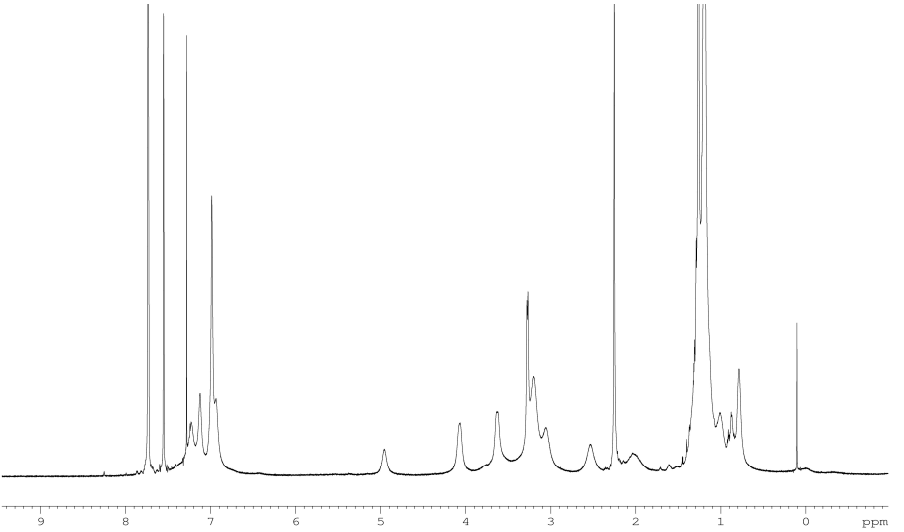

Figure 4.123. ^{1}H NMR spectrum (600 MHz, $CDCl_3$, 298 K) of 1:1 solution of **47g** (3.2 mM) and **16a**$^{+}$TFPB^{-} (3.2 mM).

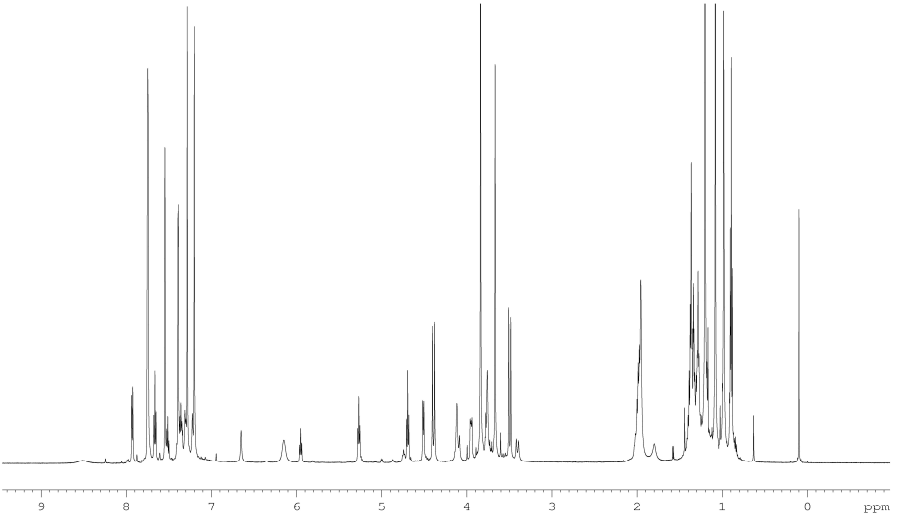

Figure 4.124. ^{1}H NMR spectrum (600 MHz, $CDCl_3$, 298 K) of 1:1 solution of **46h** (3.4 mM) and **16b**$^{+}$TFPB^{-} (3.4 mM).

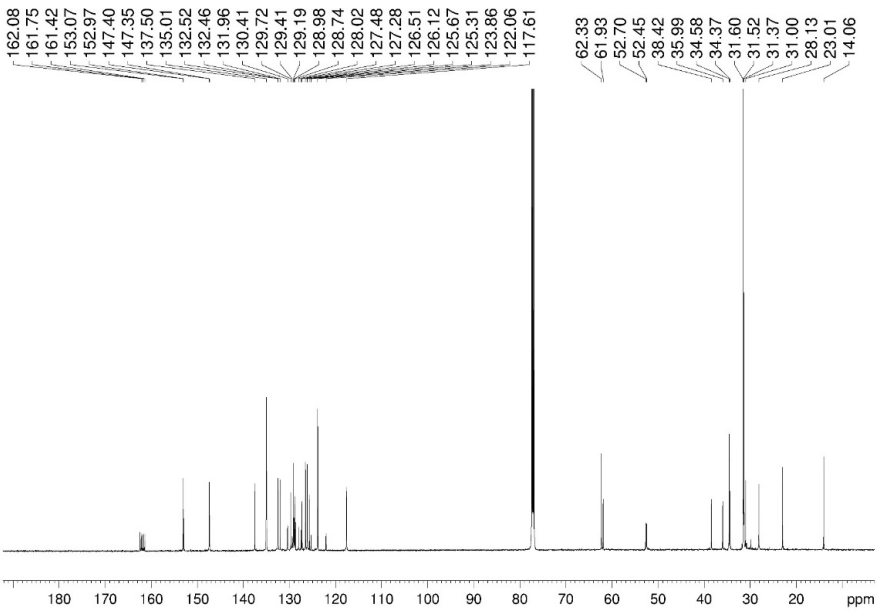

Figure 4.125. ^{13}C NMR spectrum of derivative **16b$^+$ ⊂ 46h** (150 MHz, $CDCl_3$, 298 K).

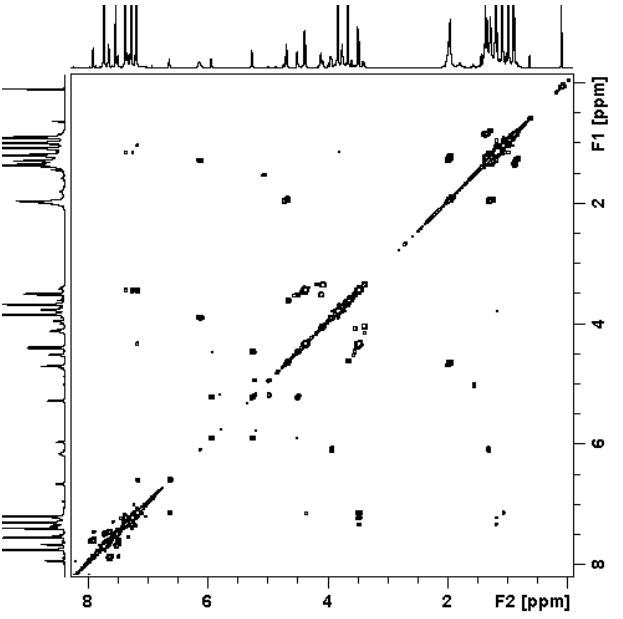

Figure 4.126. 2D COSY spectrum of derivative **16b$^+$ ⊂ 46h** ($CDCl_3$, 600 MHz, 298 K).

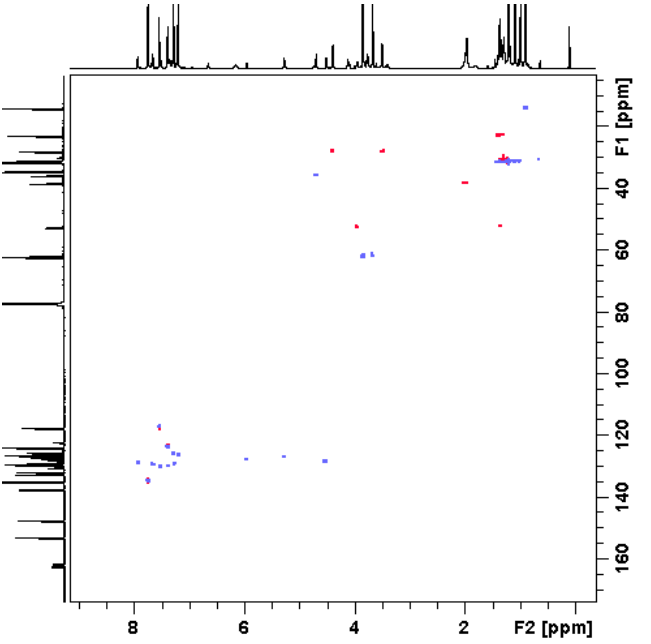

Figure 4.127. 2D HSQC spectrum of derivative **16b**$^{+}$ ⊂ **46h** (600 MHz, $CDCl_3$, 298 K).

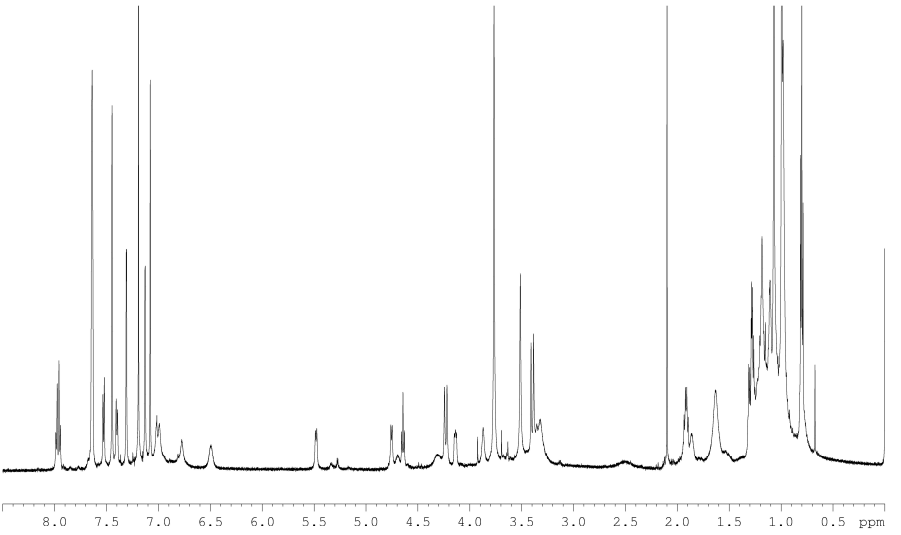

Figure 4.128. ^{1}H NMR spectrum (600 MHz, $CDCl_3$, 298 K) of 1:1 solution of **46g** (3.4 mM) and **16f**$^{+}$TFPB^{-} (3.4 mM).

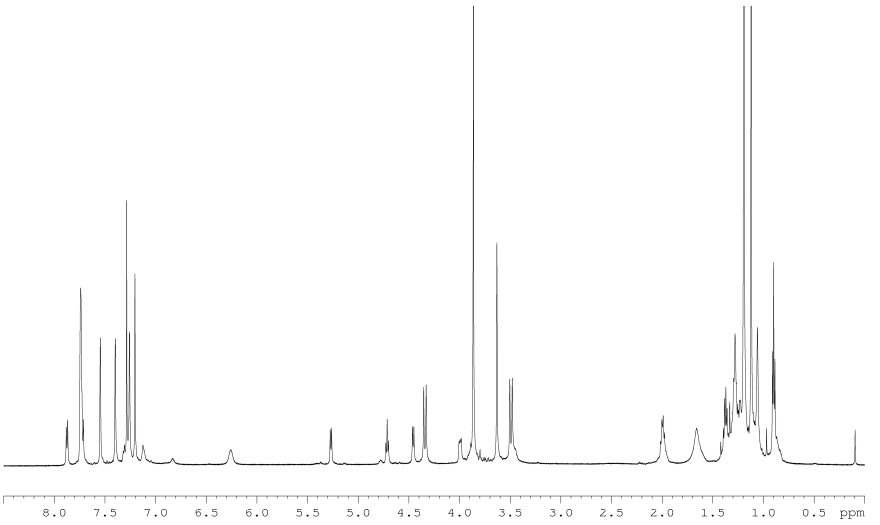

Figure 4.129. ^{1}H NMR Spectrum (600 MHz, $CDCl_3$, 298 K) of 1:1 solution of **46g** (3.4 mM) and **16f**$^{+}$TFPB^{-} (3.4 mM).

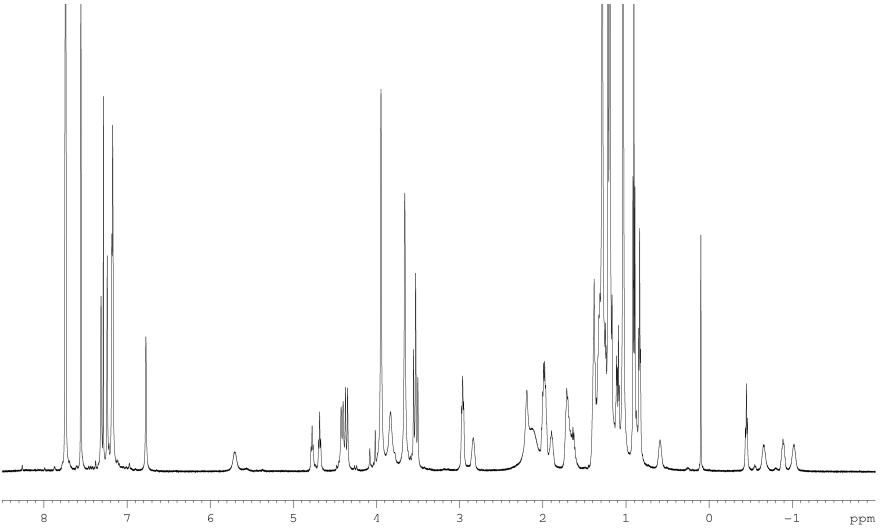

Figure 4.130. ^{1}H NMR spectrum (600 MHz, $CDCl_3$, 298 K) of 1:1 solution of **46h** (3.4 mM) and **16a**$^{+}$TFPB^{-} (3.4 mM).

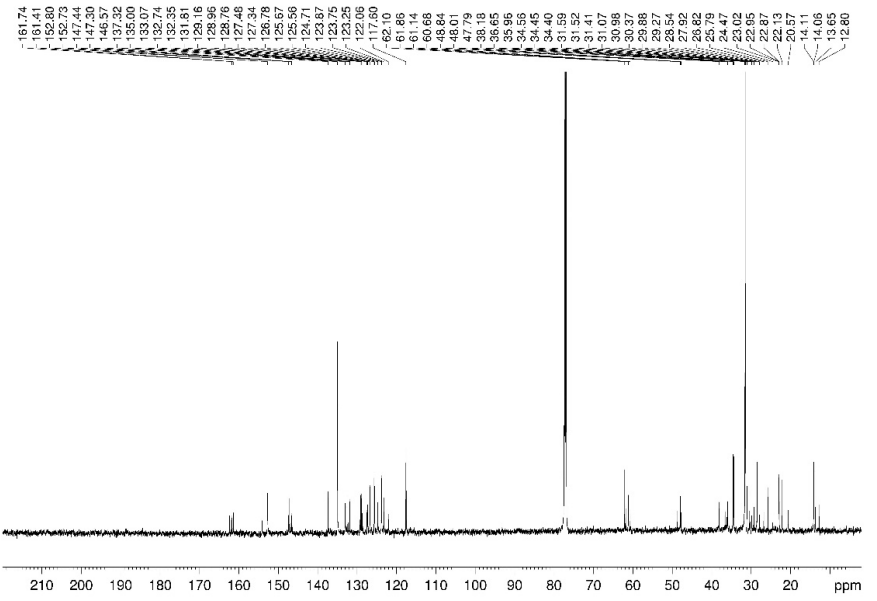

Figure 4.131. ^{13}C NMR spectrum of derivative **16a⁺ ⊂ 46h** (150 MHz, $CDCl_3$, 298 K).

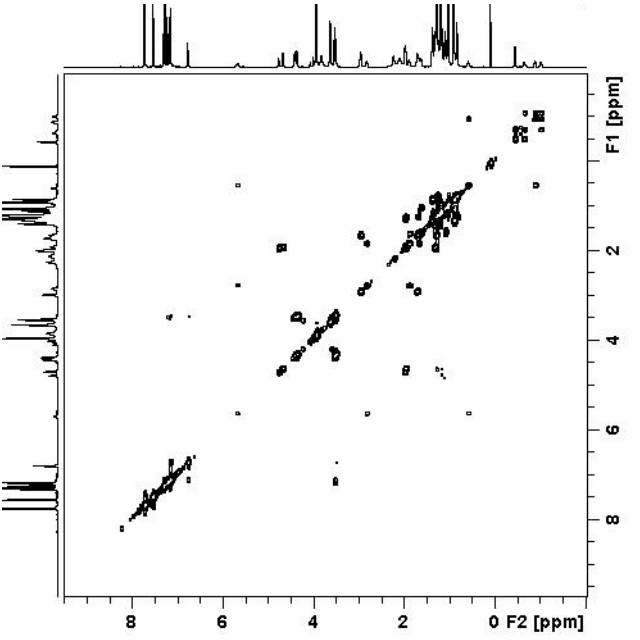

Figure 4.132. 2D COSY spectrum of derivative **16a⁺ ⊂ 46h** (600 MHz, $CDCl_3$, 298K).

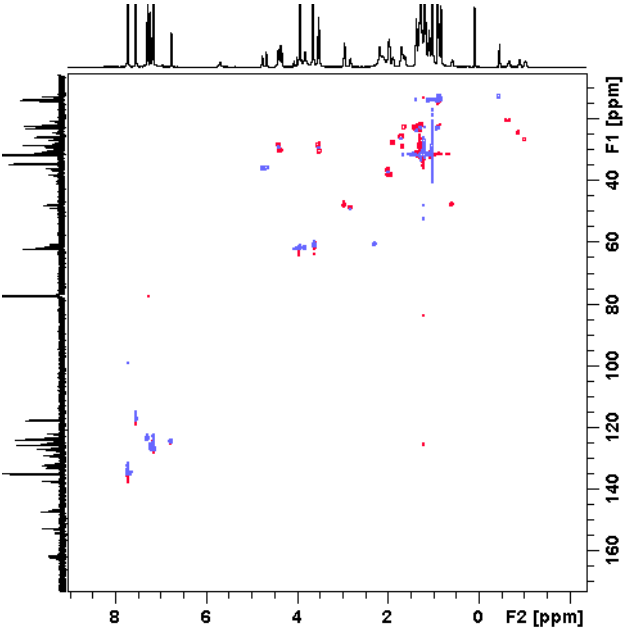

Figure 4.133. 2D HSQC spectrum of derivative **16a**$^{+}$ ⊂ **46h** (600 MHz, $CDCl_3$, 298K).

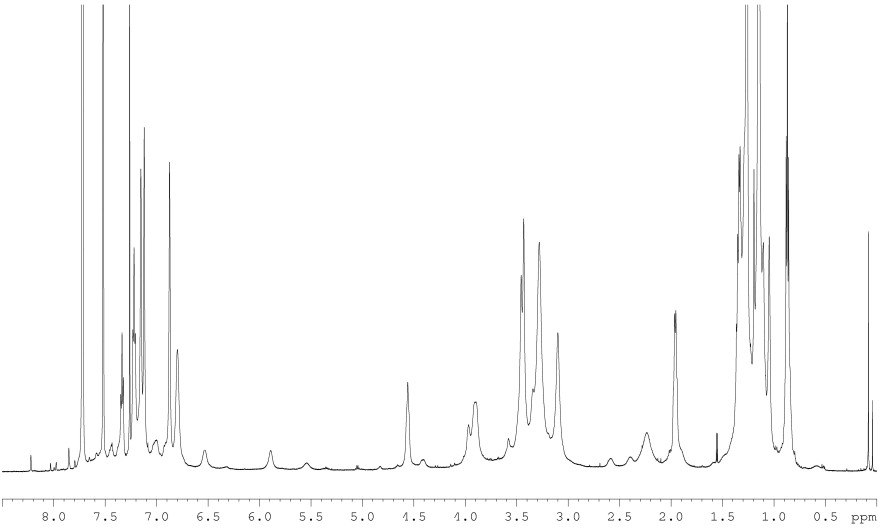

Figure 4.134. ^{1}H NMR spectrum (600 MHz, $CDCl_3$, 298 K) of 1:1 solution of **47h** (3.4 mM) and **16b**$^{+}$TFPB^{-} (3.4 mM).

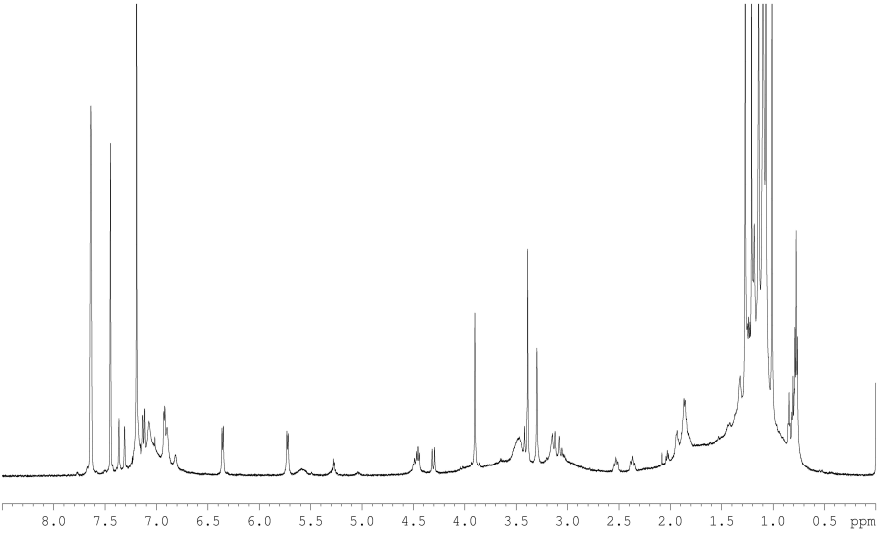

Figure 4.135. ^{1}H NMR spectrum (600 MHz, $CDCl_3$, 298 K) of 1:1 solution of **47h** (3.4 mM) and **16f**$^{+}$TFPB^{-} (3.4 mM).

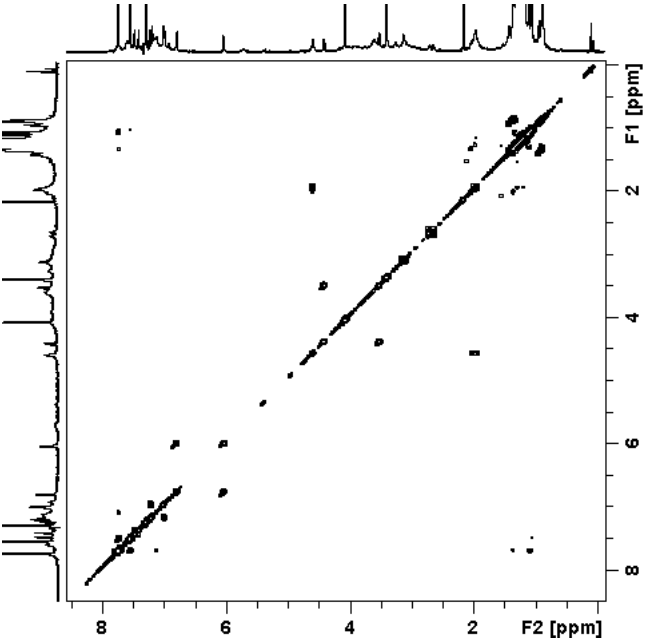

Figure 4.136. 2D COSY spectrum of derivative **16f**$^{+}$ ⊂ **47h** (600 MHz, $CDCl_3$, 298K).

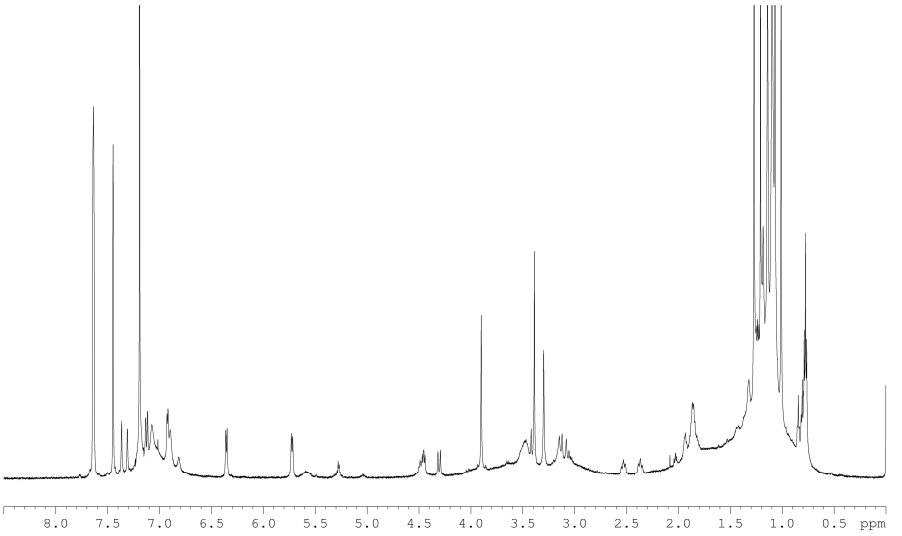

Figure 4.137. ^{1}H NMR spectrum (600 MHz, $CDCl_3$, 298 K). of 1:1 solution of **47h** (3.4 mM) and **16g**$^{+}$TFPB^{-} (3.4 mM).

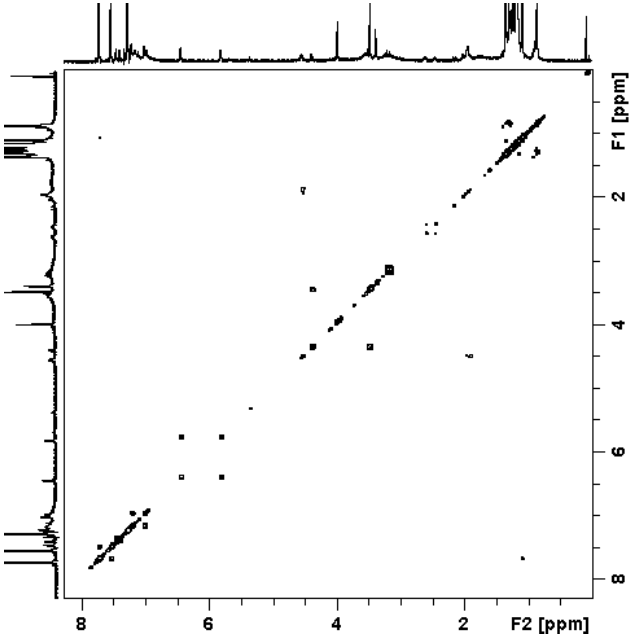

Figure4.138. 2D COSY spectrum of derivative **16g**$^{+}$ ⊂ **47h** (600 MHz, $CDCl_3$, 298K).

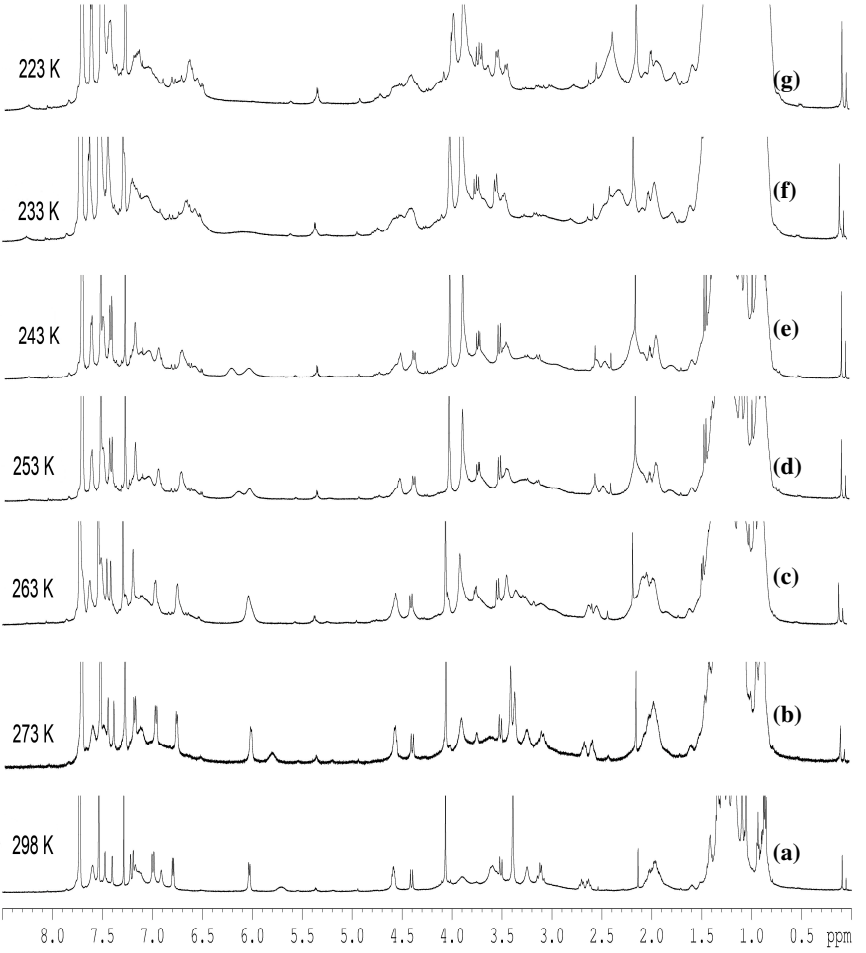

Figure 4.139. ^{1}H NMR spectra of **16f^{+}⊂47h** at different temperature: (a) 298 K, (b) 273 K, (c) 263 K, (d) 253 K, (e) 243 K, (f) 233 K, (g) 223 K (600MHz, $CDCl_3$).

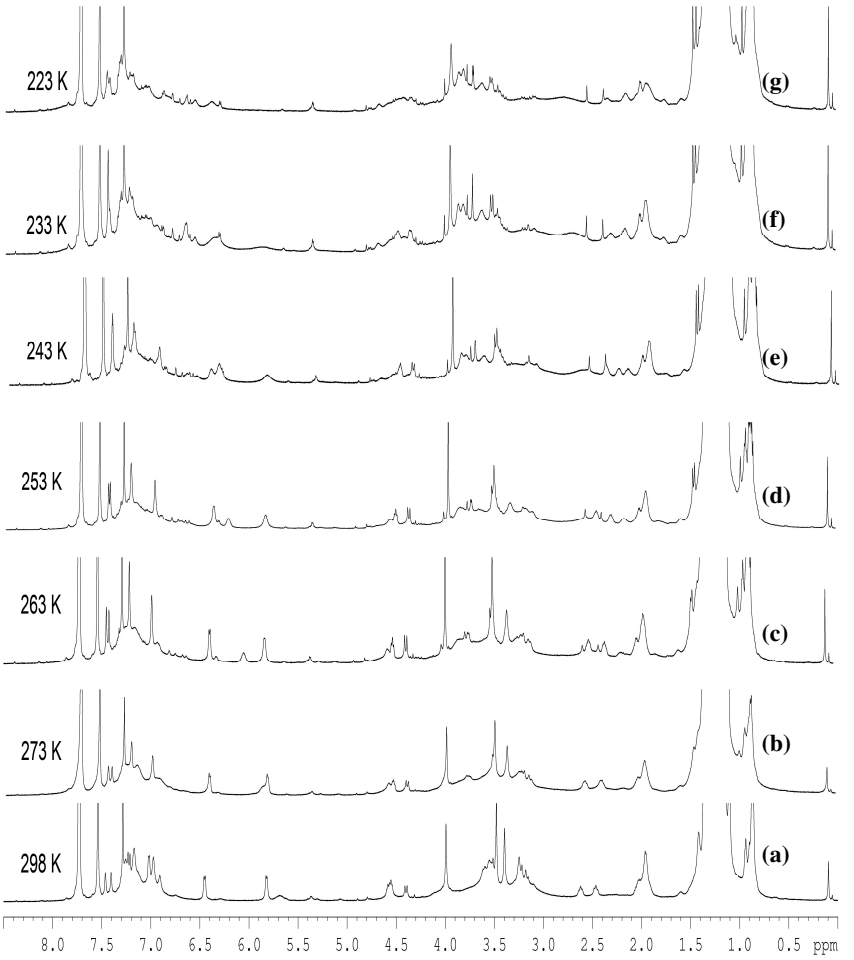

Figure 4.140. ^{1}H NMR spectra of **16g^{+}⊂47h** at different temperature: (a) 298 K, (b) 273 K, (c) 263 K, (d) 253 K, (e) 243 K, (f) 233 K, (g) 223 K (600MHz, $CDCl_3$).

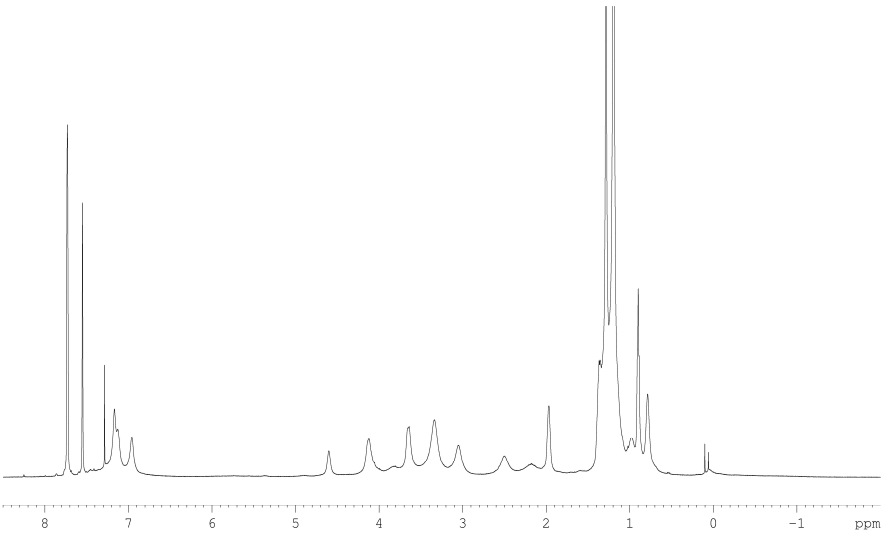

Figure 4.141. ^{1}H NMR spectrum (600 MHz, $CDCl_3$, 298 K) of 1:1 solution of **47h** (3.4 mM) and **16a**$^{+}$TFPB^{-} (3.4 mM).

4.7.3.4 ^{1}H NMR analysis determination of K_{ass} values

The association constant values of complexes were calculated by means of two methods:

a) Integration of free and complexed ^{1}H NMR signals of host or guest. In this case, an equimolar solution of host and guest was solubilized in $CDCl_3$ and equilibrated in a NMR tube.

b) Quantitative ^{1}H NMR experiments using TCE as the internal standard. In this case, ^{1}H NMR experiments were carried out on a 1:1 mixture of host and guest in 0.5 mL of $CDCl_3$ containing 1 µL of 1,1,2,2-tetrachloroethane (d= 1.586 g/mL) as internal standard. The following equation was used to obtain the moles of the complex:

$$\frac{G_a}{G_b} = \frac{F_a}{F_b} \times \frac{N_b}{N_a} \times \frac{M_a}{M_b}$$

Where:

G_a = grams of 1,1,2,2-Tetrachloroethane**;** G_b= grams of pseudorotaxane.

F_a and F_b = areas of the signal related of 1,1,2,2-tetrachloroethane and pseudorotaxane.

N_a and N_b = numbers of nuclei which cause the signals (N_a for 1,1,2,2-tetrachloroethane**;** N_b for pseudorotaxane)

M_a and M_b = molecular masses of 1,1,2,2-tetrachloroethane (a) and pseudorotaxane (b).

Derivative 16b$^+$⊂ 46g

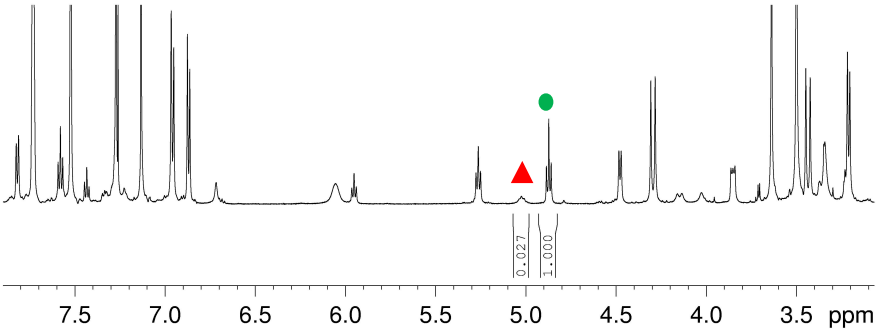

Figure 4.142. Portion of ^{1}H NMR spectrum (600 MHz, $CDCl_3$, 298 K) of a 1:1 mixture of **46g** (3.2×10^{-3} M) and **16b$^+$**TFPB$^-$ (3.2×10^{-3} M). The association constant K_a value was calculated by integration of complexed ArCH(R)Ar (▲) and free ArCH(R)Ar (●) signals of host **46g**.

Derivative 16a$^+$⊂ 46g

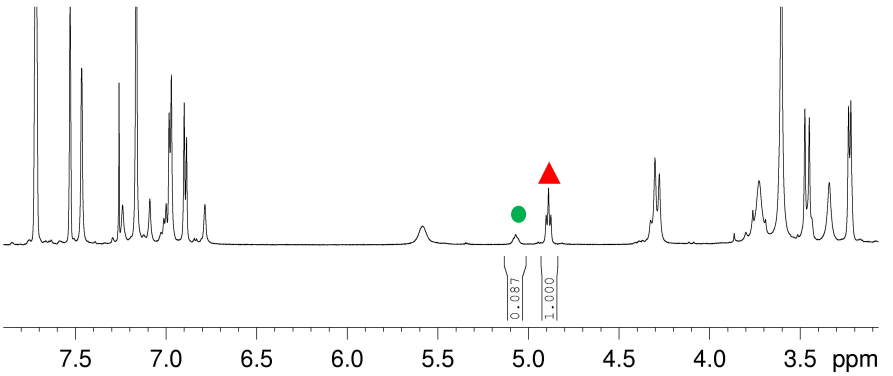

Figure 4.143. Portion of ^{1}H NMR spectrum (600 MHz, $CDCl_3$, 298 K) of a 1:1 mixture of **46g** (3.2×10^{-3} M) and **16a$^+$**TFPB$^-$ (3.2×10^{-3} M). The association constant K_a value was calculated by integration of complexed ArCH(R)Ar (▲) and free ArCH(R)Ar (●) signals of host **46g**.

Derivative 16f^{+}⊂ 47g

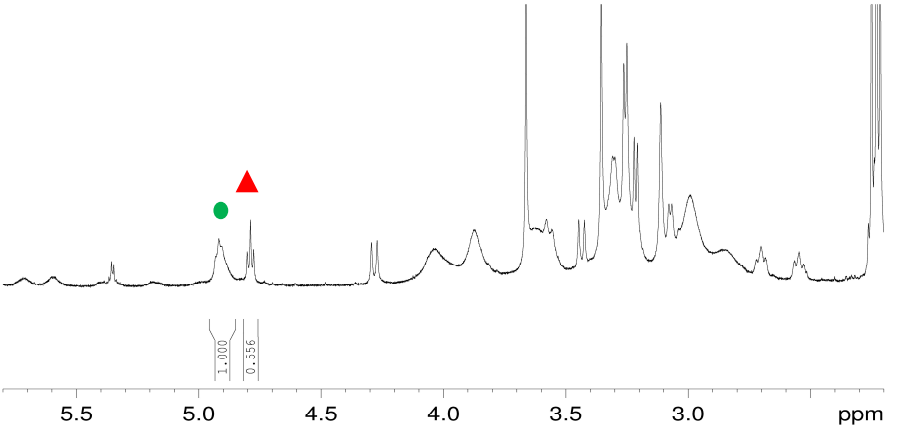

Figure 4.144. Portion of ^{1}H NMR spectrum (600 MHz, $CDCl_3$, 298 K) of a 1:1 mixture of **47g** (3.2×10^{-3} M) and **16f^{+}**TFPB^{-} (3.2×10^{-3} M). The association constant K_a value was calculated by integration of complexed ArCH(R)Ar (▲) and free ArCH(R)Ar (●) signals of host **47g**.

Derivative 16b^{+}⊂ 46h

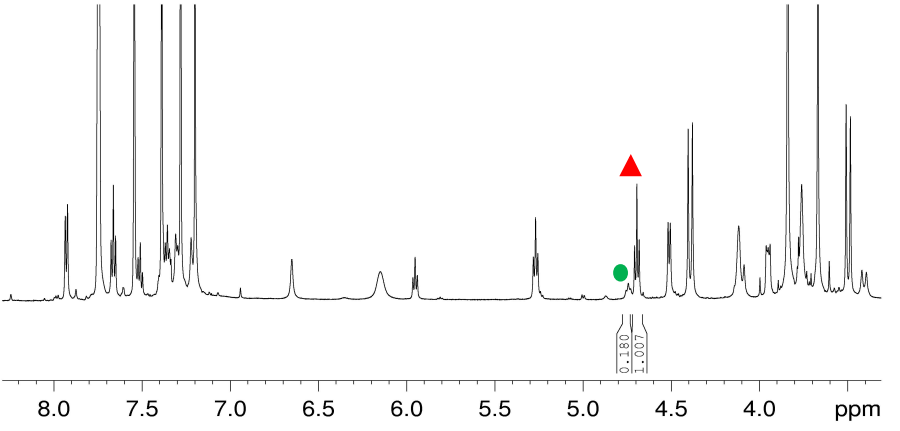

Figure 4.145. Portion of ^{1}H NMR spectrum (600 MHz, $CDCl_3$, 298 K) of a 1:1 mixture of **46h** (3.4×10^{-3} M) and **16b^{+}**TFPB^{-} (3.4×10^{-3} M). The association constant K_a value was calculated by integration of complexed ArCH(R)Ar (▲) and free ArCH(R)Ar (●) signals of host **46h**.

Derivative 16g^{+}⊂46h

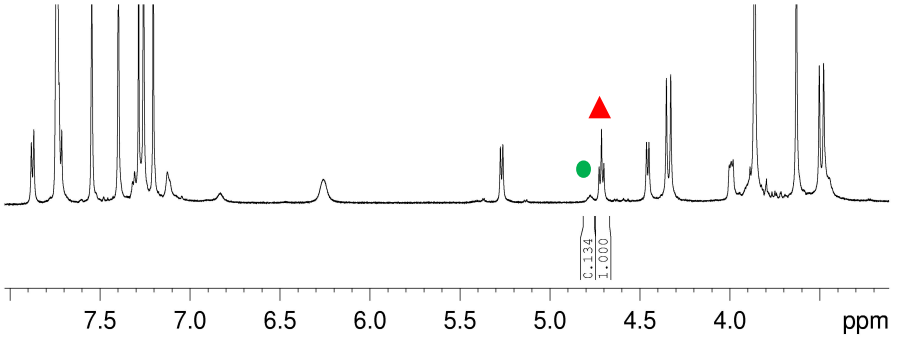

Figure 4.146. Portion of ^{1}H NMR spectrum (600 MHz, $CDCl_3$, 298 K) of a 1:1 mixture of **46h** (3.4×10^{-3} M) and **16b**$^{+}$TFPB^{-} (3.4×10^{-3} M). The association constant K_a value was calculated by integration of complexed ArCH(R)Ar (▲) and free ArCH(R)Ar (●) signals of host **46h**.

Derivative 16a^{+}⊂46h

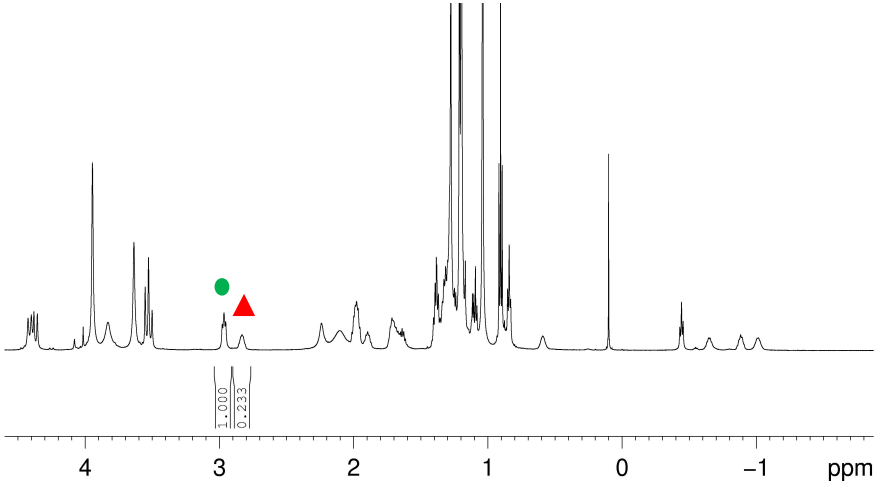

Figure 4.147. Portion of ^{1}H NMR spectrum (600 MHz, $CDCl_3$, 298 K) of a 1:1 mixture of **46h** (3.4×10^{-3} M) and **16a**$^{+}$TFPB^{-} (3.4×10^{-3} M). The association constant K_a value was calculated by integration of complexed CH_2NH_2 (▲) and free CH_2NH_2 (●) signals of guest **16a**$^{+}$TFPB^{-}.

Derivative 16f^{+}⊂ 46g

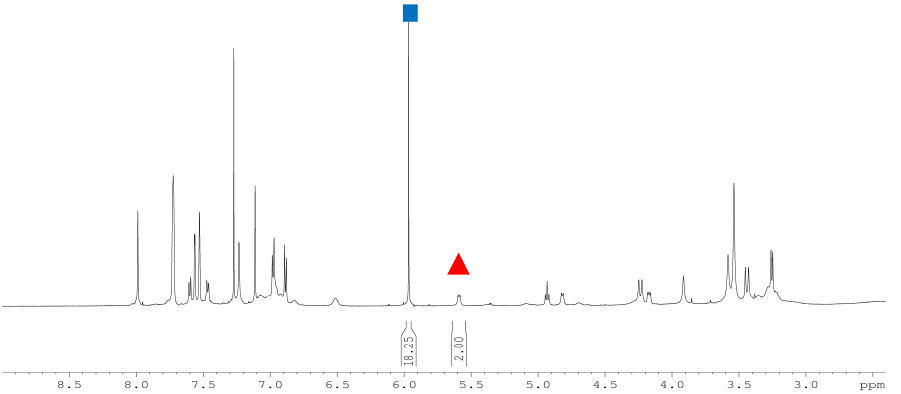

Figure 4.148. ^{1}H NMR spectra (600 MHz, $CDCl_3$, 298 K) of an equimolar solution (3.2 mM) of **46g** and **16f**$^{+}$TFPB^{-} in 0.5 mL of $CDCl_3$ containing 1 µL of 1,1,2,2-Tetrachloroethane. The association constant K_a values was calculated by integration of signal of complex **46g** (▲) and 1,1,2,2-Tetrachloroethane (■).

Derivative 16g^{+}⊂ 46g

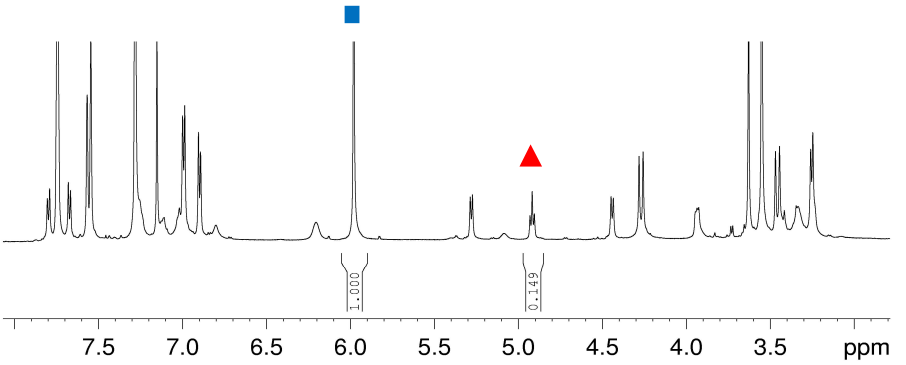

Figure 4.149. ^{1}H NMR spectra (600 MHz, $CDCl_3$, 298 K) of an equimolar solution (3.2 mM) of **46g** and **16g**$^{+}$TFPB^{-} in 0.5 mL of $CDCl_3$ containing 1 µL of 1,1,2,2-Tetrachloroethane. The association constant K_a values was calculated by integration of signal of complex **46g** (▲) and **1,1,2,2-*Tetrachloroethane*** (■).

Derivative 16g^{+}⊂ 47g

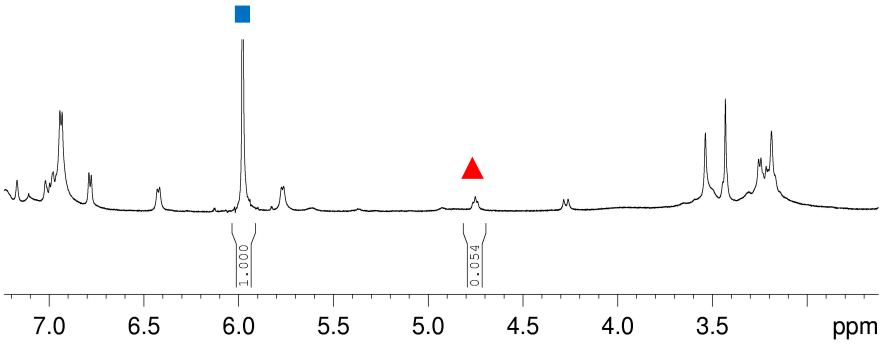

Figure 4.150. ^{1}H NMR spectra (600 MHz, $CDCl_3$, 298 K) of: (a) an equimolar solution (3.2 mM) of **47g** and **16g^{+}**TFPB^{-} in 0.5 mL of $CDCl_3$ containing 1 µL of 1,1,2,2-Tetrachloroethane. The association constant K_a values were calculated by integration of signal of complex **47g** (▲) and 1,1,2,2-Tetrachloroethane (■).

Derivative 16f^{+}⊂ 46h

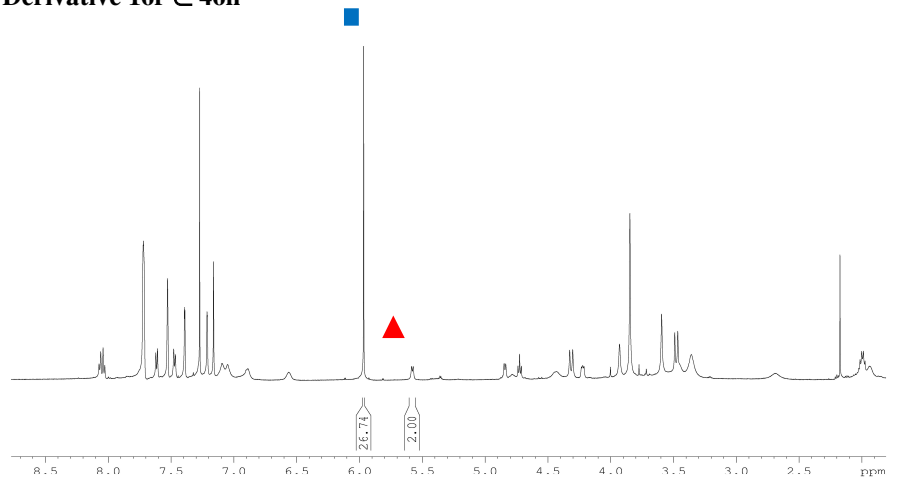

Figure 4.151. ^{1}H NMR spectra (600 MHz, $CDCl_3$, 298 K) of an equimolar solution (3.2 mM) of **46h** and **16f^{+}**TFPB^{-} in 0.5 mL of $CDCl_3$ containing 1 µL of 1,1,2,2-Tetrachloroethane. The association constant K_a values were calculated by integration of signal of complex **46h** (▲) and 1,1,2,2-Tetrachloroethane (■).

Derivative 16f^{+}⊂ 47h

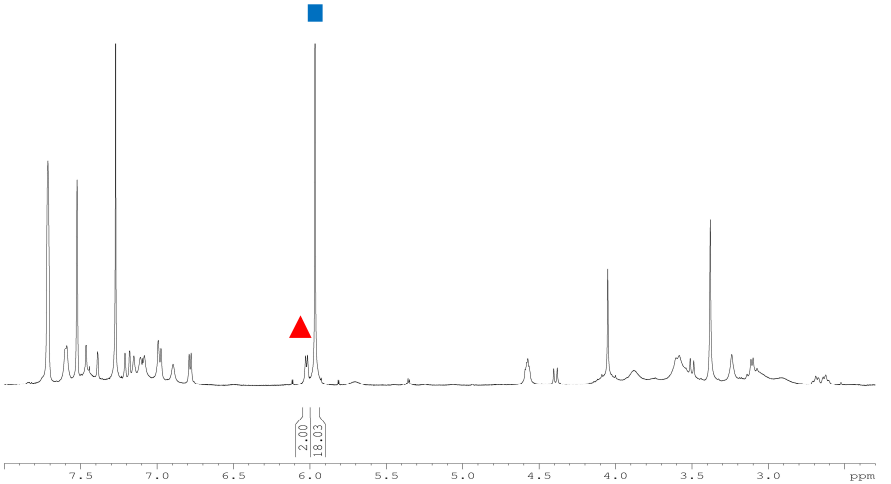

Figure 4.152. ^{1}H NMR spectra (600 MHz, $CDCl_3$, 298 K) of an equimolar solution (3.2 mM) of **47h** and **16f**$^{+}$TFPB^{-} in 0.5 mL of $CDCl_3$ containing 1 µL of 1,1,2,2-Tetrachloroethane. The association constant K_a values were calculated by integration of signal of complex **47h** (▲) and 1,1,2,2-Tetrachloroethane (■).

Derivative 16g^{+}⊂ 47h

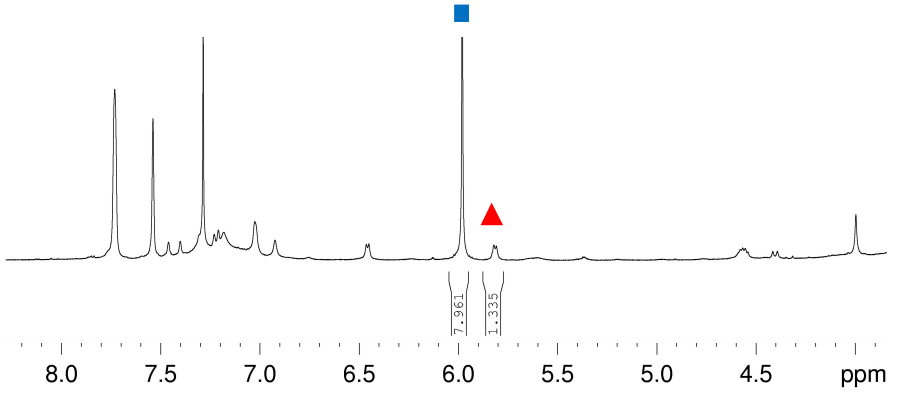

Figure 4.153. ^{1}H NMR spectra (600 MHz, $CDCl_3$, 298 K) of an equimolar solution (3.2 mM) of **47h** and **16g**$^{+}$TFPB^{-} in 0.5 mL of $CDCl_3$ containing 1 µL of 1,1,2,2-Tetrachloroethane. The association constant K_a values were calculated by integration of signal of complex **47h** (▲) and 1,1,2,2-Tetrachloroethane (■).

4.7.3.5 Crystallographic information of derivatives 46h and 47h

Derivative 46h

Colourless single crystals suitable for X-ray investigation were obtained by slow evaporation of $CHCl_3$ solution containing derivative **46h**. Data collection was carried out at the Macromolecular crystallography XRD1 beamline of the Elettra synchrotron (Trieste, Italy), employing the rotating-crystal method and the cryo-cooling technique. A single crystal of **46h** was dipped in PEG200 (cryoprotectant), mounted on a loop and flash-frozen under a liquid nitrogen stream at 100 K. Diffraction data were indexed and integrated using the XDS package.[53] Scaling was carried out with XSCALE.[54] The structure was solved by VLD methods using the SHELXT package;[55] while structure refinement was performed with SHELXL-14,[56] operating through the WinGX GUI,[57] by full-matrix least-squares (FMLS) methods on F^2.The asymmetric unit contains one molecule of derivative **46h**. The thermal parameters of all non-hydrogen atoms were refined anisotropically with exclusion of one tert-butyl group found disordered in two positions (position A: 0.8 occupancy factor, anisotropically refined with ISOR Card; position B: 0.2 occupancy factor isotropically refined). All hydrogen atoms were placed at the geometrically calculated positions and refined using the riding model. Crystal data and final refinement details for the complex are reported in **Table 4.9**.

Derivative 47h

Colourless single crystals suitable for X-ray investigation were obtained by slow evaporation of $CHCl_3/CH_3OH$ solution containing derivative **47h**. Data collection was carried out at the Macromolecular crystallography XRD1 beamline of the Elettra synchrotron (Trieste, Italy), employing the rotating-crystal method and the cryo-cooling technique. A single crystal of **47h** was dipped in glycerol (cryoprotectant), mounted on a loop and flash-frozen under a liquid nitrogen stream at 100 K. Diffraction data were indexed and integrated using the XDS package.[53] Scaling was carried out with XSCALE.[54] The structure was solved by VLD methods using the SIR 2014 package;[55] while structure refinement was performed with SHELXL-14,[56] operating through the WinGX GUI,[57] by full-matrix least-squares (FMLS) methods on F^2.The asymmetric unit contains half molecule of derivative **47h**. The thermal parameters of all non-hydrogen atoms were refined anisotropically. All hydrogen atoms were placed at the geometrically calculated positions and refined using the riding model. Crystal data and final refinement details for the complex are reported in **Table 4.10**.

Table 4.9. Crystallographic data for **46h**.

CCDC code	1906652
Formula	$C_{80}H_{112}O_6$
Formula weight	1169.69
Temperature (K)	100(2)
Wavelength (Å)	0.7
Crystal system	monoclinic
Space group	P 21/c
a (Å)	31.797(2)
b (Å)	11.539(1)
c (Å)	19.088(2)
α (°)	90
β (°)	94.402(8)
γ (°)	90
V (Å^3)	6982.8(10)
Z	4
ρ_{calc} (g.mm^{-3})	1.113
μ (mm^{-1})	0.065
F (000)	2560
Data collection θ range	1.85- 28.794
Refl. Collected / unique	118778 / 18965
R_{int}	0.0266
Completeness (%)	99.5%
Refinement method	FMLS on F^2.
Data/Restraints/Parameters	18965 / 18 / 814
GooF	1.017
R_1 / wR_2 [I>2σ(I)]	0.0535 / 0.1418
R_1 / wR_2 all data	0.0585 / 0.146
ls shift su max/mean	0.001 / 0.000
Largest. Diff. peak/hole (e. Å^3)	0.6 / -0.4

Table 4.10. Crystallographic data for **47h**.

CCDC code	1906651
Formula	$C_{80}H_{112}O_6$
Formula weight	1169.69
Temperature (K)	100(2)
Wavelength (Å)	0.7
Crystal system	monoclinic
Space group	P 21/a
a (Å)	13.341(6)
b (Å)	16.117(4)
c (Å)	17.567(6)
α (°)	90
β (°)	108.21(2)
γ (°)	90
V (Å^3)	3588(2)
Z	2
ρ_{calc} (g.mm^{-3})	1.083
μ (mm^{-1})	0.063
F (000)	1280
Data collection θ range	1.202 - 33.165
Refl. Collected / unique	74695 / 11803
R_{int}	0.0389
Completeness (%)	82.2%
Refinement method	FMLS on F^2.
Data/Restraints/Parameters	11803 / 0 / 402
GooF	1.049
R_1 / wR_2 [I>2σ(I)]	0.0500 / 0.1314
R_1 / wR_2 all data	0.0642 / 0.1427
ls shift su max/mean	0.001 / 0.000
Largest. Diff. peak/hole (e. Å^3)	0.6 / -0.3

4.7.3.6 Computational detail for pseudorotaxane 16f$^+$⊂47h

Preliminary conformational searches have been performed by molecular mechanics calculations (Spartan 02). The minimized structures were optimized by DFT calculations (Gaussian 09) at B3LYP/6-31G(d,p) level of theory using Grimme's dispersion corrections (IOp(3/124 = 3)).

Cartesian Coordinates of the DFT-optimized structure of 2b$^+$ ⊂ 6c pseudorotaxane

O	-0.133000	1.200800	-3.367900
O	2.809000	3.707900	-0.929800
O	2.940000	1.203200	1.933700
C	5.209200	0.988100	1.141000
C	5.018800	2.225800	0.258700
H	4.294400	2.872500	0.757500
C	3.383500	2.673900	-1.657500
C	0.450300	3.524200	-3.047900
C	2.868600	2.403500	-2.939500
C	4.477400	0.558200	-3.170900
C	5.526600	-1.282800	2.745200
H	5.635300	-2.152400	3.387600
C	-1.857900	2.763700	-2.678300
C	6.613900	-0.852800	1.973300
C	-0.522200	2.509000	-3.029900
C	4.154600	0.524600	1.944500
C	4.291800	-0.627300	2.737600
C	4.409000	1.887200	-1.105300
C	1.856400	3.326200	-3.609200
H	1.766600	2.996000	-4.650000
H	2.303300	4.324100	-3.672600
C	3.429900	1.351000	-3.668000
H	3.062300	1.179200	-4.676000
C	6.418700	0.278000	1.172200
H	7.240100	0.638600	0.567600
C	0.046700	4.809400	-2.680300
H	0.788500	5.601300	-2.719100
C	5.140900	-0.506500	-4.067500
C	-2.198900	4.076500	-2.320900
H	-3.228200	4.283200	-2.062600
C	6.318800	3.053200	0.068100
H	7.093300	2.434900	-0.401700
H	6.113500	3.844900	-0.661700
C	4.928000	0.838300	-1.877700
H	5.720900	0.243100	-1.442700
C	-1.271700	5.121900	-2.316200
C	-2.930200	1.686300	-2.857800
H	-3.575000	2.020400	-3.681900
H	-2.432100	0.783800	-3.200400
C	7.957100	-1.604100	2.047500
C	-1.659400	6.584000	-2.013900
C	6.860500	3.686000	1.355900
H	6.083900	4.329000	1.796600
H	7.061600	2.903900	2.098300
C	2.821800	2.210300	2.947800
H	2.892300	1.776000	3.951500
H	1.841100	2.669100	2.817200
H	3.601200	2.973900	2.842400
C	-0.267500	0.872900	-4.760400
H	0.424100	1.460100	-5.371600
H	-1.289400	1.049900	-5.109300
H	-0.031300	-0.187500	-4.859400
C	3.434200	4.992100	-1.020100
H	4.326600	5.050000	-0.388800
H	2.701000	5.720100	-0.666600
H	3.715200	5.232000	-2.051600
C	6.229700	-1.303900	-3.324400
H	7.049000	-0.661000	-2.988300
H	6.658700	-2.054700	-3.995100
H	5.828200	-1.829900	-2.451600
C	-1.375100	7.444900	-3.269200
H	-0.315400	7.438100	-3.541400
H	-1.663600	8.485400	-3.087000
H	-1.944300	7.081400	-4.130800
C	8.496800	-1.539900	3.496600
H	8.661500	-0.503500	3.808200
H	9.451000	-2.072400	3.571100
H	7.804900	-1.997300	4.209800
C	8.133000	4.513600	1.132800
H	8.907100	3.872300	0.689900
H	7.931600	5.298700	0.391200
C	9.021400	-1.000100	1.111800

H	8.712200	-1.037100	0.061700
H	9.952200	-1.568500	1.199300
H	9.248500	0.039900	1.367200
C	7.749900	-3.083500	1.645800
H	7.042500	-3.591500	2.308200
H	8.698800	-3.627800	1.698400
H	7.370600	-3.163500	0.621600
C	4.089300	-1.511800	-4.587000
H	3.633500	-2.065000	-3.758500
H	4.557300	-2.243200	-5.254200
H	3.293500	-1.016300	-5.152900
C	5.800100	0.203100	-5.275700
H	5.065800	0.745800	-5.878500
H	6.292700	-0.527900	-5.925900
H	6.554400	0.922400	-4.942200
C	-0.828600	7.127600	-0.827700
H	-1.082700	6.612200	0.103500
H	-1.037000	8.192600	-0.680100
H	0.247700	7.023800	-0.997000
C	-3.150100	6.734300	-1.656300
H	-3.801200	6.424000	-2.480200
H	-3.370900	7.785200	-1.446100
H	-3.414700	6.158100	-0.765400
C	8.670500	5.149800	2.417800
H	7.931900	5.823500	2.866800
H	9.576500	5.732400	2.225200
H	8.918300	4.387200	3.164600
O	0.511500	-1.700900	4.467100
O	-2.441400	-3.655000	1.037200
O	-2.847400	-0.891900	-1.627100
C	-4.695700	-0.397300	-0.135100
C	-4.622800	-1.807500	0.467100
H	-4.029600	-2.416400	-0.216900
C	-2.862800	-2.790800	2.048500
C	0.270200	-3.616000	3.031700
C	-2.214600	-2.862400	3.296200
C	-3.675800	-1.077800	4.137300
C	-4.853700	2.173900	-1.256600
H	-4.934100	3.145000	-1.727600
C	2.346000	-2.316800	3.021100
C	-5.784600	1.809000	-0.280500
C	1.049000	-2.548500	3.510700
C	-3.798500	0.017600	-1.137900
C	-3.847300	1.304100	-1.699000
C	-3.889400	-1.858700	1.814600
C	-1.125000	-3.889400	3.580100
H	-1.058800	-3.996600	4.667900
H	-1.438500	-4.867200	3.203700
C	-2.637800	-2.003700	4.310500
H	-2.139300	-2.074100	5.270700
C	-5.672100	0.521500	0.265000
H	-6.402800	0.209900	1.002600
C	0.848200	-4.491600	2.106900
H	0.258200	-5.343500	1.783400
C	-4.110400	-0.184800	5.315700
C	2.873600	-3.214800	2.084600
H	3.880100	-3.036900	1.729200
C	-6.019700	-2.474700	0.601400
H	-6.652500	-1.877100	1.268600
H	-5.888900	-3.432900	1.118800
C	-4.275100	-1.024500	2.876100
H	-5.074000	-0.316700	2.697800
C	2.162600	-4.337500	1.637800
C	3.151400	-1.148000	3.588600
H	3.575000	-1.464000	4.551200
H	2.446500	-0.348400	3.818100
C	-6.942500	2.727800	0.157700
C	2.823200	-5.436000	0.778100
C	-6.748700	-2.715300	-0.725600
H	-6.129100	-3.358000	-1.369300
H	-6.866200	-1.765800	-1.263100
C	-3.338800	-1.645300	-2.752800
H	-2.496900	-2.199000	-3.164500
H	-4.120100	-2.345300	-2.441000
H	-3.750200	-0.976800	-3.515500
C	0.859100	-2.022300	5.817500
H	0.322200	-1.314500	6.452200
H	0.558600	-3.044400	6.078400
H	1.934500	-1.917800	5.998900
C	-3.161500	-4.890800	0.963100
H	-3.267000	-5.353800	1.950300
H	-4.158900	-4.750800	0.532200
H	-2.583000	-5.556200	0.317600
C	-5.308700	0.716600	4.962700
H	-6.183500	0.132700	4.657700
H	-5.596400	1.304300	5.839700
H	-5.070800	1.426700	4.163900
C	3.116800	-6.646700	1.699100
H	2.196800	-7.048200	2.134700
H	3.601600	-7.450000	1.133200

H	3.779700	-6.362100	2.522200
C	-6.870400	4.117000	-0.504100
H	-6.950500	4.057100	-1.594500
H	-7.703200	4.733100	-0.152000
H	-5.943300	4.638700	-0.249100
C	-8.126000	-3.368600	-0.547000
H	-8.748600	-2.726100	0.089900
H	-8.012000	-4.315200	-0.001700
C	-8.284800	2.069600	-0.244000
H	-8.421500	1.094600	0.233600
H	-9.123600	2.706700	0.056000
H	-8.342300	1.922500	-1.327400
C	-6.910300	2.926700	1.691500
H	-5.980700	3.407700	2.007100
H	-7.743400	3.564800	2.004700
H	-7.005000	1.979900	2.231400
C	-2.931300	0.724300	5.737300
H	-2.650800	1.406400	4.928500
H	-3.210800	1.329700	6.606400
H	-2.044700	0.141900	6.004900
C	-4.521800	-1.079100	6.510000
H	-3.696200	-1.707200	6.857000
H	-4.842900	-0.459600	7.354000
H	-5.352300	-1.738900	6.238900
C	1.899000	-5.898400	-0.368500
H	1.693800	-5.084600	-1.070000
H	2.377200	-6.708600	-0.928700
H	0.940400	-6.279900	-0.006100
C	4.151800	-4.969600	0.150600
H	4.908500	-4.738000	0.905500
H	4.559000	-5.764700	-0.481700
H	4.015800	-4.081600	-0.476900
C	-8.846800	-3.625700	-1.873300
H	-8.267700	-4.297600	-2.516900
H	-9.826500	-4.085400	-1.711400
H	-9.004700	-2.692900	-2.426200
C	-1.930600	3.242800	1.672800
C	-2.324500	1.911700	1.822000
C	-1.509000	0.892700	1.342100
C	-0.311800	1.194800	0.682400
C	0.079900	2.530800	0.540800
C	-0.724300	3.551600	1.042600
H	-3.255400	1.666200	2.316700
H	-1.807400	-0.138800	1.500500
H	1.018500	2.784300	0.060900
H	-0.409500	4.582800	0.943200
C	0.575400	0.084600	0.188700
H	1.576500	0.448200	-0.042600
H	0.664300	-0.706100	0.937200
N	0.051300	-0.596300	-1.070500
H	0.029800	0.073100	-1.867400
H	-0.937100	-0.886500	-0.959900
C	0.921900	-1.783300	-1.442500
H	1.831400	-1.364800	-1.878900
H	1.186500	-2.274000	-0.502700
C	-0.962000	-4.633700	-4.063400
C	-0.067500	-3.699800	-4.588300
C	0.535700	-2.770200	-3.741500
C	0.245800	-2.759600	-2.371700
C	-0.647800	-3.708400	-1.851900
C	-1.247700	-4.640100	-2.695300
H	0.167800	-3.712600	-5.646600
H	1.256700	-2.067100	-4.145700
H	-0.878300	-3.717300	-0.789800
H	-1.931100	-5.380500	-2.294200
C	-1.674900	-5.599500	-4.977300
F	-0.972100	-5.839200	-6.101300
F	-1.903400	-6.780800	-4.368400
F	-2.877600	-5.105100	-5.351700
C	-2.836100	4.341400	2.155200
F	-3.767800	4.666800	1.216000
F	-3.522300	3.981300	3.262500
F	-2.161200	5.474900	2.437600

Energy = -4839.28065 a.u.

0 imaginary frequency

CHAPTER V

Calixarenes with aromatic EDGs and EWGs

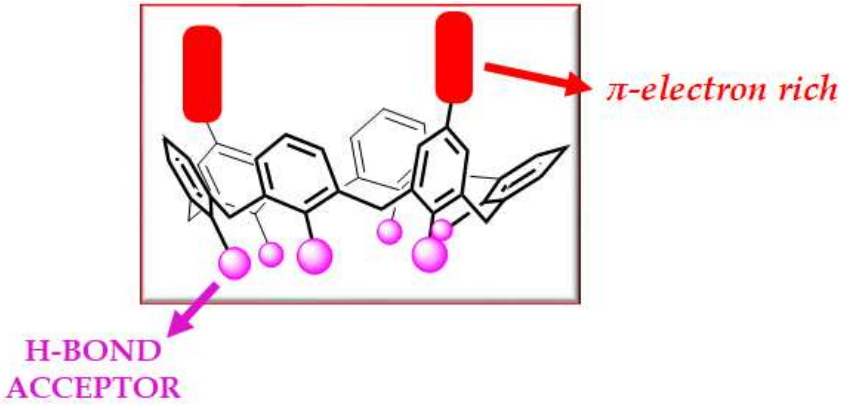

5.1 Introduction

In the previous chapters the possibilities of functionalizing the calixarene scaffold at the methylene bridges and with adamantyl groups have been explored, revealing interesting threading abilities. Hence, in this chapter, it was decided to study the influence of aromatic electron-poor or electron-rich groups towards the calixarene threading. Furthermore, it is interesting to observe that the introduction of an aromatic group on the calixarene scaffold can determine a new recognition site thanks to the formation of π-π interactions and for this reason these macrocycles can be defined as bifunctional calixarenes.

5.2 Calixarene with Electron Donating Groups

5.2.1 Synthesis of a calixarene with electron donating groups

Thanks to the results shown in the previous chapter, it was decided to focus the attention on bifunctional macrocycles with electron donating groups (EDG). Therefore, we planned to synthesize a derivative bearing an extended electron-rich aromatic substituent to the upper rim and completely alkylated at the lower rim (**Figure 5.1**).

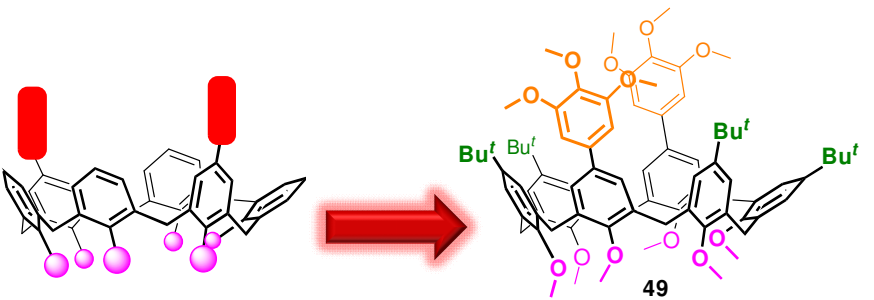

Figure 5.1. Bifunctional calix[6]arene with EDGs at the upper rim.

The synthetic strategy developed for the synthesis of such bifunctional derivative **49** is shown in **Scheme 5.1.** Starting from *p-tert*-butilcalix[6]arene, 2 out of 6 hydroxyl groups were protected by benzylation at the 1,4-positions. Then the remaining phenolic units were methylated to give derivative **50**. The previously protected sites were then freed by hydrogenolysis with Pd/C to obtain derivative **51**. This latter was then brominated (derivative **52**) at the upper rim and alkylated at the lower rim with MeI (derivative **53**). As described in chapter 3, the complete alkylation of the lower rim leads to interpenetrated complexes with a higher association constant in comparison to the partial-alkylation.

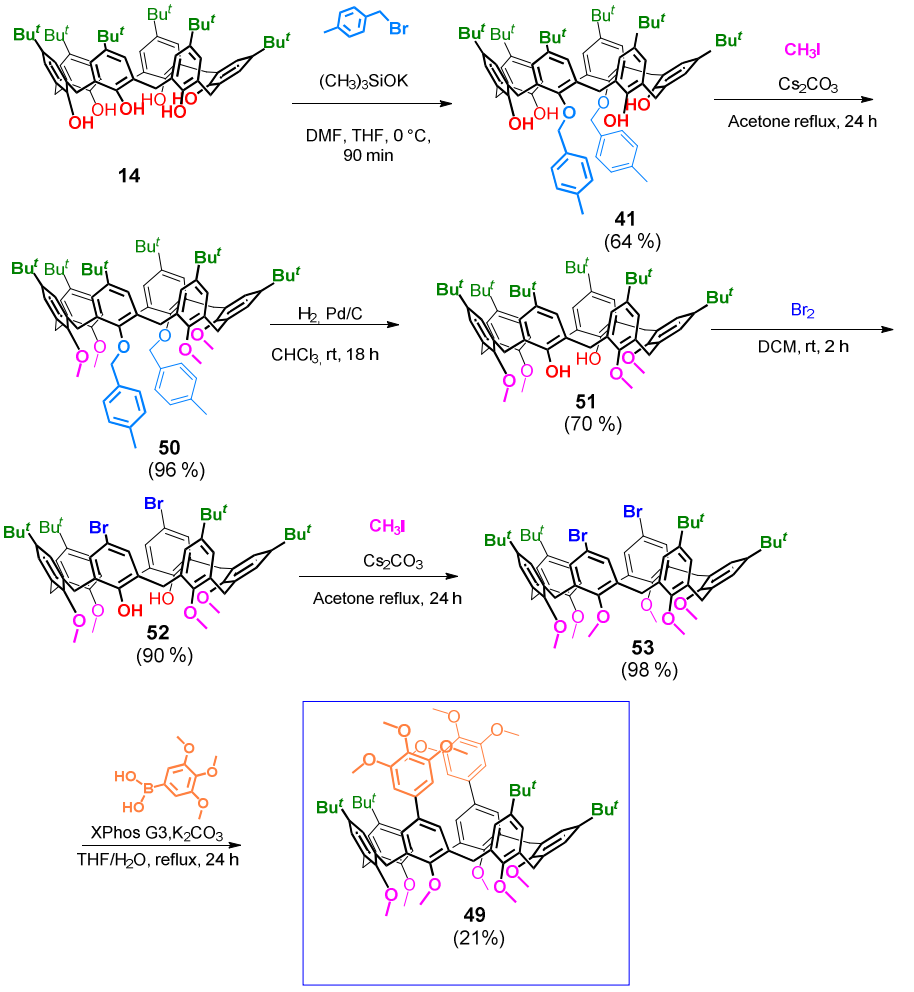

Scheme 5.1. Synthesis of derivative **49**.

Finally, electron rich aromatic substituents were introduced at the upper rim of derivative **53**, thanks to a Suzuki reaction. Given the complexity of the calixarene substrate, it was necessary to resort to a palladium-based catalyst, XPhos Pd G3 (**Figure 5.2**), which has been successfully used with other macrocycles of a similar complexity.[60]

[60] Demay-Drouhard, P.; Du, K.; Samanta, K.; Wan, X.; Yang, W.; Srinivasan, R.; Sue, A. C.-H.; Zuilhof, H. *Org. Lett.* **2019**, *21* (11), 3976–3980.

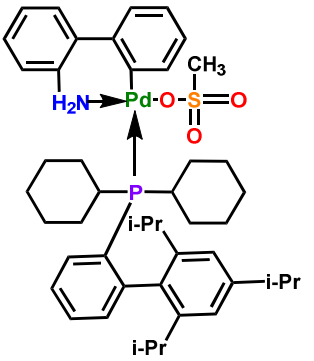

Figure 5.2. Structures of XPhos Pd G3.

The new derivative **49** was completely characterized by NMR spectroscopy and mass spectrometry. In the proton spectrum (**Figure 5.3**) it is possible to observe singlets related to the methoxy groups of the pyrogallol substituents. Furthermore, from the broad $ArCH_2Ar$ singlets at about 4 ppm, it can be deduced that this new derivative has a high conformational mobility.

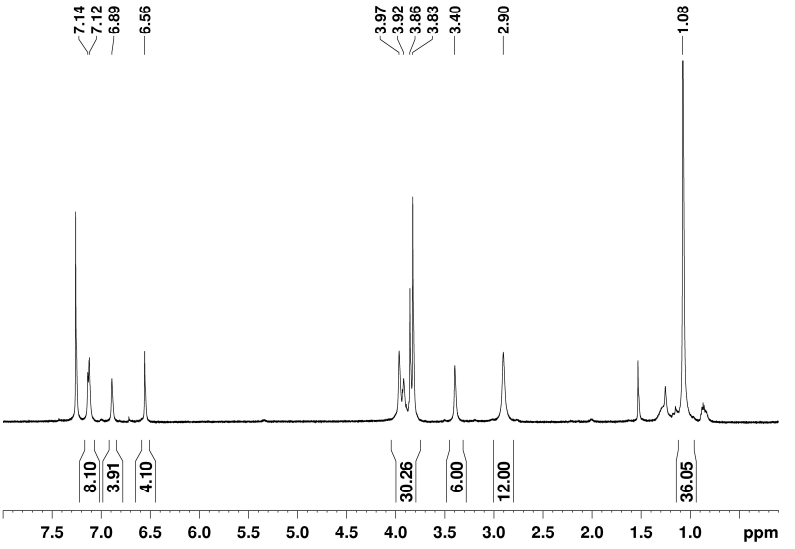

Figure 5.3. ^1H NMR spectrum of derivative **49** (600 MHz, $CDCl_3$, 298 K).

5.2.2 Threading of calixarene with EDGs

Initially, a threading study of host **53** was carried out with dibenzyl ammonium axle (**Scheme 5.2**). The proton NMR spectrum confirmed the pseudorotaxane formation driven by hydrogen bonding interactions between the calixarene oxygens and the ammonium group.

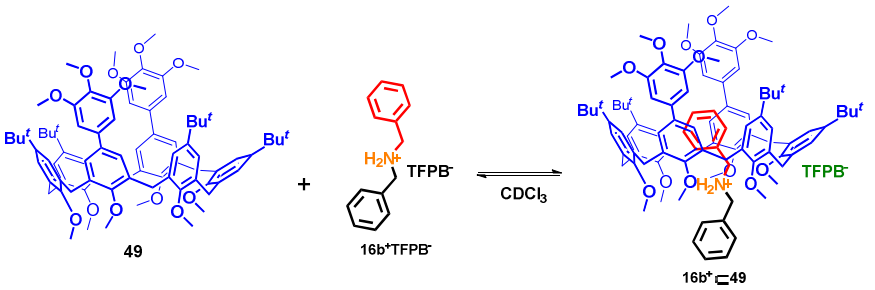

Scheme 5.2. Threading experiment between derivative **49** and derivative **16b**$^+$.

In fact, in the region between 4 and 6 ppm, the typical shielded signals of the axle (o, m, and p at 4.88, 5.74, and 6.24 ppm, respectively) can be easily seen (**Figure 5.4**). Furthermore, the calix-wheel shows a cone conformation highlighted by two $ArCH_2Ar$ AX systems (4.48/3.84 ppm and 4.36/3.52 ppm).

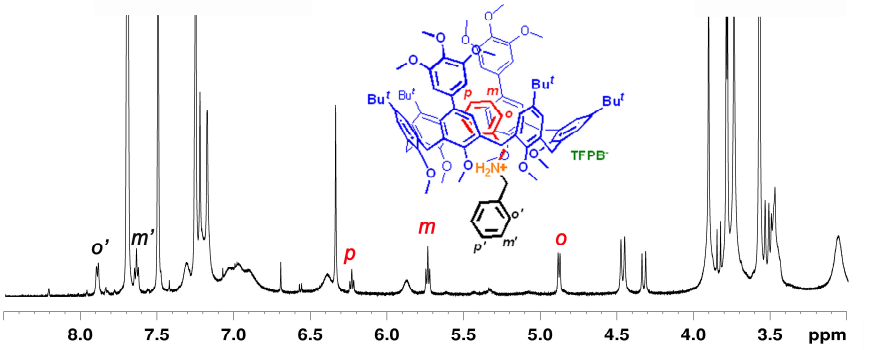

Figure 5.4. ^{1}H NMR spectra of mixture of derivative **49** and **16b**$^+$ 1:1 (600 MHz, $CDCl_3$, 298 K).

Subsequently, the threading ability of derivative **49** was extended to a non-symmetric axle, butylbenzylammonium TFPB **16e**$^+$ (**Scheme 5.3**). As in previous instances, two different stereoisomers, (endo-alkyl)-**16e**$^+$**⊂49** and (endo-benzyl)-**16e**$^+$**⊂53**, can be formed.

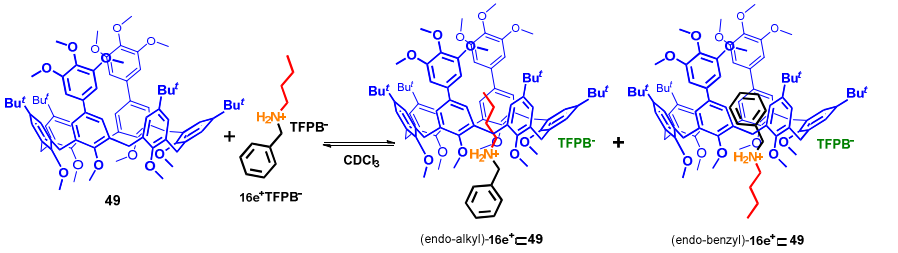

Scheme 5.3. Threading experiment between derivative **49** and derivative **16e**$^+$.

In the ^{1}H NMR spectrum of the mixture, the presence of shielded alkyl signals at negative chemical shift values and the absence of shielded benzyl resonances were

clearly visible. This confirms, that also in this case, the *endo*-alkyl rule, discussed in chapter 1, is valid. In addition, it is also clear that calixarene **49** assumes a cone conformation, as evidenced by the $ArCH_2Ar$ AX systems present between 4.5 and 3.5 ppm, when complexed by the ammonium salt (**Figure 5.5**).

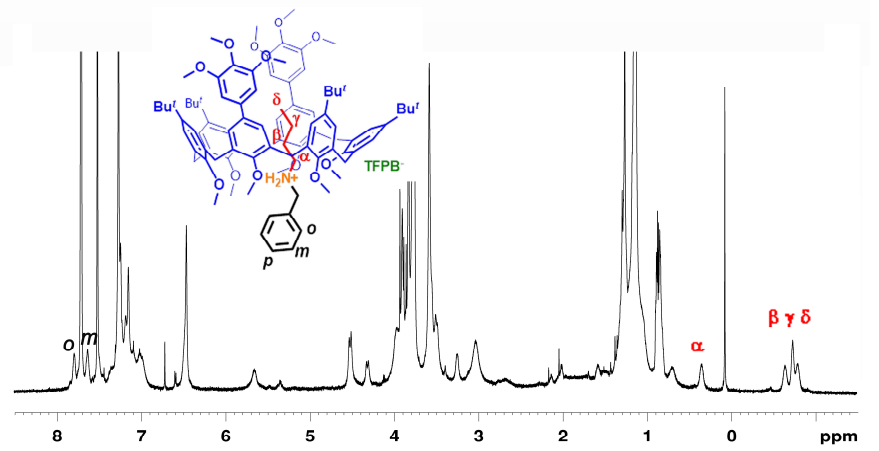

Figure 5.5. ^{1}H NMR spectrum of mixture of derivative **49** and **16e**$^+$TFPB$^-$ 1:1 (600 MHz, $CDCl_3$, 298 K).

5.3 Calixarenes with Electron Withdrawing Groups

5.3.1 Synthesis of calixarenes with EWGs

Initially, the study was focused on bifunctional calixarenes with electron withdrawing groups (EWGs) and, therefore, three different macrocycles were designed for this purpose. In detail, as EWGs were chosen pyridinium rings, viologen units, and fluorobenzyl substituents to give derivatives **54**$^{2+}$, **55**$^{4+}$, and **56**, respectively (**Figure 5.6**).

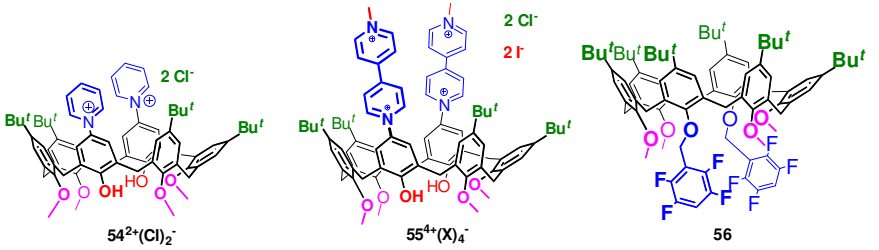

Figure 5.6. Bifunctional Calixarenes with EWGs.

The introduction of pyridinium and viologen units of derivatives $\mathbf{54}^{2+}$ and $\mathbf{55}^{4+}$ could be possible by means of the Zincke's reaction (**Scheme 5.4**), which allows the direct N-C linkage between a nitrogenous heterocycle and an aromatic nucleus.

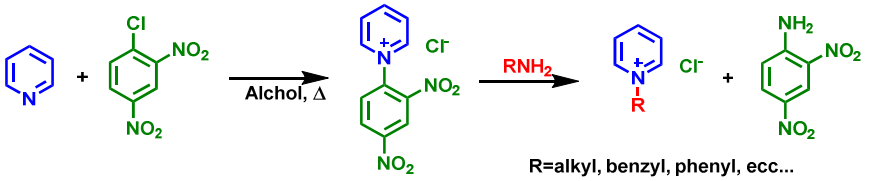

Scheme 5.4. Synthetic procedure of Zincke reaction.

Therefore, in order to obtain derivative $\mathbf{54}^{2+}$ and $\mathbf{55}^{4+}$, two different Zincke's salts[61] are necessary (**Figure 5.7**) which should be reacted with calix[6]arene **60** bearing two 4-aminophenol units in distal (1,4) positions.

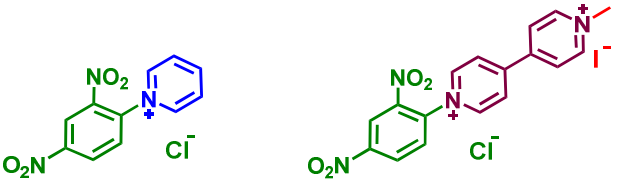

Figure 5.7. Zincke's salts **57** and **58**.

Scheme 5.5 shows the synthetic strategy developed for the synthesis of the precursor **60** obtainable from the previously described derivative **51**. In particular, two nitro groups were introduced at the 1,4 positions by ipsonitration to give **59**. This latter was subsequently reduced by Nickel/Raney in H_2 atmosphere to give **60**.

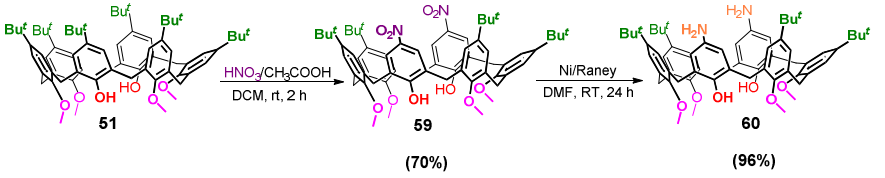

Scheme 5.5. Synthesis of derivative **60**.

The Zincke **57** was obtained by reaction of pyridine **61** with 2,4-dinitrochlorobenzene **62** (**Scheme 5.6a**). Instead, its analogue **58** was obtained by reacting 4,4'-bipyridine **63** with 2,4-dinitrochlorobenzene **62** to obtain monocation **64**. This latter was then methylated with iodomethane to obtain **59** (**Scheme 5.6b**).

[61] (a) L. Robertson, R. C. Hartley, *Tetrahedron,* **2009**, *65*, 5284; (b) V. A. Constantin; L. Cao, S. Sadaf, L. Walder, *Phys. Status Solidi B,* **2012**, *249,* 2395-2398.

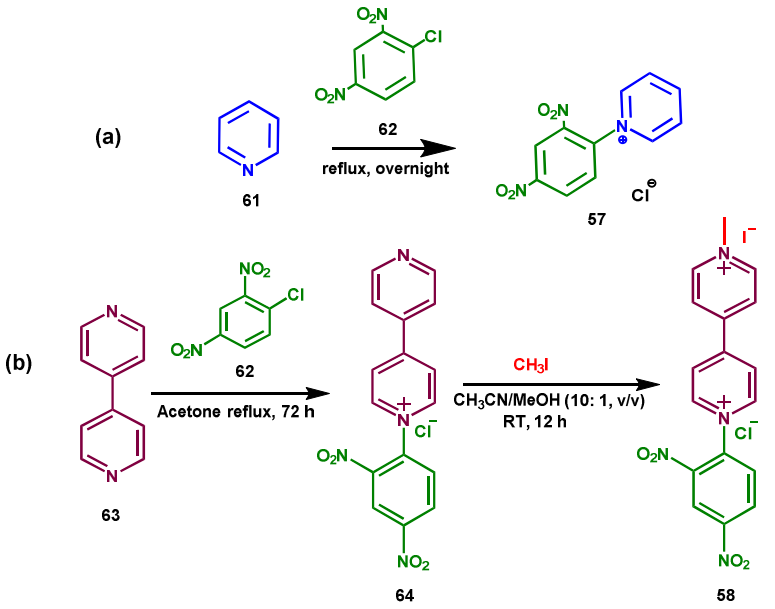

Scheme 5.6. (a) Synthesis of Zincke's salt **57**; (b) Synthesis of Zincke's salt **58**.

The reaction between derivative **60** and Zincke salt **57** (**Scheme 5.7**) under microwave irradiation, at 100 ° C and using as a solvent a mixture of $CHCl_3$, CH_3CN and H_2O (4:10:0.5), allowed the synthesis of derivative **54**, a bifunctional calix[6]arene bearing two pyridinio units at the upper rim,

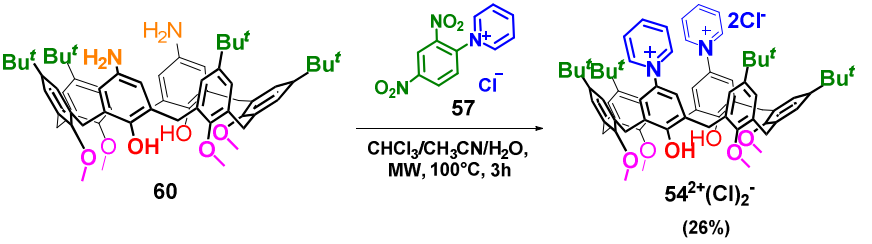

Scheme 5.7. Synthesis of derivative $\mathbf{54}^{2+}(Cl)_2^-$.

The Zincke reaction follows a complex mechanism whereby two molecules of the amino derivative react with the Zincke salt by connecting its NH_2 group to position 2 on the pyridine ring. Subsequently, there is a rearrangement and the complete opening of the nitrogenous ring. Then the breaking of the bond with the nitrobenzene group is observed, after the attack of a second amine group. Finally, the closure of a new pyridine ring occurs, which includes the nitrogen of the amino derivative (**Scheme 5.8**).

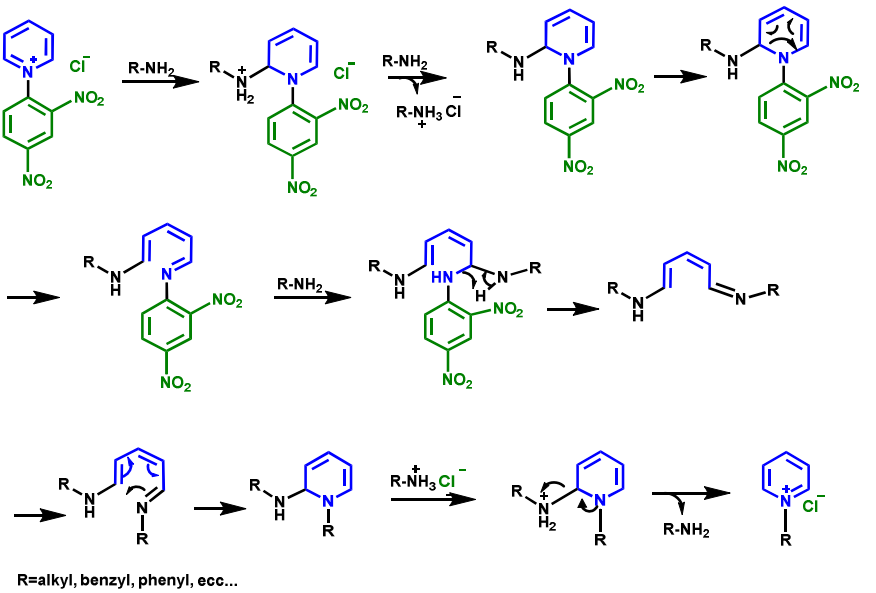

Scheme 5.8. Zincke reaction mechanism.

The new pyridinio-calix[6]arene **54**$^{2+}$ was completely characterized by NMR spectroscopy and mass spectrometry. It is important to highlight that this compound is present in solution in a preferential 1,3,5-alternate conformation, as deduced by the pattern of its $ArCH_2Ar$ signals including one tight AB system and one singlet (**Figure 5.8**).

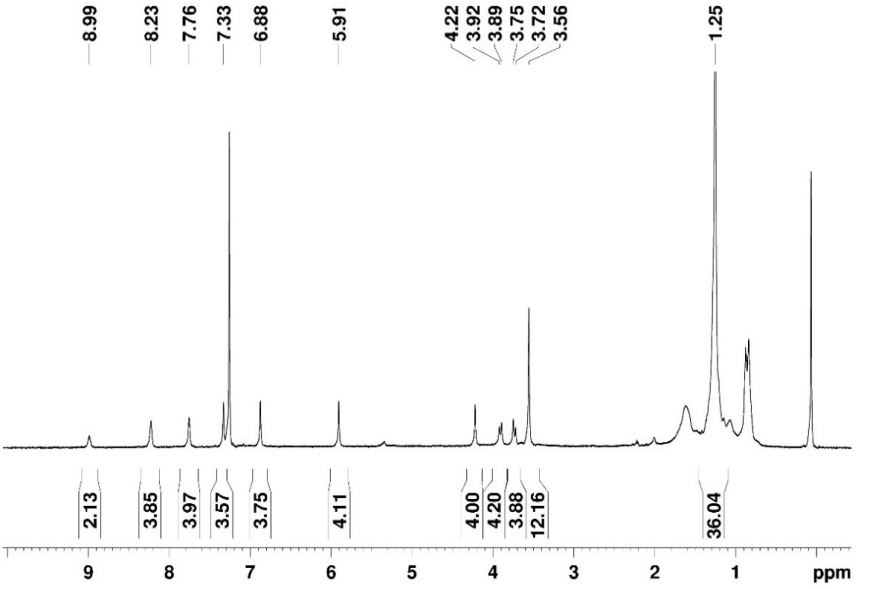

Figure 5.8. ^{1}H NMR spectrum of derivative **54**$^{2+}$$(Cl)_2^-$ (400 MHz, $CDCl_3$, 298 K).

The synthesis of bis-viologen-calix[6]arene **55**$^{4+}$ was performed in EtOH/THF 4/1 at 70 ° C, under conditions like reported by Bucher[62] in 2015 (**Scheme 5.9**).

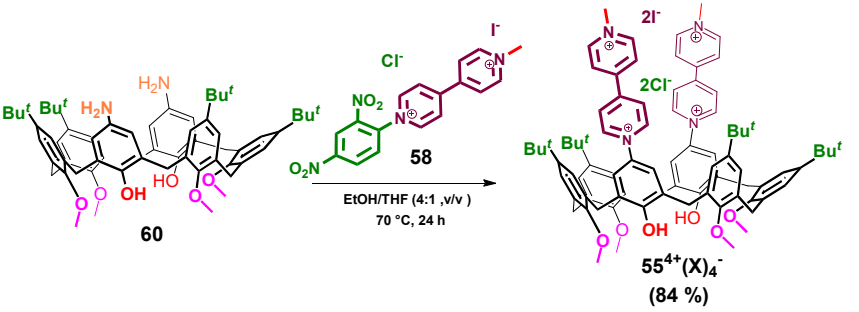

Scheme 5.9. Synthesis of derivative **55**$^{4+}$.

Compound **55**$^{4+}$ was also fully characterized by NMR spectroscopy and mass spectrometry. In this case, it is conformationally mobile (**Figure 5.9**) as testified by the broad signals in its ^{1}H NMR spectrum corresponding to interconversions occurring on the NMR timescale (**Figure 5.10**).

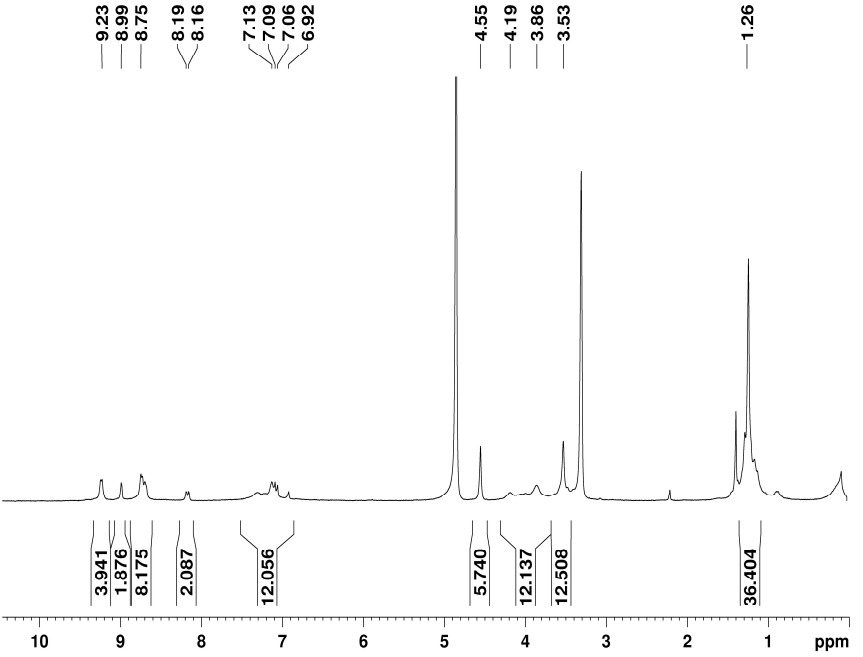

Figure 5.9. ^{1}H NMR spectrum of derivative **55**$^{4+}$ (600 MHz, CD_3OD, 298 K).

[62] C. Kahlfuss, A. Mileta, J. Wytko, J. Weiss, E. Saint-Aman, C. Bucher , *Org. Lett.,* **2015**, *17*, 4058.

The formation of **55** is confirmed by the mass spectrum due to the presence of the molecular peak at 1255.7243 (*m/z*: $[M]^+$ Calcd for $C_{84}H_{95}N_4O_6$ 1255.7246), and of the peak at 1358.6359 (*m/z*: $[M^+I]^+$ Calcd for $C_{84}H_{96}IN_4O_6$ 1358.6369), related to the molecule **55** carrying an iodide ion. These peaks are mono-charged because the viologen units are reduced in the MS source, as reported in the literature.[63]

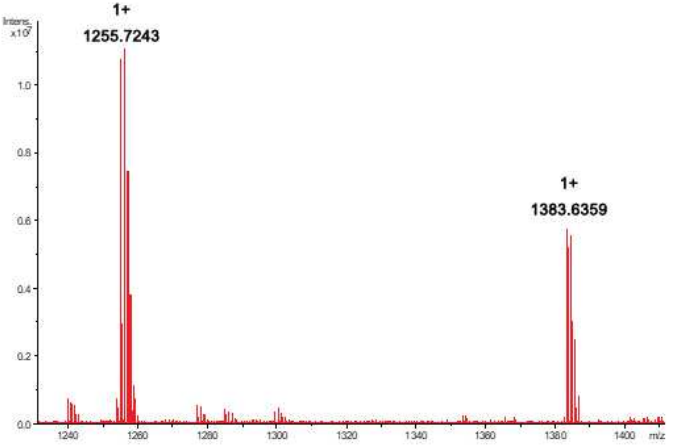

Figure 5.10. MALDI-MS spectrum of derivative $\mathbf{55}^{4+}$.

Calix[6]arene **56**, bearing two tetrafluorobenzyl EWGs, was obtained by alkylation with tetrafluorobenzyl bromide of the free phenolic groups of the known derivative **50**, in the presence cesium carbonate (**Scheme 5.10**).[64]

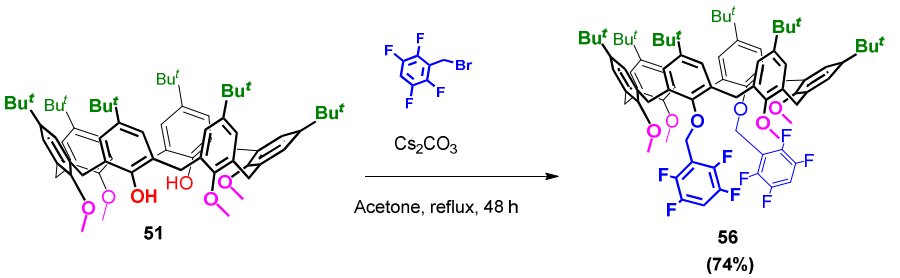

Scheme 5.10. Synthesis of derivative **56**.

56 was obtained in good yields and was exhaustively characterized by NMR spectroscopy and mass spectrometry. **Figure 5.11** shows its proton NMR spectrum from which one AX system and one singlet can be clearly seen for $ArCH_2Ar$ groups, indicating the presence of a preferred 1,2,3-alternate conformation.

[63] Svoboda, M.; Kodıcek, M. *Rapid Commun. Mass Spectrom.* **2010**, *24*, 3351.

[64] Janssen, R. G.; Verboom, W.; Reinhoudt, D. N.; Casnati, A.; Freriks, M.; Pochini, A.; Ugozzoli, F.; Ungaro, R.; Nieto, P. M.; Carramolino, M.; Cuevas, F.; Prados, P.; *Synthesis*, **1992**, *4*, 384.

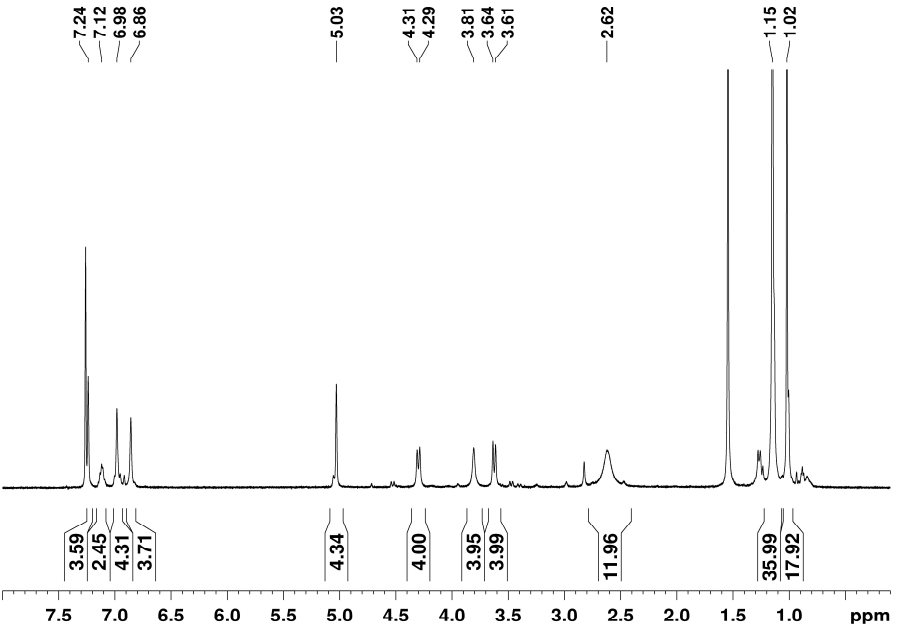

Figure 5.11. ^{1}H NMR spectrum of derivative **56** (300 MHz, $CDCl_3$, 298 K).

5.3.2 Threading of calixarenes with EWGs

The threading abilities of the above calixarenes with EWGs were studied by using two known axles having TFPB as a counterion (**Figure 5.12**). As aforementioned, this anion forms a weakly coordinating ion pair facilitating the insertion of the axle into the cavity of the macrocycle. The complexation tests were performed by mixing host and guest in a 1:1 ratio in deuterated chloroform.

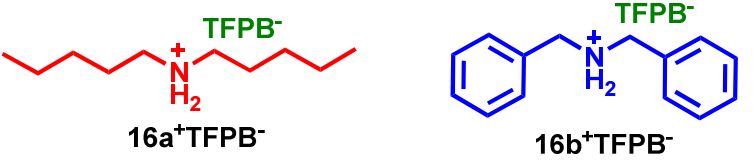

Figure 5.12. Linear ammonium systems.

Derivative **54** was initially tested with both ammonium axles (**Figure 5.13**). From the ^{1}H NMR spectra, some changes in the host signals can be observed, but there are no typical shielded signals. This indicate that no pseudorotaxanes are formed, whereas anion exchanges between host and guest are occurring.

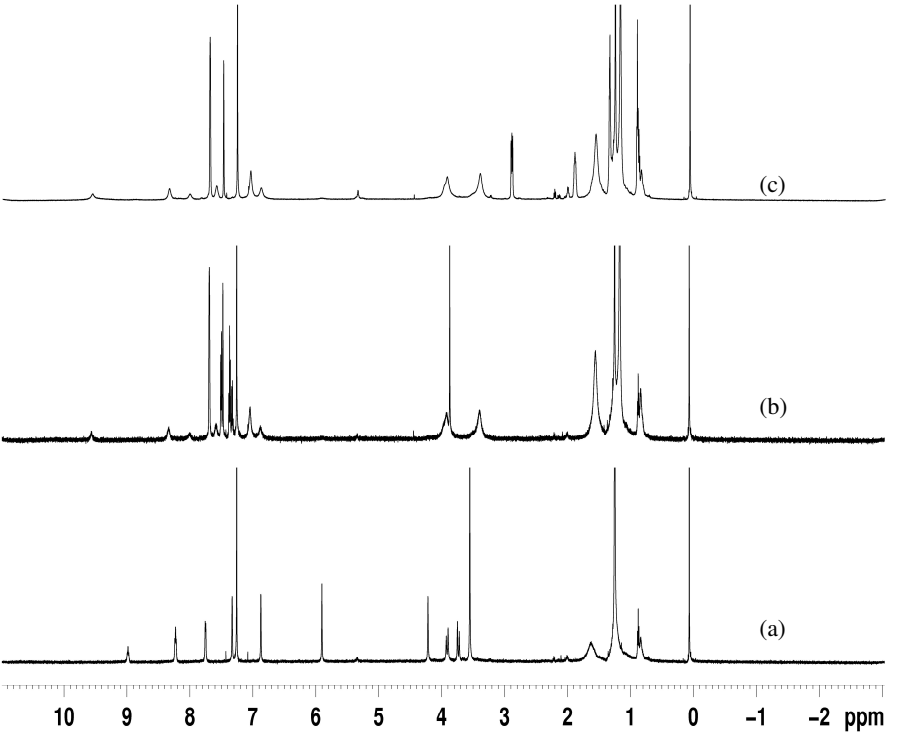

Figure 5.13. ^{1}H NMR spectra (600 MHz, $CDCl_3$, 298 K) of (a) derivative $\mathbf{54^{2+}}$, (b) mixture derivative $\mathbf{54^{2+}}$ and $\mathbf{16b^{+}}$, (c) mixture derivative $\mathbf{54^{2+}}$ and $\mathbf{16a^{+}}$.

To confirm this data, the counterion exchange on derivative $\mathbf{54^{2+}(Cl)_2^-}$ was carried out to obtain derivative $\mathbf{54^{2+}(TFPB)_2^-}$ (**Scheme 5.11**).

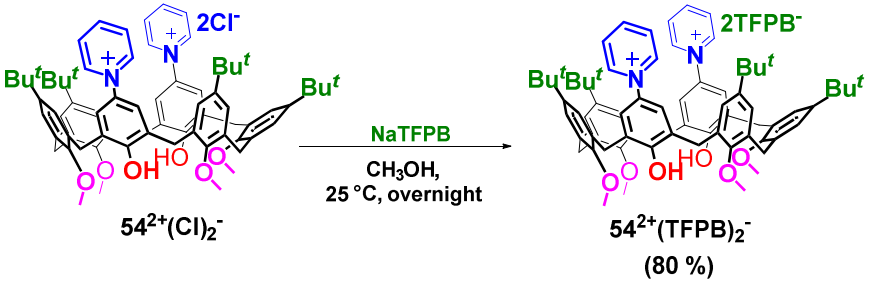

Scheme 5.11. Synthesis of derivative $\mathbf{54^{2+}}$(TFPB)$_2^-$.

The proton spectrum (**Figure 5.14**) of the new derivative $\mathbf{54^{2+}(TFPB)_2^-}$ confirms the previous hypothesis. Therefore, derivative $\mathbf{54^{2+}}$ does not form pseudorotaxane systems.

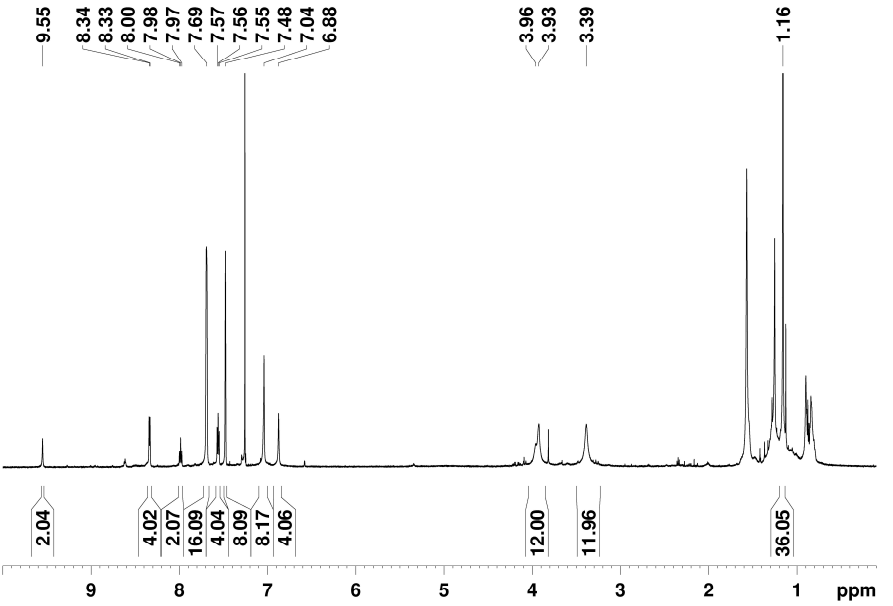

Figure 5.14. ^{1}H NMR spectrum of derivative $\mathbf{54}^{2+}(TFPB)_2^-$ (600 MHz, $CDCl_3$, 298 K).

Unfortunately, derivative $\mathbf{55}^{4+}$ is insoluble in all solvents commonly used for threading experiment. For this reason, its threading abilities remains untested.

Finally, derivative **56** was tested. When it was mixed with $\mathbf{16b}^{+}$ (1:1 ratio) in chloroform, interesting changes appeared in the ^{1}H NMR spectrum (**Figure 5.15b**) indicative of the formation of pseudorotaxane $\mathbf{16b}^{+}\subset\mathbf{56}$. Shielded benzyl signals related to the *endo*-cavity axle, were seen in the 6.5-4.5 ppm region.

In a similar way, the mixture of **56** and $\mathbf{16a}^{+}$ (1:1 ratio), led to shielded alkyl signals, related to the *endo*-cavity axle, in the negative region of the spectrum (**Figure 5.15c**).

Usually, the threading of derivatives with π-conjugated system is also studied by UV spectroscopy. Therefore, the UV absorption properties of above derivatives were explored. Although derivatives **54** and **55** did not show appreciable threading abilities, the latter exhibited interesting chromogenic properties, which will be discussed in the next paragraph.

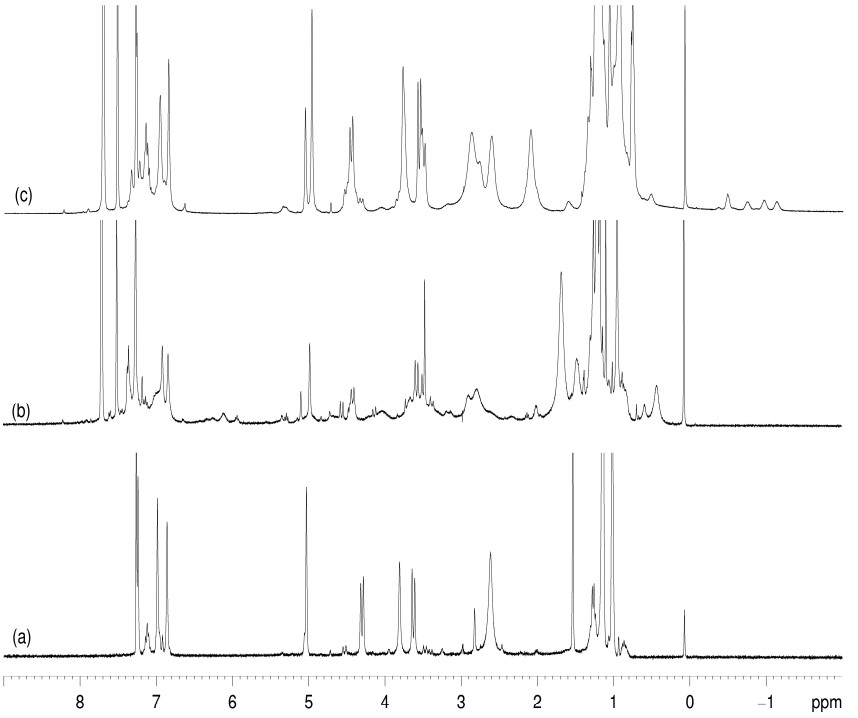

Figure 5.15. ^{1}H NMR spectra (400 MHz, $CDCl_3$, 298 K) of (a) derivative **56**, (b) mixture derivative **56** and **16b**$^{+}$, (c) mixture derivative **56** and **16a**$^{+}$.

5.4 Interesting chromogenic properties of calixarenes with EWGs

Chromogenic materials are compounds that are able to respond to one or more external stimuli by varying their optical properties. This peculiar characteristic has led, in recent years, to a growing interest in the synthesis and study of new materials with such properties. The possibility to respond to various factors leads to the possible application of these materials in various fields. The most emblematic examples are *photochromic materials*, i.e. those materials capable of responding to a variation on the received electromagnetic radiation, and *thermochromic materials*, that respond to the variation in temperature.

Chromogenic substances are given by molecules capable of absorbing in the UV/visible region, as they are made up in most cases by π-conjugated structures. The presence of *N*-heteroaromatic or *N*-heterobiaryl systems coupled to electron density donor and acceptor groups gives rise to interesting structures known as "push-pull" systems (**Figure 5.16**).

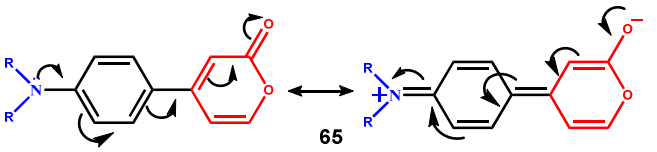

Figure 5.16. Push-Pull system.

The push-pull chromophore ensures that after the absorption of the light, the charge is transferred from the donor group to the acceptor group, thus defining an excited state with a strong variation of the dipole moment and therefore a high absorption intensity. Among the most well-known scientist in the literature for the study of these properties, Cristian Reichardt stands out, who has focused his studies on compounds having an *N*-phenoxide pyridinium group. These derivatives have shown to have different chromogenic properties, such as *piezochromism*, *thermochromism*, and *halochromism* (**Figure 5.17**).

Solvatochromism is one of the most studied chromogenic properties. This phenomenon carries out a change in absorption and/or emission spectra of a chromophore by changing the solvent polarity.[65] It is a complex phenomenon in which the secondary interactions between solvent and chromophore play a crucial role. In addition to solvatochromism, another noteworthy chromogenic property is *halochromism*, which was introduced for the first time in 1902 by Baeyer and Villiger. This phenomenon is based on the change in the colour of the solution following the change in its pH. Therefore, a chromatic response to an acid/base reaction is noticed. In detail, a variation of the electron absorption bands is observed because of the degree of protonation of the chromophore, unlike the solvatochromism, which is based on the different stabilization of the electronic states.

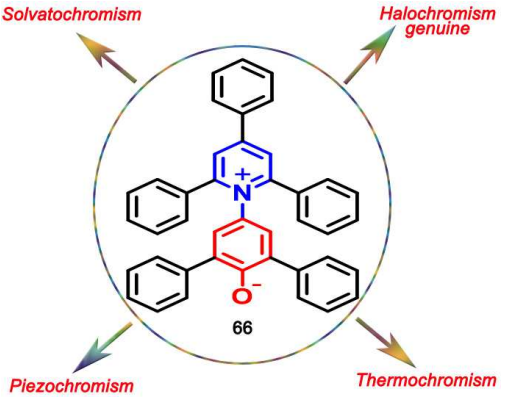

Figure 5.17. Reichardt Betaine's

[65] (a) Marini, A.; Mun˜oz-Losa, A.; Biancardi, A.; Mennucci, B. *J. Phys. Chem. B* 2010, *114*, 17128–17135. (b) Reichardt, C. *Solvent and Solvent Effects in Organic Chemistry*, 3rd ed.; Wiley-VCH: Weinheim, 2002. (c) Suppan, P.; Ghoneim, N. *Solvatochromism*; Royal Society of Chemistry: Cambridge, 1997.

Given the chromogenic properties of the *N*-phenoxide unit studied by Reichardt, it has been observed that the previously synthesized calixarene derivatives **54** and **55** have similar chromogenic units incorporated in the macrocycle scaffold (**Figure 5.18**).

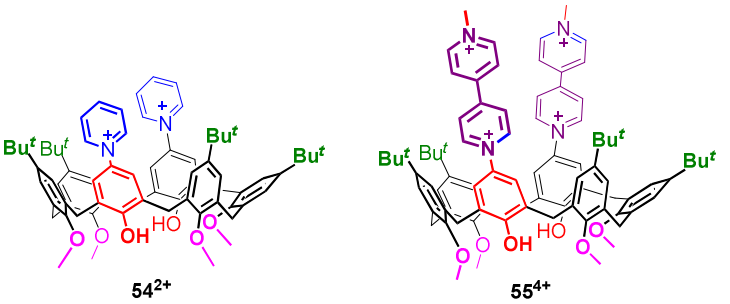

Figure 5.18. Derivatives $\mathbf{54}^{2+}$ and $\mathbf{55}^{4+}$ with chromogenic units.

5.4.1 Halochromism of derivatives 54^{2+} and 55^{4+}

To determine whether the calixarene macrocycle bearing two pyridinium units could have halochromic properties, a titration was carried out by gradually adding a solution of tetrabutylammonium hydroxide (TBAOH) as a base to the solution of $\mathbf{54}^{2+}$ in acetonitrile (**Scheme 5.12**).

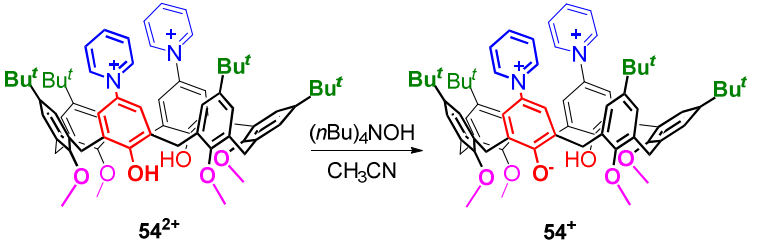

Scheme 5.12. Deprotonation of derivative $\mathbf{54}^{2+}$ with tetrabutylammonium hydroxide in acetonitrile to give $\mathbf{54}^{+}$.

What has been observed, by increasing pH, is a change in colour of the solution from colourless to pink with relative appearance of the absorption band at 487 nm (**Figure 5.19**).

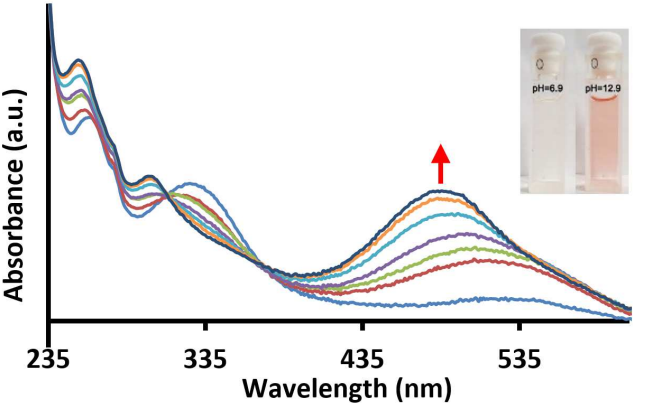

Figure 5.19. UV/vis titration of derivative $\mathbf{54^{2+}}$ with $(n\text{Bu})_4\text{NOH}$ in acetonitrile.

Subsequently, a similar study was conducted on derivative $\mathbf{55^{4+}}$ (**Scheme 5.13**). In this case, by increasing pH, a change in colour of the solution from yellow to blue (**Figure 5.20**) was observed, with relative shifting of the absorption band respectively from 386 nm to 583 nm (**Figure 5.21**). These results clearly indicate that derivatives $\mathbf{54^{2+}}$ and $\mathbf{55^{4+}}$ have interesting halochromic properties.

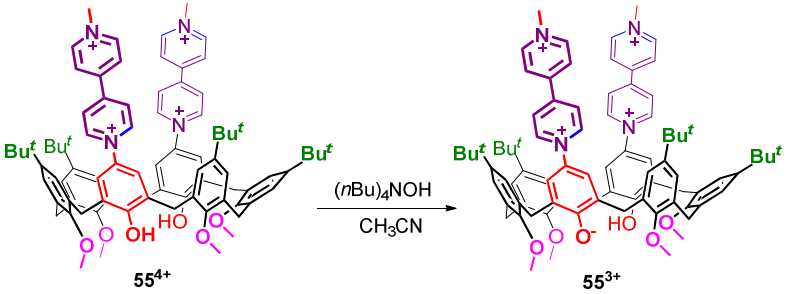

Scheme 5.13. Deprotonation of derivative $\mathbf{55^{4+}}$ with tetrabutylammonium hydroxide in acetonitrile to give $\mathbf{55^{3+}}$.

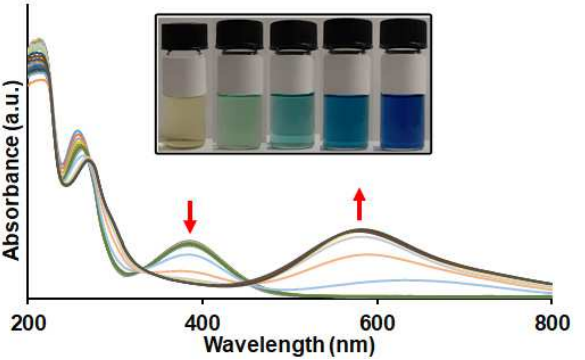

Figure 5.20. UV/vis titration of derivative $\mathbf{55^{4+}}$ with $(n\text{Bu})_4\text{NOH}$ in acetonitrile.

The further addition of base leads to a hypsochromic shift of the absorption band with consequent chromatic variation from blue (at 583 nm) to red (at 484 nm). This variation is given by the formation of the radical viologen as shown in **figure 5.21** and as previously reported in the literature.[66]

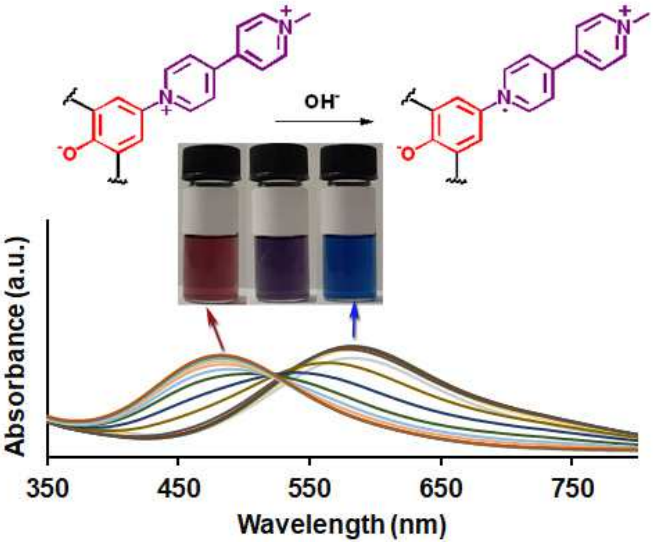

Figure 5.21. addition of a further base at derivative **55**.

5.4.2 Solvatochromism of derivatives 54^{2+} and 55^{4+}

To study the dependence of the absorption properties of $\mathbf{54^{2+}}$ on the nature of the medium, solutions of equal title in solvents of different polarity, were prepared. In **Figure 5.22**, the solvatochromic behaviour of $\mathbf{54^{2+}}$ is shown. In fact, a chromatic variation is evident as the polarity of the solvent changes. The solutions change from yellow to pink when the polarity of the medium decreases. By analysing the UV/vis spectra, this phenomenon can be defined as *negative solvatochromism*. A hypsochromic shift of the band is observed when polarity of the solvent increases. The absorption band moves from 514 nm for DMSO up to 432 nm for methanol.

[66] Shi, W.; Xing, F.; Bai, Y.-L.; Hu, M.; Zhao, Y.; Li, M.-X.; Zhu, S. *ACS Appl. Mater. Interfaces* **2015**, *7* (26), 14493–14500.

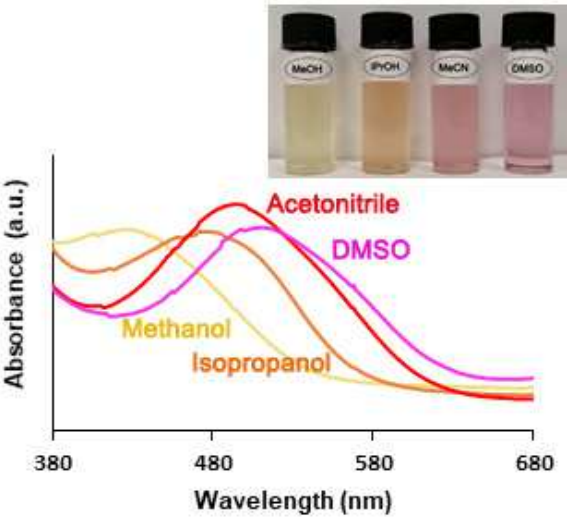

Figure 5.22. UV/Vis spectra of derivative **54**$^{2+}$ in different solvents.

The study on solvatochromic properties was then extended to derivative **55**$^{4+}$. In this case, a very strong chromatic variation is evident as the polarity of the solvent changes. The solutions change from pink to light blue when the polarity of the medium decreases. Also, in this case, it is possible observe a *negative solvatochromism*. In fact, as the polarity of the solvent increases, a hypsochromic shift of the band is observed (**Figure 5.23**) going from 700 nm for DMSO up to 510 nm for water.

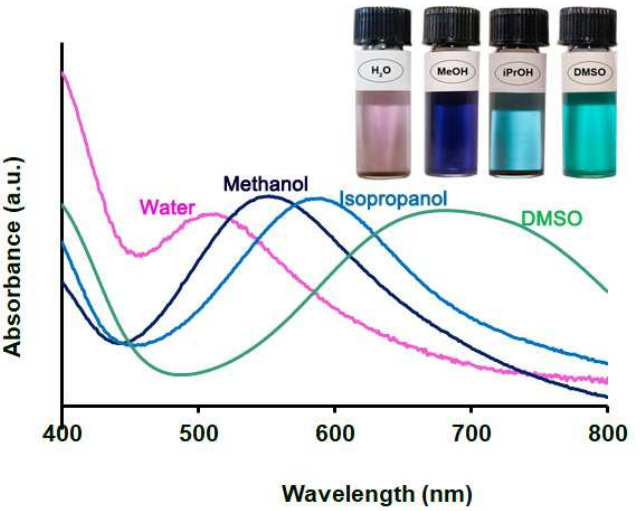

Figure 5.23. UV/Vis spectra of derivative **55**$^{4+}$ in different solvents.

5.4.3 Chromogenic properties in calix[4]arene

Given the interesting properties previously shown, it was decided to further investigate these properties on a calixarene of smaller size.[67] These derivatives were obtained in analogy to calix[6]arene macrocycle, as described in the previous paragraph (**Scheme 5.14**).

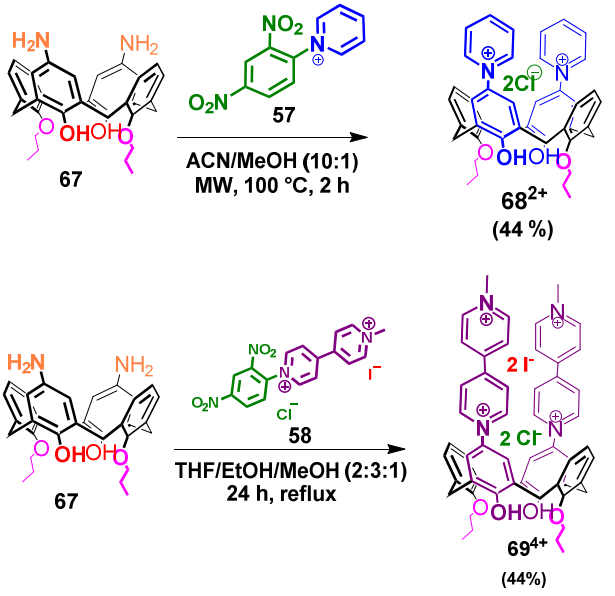

Scheme 5.14. Synthesis of derivatives **68**$^{2+}$ and **69**$^{4+}$.

Once derivative **68**$^{2+}$ was obtained, deprotonation of the hydroxyl groups was carried out by using *n*-Bu_4NOH as a base (**Scheme 5.15**). This step led to the formation of the *N*-phenoxide pyridinium unit embedded into the calix[4]arene scaffold.

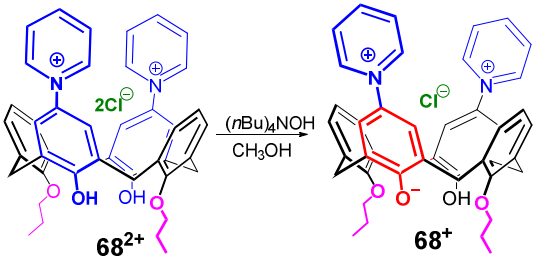

Scheme 5.15. Deprotonation of derivative **68**$^{2+}$ with tetrabutylammonium hydroxide in methanol to give **68**$^{+}$.

[67] Iuliano, V.; Talotta, C.; Gaeta, C.; Soriente, A.; De Rosa, M.; Geremia, S.; Hickey, N.; Mennucci, B.; Neri, P. *Org. Lett.* **2019**, *21* (8), 2704–2707.

This deprotonation was followed through UV/vis spectrophotometry and, from the basic titration conducted in methanol (**Figure 5.24**), the appearance of a new absorption band at 480 nm related to the formation of the chromogenic unit, was observed. In fact, as the amount of added base increases, the intensity of the new band relative to the deprotonated species increases.

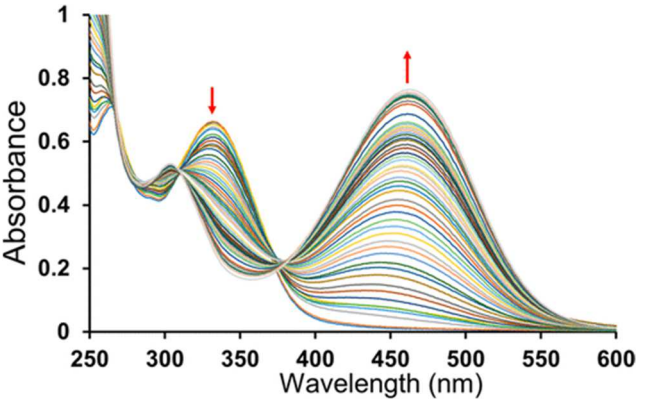

Figure 5.24. UV/vis titration of derivative **68**$^{2+}$ with (*n*-BU)$_4$NOH in methanol.

Subsequently, derivative **68**$^{+}$ was dissolved in water and from the comparison with the spectrum recorded in methanol, a *negative solvatochromic* effect was observed. In fact, the absorption band related to the phenoxide unit undergoes a hypsochromic shift from 515 nm to 420 nm as the polarity of the medium increases (**Figure 5.25**).

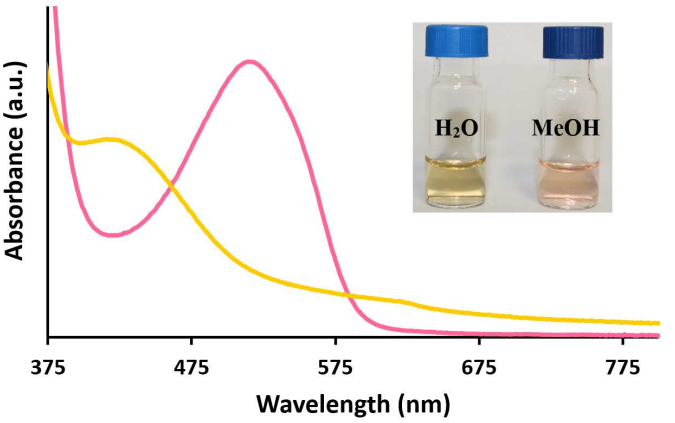

Figure 5.25. Solvatochromism of derivative **68**$^{+}$.

Subsequently, derivative **69**$^{4+}$ was also studied (**Scheme 5.16**) which, like the previous one, had never been subjected to UV / vis studies to date.

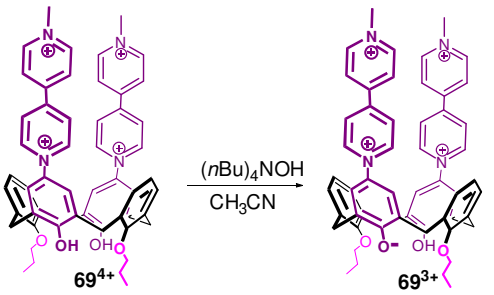

Scheme 5.16. Deprotonation of derivative **69**$^{4+}$ with tetrabutylammonium hydroxide in acetonitrile to give **69**$^{3+}$.

Initially, a new 610 nm band was observed which increases as the 366 nm band decreases following the gradual addition of (n-Bu)$_4$NOH (**Figure 5.26**).

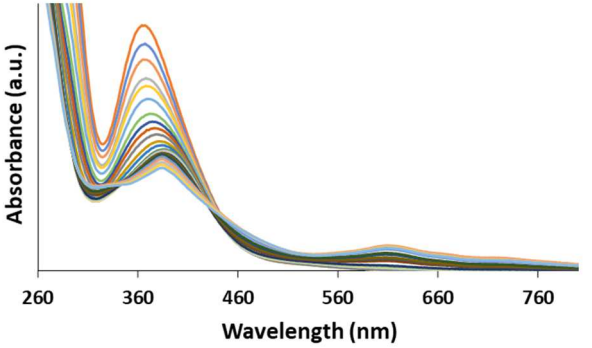

Figure 5.26. UV/vis titration of derivative **69**$^{4+}$ with (*n*-BU)$_4$NOH in acetonitrile.

However, this band does not grow high, as the subsequent addition of base leads to a drastic change in the UV spectrum and the solution turns from yellow to green and finally to brown (**Figure 5.27**).

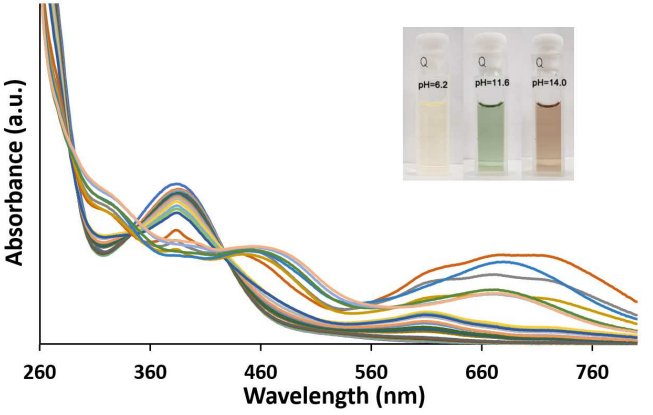

Figure 5.27. Addition of a further base at derivative **69**.

5.4.4 Computational Studies

The experimental investigation has been accompanied to and integrated with quantum chemical calculations using Density Functional Theory (DFT), and its time-dependent (TD-DFT) extension, in combination with the Polarizable Continuum Model (PCM)[17] to confirm that the colour change is due to deprotonation of the macrocycles under examination. The D3 correction proposed by Grimme[18] has been also included to account for dispersion effects. All calculations have been performed using the B3lyp functional in combination with the 6-31G(d) basis set for the geometry optimizations and the 6-31+G(d) for the electronic excitations. The excitation energies have been finally corrected for the effects of the relaxation of the solvent polarization through the corrected Linear Response model.[19] The G09 software has been used for all the calculations.[20] When the mono-deprotonated structure **54^{+}** was used to simulate the absorption spectrum, it was observed the appearance of a new low-energy excitation at 437 nm instead of 288 nm as for the protonated derivative **54^{2+}** (**Figure 5.28**). This feature leads the whole picture in much better agreement with the measured spectra.

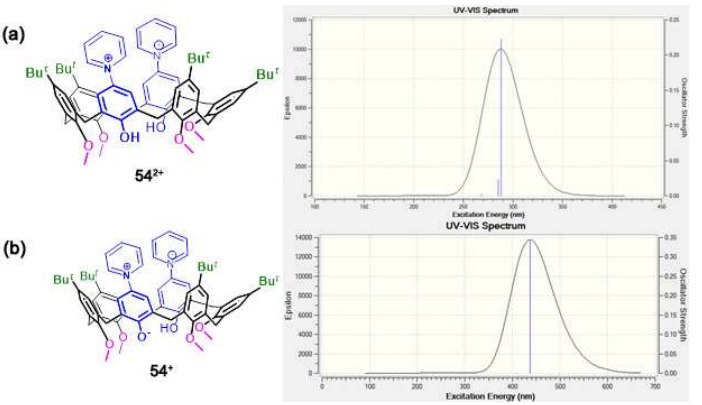

Figure 5.28. Simulated UV/vis spectra of (a) derivative **54^{2+}** and (b) derivative **54^{+}**.

Furthermore, the HOMO and the LUMO orbitals of the transition (S1←S0) were obtained (**Figure 5.29**).

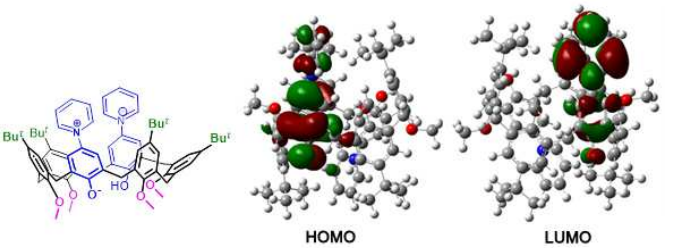

Figure 5.29. The molecular orbitals involved in the lowest excitation for the monodeprotonated betainic form **54^{+}**.

Similarly, the UV spectra of the protonated and deprotonated derivatives **55**$^{4+}$/**55**$^{3+}$, **68**$^{2+}$/**68**$^{+}$ and **69**$^{4+}$/**69**$^{3+}$ were simulated and, also, in these cases the calculations confirmed the experimental data. Furthermore, for the derivative **68**$^{+}$ the solvatochromism was also analysed by simulating the UV spectrum in the two different solvents, water, and methanol. The obtained results show that the low-energy excitation (S1←S0) moves from 481 nm to 463 nm when we include the H-bonded water molecule; the latter, in fact, stabilizes the HOMO orbital thus explaining the observed blue-shift. If now we compare this value with the one obtained in methanol, we observe that this band is characterized by a negative solvatochromism in agreement with experiments. This effect is mainly due to the larger stabilization of the HOMO orbital by hydrogen-bonding.

5.5 Conclusion

In conclusion, an efficient synthesis of four new bifunctional calixarene derivatives was reported in this chapter. These derivatives were fully characterized by NMR spectroscopy and mass spectrometry. Subsequently, the new synthesized hosts were subjected to preliminary threading studies with known monoammonium axles. The complexation tests carried out showed that a bifunctional calixarene derivative bearing EDGs has interesting complexing ability towards linear ammonium axles. Instead, derivative **56** showed only weak interactions. It has been noted that derivative **56** changes its conformation from 1,2,3-alternate to cone upon threading. Finally, derivatives **54** and **55** have shown peculiar chromogenic properties such as halochromism and solvatochromism.

5.6 Experimental Section

5.6.1 General comments

Reactions under anhydrous conditions were conducted under an inert atmosphere (nitrogen) using dry solvents. The commercial reagents were purchased by Aldrich and TCIchemicals and were used without further purification. The reactions were controlled by thin-layer chromatography (TLC) with Macherey-Nagel plates coated with silica gel (0.25 mm) with fluorescence indicator UV254 and visualized using UV light and nebulization with an indicator solution of H_2SO_4-$Ce(SO_4)_2$. The reaction temperatures were measured externally using electronic thermometers. The reaction products were purified by Macherey-Nagel silica gel chromatography (60, 70-230 mesh). NMR spectra were recorded on Bruker Avance-600 spectrometer [600 (^{1}H)

and 150 MHz (^{13}C)], Bruker Avance-400 spectrometer [400 (^{1}H) and 100 MHz (^{13}C)]. Chemical shifts are reported relative to the residual solvent peak ($CHCl_3$: δ 7.26, $CDCl_3$: δ 77.16) Standard pulse programs, provided by the manufacturer, were used for 2D NMR experiments. High-resolution Mass spectra were acquired with a Bruker Solarix spectrometer equipped with a Tesla magnet. It was used a MALDI as methods of sample ionization. DHB was used as matrix. Samples were prepared in $CHCl_3$ (1 mg / mL).

5.6.2 Calixarenes with Electron Donating Groups

5.6.2.1 Synthesis of derivative 49

Derivative 52

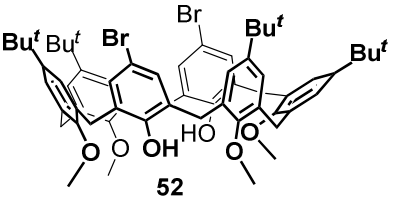

52

Derivative **51** was dissolved in dry DCM and, drop by drop, a solution of bromine in dry DCM was added. The reaction was carried out in the dark for 3 hours, after which the reaction mixture was evaporated, and the crude was purified by precipitation with methanol. Derivative **52** was obtained with a yield of 90 %. **^{1}H NMR** (300 MHz, $CDCl_3$, 298 K): *δ* 8.46 (s, -OH, 2H), *δ* 7.00 (m, ArH-OCH_3, 8H), *δ* 6.85 (s, Br-ArH-OH, 4H), *δ* 3.95 (s, -ArCH_2Ar-, 4H), *δ* 3.80 (s, -ArCH_2Ar-, 8H), *δ* 3.22 (s, -OCH_3, 12H), *δ* 1.17 (s, -C(CH_3)$_3$, 36H). **^{13}C NMR** (150 MHz, $CDCl_3$, 298 K): *δ* 152.9, 151.1, 147.1, 133.9, 131.2, 130.1, 129.9, 126.9, 126.2, 111.6, 61.3, 34.2, 31.3, 31.0. **MALDI-MS** (m/z) calcd for $[M]^+$= 1074.3832 found 1074.3850. calcd for $[M^+Na]^+$= 1097.3724 found 1097.3758. calcd for $[M^+K]^+$= 1113.3463 found 1113.3495.

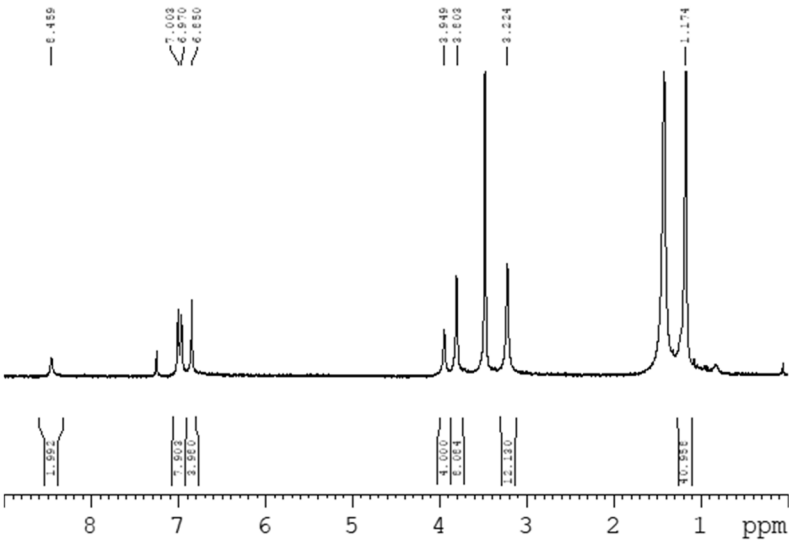

Figure 5.30. ^{1}H NMR spectrum of derivative **52** (300 MHz, $CDCl_3$, 298 K).

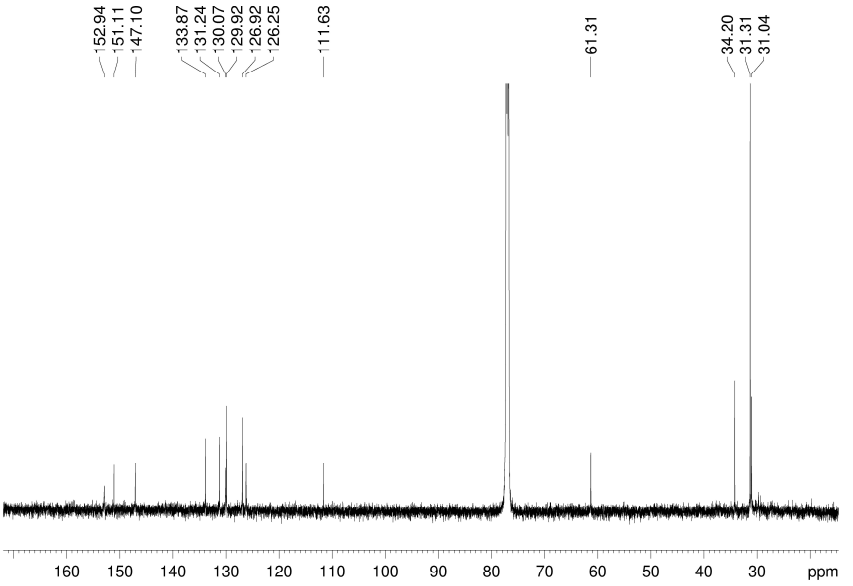

Figure 5.31. ^{13}C NMR spectrum of derivative **52** (150 MHz, $CDCl_3$, 298 K).

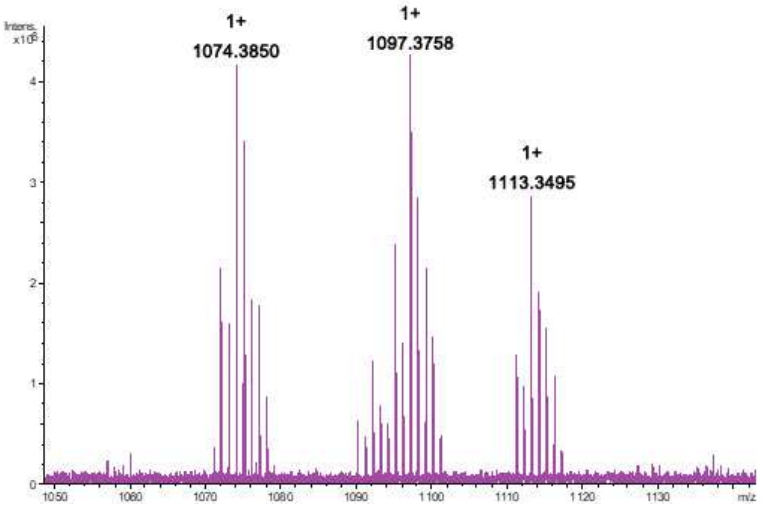

Figure 5.32. MALDI-MS spectrum of derivative **52**.

Derivative 53

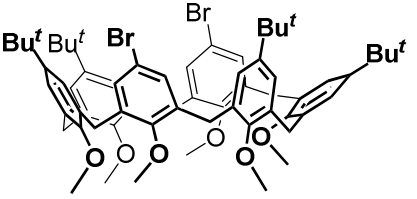

53

Derivative **52** was dissolved in acetone. Subsequently, Cesium carbonate was added to the reaction. After 30 minutes methyl iodide was added, and the reaction was carried out under reflux for about 24 hours. The reaction mixture was evaporated, and the crude was extracted with chloroform and 1N HCl. The organic phases were evaporated and subsequently purified by precipitation in methanol. Derivative **53** as a white solid was obtained with an overall yield of 98%. **^{1}H NMR** (300 MHz, $CDCl_3$, 298 K): δ 7.00 (m, Ar*H*-OCH_3, 8H), δ 6.95 (m, Ar*H*-OCH_3, 4H) δ 3.94 (s, -$ArCH_2Ar$-, 12H), δ 3.26 (s, -OCH_3, 6H), δ 3.03 (s, -OCH_3, 12H), δ 1.17 (s, -$C(CH_3)_3$, 36H). **^{13}C NMR** (100.61 MHz, $CDCl_3$, 298 K): δ 155.1, 153.8, 152.4, 146.2, 137.1, 133.7, 132.7, 131.2, 126.5, 125.8, 116.3, 60.3, 60.0, 34.2, 30.2. **MALDI-MS** (m/z) calcd for $[M]^+$= 1102.4145 found 1102.4114. calcd for $[M^+Na]^+$= 1125.4037 found 1125.4103. calcd for $[M^+K]^+$= 1141.3776 found 1141.3798.

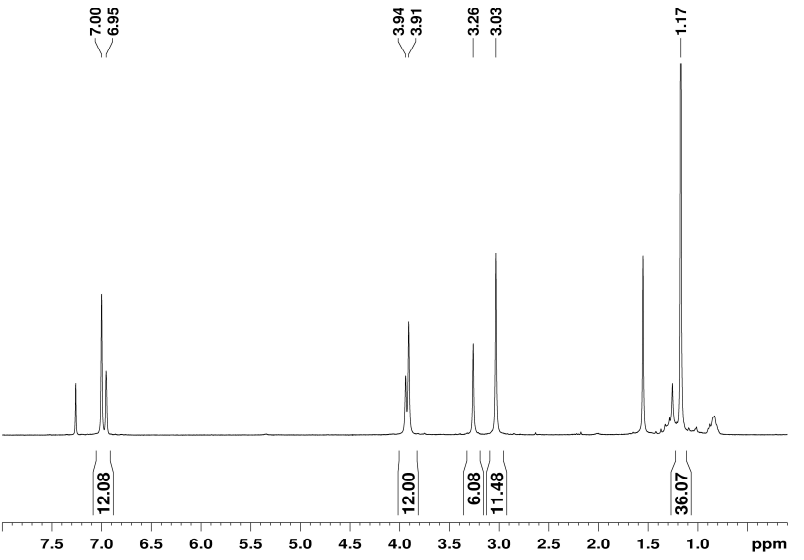

Figure 5.33. ^{1}H NMR spectrum of derivative **53** (400 MHz, $CDCl_3$, 298 K).

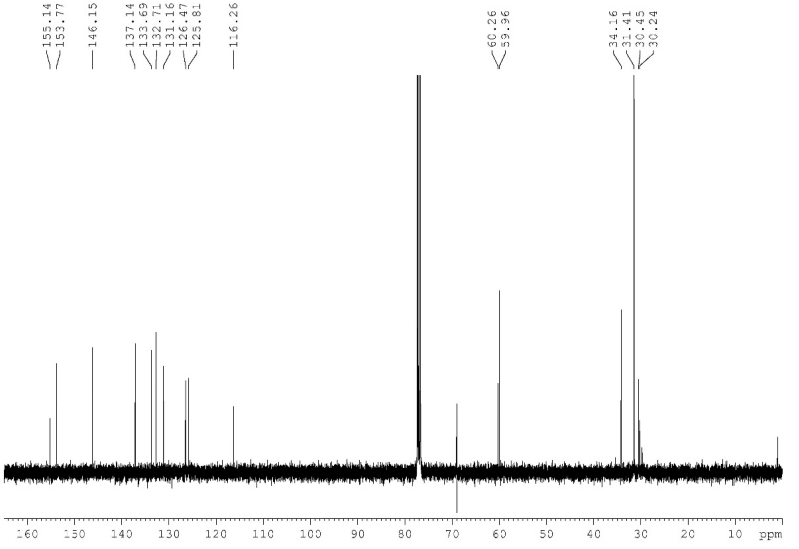

Figure 5.34. ^{13}C NMR spectrum of derivative **53** (100 MHz, $CDCl_3$, 298 K).

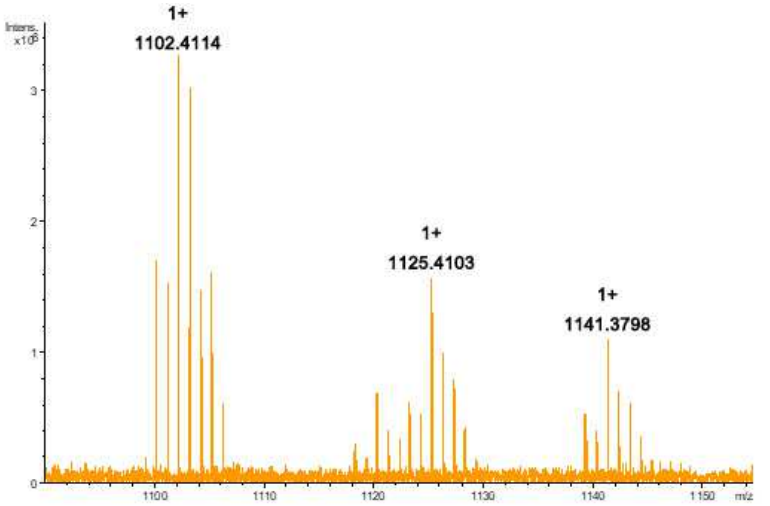

Figure 5.35. MALDI-MS spectrum of derivative **53.**

Derivative 49

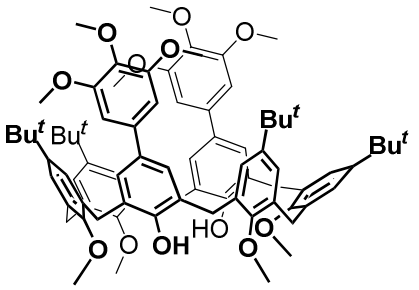

49

Derivative **53** was dissolved in 1,2-dimethoxyethane and water. After that, boric acid, XPhos Pd G3 palladium catalyst and potassium carbonate were added to the mixture reaction. The reaction was carried out at 80 degrees for 3 hours under magnetic stirring. Subsequently, the reaction mixture was cooled to room temperature. CH_2Cl_2 was added and the mixture was washed with water and a saturated solution of NaCl. The organic phases were collected, dried, and filtered. Purification was carried out by chromatography with eluents $CHCl_3/CH_3OH$ 90:10. Derivative **49** as a white solid was obtained with yield of 21 %. **^{1}H NMR** (600 MHz, $CDCl_3$, 298 K): δ 7.14 (s, Ar*H*-OCH_3, 4H), δ 7.12(s, Ar*H*-OCH_3, 4H), δ 6.90 (s, Ar*H*-OCH_3, 4H) δ 6.56 (s, Ar*H*-$(OCH_3)_3$, 4H) δ 3.97-3.92 (d,Ar-C*H*$_2$-Ar ,12H), δ 3.86-3.83 (s,OC*H*$_3$, 18H), δ 3.40 (s,Ar-OC*H*$_3$, 6H), δ 2.91 (s, Ar-OC*H*$_3$, 12H) δ 1.08 (s, -C(C*H*$_3$)$_3$, 36H). **^{13}C NMR** (150 MHz, $CDCl_3$, 298 K): δ 155.5, 154.0, 153.3, 145.9, 137.2, 136.9, 136.0 135.1, 133.8, 133.3, 126.2, 126.0, 103.9, 60.9, 60.3, 59.8, 56.3, 55.9, 34.0, 31.3, 31.3, 30.7, 30.6, 29.7. **HRMS**: (m/z) calcd for $[M^+Na]^+$= 1276.72093 found 1276.72134.

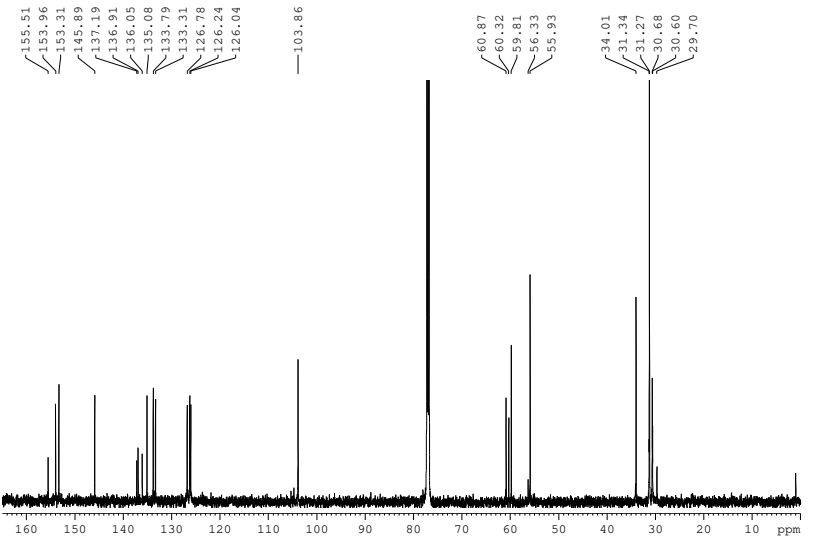

Figure 5.36. ^{13}C NMR spectrum of derivative **49** (150 MHz, $CDCl_3$, 298 K).

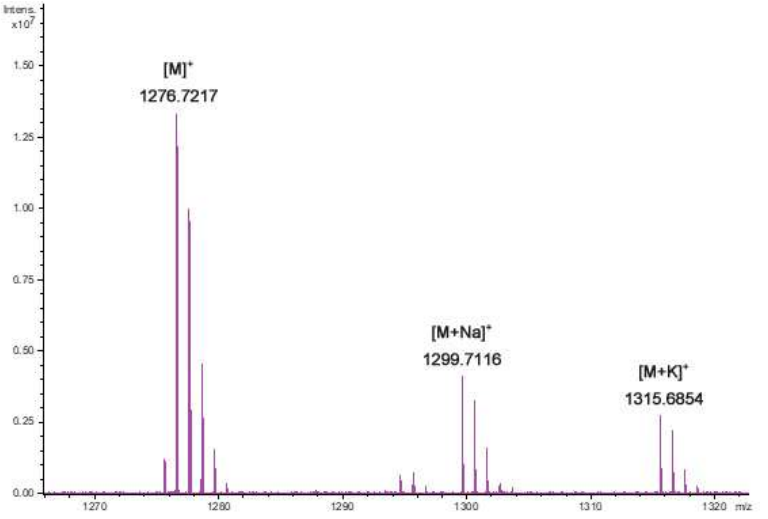

Figure 5.37. MALDI-MS spectrum of derivative 49.

5.6.2.2 Synthesis of pseudo[2]rotaxanes

A 1:1 mixture of calix[6]arene derivative and TFPB linear system was dissolved in 0.5 mL of $CDCl_3$.In detail, in **Table 5.1** we reported concentration using for calix[6]arene derivative and for axles. Then, the solution was transferred in an NMR tube for 1D and 2D NMR spectra acquisition.

Table 5.1. Amount of hosts and guests for complexation experiments.

Pseudo[2]rotaxanes	Derivative 49		Axle ($16b^+$ or $16e^+$)		$CDCl_3$
	(mg)	(mmol)	(mg)	(mmol)	(ml)
$16b^+ \subset 49$	2.01	$1.56 \cdot 10^{-3}$	1.66	$1.56 \cdot 10^{-3}$	0.5
$16e^+ \subset 49$	2.00	$1.56 \cdot 10^{-3}$	1.61	$1.56 \cdot 10^{-3}$	0.5

Pseudo[2]rotaxane $16b^+ \subset 49$

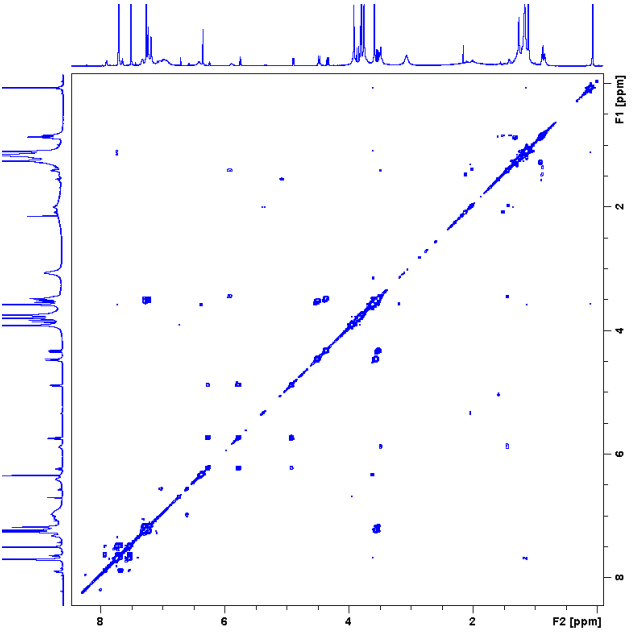

Figure 5.38. 2D COSY spectrum of **$16b^+ \subset 49$** (600 MHz, $CDCl_3$, 298 K).

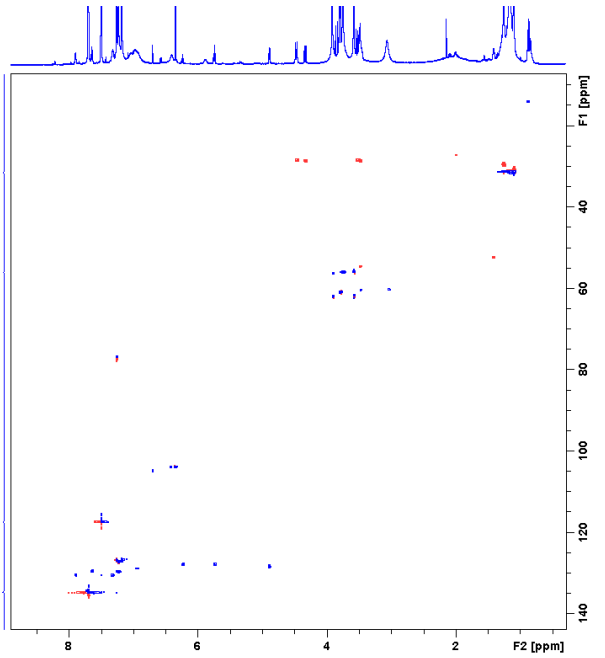

Figure 5.39. 2D HSQC spectrum of **16b⁺ ⊂ 49** (600 MHz, $CDCl_3$, 298 K).

Pseudo[2]rotaxane 16b⁺ ⊂ 49

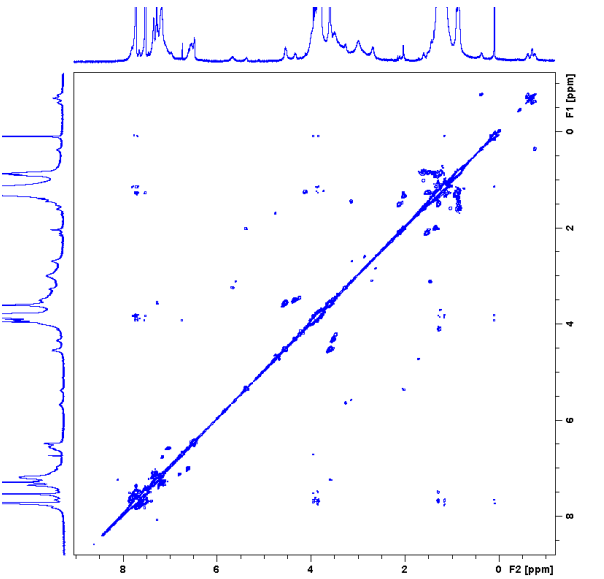

Figure 5.40. 2D COSY spectrum of **16b⁺ ⊂ 49** (600 MHz, $CDCl_3$, 298 K).

5.6.3 Calixarenes with Electron Withdrawing Groups

5.6.3.1 Synthesis of derivatives with Electron Withdrawing Groups

Derivative 60

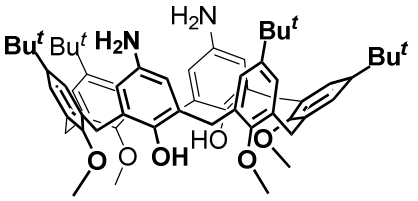

60

Derivative **59** (0.13 g, 0.129 mmol) was dissolved in 200 ml of DMF. Subsequently, Ni/Raney (previous activation) was added to the reaction mixture. Finally, vacuum / H_2 cycles have been carried out. Stirring was continued overnight at room temperature. Afterwards, reaction was stopped by filtration of solution reaction on celite and solvent was evaporated. Derivative **60** was obtained with 96 % yield (0.12 g, 0,124 mmol). **^{1}H NMR** (600 MHz, $CDCl_3$, 298 K): δ 8.03 (s, -O*H*, 2H), 7.02 (overlapped, Ar*H*, 8H), 6.08 (s, Ar*H*, 4H), 3.96-3.80 (overlapped, -ArCH_2Ar-, 12H), 3.19 (s, -OCH_3, 12H), 1.21 (s, -C(CH_3)$_3$, 36H). **^{13}C NMR** (75.48 MHz, $CDCl_3$, 298 K): δ 153.7, 147.0, 145.2, 138.8, 134.5, 132.4, 129.2, 127.0, 126.7, 115.6, 61.7, 34.6, 31.8, 31.8, 31.3, 30.1. **MALDI-MS**: m/z calcd $[M^+H]^+$= 947.5933, m/z found $[M^+H]^+$= 947.5971.

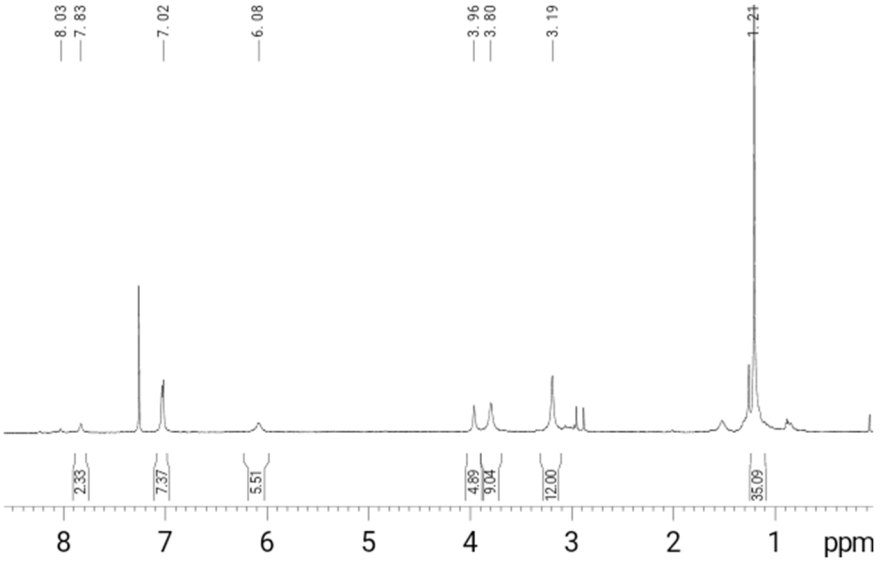

Figure 5.41. ^{1}H NMR spectrum of derivative **60** (600 MHz, $CDCl_3$, 298 K).

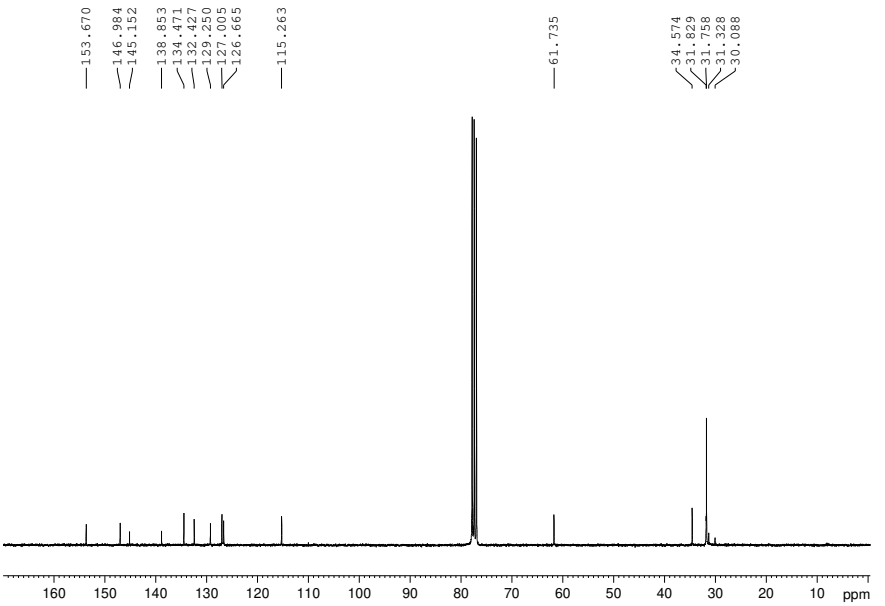

Figure 5.42. 1^{13}C NMR Spectrum of derivative **60** (75.48 MHz, $CDCl_3$, 298 K).

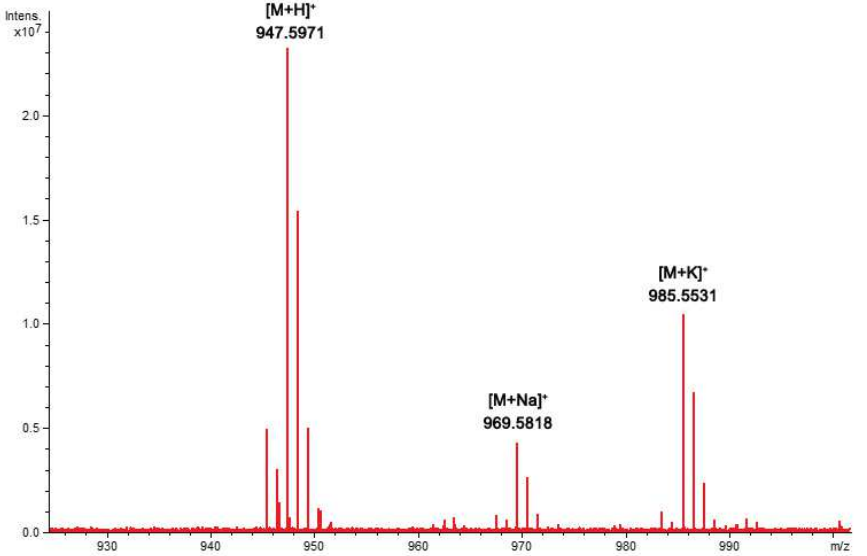

Figure 5.43. ESI-MS spectrum of derivative **60**.

Derivative 54

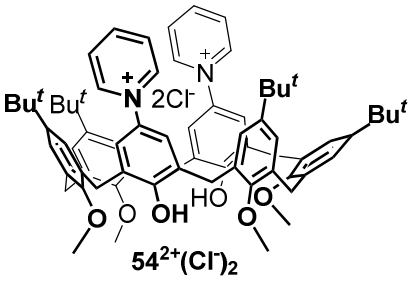

In a vessel for microwave, 31.2 mg (0.033 mmol) of derivative **60** and 66.9 mg (0.24 mmol) of Zincke's salt **57** were dissolved in a mixture of 4 mL of chloroform, 10 ml of acetonitrile and 0.5 ml of water. The reaction was carried out at MW (300 W) under stirring for three hours at 100 °C. After 3 hours, solvent was evaporated. The raw product was purified by chromatography column using as eluens $CHCl_3/CH_3OH$ 8:2 ratio, 9.2 mg of derivative $\mathbf{54^{2+}}$ were obtained (0.0087 mmol). Yield of 26 %. **^{1}H NMR** (400 MHz, $CDCl_3$, 298 K): δ 7.76-9.01 (m, -N$^+$Ar**H**, 5H), δ 5.91-7.33 (s, Ar**H**, 12H), δ 3.70-4.22 (m, -ArCH_2Ar-, 12H), δ 3.56 (s, -OCH_3, 12H), δ 1.25 (s, -C$(CH_3)_3$, 36H). **^{13}C NMR** (100 MHz, $CDCl_3$, 298 K): δ 156.1, 155.0, 147.9, 147.4, 140.4, 132.3, 130.7, 128.2, 127.4, 126.8, 119.7, 60.0, 39.4, 34.4, 31.6, 29.8, 22.8, 14.3. **HRMS** (m/z) clcd for M$^+$H]$^+$=1071.6245 found 1071.6234.

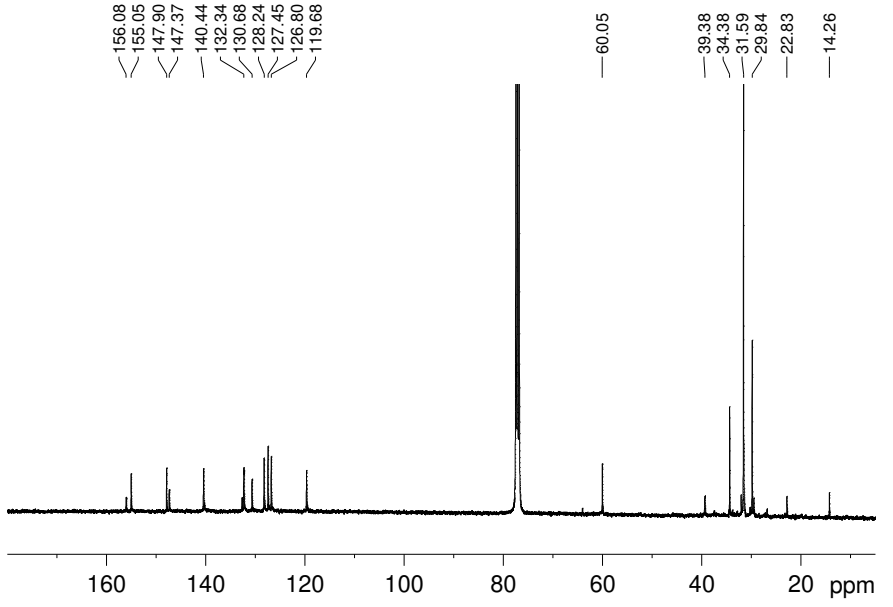

Figure 5.44. ^{13}C NMR spectrum of derivative $\mathbf{54^{2+}}$ (75.48 MHz, $CDCl_3$, 298 K).

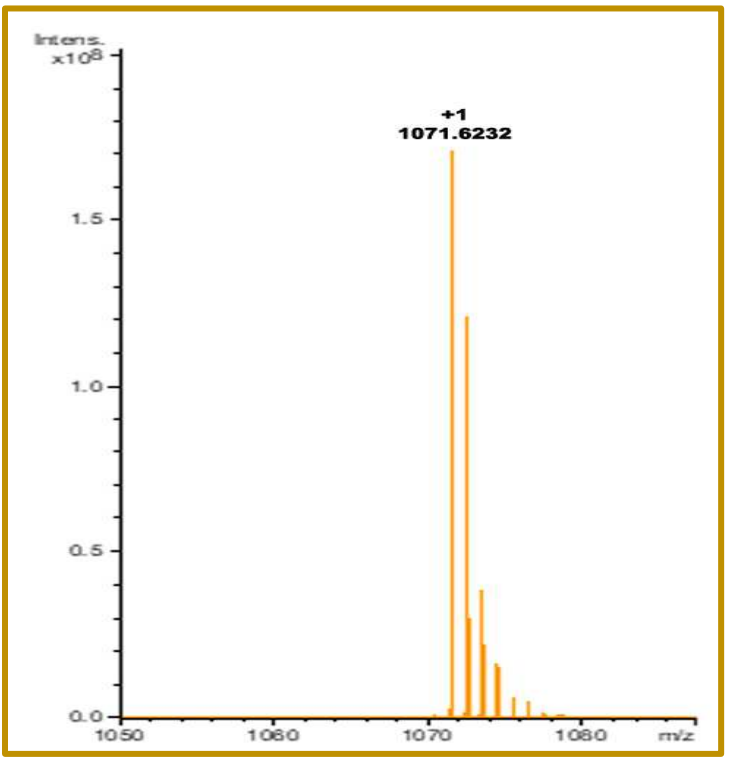

Figure 5.45. HR-MS spectrum of derivative **54**$^{2+}$.

Derivative 55

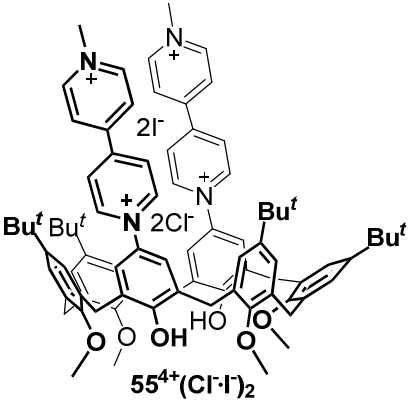

0.05 g (0.053 mmol) of derivative **60** were dissolved in 20.0 ml of ethanol and 10 ml of tetrahydrofuran. Subsequently, 0.13 g (0.27 mmol) of the Zincke **58** salt were added at reaction mixture. The reaction was carried out for 24 h under reflux at 70 ° C. After this time, raw was dried and purified by washing with water. 0.068 g of final product **55**$^{4+}$ were obtained, with an overall yield of 96%. **^{13}C NMR** (150 MHz, DMSO, 298 K): δ 155.1, 149.9, 146.5, 135.2, 132.2, 129.4, 128.8, 125.7, 123.5, 119.9, 69.9, 59.8, 48.1, 31.2. **DEPT 135** (150 MHz DMSO, 298 K): δ 129.45, 125.73, 123.47, 119.88, 69.91, 59.81, 48.11, 31.23. **HRMS** (m/z) clcd for $C_{84}H_{95}N_4O_6^{16a+}$= 1255.7235; found 1255.7243; clcd for $C_{84}H_{96}IN_4O_6^{16a+}$= 1358.6358 found = 1358.6359.

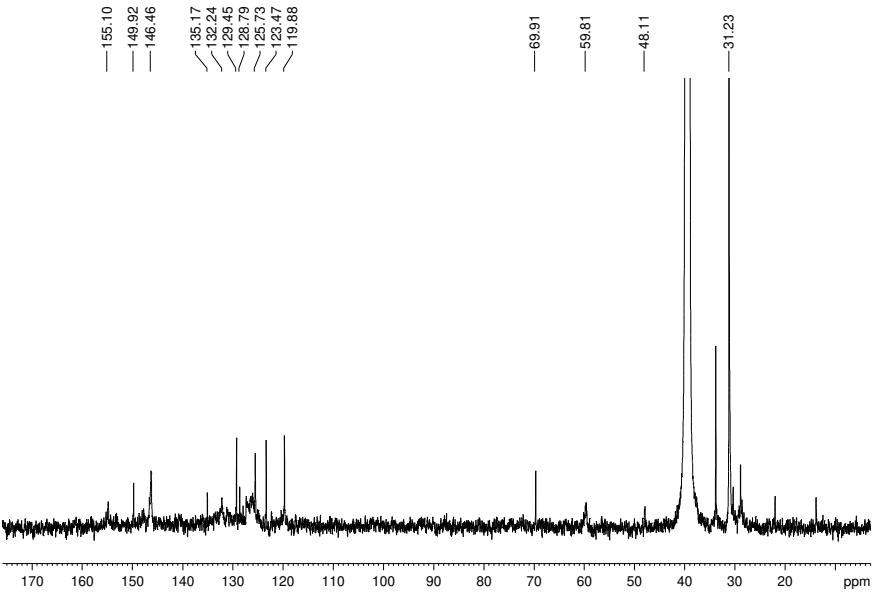

Figure 5.46. ^{13}C NMR spectrum of derivative **55**$^{4+}$.

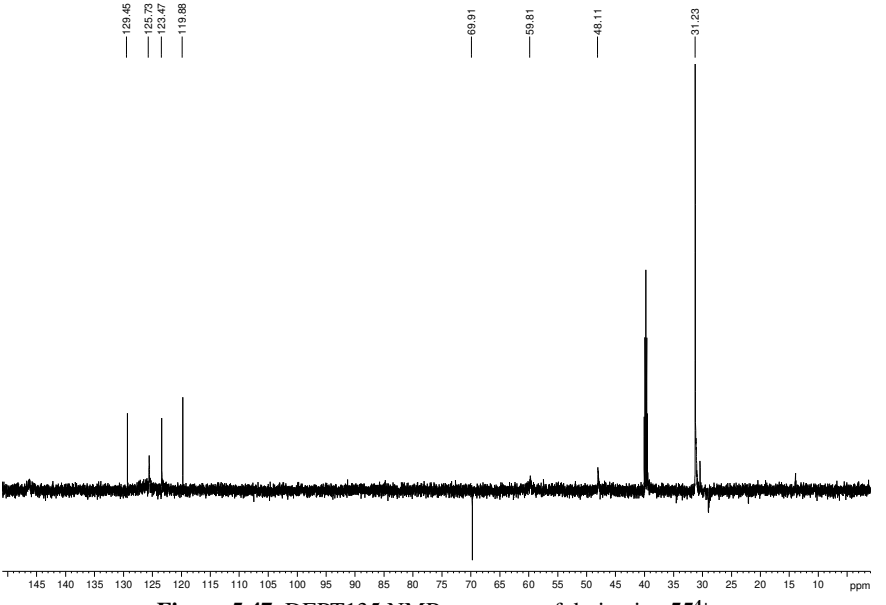

Figure 5.47. DEPT135 NMR spectrum of derivative **55**$^{4+}$.

Derivative 56

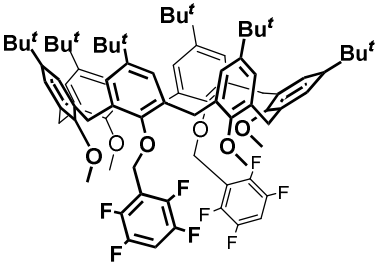

Derivative **51** (49.7 mg, 0.048 mmol) was dissolved in 10.0 ml of acetone. Subsequently, 2,3,5,6-tetrafluoro-benzyl bromide (58.7 mg, 0.242 mmol) and cesium carbonate (475 mg, 1.46 mmol) were added to the reaction mixture. Stirring was continued at reflux for 48 h. After solvent was evaporated and 1 N HCl was added to the reaction mixture. Afterwards, the solution was extracted with CH_2Cl_2. The organic phase was dried over anhydrous Na_2SO_4, filtered and evaporated of the solvent. The raw was purified through precipitated by hexane. Derivative **56** was isolated with 74 % yield (48 mg, 0.035 mmol). **^{1}H NMR** (400 MHz, $CDCl_3$, 298 K): δ 7.24 (s, -OBn(F)$_4$H, 2H), δ 6.98 (s, ArH-OCH$_3$, 8H), δ 6.86 (s, ArH-OBn(F)$_4$, 4H), δ 5.02 (s, -OCH$_{16b}$r(F)$_4$, 4H), δ 3.60-4.32 (m,-ArCH$_2$Ar-, 12H), δ 2.61 (s, -OCH$_3$, 12H), δ 1.15 (s, -C(CH$_3$)$_3$, 36H), δ 1.02 (s, -C(CH$_3$)$_3$, 18H). **^{13}C NMR** (150 MHz, $CDCl_3$, 298 K): δ 154.3, 151.6, 146.7, 145.8, 133.9, 133.6, 133.4, 127.1, 126.0, 125.2, 106.6, 61.7, 59.6, 34.2, 34.2, 31.5, 31.3, 30.9, 30.4. **MALDI-MS:** calcd m/z $[M^+H]^+$= 1353.7152, found m/z $[M^+H]^+$= 1353.7137.

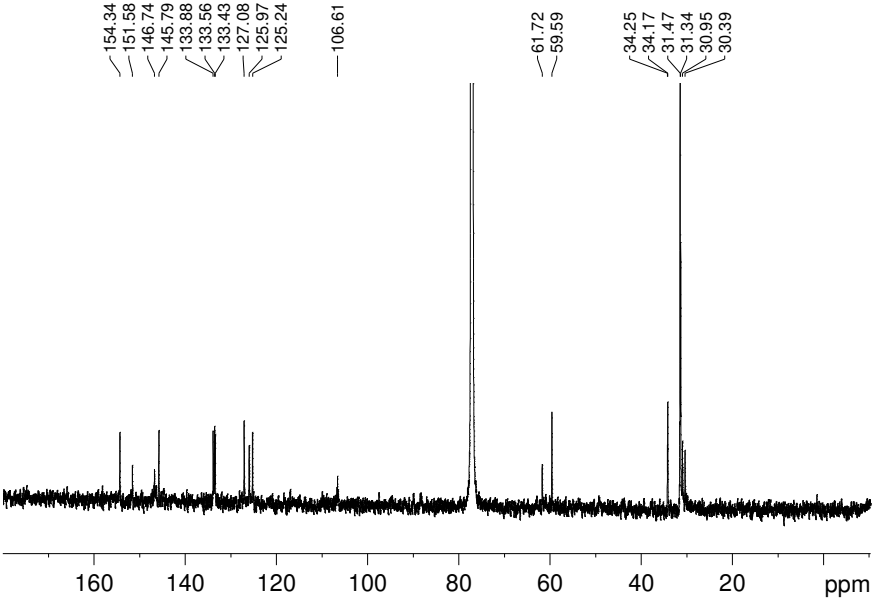

Figure 5.48. ^{13}C NMR spectrum of derivative **56** (150 MHz, $CDCl_3$, 298 K).

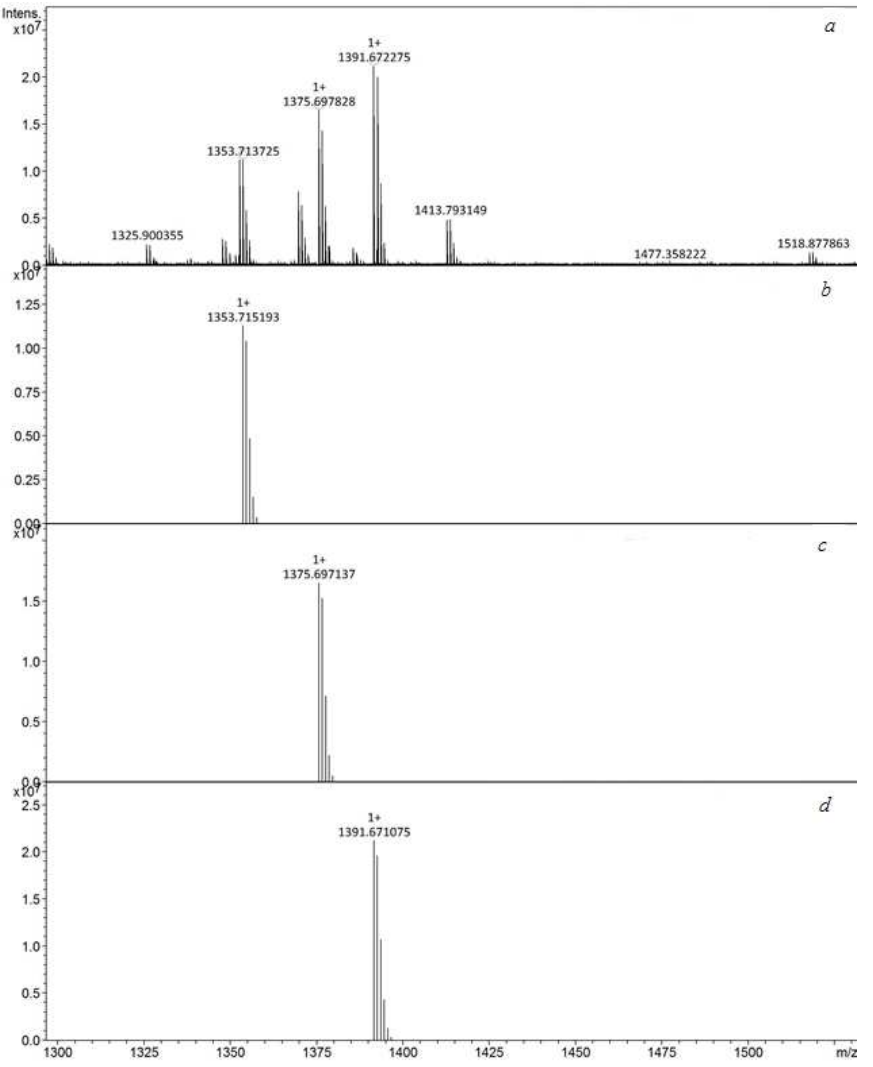

Figure 5.49. MALDI-MS spectrum of derivative **56**. a) found mass for $[M^+H]^+$ m/z=1353.7137, $[M^+Na]^+$ m/z=1375.6978, $[M^+K]^+$ m/z=1391.6723; b) calcd mass for $[M^+H]^+$ m/z=1353.7152; c) calcd mass for $[M^+Na]^+$ m/z=1375.6971; d) calcd mass for $[M^+K]^+$ m/z=1391.6711.

Derivative 68^{2+}

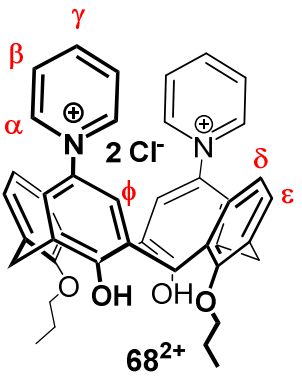

Derivative **67** (64 mg, 0.12 mmol) and the Zincke's salt **57** (133 mg, 0.48 mmol) were dissolved in an ethanol/water mixture (4/1, 10 mL). The solution was stirred for 2 h under microwave irradiation (300 W) at 100 °C. After cooling the solvent was evaporated. The crude product was purified by precipitation from acetone, to give $\mathbf{68^{2+}\cdot(Cl^-)_2}$ as a pink solid in 46 % of yield (41 mg, 0.06 mmol). **^{1}H NMR** (600 MHz, CD_3OD, 298 K): δ 9.15 (bd, 4H, Hα), 8.70 (bt, 2H, Hγ), 8.22 (bdd, 4H, Hβ), 7.66 (s, 4H, Hϕ), 7.10 (d, J = 7.0 Hz, 4H, Hε), 6.83 (t, J = 7.0 Hz, 2H, Hδ), 4.41 and 3.64 (AX system, J = 13.0 Hz, 8H, $ArCH_2Ar$), 4.07 (t, J = 5.5 Hz, 4H, $-OCH_2CH_2CH_3$), 2.11 (m, 4H, $-OCH_2CH_2CH_3$), 1.38 (t, J = 7.1 Hz, 6H, $-OCH_2CH_2CH_3$). **^{13}C NMR** (150 MHz, CD_3OD, 298 K): δ 157.4, 153.3, 146.9, 145.9, 136.0, 133.7, 131.5, 130.7, 129.4, 126.7, 125.2, 79.9, 31.8, 24.6, 11.5. **HRMS** (m/z) clcd for $C_{44}H_{43}N_2O_4^+$=663.3217 found. 663.3273.

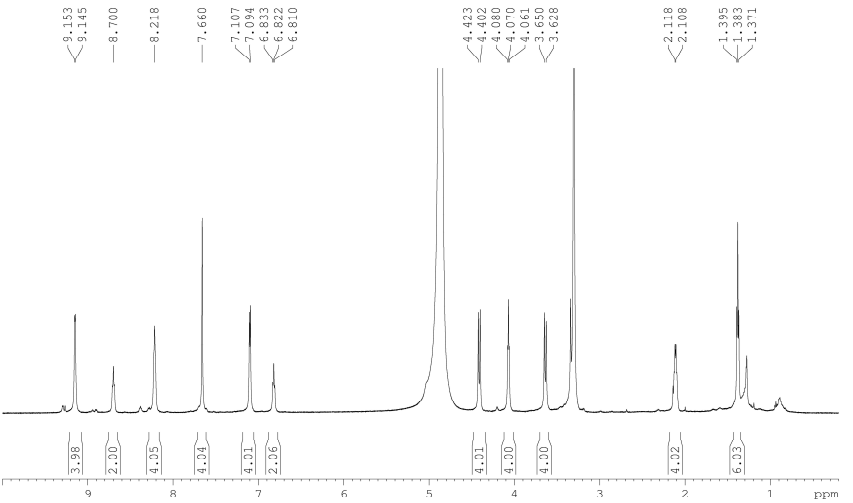

Figure 5.50. ^{1}H NMR spectrum of derivative $\mathbf{68^{2+}\cdot(Cl^-)_2}$ (600 MHz, CD_3OD, 298 K).

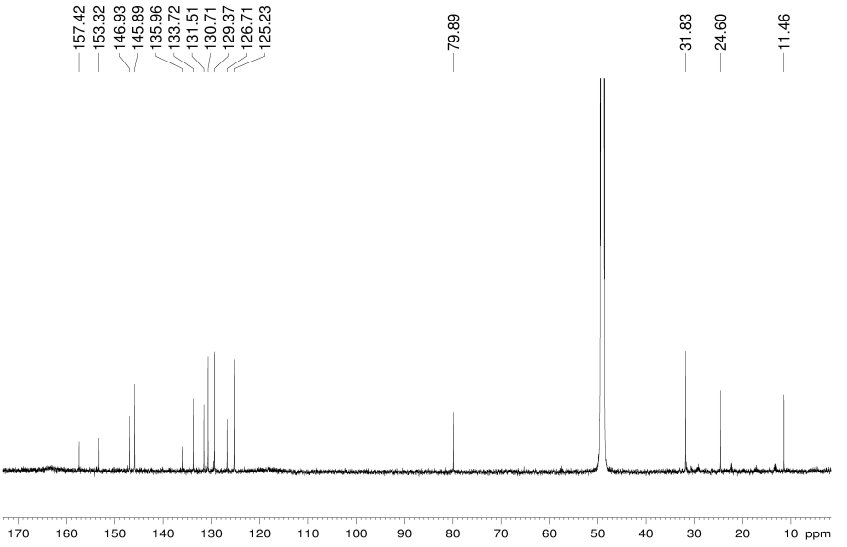

Figure 5.51. ^{13}C NMR Spectrum of derivative $\mathbf{68}^{2+}\cdot(Cl^-)_2$ (150 MHz, CD_3OD, 298 K).

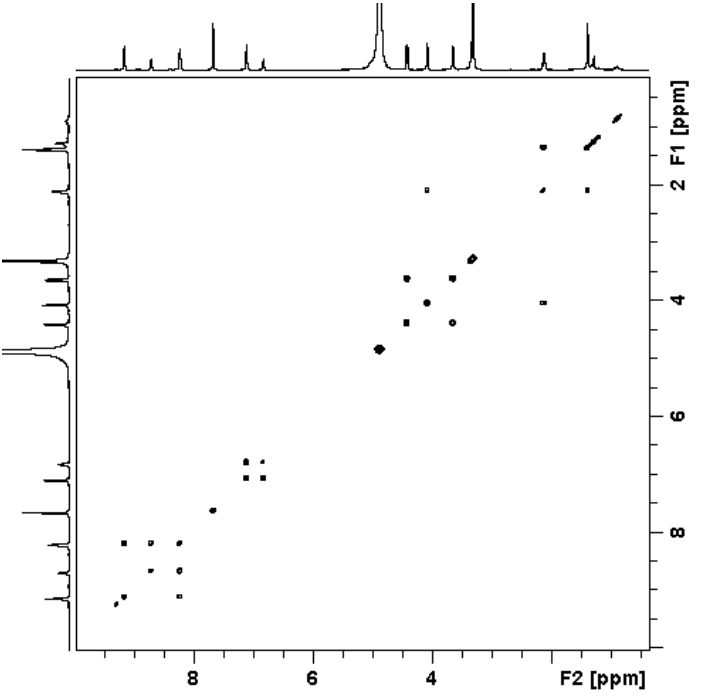

Figure 5.52. 2D COSY Spectrum of derivative $\mathbf{68}^{2+}\cdot(Cl^-)_2$ (600 MHz, CD_3OD, 298 K).

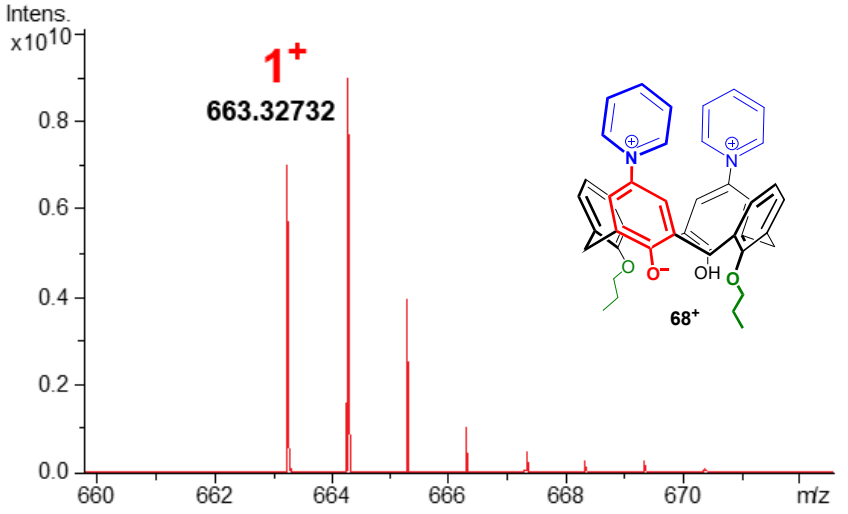

Figure 5.53. HR MALDI-FT-ICR mass spectrum of the monodeprotonated betainic form **68**$^{+}$

Derivative 69^{4+}

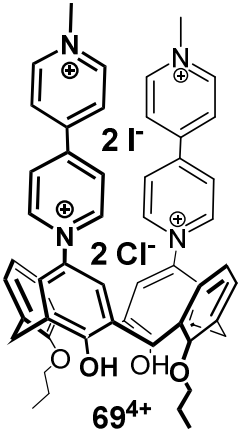

Derivative **67** (0.050g, 0.09 mmol) and the Zincke's salt **58** (0.28 g, 0.55 mmol) were dissolved in an ethanol/methanol/THF mixture (3:1:2, 60 mL). The solution was stirred for 24 h at 70 °C. After cooling the solvent was evaporated. The crude was purified by precipitation from water, to give **69**$^{4+}$·$(Cl^{-}·I^{-})_2$ as a pink solid in 44 % of yield (0.030g, 0.06 mmol). **^{1}H NMR** (600 MHz, CD_3CN, 298 K): δ 9.30 (s, -O*H*, 2H) 8.99-8.98 (d, J=5.41 Hz, Bipy-H, 4H), 8.75-8.74 (d, J= 5.60 Hz, Bipy-H, 4H), 8.42-8.41 (d. J=8.43 Hz, Bipy-H, 4H), 8.36-8.35 (d, J=5.41 Hz, Bipy-H, 4H), 7.53 (s, ArH, 4H), 7.07 (d, J=7.55, ArH, 4H), 6.77 (t, J=7.55, ArH, 2H), 4.26 (s, -NCH_3, 6H), 4.24 (overlapped, -ArCH_2Ar-, 4H), 3.94-3.92 (t, J=7 Hz, -OC$H_2$$CH_2CH_3$,4H), 3.54-3.52 (d, J= 13 Hz, -ArCH_2Ar-, 4H), 1.89-1.87 (m, -$OCH_2CH_2CH_3$, 4H), 1.22-1.19 (t, , J=7 Hz -$OCH_2CH_2CH_3$, 6H). **^{13}C NMR** (100 MHz, $CDCl_3$, 298 K): *δ* 151.0, 148.1, 146.7, 133.6, 131.7, 130.90, 130.3, 128.4, 128.3, 128.2, 128.0, 126.8, 125.3, 124.5, 120.4, 79.9, 49.6, 31.8, 24.6, 11.5. **MALDI-MS** (m/z) calcd for $[M]^{+}$= 848.4296 found 848.4318.

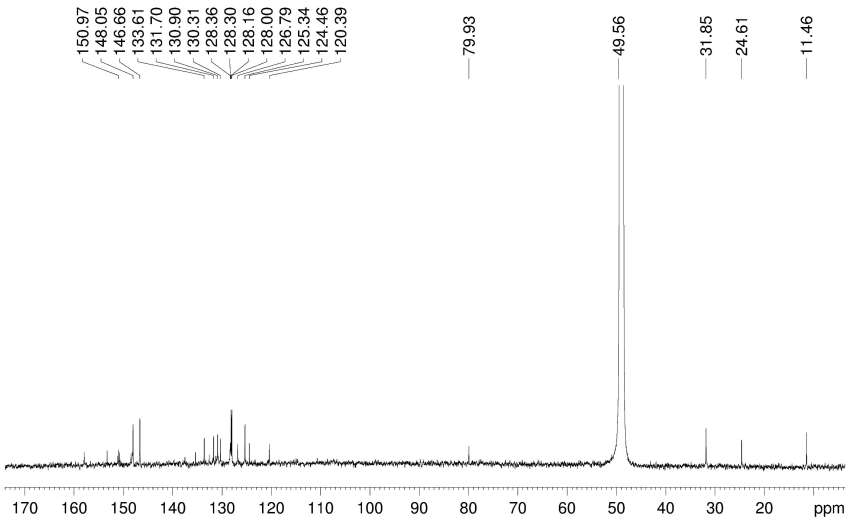

Figure 5.54. ^{13}C NMR spectrum of derivative **69**$^{4+}$ (150 MHz, CD_3OD, 298 K).

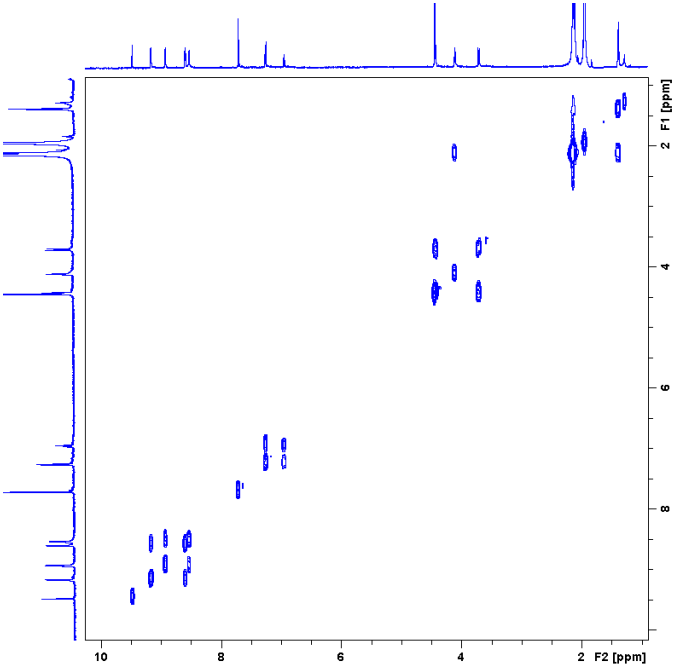

Figure 5.55. 2D COSY spectrum of derivative **69**$^{4+}$ (CD_3CN, 298 K, 600 MHz).

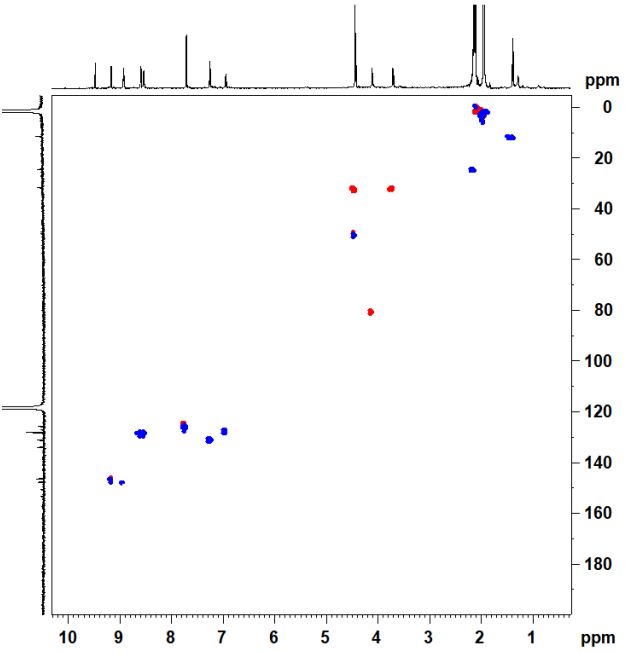

Figure 5.56. 2D HSQC spectrum of derivative **69^{4+}** (CD_3CN, 298 K, 600 MHz).

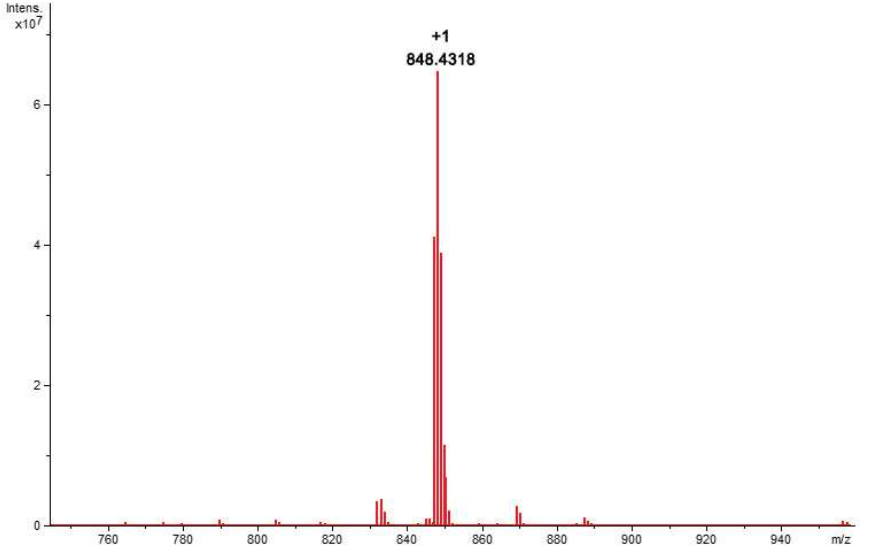

Figure 5.57. HR-MS spectrum of derivative **69^{4+}**.

5.6.3.2 UV/Vis characterization

The Uv-Vis measurements carried out on the **54**$^{2+}$, **55**$^{4+}$, **68**$^{2+}$ and **69**$^{4+}$ derivatives were recorded by first measuring the solution of the macrocyclic derivative dissolved in the appropriate solvent. subsequently UV-Vis measurements were recorded by adding from time to time a base aliquot (nBu)$_4$NOH to the prepared solution. The spectra were recorded using the Cary Uv-Vis spectrophotometer.

- **Derivatives 54^{2+}/54^{+}:** Solution was prepared dissolving 0.02 mg of derivative **54**$^{2+}$ in 2.5 ml of acetonitrile (0.007 mM). With each addition of 5 µl of (nBu)$_4$NOH (0.4 mM), a UV/vis spectrum is recorded.
- **Derivatives 55^{4+}/55^{3+}:** Solution was prepared dissolving 0.02 mg of derivative **55**$^{4+}$ in 2.5 ml of acetonitrile (0.004 mM). With each addition of 1 µl of (nBu)$_4$NOH (0.02 M), a UV/vis spectrum is recorded.
- **Derivatives 68^{2+}/68^{+}:** Solution was prepared dissolving 0.02 mg of derivative **68**$^{2+}$ in 2.5 ml of methanol (0.007 mM). With each addition of 5 µl of (nBu)$_4$NOH (0.02 M), a UV/vis spectrum is recorded.
- **Derivatives 69^{4+}/69^{3+}:**Solution was prepared dissolving 0.02 mg of derivative **69**$^{4+}$ in 2.5 ml of acetonitrile (0.04 mM). With each addition of 5 µl of (nBu)$_4$NOH (0.4 mM), a UV/vis spectrum is recorded.

5.6.3.3 Computational Details

Derivatives 54^{2+}/54^{+}

Atomic coordinate of derivative 54^{2+} in acetonitrile

N	0.10573400	2.83202200	3.51885600
C	0.96552200	3.50881700	4.31203900
C	-0.02105700	5.57538500	3.63395400
C	-0.81734000	3.48980300	2.78330800
C	-0.90721100	4.86314700	2.83441100
C	0.92933500	4.88399800	4.37554200
O	-0.48439400	2.12952000	-4.64784100
O	-4.41546700	-0.94513600	-2.35181500
O	4.34042500	-0.27212400	-2.76853400
O	4.22507700	0.77904000	2.16543600
O	0.36249900	-2.71992700	3.36876300
O	-3.92435600	0.45685700	2.43858800
C	-4.24951000	0.38125100	-1.99101600
C	1.38698100	0.74782000	3.38549300
C	-4.79101600	0.83615800	-0.78916300
C	-1.27081900	-1.01939900	-3.06253400
C	1.45301300	-0.63948200	3.38458400
C	-4.62817300	2.18199400	-0.45548200
C	0.24978600	-1.36447000	3.41896900
C	-3.50857200	1.23219200	-2.81716400
C	4.25694200	-0.47772200	1.58346300
C	3.02193900	1.73474900	-2.86369900
C	-3.37739600	2.56636500	-2.44873800
C	-3.13597600	-1.81034800	2.55806800
C	1.01729900	0.46126300	-3.73151600
C	3.69459200	-2.80934200	1.62364600
C	-1.41719200	0.19006500	-3.72535600
C	-0.26792000	0.93533400	-4.03797800
C	-0.00263300	-1.46687400	-2.73015400
C	-3.92664300	-0.83609400	1.94412500
C	1.13452300	-0.75434200	-3.06087800
C	3.57936100	-1.53661800	2.18869100
C	2.69450100	2.96759900	-2.30960700
C	-0.99485400	-0.72397300	3.54473100

C	4.45477500	-3.04771400	0.48000300	H	0.01851400	-6.01041100	-2.45808100
C	-3.94665200	3.07639600	-1.27898100	H	-0.11660900	-3.83782700	-3.69793000
C	4.00358500	0.96081200	-2.23813600	H	0.51584000	-3.72246400	1.17227400
C	4.96447000	-0.65926700	0.39071100	H	0.34917000	2.57309600	-4.84408800
C	-4.71804700	-1.14602800	0.83273100	H	-0.49740100	-3.13858200	3.50020600
C	-1.01920000	0.66534700	3.57278600	H	2.30833300	1.31065400	3.30064200
C	4.60909800	1.38654000	-1.05603000	H	-2.15392100	-1.58575200	-2.78625200
C	5.05338600	-1.94407500	-0.13209600	H	-5.06424200	2.52269400	0.47556600
C	-3.81825400	4.57090000	-0.96007800	H	-2.80902500	3.21775900	-3.10540700
C	4.24893900	2.62910400	-0.53490000	H	3.19359500	-3.62825600	2.12666500
C	-4.74052200	-2.46402900	0.38919900	H	2.12088300	-1.12941100	-2.80791600
C	0.15911900	1.38514900	3.47262500	H	1.93703800	3.56698600	-2.80623400
C	-3.99961500	-3.47850100	0.99737500	H	-1.97043700	1.16788000	3.69365500
C	3.30353200	3.44858400	-1.14796600	H	5.62218800	-2.07788100	-1.04560000
C	-3.18784700	-3.11729800	2.07039500	H	4.72733900	2.94290200	0.38387800
C	-4.13632900	-4.92203400	0.49805200	H	-5.37426400	-2.69784500	-0.45868500
C	5.31302900	1.02712200	3.05542500	H	-2.60204000	-3.87522100	2.57865100
C	-5.55915200	-1.18554700	-3.16897000	H	5.18653700	2.04247000	3.43208500
C	-4.45025200	4.93407000	0.38840800	H	5.30966800	0.32527200	3.89555900
C	-2.33303200	4.96955600	-0.92422700	H	6.27546100	0.94975300	2.54069300
C	4.68128900	-4.44832100	-0.10339300	H	-5.59549800	-2.25968600	-3.35304100
C	-4.53021200	5.38243300	-2.05773000	H	-6.47960400	-0.87261100	-2.66620900
C	-5.59196900	-5.38459300	0.69272200	H	-5.48603800	-0.65632800	-4.12471500
C	-3.78181100	-4.99225800	-0.99724300	H	-4.32078200	6.00320700	0.57794100
C	4.14917500	-4.50558200	-1.54576800	H	-5.52334100	4.72430000	0.40396300
C	6.19120100	-4.75099100	-0.11335800	H	-3.98828700	4.38908400	1.21698100
C	-3.22285300	-5.88908800	1.25937700	H	-2.22974300	6.03067600	-0.67693200
C	3.98833200	-5.54059000	0.71851900	H	-1.78813200	4.38867400	-0.17466600
C	2.91505500	4.82478800	-0.59427000	H	-1.84319300	4.80606300	-1.88722500
C	1.40414900	4.85223000	-0.30774800	H	-4.44381800	6.45430700	-1.85390400
C	3.65376100	5.15737500	0.70729300	H	-4.09746900	5.19256500	-3.04317300
C	3.25585300	5.90694400	-1.63410900	H	-5.59347000	5.12959100	-2.10217800
C	-4.94463100	0.71127800	3.40457700	H	-5.71198400	-6.41387700	0.34074500
C	5.41021300	-0.23255300	-3.71125200	H	-5.87426000	-5.35151000	1.74898100
H	1.65200600	2.91067600	4.89416500	H	-6.29295600	-4.75698100	0.13681400
H	-1.65893500	5.36366600	2.23834000	H	-3.88345800	-6.01884600	-1.36209400
H	-1.45569700	2.87679900	2.16185800	H	-4.43574900	-4.35861900	-1.60126800
H	1.63086300	5.39816900	5.01913900	H	-2.75143800	-4.67172600	-1.17109500
N	0.12121800	-2.70785700	-1.98275100	H	4.32611300	-5.49581100	-1.97666000
C	0.30026800	-2.64901600	-0.64696500	H	3.07365300	-4.31246800	-1.57538300
C	0.27634200	-5.03203400	-0.54511200	H	4.63895300	-3.76950400	-2.18812400
C	0.02197700	-3.88939000	-2.62654500	H	6.37306700	-5.74989100	-0.52178600
C	0.09912600	-5.07261600	-1.92440200	H	6.74509900	-4.03471000	-0.72491300
C	0.38032900	-3.80419800	0.10037900	H	6.60233400	-4.71831800	0.89974200
H	0.36481200	-1.65777900	-0.21893900	H	-3.34155900	-6.89869800	0.85723200

H	-2.16862400	-5.61521500	1.16287000
H	-3.46890300	-5.92727600	2.32429400
H	4.18149000	-6.51734600	0.26687700
H	4.36063600	-5.57039100	1.74637000
H	2.90488500	-5.40224100	0.75391700
H	1.11200300	5.82416000	0.10188500
H	0.81373700	4.68150100	-1.21097900
H	1.13440100	4.08152600	0.42015300
H	3.34241200	6.14402200	1.06111400
H	3.42870200	4.43543900	1.49798900
H	4.73771800	5.18392900	0.56550900
H	2.97473600	6.89567800	-1.25847700
H	4.32831000	5.91763700	-1.84913800
H	2.72532100	5.74425100	-2.57574300
H	-5.94203000	0.54440400	2.98765900
H	-4.82714200	0.07566800	4.28806200
H	-4.84702900	1.75702800	3.69699100
H	5.60075600	-1.26227100	-4.01452800
H	5.14474600	0.36221100	-4.59147800
H	6.31666500	0.18855400	-3.26550900
H	-0.07269500	6.65657700	3.68044100
H	0.33334400	-5.95425500	0.02154500
C	5.60978700	0.50930900	-0.32915600
H	6.16031000	1.13391300	0.37687100
H	6.34403200	0.11205100	-1.03315300
C	2.79680000	-1.34366200	3.47484800
H	3.40658500	-0.77427400	4.18088200
H	2.63487200	-2.32395900	3.92441300
C	-2.28864400	-1.48817000	3.77672200
H	-2.87944800	-0.90163400	4.48307700
H	-2.08135900	-2.42523000	4.30524300
C	-5.55836800	-0.09459400	0.13103900
H	-6.07946200	0.51957400	0.86745300
H	-6.33392100	-0.61434200	-0.43707000
C	-2.80421400	0.70722500	-4.05248100
H	-2.73007400	1.50198400	-4.79414400
H	-3.37873000	-0.10588700	-4.49849000
C	2.28711800	1.21826900	-4.08485300
H	2.93096400	0.54454300	-4.65175000
H	2.08621500	2.05706300	-4.75686100

Atomic coordinate of derivative 54^{+} in acetonitrile

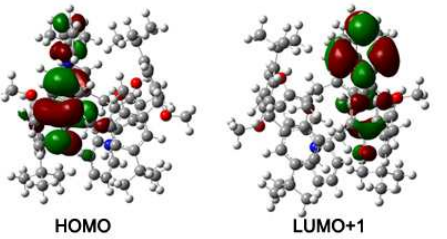

N	-0.11672600	2.77240800	-3.44639500
C	-1.05687400	3.46082200	-4.13685500
C	-0.00232500	5.53336000	-3.57684100
C	0.87917600	3.44208300	-2.81883000
C	0.96836900	4.81520400	-2.88951300
C	-1.03272700	4.83667800	-4.19644800
O	0.47363800	2.12870200	4.67877100
O	4.44826500	-0.93252500	2.37719700
O	-4.37450200	-0.23379000	2.76501600
O	-4.26015400	0.72096800	-2.16297100
O	-0.24904000	-2.77195000	-3.29889300
O	3.99641300	0.40697600	-2.40597600
C	4.28942700	0.38751200	1.99106100
C	-1.38265500	0.66972800	-3.32879500
C	4.85037200	0.82235400	0.79051700
C	1.26548200	-0.93879600	2.94096000
C	-1.43856300	-0.70946900	-3.31387000
C	4.68986500	2.16210200	0.43221900
C	-0.22593300	-1.49923500	-3.33725000
C	3.53080200	1.24933200	2.78882900
C	-4.28530800	-0.52649300	-1.55920800
C	-3.04473000	1.76565800	2.80978300
C	3.40311000	2.57699000	2.39645400
C	3.16277400	-1.85171600	-2.49095300
C	-1.02415300	0.51404500	3.66420900
C	-3.71455000	-2.85152100	-1.53561500
C	1.40993000	0.23935500	3.65903900
C	0.25976100	0.96847600	4.00436100
C	-0.00156200	-1.37300100	2.58757000
C	3.97777600	-0.88338600	-1.89924900
C	-1.13884900	-0.67301000	2.94367000
C	-3.58983100	-1.59287000	-2.13195100
C	-2.71461700	2.98621100	2.23051400
C	1.01657700	-0.76818200	-3.45704600

C	-4.49539300	-3.06892800	-0.40148300	H	-0.22914100	-5.89885900	2.18389300
C	3.99127700	3.06844600	1.22826100	H	-0.07465200	-3.76758800	3.49232500
C	-4.03774600	0.98755100	2.20840400	H	-0.33456400	-3.48765200	-1.42142500
C	-5.00895900	-0.68291900	-0.37236200	H	-0.36178500	2.55434300	4.90420200
C	4.77645600	-1.18585900	-0.79068300	H	-2.31097400	1.22452000	-3.25058000
C	1.02915300	0.60936300	-3.48442500	H	2.14864600	-1.49613200	2.64649400
C	-4.65084700	1.39398100	1.02307000	H	5.13712900	2.48701500	-0.49910600
C	-5.10691700	-1.95518200	0.17815600	H	2.81998900	3.23756800	3.03090800
C	3.85973400	4.55599300	0.87910400	H	-3.19490500	-3.67777700	-2.00625300
C	-4.28756200	2.62462000	0.47656200	H	-2.12327200	-1.03700400	2.66851400
C	4.79174000	-2.49721300	-0.32808800	H	-1.94668100	3.58801400	2.70748200
C	-0.15885800	1.33683600	-3.39745700	H	1.97809200	1.11863800	-3.61147700
C	4.02793300	-3.50850600	-0.91369300	H	-5.68951600	-2.06984300	1.08574400
C	-3.33137800	3.44936700	1.06606600	H	-4.76944300	2.92260600	-0.44560300
C	3.20129200	-3.15019600	-1.97675000	H	5.43157800	-2.72642800	0.51693300
C	4.15123600	-4.94642200	-0.39355900	H	2.56810400	-3.88910700	-2.45267300
C	-5.32208600	0.92698900	-3.09016500	H	-5.20655200	1.93737500	-3.48432500
C	5.57809000	-1.15975500	3.21544100	H	-5.27735900	0.20940600	-3.91587500
C	4.51047400	4.89748100	-0.46626400	H	-6.29949900	0.83906100	-2.60446000
C	2.37294300	4.94587100	0.81316300	H	5.61154100	-2.23083200	3.41759800
C	-4.72900300	-4.45787700	0.20687300	H	6.50673800	-0.85522800	2.72237400
C	4.55054900	5.39210700	1.97180000	H	5.49007000	-0.61515200	4.16149800
C	5.60729000	-5.41941800	-0.55796300	H	4.37861100	5.96232700	-0.67752100
C	3.77232000	-4.99756400	1.09664700	H	5.58476700	4.69317200	-0.46147100
C	-4.23263900	-4.48261000	1.66289000	H	4.06428300	4.33478600	-1.29159300
C	-6.23717400	-4.76862100	0.18642100	H	2.26862200	6.00124700	0.54244300
C	3.24822000	-5.92039900	-1.15825800	H	1.84154000	4.34733600	0.06803800
C	-4.01005100	-5.56377200	-0.57319700	H	1.87045800	4.80011300	1.77246900
C	-2.93886500	4.81290200	0.48424300	H	4.46105000	6.45962100	1.74717800
C	-1.42760400	4.83368400	0.19744700	H	4.10425500	5.21760800	2.95408500
C	-3.67715100	5.12026600	-0.82371600	H	5.61454400	5.14666400	2.03677300
C	-3.27811200	5.91609400	1.50238900	H	5.71604100	-6.44580000	-0.19343300
C	4.99272000	0.62061800	-3.40145500	H	5.90752900	-5.39912800	-1.60970400
C	-5.43556800	-0.17173000	3.71512100	H	6.30319700	-4.79038600	0.00261000
H	-1.79692500	2.86632000	-4.65170300	H	3.87408600	-6.01771600	1.48004300
H	1.78568100	5.31190500	-2.38273000	H	4.41229300	-4.34899400	1.70022900
H	1.57491700	2.83476500	-2.25758800	H	2.73697900	-4.68105100	1.24842700
H	-1.80626200	5.34770100	-4.75506300	H	-4.41562200	-5.46472000	2.11009900
N	-0.12604000	-2.58604500	1.79584400	H	-3.15923400	-4.28256500	1.71527600
C	-0.20011900	-2.48718500	0.45205300	H	-4.74193900	-3.73601100	2.27744800
C	-0.29472800	-4.85909700	0.28539200	H	-6.42541700	-5.75906500	0.61263100
C	-0.13697400	-3.78606800	2.41280500	H	-6.80907700	-4.04097500	0.76738600
C	-0.22208800	-4.94489100	1.67291600	H	-6.62320700	-4.76059600	-0.83709100
C	-0.28614800	-3.61511500	-0.33756500	H	3.36643300	-6.92824600	-0.75072200
H	-0.18150700	-1.48355900	0.04852000	H	2.19279900	-5.64946000	-1.07312200

H	3.50346100	-5.95962800	-2.22090300	H	-0.35793300	-5.76457300	-0.30770800
H	-4.20788100	-6.53186200	-0.10476500	C	-5.65514500	0.50445300	0.31564600
H	-4.35650700	-5.61850100	-1.60902600	H	-6.20024400	1.11407600	-0.40783600
H	-2.92737700	-5.41693900	-0.58508600	H	-6.39279700	0.12756100	1.02762900
H	-1.13626100	5.79681700	-0.23299900	C	-2.77261600	-1.43012800	-3.40207500
H	-0.83712400	4.68333500	1.10435500	H	-3.38747200	-0.91690500	-4.14827800
H	-1.15588700	4.04789400	-0.51309900	H	-2.55915000	-2.42824600	-3.78902900
H	-3.36157100	6.09734400	-1.19985600	C	2.29493300	-1.54448100	-3.69874600
H	-3.45594700	4.37968000	-1.59792100	H	2.89440100	-0.99817400	-4.43285600
H	-4.76089500	5.15502100	-0.68162300	H	2.01155800	-2.49585300	-4.15347500
H	-2.99500800	6.89696400	1.10789900	C	5.62237800	-0.12690500	-0.10695100
H	-4.35065600	5.93307200	1.71692800	H	6.14845600	0.47216300	-0.85275600
H	-2.74819500	5.77023100	2.44719700	H	6.39262300	-0.63865900	0.47594300
H	5.99766700	0.42807800	-3.01188400	C	2.79699000	0.74027300	4.01329500
H	4.83088900	-0.01894800	-4.27518300	H	2.71763200	1.53906700	4.74984400
H	4.91974900	1.66616400	-3.70347500	H	3.35290000	-0.07774400	4.47415200
H	-5.62636200	-1.19426600	4.04201600	C	-2.29549500	1.26438100	4.02857100
H	-5.16125300	0.44074600	4.58059700	H	-2.92980400	0.59241300	4.60851600
H	-6.34516600	0.24202200	3.26854500	H	-2.09380700	2.11355300	4.68701300
H	0.04445600	6.61427400	-3.63011800				

Derivatives $55^{4+}/55^{3+}$

The UV simulation calculations performed on the protonated derivative showed the presence of a single band at **357 nm** (experimental data = **386 nm**).

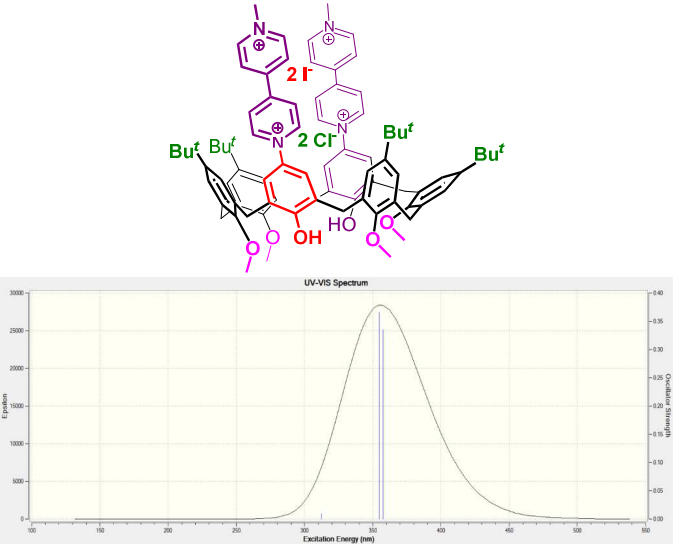

Figure 5.58. UV simulated spectrum of derivative $\mathbf{69}^{4+}$ in acetonitrile.

The analogous calculations on the monodeprotonated calixarene derivative were subsequently carried out. The presence of a band at **607 nm** was observed (experimental data = **583 nm**).

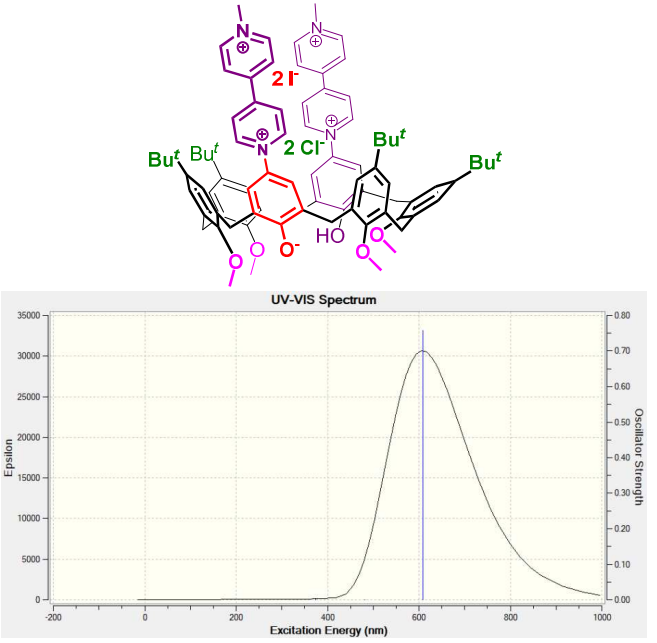

Figure 5.59. UV simulated spectrum of derivative **55**$^{3+}$ in acetonitrile.

Atomic coordinate of derivative 55^{4+} in acetonitrile

N	5.31095300	1.48868400	-2.13305500
C	5.70813800	2.29563900	-3.13994900
C	6.73684600	3.78754600	-1.56937900
C	5.60998500	1.79545900	-0.85330200
C	6.32536800	2.93012000	-0.54813800
C	6.41044000	3.45068900	-2.88373700
C	7.50140300	5.01891500	-1.26487600
C	7.21401200	5.77731100	-0.12887400
C	7.94184600	6.91565000	0.13268400
N	8.93067100	7.30691200	-0.69192500
C	9.22917200	6.59462600	-1.79312900
C	8.53029800	5.44932900	-2.10289600
C	9.66672600	8.55408200	-0.40228300
H	9.76150800	8.66493900	0.67523500
H	10.65380300	8.49336700	-0.85328400
H	9.11322600	9.39453100	-0.82034700
O	-3.08539600	-3.44134600	3.14670700
O	-0.51422600	-3.64407400	3.85043000
O	-2.71152800	-3.37118800	-0.07900100
O	0.05758300	-3.09115500	-4.21444600
O	2.59223300	-3.19042800	-3.37662000
O	2.27061800	-3.55447500	-0.25142900
C	0.15576700	-2.43835100	3.64918600
C	3.47115400	0.35527700	-3.28105300
C	1.40575600	-2.45222900	3.03039900
C	-3.49706600	0.18385000	3.34794700
C	2.76727300	-0.79539000	-3.61070200
C	2.03734300	-1.23028500	2.81162700
C	3.18408000	-2.02519600	-3.06477000
C	-0.47199300	-1.25029900	4.01723800
C	-0.49904000	-1.89531200	-3.76517700
C	-5.09801200	-3.17163300	-0.18414300
C	0.19993300	-0.05422600	3.78270000
C	3.33919600	-3.69619500	1.89422300

C	-4.58817700	-2.03066000	2.02658200
C	-0.32487600	0.46233600	-3.42497800
C	2.00651400	-3.77910400	2.59768700
C	-2.97419500	-1.07738900	3.60140800
C	-3.51940300	-2.18645900	2.92698500
C	-4.54018300	0.33379700	2.44610500
C	3.42445600	-3.61045400	0.50220900
C	-5.08722300	-0.75912900	1.78861800
C	0.23051000	-0.71761300	-3.91282600
C	-6.24828700	-3.00725000	-0.95595900
C	4.29086700	-2.09089900	-2.19861100
C	-1.57390700	0.49241900	-2.80414500
C	1.59810300	-0.70945700	-4.57260900
C	1.45992700	-0.01590400	3.18544200
C	-3.86332000	-3.26223300	-0.83047400
C	-1.73771200	-1.92267900	-3.12468400
C	4.66475300	-3.52579800	-0.13491700
C	4.97494300	-0.92542300	-1.88831700
C	-1.86405900	-1.24030900	4.62173000
C	-3.77667700	-3.18316700	-2.22260800
C	4.76301700	-3.41866400	-1.64238500
C	-2.25589900	-0.71687300	-2.65976500
C	2.15601000	1.33284100	2.96485700
C	-4.95081500	-3.01780800	-2.95288600
C	5.82048100	-3.52671800	0.64602600
C	4.56549300	0.28418900	-2.43126400
C	5.77908800	-3.60981500	2.03766800
C	-6.20569900	-2.92870600	-2.34778500
C	4.51964200	-3.69403200	2.63350100
C	7.04030300	-3.61101000	2.91025800
C	-0.28888500	-3.45775300	-5.55743100
C	-0.23748300	-4.28892600	5.10230500
C	3.50840700	1.17494700	2.26050000
C	1.26610800	2.23718000	2.09355200
C	-2.14176300	1.82274600	-2.29308300
C	2.39554800	2.01127400	4.32534700
C	7.09778100	-4.91445100	3.72665900
C	8.32332500	-3.51080600	2.07726500
C	-3.56290800	1.67041400	-1.73876800
C	-1.23759100	2.35872700	-1.16858300
C	6.99643900	-2.41025300	3.87234300
C	-2.18668400	2.84480100	-3.44268400
C	-7.46037500	-2.74888400	-3.21129100
C	-7.33830000	-1.44833900	-4.02538200
C	-7.59377200	-3.94101500	-4.17549400
C	-8.73853100	-2.66844300	-2.36888700
C	1.79145400	-4.81360000	-0.71441800
C	-2.31766500	-4.70509400	0.23010300
C	-2.44700400	-3.25252300	-2.93223200
C	-5.19081400	-3.23041800	1.32532700
H	5.45823600	1.97449100	-4.14130900
H	6.55940500	3.12828400	0.48974100
H	5.24481800	1.11491500	-0.09750200
H	6.69194700	4.07824800	-3.71930100
H	6.41622700	5.50647000	0.55038100
H	7.75424500	7.53939600	0.99638800
H	8.81657200	4.89264800	-2.98550700
H	10.03891500	6.96407700	-2.40763600
N	-5.08013300	1.65360100	2.20011800
C	-6.41268300	1.85633300	2.27575300
C	-6.11372100	4.16827700	1.71500300
C	-4.24826200	2.67217700	1.89486300
C	-4.73838400	3.93659700	1.66191500
C	-6.95223000	3.09697600	2.02581500
C	-6.66796400	5.51466100	1.44318800
C	-6.01411200	6.66267600	1.89168400
C	-6.54980400	7.90187700	1.62153400
N	-7.69579300	8.02034400	0.92693900
C	-8.34704800	6.92979100	0.48335900
C	-7.85658500	5.66713100	0.72830800
C	-8.22328100	9.36287800	0.61015500
H	-9.30808300	9.31284200	0.55976100
H	-7.92428800	10.05291600	1.39512900
H	-7.81610200	9.68357100	-0.34848400
H	-7.01333400	1.00362600	2.55944000
H	-4.03971500	4.72162500	1.40322300
H	-3.19733100	2.42927700	1.82316800
H	-8.02365400	3.22082500	2.11449500
H	-5.10167000	6.60817700	2.47096300
H	-6.08364200	8.82045200	1.95155100
H	-8.40003200	4.81659100	0.33794700
H	-9.25997800	7.10058800	-0.07129700
H	-2.15499400	-3.48002200	3.46744100
H	1.69431000	-3.09635100	-3.76829200
H	3.15604800	1.30940200	-3.68997500
H	-3.11515200	1.04204500	3.89096500
H	3.00700000	-1.24468800	2.33313400
H	-0.28371400	0.87046700	4.08230500
H	0.24088900	1.38142700	-3.54403600
H	1.27426100	-4.28496600	1.96528800

H	2.12860500	-4.41797800	3.47738300
H	-5.88612400	-0.62516300	1.06631400
H	-7.19776300	-2.94378700	-0.43710000
H	1.67379400	-1.52504500	-5.29549000
H	1.69803500	0.21468600	-5.14570600
H	5.84853000	-0.97501900	-1.24634400
H	-1.92734200	-0.41151000	5.33006500
H	-2.03831300	-2.15155400	5.19790700
H	5.80922300	-3.56306900	-1.92756400
H	4.19403100	-4.21404200	-2.12131600
H	-3.22013800	-0.73886800	-2.17074400
H	-4.86935200	-2.95865600	-4.03436300
H	6.77391100	-3.46502100	0.13430800
H	4.43913600	-3.76312700	3.71449100
H	0.04339000	-2.69650000	-6.26836300
H	0.21621900	-4.40088900	-5.76201100
H	-1.36824200	-3.59076100	-5.65318900
H	-0.51851900	-3.64691600	5.94145900
H	-0.83117000	-5.20203800	5.11921300
H	0.82228700	-4.53892100	5.17988200
H	3.96023000	2.16019900	2.11459400
H	4.20750900	0.57177700	2.84644500
H	3.38932600	0.70759600	1.27818000
H	1.75410400	3.20320100	1.93104200
H	1.08169100	1.78037500	1.11689900
H	0.29821800	2.42965100	2.56298400
H	2.88913100	2.97787900	4.18495400
H	1.45857100	2.18945300	4.85892800
H	3.03388900	1.39312500	4.96314700
H	7.99084100	-4.92551100	4.35906600
H	6.22709000	-5.02464400	4.37781300
H	7.13792900	-5.78637700	3.06737000
H	9.19128900	-3.51405800	2.74214600
H	8.42959800	-4.35541000	1.39064100
H	8.35784900	-2.58700100	1.49266300
H	-3.93451500	2.64675300	-1.41562500
H	-4.25437200	1.28601700	-2.49403900
H	-3.59383900	0.99968500	-0.87530800
H	-1.62823000	3.30721900	-0.78603300
H	-1.18891400	1.64984900	-0.33661200
H	-0.21745000	2.53405600	-1.52021700
H	7.88901800	-2.39951000	4.50545300
H	6.96197600	-1.46723000	3.31848200
H	6.12319900	-2.44719100	4.52835600
H	-2.59145800	3.79629100	-3.08453500
H	-1.19420100	3.04185800	-3.85468000
H	-2.82511500	2.48942900	-4.25662500
H	-8.22586500	-1.30805900	-4.65003300
H	-7.24782700	-0.58123100	-3.36433800
H	-6.46626500	-1.46197600	-4.68383300
H	-8.48251300	-3.82235500	-4.80293000
H	-6.72802100	-4.02691900	-4.83681600
H	-7.69073100	-4.88050400	-3.62368300
H	-9.60212300	-2.54017900	-3.02706300
H	-8.89945400	-3.57952900	-1.78570700
H	-8.71847700	-1.81926800	-1.67983400
H	0.95629800	-4.60463500	-1.38264500
H	2.56134000	-5.35757400	-1.26872600
H	1.44795200	-5.43843000	0.11726900
H	-3.12591300	-5.26078700	0.71367900
H	-2.00683200	-5.24638000	-0.67014500
H	-1.47674500	-4.63192800	0.91992600
H	-1.76528500	-3.91841100	-2.39845800
H	-2.60785900	-3.71751900	-3.90897600
H	-4.70530900	-4.12814700	1.70549100
H	-6.24687300	-3.30232100	1.60215300

Atomic coordinate of derivative 55^{3+} in acetonitrile

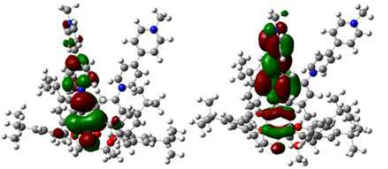

HOMO LUMO+1

N	-3.13779300	2.06233300	2.78381100
C	-2.73034000	2.91953600	3.75947300
C	-3.10730400	4.82626000	2.33994600
C	-3.51950200	2.57825700	1.58401300
C	-3.52781900	3.93094900	1.35161900
C	-2.69271800	4.27632100	3.55631300
C	-3.11145500	6.28138500	2.11387500
C	-2.90294500	6.82090100	0.84084900
C	-2.92295700	8.18398800	0.65728900
N	-3.14265600	9.01829700	1.68963200
C	-3.34374600	8.52996000	2.92991500
C	-3.33177400	7.17759600	3.16748100
C	-3.15264300	10.47884600	1.48282300

H	-3.11446700	10.68458600	0.41653400
H	-4.06911000	10.88952600	1.90276400
H	-2.28414800	10.91440300	1.97564000
O	1.33490500	-3.34388100	-4.09330700
O	-1.31498100	-2.99195200	-4.09142100
O	1.58681700	-3.78985800	-0.87080400
O	-0.63640100	-3.93040100	3.10566800
O	-3.53749900	-3.28025700	4.04770900
O	-3.34182200	-2.87582300	0.21473100
C	-1.77886900	-1.69733000	-3.85745300
C	-2.22887800	0.06945800	3.86849900
C	-2.96191600	-1.51296800	-3.14067700
C	2.23422900	0.18092200	-3.80154500
C	-2.28987300	-1.26484700	4.17499500
C	-3.40276800	-0.20535900	-2.94013400
C	-3.37901300	-2.09041700	3.68049500
C	-1.02302300	-0.62057900	-4.32154400
C	0.38364300	-3.07651500	3.47141300
C	3.94374100	-3.97518700	-1.24528000
C	-1.50626200	0.66474000	-4.09736700
C	-4.81630200	-2.42205200	-1.61947300
C	3.20166900	-2.34410900	-3.06534800
C	1.14721800	-1.16575500	4.69104100
C	-3.72347500	-2.72190700	-2.61753000
C	1.51521900	-0.95032800	-4.16712500
C	1.99166900	-2.21175300	-3.76741800
C	3.40719000	0.04777800	-3.07330300
C	-4.59335300	-2.52044600	-0.24329000
C	3.89934700	-1.19902600	-2.71313200
C	0.12156200	-2.05830300	4.39428600
C	5.22353400	-4.18470400	-0.73335800
C	-4.28959700	-1.45868000	2.73664400
C	2.40729100	-1.24342400	4.09128600
C	-1.23853700	-1.91497500	5.04779700
C	-2.70492000	0.90077700	-3.42322000
C	2.85207800	-4.03367700	-0.37535600
C	1.63617900	-3.20800200	2.86776900
C	-5.60669100	-2.21357600	0.67213100
C	-4.18909200	-0.12504800	2.44395400
C	0.29002800	-0.82124900	-5.05453100
C	3.03323400	-4.29964000	0.98482600
C	-5.38722500	-2.32515800	2.16364700
C	2.62616100	-2.27618500	3.18090300
C	-3.20717500	2.33889900	-3.24410200
C	4.32932400	-4.52474900	1.44677600
C	-6.84682000	-1.80941900	0.17630600
C	-3.17939400	0.66817100	3.02288300
C	-7.11518200	-1.71163300	-1.18911800
C	5.44762800	-4.46800200	0.61384400
C	-6.07680600	-2.02890500	-2.06506400
C	-8.47703100	-1.27461400	-1.74321600
C	-0.77524900	-5.10352100	3.89638400
C	-1.86850100	-3.62279300	-5.25705400
C	-4.57160800	2.39532600	-2.54730800
C	-2.19220300	3.13451600	-2.40427200
C	3.48697400	-0.21534800	4.45453600
C	-3.35418000	3.00594600	-4.62386400
C	-9.05648300	-2.39649200	-2.62324800
C	-9.48668200	-0.96909200	-0.63085900
C	4.79463600	-0.44815600	3.68897800
C	2.98272700	1.19992900	4.12000300
C	-8.29957200	-0.00369800	-2.59348000
C	3.79099100	-0.30188300	5.96089400
C	6.84585300	-4.72546600	1.18946100
C	7.13792700	-3.70862700	2.30730100
C	6.90370000	-6.14913400	1.77155200
C	7.94380500	-4.59650900	0.12734800
C	-3.16739900	-4.26231200	0.49270600
C	0.88742000	-4.94541600	-1.32538900
C	1.85917000	-4.38330300	1.92878900
C	3.74730300	-3.71351400	-2.72248800
H	-2.47935200	2.47486900	4.71012900
H	-3.87041100	4.27425900	0.38379800
H	-3.78926400	1.86166100	0.82355400
H	-2.34460800	4.89734600	4.37178100
H	-2.70235400	6.19255800	-0.01653200
H	-2.76128900	8.64021600	-0.30964300
H	-3.52398500	6.83279100	4.17462500
H	-3.52106700	9.25670400	3.71175200
N	4.15358700	1.23382800	-2.71066200
C	5.46834500	1.31167200	-3.00671500
C	5.58225500	3.49287800	-2.01811100
C	3.53068600	2.25241200	-2.08128300
C	4.21900500	3.39292500	-1.73669600
C	6.20373600	2.42189800	-2.66163000
C	6.34923800	4.70337700	-1.64411400
C	5.77358700	5.97036700	-1.72881800
C	6.50964700	7.08028500	-1.37548000
N	7.77714700	6.95683000	-0.94537700
C	8.35688900	5.74499800	-0.85227300

C	7.66811100	4.60514800	-1.19555900
C	8.56372600	8.15438500	-0.58616200
H	9.33865600	8.30455500	-1.33674800
H	7.90227600	9.01574600	-0.55784000
H	9.01118400	8.00117700	0.39402600
H	5.89170900	0.47230500	-3.54048400
H	3.68754500	4.17885200	-1.21622100
H	2.48424300	2.10736200	-1.85188900
H	7.25037700	2.45107000	-2.93498800
H	4.76263900	6.11354700	-2.08730900
H	6.10798200	8.08272200	-1.43080400
H	8.16372400	3.64916500	-1.08782600
H	9.37750900	5.72260400	-0.49418200
H	0.36098300	-3.19373100	-4.11316400
H	-1.39583300	0.65750200	4.24472600
H	1.90224300	1.16051300	-4.12908200
H	-4.32506800	-0.06498100	-2.39384200
H	-0.92961100	1.50073200	-4.48111600
H	0.94556300	-0.38447800	5.41839100
H	-2.99830700	-3.41539700	-2.18925200
H	-4.17796100	-3.24468400	-3.46595300
H	4.81252900	-1.28571200	-2.13292400
H	6.05664200	-4.13648900	-1.42476700
H	-1.63209300	-2.89130300	5.33165800
H	-1.10994100	-1.33083300	5.96496900
H	-4.93467100	0.32730100	1.79614300
H	0.44208800	0.03567600	-5.71438600
H	0.23372500	-1.70006800	-5.70117200
H	-6.33700700	-2.10170500	2.66372400
H	-5.13921000	-3.35083800	2.44630600
H	3.58805100	-2.37353600	2.69595100
H	4.45611400	-4.75733900	2.50011400
H	-7.62008600	-1.57326700	0.89809000
H	-6.23828700	-1.96764600	-3.13757700
H	-0.78416500	-4.86589500	4.96416000
H	-1.73164200	-5.54921500	3.62619900
H	0.03353100	-5.81573200	3.69908300
H	-1.65868900	-3.03159900	-6.15246300
H	-1.39259900	-4.59961400	-5.33726200
H	-2.94691600	-3.75040400	-5.15185400
H	-4.88574700	3.43747500	-2.44301100
H	-5.34172900	1.87198100	-3.12116000
H	-4.54303700	1.95489100	-1.54666900
H	-2.53656300	4.16541900	-2.27230700
H	-2.06276300	2.68745800	-1.41425000
H	-1.21106100	3.17054100	-2.88480100
H	-3.71576500	4.03241000	-4.50937300
H	-2.40366600	3.04670500	-5.16105600
H	-4.07008900	2.46154400	-5.24619400
H	-10.02627400	-2.09525400	-3.03141200
H	-8.39989000	-2.63264600	-3.46434800
H	-9.20230800	-3.31200500	-2.04257400
H	-10.43806600	-0.66334200	-1.07478500
H	-9.67957700	-1.84512900	-0.00522600
H	-9.14607500	-0.15508500	0.01537000
H	5.52772300	0.31005400	3.97834200
H	5.22725100	-1.42791500	3.90998100
H	4.65038000	-0.37504600	2.60714100
H	3.74169700	1.94454200	4.38014500
H	2.76633500	1.29415900	3.05170500
H	2.07159100	1.44680100	4.67058900
H	-9.26353200	0.31968500	-2.99855300
H	-7.89261700	0.81466400	-1.99188100
H	-7.62340000	-0.17046300	-3.43592000
H	4.55613000	0.43061400	6.23683600
H	2.90327500	-0.10103400	6.56580500
H	4.16140300	-1.29612100	6.22722800
H	8.13442200	-3.88163700	2.72534300
H	7.10393900	-2.68464300	1.92338100
H	6.41680700	-3.78580500	3.12495500
H	7.89442900	-6.34622700	2.19268400
H	6.16855800	-6.29145000	2.56757100
H	6.70963100	-6.89596400	0.99622300
H	8.91889300	-4.78222900	0.58580400
H	7.81543800	-5.32174100	-0.68110400
H	7.96910800	-3.59481600	-0.31134600
H	-3.95163900	-4.63989500	1.15450200
H	-3.16819500	-4.85422900	-0.43011000
H	-2.20428700	-4.35994400	0.99503300
H	1.46019500	-5.48956700	-2.08137800
H	0.66042200	-5.62380600	-0.49595100
H	-0.04227900	-4.59277700	-1.77265200
H	0.93777300	-4.53052400	1.36704100
H	1.98493800	-5.28436400	2.54096700
H	3.08078500	-4.46072100	-3.15223800
H	4.71374600	-3.83362200	-3.22153200

Derivatives $68^{2+}/68^{+}$

The UV simulation calculations performed on the protonated derivative showed the presence of a single band at **300 nm** (experimental data = **330 nm**).

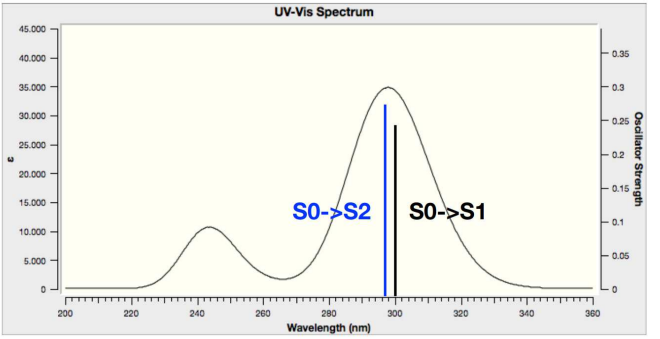

Figure 5.60. UV simulated spectrum of derivative $\mathbf{68^{2+}}$ in methanol.

The analogous calculations on the monodeprotonated calixarene derivative were subsequently carried out. The presence of a band at **465 nm** was observed (experimental data = **515 nm**). The Homo / Lumo orbitals related to the transition in question are also reported.

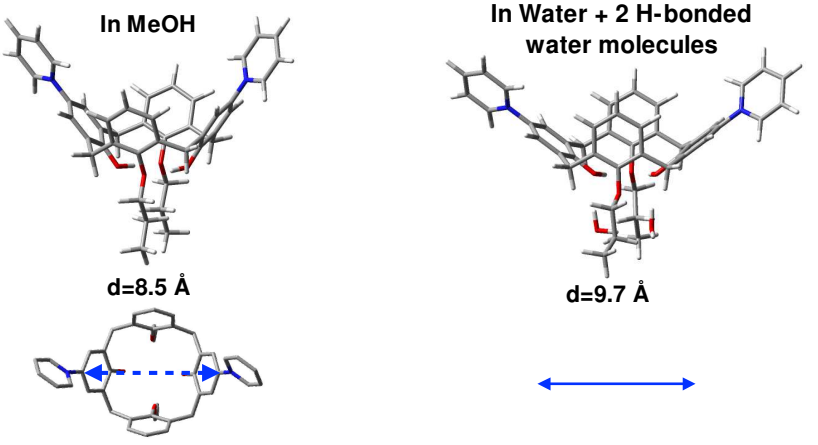

Figure 5.61. Comparison between the optimized structures in methanol and water. The distance d between the two carbon atoms linked to the pyridinium groups is here used to quantify the aperture of the cone.

Atomic coordinate of derivative 68^{2+} in methanol

6	-1.885025	4.174609	-9.988283
6	-2.307686	5.427041	-10.424611
6	-4.157170	3.719651	-9.163396
6	-2.811724	3.322968	-9.345364
8	-2.329502	2.147421	-8.888958
6	-5.176722	2.803295	-8.501644

6	-0.466631	3.700257	-10.264904
6	-0.579825	-0.503556	-13.157757
6	-5.053750	-1.658276	-10.978565
1	-1.598527	6.106848	-10.886394
1	-4.704333	2.270571	-7.671512
1	-5.968451	3.420628	-8.067049
1	-0.152071	3.017299	-9.476755
1	0.208288	4.562516	-10.251280
1	-0.101268	-1.006599	-12.312744
1	-0.051086	-0.831756	-14.057558
1	-4.444821	-1.985752	-10.136680
1	-5.820850	-2.419844	-11.154175
6	-0.379274	3.024407	-11.628529
6	-0.363036	3.799871	-12.795063
6	-0.383256	3.206488	-14.056466
6	-0.437898	1.817510	-14.171623
6	-0.443260	1.007756	-13.031384
6	-0.392509	1.629397	-11.774035
8	-0.424479	0.821158	-10.644073
1	-0.365590	3.825904	-14.948496
1	-0.342911	4.883254	-12.709669
1	-0.475167	1.353516	-15.153828
6	-2.608699	-1.141580	-14.514013
6	-4.181313	-1.538198	-12.218637
6	-2.826726	-1.150718	-12.106635
6	-2.031112	-0.950980	-13.258896
8	-2.340260	-1.027390	-10.853410
1	-2.020251	-0.964098	-15.409155
6	-6.846922	0.078879	-11.414529
6	-5.802232	1.822285	-9.483965
6	-5.250077	0.548015	-9.687252
6	-5.737387	-0.332192	-10.664645
8	-4.140442	0.188920	-8.932130
1	-7.250001	-0.588072	-12.172165
1	-3.017933	1.438422	-8.845711
1	-1.586416	-0.390208	-10.791083
6	-3.938564	-1.541798	-14.618887
6	-4.722360	-1.746517	-13.484170
1	-5.749283	-2.083504	-13.584684
6	-7.432434	1.327810	-11.212026
1	-8.295405	1.624966	-11.800812
6	-6.902465	2.199367	-10.260665
1	-7.345312	3.181421	-10.115380
6	-4.391370	-0.573357	-7.727538
1	-5.002833	0.024232	-7.038159
1	-4.957233	-1.475178	-7.990131
6	-3.038218	-0.918964	-7.128109
1	-2.455397	-1.454401	-7.886700
1	-2.500708	0.013764	-6.913827
6	-3.171561	-1.757217	-5.853787
1	-2.185264	-1.991378	-5.440398
1	-3.740413	-1.222768	-5.083767
1	-3.685456	-2.704675	-6.054591
6	0.853684	0.472089	-10.061047
1	1.396186	1.393894	-9.818995
1	1.447452	-0.090458	-10.793970
6	0.568540	-0.350043	-8.815125
1	-0.078313	0.240596	-8.155870
1	-0.002063	-1.241629	-9.105498
6	1.854228	-0.757724	-8.090295
1	1.624055	-1.349610	-7.198585
1	2.500881	-1.362264	-8.737248
1	2.425491	0.122137	-7.771578
6	-3.636241	5.812664	-10.252050
6	-4.557326	4.969878	-9.634599
1	-5.593368	5.277178	-9.529419
6	-5.640062	-2.124750	-18.425966
6	-6.284952	-1.329819	-17.476556
6	-5.700996	-1.142603	-16.237369
7	-4.521496	-1.743844	-15.929953
6	-3.885904	-2.529037	-16.838700
6	-4.422292	-2.723826	-18.098380
1	-6.079689	-2.274567	-19.405851
1	-7.226203	-0.838844	-17.691977
1	-6.126514	-0.510053	-15.470039
1	-2.966295	-2.992104	-16.507350
1	-3.892632	-3.354331	-18.802119
6	-4.879481	9.584254	-11.651328
6	-5.180128	9.180604	-10.349203
6	-4.752508	7.942735	-9.905086
7	-4.065329	7.110971	-10.731005
6	-3.775252	7.483202	-12.005774
6	-4.162853	8.721640	-12.482947
1	-5.198800	10.555639	-12.012567
1	-5.726394	9.821870	-9.668237
1	-4.918251	7.584015	-8.898261
1	-3.251062	6.752687	-12.607228
1	-3.916733	8.991083	-13.502877

Atomic coordinate of derivative 68^{+} in methanol

6	-1.698396	3.968603	-9.989164
6	-2.301152	4.858888	-10.853782
6	-3.904413	3.509634	-8.979947
6	-2.458578	3.297273	-8.937864
8	-1.903364	2.586740	-8.053018
6	-4.809854	2.640404	-8.114661
6	-0.217070	3.655060	-10.149340
6	-0.523038	-0.454769	-13.115344
6	-5.003150	-1.588460	-10.909619
1	-1.688375	5.385769	-11.580761
1	-4.176918	2.094093	-7.414613
1	-5.500599	3.266342	-7.536075
1	0.074785	3.015113	-9.316149
1	0.380603	4.573243	-10.091649
1	-0.113909	-1.052530	-12.296202
1	-0.064197	-0.823668	-14.037968
1	-4.358421	-2.025687	-10.148111
1	-5.763220	-2.329910	-11.179655
6	0.033967	2.990923	-11.493215
6	0.356535	3.751335	-12.624935
6	0.415794	3.170221	-13.892782
6	0.138099	1.812797	-14.051130
6	-0.159982	1.011907	-12.941535
6	-0.179542	1.615270	-11.677276
8	-0.450381	0.826359	-10.562273
1	0.668768	3.777454	-14.757398
1	0.551304	4.814634	-12.508610
1	0.165113	1.362628	-15.040320
6	-2.684688	-0.511335	-14.415879
6	-4.173547	-1.262603	-12.144754
6	-2.781110	-1.045923	-12.059029
6	-2.026912	-0.681949	-13.198433
8	-2.182185	-1.239512	-10.856989
1	-2.127136	-0.194946	-15.292430
6	-6.913899	0.088042	-10.901799
6	-5.613853	1.690934	-8.989696
6	-5.076572	0.453150	-9.386698
6	-5.690323	-0.340267	-10.370493
8	-3.907022	0.011795	-8.801292
1	-7.412109	-0.521136	-11.652225
1	-1.538721	-0.508142	-10.690248
6	-4.057748	-0.729519	-14.497174
6	-4.799208	-1.111922	-13.381237
1	-5.864638	-1.298532	-13.473406
6	-7.504186	1.274351	-10.466886
1	-8.465969	1.582700	-10.867803
6	-6.848336	2.073887	-9.529080
1	-7.297571	3.012140	-9.211840
6	-4.144843	-0.747051	-7.603105
1	-4.651814	-0.113941	-6.859251
1	-4.815692	-1.590050	-7.829020
6	-2.813687	-1.245975	-7.071107
1	-2.336889	-1.852559	-7.849756
1	-2.163997	-0.381494	-6.898029
6	-2.978043	-2.059761	-5.784372
1	-2.007172	-2.410112	-5.417914
1	-3.438438	-1.459007	-4.990502
1	-3.612173	-2.939877	-5.947296
6	0.732235	0.422250	-9.821297
1	1.380335	1.295981	-9.690229
1	1.284535	-0.323592	-10.409624
6	0.271560	-0.124414	-8.483876
1	-0.368199	0.636869	-8.024649
1	-0.350774	-1.009471	-8.658636
6	1.448459	-0.486791	-7.574090
1	1.089143	-0.888626	-6.620707
1	2.094219	-1.244411	-8.034670
1	2.066370	0.392553	-7.355743
6	-3.679498	5.121153	-10.783297
6	-4.466103	4.418450	-9.853098
1	-5.547047	4.532244	-9.877928
6	-6.024515	-0.206992	-18.183394
6	-6.511573	0.406927	-17.027933
6	-5.842165	0.230198	-15.830972
7	-4.732801	-0.551846	-15.767828
6	-4.251710	-1.165549	-16.880200
6	-4.876370	-0.997167	-18.102483
1	-6.531869	-0.071703	-19.132223
1	-7.393976	1.034900	-17.047529
1	-6.142241	0.705121	-14.906577
1	-3.381275	-1.792094	-16.739589
1	-4.469686	-1.498094	-18.972594
6	-5.486128	7.856766	-13.437097
6	-5.919820	7.748398	-12.114022
6	-5.298130	6.864689	-11.252915
7	-4.285758	6.050307	-11.680080
6	-3.870217	6.132708	-12.981142

6	-4.436247	7.036916	-13.858339
1	-5.951947	8.558534	-14.119567
1	-6.720554	8.369151	-11.728934
1	-5.550537	6.793393	-10.204531
1	-3.105965	5.429240	-13.279399
1	-4.068946	7.067627	-14.877664

Atomic coordinate of derivative 68^{2+} in water

6	-1.999721	4.270064	-9.836181
6	-2.249620	5.633797	-9.948439
6	-4.328573	3.917925	-9.121135
6	-3.040542	3.421597	-9.402996
8	-2.712100	2.111745	-9.287205
6	-5.463070	2.993694	-8.707911
6	-0.670239	3.667677	-10.244101
6	-0.841962	-0.709100	-12.848977
6	-5.630766	-1.419955	-11.283241
1	-1.452560	6.306284	-10.250303
1	-5.133648	2.356792	-7.881444
1	-6.279493	3.602979	-8.309941
1	-0.314508	2.987172	-9.467793
1	0.071567	4.466563	-10.350736
1	-0.432076	-1.078227	-11.906815
1	-0.170717	-1.037278	-13.649750
1	-5.281213	-1.841422	-10.336221
1	-6.494651	-2.021260	-11.580199
6	-0.827537	2.910616	-11.557282
6	-1.295190	3.582717	-12.691956
6	-1.552887	2.897128	-13.877953
6	-1.386156	1.514219	-13.922358
6	-0.913976	0.810769	-12.808753
6	-0.603052	1.526052	-11.641071
8	-0.083469	0.844637	-10.553505
1	-1.909564	3.433376	-14.752768
1	-1.478100	4.652903	-12.633603
1	-1.638639	0.964652	-14.825830
6	-2.563580	-1.844189	-14.320958
6	-4.548502	-1.575578	-12.340072
6	-3.220032	-1.172525	-12.100737
6	-2.221934	-1.289337	-13.091432
8	-2.818936	-0.636743	-10.918835
1	-1.817483	-1.914081	-15.106275
6	-6.954833	0.618390	-12.016273
6	-6.004860	2.148201	-9.854527
6	-5.631997	0.809627	-10.029166
6	-6.086690	0.022431	-11.095158
8	-4.683709	0.258143	-9.153786
1	-7.319931	0.032549	-12.855591
1	-3.467028	1.532803	-9.042882
1	-3.553321	-0.483584	-10.283377
6	-3.873679	-2.262367	-14.555927
6	-4.860483	-2.128285	-13.583450
1	-5.868321	-2.482555	-13.775253
6	-7.347129	1.948846	-11.869619
1	-8.023499	2.396085	-12.591828
6	-6.873942	2.706556	-10.798512
1	-7.175895	3.744864	-10.690787
6	-5.195601	-0.438094	-7.971899
1	-5.712073	0.293838	-7.341532
1	-5.925657	-1.184736	-8.302223
6	-4.010116	-1.066945	-7.264815
1	-3.521818	-1.775023	-7.945023
1	-3.268034	-0.290657	-7.044545
6	-4.441441	-1.779413	-5.978640
1	-3.575368	-2.228306	-5.482010
1	-4.907966	-1.080806	-5.274170
1	-5.161629	-2.579596	-6.186513
6	1.355306	0.944684	-10.475266
1	1.637977	1.997126	-10.329899
1	1.794710	0.610829	-11.425973
6	1.850247	0.097429	-9.314452
1	1.252327	0.343040	-8.430284
1	1.677435	-0.961841	-9.547703
6	3.342034	0.320224	-9.046868
1	3.689567	-0.315197	-8.225678
1	3.946260	0.085192	-9.931461
1	3.540943	1.363077	-8.772589
6	-3.519528	6.131791	-9.653559
6	-4.553542	5.289259	-9.254910
1	-5.542926	5.693432	-9.064807
6	-4.853991	-3.922750	-18.298398
6	-5.632667	-2.899976	-17.753468
6	-5.287512	-2.362634	-16.527117
7	-4.214635	-2.837559	-15.841152
6	-3.453588	-3.841350	-16.351197
6	-3.748863	-4.390735	-17.585107
1	-5.104218	-4.348274	-19.263910
1	-6.493314	-2.501379	-18.276586

1	-5.822827	-1.543367	-16.066587
1	-2.635311	-4.181973	-15.731236
1	-3.122871	-5.188221	-17.966385
6	-4.252850	10.261716	-10.009333
6	-4.585074	9.584151	-8.834761
6	-4.324664	8.229773	-8.734423
7	-3.770970	7.553925	-9.774899
6	-3.451684	8.195342	-10.929396
6	-3.673812	9.553420	-11.064062
1	-4.442094	11.325502	-10.101315
1	-5.028210	10.096838	-7.989715
1	-4.523637	7.651337	-7.842260
1	-3.041894	7.579208	-11.718291
1	-3.408392	10.038490	-11.995485
8	-1.068308	-1.673451	-8.950729
8	-1.005363	0.700539	-7.410367
1	-1.321649	1.281224	-8.124852
1	-0.988926	-0.175280	-7.855836
1	-1.447157	-1.221524	-9.730821
1	-0.137078	-1.805383	-9.184393

Atomic coordinate of derivative 68^{+} in water

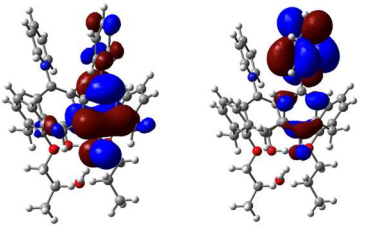

6	-1.708917	3.982003	-10.031149
6	-2.299633	4.884766	-10.894745
6	-3.913251	3.552368	-9.016275
6	-2.478602	3.319630	-8.990749
8	-1.905514	2.584977	-8.120714
6	-4.852901	2.711513	-8.157583
6	-0.229694	3.654980	-10.192017
6	-0.516312	-0.494446	-13.105486
6	-5.002527	-1.569306	-10.879612
1	-1.681864	5.406183	-11.620968
1	-4.274066	2.175732	-7.407472
1	-5.558660	3.365493	-7.630398
1	0.064023	3.022293	-9.354541
1	0.370761	4.571834	-10.146662
1	-0.104665	-1.081169	-12.279784
1	-0.058990	-0.873556	-14.024638
1	-4.359247	-1.988332	-10.106849
1	-5.758663	-2.319312	-11.136984
6	0.016129	2.975064	-11.529276
6	0.322622	3.725030	-12.672502
6	0.382856	3.128698	-13.932987
6	0.120928	1.766094	-14.072278
6	-0.160734	0.975972	-12.950910
6	-0.180107	1.594434	-11.693749
8	-0.427967	0.814186	-10.566647
1	0.623538	3.727945	-14.806565
1	0.505825	4.791825	-12.570938
1	0.146716	1.303841	-15.055848
6	-2.679729	-0.552896	-14.400293
6	-4.169477	-1.266673	-12.118170
6	-2.774669	-1.064866	-12.037781
6	-2.020722	-0.719081	-13.182907
8	-2.173120	-1.254666	-10.835394
1	-2.121151	-0.248704	-15.280391
6	-6.924996	0.093663	-10.910096
6	-5.638274	1.746512	-9.032698
6	-5.087063	0.507900	-9.406369
6	-5.697779	-0.312845	-10.370454
8	-3.907350	0.093672	-8.825848
1	-7.420161	-0.536851	-11.644705
1	-1.518931	-0.531431	-10.677845
6	-4.054989	-0.757870	-14.476423
6	-4.796644	-1.121892	-13.354869
1	-5.864201	-1.297955	-13.442004
6	-7.521850	1.287610	-10.505751
1	-8.484190	1.581509	-10.916005
6	-6.872530	2.111578	-9.584799
1	-7.328157	3.053666	-9.288655
6	-4.116140	-0.680597	-7.628328
1	-4.506283	-0.030177	-6.834869
1	-4.861827	-1.465089	-7.827841
6	-2.792045	-1.288794	-7.208493
1	-2.413550	-1.904034	-8.033598
1	-2.081669	-0.474113	-7.050502
6	-2.926435	-2.116205	-5.927659
1	-1.965010	-2.559491	-5.645578
1	-3.263115	-1.488484	-5.094129

1	-3.648792	-2.933228	-6.048643
6	0.772243	0.433521	-9.841352
1	1.413336	1.315973	-9.736362
1	1.321216	-0.315416	-10.428735
6	0.347461	-0.098900	-8.486396
1	-0.280786	0.664845	-8.015463
1	-0.277500	-0.986945	-8.634311
6	1.549838	-0.448842	-7.605235
1	1.217728	-0.839190	-6.637407
1	2.182838	-1.211537	-8.074870
1	2.172836	0.433498	-7.415326
6	-3.671965	5.160836	-10.820349
6	-4.464454	4.471960	-9.891027
1	-5.543218	4.605534	-9.907486
6	-6.026840	-0.238876	-18.160254
6	-6.505590	0.385475	-17.006946
6	-5.834857	0.209234	-15.810729
7	-4.732123	-0.582132	-15.746215
6	-4.259188	-1.206001	-16.856442
6	-4.885546	-1.038736	-18.077968
1	-6.535265	-0.104009	-19.108554
1	-7.382420	1.021128	-17.027738
1	-6.128816	0.691830	-14.888363
1	-3.393703	-1.839140	-16.714906
1	-4.485435	-1.547784	-18.946373
6	-5.440829	7.929466	-13.462723
6	-5.845051	7.857220	-12.128202
6	-5.236154	6.959020	-11.272237
7	-4.269396	6.104129	-11.717072
6	-3.882757	6.150629	-13.025990
6	-4.436263	7.064343	-13.902182
1	-5.896542	8.640500	-14.142553
1	-6.611166	8.513706	-11.732621
1	-5.465709	6.905528	-10.217332
1	-3.150864	5.415763	-13.330479
1	-4.095465	7.068947	-14.930907
8	-2.648072	1.629391	-5.690859
1	-2.426079	1.945653	-6.605520
1	-3.039704	2.414587	-5.278954

Derivatives 69^{4+}/69^{3+}

The UV simulation calculations performed on the protonated derivative showed the presence of a single band at **355 nm** (experimental data = **367 nm**).

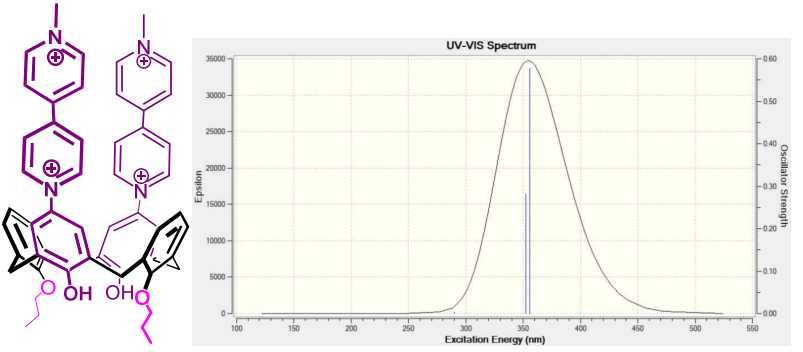

Figure 5.62. UV simulated spectrum of derivative $\mathbf{69^{4+}}$ in acetonitrile.

The analogous calculations on the monodeprotonated calixarene derivative were subsequently carried out. The presence of a band at **594 nm** was observed (experimental data = **610 nm**).

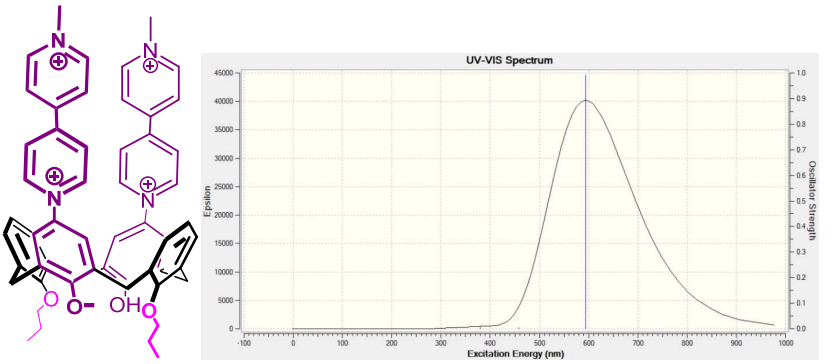

Figure 5.63. UV simulated spectrum of derivative **69**$^{3+}$ in acetonitrile.

Atomic coordinate of derivative 69^{4+}

O	7.1725	7.8151	8.8095
O	3.5723	6.4946	7.7176
O	5.0754	9.0892	8.0778
H	5.8897	8.6058	8.3221
O	5.6736	5.3172	8.5385
H	4.861	5.75	8.2092
N	5.1966	2.7273	13.5234
C	2.5252	6.4697	8.6025
N	2.6814	11.6324	12.4963
C	5.5317	4.7132	9.7568
C	2.2026	8.9882	8.2923
H	2.7058	8.8675	7.3327
H	1.3251	9.5923	8.0602
C	1.7687	7.6286	8.8452
C	3.1291	4.0516	9.1418
H	2.5475	3.1411	9.2982
H	3.4885	3.9557	8.1151
C	4.2188	3.435	11.3405
H	3.2941	2.9188	11.5584
C	2.5221	10.4135	10.3493
H	1.4466	10.3636	10.4382
C	4.5068	9.7426	9.1361
C	2.2187	5.2734	9.2694
C	6.4993	4.0557	11.8758
H	7.3462	4.0952	12.5456
C	5.314	10.3838	10.0934
C	3.1762	6.2611	6.362
H	2.4537	7.0067	6.0229
H	2.6908	5.2876	6.2657
C	3.1086	9.7417	9.2741
C	8.0045	6.8573	10.8659
C	4.7123	11.037	11.1756
H	5.3535	11.5433	11.884
C	0.5996	7.5325	9.6072
H	-0.0335	8.3965	9.7477
C	6.6138	4.7214	10.6522
C	7.4941	9.2337	10.7081
C	3.3145	11.0464	11.3197
C	1.051	5.1981	10.0361
H	0.76	4.2683	10.5042
C	7.9306	5.4324	10.309
H	8.0705	5.4406	9.2282
H	8.7753	4.8491	10.6773
C	7.5581	7.9621	10.1178
C	6.8423	10.4029	9.9718
H	7.138	10.397	8.9206
H	7.2365	11.3493	10.3481
C	5.3048	3.4076	12.2345
C	8.0426	9.4287	11.9795
H	8.0645	10.4146	12.4225
C	0.2324	6.3177	10.1844
H	-0.6855	6.2456	10.7518
C	8.549	7.072	12.1369
H	8.9596	6.2478	12.7017
C	1.352	12.5194	14.8077
C	8.5875	8.3548	12.6818
H	9.0373	8.517	13.6518
C	0.7757	12.6654	13.5378
H	-0.2109	13.0985	13.4268

C	4.4243	6.3062	5.475
H	5.1441	5.564	5.8217
H	4.9037	7.2795	5.5819
C	4.3212	4.0889	10.1071
C	6.2906	2.1393	14.0838
H	7.1988	2.1403	13.4941
C	5.0133	1.5107	16.0542
C	1.4542	12.2137	12.3988
H	1.0479	12.3162	11.3998
C	3.2895	11.5436	13.7103
H	4.2604	11.0668	13.7335
C	4.0071	2.6963	14.1853
H	3.1732	3.1929	13.7086
C	8.2594	7.8793	7.8809
H	9.0543	7.179	8.1443
H	8.7065	8.8751	7.8803
C	7.7222	7.5454	6.4848
H	6.9587	8.2726	6.2051
H	7.2283	6.5731	6.5165
C	3.8959	2.1024	15.4496
H	2.9366	2.1001	15.9521
C	6.2202	1.5242	15.3404
H	7.1121	1.0717	15.7569
C	4.1243	6.0609	3.9884
H	3.6759	5.0802	3.8218
H	5.0392	6.1058	3.3951
H	3.4419	6.8128	3.5897
C	2.6414	11.9716	14.8759
H	3.1407	11.8631	15.8308
C	8.8095	7.517	5.3992
H	9.3069	8.4826	5.3026
H	8.3805	7.2727	4.4264
H	9.5717	6.7674	5.615
C	4.9242	0.903	17.4154
C	4.3892	1.6268	18.4946
C	4.3228	1.0506	19.7695
N	4.7649	-0.2171	19.9626
C	5.295	-0.9491	18.9502
C	5.3811	-0.4017	17.6625
H	4.043	2.6441	18.3556
H	3.9375	1.5703	20.6411
C	4.7037	-0.7899	21.3253
H	5.637	-1.949	19.1972
H	5.7937	-1.0012	16.8584
C	0.4631	11.984	17.0998
C	0.6041	12.8985	16.0428
C	-0.0001	14.1595	16.1807
C	-0.7247	14.4717	17.3401
N	-0.8523	13.5505	18.3279
C	-0.2716	12.3278	18.2413
H	0.9022	10.9961	17.032
H	0.0967	14.9041	15.3977
H	-1.2063	15.4308	17.5048
C	-1.6229	13.9088	19.5391
H	-0.4159	11.6565	19.0809
H	4.7302	-1.8813	21.2774
H	5.5625	-0.4155	21.8885
H	3.7684	-0.4869	21.8039
H	-1.8575	13.0155	20.1233
H	-1.0185	14.5969	20.1357
H	-2.5601	14.3825	19.2351

Atomic coordinate of derivative 69^{3+}

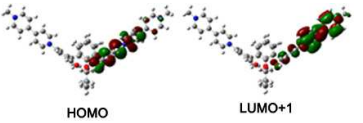

O	-0.02562900	-3.37227900	2.57742300
O	-0.09509500	-3.07191300	-2.49128300
O	1.63495800	-2.74511300	-0.02991900
O	-1.66318200	-2.84368700	-0.26561400
H	-1.19729800	-2.98494100	-1.11731100
N	-6.03588000	0.56163400	-0.12375000
C	0.02145800	-1.71831300	-2.76588200
N	6.04896800	0.53572500	0.07624800
C	-2.68768100	-1.98154200	-0.29853700
C	2.56351400	-1.88231200	-2.52177700
H	2.33269000	-2.94721900	-2.47323800
H	3.25376400	-1.71781700	-3.35529900
C	1.28111600	-1.11297400	-2.78892100
C	-2.51908600	-1.66225100	-2.82306500
H	-3.17504900	-1.28103700	-3.60876800
H	-2.42774100	-2.73748600	-2.99001300
C	-4.29071400	-0.57330500	-1.40736900
H	-4.70782100	-0.15672400	-2.31811300
C	4.34356800	-0.68713200	-1.18153000
H	4.77418300	-0.32264200	-2.11030900
C	2.60967800	-1.96246200	-0.00348100

C	-1.16061400	-0.99230900	-2.94606600
C	-4.37005800	-0.84170700	0.99554100
H	-4.81120200	-0.58238800	1.95238400
C	3.17269400	-1.48874100	1.25001100
C	-0.04988000	-3.93947100	-3.63427000
H	0.89780400	-3.78004400	-4.16132900
H	-0.86474500	-3.68507800	-4.32395700
C	3.22789500	-1.48152300	-1.22648500
C	-1.31993500	-1.35948600	2.49315600
C	4.28036000	-0.68216600	1.25641500
H	4.71825000	-0.39343400	2.20794900
C	1.32989900	0.25783900	-3.04037500
H	2.29699900	0.75165800	-3.05979700
C	-3.25880800	-1.66733900	0.95267200
C	1.11436600	-1.25946600	2.63905200
C	4.89302100	-0.28245600	0.05117700
C	-1.06702200	0.37517700	-3.19307400
H	-1.97477900	0.95371300	-3.33784800
C	-2.59140400	-2.14852600	2.22174200
H	-2.33631000	-3.20431100	2.13259700
H	-3.29150700	-2.03930500	3.05553700
C	-0.07570000	-1.99562000	2.57907000
C	2.47428300	-1.92400000	2.51623800
H	2.33154100	-3.00553900	2.49870900
H	3.09289600	-1.67238200	3.38397000
C	-4.88201600	-0.30873400	-0.18198200
C	1.02829900	0.12826700	2.72712500
H	1.94585200	0.70792900	2.77466400
C	0.17324300	0.99721000	-3.25091300
H	0.23810200	2.06172000	-3.45062500
C	-1.36416900	0.03094600	2.58608200
H	-2.32373100	0.53606900	2.52741100
C	8.31969100	2.16881700	0.10831700
C	-0.20104300	0.77398900	2.73179600
H	-0.25069900	1.85498800	2.81416900
C	8.13652300	1.19260700	-0.87457100
H	8.86122200	1.03977300	-1.66404300
C	-0.16905700	-5.36856600	-3.14874800
H	-1.10725400	-5.47515600	-2.59345600
H	0.64247200	-5.56427200	-2.44068500
C	-3.18075600	-1.40651400	-1.48386900
C	-7.14055700	0.16894300	0.54550100
H	-7.10810100	-0.81554000	0.99069500
C	-8.22728600	2.23620000	0.00297700
C	7.02325500	0.38915200	-0.86219400
H	6.88458900	-0.41067400	-1.57357000
C	6.20584000	1.48861700	1.03476200
H	5.39158600	1.60175700	1.73401800
C	-5.99543500	1.76542500	-0.73345300
H	-5.07071000	2.02147500	-1.23120100
C	-0.08886000	-3.94863400	3.88109600
H	-1.01995700	-3.64486100	4.38008300
H	0.74761700	-3.58046500	4.49139900
C	-0.02538800	-5.45594700	3.74059800
H	0.89777400	-5.71936600	3.21361500
H	-0.85562900	-5.78364200	3.10590200
C	-7.07780400	2.61333200	-0.69228900
H	-7.01133200	3.56259100	-1.20772300
C	-8.24217200	0.98928900	0.62899400
H	-9.10151700	0.64688900	1.19072900
C	-0.12240900	-6.36702800	-4.30108200
H	-0.94047400	-6.19755100	-5.00758400
H	-0.20894300	-7.39104100	-3.93113800
H	0.81821700	-6.29091700	-4.85462500
C	7.32014000	2.28872700	1.07797100
H	7.39079300	3.01326200	1.87923000
C	-0.08282900	-6.16122000	5.09184300
H	0.75315800	-5.86243100	5.73164100
H	-0.03647000	-7.24583700	4.96953200
H	-1.00957700	-5.92559400	5.62397200
C	-9.39718200	3.14058500	0.07972300
C	-9.22403800	4.51550500	0.23625000
C	-10.32601100	5.33834200	0.30902400
N	-11.56900200	4.83246900	0.22446000
C	-11.76448300	3.50936300	0.07086300
C	-10.69872400	2.64209100	-0.00073100
H	-8.24026300	4.95791900	0.32302000
H	-10.24324500	6.40886200	0.43771000
C	-12.74018300	5.72504600	0.33905600
H	-12.79180800	3.17653800	0.00664400
H	-10.89696100	1.58780200	-0.14265000
C	9.44082300	4.35267400	0.58791700
C	9.50916500	3.03756500	0.11756800
C	10.74627900	2.58032800	-0.35103500
C	11.83731600	3.41524500	-0.33949300
N	11.73803500	4.67913300	0.11695300
C	10.56281200	5.14771900	0.57605000
H	8.51204600	4.78182800	0.93975100
H	10.87778300	1.56812000	-0.70965300
H	12.81331200	3.10134300	-0.68551400

C	12.93880100	5.53577100	0.14454600
H	10.55051200	6.17245700	0.92154900
H	-13.49297700	5.41317900	-0.38144600
H	-13.13637900	5.65758500	1.35186300
H	-12.42901700	6.74445300	0.12672500
H	12.62892400	6.57599800	0.20183000
H	13.53992200	5.27667600	1.01596600
H	13.50983600	5.37415900	-0.76724100

CHAPTER VI

Goals and Outline – Part II

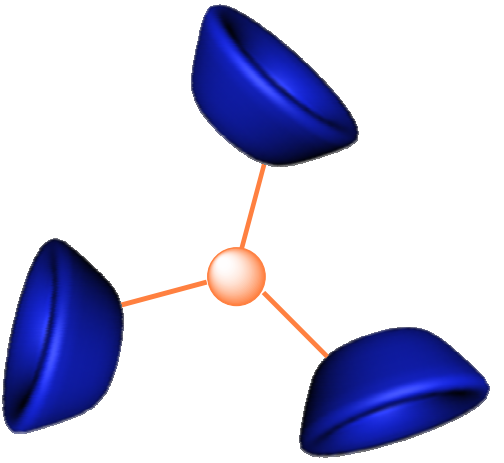

6.1 Goals and Outline – Part II

In the context of the study of calixarene derivatives for the possible construction of molecular machines, it was decided to extend our investigation to multivalent systems, which could give rise to more complex supramolecular behaviours. These systems are characterized by the presence of more recognition sites that can interact with more guest molecules (**Figure 6.1**).

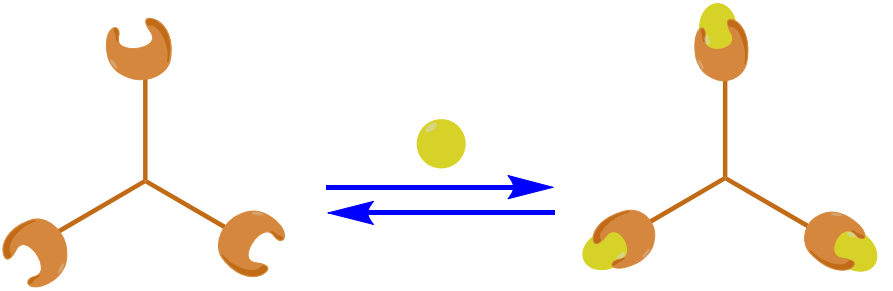

Figure 6.1. Schematic multivalent system.

In the following chapters, two different multivalent systems will be described (**Figure 6.2**). The first is a trivalent host, while the second is a bivalent axle. In the first instance, the multiple threading will be examined, while in the latter case, the self-sorting properties will be considered.

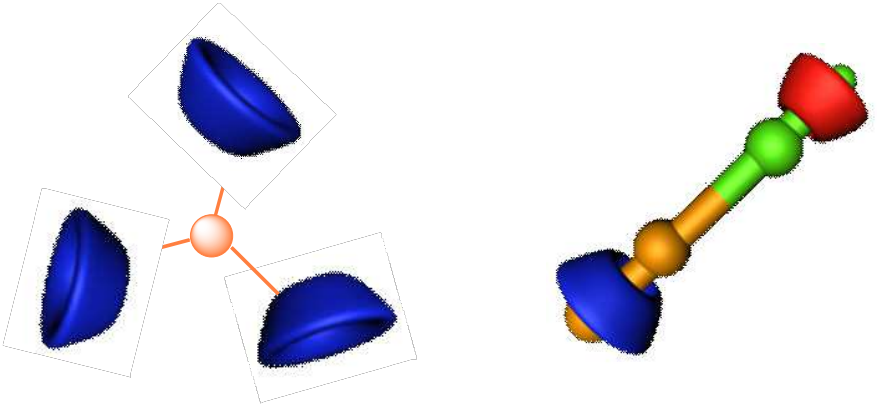

Figure 6.2. Multivalent systems.

CHAPTER VII

Multiple-Threading of a Tris-calix[6]arene

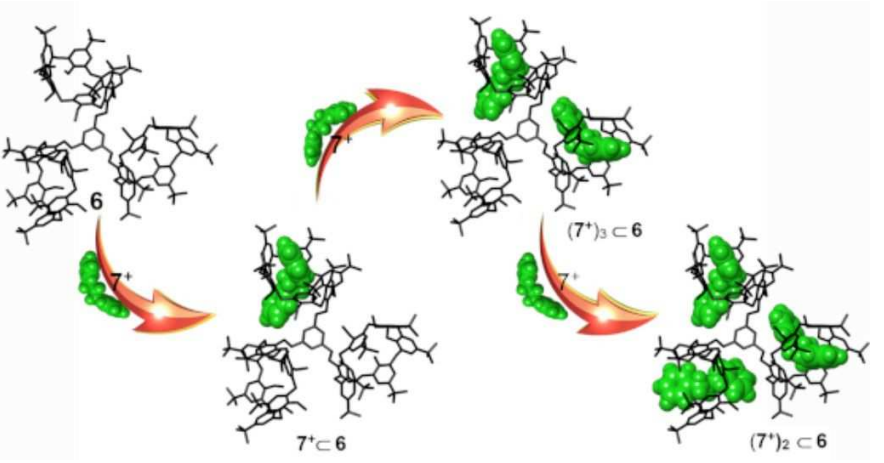

ù

7.1 Multivalent hosts

Macrocyclic hosts with multiple cavities and/or multiple recognition sites have attracted increasing attention thanks to their usefulness for developing nontrivial interlocked architectures. At this regard, interpenetrated systems in which two rings are linked to one another in a handcuff-like fashion have represented a significant synthetic challenge. Based on the template-directed threading[68] of linear axles through such double-macrocycles, beautiful handcuff-like architectures have been reported, which shows interesting properties and functions (**Figure 7.1**).

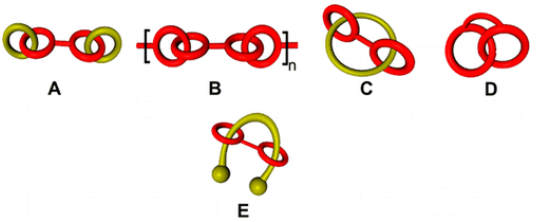

Figure 7.1. Schematic representation of the currently known prototypical examples of handcuff-derived architectures.

An interesting example of handcuff catenane is that reported by Beer in 2011 (**Figure 7.2**), whose synthesis exploited a chloride anion templated.

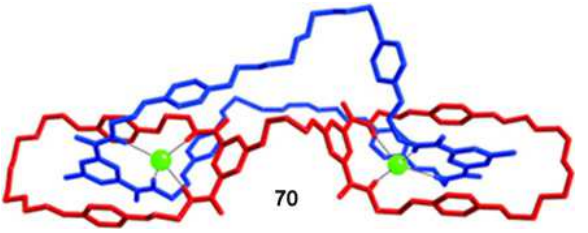

Figure 7.2. Crystal structure of handcuff catenane **70**.

The synthetic strategy undertaken to prepare such handcuff catenane is illustrated in **Figure 7.3**. Two identical *N*-methylpyridinium molecules thread, by anion templated, through a handcuff-like bis-macrocycle. Each macrocycle contains an isophthalamide group able to hydrogen bonding to the chloride anion. Pseudorotaxane formation is also supported by π–π stacking between the electron-rich hydroquinone groups of the bis-macrocycle and electron-poor pyridinium rings of the threading components. Subsequent cyclization led to the formation of the desired handcuff catenane.

[68](a) Badjić, J. D.; Balzani, V.; Credi, A.; Silvi, S.; Stoddart, J. F. Science 2004, 303, 1845. 89 (b)Evans, N. H.; Serpell, C. J.; Beer, P. D., Angew. Chem. Int. Ed. 2011, 50, 2507. (c) Zhang, Z.-J.; Han M.; Zhang, H.-Y.; Liu, Y. Org. Lett. 2013, 15, 1698;

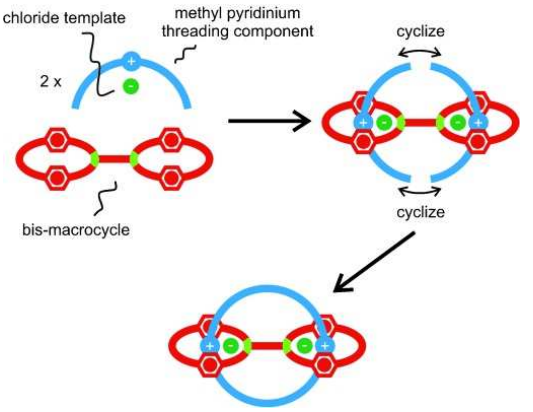

Figure 7.3. Synthesis of "handcuff" catenane.

In addition to the chain handcuff systems just described, there are also numerous examples of handcuff rotaxane in the literature and among them a recent example was reported by Champness in 2019.[69] In particular, such "handcuff" rotaxane includes two pillar[5]arenes linked together by an aromatic bridge as cyclic system and a molecule with two imidazole groups as a linear system (**Figure 7.4**). The formation of the supramolecular system occurs thanks to the robust interaction between pillararenes and imidazole units. The interaction between these moieties provides a reliable method for the formation of the two pseudorotaxane moieties, which can be readily locked in place through reaction with appropriate plug sets.

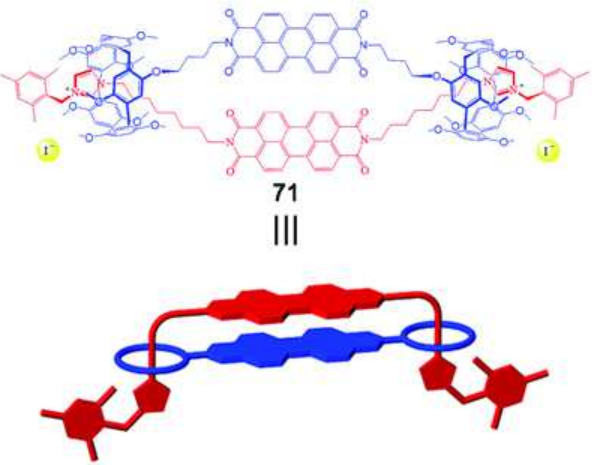

Figure 7.4. "handcuff" rotaxane **71**.

Other examples calixarene-based handcuff systems were described in chapter 2.

[69] Yang, L.; Langer, P.; Davies, E. S.; Baldoni, M.; Wickham, K.; Besley, N. A.; Besley, E.; Champness, N. R. *Chem. Sci.* **2019**, *10* (13), 3723–3732.

Regarding double-calixarene systems, their threading with dialkylammonium axles was explored. Initially, the study was conducted with symmetric axles leading to the formation of the expected symmetrical pseudo[3]rotaxane (**Figure 7.5**).

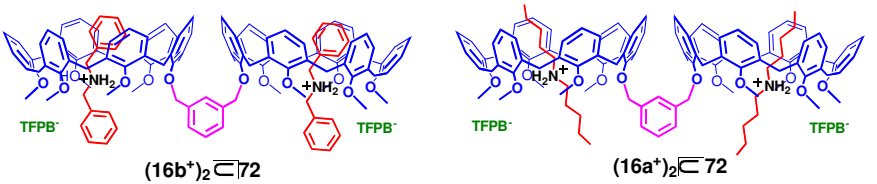

$(16b^+)_2\supset 72$ $(16a^+)_2\supset 72$

Figure 7.5. Double-calixarene based pseudo[3]rotaxanes

Instead, when the study was extended to the non-symmetrical alkylbenzyl ammonium axle, only one supramolecular system was formed out of the three possible ones (**Figure 7.6**).

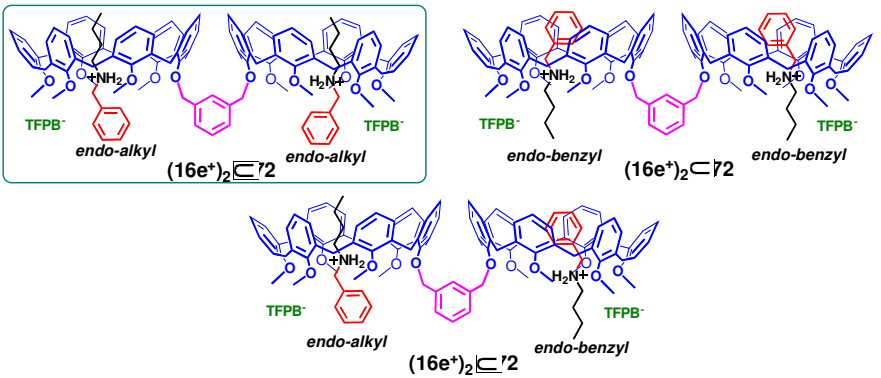

$(16e^+)_2\supset 72$ $(16e^+)_2\supset 72$ $(16e^+)_2\supset 72$

Figure 7.6. Double-calixarene based pseudo[3]rotaxanes with a non-symmetric axle.

7.2 Tris-calix[6]arene[70]

With the aim of forming more complex supramolecular systems, we decided to synthesize a homotritopic host **73** (**Figure 7.7**), bearing three calix[6]arene wheels linked to a central benzene unit and resembling the host component of molecular elevator synthesized by Stoddart (see Chapter 1).

[70] Iuliano, V.; Ciao, R.; Vignola, E.; Talotta, C.; Iannece, P.; De Rosa, M.; Soriente, A.; Gaeta, C.; Neri, P. *Beilstein J. Org. Chem.* **2019**, *15*, 2092–2104.

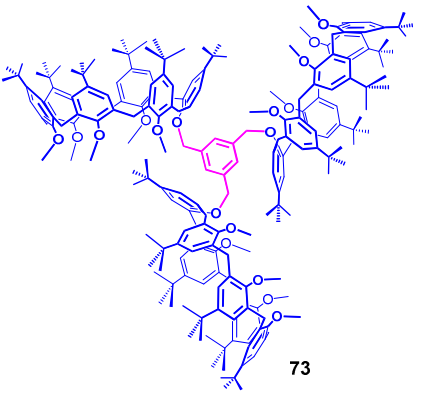

Figure 7.7. Multivalent host **73**.

7.2.1 Synthesis of triple-calix[6]arene 73

Scheme 7.1 shows the synthetic strategy developed for the synthesis of derivative **73**. In detail, mono-ol **75**, previously obtained according to the procedure reported in literature,[71] was reacted with 1,3,5-tris(bromomethyl)benzene in the presence of NaH as base, in a mixture of dry THF/DMF (7/3 v/v) for 12 h at reflux.

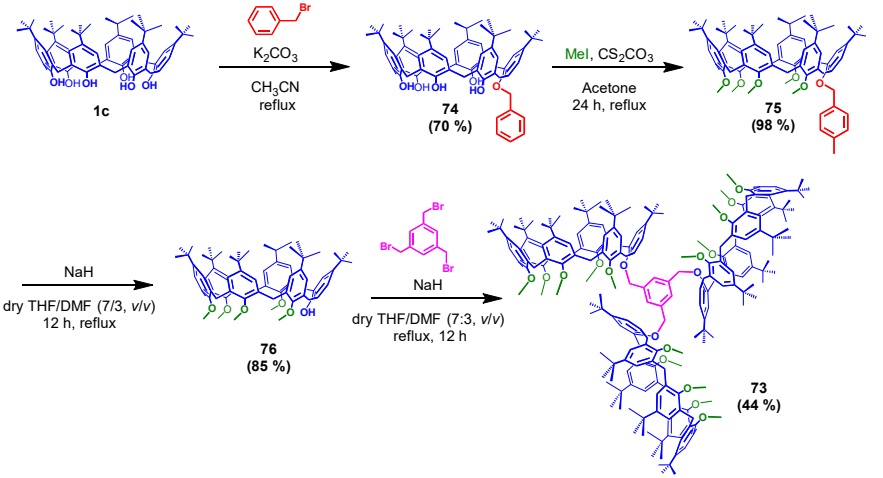

Scheme 7.1. Synthesis of derivative **73**.

The ^{1}H NMR spectrum confirms the formation of multivalent host **73** (**Figure 7.8a**). In fact, three ArCH$_2$Ar AX systems can be seen in the 4.5-3.5 ppm region, while one

[71] (a) de Mendoza, J.; Carramolino, M.; Cuevas, F.; Nieto, P. M.; Prados, P.; Reinhoudt, D. N.; Verboom, W.; Ungaro, R.; Casnati, A. *Synthesis* **1994**, 47–50. (b) De Rosa, M.; Soriente, A.; Concilio, G.; Talotta, C.; Gaeta, C.; Neri, P. *J. Org. Chem.* **2015**, 80, 7295–7300.

OCH_2 (6H) singlet resonates at 5 ppm. A further confirmation is given by the HR-ESI-FT-ICR mass spectrum (*m/z* calcd for $C_{222}H_{288}KO_{18}^+$ 3283.1319 found 3283.1748, **Figure 7.8b**).

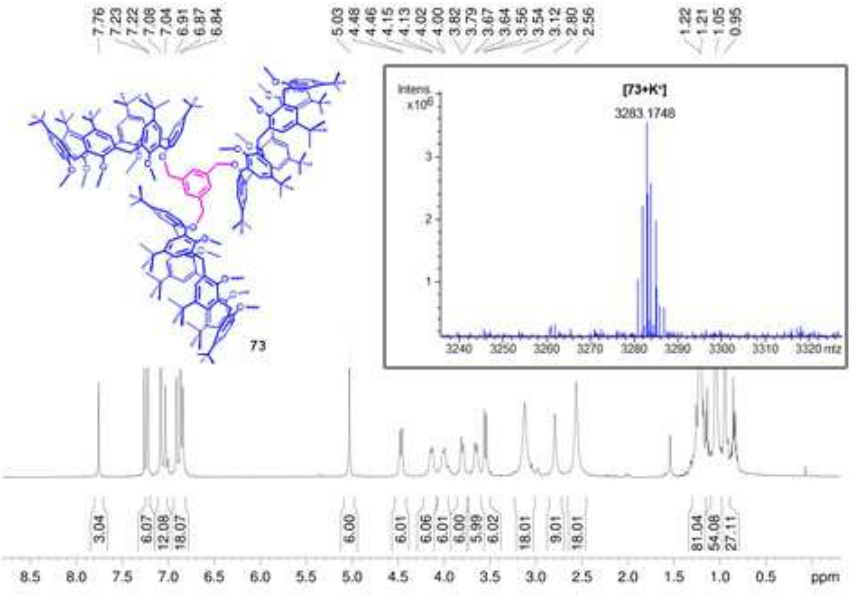

Figure 7.8. ^{1}H NMR and HR-ESI-FT-ICR mass spectra of derivative **73**.

7.2.2 Threading studies of derivative 73

Initially, the threading of **73** with a symmetrical dibenzylammonium axle **16b**$^+$ was studied. Given the presence of three cavities, the study was carried out with different guest/host ratios, namely 1:1, 2:1, and 3:1, to form pseudo[2]-, -[3]-, and -[4]rotaxanes (**Scheme 7.2**).

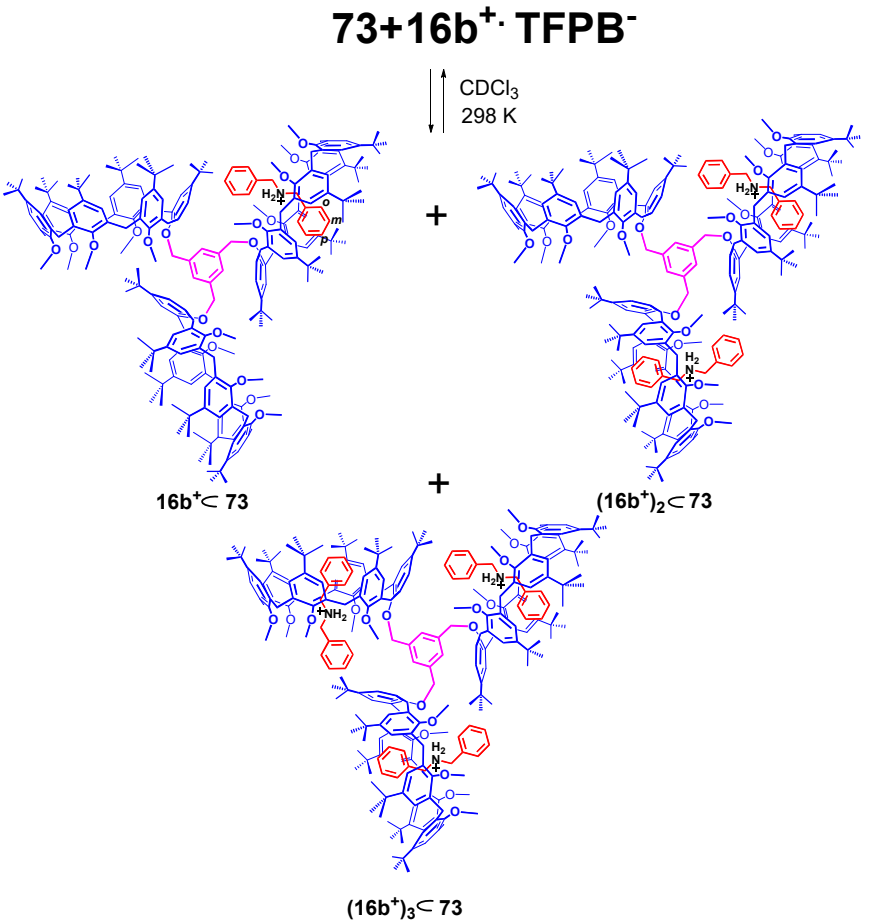

Scheme 7.2. Formation of the **16b**$^+$ ⊂ **73**, (**16b**$^+$)$_2$ ⊂ **73**, (**16b**$^+$)$_3$ ⊂ **73** pseudorotaxane architectures by multiple-threading of **73** with **16b**$^+$ as TFPB$^-$ salt.

The formation of pseudo[*n*]rotaxanes by threading of **73** with dibenzylammonium axle **16b**$^+$ was studied by HR-ESI-FT-ICR mass spectrometry and 1D/2D NMR (**Figure 7.9**). The ^{1}H NMR spectrum (**Figure 7.9b**) of a 1:1 mixture of **73** and **16b**$^+$**·TFPB**$^-$ in $CDCl_3$ at 298 K, shows the formation of the **16b**$^+$**⊂ 73** pseudo[2]rotaxane in $CDCl_3$ solution. In details, a set of shielded benzyl resonances was observed in the 4.5–6.5 region of the ^{1}H NMR spectrum, at 5.99 (t, 1H), 5.34 (dd, 2H), and 4.77 ppm (d, 2H), corresponding to its *endo*-cavity disposition and consequently indicative of the formation of the **16b**$^+$**⊂ 73** pseudo[2]rotaxane. Further confirmation comes from the ESI FT ICR MS spectrometry (**Figure 7.9c**). In fact, the presence of a molecular ion peak at 3442.2979 *m/z* attributable to **16b**$^+$**⊂ 73** pseudo[2]rotaxane was observed.

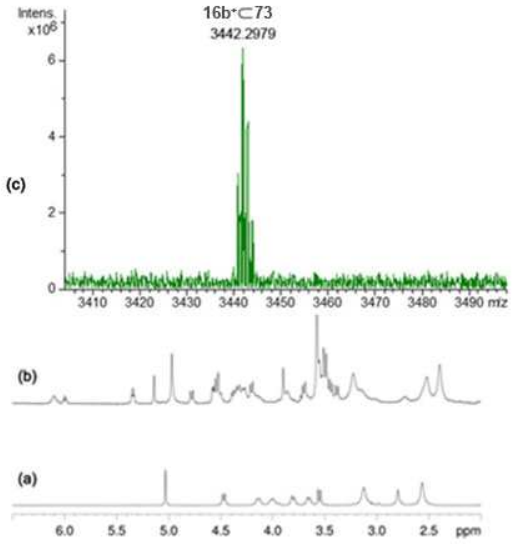

Figure 7.9. (a) Portion of ^{1}H NMR spectrum of **73** ($CDCl_3$, 298 K, 600 MHz); (b) Portion of ^{1}H NMR spectrum of a 1:1 mixture of **73** and **16b**$^+$·$TFPB^-$ ($CDCl_3$, 298 K, 600 MHz); (c) Portion of the ESI FT-ICR mass spectrum of **16b**$^+$ ⊂ **73**.

By adding 1 equivalent of salt to the previously analysed 1:1 mixture, we observed the appearance of further shielded aromatic signals in agreement with the formation of pseudo[3]rotaxane **(16b**$^+$**)$_2$⊂ 73**. Confirmation of the formation of this supramolecular system comes from ESI FT-ICR mass spectrometry. In fact, the doubly charged molecular peak at 1820.2282 *m/z* relative to the pseudo[3]rotaxane is clearly evident. An ESI-CID MS/MS experiment was then carried out which showed the appearance of a singly charged peak at 3442.2979 *m/z* related to the formation of the pseudo[2]rotaxane following the extraction of an ammonium axle from the pseudo[3]rotaxane system previously formed (**Figure 7.10**).

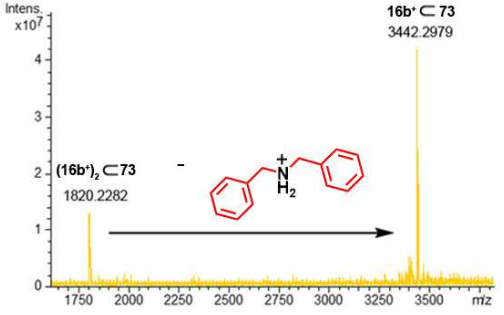

Figure 7.10. HR ESI-FT-ICR-CID mass spectrum of **(16b**$^+$**)$_2$ ⊂ 73**.

Subsequently, the guest/host ratio was increased to 3:1. From analysis of the NMR spectra, it was observed that pseudo[3]rotaxane was the specie most abundant as evidenced by the presence of two singlet in 1:2 ratio at 5.08 and 5.06 ppm attributable to the benzylic methylene groups of the central benzene core of **73** in **$(16b^+)_2 \subset 71$** pseudo[3]rotaxane. A close inspection of the region between 4.8 and 5.2 ppm in the 1D and 2D NMR spectra, revealed the presence of the **$(16b^+)_3 \subset 73$** pseudo[4]rotaxane as a less abundant species. These data suggested that in a 1:3 mixture of **73** and **$16b^+ \cdot TFPB^-$** in $CDCl_3$ (**Figure 7.11b**), the **$(16b^+)_2 \subset 73$** and **$(16b^+)_3 \subset 73$** pseudorotaxanes were present.

Finally, increasing the guest/host ratio to 6:1, we observed the intensification of the signals related to the pseudo[4]rotaxane system at the expense of the pseudo[3]rotaxane (**Figure 7.11g**).

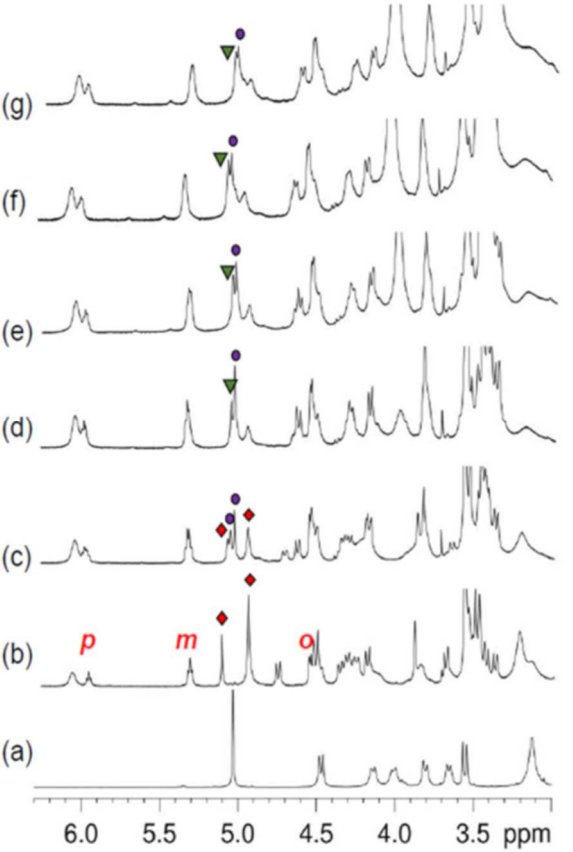

Figure 7.11. ^1H NMR titration of **73** with **$16b^+ \cdot$**TFPB– ($CDCl_3$, 298 K, 600 MHz). Significant portions of the ^1H NMR spectra of: (a) 6; (b) 1:1, (c) 1:2, (d) 1:3, (e) 1:4, (f) 1:5 and (g) 1:6 mixture of **73** and **$16b^+ \cdot$**TFPB–. Marked: red diamond = **$16b^+ \subset 6$**; purple circle = **$(16b^+)_2 \subset 73$**; green triangle = **$(16b^+)_3 \subset 73$**.

Then, a similar study was conducted using dipentylammonium as the linear axle, in different host/guest ratios (**Scheme 7.3**). Initially, the 1:1 mixture showed the formation of the pseudo[2]rotaxane system as confirmed by mass spectrometry and NMR spectroscopy.

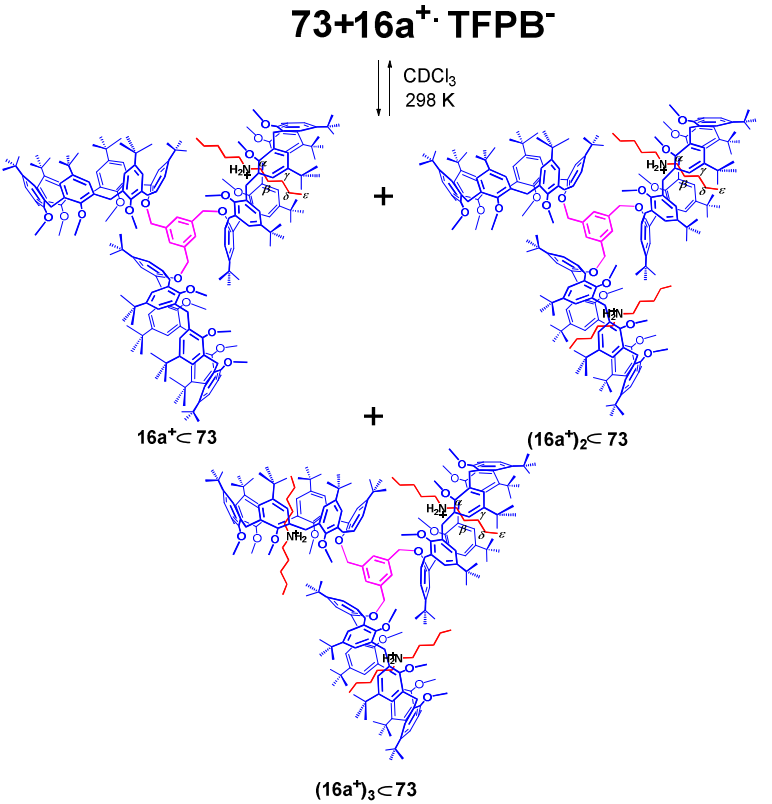

Scheme 7.3. Formation of the **16a**$^+$⊂**73**, (**16a**$^+$)$_2$ ⊂ **73**, (**16a**$^+$)$_3$ ⊂ **73** pseudorotaxane architectures by multiple-threading of **73** with **16a**$^+$ as TFPB$^-$ salt.

In detail, HR ESI FT–ICR mass spectrum (**Figure 7.12e**) of the 1:1 mixture of **73** and **16a**$^+$·**TFPB**$^-$ clearly evidenced the presence of a molecular ion peak at 3402.3809 *m/z*. Moreover, the analysis of NMR spectrum showed shielded signals at negative values of chemical shifts at –0.99, –0.88, –0.57, –0.40, and 0.64 ppm attributable, respectively, to the β, γ, δ, ε, and α H-atoms of the pentyl chain of linear system in the calix-cavity of **6**. By bringing the mixture to a 1:2 ratio between host and guest, it is possible to observe the presence of the molecular peak related to the 3-component supramolecular system by using ESI FT-ICR MS (**Figure 7.12f**). At the end, with an excess of **16a**$^+$·**TFPB**$^-$, the formation of the (**16a**$^+$)$_3$ ⊂ **71** pseudo[4]rotaxane was evidenced by ^{1}H NMR (**Figure 7.12d**).

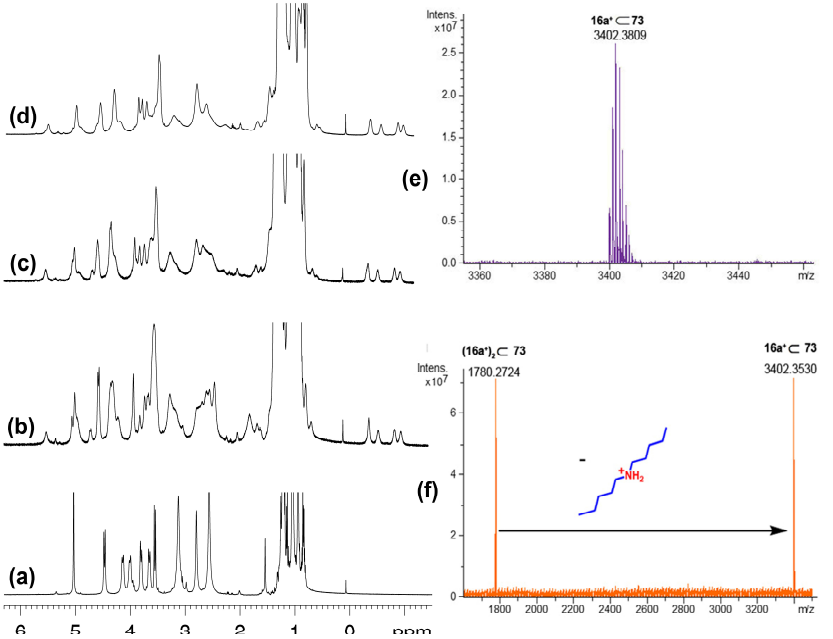

Figure 7.12. (a-d) ^{1}H NMR titration of **73** with **16a**$^+$·TFPB$^-$ ($CDCl_3$, 298 K, 600 MHz). Significant portions of the ^{1}H NMR spectra of: (a) 73; (b) 1:1, (c) 1:2, (d) 1:3, mixture of **73** and **16a**$^+$·TFPB$^-$. (e) HR ESI-FT-ICR mass spectrum of **16a**$^+$**⊂ 73**. (f) HR ESI-FT-ICR-CID mass spectrum of **(16a**$^+$**)$_2$ ⊂ 73**.

Subsequently, the threading of the multivalent host with the directional butylbenzyl ammonium axle **16e**$^+$ was studied. In this case, given the non-symmetry of the linear system, the *endo*-alkyl and the *endo*-benzyl adducts can be formed for each calixarene cavity and this implies that up to 4 supramolecular pseudo[4]rotaxane stereoisomers can be formed (**Figure 7.13**).

By mixing derivative **73** with 1 equiv. of butylbenzylammonium cation **16e**$^+$ as TFPB$^-$ salt in $CDCl_3$, the formation of the (*endo*–alkyl)–**16e**$^+$**⊂ 73** pseudo[2]rotaxane was observed by the presence in the ^{1}H NMR spectrum of shielded signals related to alkyl chain at negative value of chemical shift between –0.73 to –0.82 ppm. No evidence of the (*endo*–benzyl)–**16e**$^+$**⊂ 73** pseudo[2]rotaxane stereoisomer was observed in the ^{1}H NMR spectrum of the 1:1 mixture of **16e**$^+$ and **73.**

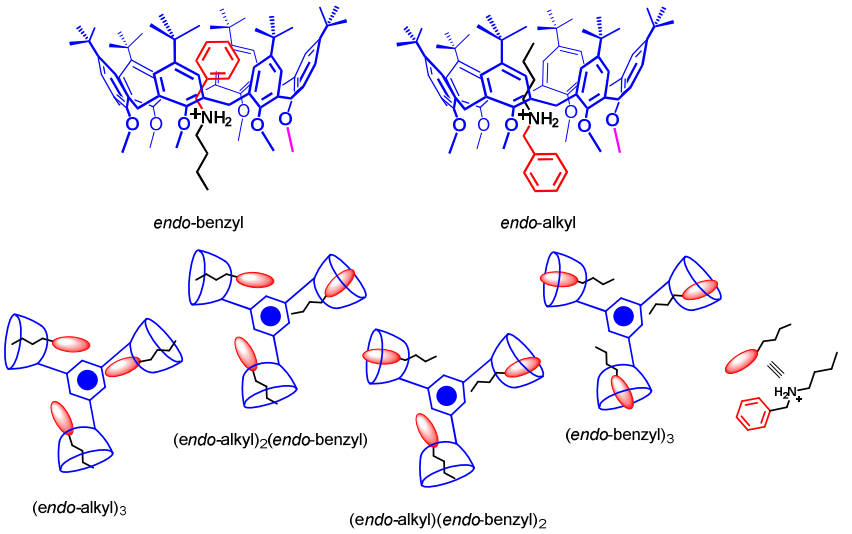

Figure 7.13. (top) Possible endo-benzyl and endo-alkyl stereoisomer obtainable by directional threading of calix[6]arene-wheel with alkylbenzylammonium axles. (Bottom) Sketch of the possible pseudo[4]rotaxane stereoisomers obtainable by triple-threading of **73** with **16e**$^+$.

MS analysis of this mixture confirmed the formation of **16e**$^+$**⊂73** pseudo[2]rotaxane. In fact, a molecular ion peak was present at 3408.3230 *m*/*z* (**Figure 7.14**). Afterwards, a mass spectrum of the 1:2 mixture of **73/16e**$^+$**·TFPB**$^-$ revealed the presence of singly-charged **16e**$^+$**⊂73** and doubly-charged **(16e**$^+$**)**$_2$**⊂73** pseudorotaxanes. ESI-CID MS/MS experiment revealed that **(16e**$^+$**)**$_2$**⊂73** pseudo[3]rotaxane was collisionally dissociated to **16e**$^+$**⊂73** pseudo[2]rotaxane by de-threading of one ammonium axle.

Finally, a ^{1}H NMR spectrum of the 1:3 mixture of **16e**$^+$**·TFPB**$^-$ and **73** was recorded and, again, no shielded benzylic resonances in the 4–6 ppm region could be evidenced. This is a clear proof that *endo*-butyl pseud[*n*]rotaxanes were selectively formed.

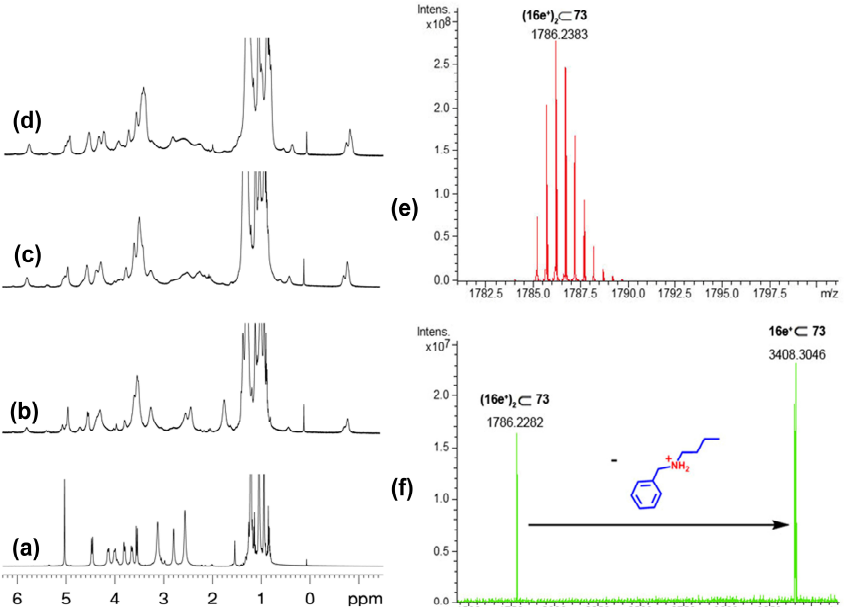

Figure 7.14. (a-d) ^{1}H NMR titration of **73** with **16e**$^{+}$·TFPB^{-} ($CDCl_3$, 298 K, 600 MHz). Significant portions of the ^{1}H NMR spectra of: (a) 6; (b) 1:1, (c) 1:2, (d) 1:3, mixture of **73** and **16e**$^{+}$·TFPB^{-}. (e) HR ESI-FT-ICR mass spectrum of **16e**$^{+}$⊂**73**. (f) HR ESI-FT-ICR-CID mass spectrum of (**16e**$^{+}$)$_2$⊂**73**.

7.3 Conclusions

In this chapter, the synthesis of an interesting multivalent host is shown. The threading ability of triple-calix[6]arene derivative **73** was tested with classical ammonium salt used for calixarene threading. It was demonstrated that derivative **73** is able to give a multiple-threading process with each axle used. The formation of pseudo[2]rotaxane, pseudo[3]rotaxane, and pseudo[4]rotaxane in $CDCl_3$ solution was ascertained by 1D and 2D NMR, and ESI FT-ICR MS/MS experiments. Furthermore, in the presence of a directional butylbenzylammonium axle, the stereoselective formation of *endo*-alkyl pseudorotaxane stereoisomers was observed.

7.4 Experimental Section

7.4.1 General Comments

Reactions under anhydrous conditions were conducted under an inert atmosphere (nitrogen) using dry solvents. The commercial reagents were purchased by Aldrich and TCIchemicals and were used without further purification. The reactions were controlled by thin-layer chromatography (TLC) with Macherey-Nagel plates coated with silica gel (0.25 mm) with fluorescence indicator UV254 and visualized using UV light and nebulization with an indicator solution of H_2SO_4-$Ce(SO_4)_2$. The reaction temperatures were measured externally using electronic thermometers. The reaction products were purified by Macherey-Nagel silica gel chromatography (60, 70-230 mesh). NMR spectra were recorded on Bruker Avance-600 spectrometer [600 (^{1}H) and 150 MHz (^{13}C)], Bruker Avance-400 spectrometer [400 (^{1}H) and 100 MHz (^{13}C)]. Chemical shifts are reported relative to the residual solvent peak ($CHCl_3$: δ 7.26, $CDCl_3$: δ 77.16) Standard pulse programs, provided by the manufacturer, were used for 2D NMR experiments. High-resolution Mass spectra were acquired with a Bruker Solarix spectrometer equipped with a Tesla magnet. It was used a MALDI as methods of sample ionization. DHB was used as matrix. Samples were prepared in $CHCl_3$ (1 mg / mL).

7.4.2 Synthesis of derivative 73

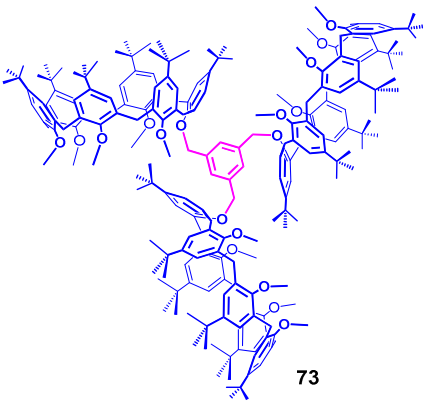

In a dry round flask, under N_2, derivative **76** (3.11 g, 2.98 mmol) was dissolved in dry THF/DMF (180 mL, 7:3 v/v). Subsequently, NaH (1.05 g, 43.86 mmol) was added at 0 °C. After 15 minutes, 1,3,5-tris(bromomethyl)benzene (0.36 g, 1.00 mmol) was added to the reaction mixture at room temperature. The reaction was stirred at reflux for 24 h under a nitrogen atmosphere. Afterwards the reaction was stopped by addition of 1 N HCl and the solution was extracted with chloroform. The organic phase was dried over anhydrous Na_2SO_4, filtered, and evaporated of the solvent. The raw was purified through chromatography column on silica gel and using solvent mixture dichloromethane/diethyl ether 96:4 as eluents. Derivative **73** was isolated with 68 % yield (2.20 g, 0.67 mmol). **^{1}HNMR** (400 MHz, $CDCl_3$, 298 K): δ 7.78 (s, Ar*H*, 3H), 7.28 - 7.26 (overlapped, ArH_{calix}, 6H), 7.11 - 7.06 (overlapped, ArH_{calix}, 12H), 6.94 – 6.87 (overlapped, ArH_{calix}, 18H), 5.06 (s, OCH_2Ar,6H), 4.50 and 3.58 (AX system,

$ArCH_2Ar$, J = 14.7 Hz, 12H), 4.17 and 4.04 (AX system, $ArCH_2Ar$, J = 14.5 Hz, 12H), 3.83 and 3.68 (AX system, $ArCH_2Ar$, J = 15.1 Hz, 12H), 3.15 (s, OCH_3, 18H), 2.82 (s, OCH_3, 9H), 2.58 (s, OCH_3, 18H), 1.24 - 1.22 (overlapped, $C(CH_3)_3$, 81H), 1.07 (s, $C(CH_3)_3$, 54H), 0.97 (s, $C(CH_3)_3$, 26H). **^{13}CNMR** (75 MHz, $CDCl_3$, 298 K): δ 154.5, 154.4, 153.9, 152.4, 145.9, 145.7, 138.8, 134.1, 133.9, 133.7, 133.6, 133.4, 127.5, 126.9, 125.5, 125.3, 124.8, 77.5, 75.9, 74.8, 60.2, 60.0, 34.3 (2), 31.8, 31.7(2), 31.5 (2),30.8, 30.6, 22.7, 14.4. **HRMS** (*m*/*z*) calcd for $C_{222}H_{288}KO_{18}^+$ 3283.1319 found 3283.1748.

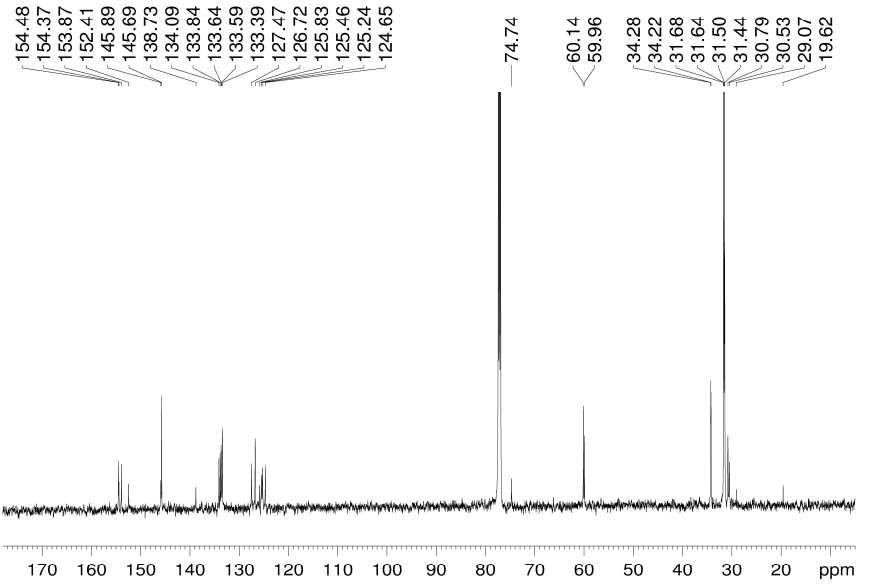

Figure 7.15. ^{13}C NMR spectrum of derivative **73** (150 MHz, $CDCl_3$, 298 K).

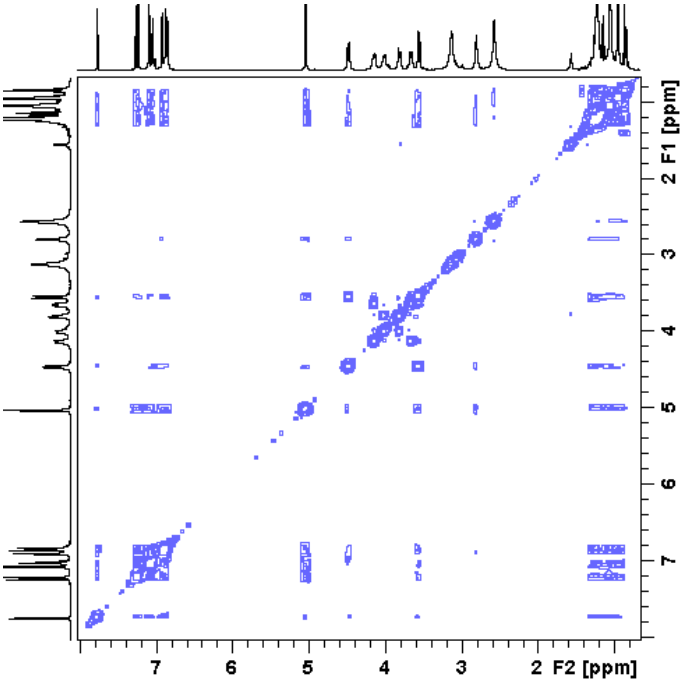

Figure 7.16. 2D COSY spectrum of derivative **73** (600 MHz, $CDCl_3$, 298 K).

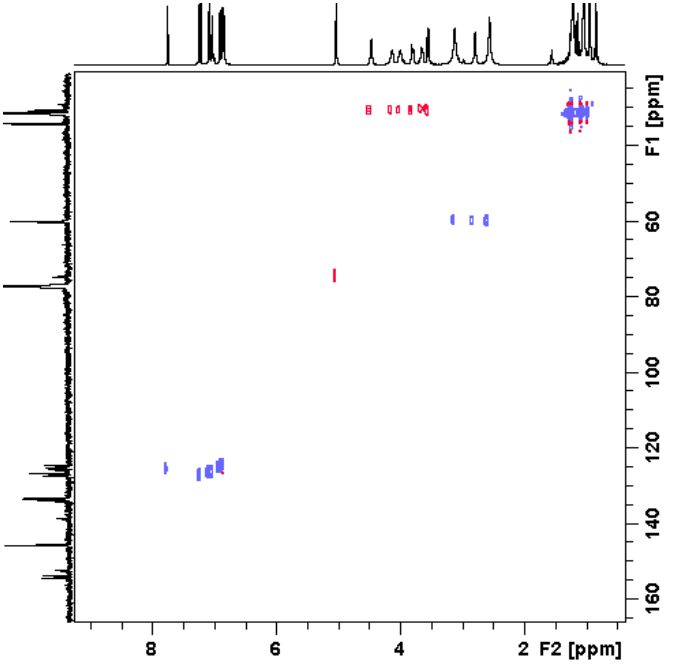

Figure 7.17. 2D HSQC spectrum of derivative **73** (600 MHz, $CDCl_3$, 298 K).

7.4.3 Threading of derivative 73

Mixtures of calix[6]arene derivative and TFPB linear system were dissolved in 0.5 mL of $CDCl_3$.Then, solutions were transferred in an NMR tube for 1D and 2D NMR spectra acquisition.

Table 7.1. Amount of hosts and guests for complexation experiments.

Pseudo[n]rotaxanes	**Calix[6]arene**		**Axles**		**$CDCl_3$**
	(mg)	**(mmol)**	**(mg)**	**(mmol)**	**(ml)**
$16b^+ \subset 73$	5.00	$1.5 \cdot 10^{-3}$	1.63	$1.5 \cdot 10^{-3}$	0.5
$(16b^+)_2 \subset 73$	5.00	$1.5 \cdot 10^{-3}$	3.26	$3.0 \cdot 10^{-3}$	0.5
$(16b^+)_3 \subset 73$	5.00	$1.5 \cdot 10^{-3}$	4.89	$4.5 \cdot 10^{-3}$	0.5
$16a^+ \subset 73$	5.00	$1.5 \cdot 10^{-3}$	1.57	$1.5 \cdot 10^{-3}$	0.5
$(16a^+)_2 \subset 73$	5.00	$1.5 \cdot 10^{-3}$	3.14	$3.0 \cdot 10^{-3}$	0.5
$(16a^+)_3 \subset 73$	5.00	$1.5 \cdot 10^{-3}$	4.71	$4.5 \cdot 10^{-3}$	0.5
$16e^+ \subset 73$	5.00	$1.5 \cdot 10^{-3}$	1.58	$1.5 \cdot 10^{-3}$	0.5
$(16e^+)_2 \subset 73$	5.00	$1.5 \cdot 10^{-3}$	3.16	$3.0 \cdot 10^{-3}$	0.5
$(16e^+)_3 \subset 73$	5.00	$1.5 \cdot 10^{-3}$	4.74	$4.5 \cdot 10^{-3}$	0.5

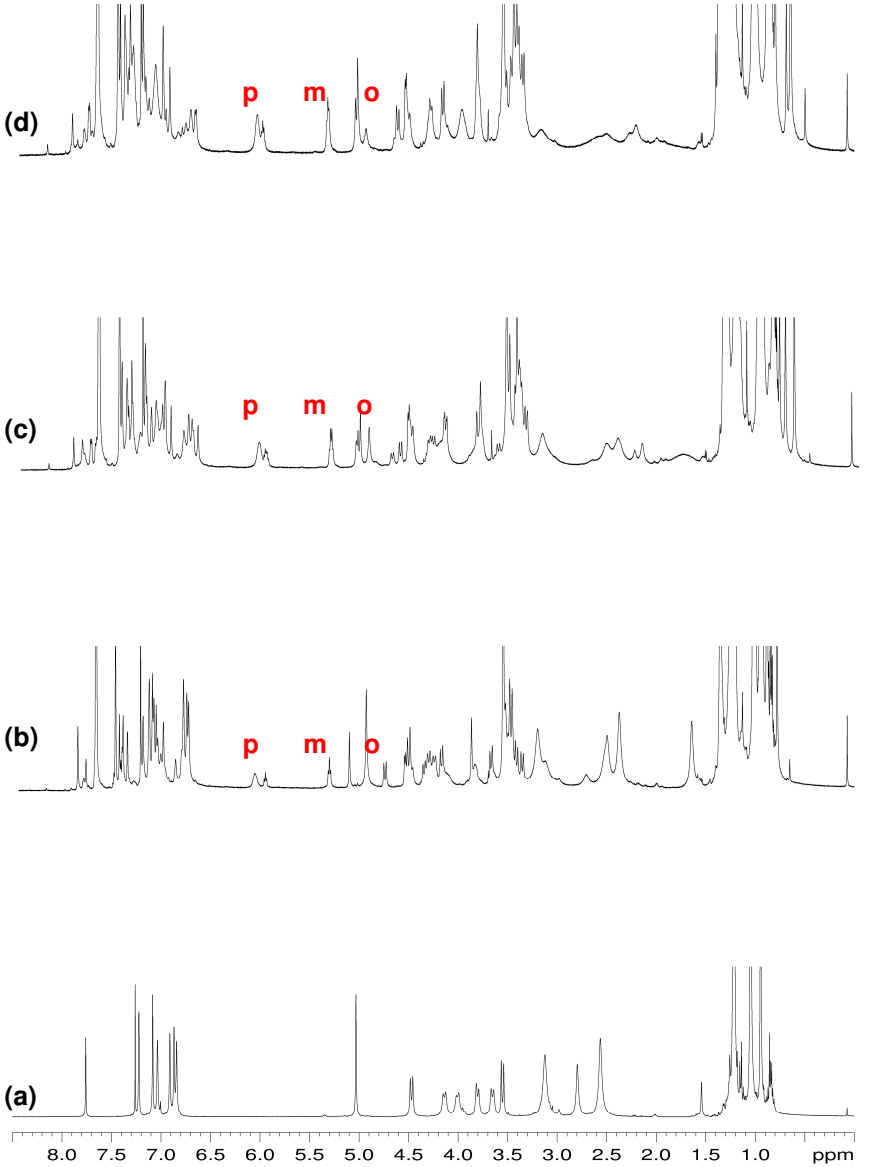

Figure 7.18. (a) ^{1}H NMR spectrum of derivative **73**; (b) ^{1}H NMR spectrum of derivative **73** and **16b**$^{+}$TFPB^{-} in mixture 1:1; (c) ^{1}H NMR spectrum of derivative **73** and **16b**$^{+}$TFPB^{-} in mixture 1:2; (d) ^{1}H NMR spectrum of derivative **73** and **16b**$^{+}$TFPB^{-} in mixture 1:3 (600 MHz, $CDCl_3$, 298 K).

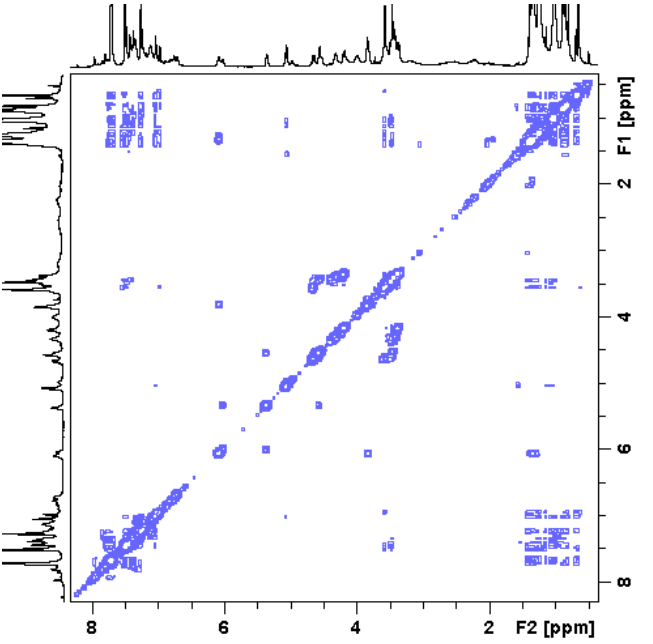

Figure 7.19. 2D COSY spectrum of derivative **(16b$^+$)$_3$ ⊂ 73** (600 MHz, $CDCl_3$, 298 K).

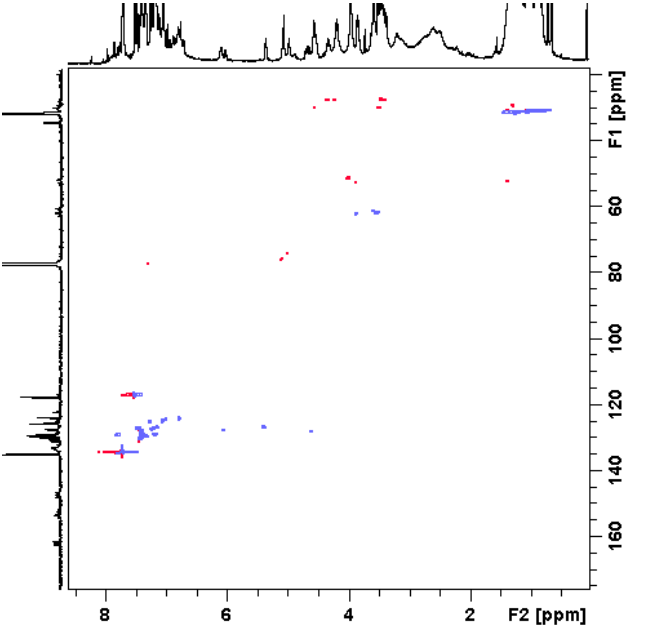

Figure 7.20. 2D HSQC spectrum of derivative **(16b$^+$)$_3$ ⊂ 73** (600 MHz, $CDCl_3$, 298 K).

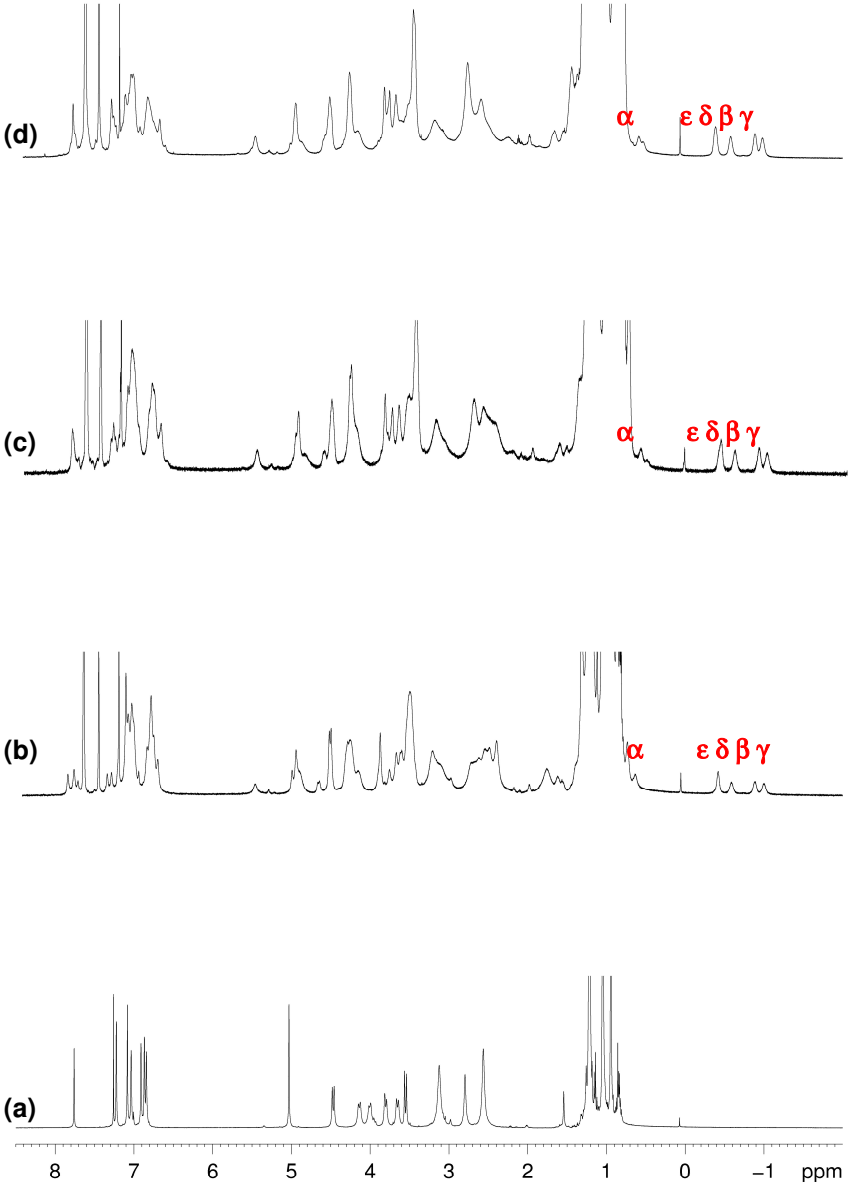

Figure 7.21. (a) ^{1}H NMR spectrum of derivative **73**; (b) ^{1}H NMR spectrum of derivative **73** and **16a**$^{+}$TFPB^{-} in mixture 1:1; (c) ^{1}H NMR spectrum of derivative **73** and **16a**$^{+}$TFPB^{-} in mixture 1:2; (d) ^{1}H NMR spectrum of derivative **73** and **16a**$^{+}$TFPB^{-} in mixture 1:3 (600 MHz, $CDCl_3$, 298 K).

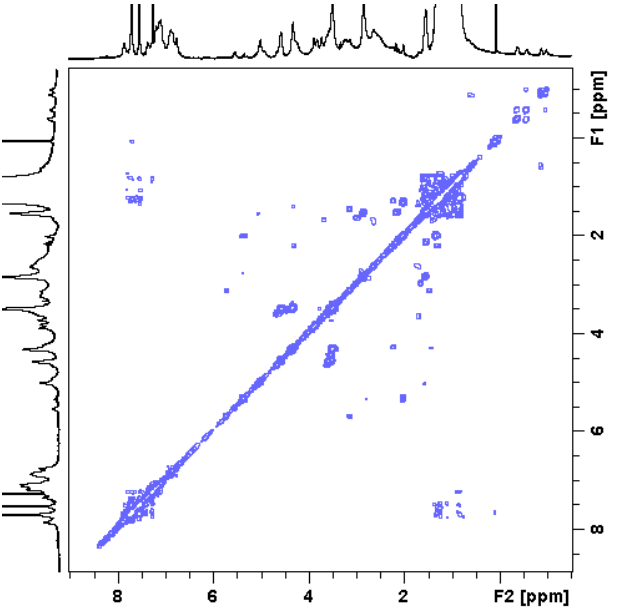

Figure 7.22. 2D COSY spectrum of derivative **(16a^{+})$_3$ ⊂ 73** (600 MHz, $CDCl_3$, 298 K).

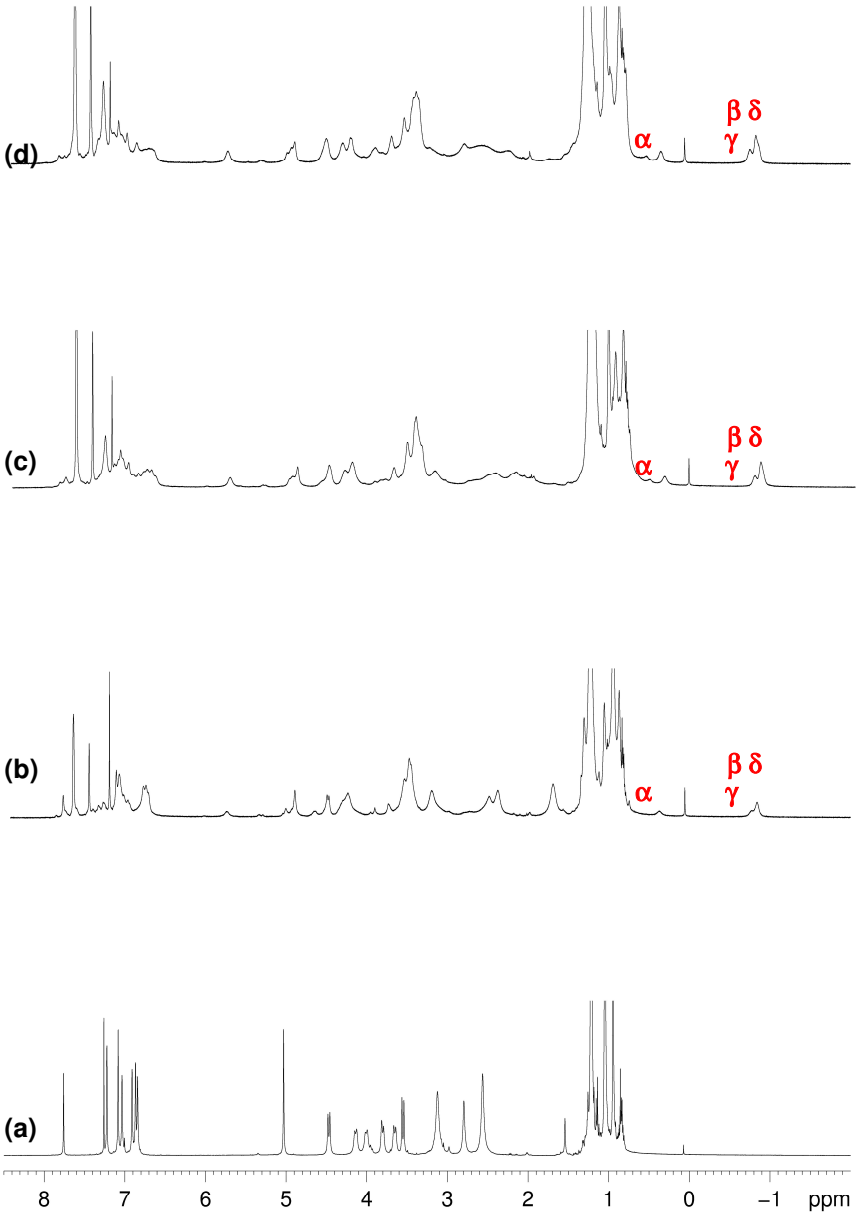

Figure 7.23. (a) ^{1}H NMR spectrum of derivative **73**; (b) ^{1}H NMR spectrum of derivative **73** and **16e**$^{+}$TFPB^{-} in mixture 1:1; (c) ^{1}H NMR spectrum of derivative **73** and **16e**$^{+}$TFPB^{-} in mixture 1:2; (d) ^{1}H NMR spectrum of derivative **73** and **16e**$^{+}$TFPB^{-} in mixture 1:3 (600 MHz, $CDCl_3$, 298 K).

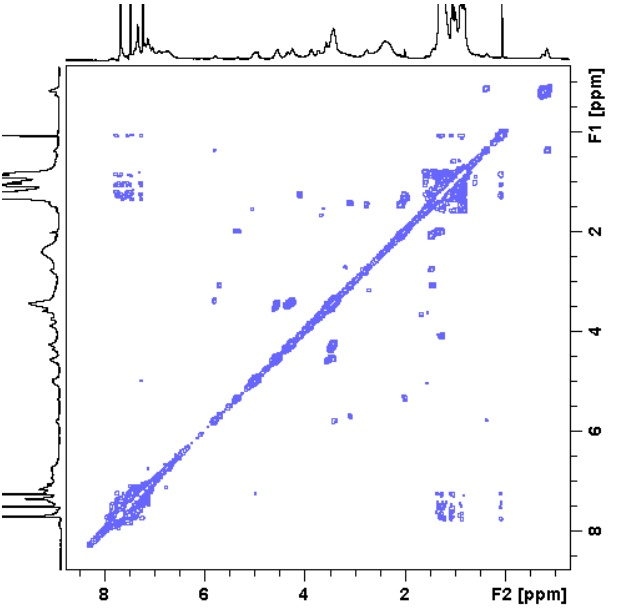

Figure 7.24. 2D COSY spectrum of derivative **(16e⁺)₃ ⊂ 73** (600 MHz, CDCl3, 298 K).

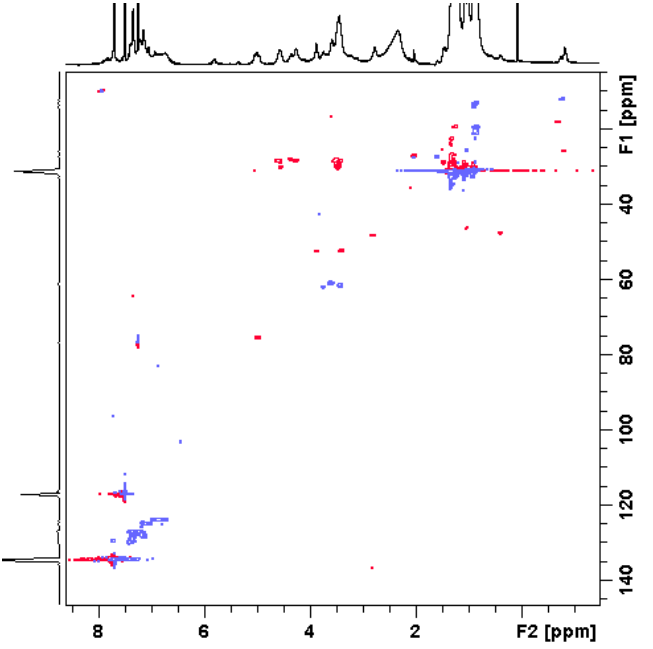

Figure 7.25. 2D HSQC spectrum of derivative **(16e⁺)₃ ⊂ 73** (600 MHz, $CDCl_3$, 298 K).

CHAPTER VIII

Self-sorting processes in pseudo[3]rotaxane systems

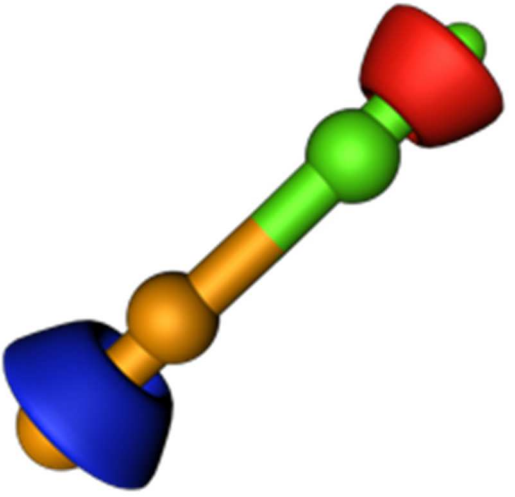

8.1 Self-sorting processes

A new frontier of supramolecular chemistry is the realization of complex molecular devices that are based on self-sorting processes. Through these processes, it is possible to observe in multicomponent mixtures molecular recognition phenomena that lead to the formation of a small number of supramolecular aggregates compared to a higher number of possibilities. Therefore, self-sorting refers to supramolecular systems that can self-select.

The concept behind self-sorting processes originates from nature itself, which controls the organization of complex biological systems, such as proteins, nucleic acids, and lipids within larger functional assemblies. Such organized biological systems must have specific characteristics that lead to their functions (e.g., DNA, ribosomes, or membranes). The most emblematic example in nature is represented by the 4 nitrogenous bases of DNA, because to form the double helix structure, the selective complementary pairing between adenine and thymine, cytosine and guanine (**Figure 8.1**) is necessary.

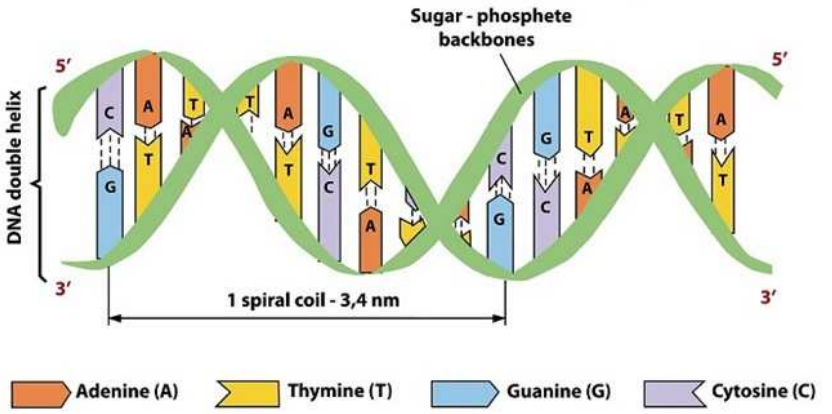

Figure 8.1. Double Helix of DNA.

From a synthetic point of view, these phenomena can be observed thanks to the construction of specific "molecular codes". By this term, it is meant the intrinsic structural information of a given interacting species on which depend the strength and selectivity of the interactions with the components of the system. The molecules, therefore, will tend to bind establishing the maximum number of possible interactions, otherwise, discrimination events will be observed. There are different "molecular codes" (**Figure 8.2**), both in synthetic and biological systems, including geometric complementarity (due to the size and shape of the interacting species) and interactional complementarity (between donors and acceptors of hydrogen-bonds, opposite charges, metal-ligand coordination, etc.).

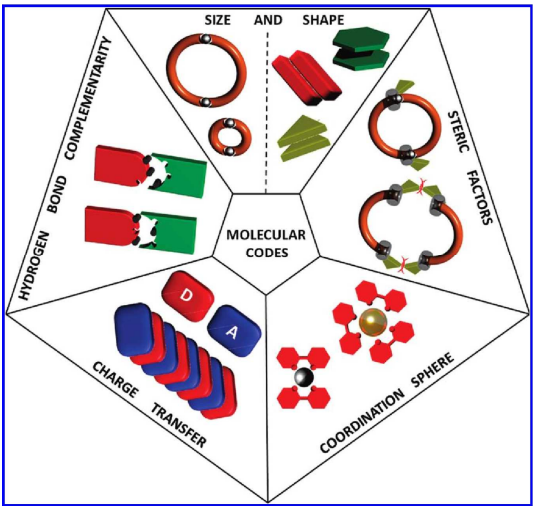

Figure 8.2. Molecular codes in self sorting systems.

The main differentiations processes can be classified as *narcissistic self-sorting*[72] or *social self-sorting*.[73] In the first instance, the molecule or ion manifests the affinity only towards itself, while in the second case it is able to selectively discriminate one constituent among many others.

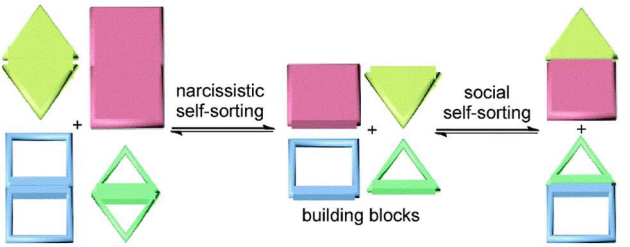

Figure 8.3. Schematic representation of narcissistic and social self-sorting

A further classification can be that of *non-integrative* and *integrative self-sorting* (**Figure 8.4**). Through the first type of process, it is possible to obtain more supramolecular systems each consisting of a subunit able to interact in a specific and selective way. Instead, in the second type all the subunits are connected leading to a single *integrative* supramolecular complex.

[72] A. Wu, L. Isaacs; *J. Am. Chem. Soc.*; **2003**, *125*, 4831.
[73] A. Shivanyuk, J. Jr. Rebek; *J. Am. Chem. Soc.*; **2002**, *124*, 12074.

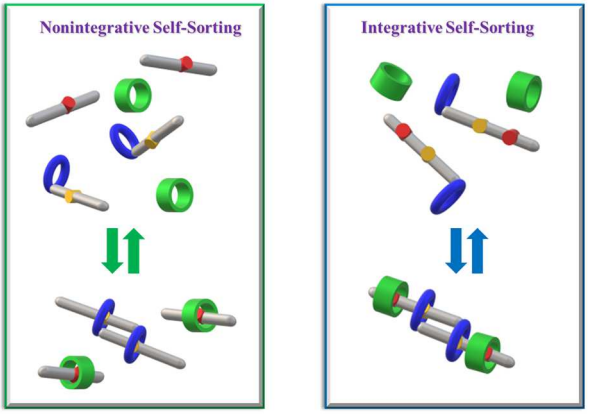

Figure 8.4. nonintegrative and integrative self-sorting.

8.2 Self-sorting in supramolecular chemistry

One of the most significant examples of synthetic self-sorting processes was reported in 2008 by Schalley and coll.[74] In detail, a hetero[3]rotaxane system was formed by integrative self-sorting (**Scheme 8.1**) exploiting two crown ethers, **77** and **78**, of different size and an axle bearing two different ammonium sites, **79**.

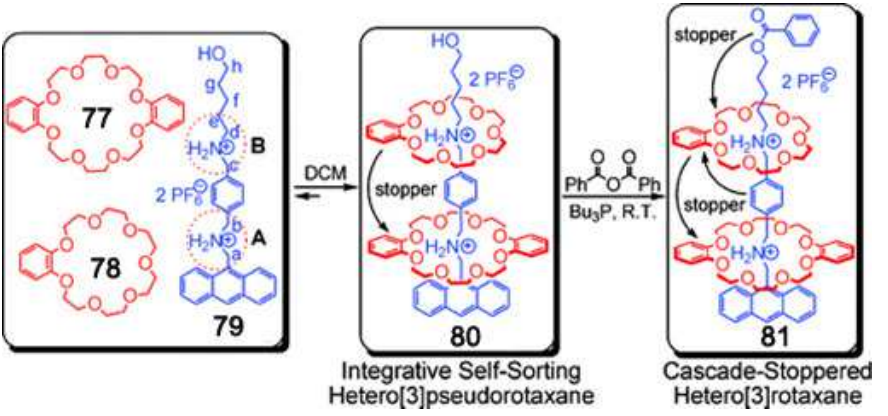

Scheme 8.1. Sequence-specific formation of hetero[3]pseudorotaxane **80** based on an integrative self-sorting process and the synthesis of "cascade-stoppered" hetero[3]rotaxane **81**.

[74] Jiang, W.; Winkler, H. D. F.; Schalley, C. A. *J. Am. Chem. Soc.* **2008**, *130* (42), 13852–13853.

The benzo-21-crown-7 wheel **78** has a very small cavity which cannot be crossed by benzyl groups. Therefore, this macrocycle can only integrate the ammonium site B of the axle **79**. Instead, the larger dibenzo-24-crown-8 unit **77** is able to reach site A of the axle **79**.

Other examples of interesting self-sorting based on calixarene pseudorotaxanes were reported in 2013.[75] In detail, by mixing very similar calix[6]arene macrocycles with bis-ammonium axles, it was observed that each calixarene is able to select its own axle leading to the formation of only two pseudorotaxanes out of twenty possible ones (**Scheme 8.2**).

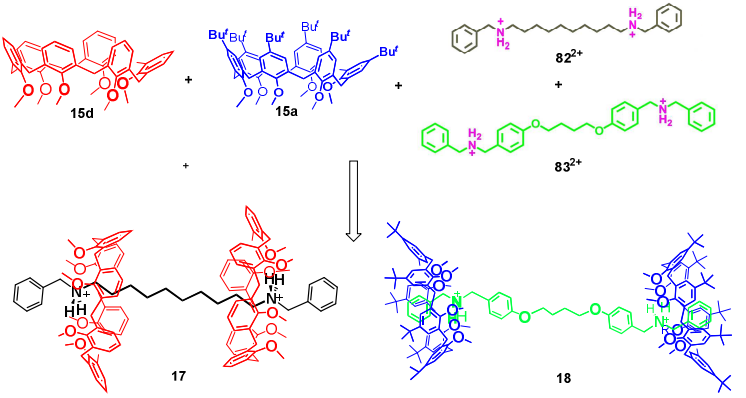

Scheme 8.2. Nonintegrative Self-sorting of calixarene pseudo[3]rotaxane systems.

The experiment described in **Scheme 8.2** led to the writing of the following molecular code:

- **Rule 1** (social behavior): benzylalkylammonium sites on bis-ammonium axles select non-*tert*-butylated calix[6]arene wheels in preference to *tert*-butylated ones, which thus remain uncomplexed.
- **Rule 2** (stereochemistry): threading of a directional alkylbenzylammonium station through a non-*tert*-butylated hexaalkoxycalix[6]arene occurs with preference for the *endo*-alkyl orientation.
- **Rule 3** (social behavior): benzyl-*p*-alkoxybenzylammonium sites on a bis-ammonium axle select *tert*-butylated calix[6]arenes over non-*tert*-butylated ones, which remain uncomplexed.
- **Rule 4** (stereochemistry): threading of a benzyl-*p*-alkoxybenzylammonium site through a *tert*-butylated hexaalkoxycalix[6]arene occurs with preference for the *endo*-benzyl configuration.

The definition of the above molecular code led to the design of a directional bis-ammonium axle **84²⁺**, which is constitutionally non-symmetric (**Figure 8.5**).

[75] Talotta, C.; Gaeta, C.; Qi, Z.; Schalley, C. A.; Neri, P. *Angew. Chem. Int. Ed.* **2013**, *52* (29), 7437–7441.

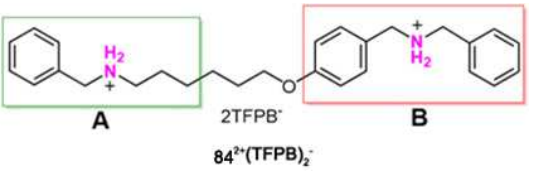

Figure 8.5. Derivative $\mathbf{84}^{2+}(TFPB)_2^-$.

The mixing of axle $\mathbf{84}^{2+}$ with the two calix[6]arene wheels **15d** and **15a** led to the sorting of only one interpenetrate system out of 16 stereo-adducts potentially possible. (**Figure 8.6**). This is the first example in the literature in which an integrative self-sorting process is able to discriminate at the same time both sequence and stereochemistry of the wheels.

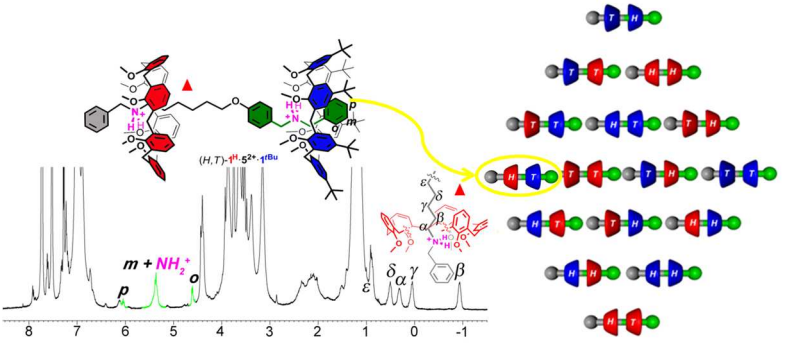

Figure 8.6. ^{1}H NMR spectrum of pseudo[3]rotaxane self-sorted (400 MHz, 298 K, $CDCl_3$).

8.3 Self-sorting in a heteropseudo[3]rotaxane system

On the basis of the above information, it was decided to study the stereoselective integrative self-sorting of a heteropseudo[3]rotaxane (**Figure 8.7**) by exploiting two calixarene wheels of different size and a specifically designed axle. The non-symmetrical bis-ammonium axle $\mathbf{85}^{2+}$ was designed by including an alkylbenzyl and a bis-benzyl site (**Figure 8.7**) counterbalanced by TFPB- "superweak anion". This system was designed by integrating the previously described molecular code with the additional information obtained from threading studies on calix[5]arene wheels. In fact, it was observed that the smaller calix[5]arene annulus does not allow the passage of a benzyl group. Therefore, in the presence of an alkylbenzylammonium axle it only gives the *endo*-alkyl adduct.

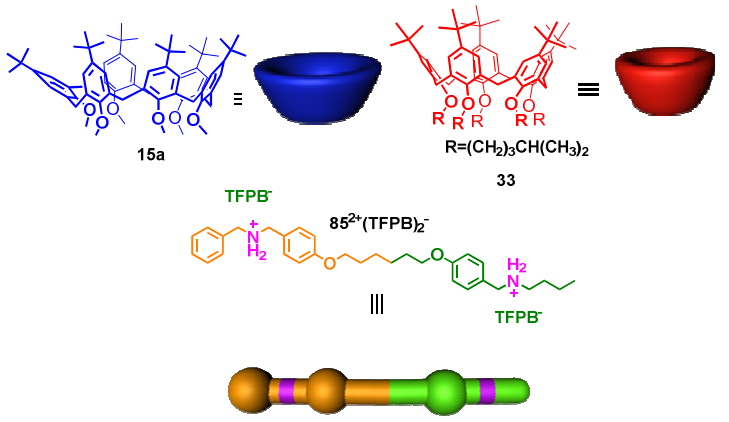

Figure 8.7. Components for Heteropseudo[3]rotaxane.

8.3.1 Synthesis of linear system $85^{2+}(TFPB)_2^-$

Linear system **85** was obtained with the synthetic procedure shown in **Scheme 8.3**.

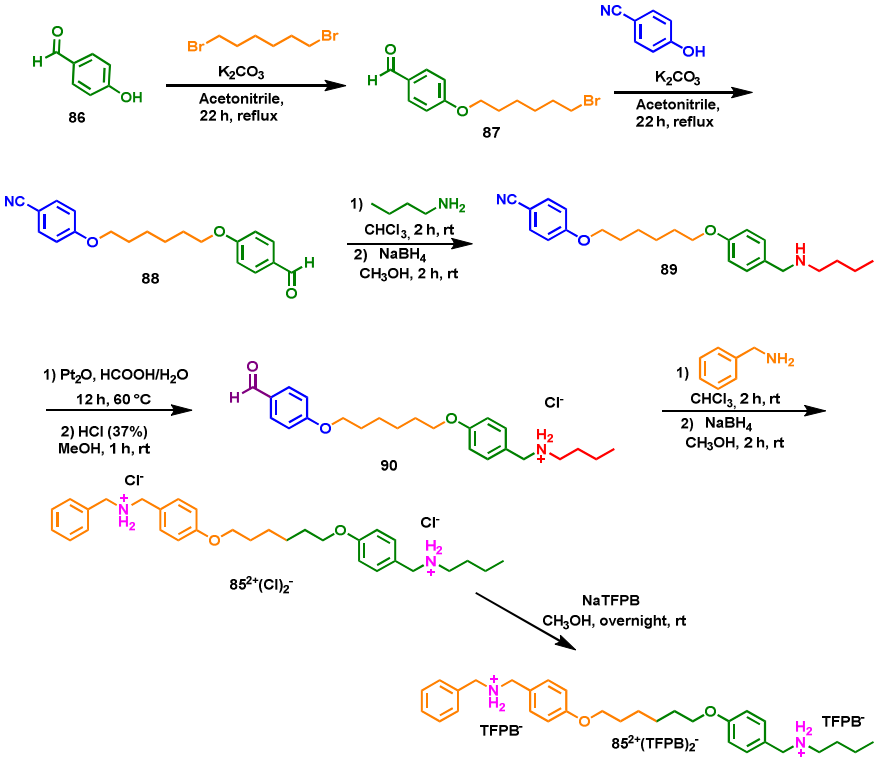

Scheme 8.3. Synthesis of derivative $\mathbf{85}^{2+}(TFPB)_2^-$.

Initially, a reductive amination reaction was performed between butylamine and aldehyde **86**. Subsequently, the cyano group was transformed into an aldehyde **88**, which in turn was reacted in a second amination reaction with benzylamine. Once the non-symmetric diamine was obtained, a salification step was carried out $\mathbf{85^{2+}(Cl)_2^-}$. Finally, an anion exchange with NaTFPB led to the desired axle $\mathbf{85^{2+}(TFPB)_2^-}$**.**The linear system was characterized by NMR spectroscopy. In detail, an analysis of the proton spectrum evidenced three N-CH_2-Ar singlets (4.11, 4.16, and 4.20 ppm) and one N-CH_2-CH_2 triplet at 3.0 ppm. Finally, in the 7.0-7.5 ppm aromatic zone, there are signals related to benzyl rings and to the TFPB anion.

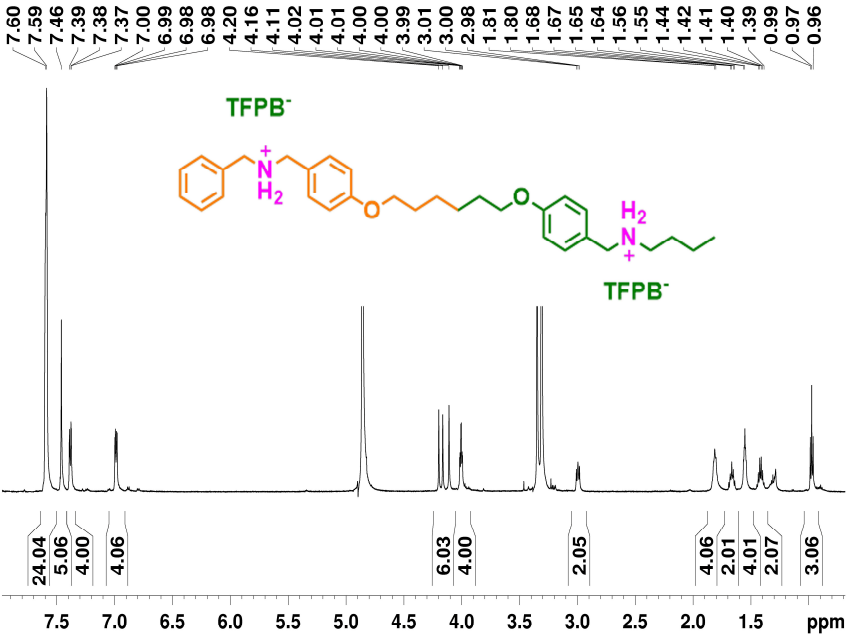

Figure 8.8. ^{1}H NMR spectrum of derivative $\mathbf{85^{2+}}(TFPB)_2^-$ (CD_3OD, 600 MHz, 298 K).

8.3.2 Threading of linear system $\mathbf{85^{2+}(TFPB)_2^-}$

With the bis-ammonium axle in hand, its threading abilities were studied with the two calix[5 and 6]arenes previously mentioned. Given the directionality of both axle and wheels, by their combination 16 different pseudo[3]rotaxanes can be obtained. These include the three possible *head-to-head* (*H-H*), *tail-to-tail* (*T-T*), and *head-to-tail* (*H-T*) relative orientations of the wheels (**Figure 8.9**).

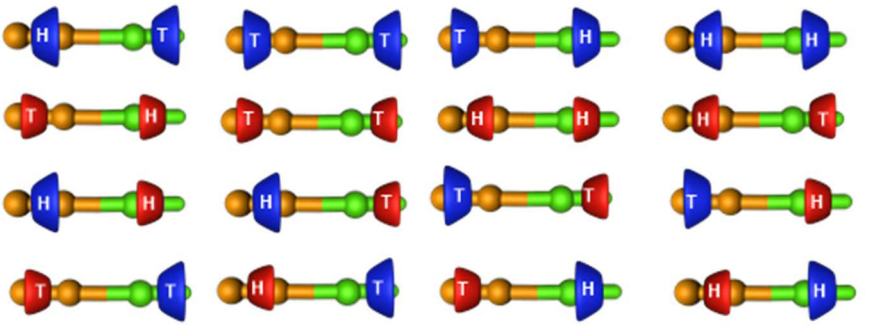

Figure 8.9. 16 possible interpenetrated systems.

Initially, preliminary tests were carried out by mixing axle $\mathbf{85}^{2+}$ with calix[6]-wheel **15a** in a 1:2 ratio. An inspection of the proton spectrum revealed the formation of one pseudo[3]rotaxane system (**Figure 8.10**). In fact, only the *T*-*T* adduct was obtained with respect to the four possible ones, which differ only by the spatial relative orientation of the wheels along the axle.

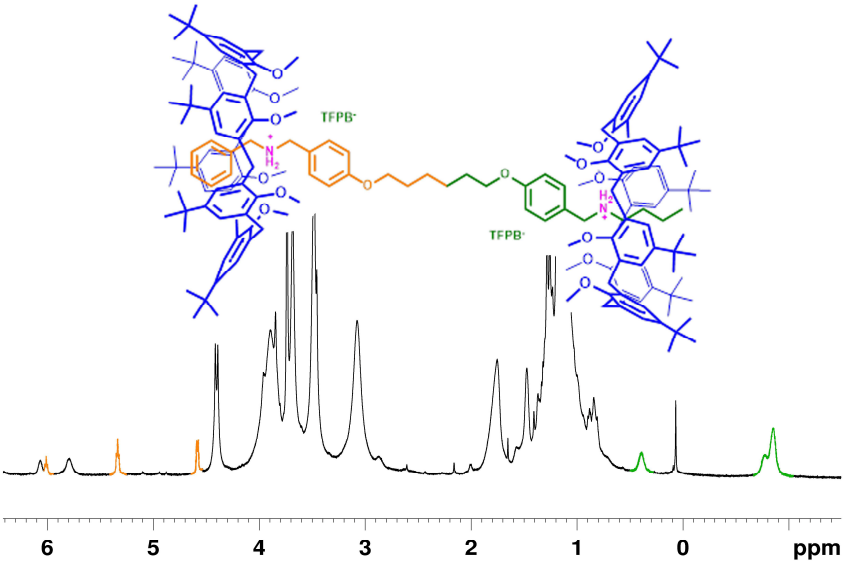

Figure 8.10. ^{1}H NMR spectrum of mixture 1:2 between derivatives $\mathbf{85}^{2+}$ $(TFPB)_2^-$ and **15a** ($CDCl_3$, 600 MHz, 298 K).

Subsequently, the NMR study was extended to the 1:2 mixture of axle $\mathbf{85}^{2+}$ and calix[5]-wheel **33**. Also, in this case, only one supramolecular system was formed. In fact, since the benzyl groups are too big to thread the calix[5]arene annulus, only the *endo*-alkyl pseudo[2]rotaxane can be obtained (**Figure 8.11**).

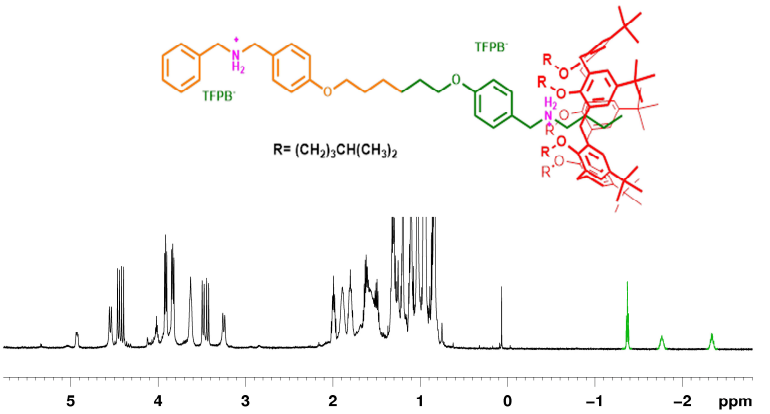

Figure 8.11. ^{1}H NMR spectrum of mixture 1:2 between derivatives **85**$^{2+}$ $(TFPB)_2^-$ and **33** ($CDCl_3$, 600 MHz, 298 K).

Given these good results, a sorting experiment was carried out by mixing bis-ammonium axle **85**$^{2+}$ **(TFPB)**$_2^-$ with the two wheels **15a** and **33** in a 1:1:1 ratio. The ^{1}H NMR spectrum revealed again the formation of only one pseudo[3]rotaxane out of the 16 possible ones. In particular, the (*T*-*T*)-heteropseudo[3]rotaxane depicted in **Figure 8.12** was obtained, in which the calix[5] and calix[6] wheels are resident in the alkylbenzyl and bis-benzyl site, respectively.

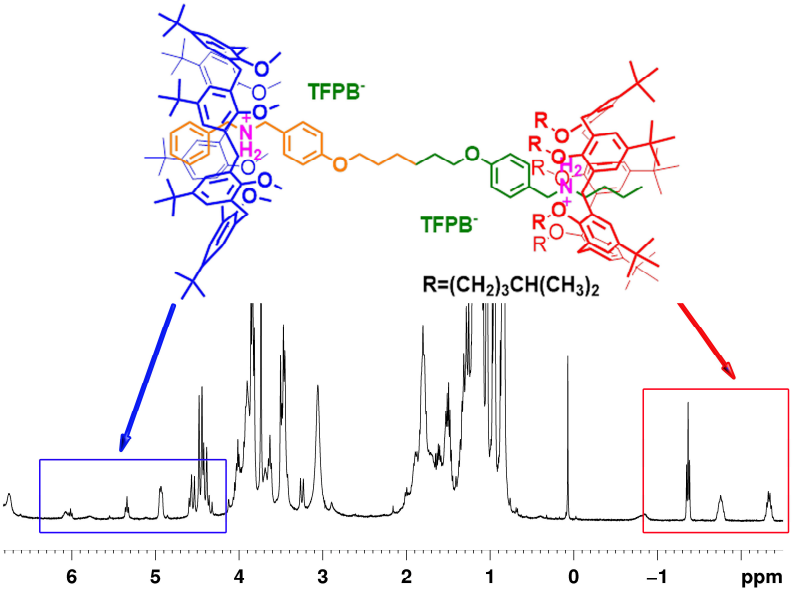

Figure 8.12. ^{1}H NMR spectrum of mixture 1:1:1 between derivatives **85**$^{2+}$ $(TFPB)_2^-$, **15a** and **33** ($CDCl_3$, 600 MHz, 298 K).

8.4 Conclusion

In conclusion, this chapter describes a self-sorting pseudo[3]rotaxane system based on a non-symmetric bis-ammonium axle and two different calixarene macrocycles that differ in the size of their cavity. The two different sites of the axle are able to discriminate the two different macrocycles. In addition, their binding is also stereoselective in terms of their relative spatial orientation.

8.5 Experimental Section

8.5.1 General Comments

Reactions under anhydrous conditions were conducted under an inert atmosphere (nitrogen) using dry solvents. The commercial reagents were purchased by Aldrich and TCIchemicals and were used without further purification. The reactions were controlled by thin-layer chromatography (TLC) with Macherey-Nagel plates coated with silica gel (0.25 mm) with fluorescence indicator UV254 and visualized using UV light and nebulization with an indicator solution of H_2SO_4-$Ce(SO_4)_2$. The reaction temperatures were measured externally using electronic thermometers. The reaction products were purified by Macherey-Nagel silica gel chromatography (60, 70-230 mesh). NMR spectra were recorded on Bruker Avance-600 spectrometer [600 (^{1}H) and 150 MHz (^{13}C)], Bruker Avance-400 spectrometer [400 (^{1}H) and 100 MHz (^{13}C)]. Chemical shifts are reported relative to the residual solvent peak (C*H*Cl_3: δ 7.26, *C*DCl_3: δ 77.16) Standard pulse programs, provided by the manufacturer, were used for 2D NMR experiments. High-resolution Mass spectra were acquired with a Bruker Solarix spectrometer equipped with a Tesla magnet. It was used a MALDI as methods of sample ionization. DHB was used as matrix. Samples were prepared in $CHCl_3$ (1 mg / mL).

8.5.2 Synthesis of derivative $85^{2+}(TFPB)_2^-$

Derivative 89

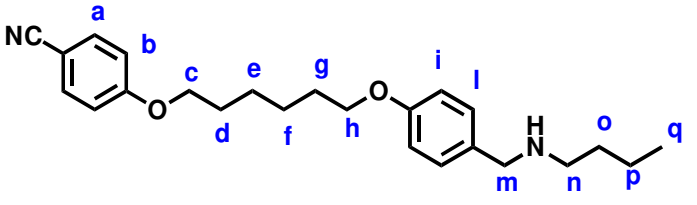

A mixture of derivative **88** (0.50 g, 1.55 mmol) and butylamine (0.11 g, 1.55 mmol) in $CHCl_3$ (5 mL) was stirred at room temperature for 2 h. The solvent was evaporated under reduced pressure to give the imine intermediate as a yellow oil in a quantitative yield. The imine intermediate was used for the next step without further purification. The imine was dissolved in THF (5 mL), and $NaBH_4$ (0.58 g, 15.46 mmol) was added at 0 °C and then the mixture was allowed to warm at room temperature. The solution was kept under stirring for 2 h. The solvent was removed under reduced pressure and the residue partitioned between AcOEt (50 mL) and an aqueous saturated solution of $NaHCO_3$ (100 mL). The organic layer was dried over $NaSO_4$ and the solvent was removed under reduced pressure, to give derivative **89** as a yellow oil 92 % (0.54 g, 1.42 mmol). **^{1}H NMR** ($CDCl_3$, 300 MHz, 298 K): δ 7.57 (d, H_l, 2H, J=8.7), 7.22 (d, H_a, 2H, J=8.2), 6.92 (d, H_b, 2H, J=8.2), 6.85 (d, H_i, 2H, J=8.7), 3.98 (overlapped, $H_{c,h}$, 4H), 3.72 (s, H_m, 2H), 2.61 (t, H_n, 2H, J=7.2), 1.82 (overlapped, $H_{d,g}$, 4H), 1.50 (overlapped, $H_{e,f,o}$, 6H), 1.32 (m, H_p, 2H), 0.93 (t, H_q, 3H). **^{13}C NMR** ($CDCl_3$, 75 MHz, 298 K): δ 162.6, 158.2, 134.1, 132.9, 129.4, 119.5, 115.3, 114.5, 103.9, 68.4, 67.9, 53.7, 49.3, 32.4, 29.4, 29.1, 26.0, 25.9, 20.7, 14.2. **MALDI-MS** (m/z) calcd for $[M+H]^+$= 381.2537 found 381.2557.

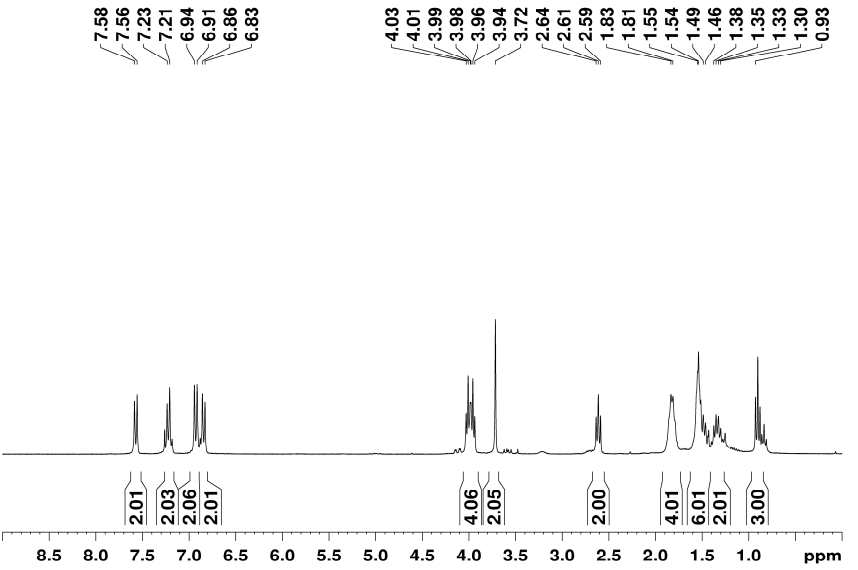

Figure 8.13. ^{1}H NMR of derivative **89** ($CDCl_3$, 400 MHz, 298 K).

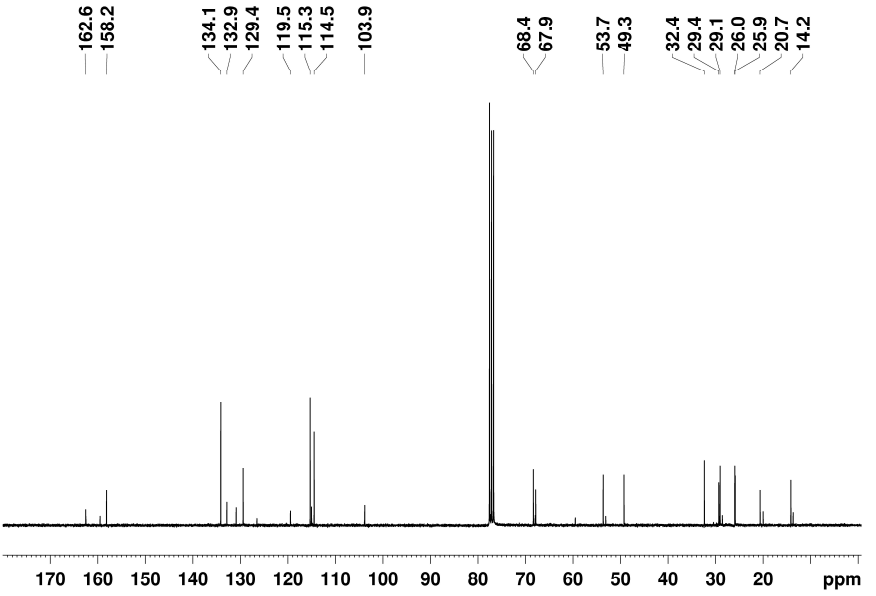

Figure 8.14. ^{13}C NMR of derivative **89** ($CDCl_3$, 100 MHz, 298 K).

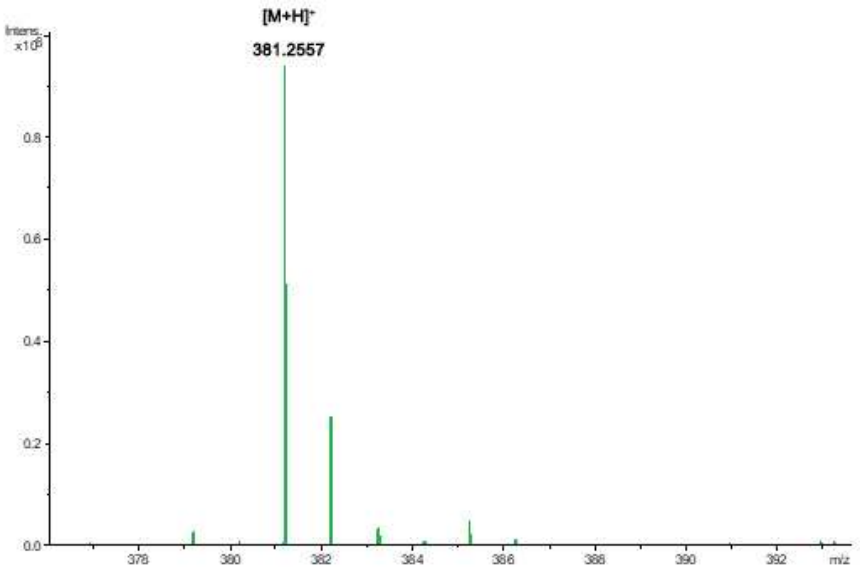

Figure 8.15. MALDI-MS spectrum of derivative **89**.

Derivative 90

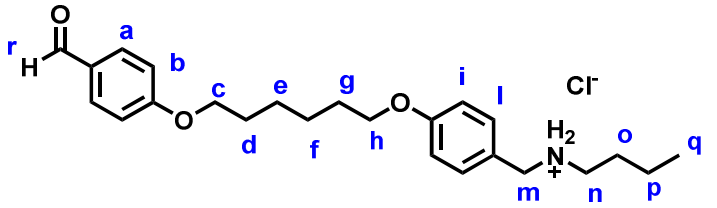

To a solution of derivative **89** (0.52 g, 1.37 mmol) and HCOOH/H_2O (80 % w/w 8 ml + 2 ml); was added (0.03 g, 0.14 mmol) and the reaction was stirred at 60 °C for 12h. The solution was cooled at room temperature and the catalyst was filtered. The crude product was extracted with AcOEt and the organic layer was dried over $NaSO_4$ and the solvent was removed under reduced pressure. Subsequently, raw was treated with HCl (37 %) in methanol at room temperature for 1 hour. The solvent was removed under reduced pressure and the crude was precipitated in acetonitrile to give derivative **90** (0.14 g, 28 %) as a white solid. **^{1}H NMR** (CD_3OD, 250 MHz, 298 K): δ 9.82 (s, H_r, 1H,), 7.85 (d, H_l, 2H, J=8.7), 7.36 (d, H_a, 2H, J=8.2), .7.06 (d, H_b, 2H, J=8.2), 6.97 (d, H_i, 2H, J=8.7), 4.05 (overlapped, $H_{c,h,m}$, 6H), 2.96 (t, H_n, 2H, J=7.2), 1.57 (overlapped, $H_{d,g,e,f,o,p}$, 12H), 1.00 (t, H_q, 3H). **^{13}C NMR** (CD_3OD, 62.5 MHz, 298 K): δ 191.3, 159.9, 131.6, 130.8, 114.5, 114.4, 67.9, 67.4, 50.5, 28.7, 27.9, 25.3, 19.4, 12.4. **MALDI-MS** (m/z) calcd for $[M]^+$= 384.2533 found 384.2565.

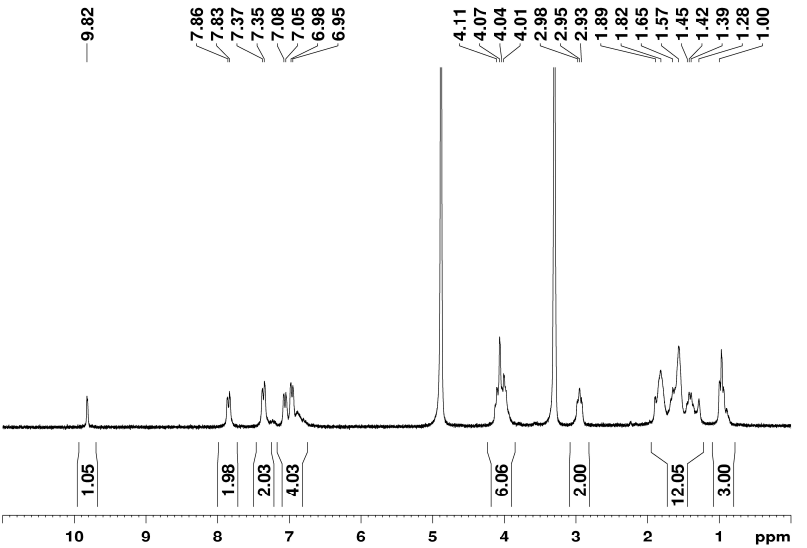

Figure 8.16. ^{1}H NMR of derivative **90** (CD_3OD, 250 MHz, 298 K).

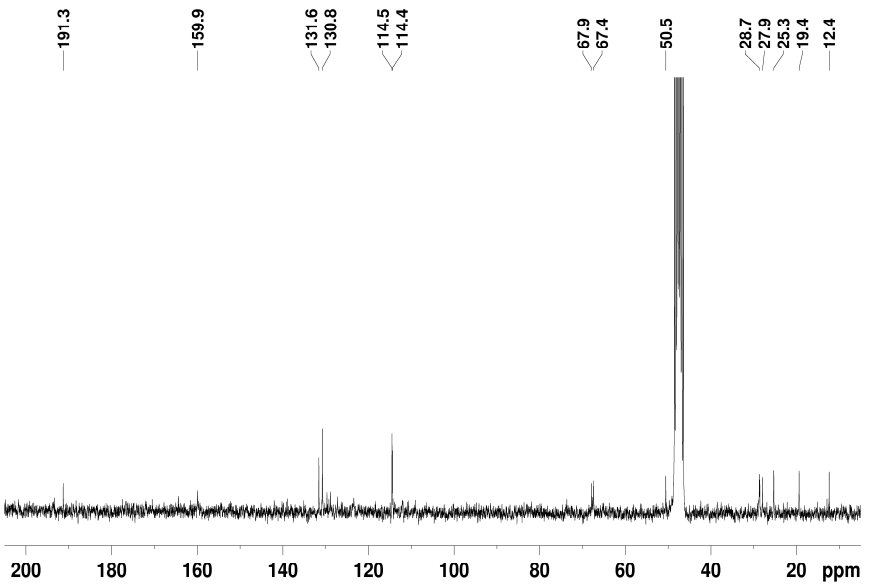

Figure 8.17. ^{13}C NMR of derivative **90** ($CDCl_3$, 62.5 MHz, 298 K).

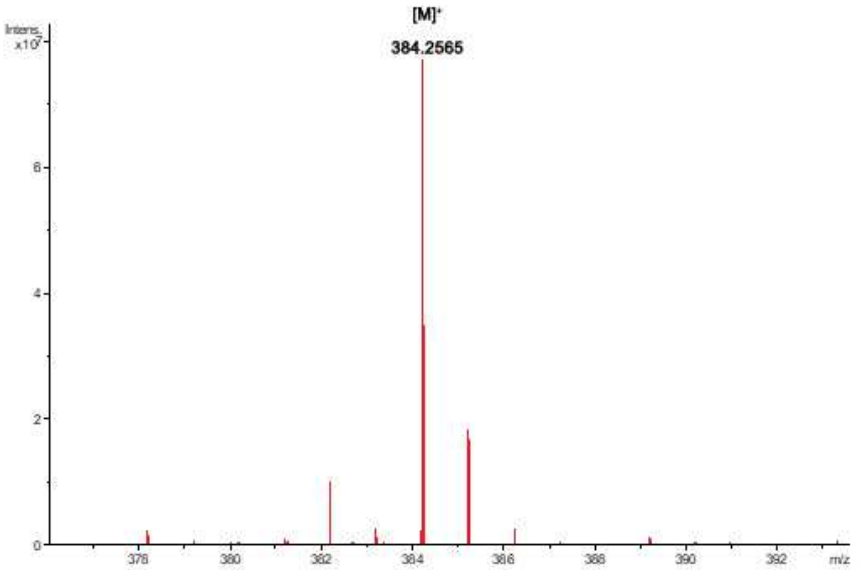

Figure 8.18. MALDI-MS spectrum of derivative **90**.

Derivative $85^{2+}(Cl)_2^-$

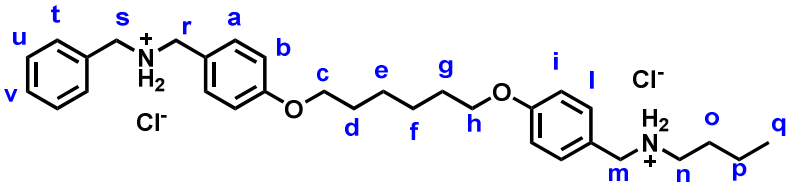

A mixture of derivative **90** (0.50 g, 1.55 mmol) and benzylamine (0.11 g, 1.55 mmol) in $CHCl_3$ (5 mL) was stirred at room temperature for 2 h. The solvent was evaporated under reduced pressure to give the imine intermediate as a yellow oil in a quantitative yield. The imine intermediate was used for the next step without further purification. The imine was dissolved in THF (5 mL), and $NaBH_4$ (0.58 g, 15.46 mmol) was added at 0 °C and then the mixture was allowed to warm at room temperature. The solution was kept under stirring for 2 h. The solvent was removed under reduced pressure and the residue partitioned between AcOEt (50 mL) and an aqueous saturated solution of $NaHCO_3$ (100 mL). The organic layer was dried over $NaSO_4$ and the solvent was removed under reduced pressure, to give derivative **$85^{2+}(Cl)_2^-$** as a yellow oil. The amine was treated with HCl 37% (2 ml) in methanol. (5 ml). Reaction was stirred at room temperature for 30 min. Solvent was evaporated. Raw was triturated in acetonitrile. The product was obtained as white solid, 92 % (0.54 g, 1.42 mmol). **^{1}H NMR** (CD_3OD, 400 MHz, 298 K): δ 7.46 (overlapped, $H_{t,u,v}$, 5H),), 7.39 (overlapped, $H_{a,l}$, 4H), 6.99 (overlapped, $H_{b,i}$, 4H), 4.16 (overlapped, $H_{m,r,s}$, 6H), 4.01 (overlapped, $H_{c,h}$, 4H), 3.00 (t, H_n, 2H), 1.82 (overlapped, $H_{d,g}$, 4H), 1.67 (m, H_o, 2H), 1.56 (overlapped, $H_{e,f}$, 4H), 1.42 (m, H_p, 2H), 0.98 (t, H_q, 3H). **^{13}C NMR** (CD_3OD, 100 MHz, 298 K): δ 161.6, 132.6, 132.5, 131.0, 130.7, 130.4, 124.2, 124.0, 116.1, 116.1, 69.1, 51.9, 51.8, 51.7, 48.1, 30.3, 29.2, 27.0, 20.9, 13.8

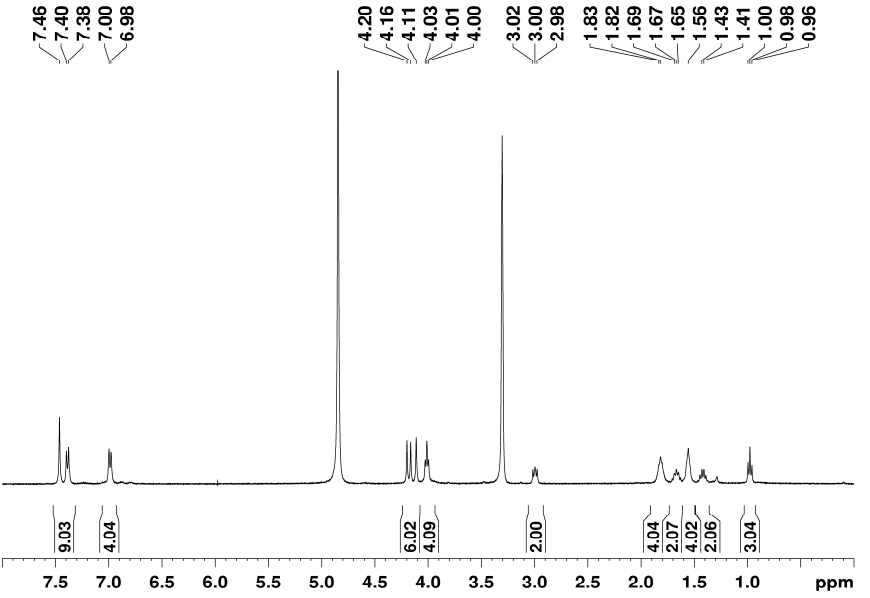

Figure 8.19. ^{1}H NMR of derivative **85**$^{2+}$$(Cl)_2^-$ (CD_3OD, 400 MHz, 298 K).

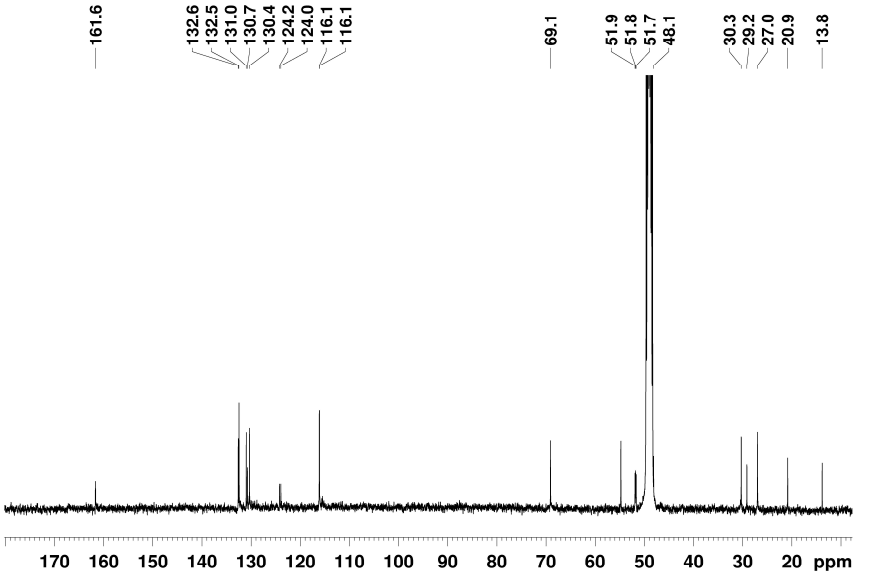

Figure 8.20. ^{13}C NMR of derivative **85**$^{2+}$$(Cl)_2^-$ (CD_3OD, 100 MHz, 298 K).

Derivative $85^{2+}(TFPB)_2^-$

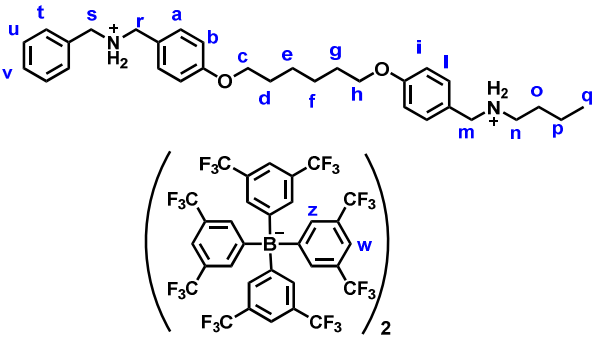

Derivative $\mathbf{85^{2+}(Cl)_2^-}$ (0.08 g, 0.17 mmol was dissolved in methanol (5 mL), then sodium tetrakis[3,5- bis(trifluoromethyl)phenyl]borate4 (0.30 g, 0.34 mmol) was added. The mixture was kept under stirring overnight in the dark. The solvent was removed and deionized water was added, obtaining a brown precipitate that was filtered off and dried under vacuum for 48 h to give derivative $\mathbf{85^{2+}(TFPB)_2^-}$ as a brown solid (0.32 g, 0.14 mmol, 84%). **^{1}H NMR** (300 MHz, $CDCl_3$, 298 K): δ 8.46 (s, -OH, 2H), δ 7.00 (m, ArH-OCH_3, 8H), δ 6.85 (s, Br-ArH-OH, 4H), δ 3.95 (s, -$ArCH_2Ar$-, 4H), δ 3.80 (s, -$ArCH_2Ar$-, 8H), δ 3.22 (s, -OCH_3, 12H), δ 1.17 (s, -$C(CH_3)_3$, 36H). **^{13}C NMR** (150 MHz, $CDCl_3$, 298 K): δ 161.6, 135.8, 132.6, 132.4, 130.3, 128.5, 126.7, 124.9, 123.1, 118.5, 116.1, 116.1, 69.1, 51.9, 51.8, 51.7, 48.1, 30.3, 29.1, 27.0, 20.8, 13.8. **MALDI-MS** (m/z) calcd for $[M]^+$= 475.3319 found 475.3334. calcd for $[M^+TFPB]^+$= 1339.4046 found 1339.4090.

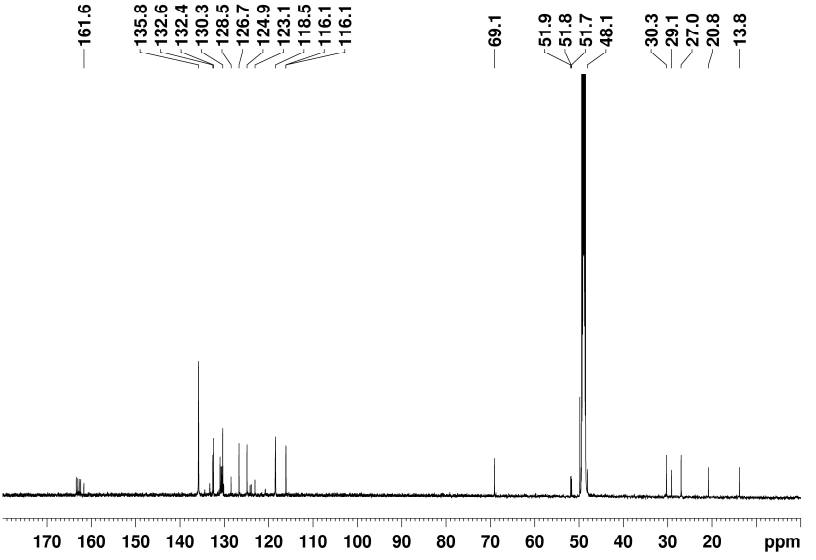

Figure 8.21. ^{13}C NMR of derivative $\mathbf{85^{2+}}(TFPB)_2^-$ ($CDCl_3$, 150 MHz, 298 K).

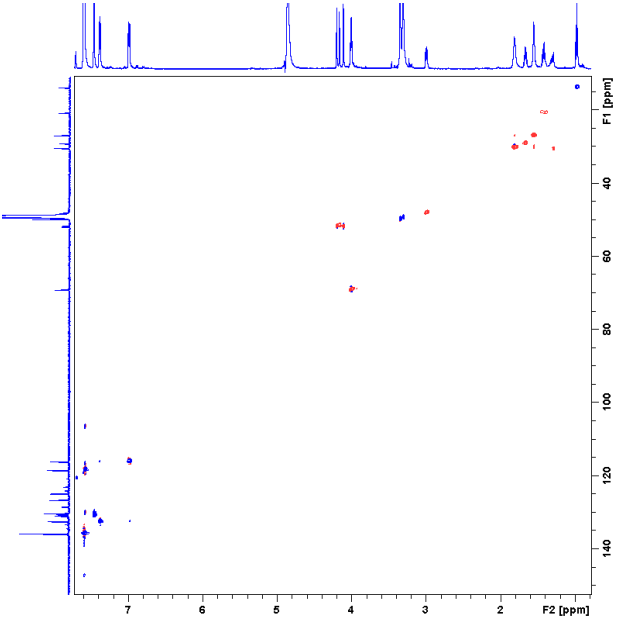

Figure 8.22. 2D HSQC of derivative **85**$^{2+}$(TFPB)$_2^-$ ($CDCl_3$, 600 MHz, 298 K).

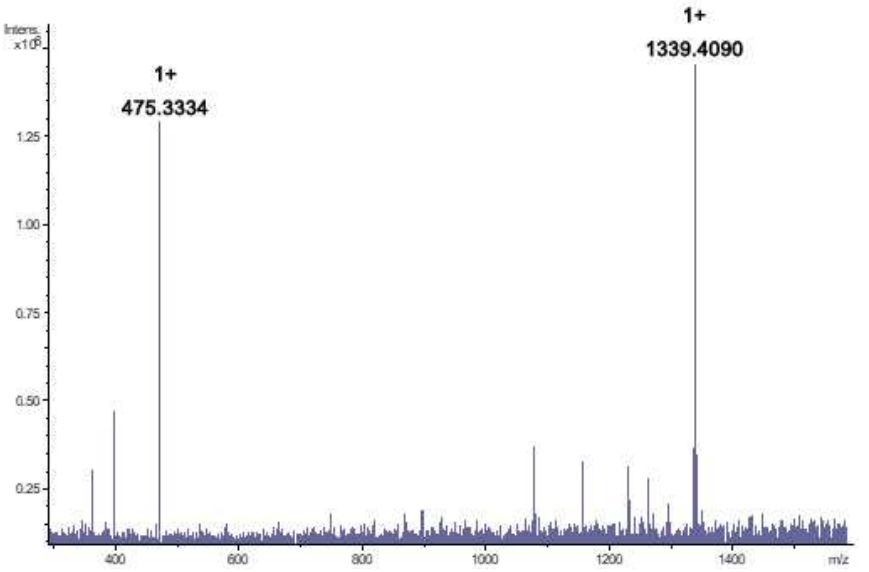

Figure 8.23. MALDI-MS spectrum of derivative **85**$^{2+}$(TFPB)$_2^-$.

8.5.3 Synthesis of pseudo[n]rotaxane systems

A mixture of host and guest was dissolved in $CDCl_3$ and was transferred in a NMR tube. In detail, in **Table 8.1** it was reported concentration using for calixarenes derivative and for axle. Then, the solution was transferred in an NMR tube for 1D and 2D NMR spectra acquisition.

Table 8.1. Amount of host and guests for complexation experiments.

		Pseudo[n]rotaxanes		
		$85^{2+}\subset$15a	**$85^{2+}\subset$33**	**$85^{2+}\subset$(15a·33)**
15a	**(mg)**	5.44		2.24
	(mmol)	$5.2 \cdot 10^{-3}$		$2.1 \cdot 10^{-3}$
33	**(mg)**		6.00	2.60
	(mmol)		$4.8 \cdot 10^{-3}$	$2.1 \cdot 10^{-3}$
$85^{2+}(TFPB)_2^-$	**(mg)**	5.67	5.37	4.66
	(mmol)	$2.6 \cdot 10^{-3}$	$2.4 \cdot 10^{-3}$	$2.1 \cdot 10^{-3}$
$CDCl_3$	**(ml)**	0.7	0.7	0.6

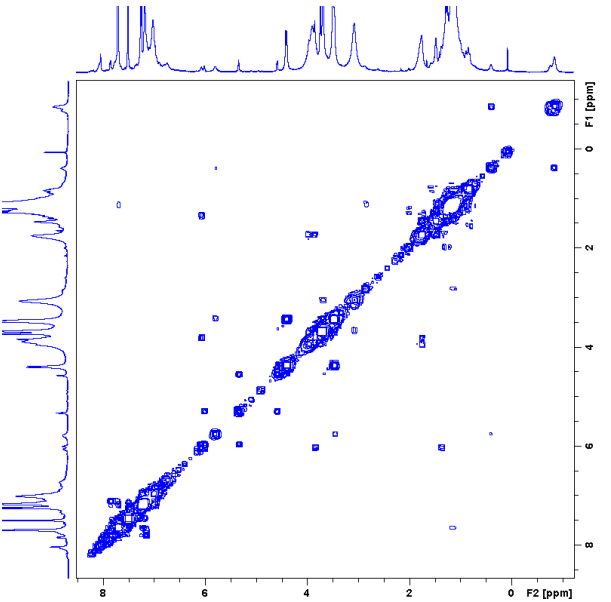

Figure 8.24. 2D COSY of mixture **15a/85^{2+}**$(TFPB)_2^-$ 2:1 ($CDCl_3$, 600 MHz, 298 K).

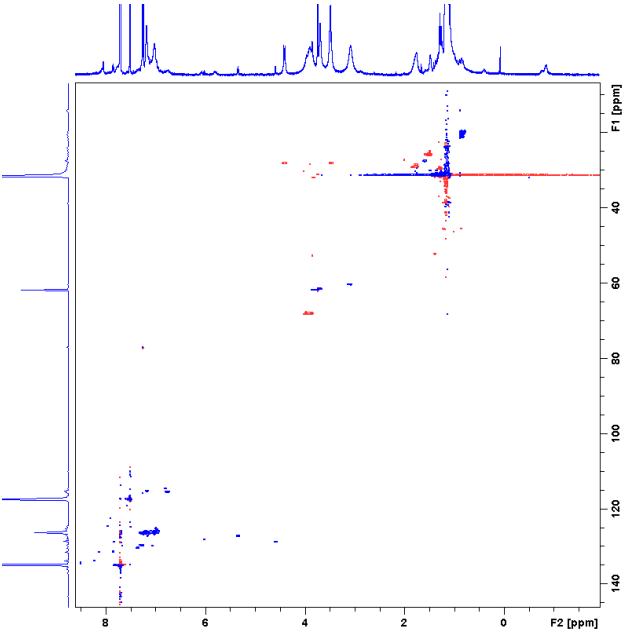

Figure 8.25. 2D HSQC of mixture **15a/85**$^{2+}$(TFPB)$_2^-$ 2:1 ($CDCl_3$, 600 MHz, 298 K).

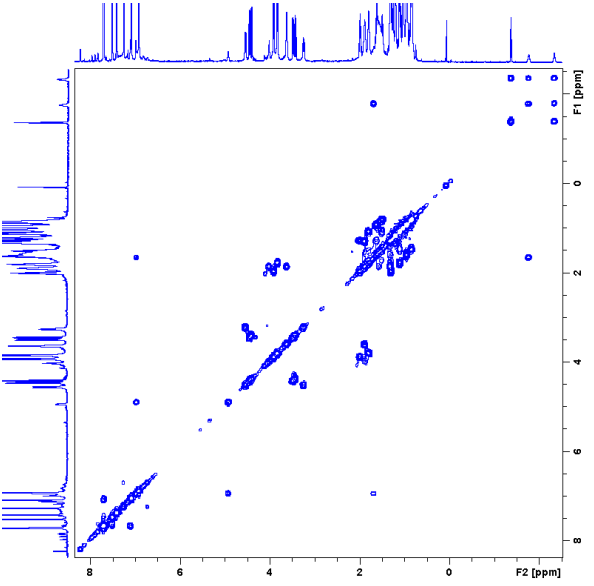

Figure 8.26. 2D COSY of mixture **33/85**$^{2+}$(TFPB)$_2^-$ 2:1 ($CDCl_3$, 600 MHz, 298 K).

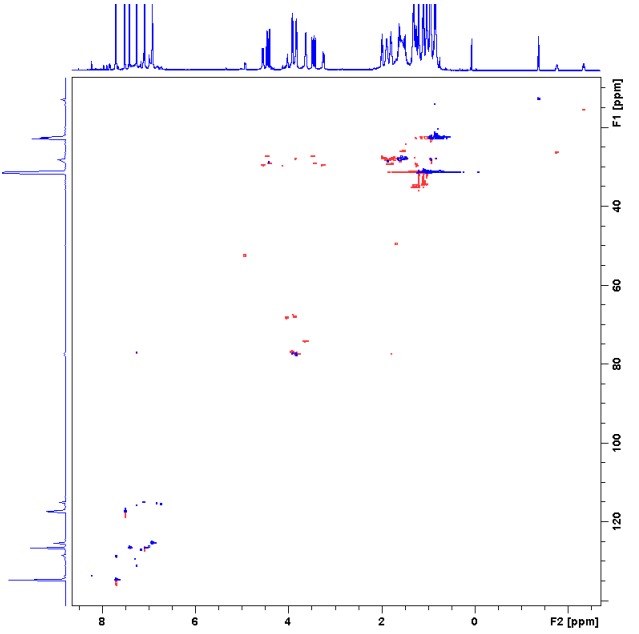

Figure 8.27. 2D HSQC of mixture **33/85**$^{2+}$(TFPB)$_2^-$ 2:1 ($CDCl_3$, 600 MHz, 298 K).

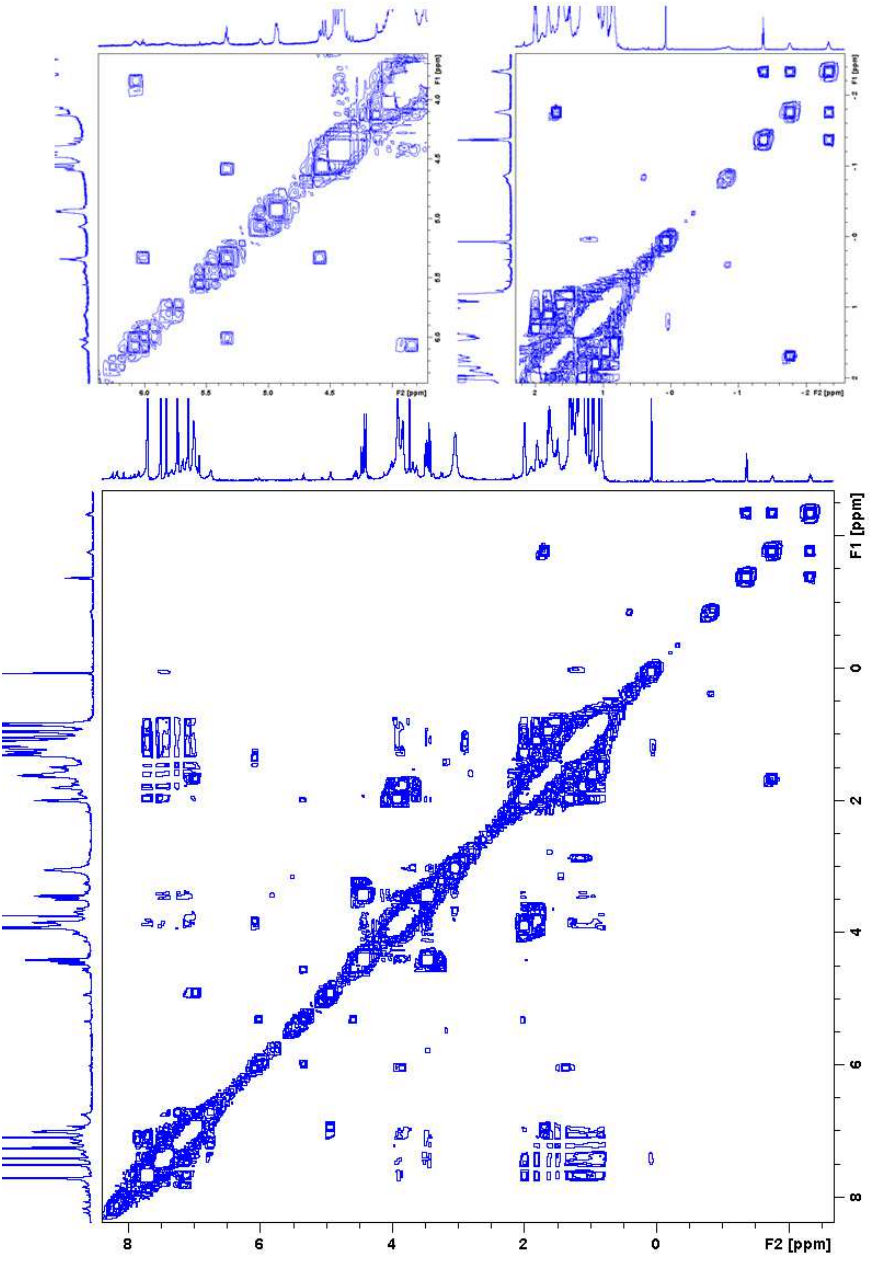

Figure 8.28. 2D COSY of mixture **15a/33/85**$^{2+}$ $(TFPB)_2^-$ 1:1:1 ($CDCl_3$, 600 MHz, 298 K).

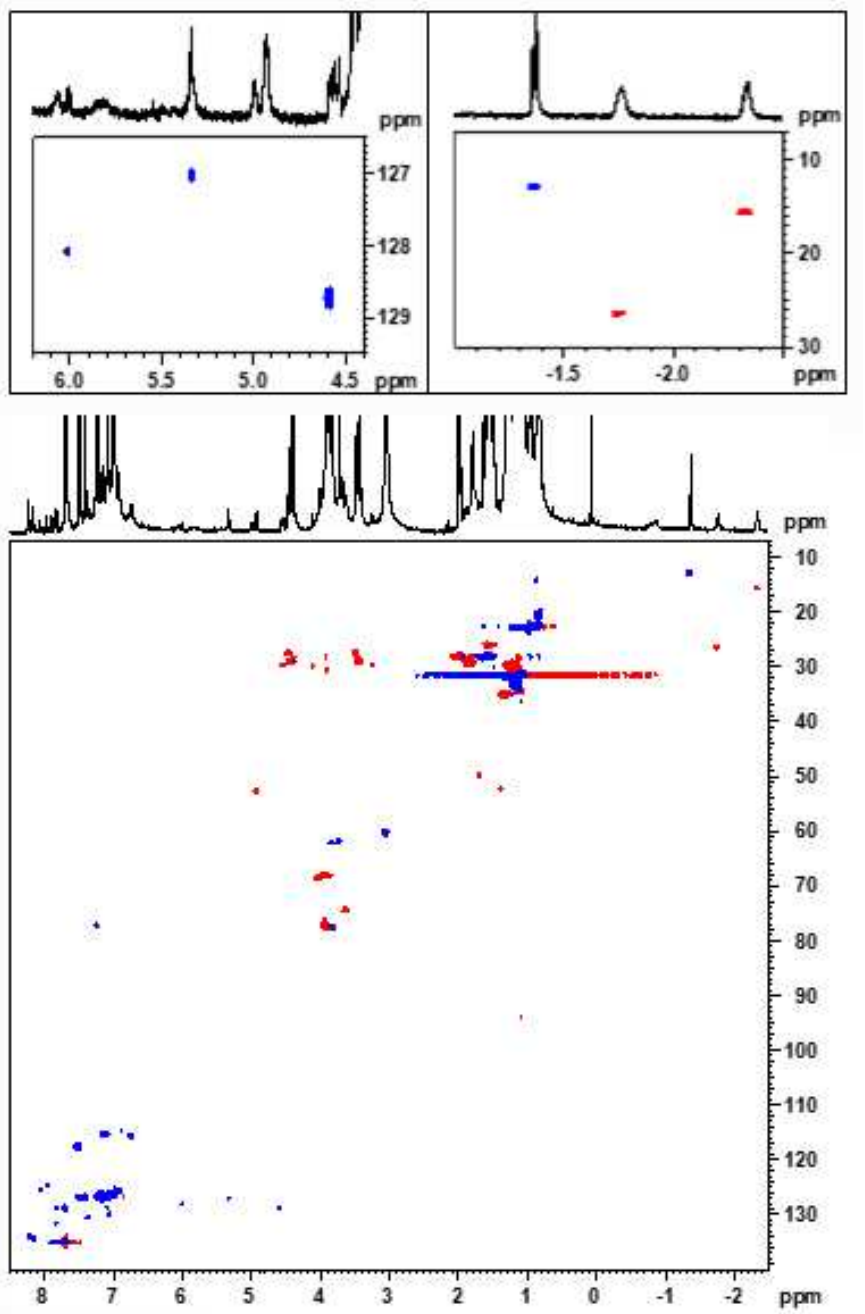

Figure 8.29. 2D HSQC of mixture **15a/33/85**$^{2+}$ $(TFPB)_2^-$ 1:1:1 ($CDCl_3$, 600 MHz, 298 K).

CHAPTER IX

Conclusion

9.1 Conclusions

In conclusion, in this PhD project the attention was focused on the threading abilities of calixarene macrocycles to provide useful information for the future construction of mechanically interlocked molecular machines.

Initially, the threading abilities of calix[6]arenes specifically functionalized at the upper rim, lower rim, or methylene bridges have been investigated. This study demonstrated that a better association with ammonium axles is obtained when the calix[6]arene macrocycle bears bulky groups, such as adamantyls, at the upper rim and when it is totally alkylated at the lower rim. Furthermore, it was observed that alkylation of the methylene bridges leads to a greater preorganization of the cavity and, consequently, to higher association constants.

The threading study was then extended to bifunctional calixarenes bearing electron rich or electron poor aromatic groups. It was observed that threading occurs with EDGs while EWGs do not lead to the formation of interpenetrated systems. On the other hand, calixarenes bearing EWGs have shown interesting chromogenic properties, such as halochromism and solvatochromism.

The possible application of multivalent systems for the future construction of molecular machines was then evaluated by studying the threading abilities of a triple-calix[6]arene host. It was demonstrated that this triple-host can give multiple-threading processes when mixed with various ammonium axles. Furthermore, in the presence of a directional alkylbenzylammonium axle, the stereoselective formation of multiple *endo*-alkyl pseudorotaxane stereoisomers was observed.

Finally, a self-sorting interpenetrated system was obtained, which is based on a non-symmetric bis-ammonium linear axle and two different calixarene macrocycles that differ in the size of their cavity. The two different recognition sites of the axle can selectively bind each own specific macrocycle. Interestingly, the relative spatial orientation of the two macrocycles is also stereoselectively fixed during the self-sorting binding process.